SEISMIC SAFETY AND RISK ASSESSMENT OF EXISTING STEEL BUILDINGS

A thesis submitted to the Faculty of Engineering of the University of Porto for the degree of Doctor of Philosophy in Civil Engineering

By

Miguel Neves Martins Ferreira de Araújo

January 2016

Department of Civil Engineering
Faculty of Engineering
University of Porto

Seismic Safety and Risk Assessment of Existing Steel Buildings

Miguel Neves Martins Ferreira de Araújo

Doctoral Program in Civil Engineering

Thesis Examining Committee:

President: Dr Rui Manuel Carvalho Marques de Faria, Full Professor at the Civil Engineering Department of the Faculty of Engineering of the University of Porto, Portugal.
Examiner: Dr Dimitrios Lignos, Associate Professor at École Polytechnique Fédérale de Lausanne, Switzerland.
Examiner: Dr Rita Nogueira Leite Pereira Bento, Associate Professor at the Civil Engineering Department of the Technical Institute of the University of Lisbon, Portugal.
Examiner: Dr Raimundo Moreno Delgado, Full Professor at the Civil Engineering Department of the Faculty of Engineering of the University of Porto, Portugal.
Examiner: Dr Xavier das Neves Romão, Assistant Professor at the Civil Engineering Department of the Faculty of Engineering of the University of Porto, Portugal.
Supervisor: Dr José Miguel de Freitas Castro, Assistant Professor at the Civil Engineering Department of the Faculty of Engineering of the University of Porto, Portugal

December 12, 2018

Abstract

This thesis deals with the seismic safety and risk assessment of existing steel buildings and aims, in brief, at contributing to the current lack of knowledge regarding the adequacy of the seismic safety assessment procedures preconized within the part 3 of Eurocode 8 (EC8-3) and at providing a first projection of the potential industrial seismic losses for Mainland Portugal.

The work is divided into two main parts. The first is devoted to the review of the current conceptual frameworks and procedures preconized in different guidelines and codes for seismic safety assessment of existing buildings. Particular attention is given to numerous inconsistencies identified in the use of EC8-3. The consistency, efficiency and sufficiency of different code-based record selection and scaling methods are assessed. The reliability of the EC8-3 linear analysis procedures is also investigated alongside with the criterion established to verify their applicability. A novel simplified procedure for estimating local inelastic deformation demands using linear-elastic methods of analysis is proposed. Concomitantly, the adequacy of the deformation capacity limits preconized by EC8-3 is addressed. Prediction equations for quantifying the deformation capacity of laterally retrained steel members with any European cross-section profile that account for fracture initiation and the onset of local buckling are derived.

In the second part of the thesis, the focus is on the development of an industrial seismic risk model for Mainland Portugal. A review of the most common types of property damage to industrial steel buildings, as well as the factors that influence the most business interruption, is presented. The three components of seismic risk – hazard, exposure and vulnerability – are covered. A comprehensive industrial exposure model that incorporates economic statistical information respective to the 2-digit industrial activities of the Portuguese CAE System and the geographical distribution of the as-built building stock based on information collected from existing databases is developed. A novel vulnerability model for industrial steel buildings is proposed using statistical information gathered from hundreds of real surveyed buildings. Losses to industrial property, including structural and non-structural components and contents, and direct and indirect losses to industrial activity and production are quantified.

Resumo

Esta dissertação aborda o tema da avaliação da segurança e risco sísmicos de edifícios existentes em aço e procura contribuir para a atual falta de conhecimento relativo à robustez dos procedimentos para a avaliação da segurança sísmica preconizados na parte 3 do Eurocódigo 8 (EC8-3), bem como fornecer uma primeira projeção das perdas sísmicas potenciais sobre a atividade e propriedade industrial existentes em Portugal Continental.

Este trabalho encontra-se dividido em duas partes. A primeira dedica-se à revisão das atuais metodologias e procedimentos para a avaliação da segurança sísmica de edifícios existentes propostos em diferentes códigos e documentos orientadores. Particular atenção é prestada às inconsistências identificadas na aplicação do EC8-3. A consistência, eficiência e suficiência dos métodos de seleção e escalamento de registos sísmicos reais propostos em diferentes documentos normativos é igualmente avaliada, bem como a fiabilidade dos procedimentos de análise linear do EC8-3 e do critério proposto pela norma Europeia para a verificação da sua aplicabilidade. Nesta dissertação é proposto um novo procedimento simplificado para a quantificação das deformações inelásticas locais através do uso de métodos de análise linear-elásticos. Os limites propostos pelo EC8-3 para a definição da capacidade de deformação de elementos à flexão em aço são igualmente avaliados e um conjunto de equações de previsão que permitem estimar a capacidade de deformação de elementos em aço com perfis Europeus e restringidos lateralmente é apresentado.

A segunda parte desta dissertação foca-se no desenvolvimento de um modelo de risco sísmico relativo à atividade e propriedade industrial existentes em Portugal Continental. A revisão dos principais tipos de dano sobre a propriedade observados em edifícios industriais em aço, bem como dos fatores que influenciam as perdas por interrupção da produção é apresentada. As três componentes do risco sísmico – perigosidade, exposição e vulnerabilidade – são cobertos. Nesta dissertação é desenvolvido um modelo de exposição industrial exaustivo que incorpora informação económica relativa às atividades industriais de 2-dígitos definidas pelo CAE Português e à distribuição geográfica do parque industrial existente. Um novo modelo de vulnerabilidade para edifícios industriais em aço é proposto com base em informação estatística recolhida através do levantamento de centenas de edifícios reais. Perdas à escala nacional sobre a propriedade industrial, incluindo os componentes estruturais e não estruturais e o recheio, e sobre a atividade industrial, incluindo as perdas diretas e indiretas, são analisadas.

Acknowledgements

I would like to begin by expressing my sincere gratitude and admiration to my supervisor Professor José Miguel Castro for his unconditional support, constant encouragement and true friendship, for having such a positive impact in my personal development and for persuading me to attend the ROSE School course. His strong technical guidance was of upmost importance for the successful accomplishment of this academic work.

I am deeply grateful to Professor Raimundo Delgado for his sympathy, constant support, guidance during the first steps of my academic experience and for having introduced me to the field of Earthquake Engineering and Structural Dynamics with such fortitude.

To Dr Mário Marques, I would like to express my great gratitude for his strong friendship, indisputable support, entrepreneurship ideas and technical contributions to this thesis. To him, I owe the knowledge acquired through the many endless discussions and numerous great experiences lived throughout this stage. I also want to express my deep gratitude to Mr Luís Macedo for his unquestionable contribution to this thesis.

Over the past few years I greatly benefited, both technically and personally, from the interaction with many colleagues and friends from the University of Porto and abroad. I am truly thankful to Dr Miguel Amaral, Mr Nuno Martins, Dr Alejandro Tejada and family, Dr Sérgio Neves, Dr João Barbosa, Dr Fernando Bastos, Mr Luís Martins, Mr Nuno Pereira, Dr Ádám Zsarnóczay, Mrs Cecilia Nievas, and so many others.

A special word of thanks goes to all my companions and dear friends, Fernando Ochoa, Eduardo Cruz, Tiago Freitas, Lourenço Leite, Guilherme Sampaio, Diogo Codeço, Arnaldo Fonseca, Gonçalo Maçães, for their unconditional friendship over the course of my life.

To Julia, I would like to express my deepest and most truthful thanks for her strong love, constant care, understanding and patience, and for all wonderful moments experienced along the way. I cannot but offer my heartfelt thanks to the Högemann family.

Finally, and most importantly, to my family, to whom I dedicate this thesis I would like to express my deepest and sincere thanks. I am especially gratefully to my parents, Manuel and Maria Alina, and to my sister, Patrícia, for providing me always with such unconditional love, endless care and constant encouragement. Muito obrigado, família!

Contents

List of Figures

List of Tables

List of Abbreviations

L	member length
q	uniformly distributed gravity load
V	point load applied at the top of the simplified cantilever system
d	displacement of the free node of the simplified cantilever system
d_2	displacement of node 2
$d_{L/2}$	displacement at the mid-span
M_E	bending moment due to earthquake load
M_{E+Q}	bending moment due to combined earthquake and gravity loads
N_{E+Q}	axial force due to combined earthquake and gravity loads
N_{pl}	axial capacity of the member
M_{pl}	plastic bending moment
M_y	yielding bending moment
M_2	bending moment at node 2
L_{ph}	plastic hinge length
Φ_u	ultimate member curvature
Φ_y	yielding member curvature
x	abscissa of the cross-section within the member length L
$\Phi(x)$	member curvature at abscissa x
$\Phi_{pl}(x)$	plastic member curvature at abscissa x
θ_{pl}	plastic rotation
θ_{el}	elastic rotation
θ_t	total rotation
x_{Ls}	abscissa of the point of contraflexure
δ_2	distance between the member deflection at x_{Ls} and the tangent to the member axis at node 2
x^*	distance of the intersection point between the tangent to the member axis at node 2 and the perpendicular that intersects the member deflection at x_{Ls} to node 2.
θ_1	member chord rotations at node 1
θ_2	member chord rotations at node 2
θ_{1a}	contribution of the deflection at x_{Ls} with respect to the initial member configuration to the member chord rotations at node 1
θ_{2a}	contribution of the deflection at x_{Ls} with respect to the initial member configuration to the member chord rotations at node 2

θ_{1b}	contribution of the nodal rotation to the member chord rotations at node 1
θ_{2b}	contribution of the nodal rotation to the member chord rotations at node 2
d_y	relative transverse displacements of the sections at nodes 1 and 2, neglecting the contribution of the axial deformation of the member
θ_y	yielding chord rotation
$\theta_{y,ASCE41}$	yielding chord rotation quantified using the ASCE41-13 approach
θ	inter-storey drift sensitivity coefficient
DCR	demand-to-capacity ratio
m	ASCE41-13 member capacity factor that defines the acceptance criteria for linear procedures
k	ASCE41-13 knowledge factor
θ_D	deformation demands obtained from structural analysis, defined in terms of plastic rotations by EC8-3 for steel structures
θ_C	deformation capacity, defined in terms of plastic rotations by EC8-3 for steel structures
CF	EC8-3 confidence factor
E	modulus of elasticity of steel
I	moment of inertia of the member cross-section
Q_f	quantity whose level of error is under evaluation
Q_R	quantity used as reference to estimate the level of error associated to Q_f
ΔQ	local error of quantity Q_f with respect to quantity Q_R
$RMSE$	Root Mean Square Error
n	number of element sections or number of stories
m_i	masses at storey i
h_i	Heights of the masses m_i above the level of application of the seismic action
T	period of vibration of the structure
e	exponent that is function of the period of vibration of the structure,
$mDCR_i$	maximum DCR within a floor i
$\overline{\boldsymbol{DCR_i}}$	mean DCR within a floor i

Chapter 1
Introduction

1.1 The disastrous impacts of earthquakes to steel structures

Earthquakes are, undoubtedly, among the most powerful and destructive natural hazards striking on earth, producing heavy physical, social, economic, ambient and cultural losses. During the past three decades, earthquakes have claimed close to 600 000 lives and caused over 400 billion United States Dollars (USD) in economic loss. The worldwide economic losses averaged around 5 billion USD a year until the 1994 Northridge earthquake nearly quintupled to 24 billion USD with the occurrence of a series of large earthquakes around the world, such as Northridge 1994, Kobe 1995, Kocaeli-Izmit 1999, Chi Chi 1999, Indonesia 2004 and Wenchuan 2008 (Jaiswal and Wald, 2011). The 2008 Wenchuan earthquake, alone, resulted in 69 227 human losses with other 17 923 people being listed as missing and 374 643 injured. About 5.4 million buildings collapsed and a total of 21 million buildings were damaged. At least 15 million people were evacuated from their homes and more than 5 million were, at the time, reported to be homeless. The direct economic loss was estimated to be around 125.6 billion USD (Zhao et al., 2010). Very recently, in the year of 2011, designated by The Geneva Association (2012) as *Annus Horribilis*, almost 47% of the total natural disasters economic losses were due to seismic hazards. Indeed, the earthquakes of Japan and New Zealand turned 2011 as the costliest year yet for insurance industry of natural disasters, resulting in an overall economic toll of 210 billion USD and 16 billion USD, respectively, and insured losses of more than 48 billion USD (Munich Re, 2012). In today's world, 370 million people live in regions prone to the occurrence of earthquakes and are expected to more than double in 2050 (Lall and Deichmann, 2009). The worldwide mass migrations from rural to urban areas, and the

consequent growth of urban slums, the lack of seismic provisions in the design of new buildings over the past and the fact that most earthquakes tend to occur in countries with poorer societies and lower development standards, are some of the manifold causes for such high vulnerability and low resilience for human and economic losses (Guha-Sapir and Vos, 2011; Ferreira, 2012). Nevertheless, the 2011 Tohoku-Oki Japan earthquake and tsunami are reminders that even the most-prepared communities in the most-prepared countries can be overwhelmed. Becoming resilient is more than just building stronger structures, it is also about building social structures that create stronger communities (Eisne, 2013).

In 1994, the Northbridge earthquake dramatically demystified the pre-conceptualized idea that steel structures are capable of withstanding severe earthquakes with no or limited damage, revealing many unexpected structural flaws. The inadequate ductility and toughness of connections due to lack of understanding of the welding process and the underestimation of their deformation demands in cases where beam sizes were greater than those tested in the past, were the most prominent causes of damage (Leon, 2003). Over 200 welded steel moment frames buildings suffered brittle fractures at connections (Porter et al., 2001; Kircher, 2003). The underestimation of actual forces in connections with relatively weak panel zones due to ignoring both material over-strength and local stress concentration and the poor detailing practice were other causes of severe damage (FEMA, 2000a). A recent simulation of a future massive Southern California quake revealed that the pre-1994 Northridge earthquake welding technique is still a rather problematic issue in many tall buildings (Chong, 2009). A year later, in 1995, the Kobe earthquake in Japan resulted in an even more disturbing level of damage, with 10% of the steel buildings in Kobe designed to the Japanese building standards in force at that time having collapsed (Trembley et al., 1996; Nakashima and Tada, 1998). The 1999 Chi-Chi earthquake in Taiwan equally caused tremendous steel property losses, resulting in more than 1600 steel or composite-steel buildings with severe damage (Lee et al., 2002). More recently, the 2010 and 2011 series of earthquakes in New Zealand evidenced the potential damaging effects that strain ageing may imply to steel structures (Bruneau et al., 2010; Clifton et al., 2011), which resulted from the accumulation of short ground shakings with 10 to 15 seconds to an overall cumulative duration of 60 seconds. Many warehouses close to the epicentre suffered stretching of sagging braces due to yielding and roof beams buckled in compression by the inward movement of the tilt-up panels.

1.2 Coping with seismic risk to existing building stocks

1.2.1 The role of seismic safety assessment codes

The 1994 Northbridge earthquake propelled in mid-1994 the formation of a working group, the SAC Joint Venture, with the main goal of developing reliable, practical, and cost-effective guidelines and standards for the repair and upgrading of damaged steel moment frame buildings, the design of new steel buildings and the identification of at-risk steel buildings (FEMA, 2000b; FEMA, 2000c). The outcomes of this working group constituted a turning point in the comprehension and analysis of the seismic behaviour of steel structures mainly through the introduction of performance-based engineering principles. The 1999 Chi-Chi and 2011 Tohoku earthquakes were some examples of past events where the extent of structural damage was seen to be greatly dependent on whether buildings were seismically designed, or not (Lee et al., 2003; Midorikawa and Okazaki, 2012).

With the intention of preventing and reducing the impact of earthquakes in people's lives and economies, the past fifteen years have hence witnessed the development and wide dissemination of the performance-based earthquake engineering philosophy (Romão et al., 2012; FEMA 2012), which fundamental principles aim at improving the adequate quantification of the behaviour of structures subjected to earthquake loading in order to predict their performance with sufficient confidence and to contribute for the development of more effective risk mitigation measures (Fajfar and Krawinkler, 2004). Performance-based earthquake engineering principles set, nowadays, the basis of many guidelines and codes for seismic design and assessment of buildings. Whilst in the United States the procedures for seismic safety assessment were made available few years after the 1994 Northridge earthquake, in Europe, however, the introduction of a part of the Eurocode that specifically addresses the seismic safety assessment and retrofitting of existing buildings only took place few years ago with the publication of Part 3 of Eurocode 8 (EC8-3) (CEN, 2005). The experience with the application of this specific part of the European code is, therefore, currently very limited, and no practical studies have yet been conducted with respect to its application to existing steel buildings. Nevertheless, despite the urge need of further studies focusing on the practical application of EC8-3 in order to verify its consistency and reliability, and an eventual need for further modifications in future

generations of Eurocodes, its revision has not been yet established as a first priority by current European technical committees (Degee and Landolfo, 2014; Landolfo, 2015).

Moreover, American practitioners have alarmingly demonstrated a clear distrust and lack of confidence in current American codes for seismic safety assessment and strengthening of existing buildings (Gray et al., 2008; Paret et al., 2011), claiming that these standards are much more likely to result in nonsensical answers when used by the inexperienced engineer, provide results that are often not accurate at all and are too complicate to use. Toranzo-Dianderas (2009) has equally emphasized that linear analysis elastic methods of analysis are, and will continue to be, used due to their simplicity and acquaintance of most design practitioners, although current seismic safety assessment codes are clearly oriented towards the use of nonlinear methods of analysis. Similarly, despite the unequivocal breakthrough and advantages of implementing probabilistic frameworks in current safety assessment procedures to deal with the uncertainties associated with the lack of knowledge of existing buildings (Pinto and Franchin, 2014a; 2014b; Romão et al., 2014), they will most probably contribute to these adverse feeling of most practitioners towards seismic safety assessment codes, requiring, as recognized by Pinto and Franchin (2014a), time to be disseminated into a wider audience.

1.2.2 The role of seismic risk assessments at different scales

Seismic risk assessment studies have paramount importance in evaluating the expected probability of losses of a certain building within a given reference point and in providing more meaningful and useful information to property owners, stakeholders and public authorities in terms of the expected potential casualties or repair costs and times (Bradley, 2009). They thus take a step forward in comparison to the discrete performance levels preconized in current safety assessment codes. Furthermore, seismic risk studies can be extended to broader territorial, regional or national, scales, thus providing the big picture of expected losses, which is of primordial importance in supporting future earthquake preparedness and response plans, in prioritizing regions for risk reduction and implementation of retrofitting mitigation strategies and raising awareness of national and local communities for the level of risk that they might be exposed to (Petruzzelli, 2013; Silva, 2013).

Preforming seismic risk assessments at different scales is not, however, a straightforward task, requiring apart from the exposure and the hazard modelling, the characterization of the expected level of vulnerability of the considered portfolio of

buildings. In the latter case, although substantial developments have been made in the case of RC and masonry buildings (Pitilakis et al., 2014; Ramirez et al., 2008; Liel and Deierlein 2012), very few works have yet been conducted focusing on the characterization of the seismic fragility of steel buildings (Kazantzi et al., 2008a; 2008b; 2011; Petruzzelli, 2013; Rossetto et al., 2013; Hwang and Lignos 2017a,b) and aiming at the definition of damage-to-loss consequence models for such building typology, which most acknowledged model is that simply based on expert opinion provided within the Hazus-MH MR5 framework (FEMA, 2010). Global steel building inventories for rapid and effective loss analysis are thus clearly needed (Daniell et al., 2011; Jaiswal et al., 2011; Porter, 2011). Additionally, most of the widespread damage in steel structures, as observed in the aftermath of the 2011 Tohoku earthquake (Midorikawa and Okazaki, 2012), is expected to be related to industrial and commercial facilities, which are oftentimes associated to direct and indirect business interruption losses many times greater than their structural counterparts (Cochrane, 1996; Durukal and Erdik, 2008; Durukal et al., 2008). Complex holistic seismic risk assessment frameworks that account not only for direct property and business interruption losses, but also for indirect production losses resultant form input factor, infrastructure and supply chain disruptions (Merz et al, 2013) should be thus implemented in such cases in order to provide more reliable information in support of risk management decision-making (Olson and Wu, 2010).

1.3 Current perception of Portuguese practitioners and public authorities

Portugal has its past marked by the occurrence of heavily destructive earthquakes (Silva, 2013). After the 1755 Lisbon earthquake, nearly 70% of Lisbon's dwellings, around 23 000 buildings, were destroyed or substantially damaged by the combined effects of shaking, fire and tsunami. In total, economic losses of 64 000 to 72 000 thousand Escudos, about 32% to 48% of the Portuguese GDP at the time, were estimated (Pereira, 2003). Today, for what concerns the seismic risk of the current Portuguese residential building stock, a potential economic toll of 15.7% of the total stock value, about 56 billion Euros, has been estimated for a return period of 475 years (Silva, 2013), which is commonly adopted in the current design of new structures. These losses are expected to be mainly concentrated in the Metropolitan Area of Lisbon and in the south of mainland Portugal (Sousa, 2008; Costa et al., 2010; Silva, 2013). The raise of public awareness to seismic risk

in Portugal motivated the Portuguese Authority for Civil Protection to recently promote an initiative dedicated to the seismic risk assessment of lifeline systems located in the regions of Great Lisbon and Algarve (ANPC, 2010; Azevedo et al., 2010) and the Assembly of the Portuguese Republic (2010) to issue a resolution that identifies the need for future measures in seismic risk reduction. However, all seismic risk studies conduct up to date for Portugal have neglected the potential losses associated to steel buildings, which assumes critical relevance since, although the Portuguese steel residential building stock only comprises some high-rise buildings mostly located in Lisbon (Lamas, 2006), the majority of the country's industrial building stock is made of steel (RFCS, 2013). The lessons learned from the potentially devastating impacts observed in fairly industrialized regions in past earthquake events (Durukal and Erdik, 2008; Durukal et al., 2008; EPICentre, 2012) should aware the Portuguese authorities, the financial sector and company owners to the high industrial and economic burden that the country may be exposed to. Industrial seismic risk assessment studies for Portugal are thus of critical relevance, particularly in the today's economic situation of the country, which lost more than 10% of the industrial capacity with the European debt crisis that stuck in the year of 2009 (Bank of Portugal, 2015) and is grounded on rather vulnerable microenterprises that fulfil 95% of the country's overall business structure and are heavily dependent on the domestic banking sector (European Commission, 2015).

Portugal was one of the first countries to endorse a seismic design code in the mid-50s. Over the last 60 years, a number of new seismic design regulations has been introduced (Silva, 2013), forcing Portuguese practitioners to adapt to such constant changes in the seismic design and assessment of structures. To evaluate the current design and assessment practices of Portuguese practitioners and, in particular, their level of acquaintance with EC8-3, a short survey was conducted, which had 79 respondents and revealed rather interesting scenarios (Figure 1.1). Firstly, when Portuguese practitioners were questioned about which standard they commonly adopt in the seismic design of new structures, half of participants confirmed using Part 1 of Eurocode 8 (CEN, 2004a), although a significant percentage (42%) still uses the former normative document that preconizes criteria for designing the seismic action (RSA, 1983), in combination with Eurocode 2 (CEN, 2004b) or with the older Portuguese normative for design of RC structures (REBAP, 1984). Secondly, when they were asked about if they had ever dealt with a seismic safety assessment problem, 45% of participants responded positively, although only 8% of those have actually applied Part 3 of Eurocode 8. Among the reasons

not to apply EC8-3, 35% of participants responded to be unaware of its existence and 36% consider it too complex to be applied in practice.

Figure 1.1 – Responses given by Portuguese practitioners.

For what concerns the level of acquaintance of Portuguese practitioners with respect to seismic safety assessment procedures, almost half of respondents revealed not being familiarized at all with nonlinear methods of analysis and only 20% of those who said to be have already applied nonlinear analysis in practice. It is thus clear the generalized unawareness of Portuguese practitioners with respect to EC8-3 and the reduced percentage of practitioners (11.6%) that might truly exploit the maximum code potential in terms of the use of nonlinear methods of analysis. Future workshops and training programs aiming at demystifying and acquainting practitioners with EC8-3 are clearly deemed necessary.

1.4 Objectives

Based on the aforementioned issues regarding the seismic safety and risk assessment of existing steel buildings and, in particular, the current perception of Portuguese practitioners and public authorities towards such issues, the purpose of this dissertation is to scrutinize the limitations of current guidelines and codes for seismic assessment of existing buildings, with particular emphasis on EC8-3, and to provide a first projection of the industrial seismic risk for Mainland Portugal, as briefly described below.

1.4.1 Scrutinize limitations of EC8-3 and propose simplified procedures

On the one hand, this thesis covers a first comprehensive review of existing guidelines and codes for seismic safety assessment of existing steel buildings, which aims at pointing out the main limitations and conceptual inconsistencies of EC8-3 in comparison to more mature normative documents, such the American standard ASCE 41-13 (ASCE, 2014). The encountered difficulties are highlighted and set as the basis of the further studies conducted in this dissertation.

Current codes implicitly recognize the variability in seismic responses introduced by input ground-motions and preconize a number of techniques for such uncertainty reduction (e.g., minimum number of records, selection of records based in the expected seismogenic characteristics, range of periods of interest for record scaling) that aim at providing more consistent mean estimates of structural responses. However, the different approaches followed by various codes reveal the current lack of consensus on the appropriateness of such techniques. Some insights on the influence of current code-based record selection methods on demand-based assessments of buildings are provided in this thesis and the probabilistic approach proposed by Bradley (2011) is assessed with the aim of enforcing its implementation in future generations of codes.

In line with the lack of familiarization of Portuguese practitioners with nonlinear methods of analysis, this thesis places particular emphasis on the assessment of the trustworthiness of the EC8-3 linear-elastic procedures and in scrutinizing a demand parameter compatible with plastic rotation demands that can be quantified from linear analysis. A simplified procedure capable of quantifying beam inelastic chord rotation demands using linear-elastic analysis in an expeditious and conservative way is sought.

At last, the resemblance between the deformation capacity limits preconized by EC8-3 and those defined in ASCE 41-13, which suggest a direct reproduction from the latter

document despite the fact that American cross-section sizes are significantly different from those adopted in Europe, motivates the assessment of the adequacy of the EC8-3 deformation capacity limits on the basis of detailed Finite Element models that incorporate local imperfections, the influence of axial load and different loading regimes.

This work was performed within the framework of the research project 'Development and calibration of seismic safety assessment methodologies for existing buildings according to the Eurocode 8 – Part 3' founded by Foundation of Science and Technology (FCT) of Portugal.

1.4.2 Predict the industrial seismic risk for Mainland Portugal

On the other hand, this thesis discusses the various aspects related with seismic risk assessment and presents a novel comprehensive industrial seismic risk model for Mainland Portugal, developed with the aim of providing a first projection of the potential economic losses to which the country may be exposed to, namely in terms of industrial property losses, mostly composed of industrial steel buildings, direct and indirect business interruption losses, relocation expenses and employment losses.

On the exposure side, the estimation of the industrial assets at risk for Portugal, including all industrial activity firms defined according to the 2-digit Portuguese Standard Industrial Classification System, is tackled and new industrial building taxonomies for Portugal are investigated by employing analytical methodologies consisting of randomly generating populations of synthetic buildings representative of the as-built building stock.

On the vulnerability side, the derivation of industry-specific loss functions is discussed, alongside with the development of a comprehensive 3-dimensional numerical model capable of accounting for the main failure modes observed in past post-earthquake reconnaissance campaigns.

This work was performed within the framework of the research project 'PRISE - Earthquake loss of the Portuguese building stock' founded by Foundation of Science and Technology (FCT) of Portugal.

1.5 Outline of the thesis

This thesis consists of ten chapters divided into two parts according to the objectives above discussed. The first part, which comprises Chapters 2 to 6, addresses the limitations encountered in the use of the seismic safety assessment procedures preconized by Part 3 of

Eurocode 8 and the proposal of alternative simplified procedures, while the second part, consisting of Chapter 7 to 9, is devoted to the industrial seismic risk assessment at a national scale for Mainland Portugal.

Chapter 2 presents a critical review of Part 3 of Eurocode 8 (CEN, 2005), the North America ASCE 41-13 (ASCE, 2014) and the New Zealand guidelines (NZSEE, 2006) for seismic safety assessment of existing steel buildings. A commented application of each document to a set of four steel buildings designed according to different criteria is provided using every method of analysis made available by each code and guideline.

Chapter 3 investigates the impact of the Eurocode 8 (CEN, 2004a), ASCE 41-13 (ASCE, 2014), and New Zealand NZS1170.5:2004 (NZS, 2004) record selection methods in the seismic performance assessment of steel buildings. Special attention is devoted to the influence of the number of real ground motion records selected on the estimation of the "true" mean seismic response and to the efficiency that is achieved when an additional selection criteria based on the control of the spectral mismatch of each individual record with respect to the reference response spectrum is adopted. The sufficiency of the methods with respect to the pairs of *M*-*R* of the selected group of records and the robustness of the scaling procedure are also examined. The chapter closes with a study which demonstrates the suitability of a simplified probability-based approach recently proposed for estimating mean seismic demands.

The Part 3 of Eurocode 8 (EC8-3) requires analysts to quantify plastic rotations even when linear methods of analysis are used. Hence, Chapter 4 examines chord rotations as a demand parameter compatible with plastic rotation demands that can be quantified from linear methods analysis and addresses the question of how reliable are the EC8-3 linear analysis procedures. The chapter ends with the investigation of the adequacy of the linear analysis applicability criterion preconized by EC8-3.

Chapter 5 further extends the work conducted in Chapter 4 by examining the pertinence of a simplified procedure to quantify local inelastic chord rotations using linear-elastic analysis at the beams of buildings where column-sway mechanisms are not expected to occur. A number of moment-resisting steel frames design according to different criteria and exhibiting different column-to-beam moment ratios are analysed so as to broaden the validity of the proposed procedure.

Chapter 6 addresses the question of how adequate are the deformation capacity limits preconized by EC8-3 and focuses on the estimation of the deformation capacity of steel elements with a wide range of European cross-section sizes on the basis of detailed FE

analysis. The influence of geometrical imperfections, axial load, loading conditions and ductile fracture is investigated. Multivariate regression analysis is employed so as to provide empirical equations for quantifying the deformation capacity of laterally restrained steel members with European profiles in a sufficiently accurate and expeditious way.

Chapter 7 deals with the seismic property loss estimation of typical industrial steel buildings and with the development of a comprehensive 3-dimensional model capable of accurately capturing the main failure modes observed in previous post-earthquake reconnaissance campaigns. Every particular modelling aspect is discussed. Novel physical fragility and vulnerability functions for typical industrial steel buildings are proposed, accounting not only for structural components, but also for non-structural components and contents.

Chapter 8 gives continuity to Chapter 7, and focuses on the estimation of direct and indirect seismic business losses associated to a typical industrial steel building with any of the 27 industrial activities of the 2-digit Portuguese Standard Industrial Classification System (CAE). The Hazus – MH MR5 framework (FEMA, 2010) is employed as benchmark and industrial business vulnerability functions are derived accounting to inventories losses, direct production losses, indirect production losses resultant from input, infrastructure and supply chain disruptions and relocation expenses.

Chapter 9 provides a first projection of the seismic losses to industrial property and economic activity at a national scale for mainland Portugal. For such, comprehensive industrial exposure and vulnerability models are developed based on economic statistical information collected from the Portuguese National Institute of Statistics (INE), considering every industrial activity from the 2-digit Portuguese Standard Industrial Classification (CAE) system, and based on an extensive survey of more than 200 industrial building design projects and site-visits to national firms. The industrial property and activity vulnerability models discussed in Chapters 7 and 8 are extended to account for the uncertainty introduced by the variability in the characteristics of the existing industrial building stock. The hazard, exposure, vulnerability models are afterwards implemented in a web-based seismic loss estimation platform created at the University of Porto under the nationally founded PRISE project.

The thesis closes with Chapter 10, which discusses the key contributions of this dissertation in the field of seismic safety and risk assessment of existing steel buildings. Limitation in the contributions presented are identified alongside with future research recommendations.

1.6 References

ANPC (2010) Study of the seismic risk and tsunami in Algrave, Portuguese Authority for Civil Protection, Carnaxide, Lisbon, Portugal.

ASCE (2014) Seismic evaluation and retrofit of existing buildings (ASCE/SEI 41-13), American Society of Civil Engineers.

Assembly of the Portuguese Republic (2010) Measures to reduce the seismic risk, Resolution from the Assembly of the Portuguese Republic n.º 102/2010, in Dário da República.

Azevedo J, Guerreiro L, Beto R, Lopes M, Proença J (2010) Seismic vulnerability of lifelines in the greater Lisbon area, Bulletin of Earthquake Engineering, 8, 157–180.

Bank of Portugal (2015) Projections for the Portuguese Economy: 2015-2017. Projection assumptions, Economic Bulletin, Bank of Portugal, Lisbon, Portugal.

Bradley B (2011) Design seismic demands from seismic response analyses: A probability-based approach, Earthquake Spectra, 27, 213-224.

Bradley BA (2009) Structure-specific probabilistic seismic risk assessment, PhD dissertation, Department of Civil and Natural Resources Engineering, College of Engineering, University of Canterbury, Christchurch, New Zealand.

Burneau M, Anagnostopoulou M, MacRae G, Clifton C, Fussell A (2010). Preliminary report on steel building damage from the Darfield earthquake of September 4, 2010, Bulletin of the New Zealand Society for Earthquake Engineering, 43, 351-369.

CEN (2004a) ENV 1998-1 Eurocode 8: Design of structures for earthquake resistance - Part 1: General rules, seismic actions and rules for buildings, European Committee for Standardization, Brussels, Belgium.

CEN (2004b) ENV 1992-1-1 Eurocode 2: Design of concrete structures - Part 1-1: General rules and rules for buildings, European Committee for Standardization, Brussels, Belgium.

CEN (2005) ENV 1998-3 Eurocode 8: Design of structures for earthquake resistance - Part 3: Assessment and retrofitting of buildings, European Committee for Standardization, Brussels, Belgium.

Chong JR (2009) Earthquake drill finds weakness in steel high-rises, Los Angeles Times, January 2, Los Angeles.

Clifton C, Bruneau M, MacRae G (2011) Steel structures damage from the Christchurch earthquake series of 2010 and 2011, Bulletin of the New Zealand Society for Earthquake Engineering, 44, 297-318.

Cochrane, H (1996) Catastrophic earthquakes and the prospect of indirect losses, Post-Earthquake Rehabilitation and Reconstruction, eds. F. Y. Cheng and Y. Y. Wang, Elsevier B.V., Oxford, U.K.

Costa AC, Sousa ML, Carvalho A, Coelho (2010) Evaluation of seismic risk and mitigation strategies for the existing building stock: application of LNECloss to the metropolitan area of Lisbon, Bulletin of Earthquake Engineering, 8, 119-134.

Daniell J, Wenzel F, Khazai B, Vervaeck A (2011) A Country-by-Country building inventory and vulnerability index for Earthquakes in comparison to historical CATDAT damaging earthquakes database losses. Proceedings of the Australian Earthquake Engineering Society 2011 Conference. Barossa Valley, South Australia.

Degee H, Landolfo R (2014) Perspectives for EN 1998 evolution regarding steel structures, Proceedings of the 2nd European Conference on Earthquake Engineering and Seismology, Istanbul, Turkey.

Durukal E, Erdik M (2008) Physical and economic losses sustained by the industry in the 1999 Kocaeli, Turkey earthquake, Natural Hazards, 46, 153-178.

Durukal E, Erdik M, Uçkan E (2008) Earthquake risk to industry in Istanbul and its management, Natural Hazards, 44, 199-212.

Eisne R (2013) Preparing for the wort case…because it just might happen, Earthquake Spectra, 29, S339-S340.

EPICentre (2012) The 29th May 2012 Emilia Romagna Earthquake, EPICentre Field Observation Report, University College London, London, United Kingdom.

European Commission (2015) Country Report Portugal 2015 including an in-depth review on the prevention and correction of macroeconomic imbalances, European Commission, Brussel, Belgium.

Fajfar P, Krawinkler H (2004) Performance-based seismic design concepts and implementation, The Pacific Earthquake Engineering Research Centre, Bled, Slovenia.

FEMA (2000a) FEMA 355E State of the arte report on past performance of steel moment-frame buildings in earthquakes, Report developed by the SAC joint venture for the Federal Emergency Management Agency, Washington, D.C.

FEMA (2000b) FEMA 351 Recommended seismic evaluation and upgrade criteria for existing welded steel moment-frame buildings, Report developed by the SAC joint venture for the Federal Emergency Management Agency, Washington, D.C.

FEMA (2000c) FEMA 350 Recommended seismic design criteria for new Steel moment-frame buildings, Report developed by the SAC joint venture for the Federal Emergency Management Agency, Washington, D.C.

FEMA (2010) Multi-hazard loss estimation methodology. Earthquake Model. HAZUS – MH MR5 Technical Manual, Federal Emergency Management Agency, Mitigation Division, Washington, D. C.

FEMA (2012) FEMA P-58-1 Seismic performance assessment of buildings. Volume 1 – Methodology, Federal Emergency Management Agency, Washington, D.C., U.S.A.

Ferreira M (2012) Seismic risk in urban areas, PhD dissertation, Department of Civil Engineering, Technical University of Lisbon, Lisbon, Portugal.

Geneva Association (2012) Extreme events and insurance: 2011 annus horribilis. The Geneva Reports series, Geneva, Switzerland.

Guha-Sapir D, Vos F (2011) Earthquakes, an epidemiological perspective on patterns and trends, In Spence R, So E, Scwthorn C (eds.), Human Casualties in Earthquakes: Progress in Modelling and Mitigation, Springer, Dordrecht, The Netherlands.

Hwang S-H, Lignos D (2017a) Effect of modelling assumptions on the earthquake-induced losses and collapse risk of steel-frame buildings with special concentrically braced frames, Journal of Structural Engineering.

Hwang S-H, Lignos D (2017b) Earthquake-induced loss assessment of steel frame buildings with special moment frames designed to highly seismic regions, Earthquake Engineering and Structural Dynamics.

Jaiswal K, Wald D, D'Ayala D (2011) Developing empirical collapse fragility functions for global building types, Earthquake Spectra, 27, 775-795.

Jaiswal KS, Wald DJ (2011) Rapid estimation of the economic consequences of global earthquakes, U.S. Geological Survey, Denver, USA.

Kazantzi AK, Righiniotis TD, Chryssanthopoulos MK (2008) Fragility and hazard analysis of a welded steel moment resisting frame, Journal of Earthquake Engineering, 12, 596-615.

Kazantzi AK, Righiniotis TD, Chryssanthopoulos MK (2008) The effect of joint ductility on the seismic fragility of a regular moment resisting steel frame designed to EC8 provisions, Journal of Constructional Steel Research, 64, 987-996.

Kazantzi AK, Righiniotis TD, Chryssanthopoulos MK (2011) A simplified fragility methodology for regular steel MRFs, Journal of Earthquake Engineering, 15, 390-403.

Kircher CA (2003) Earthquake loss estimation methods for welded steel moment-frame buildings, Earthquake Spectra, 19, 365-384.

Lall SV, Deichmann U (2009) Density and disasters: economics of urban hazard risk, Policy Research Working Paper, The World Bank, Economics and Urban Department and Development Research Group, Energy and Environment Team, Washington, D.C.

Lama ARG (2006) The development of steel structures in Portugal – the influence of Patrick Dowling, Journal of Constructional Steel Research, 63, 1161-1164.

Landolfo R (2015) Bridging the gap between research and standards: the activities of the ECCS-TC13 Seismic Committee, Proceedings of the 8th International Conference on Behaviour of Steel Structures in Seismic Areas, Tongji University, Shangai, China.

Lee BJ, Chou TY, Hsiao CP, Chung LK, Huang PH, Wu YB (2002) The statistics and analysis of building damage on Chi-Chi earthquake. In: International training programs for seismic design of building structures, Taipei, Taiwan. National Centre for Research on Earthquake Engineering, Taipei, Taiwan.

Leon R (2003) Evaluation, strengthening and repair of old structures, Proceedings of the IV Portuguese Conference on Steel and Composite Construction, Lisbon, Portugal.

Merz M, Hiete M, Comes T, Schultmann F (2013) A composite indicator model to access natural disaster risks in industry on a spatial level, Journal of Risk Research, 16, 1077-1099.

Midorikawa M, Okazaki T (2012) Earthquake and Tsunami Damage to Steel Structures, Proceedings of the ASCE Structures Congress, Chicago, Illinois.

Munich Re (2012) Group annual report 2012, Munich Re, Munich, Germany.

Nakashima M, Tada KM (1998) Classification of damage to steel buildings observed in the 1995 Hyogoken-Nanbu earthquake, Engineering Structures, 20, 271-281.

NZS (2004) NZS 1170.5:2004 Structural design actions. Part 5: Earthquake actions – New Zealand, New Zealand Standard, Wellington, New Zealand.

NZSEE (2006) Assessment and improvement of the structural performance of buildings in earthquake, Recommendations of a NZSEE Study Group on Earthquake Risk Buildings, New Zealand Society for Earthquake Engineering, New Zealand.

Olson DL, Wu D (2010) Enterprise risk management models, Springer - Verlag Berlin Heidelberg, Berlin, Germany.

Paret TF, Searer GR, Freeman SA (2011) ASCE 31 and 41: Apocalypse Now. Proceedings of the ASCE Structures Congress 2011, Las Vegas, Nevada.

Pereira AS (2003) The opportunity of a disaster: the economic impact of the 1755 Lisbon earthquake, Department of Economics, University of York, York, UK.

Petruzzelli F (2013) Scale-dependent procedures for seismic risk assessment and management of industrial buildings portfolios, PhD dissertation, Department of Structures for Engineering and Architecture, University of Naples Federico II, Naples, Italy.

Pinto PE, Franchin P (2014a) Performance-based assessment of existing buildings in Europe: Problems and Perspectives, In Fischinger M (eds.), Performance-Based Seismic Engineering: Vision for an Earthquake Resilient Society, Geotechnical, Geological and Earthquake Engineering, Springer, Dordrecht, The Netherlands.

Pinto PE, Franchin P (2014b) Existing buildings: the new Italian provisions for probabilistic seismic assessment, In Ansal A (eds.), Perspectives on European Earthquake Engineering and Seismology Volume 1, Geotechnical, Geological and Earthquake Engineering, Springer Open, Dordrecht, The Netherlands.

Pitilakis K, Crowley H, Kaynia AM (2014) SYNER-G: Typology definition and fragility functions for physical elements at seismic risk. Buildings, lifelines, transportation networks and critical facilities, Geotechnical, Geological and Earthquake Engineering, Springer, Dordrecht, The Netherlands.

Porter K (2011) GEM Vulnerability rating system, GEM Foundation, Pavia, Italy.

Porter KA, Kiremidjian AS, LeGrue JS (2001) Assembly-based vulnerability of buildings and its uses in seismic performance evaluation, Earthquake Spectra, 17, 291-312.

RFCS (2013) Prefabricated steel structures for low-rise buildings in seismic areas, Research Found for Coal and Steel, European Commission, Brussels, Belgium.

Romão X (2012) Deterministic and probabilistic methods for structural seismic safety assessment, PhD dissertation, Department of Civil Engineering, Faculty of Engineering of the University of Porto, Porto, Portugal.

Romão X, Delgado R, Costa A (2014) Probabilistic Performance Analysis of Existing Buildings under Earthquake Loading, Journal of Earthquake Engineering, 18, 1241-1265.

Rossetto T, Ioannou I, Grant DN (2013) Existing empirical vulnerability and fragility functions: compendium and guide for selection, GEM Foundation, Pavia, Italy.

RSA (1983) Regulamento de segurança e acções para estruturas de edifícios e pontes, Decreto-Lei nº 235/83, Imprensa Nacional - Casa da Moeda, Lisbon, Portugal.

RSA (1984) Regulamento de Estruturas de Betão Armado e Pré-Esforçado, Decreto-Lei nº 349-C/83, Imprensa Nacional - Casa da Moeda, Lisbon, Portugal.

Searer GR, Paret TF, Freeman SA (2008) ASCE 31 and ASCE 41: What good are they? Proceedings of the ASCE Structures Congress 2008, Vancouver, Canada.

Silva V (2013) Development of open models and tools for seismic risk assessment: application to Portugal, PhD dissertation, Department of Civil Engineering, University of Aveiro, Aveiro, Portugal.

Sousa ML (2008) Annualized economic and human earthquake for mainland Portugal, Proceedings of the 14th World Conference on Earthquake Engineering, Beijing, China.

Toranzo-Dianderas L (2009) Evaluation of the ASCE 41 linear elastic procedure for seismic retrofit of existing structures: Pros and cons of the method, Proceedings of the 2009 ATC & SEI Conference on Improving the Seismic Performance of Existing Buildings and Other Structures, San Francisco, CA.

Toranzo-Dianderas L (2009) Evaluation of the ASCE 41 linear elastic procedure for seismic retrofit of existing structures: Pros and cons of the method, Proceedings of the 2009 ATC & SEI Conference on Improving the Seismic Performance of Existing Buildings and Other Structures.

Tremblay R, Bruneau M, Nakashima M, Prion HGJ, Filiatrault A, DeVall R (1996) Seismic design of steel buildings: lessons from the 1995 Hyogo-Ken Nanbu earthquake, Canadian Journal of Civil Engineers, 23, 727-756.

Zhao B, Taucer F, Lu X (2010) Lesson Learned from Wenchuan Earthquake of 12 May 2008, Proceedings of the EU-China Science and Technology Week. Shanghai.

Chapter 2

Critical review of guidelines and codes for seismic assessment of existing steel buildings

Araujo M, Castro JM (2018) A Critical Review of European and American Provisions for the Seismic Assessment of Existing Steel Moment-Resisting Frame Buildings. Journal of Earthquake Engineering 22:1336-1364. [1]

2.1 Summary

In Europe, the introduction of a specific part of the Eurocode for seismic safety assessment of existing buildings only took place few years ago with the publication of Part 3 of Eurocode 8 (EC8-3). Few studies related to the application of the EC8-3 procedures to RC structures have already been conducted, but none have yet been performed for steel structures. In this chapter a critical review and practical application of guidelines and codes for seismic safety assessment of existing steel buildings is carried out. The main results obtained are discussed and the difficulties in the application of each code are identified.

2.2 Introduction

The recent widespread awareness of earthquake experts and public authorities for the need of a correct evaluation of the seismic vulnerability of the existing building stock, as well as the acknowledgment that current codified seismic assessment procedures are associated with strongly varying accuracy levels, stood the revision of guidelines and

[1] The published version of this work provides further insights to this study and adds to the discussion around the performance requirements defined in both part 1 and 3 of Eurocode 8. The author fully recommends the reader to visit this manuscript. Moreover, the American ASCE 41-13 standard has recently been superseded by ASCE 41-17 and changes are expected regarding safety verifications, which now includes drift checks, and treatment of uncertainty, which is now reliability-based. Additionally, the Portuguese National Annex of Part 3 of Eurocode 8 in now in force and thus could lead to different conclusions to those herein presented.

codes that specifically address this issue on the top of the agenda. Most of these documents (NRC-CNRC, 1993; BRI, 2001; CEN, 2005a; IITK-GSDMA, 2005; NZSEE, 2006; ASCE, 2007; TSDC, 2007; ASCE, 2014) introduce comprehensive frameworks that include structural characterization, analysis and verification procedures that are generally more detailed and lengthy than those used in the design of new structures, thus requiring extensive evaluation through practical application in order to verify their adequacy and to determine the need to modify some of them.

A critical review of the state-of-the-practice of seismic assessment of existing buildings conducted by Holmes (1996) highlighted the needed for more efficient and reliable safety assessment methodologies. In this work, Holmes (1996) provides a thorough discussion on a number of issues related with: (i) the use of unreliable methods for damage data collection; (ii) the need of standardized damage state scales; (iii) the proposal of new practical methodologies, which should be displacement-based rather than force-based; (iv) and the lack of knowledge in material/component acceptability criteria. Moreover, although few comparative studies on current guidelines and codes for seismic assessment of existing buildings have already been conducted up to date (Lupoi, 2003; Lupoi et al., 2004; Mahalov, 2006; Öztürk, 2006; Boroujeni and Sadeghazar, 2006; Mpampatsikos et al., 2008a; Mola and Negro, 2009), all were simply applied to existing RC buildings, and none has yet been applied to existing steel buildings.

Chrysostomou (2005) provided one of the first contributions to the assessment of Part 3 of Eurocode 8 (EC8-3) (CEN, 2005a), concluding that the application of EC8-3 as a screening method to identify deficient structures is rather costly and the proposed confidence factors seem to have a marginal influence on the final safety assessment results. More recently, Romão et al. (2010) found that, depending on the selected limit state, the increase in the knowledge of the structural properties by visual inspection or in-situ testing, which will affect the selection of the confidence factors, must be carefully evaluated due to the amount of work, costs and on-site difficulties that may be implied. A number of studies focused on the assessment of the consistency of EC8-3 have been also systematically demonstrating that the EC8-3 linear methods of analysis tend to lead to higher levels of demand when compared to nonlinear dynamic analysis and that the prescribed stringent EC8-3 linear analysis applicability criterion will be most probably not verified by many existing buildings (Masi et al., 2008; Mpampatsikos et al., 2008b; Pinto and Franchin, 2008; Romão et al., 2010). Moreover, for what concerns the comparison between different guidelines and codes, Lupoi et al. (2004) carried out a commented application work of the

American FEMA 356 (FEMA, 2000), the New Zealand guidelines (NZSEE, 2006) and the Japanese Standard (BRI, 2001), reporting significant differences in the determination of the ultimate capacity of buildings as a result of the conceptually different approaches followed by each document. Additionally, Parker et al. (2012) have also concluded that, although ASCE 41-13 (ASCE, 2014) and NZS1170.5 (NZS, 2004) may yield similar results, there were notable exceptions, particularly with respect to the maximum earthquake response, where the NZS1170.5 tends to significantly penalized components demands compared to ASCE 41-13.

Clearly, continuous comprehensive studies focused on the assessment of current guidelines and codes, particularly in the case of existing steel building, which have not been the focus of previous studies, are deemed necessary. The lack of consensus on the most adequate safety assessment methodologies and the conceptually different approaches followed by various guidelines and codes, should motivate the revision and development of new assessment procedures that may be further implemented in future generations of codes. Hence, this chapter aims at providing a first contribute to the review of guidelines and codes that specifically address the seismic safety assessment of existing steel buildings. The European EC8-3 (CEN, 2005a), the American ASCE 41-13 (ASCE, 2014) and the New Zealand NZSEE guidelines (NZSEE, 2006) were employed in the seismic safety assessment of four different steel buildings. Special attention was devoted to the use of linear elastic methods of analysis, both in terms of their applicability criteria and corresponding safety checks. The main results of this study will be discussed and the encountered difficulties and inconsistencies highlighted.

2.3 How familiar are Portuguese practitioners with the Part 3 of Eurocode 8

In order to assess the degree of acquaintance of the civil engineering community with Part 3 of Eurocode 8 and their seismic assessment and design practices, a survey was conducted among Portuguese practitioners, which had 79 respondents. Although more than half of the participants (52%) confirmed using Part 1 of Eurocode 8, EC8-1 (CEN, 2004a) in the design of new structures, a considerable percentage still uses the former Portuguese normative document (RSA, 1938) that preconizes criteria for the definition of the seismic action, in combination with Eurocode 2 (CEN, 2004b) and the older Portuguese normative document for the design of reinforced concrete and pre-stressed concrete structures

(REBAP, 1984). When practitioners were asked if they had ever dealt with a seismic safety assessment problem, 45% of the respondents said yes. However, when they were asked which normative document they use to assess existing buildings, only 8% replied EC8-3. Among the reasons not to use EC8-3, 35% of the respondents said that they are unaware of its existence, while 36% consider it too complex to be applied in practice (Figure 2.1Figure 2.1). It is thus evident the unawareness of the civil engineering community with respect to EC8-3 and the need for future workshops and training programs that may help demystifying and acquainting practitioners with this European code. Moreover, almost half of the engineers (42%) said that they are not familiarized with nonlinear static and dynamic procedures and only 20% of those who said yes have already applied them in practice.

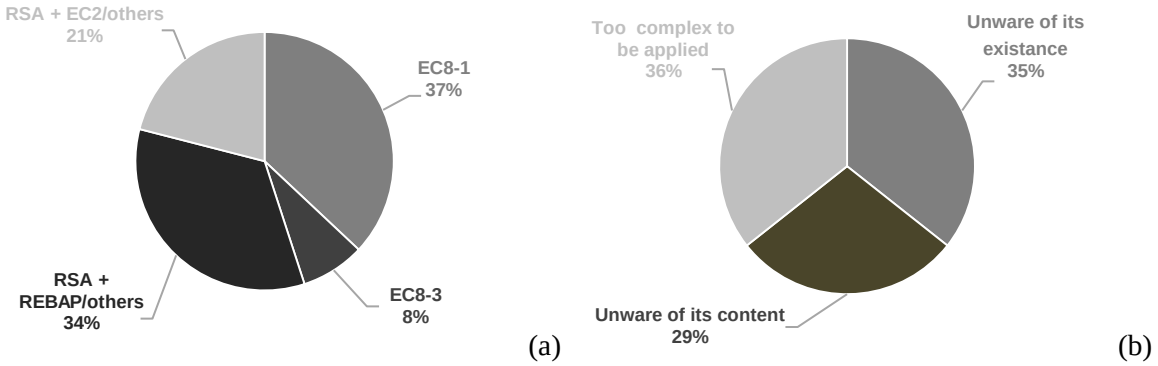

Figure 2.1 – (a) Normative documents adopted in the seismic safety assessment of existing structures and (b) reasons not to apply EC8-3.

2.4 Guidelines and codes for seismic safety assessment of existing buildings

The codification of procedures for seismic safety assessment of existing buildings closely followed the evolution and incorporation of state-of-the-art concepts such as the capacity design and the establishment of performance levels and the definition of acceptance criteria. The European EC8-3 (CEN, 2005a), the American ASCE 41-13 (ASCE, 2013) and the New Zealand NZSEE guidelines (NZSEE, 2006) will be considered herein.

2.4.1 Performance requirements and compliance criteria

Post-earthquake damage and loss collection have demonstrated that, in many cases, buildings non-compliant with modern seismic design codes are not necessarily associated with unacceptable performance levels, so that no rehabilitation measures would be needed

in these cases (Mola and Negro, 2009). The seismic safety assessment objective should not be aimed at the upgrading of buildings to comply with design codes for new buildings, as the costs of rehabilitation would be prohibitive, but to ensure acceptable levels of damage or to prevent collapse for a ground shaking with a given probability of exceedance. Performance-based approaches (SEAOC, 1995; Mazzolani et al., 2000; Grecea et al., 2004) are thus usually adopted by current guidelines and codes for seismic safety assessment of existing buildings, according to which the performance requirements and compliance criteria are expressed in terms of a set of performance objectives, characterized by limits to inter-storey drifts, plastic or chord rotations, ductility or damage indices, that are paired with different levels of seismic hazard.

Although the European EC8-3 and the American ASCE 41-13 belong to the last generation of assessment codes, their assessment procedures follow conceptually different approaches. According to EC8-3, appropriate levels of protection are considered to be achieved if three limit states (LSs) are satisfied, namely: (i) the Damage Limitation (DL) limit state; (ii) the Significant Damage (SD) limit state; (iii) and, the Near Collapse (NC) limit state. Whereas the NC LS refers to a damage level that aims to reflect the actual collapse of the building, the SD LS is roughly equivalent to the non-collapse requirement preconized by Part 1 of Eurocode 8 (EC8-1) for the seismic design of new buildings (CEN, 2004a). In turn, the DL LS refers to cases of light structural damage without significant yielding of structural members. The return periods ascribed by EC8-3 for the various limit states are defined in accordance with levels of protection normally established for ordinary new buildings, having values of 2475, 475 and 225 years for the NC, SD and DL limit states, respectively, and being associated to probabilities of exceedance of 2%, 10% and 20% in 50 years. It will be the national authorities' responsibility to decide whether all three LSs shall be checked, just two, or simply one of them. Different return periods may be also ascribed to the various LSs depending on the socio-economic impact of the building or facility under analysis. Importance factors, γ_I, varying from 0.8 to 1.4 can be adopted depending on the consequences of the building collapse and its importance to civil protection.

The ASCE 41-13, on the other hand, which is a direct descendant of the former Vision 2000 (SEAOC, 1995), FEMA 273 (2005) and FEMA 356 (FEMA, 2000) guidelines, considers that a certain rehabilitation objective, defined in accordance with certain pre-defined requirement goals, will be achieved if four performance levels are achieved: (i) the Operation (OP) performance level; (ii) the Immediate Occupancy (IO)

performance level; (iii) the Life Safety (LS) performance level; (iv) and the Collapse Prevention (CP) performance level. In other words, depending on the economical, architectural and historical impacts of the building and its lifetime and rehabilitation costs, the analyst is invited to select one of the following rehabilitation objectives: (i) Limited objective; (ii) Basic Safety (BSO) objective; (iii) or Enhanced objective; which are related to the various performance levels. Therefore, the American standard provides greater flexibility in the decision-making and definition of the rehabilitation requirements, being the Enhanced Objective achieved if the *f*, *k* and *p* performance requirements shown in Figure 2.2 are attained. This objective is the one that better matches the performance requirements preconized by EC8-3, although there is still a significant conceptual difference between both procedures. Whereas explicit performance-based approaches, such as that of ASCE 41-13, set different rehabilitation objectives by changing the allowable drifts or displacement values, implied performance-based approaches, such as that of EC8-3, establish different performance levels by using importance factors to increase or reduce lateral forces (Bommer and Pinho, 2006).

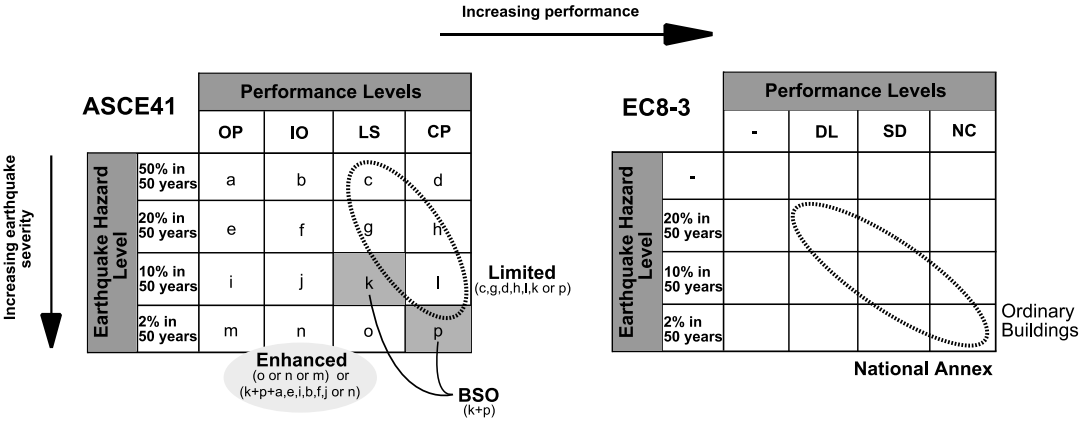

Figure 2.2 – ASCE31-13 rehabilitation objectives and EC8-3 performance requirements.

With respect to compliance criteria, EC8-3 formulates the requirements for each limit state, or performance level, in qualitative terms, referring to more or less severe damage states that characterize the structural damage as a whole. However, when going into the safety verification stage, EC8-3 asks the analyst to conduct individual safety checks at every single structural element, thus implying that a building may collapse if at least one element fails its safety verifications. This issue has already been discussed by Pinto and Franchin (2008), who proposed an alternative procedure, based on a fault-tree representation. ASCE 41-13 equally preconizes the acceptance criteria to be checked individually at a member scale, although still defining a set of other damage measures,

such as inter-storey drift limits of 5%, 2.5% and 0.7% for the CP, LS and IO performance levels, respectively. The correlation of damage metrics, such as inter-storey drift limits, with the various performance levels has been a matter of continuous and intensive research (Bertero and Bertero, 2000; Bertero and Bertero, 2002; Gioncu and Mazzolani, 2002; Sullivan et al., 2012; Kamaris et al., 2015).

Contrarily to EC8-3 and ASCE 41-13, the NZSEE guidelines exhibit a clearer practice-oriented character, proposing assessment tools that simply intend to evaluate, with greater or lower accuracy, the performance of an existing building at a single ultimate limit state (ULS), which refers to a collapse-prevention requirement. For such, the NZSEE guidelines establish two distinct evaluation procedures: (i) a so-called Initial Evaluation Procedure (IEP), which is intended to be a coarse screening method involving as few resources as reasonably possible; (ii) and a Detailed Assessment Procedure (DAP), which provides more accurate performance assessments and allows the analyst to look in more detail at the response of the building under a certain ground motion. The performance of the structure is evaluated by comparing the maximum design seismic action achieved, with respect to ULS, with the recommended design seismic action for new buildings. A certain existing building will be thus considered to exhibit low to moderate seismic risk if the ratio between the maximum design seismic action achieved and the recommended design action for new buildings is not less than 67% and 33%, respectively, and to exhibit high seismic risk if the ratio is less than 33%.

2.4.2 Data collection requirements and treatment of uncertainty

An important distinctive feature of existing buildings when compared to new ones is the fact that their structural properties can be obtained to a certain extent during the assessment process. The gathering of this information implies carrying out visual and field surveys on a building-by-building basis, which effectiveness vary greatly depending on the inventory. Although techniques for in situ testing may be considered to be reasonably well developed, they involve measurement errors and the results may lead to a considerable degree of uncertainty (Romão et al., 2012b). As a result, it is oftentimes difficult to obtain trustful data to define the exact material, geometrical and detailing characteristics of the building, being this incompleteness of knowledge always present in any seismic safety assessment study of existing structures.

Both American and European documents try to account for this type of epistemic uncertainty through the definition of different knowledge levels, which are related to the

amount and quality of usable information, and the use of a single factor that aims to covers all types of uncertainties, denoted as Confidence Factor (CF) in EC8-3 and Knowledge Factor (k) in ASCE 41-13. In both standards, these factors act as partial safety factors in the safety verification stage. Figure 2.3 depicts a comparison between the different ways of ASCE 41-13 and EC8-3 in treating uncertainty. Whilst in EC8-3 the level of knowledge only establishes the method of analysis and the CF value to be adopted, in ASCE 41-13 the level of knowledge also influences the selection of the rehabilitation objective. Therefore, another important conceptual difference between EC8-3 and ASCE 41-13 may be identified for minimum or limited levels of knowledge. ASCE 41-13 not only considers that simplified elastic methods of analysis (Linear Static Procedures, LSP, and Linear Dynamic Procedures, LDP) should be adopted in this case, similarly to EC8-3, but also the IO performance level may be neglected. Such an approach could be due to the fact that in the IO performance level, as in the DL limit state of EC8-3, no yielding is expected to occur in any structural element, both ductile and brittle, and hence the verification of this performance level could lead to poor estimates of the actual response of the building.

ASCE41

Data	Knowledge Levels			
	Minimum	Usual		Comprehensive
Rehabilitation Objectives	BSO or Lower LS+CP	BSO or Lower	Enhanced	Enhanced
Analysis Procedures	LSP, LDP	ALL	ALL	ALL
Knowledge Factor (k)	0.75	1.00	0.75	1.00

EC8-3

Data	Knowledge Levels		
	Limited (KL1)	Normal (KL2)	Full (KL3)
Rehabilitation Objectives	-	-	-
Analysis Procedures	LF, MRS	ALL	ALL
Confidence Factor (CF)	1.35	1.20	1.00

Figure 2.3 – Comparison between the ASCE41-13 and EC8-3 ways of treating uncertainty.

A number of controversial features associated with knowledge factors have already been highlighted by Romão et al., (2008) and Franchin et al. (2009; 2010), such as the fact that they are not differentiated with respect to the method of analysis or structural type, the complete knowledge level does not actually correspond to a state of perfect knowledge and the use of mean values of material properties within the model tends to led to non-conservative values, underestimating the demand-to-capacity ratios. For what concerns the NZSEE guidelines, no explicit reference is made on the way uncertainty is treated, being just prescribed that probable values of strengths should be adopted when determining the strength and deformation capacities of an existing building. In the case of steel, the probable strength is the minimum yield stress or tensile strength obtained from published data or test results.

2.4.3 Analysis procedures

In the assessment of an existing building, the accuracy of the method of analysis that will be employed is of crucial importance, since conservative methods may indicate unnecessary expensive interventions, while non-conservative ones may leave the building exposed to excessive risk. In this sense, both EC8-3 and ASCE 41-13 recommend the use of similar methods of analysis in the assessment of existing structures, which can range from simpler force-based elastic methods, as the well-known lateral force method, designated by Linear Static Procedure (LSP) in ASCE 41-13 and by Lateral Force method (LF) in EC8-3, or the modal response spectrum method, designated by Linear Dynamic Procedure (LDP) in ASCE 41-13 and Modal Response Spectrum Analysis (MRS) in EC8-3, to more complex nonlinear methods, as the pushover or the time-history dynamic analysis methods. By allowing the analyst to select one method of analysis from a wide range of alternatives, both standards intend to own a practice-oriented character and to encourage engineering judgment. EC8-3 also allows the use of the *q*-factor approach, which is the baseline design method prescribed in EC8-1 (CEN, 2004a), by setting a default value for the behaviour factor, *q*, equal to 2.0. This value should be increased by one-third to check the NC limit state or to higher values if analytically justified. Nevertheless, the EC8-3 itself refers to this type of approach as generally not suitable to check the NC limit state and, with such small values of *q*, is expected to be too conservative. Hence, it should only find application in the case of buildings with an apparent overcapacity and/or located in low seismicity regions (Pinto and Franchin, 2008).

The use of linear methods of analysis is not straightforward and depends, as seen before, on the knowledge of the structure and on specific criteria related with the distribution of inelastic demands height-wise. To assess this inelastic distribution of demands, the ratio between the elastic demands obtained from the un-reduced seismic action and the corresponding capacity, denoted as $\rho_i = D_i / C_i$ in EC8-3 and DCR_i in ASCE 41-13, should be determined over all *i*-th ductile primary elements of the structure and compared with the limits prescribed by both codes. According to EC8-3, linear methods of analysis can be applied if the ratio ρ_{max} / ρ_{min}, defined over all ductile primary elements with $\rho_i > 1.0$, does not exceed a maximum acceptable value in the range between 2 and 3, being 2.5 the recommended value. Around beam-column joints, the ratio ρ_i only needs to be evaluated at the sections where plastic hinges are expected to form on the basis of capacity design principles. The assumption underlying this criterion is that if a structure

goes into inelastic range with a uniform distribution of inelastic demands, which results from a regular distribution of stiffness, mass and strength, its response, in terms of displacements, would be acceptably accurate on the basis of the equal displacement rule, which is approximately valid for a single-degree-of-freedom oscillator.

With respect to ASCE 41-13, linear methods of analysis could be employed if all component verify the condition *DCRs* ≤ 2.0, which assumes that no significant nonlinear incursions would occur. Still, ASCE 41-13 extends its applicability to structures with one or more *DCRs* greater than 2.0 if they verify a set of criteria related to structural irregularity, such as: (i) in-plane and out-of-plane discontinuity irregularities; (ii) torsional strength irregularity, which shall be considered if the ratio of the critical element *DCRs* for primary elements on one side of the centre of resistance of a storey to those on the other side exceeds 1.5; (iii) and weak storey irregularity, that shall be considered to exist if the ratio between the average shear *DCR* of any storey to that of an adjacent storey exceeds 125%, being the average *DCR* of a storey, $\overline{DCR}$, given by:

$$\overline{DCR} = \frac{\sum_{1}^{n} DCR_i V_i}{\sum_{1}^{n} V_i} \tag{2.1}$$

where DCR_i is the critical action *DCR* of the *i* element of the storey, which is the largest *DCR* obtained for each action (i.e., axial force, moment or shear), V_i is the total calculated lateral shear force for the *i* element due to earthquake response, assuming that the structure remains elastic, and *n* is the total number of elements in the storey. This expression represents a weighted average of the elements *DCRs* of a storey by considering the elastic shear forces developed at each element over the entire storey. An identical approach is adopted by the New Zealand NZSEE guidelines, though no quantitative ways of characterizing these irregularities are given.

Once verified the linear analysis applicability criteria, the analyst can afterwards perform linear analysis, which, as referred above, could be conducted using a simple lateral force method based on the fundamental mode of vibration of the structure or a modal response spectrum method. With respect to the lateral force method, while EC8-3 defines the total base shear as $V_b = S_a m\lambda$, where S_a is the elastic spectral acceleration at the fundamental period of vibration of the building in the direction under consideration, *m* is the total mass of the building and λ a is correction factor of 0.85 or 1.0 depending on the type and period of vibration of the structure, ASCE 41-13 defines the base shear as

$V_b = C_1 C_2 C_m S_a m$, being C_1 a modification factor that relates the expected maximum inelastic displacements with those computed from the elastic analysis, C_2 a modification factor that represents the effect of pinched hysteresis shapes and cyclic stiffness and strength degradation on the maximum displacement response and C_m is the effective mass factor that accounts for higher mode effects. Since the product of C_1C_2 may lead to values slightly higher than the unity and C_m is roughly equal to λ, one may expect that ASCE 41-13 would result in higher base shear demands comparing to EC8-3. Additionally, in terms of the distribution of the horizontal forces along the height of the building, ASCE 41-13 proposes the following expression:

$$F_i = \frac{m_i h_i^k}{\sum_1^n m_i h_i^k} V_b \tag{2.2}$$

where m_i are the storey masses, h_i are the heights of masses m_i above the level of application of the seismic action (foundation or top of a rigid basement), and k is a constant function of the period of vibration of the structure, T, being equal to 2.0 if $T \geq 2.5$ sec and 1.0 if $T \leq 0.5$ sec, while for values of T within this interval a linear interpolation shall be used. A similar pattern is proposed by EC8-3 at Annex B, being also suggested the use of the pattern defined for the design of new structures (CEN, 2004a), which is simply linearly proportional to the storey masses and heights. It may be referred that the NZSEE guidelines follow the same provisions as prescribed by ASCE 41-13.

When linear analysis is not applicable, alternative nonlinear methods of analysis shall be used, which may be static or dynamic. In the case of nonlinear static analysis, commonly designated as Pushover Analysis (PA), no applicability conditions are imposed, being just referred by EC8-3 that in the case of buildings not conforming to in-plan regularity criteria (EC8-1) a spatial model shall be adopted. Still, the NZSEE guidelines make a note on the applicability of this type of analysis, which should be limited to cases where higher mode effects are not critical, also highlighted by Krawinkler and Seneviratna (1998). No limitations are established to the use of Nonlinear Dynamic Analysis (NDA).

In order to conduct pushover analysis, two main steps may be distinguished (Pinho et al., 2013): (i) one that involves the definition of the so-called capacity curve, which relates the total base shear with the control node displacement, taken at the centre of mass of the roof of the building; (ii) and another related to the target displacement, or performance point, determination. In the former step, EC8-3 recommends the use of at least three load patterns to compute the capacity curve: (i) a uniform pattern; (ii) a first mode proportional

pattern, as suggested by EC8-1; (iii) and the pattern of equation (2.2), as referred in Annex B. ASCE 41-13, relying on FEMA 440 (FEMA, 2005), simply recommends a single pattern based on the first mode shape, considering that multiple load patterns have little effect in improving the accuracy of pushover analysis. In line with the most recent advances in pushover analysis (Chopra and Goel, 2002; Antoniou and Pinho, 2004; Kalkan and Kunnath, 2006), the New Zealand document suggests, as an alternative to first mode proportional and constant patterns, the use of a modal load pattern, obtained by combining modal responses from a response spectrum analysis with sufficient modes to capture at least 90% of the total building mass, and an adaptive load pattern, that changes as the structure displaces as yielding progresses. In the second step, EC8-3 follows the N2 method proposed by Fajfar (1999) to determine the target displacement value d_t, which is based on an idealized bilinear SDOF system defined by an elastic-perfectly plastic force-displacement relationship (Figure 2.4 (A)), with effective period T^* and corresponding elastic spectral displacement, d_{et}^*. According to this approach, if T^* is equal or greater than the corner period T_c, which sets the boundary between the constant velocity and the constant acceleration branches of the spectrum, the final inelastic displacement demand of the SDOF system is equal to the elastic one, otherwise a reduction factor is applied (Fajfar, 1999; CEN, 2004a). In turn, the American standard is based on the improved Displacement Coefficient Method initially proposed by FEMA 356 (FEMA, 2000) and used by FEMA 440 (FEMA, 2005), which defines the target displacement as $\delta_t = C_o C_1 C_2 S_a T_e^2 / 4\pi^2 g$, where C_1 and C_2 are the modification factors already described above, C_o is a modification factor that relates the spectral displacement of an equivalent SDOF system to the roof displacement of the building and T_e is the effective fundamental period defined considering an idealized bilinear force-displacement relationship as presented in Figure 2.4 (B).

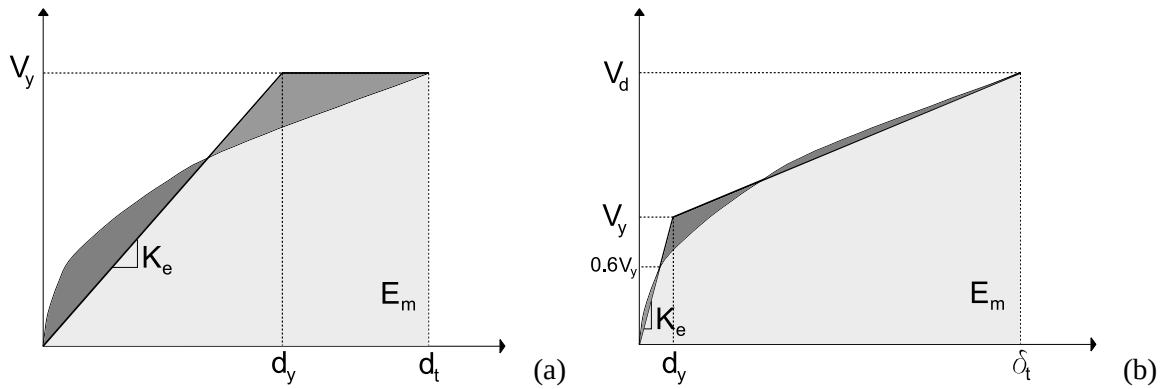

Figure 2.4 – Bilinear curve idealization according to: (a) EC8-3 and (b) ASCE 41-13.

The effective period is a key parameter in the definition of the target displacement value, which directly dependents on the yield displacement, d_y, that may be defined according to the equivalent energy rule in EC8-3, so that:

$$d_y = 2\left(d_t - \frac{E_m}{V_y} \right) \tag{2.3}$$

being E_m the deformation energy up to the target displacement of the SDOF system and V_y the effective yield force, and in ASCE 41-13 as:

$$d_y = \frac{\delta_t \left(V_d + V_y \right) - 2E_m}{V_d} \tag{2.4}$$

wherein the effective stiffness K_e should be defined as secant at the ordinate $0.6V_y$ of the real capacity curve. Since the yield displacement, d_y, and the yield force, V_y, are unknowns in equation (2.4), an iterative calculation is needed to determine both. For such, a first value of d_y may be guess and the computed value of V_y should be afterwards checked against the one picked up from the real capacity curve at abscissa $0.6d_y$. The final idealized curve is obtained when convergence is achieved. EC8-3 defines the effective period of the equivalent SDOF system as $T^* = 2\pi\sqrt{m^* d_y^* / V_y^*}$, where m^*, d_y^*, and V_y^* are the properties of the idealized single-degree-of-freedom system, while ASCE 41-13 defines the effective period as $T_e = T_i \sqrt{K_i / K_e}$, being T_i and K_i the elastic fundamental period and the elastic lateral stiffness, respectively. The NZSEE guidelines also suggest the procedure proposed by FEMA 356 (FEMA, 2000) to conduct pushover analysis.

In comparison to elastic methods of analysis, the advantages of pushover analysis as an assessment tool are manifold, not only providing more detailed evaluations and a more reliable prediction of failure mechanisms, but also providing a complete picture and a step-by-step monitoring of the response of the structure. Still, pushover analysis have proved to be quite inaccurate in many situations, such the cases of plan irregular structures or in case where higher mode effects cannot be neglected (Krawinkler and Seneviratna, 1998). The alternative should be the use of more accurate and robust nonlinear dynamic analysis, in which, apart from the complexity of the mathematical model formulation, major issues arise in the definition of the seismic action. A thorough discussion on the impact of the record selection methods proposed for seismic performance assessment of buildings by the codes and guidelines under analysis is presented in Chapter 2.

2.4.4 Acceptance criteria

The last stage of the seismic safety assessment process corresponds to safety verifications. In order to conduct such safety verifications, both EC8-3 and ASCE 41-13 preconize that an initial distinction has to be made between the nature of the failure mechanism of each individual member (i.e. brittle or ductile), and the type of analysis adopted (i.e. linear or nonlinear). If nonlinear methods of analysis are used, the demands should be directly obtained from the analysis using mean values for the material properties. For what concerns ductile members, safety verifications are performed by comparing the plastic deformations demands θ_{demand} with the corresponding deformation capacities $\theta_{capacity}$ defined by the codes. In the case of steel moment resisting frames, the safety checks shall be performed in terms of plastic hinge rotations. Also, in order to account for the uncertainties associated to the level of knowledge of the structure, the deformation capacity values should be affected by a knowledge or confidence factor (k or CF), as represented in Figure 2.5. With respect to brittle members, both codes similarly prescribe safety verifications based on the comparison of the member internal forces, Q_{demand}, with the corresponding member strength capacity, $Q_{capacity}$. On the other hand, if linear methods of analysis are used, the fulfilment of safety verifications is not straightforward. EC8-3 preconizes that brittle member demands shall be quantified by means of capacity design principles, considering the contribution of ductile members, so that: (i) they shall be taken equal to the demands obtained from linear analysis if ductile members are behaving elastically ($\rho \leq 1.0$); (ii) or they shall be taken equal to the capacity of the ductile members if ductile members are behaving inelastically ($\rho > 1.0$). Likewise, ASCE 41-13 prescribes that the force-control actions (i.e. brittle shear or axial load actions), shall be calculated so that $Q_{demand} = Q_G \pm Q_E / C_1 C_2 J$, where Q_G is the action due to gravity loads, Q_E is the action due to earthquake loads and J is the force-delivered reduction factor taken as the smallest *DCR* of the components in the load path delivering force to the member under analysis. Major differences between both standards arise in the safety verifications stage of ductile members or deformation-controlled actions (i.e. bending moment actions) using linear analysis. While ASCE 41-13 defines the acceptance criteria in terms of member strengths, by considering a so-called component demand modification factor, m, that accounts for the expected ductility associated with deformation-controlled actions, EC8-3 considers that safety verifications shall be always conducted in terms of member deformations. Naturally, EC8-3 proposes a rather questionable approach, as it is

controversially requiring analysts to evaluate the safety of ductile members in terms of plastic rotations using a linear elastic structural model. Moreover, it may be noted that the values of the *m* factor proposed by ASCE 41-13 are quite similar to those defined by the same standard for the ductility capacity of steel members. Figure 2.5 summarizes the safety verification approaches proposed by both codes. It should be also referred that, unlike EC8-3, which only treats columns as ductile members at the NC limit state, ASCE 41-13 considers that both beam and column elements shall be treated as ductile elements in moment-resisting frames.

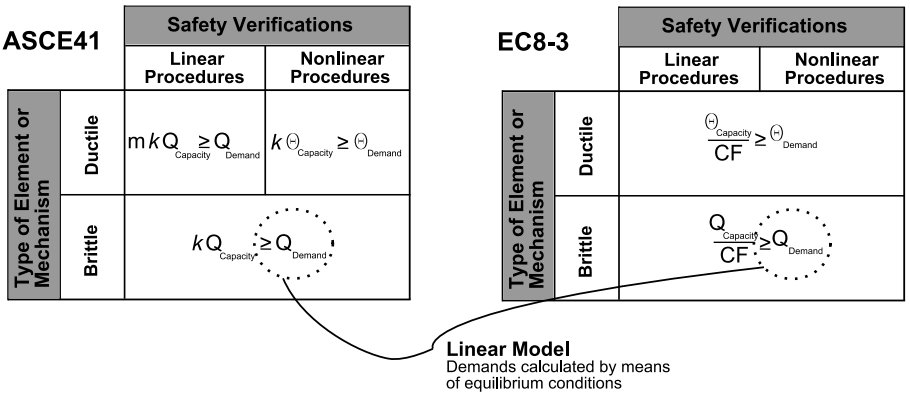

Figure 2.5 – Summary of the safety verifications proposed by ASCE 41-13 and EC8-3.

2.5 Comparative study between different procedures for seismic safety assessment of existing steel buildings

2.5.1 Case study description, numerical modelling and seismic action definition

The study presented herein was conducted considering four different 5-storey moment resisting steel frame buildings with a regular configuration in plan and elevation. The plan layout and the elevation views of the internal moment-resisting frame of the analysed buildings are illustrated in Figure 2.6. Each building was designed according to different criteria. The first building, denoted as GB, was designed accounting only for gravity loads following the rules prescribed in Eurocode 3 (CEN, 2005b). The remaining three buildings were seismically designed according to Part 1 of EC8 (CEN, 2004a) assuming a DCM ductility class, with a behaviour factor, *q*, of 4.0. The difference between the three buildings is found on the different limits considered for the inter-storey drift sensitivity coefficient, θ, which is the parameter used to check for the need to consider second-order effects in the analysis and design process. Thus, the SB1 building was

designed assuming $0.2< \theta < 0.3$, the SB2 building was designed considering $0.1< \theta \leq 0.2$, being the second-order effects taken into account by multiplying the relevant seismic action effects by a factor equal to $1/(1 - \theta)$, and finally the SB3 building was designed in order to minimize the relevance of second-order effects ($\theta \leq 0.1$). The members of the analysed buildings are presented in Table 2.1, being assumed a grade S275 for the structural steel.

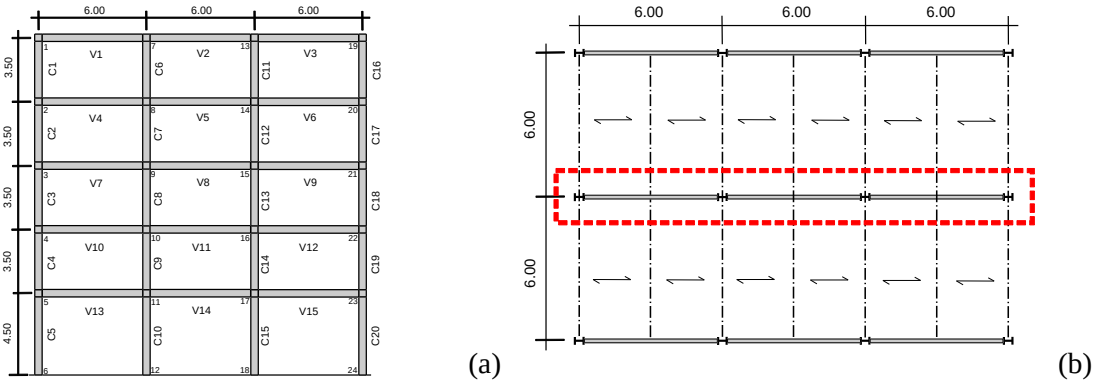

Figure 2.6 – Dimensions, structural elements and nodes naming: (a) elevation view; (b) and plan view.

Table 2.1 – Characteristics of the buildings analysed.

Storey	Building GB			Building SB1		Building SB2		Building SB3	
	Outer Columns	Inner Columns	Beams	Columns	Beams	Columns	Beams	Columns	Beams
5	HE240B	HE280B	IPE300	HE280B	IPE300	HE300B	IPE300	HE500B	IPE300
4	HE240B	HE280B	IPE300	HE280B	IPE300	HE300B	IPE300	HE500B	IPE400
3	HE240B	HE280B	IPE300	HE280B	IPE300	HE400B	IPE300	HE500B	IPE400
2	HE260B	HE300B	IPE300	HE300B	IPE330	HE400B	IPE330	HE500B	IPE450
1	HE260B	HE300B	IPE300	HE300B	IPE330	HE450B	IPE330	HE500B	IPE450

The analyses were carried out using the open source software OpenSees (PEER, 2011) and two sets of structural models were developed in line with the type of analysis performed, linear and nonlinear. For the development of the numerical models for linear analysis, the previously presented data is sufficient. Nonetheless, it should be referred that instead of the exact manufactured cross-section properties, approximate properties were used by neglecting the representation of the root radius between the flange and the web of the cross-sections. The aim was to provide a perfect fit between the results obtained from both linear and nonlinear analysis. With respect to the models used for nonlinear analysis,

force-based beam-column elements (Scott et al., 2008; Spacone et al., 1992) were adopted considering 10 Gauss-Lobatto integration points along its length, which offers a superior solution to the classical Gauss integration method when it is important to include in the integration the end points of the element. Also a cross-section discretization solution by fibers was followed and a bilinear elasto-plastic material model with 0.5% hardening was adopted for the structural steel. The effect of the panel zones was neglected in this study. Special attention was given to the modelling of the elastic viscous damping using the Rayleigh approach, having the mass proportional damping been neglected, since it does not have a real physically meaning (Petrini et al., 2008), and a tangent-stiffness proportional damping assumed, which greatly reduces the elastic damping force when the structural stiffness drops to the post-yield level (Priestely and Grant, 2005; Charney, 2008). A fraction of critical damping equal to 2% was considered. The gravity loading assumed in the analysis merely consists of simple point loads applied at the mid-span of the beams and at each alignment of columns, which represent the vertical loads transmitted from secondary frames. On the top floor, both dead and live loads were set as G_k =85.5kN and Q_k =18kN at the inner alignment of columns and mid-span of beams and as G_k = 42.75kN and Q_k =9kN at the outer alignment of columns. On the remaining storeys the dead and live loads were defined as G_k =103.5kN and Q_k =36kN at the inner alignment of columns and mid-span of beams and as G_k =51.75kN and Q_k =18kN at the outer alignment of columns. The combination factor ψ_2 proposed in the Eurocode 0 (CEN, 2002) seismic combination of loads was defined as 0.0 at the top floor and 0.3 at the remaining storeys. The masses were lumped at each node of the various floors and P-Δ effects were directly included in the numerical analysis. At last, as the type 1 seismic action defined in EC8-1, which represents an inter-plates earthquake, was found to be the critical one during the design, it served as the basis for the assessment study presented hereafter, being characterized by PGA values of 0.091g, 0.15g and 0.451g for the DL, SD and NC limit states, respectively. Figure 2.7 presents the elastic response spectra corresponding to these conditions.

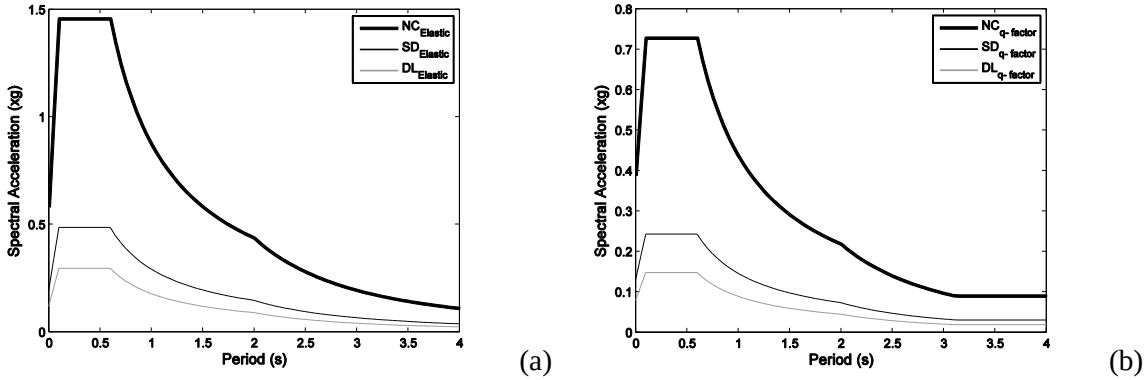

Figure 2.7 – Response spectra defined for the DL, SD and NC limit states: (a) elastic spectra; (b) and design spectra obtained using the *q* values recommend by EC8-3 for steel buildings.

For the sake of convenience and since a direct correspondence between the EC8-3 limit states and the ASCE 41-13 performance levels may be established, the IO, LS and CP performance levels will be henceforth referred to as DL, SD and NC limit states, respectively. Modal analysis was carried out for each frame to identify the dynamic characteristics of the buildings, which are listed in Table 2.2.

Table 2.2 – Dynamic characteristics of the buildings.

Building	Periods of vibrations (s)			Mass Participation Ratios (%)		
	Mode 1	Mode 2	Mode 3	Mode 1	Mode 2	Mode 3
GB	1.63	0.50	0.26	85.49	9.24	3.40
SB1	1.50	0.48	0.25	83.86	10.41	3.58
SB2	1.20	0.39	0.20	78.73	12.06	5.34
SB3	0.90	0.28	0.13	80.56	13.22	4.33

Prior to the seismic safety assessment study that will be presented further on, some questions may be previously raised regarding the seismically designed buildings, which despite complying with EC8-1, feature completely different lateral stiffness levels. In a comparative study between the European and American approaches for consideration of P-Δ effects in seismic design, Peres (2010) concluded that the adoption of EC8-1 tends to result in stiffer, stronger and, consequently, more expensive structures. Hence, the comparative study conducted in this work will not only intend to understand how reliable the various available assessment methods for existing steel buildings are, by setting nonlinear dynamic analysis as benchmark, and to evaluate the level of variance associated with the response estimates, defined in terms of global drifts, inter-storey drifts and demand-to-capacity ratios, but also to assess how conservative the second-order effects condition proposed by EC8-1 may be.

2.5.2 Results from linear analysis

Four linear analyses were employed in this study: (i) the EC8-3 Lateral Force (LF) analysis using a force pattern linearly proportional to the storey masses and heights, designated as EC8-3; (ii) the EC8-3 LF analysis with a force pattern defined by expression (2.2), designated as EC8-3 Annex B; (iii) the ASCE 41-13 LSP analysis also admitting the force pattern of expression (2.2), named as ASCE 41-06; (iv) and a modal response spectrum analysis designated as LDA. It was found that the EC8-3 and the EC8-3 Annex B methods are slightly more conservative when compared the ASCE 41-13 method for buildings GB and SB1, mainly because of the effect of the EC8-1 correction factor (λ), which is equal to 1.0 when $T_1 \geq 2T_C$. In turn, the product between the modification factors $C_1C_2C_m$ defined by ASCE41-13 is approximately equal to 0.9. Additionally, not only the force pattern of expression (2.2) was seen to lead to more severe results when compared to the linearly proportional pattern, but also the simplified LF method led to higher seismic demands comparing to the MRS method in all buildings. Since the plastic rotation demands at beams located at a certain level may be approximately estimated by the inter-storey drift of that same level (Gioncu, 2000), a considerable decrease in the local plastic demands along the building height was observed with the increase in the lateral stiffness of buildings, as it would be expected. It should be noted that the NZSEE and EC8-1 capacity design criteria were verified at all storey joints and thus a beam-sway mechanism is likely to be developed in all buildings. Table 3 summarizes the results obtained in terms of global drift ratios, defined as $\Delta u / H$, for the various buildings and methods of analysis. It may be recalled that values of 0.025 and 0.04 of maximum interstorey drift ratios are usually associated with the SD and NC limit states, respectively [Karavasilis et al., 2006], corresponding the latter to global drift ratios of approximately 3% [Grecea et al., 2004]. The DL limit state is generally associated with the occurrence of the first plastic hinge in the structure. As a result, buildings GB and SB1 are expected to fail at the NC limit state using linear static methods of analysis, but not using the LDA method.

Table 2.3 – Global drift ratios obtained for each linear method of analysis (%).

Building	GB			SB1			SB2			SB2		
	DL	SD	NC	DL	SD	NC	DL	SD	NC	DL	SD	NC
EC8-3	0.70	1.12	3.31	0.65	1.06	3.12	0.48	0.78	2.30	0.33	0.53	1.58
EC8-3 Annex B	0.75	1.21	3.56	0.70	1.13	3.35	0.51	0.83	2.45	0.34	0.55	1.64
ASCE 41-13	0.68	1.09	3.23	0.63	1.02	3.03	0.54	0.87	2.61	0.36	0.58	1.75
LDA	0.62	1.00	2.93	0.57	0.93	2.74	0.48	0.77	2.29	0.33	0.53	1.57

As it has been previously discussed, before the assessment of any existing building using linear methods of analysis, its applicability shall be firstly verified. To this end, the distribution of the inelastic demands within the structure has to be evaluated, which is defined in terms of *DCRs* or ρ_i in EC8-3. Figure 2.8 displays the *DCR* values at the control sections of the GB and SB1 buildings, for the NC limit state, providing a picture of the seismic demand distribution along the structures and a hint on the applicability of the analysis. The nomenclature used for the control sections is set by putting together the names of its element and node with reference to Figure 2.6.

The demand-to-capacity ratios were obtained according to EC8-3. The flexural demands were directly picked up from the analysis, whilst the capacities were defined for the beams as $M_{pb,Rd} = W_{pl,b}\, f_{yb}$, where $W_{pl,b}$ is the effective plastic modulus computed with reference to the actual measured size of the section and f_{yb} is the yield strength of the steel in each beam that may be taken equal to the mean value obtained from in-situ tests and from the additional sources of information, appropriately affected by the knowledge factor; and for columns as $M_{pc,Rd} = W_{pl,c}\ (f_{yd,c} - N_{Ed} / A_c)$, being $W_{pl,c}$ the plastic modulus of the column section, with area A_c, evaluated on the basis of actual geometric properties, if available, and taking into account haunches, if any, N_{Ed} the axial load in the seismic design situation and $f_{yd,c}$ the yield strength of the steel in each column computed as referred for the case of beams. For comparison purposes, whereas the expected strength of beams is estimated similarly by ASCE 41-13, the American standard overestimates the strength capacity of columns by 18%. In the present study a comprehensive level of knowledge of the structure was assumed and values of CF and KF equal to 1.0 were adopted. It is worth recalling that, according to EC8-3, linear methods of analysis may only be applied if the ratio DCR_{max} /*DCRmin*, defined over all ductile primary elements with *DCRi* > 1.0 and sections where plastic hinges are expected to form on the basis of capacity design principles, does not exceed a maximum acceptable value in the range between 2.0 and 3.0. Since beam-sway mechanisms are expected to be developed in all buildings and no hinging should occur at columns according to EC8-3, only the bottom sections of the first storey columns were monitored.

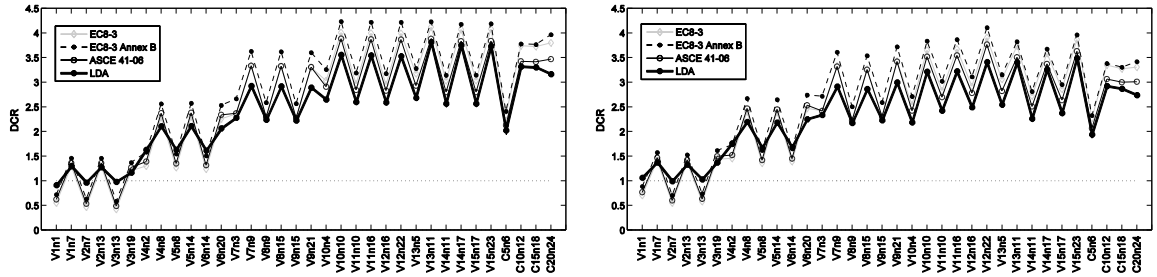

Figure 2.8 – *DCRs* at the control sections for the NC limit state and considering various linear methods of analysis of building GB (*left*) and building SB1 (*right*).

It may be observed from Figure 2.8 (a) that building GB fails to meet the $DCR_{max}/DCRmin$ condition in the NC limit state for both LF and MRS methods, resulting in ratios of 3.41 and 3.26, respectively. Additionally, despite of leading to a higher DCR_{max} value of 4.23, the LF analysis using the pattern of expression (2.2) resulted in a lower DCR_{max} /*DCRmin* ratio of 3.08. This value is practically within the EC8-3 allowable limit and results from a more uniform distribution of inertial forces along the height of the building. On the other hand, in the case of building SB1 (Figure 2.8 (b)), although the MRS method fails in terms of its applicability requirements, corresponding to a ratio of 3.38, the safety assessment may still be carried out using the LF analysis, which yielded a ratio of 2.87. A major question may be thus raised with respect to the linear analysis applicability criterion defined by EC8-3: Is it coherent to allow the assessment of a building using a simpler lateral force method, but not using a supposedly more accurate modal response spectrum analysis? The reason for such inconsistency is related with the impact of higher modes effects in the MRS method, which makes the left node of the beams at the top floor to initiate yielding, thus resulted in a *DCRmin* value practically equal to 1.0. This value, when compared to DCR_{max}, result in a ratio greater than the code limit, although the maximum level of demands obtained from the MRS analysis is considerably lower than that of the LF method. For what concerns buildings SB2 and SB3, it was observed that both buildings comply with the requirements for applicability of linear methods of analysis in the NC limit state, being only interesting to point out the ratio of 2.94 obtained using the MRS analysis in building SB2, which is right on the threshold of the code limit. No applicability limitations were observed at the remaining limit states for all buildings, as listed in Table 2.4. Since for ordinary buildings, EC8-3 establishes that safety verifications have to be conducted for all limit states, nonlinear methods of analysis would have to be employed in building GB in order to carry out with the seismic safety assessment procedure. Building SB1 could only be assessed elastically using the simplified

LF method of analysis. With the exception of building SB3, all buildings exhibit a maximum *DCR* higher than 1.0 in the DL limit state, implying that yielding has already been developed. According to EC8-3, the capacities of both ductile and brittle elements shall be defined by their yield strengths at the DL limit state, foreseeing that no yielding should occur at any structural element. Nevertheless, EC8-3 allows the development of plastic rotations in primary structural components at the DL limit state when nonlinear analysis are adopted, hence some lack of conceptual coherence in the definition of the performance objectives of this limit state seem to exist.

Table 2.4 – Applicability of linear methods of analysis according to EC8-3.

Building	Lateral Force Method (LF)			Modal Response Spectrum Analysis (MRS)		
	NC	SD	DL	NC	SD	DL
GB	Not Applicable	Applicable	Applicable	Not Applicable	Applicable	Applicable
SB1	Applicable	Applicable	Applicable	Not Applicable	Applicable	Applicable
SB2	Applicable	Applicable	Applicable	Applicable	Applicable	Applicable
SB3	Applicable	Applicable	Applicable	Applicable	Applicable	Applicable

With respect to the verification of the applicability criteria defined by ASCE 41-13, it was observed that linear methods of analysis cannot be applied at the CP performance level in any building (Table 2.5). This is due to the fact that, neither the $DCR_i \leq 2.0$ condition, nor the structural weak storey irregularity criterion are verified, even in building SB3. ASCE 41-13 establishes that the latter regularity criterion is verified if the ratio between the $\overline{DCR}$ of two adjacent storeys does not exceed 125%. It was observed that this regularity criterion is unlikely to be meet when comparing the first and second storey $\overline{DCR}$ values of all buildings. Buildings GB, SB1, SB2 and SB3 exhibit $\overline{DCR_1}/\overline{DCR_2}$ ratios equal to 2.07, 1.78, 1.62 and 2.02, respectively.

Table 2.5 – Applicability of linear methods of analysis according to ASCE 41-13.

Building	Linear Static Procedure (LSP)		
	CP	LS	IO
GB	Not Applicable	Applicable	Applicable
SB1	Not Applicable	Applicable	Applicable
SB2	Not Applicable	Applicable	Applicable
SB3	Not Applicable	Applicable	Applicable

Summing up the foregoing, while EC8-3 admits that the ratio DCR_{max} /*DCRmin* should be lower than a certain value ranging from 2 to 3, imposing inelastic demands to be regularly distributed height-wise regardless of the intensity of the seismic action, the $DCR_i \leq 2.0$ condition prescribed by ASCE 41-13 is easily violated for increasing levels of seismic intensity. One should recall that the satisfaction of the Basic Safety Objective requires the check of both CP and LS performance levels and thus nonlinear methods of analysis would have to be employed to assess all buildings according to ASCE 41-13. Furthermore, as was already concluded by Romão et al. (2010) for RC buildings, both EC8-3 and ASCE 41-13 prescribe rather stringent linear analysis applicability conditions that are not expected to be satisfied by many existing buildings, especially those not seismically designed. In addition, regardless the lateral stiffness and strength of the buildings analysed, all buildings failed or verified the linear analysis applicability criterion proposed by EC8-3 with very little margin, i.e. the maximum DCR_{max} /*DCRmin* ratio was found to be always right on the threshold of the maximum limit value of 3.0., which raised another pertinent question: How confident should analysts be on the results obtained using linear methods of analysis, particularly when assessing the structural response at the Near Collapse limit state, where high nonlinear incursions are expected to occur?

2.5.3 Results from *q*-factor approach

Despite referring the *q*-factor approach as generally not suitable for checking the NC limit state, EC8-3 allows its use. The results obtained with the use of this alternative approach are presented in Table 2.6, for each building and limit state. Again, the SB3 building was seen to verify all safety requirements and the admissible inter-storey drifts imposed at the DL limit state. These observations are in agreement with those previously obtained for the LF and MRS methods of analysis. However, as expected, this method led to rather conservative results, especially in the case of the SB1 and SB2 buildings, which were designed according to EC8-1 considering a behaviour factor *q* equal to 4.

Table 2.6 – Safety verifications according to the EC8-3 *q*-factor approach.

Building	*q*-factor approach		
	NC	SD	DL
GB	Not Safe	Safe	Not Safe
SB1	Not Safe	Safe	Not Safe
SB2	Not Safe	Safe	Safe
SB3	Safe	Safe	Safe

2.5.4 Results from nonlinear pushover analysis

Seven pushover analyses were carried out herein. The analyses, henceforward designated by $PA_{EC8}N2$, $PA_{EC8\text{-}3B}N2$ and PA_cN2, where conducted using the EC8-3 linearly proportional to the storey masses and heights lateral pattern (PA_{EC8}), the lateral pattern of expression (2.2) ($PA_{EC8\text{-}3B}$) and a constant lateral pattern along the height (PA_c), respectively, while the performance points were determined according to the N2 method. Despite ASCE 41-13 only recommends the use of a single force pattern based on the first mode shape, designated herein as PA_mDCM, an additional constant pattern along the height was equally adopted, termed as PA_cDCM. In both cases the target displacement was predicted using the Displacement Coefficient Method. Finally, based on the guidelines of NZSEE, an additional Modal Adaptive Pushover Analysis (MAPA) was conducted, so that: (i) *n*th lateral load patterns was firstly defined for each *n*th-mode considering all peak modal contributions (Antoniou and Pinho, 2004; Kunnath, 2004; Park et al., 2007) as $f_n = \Gamma_n\, m\, \phi_n\, S_a\,(\xi_n, T_n)$, where $S_a\,(\xi_n, T_n)$ is the spectral acceleration for the given earthquake loading at a frequency corresponding to the period and damping of mode n, Γ_n is the modal participation factor, ϕ_n is the nth mode shape and m is the mass matrix of the multi-degree-of-freedom system; (ii) secondly, the final load pattern was calculated combining the modal inertial forces using SRSS or other combination rule (Reinhorn, 1997) and re-calculated every time the system properties changed due to inelastic action. The N2 method was used to derive the target displacement values (MAPA N2) and the influence of the spectral amplification was equally accounted for in the derivation of *n*th mode lateral load patterns in an additional analysis designated as $MAPA_{RSA}N2$.

As expected from previous studies (Kalkan and Kunnath, 2007; Pinho et al., 2013), the constant along the height pattern was found to work as higher bound of structural responses, while the first mode and expression (2.2) patterns were seen to set the lower bound. It may be anticipated based on the dynamic characteristics of the buildings (Table 2.2) that their dynamic responses will be mostly governed by their first mode of vibration. As a result, an almost perfect fit between the MAPA and the first mode shape capacity curves was found for all buildings and for low and medium seismic intensities. However, for higher seismic intensities the MAPA capacity curves fitted better those obtained using the constant along the height pattern. This was due to the structural degradation of the buildings and consequent lengthening of the first mode period of vibration, which mass participation ratios grew in all buildings from 80% to more than 90%, resulting in updated

inertial forces with a progressively constant distribution along height of the buildings. The inclusion of spectral amplifications ($MAPA_{RSA}$) accentuated these differences in favour of the constant along the height pattern. In other words, looking into detail at the evolution of the ratio between the first mode $\Gamma_1 S_a$ (ξ_1, T_1) and the second mode $\Gamma_2 S_a$ (ξ_2, T_2) for building GB, a reduction of 3.4 to 1.4 was observed between global drifts of 0.5% and 1.0%, which correspond to the DL and SD limit states, demonstrating the increase in the importance of the participation of the second mode in the response of the building as a result of the spectral amplification. In addition, when comparing the target displacements obtained using the EC8-3 and the ASCE 41-13 approaches (Table 2.7), it was observed that PA_mDCM always results in higher response demands at every limit state, particularly in buildings SB3. Recall that this is the only pushover analysis recommended by ASCE 41-13. On the other hand, the non-preconized PA_cDCM procedure and PA_cN2 were the ones leading to better results in comparison to the supposedly more accurate $MAPA_{RSA}N2$. Notwithstanding these findings, since during the safety verifications the maximum demand value obtained from each pushover analyses is the one that governs the assessment process, the American and European standards may lead to overall similar, with the exception of building SB3. In this case and for the SD limit state, the PA_mDCM overestimated the building demands at the upper storeys.

Table 2.7 – Global drift ratios obtained for each nonlinear method of analysis (%).

Building	GB			SB1			SB2			SB3		
	DL	SD	NC	DL	SD	NC	DL	SD	NC	DL	SD	NC
$PA_{EC8}N2$	0.52	0.89	3.08	0.49	0.82	2.74	0.42	0.70	2.43	0.30	0.49	1.58
$PA_{EC8\text{-}3B}N2$	0.53	0.91	3.10	0.51	0.87	2.84	0.43	0.74	2.54	0.31	0.48	1.66
PA_cN2	0.47	0.80	2.81	0.45	0.76	2.52	0.38	0.63	2.13	0.27	0.43	1.37
PA_cDCM	0.54	0.89	2.67	0.50	0.82	2.47	0.43	0.70	2.11	0.30	0.50	1.50
PA_mDCM	0.64	1.05	3.16	0.61	1.00	3.01	0.55	0.90	2.71	0.38	0.62	1.87
MAPA N2	0.52	0.91	2.90	0.49	0.84	2.79	0.41	0.71	2.41	0.29	0.48	1.58
$MAPA_{RSA}N2$	0.52	0.86	2.84	0.49	0.80	2.63	0.40	0.67	2.31	0.29	0.48	1.58

With respect to the quantification of the local demand-to-capacity ratios, the EC8-3 plastic rotation capacities were adopted herein, which, however, resemble those from ASCE 41-13. To compute the plastic rotation capacities two alternative approaches were adopted in the definition of the chord rotation at yielding (θ_y), namely: (i) the simplified expressions proposed by ASCE 41-13 that are defined for beams as $\theta_y = M_{pb,Rd}\, l_b / 6EI_b$ and for columns as $\theta_y = M_{pc,Rd}\, l_c / 6EI_b\, (1 - N_{Ed} / N_{p,Rd})$, where l_b and l_c are the beam and column

lengths, respectively, I_b and I_c its moments of inertia and $N_{p,Rd}$ is the expected axial yield force of the element. These expressions were used in the PA_mDCM and PA_cDCM analyses. (ii) and, the actual value of the chord rotation at yield by considering the exact shear span length (x_{Ls}), thus $\theta_y = M_{pb,Rd}\, x_{Ls} / 3EI_b$. Since EC8-3 does not provide any guidance on how to estimate θ_y, the second approach was used in the PA_{EC8}N2, $PA_{EC8\text{-}3B}$N2, PA_cN2, MAPA N2 and $MAPA_{RSA}$N2 analyses. Figure 2.9 graphically represents the differences between using both approaches. The ASCE41-13 simplified expressions assume the shear span length (x_{Ls}) to be always equal to half of the member span length (L/2), which is equivalent to neglect the effect of gravity loads and assume that chord rotations at both member ends, $\theta_{1,E}$ and $\theta_{2,E}$, are equal. However, the effect of the gravity loads, which will be more relevant at lower seismic intensity levels, would lead to asymmetric values of chord rotations at nodes 1 and 2. In fact, by looking into detail at node 2, the ratio $\theta_{2,E} / \theta_{2,G+E}$ seems to be roughly equal to (L/2) /x_{Ls}. Hence, the ASCE41-13 approach may be overestimating the chord rotation capacities in this order of magnitude. Therefore, since the plastic rotation capacity of steel members is merely defined as a function of θ_y, the estimation of θ_y plays a critical role in the seismic safety assessment process, particularly due to the fact that x_{Ls} changes with the intensity of the seismic action. At last, the plastic rotation demands, θ_p, were determined by numerically integrating plastic curvatures along the length of the element using the previously referred Gauss-Lobatto quadrature rule. The demand-to-capacity ratios were thus defined as DCR = ($\theta_p + \theta_y$) / (θ_y (m_{NL} +1)), where m_{NL} is the EC8-3 constant that multiplies to θ_y to define the rotation capacity of steel members.

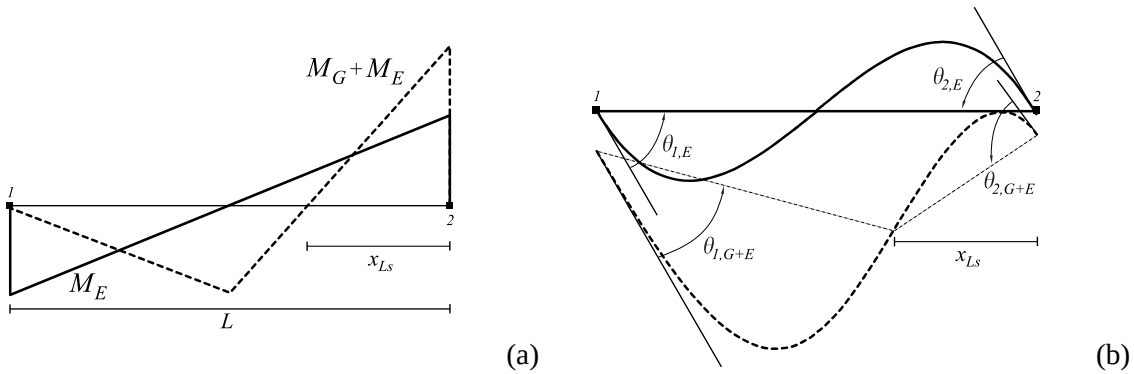

Figure 2.9 – Chord rotation definition considering the influence of seismic loads alone (E) and both gravity and seismic loads ($G + E$) in a beam element: (a) diagram of flexural moments; (b) chord rotation definition.

Figure 2.10 depicts the demand-to-capacity ratios obtained for building GB at the NC and DL limit states. It was seen that building GB is the only to fail safety verifications at the NC limit state and that the use of the ASCE41-13 approach, mainly because of the

quantification of θ_y, considerably underestimates local responses at the NC limit state. A difference of around 50% between the maximum *DCR* values obtained from MAPA$_{RSA}$N2 and PA$_m$DCM at the NC limit state was found. The results also indicate that the NC limit state seems to be the governing one for all buildings, contrarily to what was observed by Romão et al. (2010), who concluded that the DL limit state typically governs the assessment of existing RC buildings.

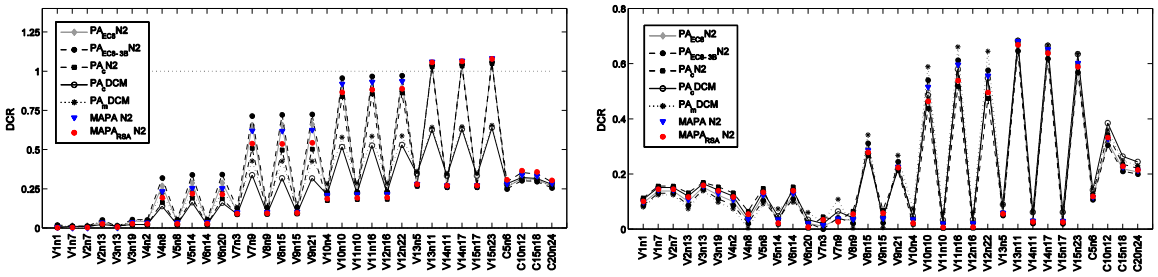

Figure 2.10 – *DCRs* at the control sections of the GB building for the NC (*left*) and DL (*right*) limit states and considering the various nonlinear pushover methods of analysis.

With respect to the inclusion of P-Δ effects in the design of steel moment resisting frame buildings, to the extent of this work, it may be observed that excessively laterally stiffer, and consequently more expensive, buildings would be designed if analysts opt to neglect P-Δ effects. Building SB3 features a lateral capacity that is almost 50% of the seismic demand. On the other hand, if *P*-Δ effects are simply turned on during design, as the majority of commercial programmes now enable, more reasonable solutions would be obtained. Yet, it is interesting to refer that although building SB1 could not be assessed according to EC8-3 using the MRS method of analysis, this method was adopted in the design.

2.5.5 Results from nonlinear dynamic analysis

EC8-3, ASCE 41-13 and NZSEE establish that the maximum value of all structural responses should be taken when groups of three to six records are adopted in nonlinear dynamic analyses and that mean values should be taken when groups with a higher number of records are used. Therefore, two groups of three (G3) and seven (G7) real ground motion records were selected and scaled according to the methods proposed by EC8-3, ASCE 41-13 and NZSEE. More information about the selection and scaling of these groups is provided in Chapter 3. Table 2.8 lists the global responses obtained for each case. In brief, it may be seen that the use of groups with only three records tends to considerably overestimate global response demands, with deviations from the responses obtained using

groups of seven records that reached more than two times. Still, these deviations reduced with the reduction of seismic intensity, i.e. for the SD and DL limit states, and with the increase in the lateral stiffness and strength of the buildings. Also, it may be seen that EC8-3 systematically leads to lower global deformation demands when compared ASCE 41-13. In turn, the results obtained using NZSEE seem to be always nearer to those of EC8-3.

Table 2.8 – Global drift ratios obtained for each nonlinear dynamic method of analysis (%).

Building	GB			SB1			SB2			SB3		
	DL	SD	NC	DL	SD	NC	DL	SD	NC	DL	SD	NC
EC8-3 G3	0.93	1.24	4.67	0.81	1.18	4.19	0.72	1.08	3.69	0.62	0.86	1.78
EC8-3 G7	0.53	0.77	2.37	0.56	0.80	1.97	0.49	0.69	1.68	0.37	0.56	1.68
ASCE41-13 G3	0.90	1.63	5.17	0.93	1.32	6.46	0.96	1.38	3.81	0.46	0.78	3.14
ASCE41-13 G7	0.54	0.81	2.54	0.62	0.90	1.99	0.52	0.84	1.83	0.42	0.62	1.84
NZSEE G3	0.80	1.23	4.51	0.67	1.02	5.54	0.67	0.95	2.69	0.47	0.67	1.80
NZSEE G7	0.59	0.88	1.94	0.56	0.86	2.19	0.54	0.82	1.74	0.35	0.54	1.50

Nevertheless, EC8-3, ASCE 41-13 and NZSEE do not provide an idea of the level of consistency associated with the nonlinear dynamic analysis results obtained from a certain group of ground motions selected. Hence, a pertinent question could be placed: Would it be expected to obtain similar nonlinear dynamic analysis results if different groups of ground motion records were selected?

With respect to local demands, Figure 2.11 shows the *DCR* values obtained for building GB at the NC and DL limit states using nonlinear dynamic analysis. Rolling out from the outset the results of the groups with three ground motions, which provided too conservative results, one may conclude that all buildings verify safety. Also, comparing these results with those previously obtained from pushover analysis, it may be concluded that pushover analysis systematically overestimate both local and global deformation demands, particularly at the NC limit state.

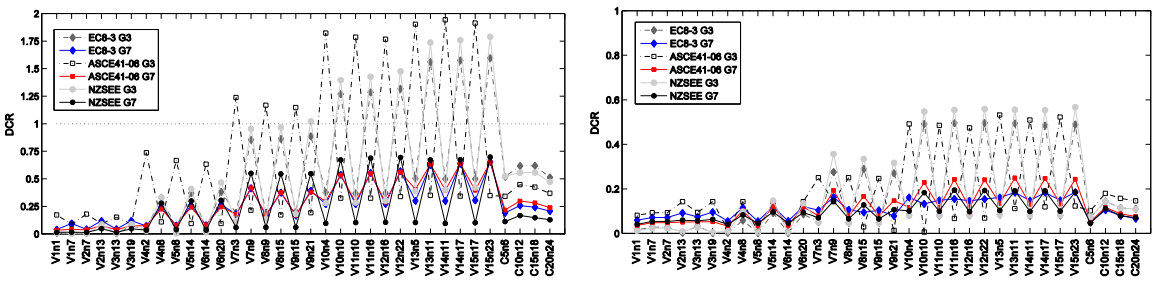

Figure 2.11 – *DCRs* at the control sections of the GB building for the NC (*left*) and DL (*right*) limit states and considering the various nonlinear dynamic methods of analysis.

2.6 Expected probabilities of collapse at different seismic levels

As above mentioned, EC8-3 establishes performance requirements that aim at being more adequate to existing structures and relaxed in comparison to those of EC8-1. Both documents define somewhat similar qualitative near- or no-collapse requirements, although not being totally evident the baseline level of damage, nor the acceptable probabilities of collapse, associated to steel buildings designed and assessed to those limit states. More clarifying information may be found in the background document of EC8-1 (Fardis et al., 2005), which refers that the no-(local-)collapse requirement is implicitly associated to a performance level that provides a safety factor between 1.5 and 2 against substantial loss of lateral load resistance. Conversely, EC8-3 specifically refers that at the near collapse limit state, local buckling is expect to have occurred at beams, indicating that loss of lateral load resistance would have already initiated. Hence, since Eurocode 8 conceptually establishes different performance levels by affecting importance factors (Bommer and Pinho, 2006), i.e. the level of seismic action, rather than allowable drifts or displacement values, one may interpret that the EC8-1 no-(local-)collapse requirement is implicitly designing new buildings that are expected to collapse (i.e. loss of substantial lateral load resistance) at a seismic action 2 times greater than that adopted in design with 1.3% probability of exceedance in 50 years (return period equal to 3800 years defined considering an importance factor γ_1 equal to 2.0 and an exponent k equal to 3.0), whereas EC8-3 considers a 2% probability of exceedance in 50 years that corresponds to an importance factor γ_1 equal to 1.73. Consistency does seem to exist between EC8-1 and EC8-3, as the latter is assessing existing buildings to attain collapse at a seismic action 0.87 times lower than that of new buildings. However, this observation does not hold true for the particular case of this study. According to the current Portuguese National Annex, the EC8-3 near collapse seismic action is associated to an importance factor γ_1 equal to 3.0 (exponent k equal to 1.5 for the Type I seismic action) that is implicitly, and more conservatively, assessing existing buildings to attain collapse at a seismic action 1.5 times greater than that of new buildings. It should be recalled, however, that the present case study was conducted using the EC8-3 version currently in force in Portugal, although a draft version of the Portuguese National Annex is being elaborated, which defines a seismic action at the EC8-3 near collapse limit state similar to that of EC8-1 at the non-collapse performance level (Castro, 2013). Nevertheless, another question may be raised:

Does it seem reasonable to assess existing buildings to attain collapse at a seismic action 0.5 times lower than that of new buildings?

To briefly contribute to a discussion in this topic, and due to the particular features of the buildings analysed in this study, the probabilities of collapse at different seismic levels, PC|*gm* (Silva et al., 2015), were estimated for buildings GB and SB3, as presented in Figure 2.12. Recall that building GB fails its seismic design according to EC8-1, but verifies safety to EC8-3 considering an importance factor γ_1 equal to 3.0, whereas building SB3 was previously designed to EC8-1 using a simplified procedure that excludes *P*-Δ effects. It should be referred that the fragility curves presented in Figure 2.12 were derived by adopting a group of 20 ground motions selected and scaled to match a more rigorous target spectrum obtained for the city of Lisbon, as discussed in Marques et al. (2014a; 2014b), using the Conditional Mean Spectrum (CMS) method proposed by Baker (2011). For consistency, the local deformation capacities were defined according to EC8-3. Hence, it may be observed that at the EC8-1 design seismic level, building GB is associated to a PC|*gm* of 1.01×10^{-3} and that collapse occurs, say PC|*gm* equal to 0.5, at a seismic action 4 times greater than that adopted in design. Based on these findings, three conclusions may be readily drawn: (i) EC8-1 seems to be designing steel buildings that are capable of resisting seismic loads, at least, 2 times higher than those initially intended; (ii) EC8-3 is assessing existing steel buildings to attain collapse at a seismic action that is, in fact, at least 0.43 times lower than that of new steel buildings; (iii) and, finally, the future version of the Portuguese National Annex is going to assess existing steel buildings to attain collapse at a seismic action that is, in fact, at least 0.25 times lower than that of new steel buildings. For what concerns Building SB3, an interesting PC|*gm* of zero was obtained, being thus clear that the simplified procedure proposed by EC8-1 to design new buildings excluding *P*-Δ effects is, in fact, significantly overdesigning steel moment-resisting frame structures. Likewise, it seems that the lateral stiffness imposed to building GB by controlling α_{cr} in gravity design (CEN, 2005b; Peres, 2010) provides sufficient lateral resistance to comply with the EC8-1 performance requirements.

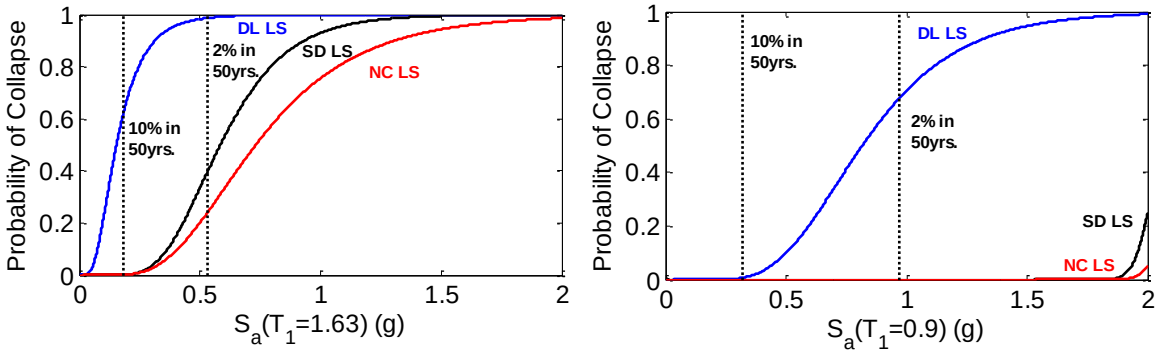

Figure 2.12 – Fragility curves of buildings GB (*left*) and SB3 (*right*) at the various limit.

Despite the conclusions drawn above, looking at PC|*gm* does not provide a tangible measure of the socio-economic impacts associated to the probability of collapse of buildings (Diamantidis and Bazzurro, 2007). Hence, the annual probability of failure, p_f, was additionally quantified. According to the Joint Committee for Structural Safety (JCSS, 2001), the annual probability of failure at the ultimate limit state of new buildings should be $\approx 10^{-5}$ (β=4.2) and of existing buildings $\approx 0.5\text{x}10^{-3}$ (β=3.3). Building GB was found to be associated to a p_f value of $0.13\text{x}10^{-4}$ (β=4.19), which is right on the value suggested by JCSS (2001) for new buildings. Although this p_f value seems to somehow support the previous findings that the gravity building would satisfy the performance requirements of a new seismically design building, the fact that building GB is right on the socio-economic limit state proposed by JCSS (2001) may question the conclusions above made, which rely on considering that collapse occurs for a PC|*gm* equal to 0.5. Hence, since building GB is on the threshold of what is acceptable from a socio-economic point of view, and by looking at the building's fragility curve, it seems that EC8-1 is assuming a probability of collapse PC|*gm* at a seismic action expected to cause substantial loss of lateral load resistance (2.0 times that adopted in design) lower than 0.06, without accounting for material and geometrical uncertainties and assuming the EC8-3 deformation capacity limits.

2.7 Conclusions

In this chapter a critical review of various guidelines and codes for the seismic safety assessment of existing steel buildings was presented. Particular attention was paid to the comparison between the Part 3 of Eurocode 8 (EC8-3) and the American ASCE 41-13, which aimed at pointing out the different conceptual approaches followed by both documents and, most importantly, at highlighting the existing deficiencies in the current

version of EC8-3. Indeed, it was demonstrated that the procedure prescribed by EC8-3 for the seismic safety assessment of existing steel buildings deeply lacks on consistency and urges for further revision and research. For what concerns linear elastic methods of analysis, a major basilar deficiency was found to exist in the safety verifications stage. Since safety verifications shall be carried out in terms of deformations regardless the type of analysis adopted, the analyst will be confronted with a rather ambiguous scenario: How could safety verifications be performed if plastic rotation demands cannot be obtained from linear elastic methods of analysis? This conceptual deficiency could be, eventually, solved by conducting the safety verifications in terms of forces similarly to what is proposed by ASCE 41-13. The linear analysis applicability criterion preconized by EC8-3 was also found to lead to ambiguous situations, allowing the use of simplified methods of analysis and rejecting the use of supposedly more accurate linear dynamic methods of analysis for the same building. With respect to nonlinear methods of analysis, static procedures were found to systematically lead to conservative estimates of structural demands, which will influence its use in future practice, whereas further studies seem to be deemed necessary to assess the level of robustness associated with the results obtained from nonlinear dynamic analysis. To conclude, it became clear in this work that further studies focusing on the revision of the seismic safety assessment procedures prescribed by EC8-3 should be taken as a priority, as well as the promotion of future workshops and training programs aimed at demystifying and acquainting practitioners with this particular part of the Eurocode.

2.8 Acknowledgments

This work was performed within the framework of the research project ‘Development and calibration of seismic safety assessment methodologies for existing buildings according to the Eurocode 8 – Part 3’ founded by Foundation of Science and Technology (FCT) of Portugal.

2.9 References

Antoniou S, Pinho R (2004) Advantages and limitations of adaptive and non-adaptive force-based pushover procedures, Journal of Earthquake Engineering, 8, 497–522.

ASCE (2014) Seismic evaluation and retrofit of existing buildings (ASCE/SEI 41-13), American Society of Civil Engineers, Reston, Virginia, USA.

Baker JW (2011) Conditional Mean Spectrum: Tool for ground motion selection, Journal of Structural Engineering, 137, 322-311.

Bertero RD, Bertero VV (2000) Application of a comprehensive approach for the performance-based earthquake-resistant design of buildings, Proceedings of the 12th World Conference on Earthquake Engineering, Auckland, New Zealand.

Bertero RD, Bertero VV (2002) Performance-based seismic engineering: the need for a reliable conceptual comprehensive approach, Earthquake Engineering and Structural Dynamics 31, 627–652.

Bommer JJ, Pinho R (2006) Adapting earthquake actions in Eurocode 8 for performance-based seismic design, Earthquake Engineering and Structural dynamics 35, 39–55.

Boroujeni ARk, Sadeghazar M (2006) Evaluation of the Iranian guideline for seismic rehabilitation of existing buildings, Earthquake Engineering and Engineering Vibration 5, 297-307.

BRI (2001) Standard for seismic evaluation of existing reinforced concrete buildings, Building Research Institute, Japan Building Disaster Prevention Association, Tokyo, Japan.

Castro JM (2013) Novos desafios associados à implementação da regulamentação Europeia para avaliação da segurança sísmica de estruturas de edifícios, Construção Magazine, 57, 52-53.

CEN (2002) ENV 1990 Eurocode: Basis of structural design, European Committee for Standardization, Brussels, Belgium.

CEN (2004a) ENV 1998-1 Eurocode 8: Design of structures for earthquake resistance - Part 1: General rules, seismic actions and rules for buildings, European Committee for Standardization, Brussels, Belgium.

CEN (2004b) ENV 1992-1-1 Eurocode 2: Design of concrete structures, General rules and rules for buildings, European Committee for Standardization, Brussels, Belgium.

CEN (2005a) ENV 1998-3 Eurocode 8: Design of structures for earthquake resistance - Part 3: Assessment and retrofitting of buildings, European Committee for Standardization, Brussels, Belgium.

CEN (2005b) ENV 1993-1 Eurocode 3: Design of steel structures - Part 1-1: General rules and rules for buildings, European Committee for Standardization, Brussels, Belgium.

Charney FA (2008) Unintended consequences of modeling damping in structures, Journal of Structural Engineering 134, 581-592.

Chopra AK, Goel RK (2002) A modal pushover analysis procedure for estimating seismic demands for buildings, Earthquake Engineering and Structural Dynamics 31, 561-582.

Chrysostomou CZ (2005) A pilot application of Eurocode 8 for the seismic assessment and retrofitting of a real building, Proceeding of the 250th Anniversary of the 1755 Lisbon Earthquake, Lisbon, Portugal.

Diamantidis D, Bazzurro P (2007) Safety acceptance criteria for existing structures, Workshop on Risk Acceptance and Risk Communication, Stanford University, C.A.

Fajfar P (1999) Capacity spectrum method based on inelastic demand spectra Earthquake, Engineering and Structural Dynamics 28, 979-993.

Fardis MN, Carvalho E, Elnashai A, Faccioli E, Pinto P, Plumier A (2005) Designers' guide to EN 1998-1 and EN 1998-5. Eurocode 8: Design of structures for earthquake resistance. General rules, seismic actions, design rules for buildings, foundations and retaining structures, Gulvanessian H (eds.), Thomas Telford, UK.

FEMA (2000) FEMA 356 Pre-standard and commentary for the seismic rehabilitation of buildings, Federal Emergency Management Agency, Washington DC, Maryland, USA.

FEMA (2005) FEMA 440 Improvement of nonlinear static seismic analysis procedures, Federal Emergency Management Agency, Washington DC, Maryland, USA.

Franchin P, Pinto PE, and Rajeev, P (2009) Confidence in the confidence factor, Proceeding of the Eurocode 8 - Perspectives from the Italian Standpoint Workshop, Napoli, Italy.

Franchin P, Pinto PE, Rajeev P (2010) Confidence Factor?, Journal of Earthquake Engineering 14, 989-1007.

Gioncu V (2000) Framed structures Ductility and seismic response General Report, Journal of Constructional Steel Research, 55, 125–154.

Gioncu V, Mazzolani F (2002) Ductility of seismic resistant steel structures, Spon Press, Taylor & Francis Group, London, Great Britain.

Grecea D, Dinu F, Dubina D (2004) Performance criteria for MR steel frames in seismic zones, Journal of Constructional Steel Research, 60, 739–749.

Holmes WT (1996) Seismic evaluation of existing building State of the practice, Proceedings of the 11th World Conference on Earthquake Engineering, Acapulco, Mexico.

IITK-GSDMA (2005) Guidelines for seismic evaluation and strengthening of buildings Provisions with commentary and explanatory examples, Indian Institute of Technology Kanpur, Kanpur, India.

JCSS (2001) Probabilistic Model Code. Part 1 – Basis of design, Joint Committee on Structural Safety, ISBN 978-3-909386-79-6.

Kalkan E, Kunnath S (2007) Assessment of current nonlinear static procedures for seismic evaluation of buildings, Engineering Structures, 29, 305–316.

Kalkan E, Kunnath SK (2006) Adaptive modal combination procedure for nonlinear static analysis of building structures, Journal of Structural Engineering, 132, 1721-1731.

Kamaris GS, Hatzigeorgiou GD, Beskos DE (2015) Direct damage controlled seismic design of plane steel degrading frames, Bulletin of Earthquake Engineering, 13, 587-612.

Karavasilis TL, Bazeos N, Beskos DE (2006) Maximum displacement profiles for the performance based seismic design of plane steel moment resisting frames, Engineering Structures, 28, 9–22.

Krawinkler H, Seneviratna K (1998) Pros and cons of a pushover analysis of seismic performance evaluation, Engineering Structure, 20, 452-464.

Kunnath S (2004) Identification of modal combinations for nonlinear static analysis of building structures, Computer-Aided Civil and Infrastructure Engineering, 19, 246–259.

Lupoi G (2003) Limitations and performances of different approaches for seismic assessment of existing buildings, European School of Advanced Studies in Reduction of Seismic Risk, Istituto Universitario di Studi Superiori di Pavia, Pavia, Italy.

Lupoi G, Calvi GM, Lupoi A, Pinto PE (2004) Comparison of different approaches for seismic assessment of existing buildings, Journal of Earthquake Engineering, 8, 121-160.

Mahalov B (2006) Analysis of code procedures for seismic assessment of existing buildings: Italian Seismic Code, EC8, ATC-40, FEMA356, FEMA440, European School of Advanced Studies in Reduction of Seismic Risk, Istituto Universitario di Studi Superiori di Pavia, Pavia, Italy.

Marques M, Araújo M, Macedo L, Martins L, Castro JM, Sousa L, Silva V, Delgado (2014b) Ground motion selection and modification methods for seismic risk assessments, Proceedings of the 2nd European Conference on Earthquake Engineering, Istanbul, Turkey.

Marques M, Macedo L, Araújo M, Martins L, Castro JM, Sousa L, Silva V, Delgado R (2014a) Influence of record selection procedures on seismic loss estimation, Vulnerability, Uncertainty and Risk, 1756-1766.

Masi A, Vona M, Manfredi V (2008) A parametric study on RC existing buildings to compare different analysis methods considered in the European seismic code (EC8-3), Proceedings of the 14th World Conference on Earthquake Engineering, Beijing, China.

Mazzolani F, Montuori R, Piluso V (2000) Performance based design of seismic-resistant MR frames, Proceedings of the 3rd International Conference STESSA 2000: Behaviour of Steel Structures in Seismic Areas, Montreal, Canada.

Mola E, Negro P (2009) A critical review of current assessment procedures, *In* Seismic Risk Assessment and Retrofitting: With Special Emphasis on Existing Low Rise Structures, Eds. Ilki, Karadogan, Pala and Yuksel, Vol 10 Springer, Netherlands.

Mpampatsikos V, Nascimbene R, Petrini L (2008a) A critical review of the RC frame existing building assessment procedure according to Eurocode 8 and Italian Seismic Code, Journal of Earthquake Engineering, 12, 52-82.

Mpampatsikos V, Nascimbene R, Petrini L (2008b) Some considerations about the Eurocode 8 RC frame building assessment procedure, Proceedings of the 14th World Conference on Earthquake Engineering, Beijing, China.

NRC-CNRC (1993) Guidelines for seismic evaluation of existing buildings, Institute for Research in Construction, National Research Council Canada, Canada.

NZSEE (2006) Assessment and improvement of the structural performance of buildings in earthquake, Recommendations of a NZSEE Study Group on Earthquake Risk Buildings, New Zealand Society for Earthquake Engineering, New Zealand.

Öztürk İ (2006) A comparative assessment of an existing reinforced concrete building by using different seismic rehabilitation codes and procedures, Middle East Technical University, Ankara, Turkey.

Park H-G, Eom T, Lee H (2007) Factored modal combination for evaluation of earthquake load profile, Journal of Structural Engineering, 133, 956-968.

Parker W, Thompson J, Cordova PP, Tam KT, Meyer JD (2012) Performance Based Design, would it have made a difference in Christchurch? Proceedings of the NZSEE Annual Conference, Christchurch, New Zealand.

PEER (2011) OpenSees: Open system for earthquake engineering simulation, Pacific Earthquake Engineering Research Center, University of California, Berkeley, CA.

Peres R (2010) Comparison of European and American approaches for consideration of P-Δ effects in seismic design, European School of Advanced Studies in Reduction of Seismic Risk, Istituto Universitario di Studi Superiori di Pavia, Pavia, Italy.

Petrini L, Maggi C, Priestley MJN, Calvi GM (2008) Experimental verification of viscous damping modeling for inelastic time history analyses, Journal of Earthquake Engineering, 12, 125-145.

Pinho R, Marques M, Monteiro R, Casarotti C, Delgado R (2013) Evaluation of nonlinear static procedures in the assessment of frame buildings, Earthquake Spectra, 29, 1459-1476.

Pinto PE, Franchin P (2008) Assessing existing buildings with Eurocode 8 Part 3: a discussion with some proposals, Proceedings of the Background documents for the Eurocodes: Background and applications workshop, Brussels, Belgium.

Priestley MJN, Grant DN (2005) Viscous damping in seismic design and analysis, Journal of Earthquake Engineering, 9, 229-255.

REBAP (1984) Regulamento de Estruturas de Betão Armado e Pré-Esforçado, Decreto-Lei nº 349-C/83, Imprensa Nacional - Casa da Moeda, Lisbon.

Reinhorn AM (1997) Inelastic analysis techniques in seismic evaluations, Proceedings of the International Workshop on Seismic Design Methodologies for the Next Generation of Codes, Bled, Slovenia.

Romão X, Delgado R, Guedes J, Costa A (2010) A comparative application of different EC8-3 procedures for the seismic safety assessment of existing structures, Bulletin of Earthquake Engineering, 8, 91–118.

Romão X, Gonçalves R, Costa A, Delgado R (2012b) Evaluation of the EC8-3 confidence factors for the characterization of concrete strength in existing structures, Materials and Structures, 45, 1737–1758.

Romão X, Guedes J, Costa A, Delgado R (2008) Adequacy of the EC8-Part 3 proposed confidence factors for the assessment of existing RC structures, Proceeding of the 14th World Conference on Earthquake Engineering, Beijing, China.

RSA (1983) Regulamento de Segurança e Acções, Decreto-Lei nº 235/83, Imprensa Nacional - Casa da Moeda, Lisboa.

Scott M, Fenves G, McKenna F, Filippou F (2008) Software patterns for nonlinear beam-column models, Journal of Structural Engineering, 234, 562-571.

SEAOC (1995) Vision 2000: Performance Based Seismic Engineering of Buildings Structural Engineers Association of California, Sacramento, USA.

Sextos A, Katsanos G, Manolis G (2011) EC8-based earthquake record selection procedure evaluation: validation study based on observed damage of an irregular R/C building, Soil Dynamics and Earthquake Engineering, 31, 583-597.

Silva V, Crowley H, Bazzurro P (2015) Exploring risk-targeted hazard maps for Europe, Earthquake Spectra, in press.

Spacone E, Ciampi V, Filippou F (1992) A beam element for seismic damage analysis, Report No UCB/EERC-92/07, Earthquake Engineering Research Centre, University of California, Berkeley, CA.

Sullivan TJ, Priestley MJN, Calvi GM (2012) A model code for the displacement-based seismic design of structures, IUSS Press, Pavia, Italy.

TSDC (2007) Turkish Seismic Design Code Official Gazette, Turkey (in Turkish).

Chapter 3

Code-based record selection methods for seismic performance assessment of buildings

Araújo M, Macedo L, Marques M, Castro JM (2016) Code-based record selection methods for seismic performance assessment of buildings, *Earthquake Engineering and Structural Dynamics*, 45(1):129-148.

3.1 Summary

The recent concerns regarding the seismic safety of the existing building stock have highlighted the need for an improvement of current seismic assessment procedures. Alongside with the development of more advanced commercial software tools and computational capacities, nonlinear dynamic analysis is progressively becoming a common and preferable procedure in the seismic assessment of buildings. Besides the complexity associated with the formulation of the mathematical model, major issues arise related with the definition of the seismic action, which can lead to different levels of uncertainty in terms of local and global building response. Aiming to address this issue, a comparative study of different code-based record selection methods proposed by Eurocode 8, ASCE41-13 and NZS1170.5:2004 is presented herein. The various methods are employed in the seismic assessment of four steel buildings, designed according to different criteria, and the obtained results are compared and discussed. Special attention is devoted to the influence of the number of real ground motion records selected on the estimation of the mean seismic response and, importantly, to the efficiency that is achieved when an additional selection criteria, based on the control of the spectral mismatch of each individual record with respect to the reference response spectrum, is adopted. The sufficiency of the methods with respect to the pairs of *M-R* of the selected group of records and the robustness of the scaling procedure are also examined. The work closes with a study which demonstrates the

suitability of a simplified probability-based approach recently proposed for estimating mean seismic demands.

3.2 Introduction

Nonlinear dynamic analysis is recognized as the most reliable tool to assess the seismic performance of structures, particularly in the case of irregular ones. The constant increase in computational power and the wide number of advanced structural analysis software tools available have set this type of analysis as the preferable procedure for code-based seismic assessment of structures as well as probabilistic seismic risk assessment. However, besides the complexity associated with the formulation of the mathematical model, major issues arise related with the definition of the input ground-motion records.

A number of scientific studies focusing on the influence of ground motion records on the structural response of buildings have been performed in the past (Kappos and Kyriakakis, 2000; Bommer and Acevedo, 2004; Iervolino and Manfredi, 2008; Iervolino et al., 2008; Katsanos et al., 2010). Among the various findings, the structural response estimates were seen to be highly dependent on the type of ground motions, i.e., artificial, real or simulated, as well as on the methods utilized for selection and scaling of the records (Cimellaro et al., 2011; Grant and Diaferia, 2013; Cantagallo et al., 2014). Current codes implicitly recognize the variability of the seismic response of buildings introduced by input ground-motions by setting a minimum number of records, which varies from code to code, to be selected and scaled with the aim of providing realistic estimates of mean seismic demands (Baker and Cornell, 2006; Bradley, 2011; Ay and Akkar, 2012). This uncertainty is usually biased when using code-based record selection methods which is due to the fact that the uncertainty in the ground motion intensity is not properly addressed when selection and scaling is performed to reduce the mismatch in relation to a target spectrum, and thus cannot be used to capture the dispersion in the structural responses (Haung et al., 2011; Haselton et al., 2012). Moreover, most codes recommend a selection of records based on the expected seismological characteristics of the events that are most likely to strike the structure. This pre-selection is expected to provide unbiased mean seismic demand estimates, although previous studies have shown no consensual results (Shome et al., 1998; Krawinkler et al., 2003; Iervolino and Cornell, 2005; Luco and Bazzurro, 2007). An additional source of bias induced in mean structural responses is related to the amplitude of the scale factors and the manner in which it changes the ground motion intensity measures

of the selected ground motion time series related to those which would be expected for the considered scenario (Bradley, 2013). Values varying from one to 10, or more, are considered acceptable within the scientific community, still no definitive conclusions were found (Iervolino and Cornell, 2005; Watson-Lamprey and Abrahamson, 2006).

This lack of consensus on how to appropriately select and scale the ground motions for code-based design and assessment of buildings is reflected on the different approaches proposed by current codes (CEN, 2004; NZS, 2004; ASCE, 2014; NZS, 2004). Past studies have already highlighted the need for further improvements in existing code-based record selection methods (Beyer and Bommer, 2007; Sextos et al., 2011) and identified several important deficiencies. An issue of particular importance is related to the fact that current codes address variability in seismic responses in a deterministic manner, not being clear what is the likelihood of the maximum of three seismic responses, or the mean of seven or more seismic responses, being smaller than the "true" mean seismic response (Bradley, 2011). Moreover, codes do not provide explicit guidance on how the mean seismic response is affected by the number of records of the suite and also by the mismatch between the spectra of the individual records and the target response spectrum. Additionally, no account is made for the fact that some engineering demand parameters are significantly more sensitive to the input ground motion than others (Krawinkler et al., 2003). Motivated by such deficiencies, Bradley (2011) proposed a probability-based approach for estimating deterministic design seismic demands with constant and known likelihood, equal to 16%, of being below the "true" mean value, regardless of the number of records and the variability associated with the input ground-motions.

The purpose of this chapter is to investigate the influence of the code-based record selection methods proposed by Part 1 of Eurocode 8 (EC8-1) (CEN, 2004), the American Standard ASCE41-13 (ASCE, 2014) and the New Zealand Standard NZS 1170.5:2004 (NZS, 2004) on demand-based assessments of buildings, while addressing the various issues discussed above and evaluating their efficiency to provide consistent and unbiased estimates of seismic response. The accuracy and efficiency of the methods are evaluated through a detailed analysis of the variability between the "true" mean responses and the responses computed with each group of records. The "true" mean response is herein defined to be obtained from a large record set (105 records) selected and scaled to match the code target spectrum, which is considered to be a reasonable assumption within the context of code demand-based assessments. However, it should be recognized that the use of code target spectra is expected to result in conservative demand estimates, particularly

in multi-degree of freedom and/or nonlinear systems, in comparison to more rigorous target scenario spectra (e.g. Conditional or Conditional Mean Spectra) (Haselton et al., 2012). Additionally, the consistency of the methods is evaluated based on the analysis of the accuracy and efficiency of the group-to-group variability (Reyes and Kalkan, 2012). The number of ground motion records and the influence of the scale factors and pairs of *M*-*R* on the seismic demand estimates are also examined. This comparative study between different code-based record selection methods aims at providing further insights on the adequacy and robustness of each method and on highlighting the advantages and the limitations between them. Moreover, since it has been found that both the required number of records and bias systematically decrease when records with a spectral shape similar to the target spectrum are adopted and additional constraints on the selection and scaling of the records are considered (Luco and Bazzurro, 2007; Hancock et al., 2008), the advantage of including a simple and expeditious additional criterion in the selection of each individual record by limiting the spectral mismatch relative to the target spectrum to ±50% is investigated. Finally, the simplified probability-based method proposed by Bradley (2011) for determining design seismic demands is applied to the case study buildings so as to demonstrate its accuracy and applicability and to enforce its implementation in future generations of design and assessment codes, as it clearly provides an important breakthrough in terms of the estimation of robust mean design seismic demands regardless of the record selection and scaling method adopted.

3.3 Brief review of code-based record selection methods

In general, all codes (CEN, 2004; NZS, 2004; ASCE, 2014; NZS, 2004) recommend the use of groups with at least three ground motion records for nonlinear dynamic analysis. The records may be obtained either from real earthquake events or artificially simulated, although preference is given to the former. As referred above, most of the code-based record selection methods suggest that a careful preliminary selection from a bin of random real events should be carried out considering the expected magnitude, source-to-site distance, rupture mechanism and soil profile that are consistent with the seismic hazard scenario associated with the structure under analysis. If ground motion records having these characteristics are not available, simulated data sets with equivalent duration and spectral content should be used to make up the total number required (CEN, 2004; NZS, 2004; ASCE, 2014; NZS, 2004). Code prescriptions typically require control of the

average spectral ordinates of the chosen record set in relation with the target spectrum. The set has to consist of at least seven records so that the mean response of a given parameter can be considered. Otherwise, if the set comprises three to six records, the maximum response obtained among all the records within the set should be considered (CEN, 2004; NZS, 2004; ASCE, 2014; NZS, 2004). Alternatively, ASCE41-13 requires a higher number of ground motion records to compute mean structural responses, which is typically equal or greater than 10 and depends on the type of seismic action and performance objective. The ground motion record selection and scaling methods proposed in the European, American and New Zealand standards are presented next.

3.3.1 Eurocode 8

Part 1 of Eurocode 8 (EC8-1) establishes the following criteria for the selection and scaling of ground motion records in the context of demand-based assessments of buildings: (i) the mean of the zero period spectral response acceleration values calculated from the individual time histories should not be smaller than the value of $a_g\ S$ for the site under study, being a_g the design ground acceleration on rock and S the soil parameter; (ii) and, in the range of periods between $0.2T_1$ and $2.0T_1$, where T_1 is the fundamental period of the structure in the direction where the record will be applied, no value of the mean 5% damping elastic spectrum, calculated from all time histories, should be less than 90% of the corresponding value of the 5% damping elastic response spectrum.

3.3.2 American Standard

ASCE41-13 establishes that, when bidirectional planar analysis is to be performed, the square root of the sum of the squares (SRSS) of the two principal horizontal components of the records shall be scaled such that the average value of the set of 5% damping constructed spectra does not fall below the corresponding ordinate of the target response spectrum for periods between $0.2T_1$ and $1.5T_1$. This record scaling approach is in line with ASCE 7-10 (ASCE, 2010), which defines the target spectrum as 1.0 times the design spectrum, recognizing that the design spectrum is based on the maximum response of the horizontal plane, rather than on the average horizontal response, as assumed in the former version of ASCE41 (NEHRP, 2011). The intent of ASCE 7-10 is that the records should be scaled such that the maximum responses in the horizontal plane of the scaled records are, on average, equal to, but not less, than the design spectrum over the defined period range (NEHRP, 2011).

3.3.3 New Zealand Standard

According to NZS 1170.5:2004 (NZS, 2004), the ground motion records shall be scaled by a record scale factor k_1 and a family scale factor k_2, both applied in the time domain, i.e. the record ordinates shall be multiplied by the product k_1k_2. The record scale factor, k_1, is defined as the scalar value that minimizes, in a least square sense, the function $log(k_1SA_c/SA_t)$, where SA_c refers to the spectrum constructed for each record component and SA_t to the code target spectrum for the given site, over the period range of interest, between $0.4T_1$ and $1.3T_1$. It is recommended in the document that $0.33 < k_1 < 3.0$ and that the record selected should exhibit a reasonable fit to the target spectrum. The latter condition may be met by ensuring that $D_1 < log(1.5)$, where.

$$D_1 = \sqrt{\frac{1}{n}\sum\left(log\left(SA_c\right) - log\left(SA_t\right)\right)^2} \tag{3.1}$$

The family scale factor, k_2, is defined as the maximum value of the ratio $SA_t/max(SA_c)>1.0$ over the period range of interest for the direction under consideration, where $max(SA_c)$ is the maximum component of each record within a family at each period considered. It shall be verified that $1.0 < k_2 <1.3$.

3.4 Description of the case study and record selection

The study presented herein was conducted considering the four 5-storey 3-bay steel buildings presented in Chapter 2. The design seismic action adopted was that proposed in the Portuguese National Annex of Eurocode 8 (CEN, 2010), considering that the structures were located in Lisbon and assuming a soil type B, characterized by a soil factor, S, equal to 1.29 according to the same National Annex. The nonlinear dynamic analyses were conducted using the open source software OpenSees (PEER, 2011). Seismic action Type 1, which represents inter-plates earthquakes, was found to be the governing action during the design stage. Therefore, it served as the basis for the assessment study presented hereafter. It is characterized by PGA values of 0.091g, 0.15g and 0.451g for the Damage Limitation (DL), Significant Damage (SD) and Near Collapse (NC) limit states, respectively, which are associated, according to Part 3 of Eurocode 8 (EC8-3) (CEN, 2005), to return periods, T_r, of 225, 475 and 2475 years. The real ground-motion sets were defined using the SelEQ tool (Macedo et al., 2013), which consists of a software application for record selection developed at the Faculty of Engineering of the University of Porto (FEUP). SelEQ features a wide variety of filtering criteria and incorporates several meta-heuristic algorithms

allowing, in this way, the selection of seismic records or groups of seismic records that are compatible with any type of target response spectrum, either obtained from a design code or derived from a probabilistic seismic hazard assessment, namely the Conditional Mean Spectrum (CMS) proposed by Baker (Baker, 2011) or the Generalized Conditional Intensity Measure (GCIM) approach proposed by Bradley (2010; 2012). On the basis of the seismological characteristics of the events that define the Portuguese Type 1 and Zone 3 seismic action, magnitudes and epicentral distances higher than 5.5 and 20km, respectively, were considered for the preliminary search. Also, an interval of values of the average shear wave velocity, $v_{s,30}$, between 360m/s and 800m/s was adopted, in agreement with soil type B defined in EC8-1. Regarding the scale factors adopted, it is worth noting that the records were scaled to match the elastic spectrum corresponding to the SD limit state, being afterwards linearly scaled to match the elastic spectra associated with the DL and NC limit states. Groups of three and seven records were selected and scaled according to EC8-1, ASCE41-13 and NZS 1170.5:2004 methods. Moreover, and with the aim of finding a simple and efficient way of reducing the record-to-record variability of each set, an additional criterion was considered in the selection, which consisted of imposing spectral mismatch limits relative to the target spectrum of ±50% for each individual record. Also, it may be noted that since the NZS1170.5 already considers criteria for scaling each record individually, no control of the mismatch relative to the target spectrum was adopted in this case. The groups of records considered are summarized in Figure 3.1.

Table 3.1 – Identification of the groups of records considered. *I* identifies the groups with mismatch control.

Selection and Scaling Method	Number of records / Control of mismatch relative to target spectrum			
EC8	3/no (G3)	3/yes (G3I)	7/no (G7)	7/yes (G7I)
ASCE 41-13	3/no (G3)	3/yes (G3I)	7/no (G7)	7/yes (G7I)
NZS1170.5:2004	3 (G3I)		7 (G7I)	

The inspection of Figure 3.1 provides an understanding of the features of the various groups of records that will be key in interpreting the findings and conclusions made throughout this chapter. It may be observed that: (i) the inclusion of additional control of spectral mismatch significantly contributes for reducing the record-to-record variability within the period range of interest, still providing average spectra consistent with the EC8 lower bound limit defined by 90% of the target spectrum (Figure 3.1 (a) and (v)); (ii) ASCE41-13 provides a more conservative average spectrum defined by a lower bound

limit equal to the target spectrum (Figure 3.1 (c)); (iii) the NZS1170.5:2004 method ensures record-to-record variability levels similar to those obtained when the additional control of spectral mismatch is considered and an average spectrum relatively similar to that of EC8, particularly at the fundamental periods of vibration of the case study buildings (Figure 3.1 (d)); (iv) the control of the record-to-record variability contributes to the elimination of outlier sets of records, which may lead to large undesirable, or non-converged, structural responses that can bias the mean seismic demand estimates.

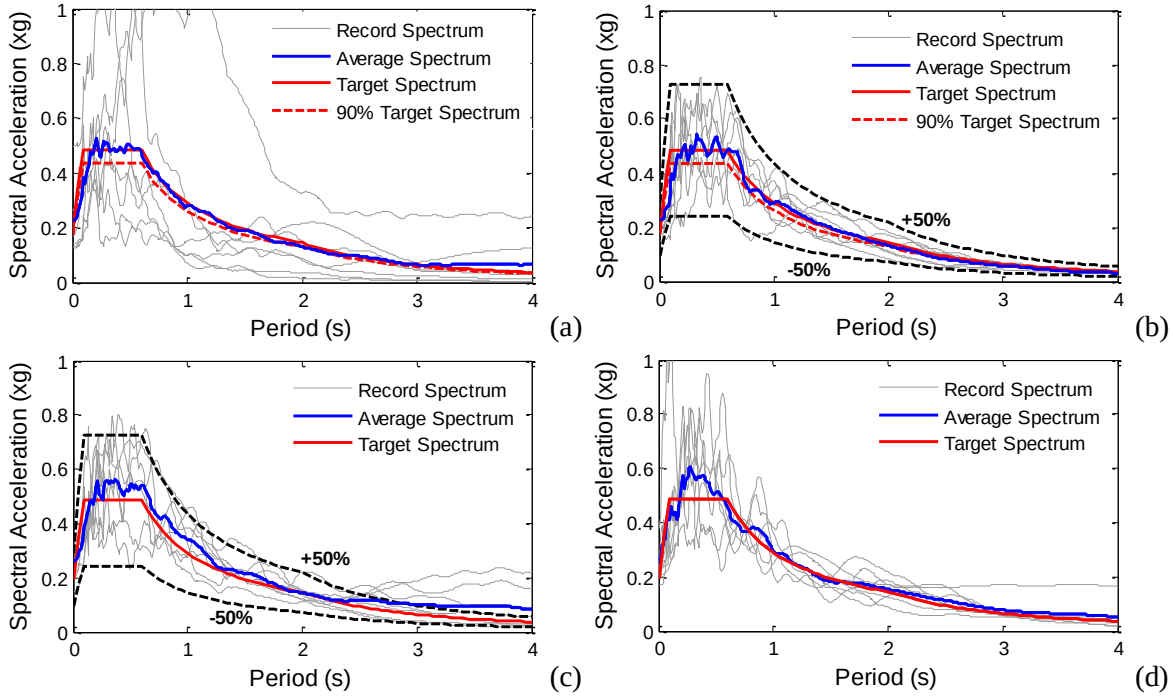

Figure 3.1 – Elastic response spectra of different groups and target spectrum: (a) EC8 G7; (b) EC8 G7I; (c) ASCE41-13 G7I; (d) and NZS 1170.5:2004 G7.

Finally, in order to evaluate the impact of different groups of ground motions selected and scaled according to the same criteria and with the same number of records, the so-called group-to-group variability, each group of records identified in Table I was replicated 15 times.

3.5 Demand-based assessment

The reliability of code-based assessment procedures largely depends on the accuracy of the structural demand estimates. Since most codes prescribe that just one group of ground motion records is required to conduct nonlinear dynamic analysis, it should be ensured that the demands estimated from that single group consist of a realistic representation of the expected seismic demands that are to be imposed to the structure. In other words, it should be expected that a certain building is considered safe, or unsafe,

regardless of the group of ground motions selected. Hence, aiming to evaluate the impact of the various code-based record selection methods on the accuracy of the structural demand estimates, Figure 3.2 displays the mean global drift ratios of building GB (i.e. top displacement of the building divided by its height) and its respective coefficient of variation (CoV) defined over the 15 sets of each group type. Figure 2 presents just a fraction of illustrative results regarding building GB. The full compilation of results for every building may be found in Araújo et al. (2013). It should be referred that, on the basis of the code prescriptions, mG3 and mG3I are vectors of values of the maximum response of each group comprising three records and aG7 and aG7I are vectors of values representing the average response of each group of seven records.

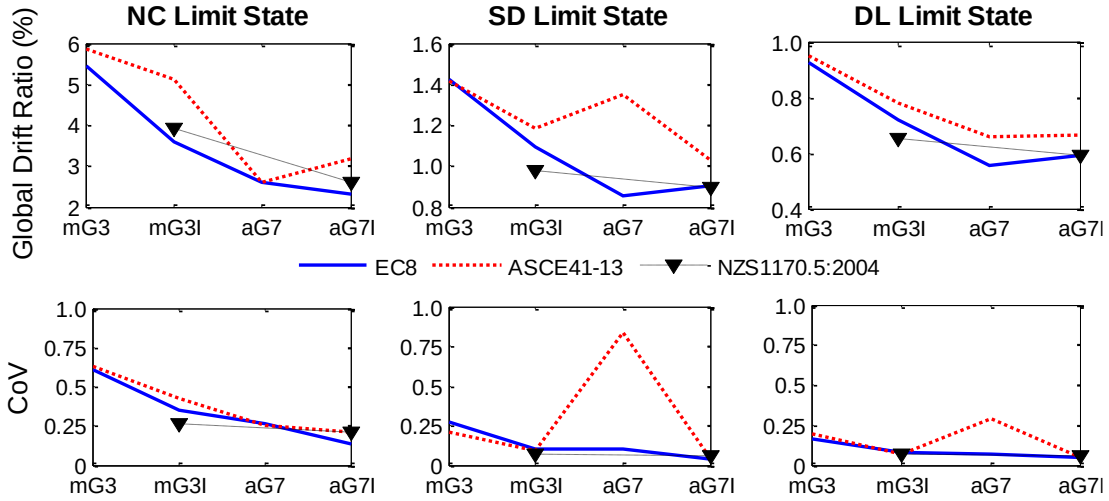

Figure 3.2 – Mean global drift ratios and respective CoV of building GB using the 15 sets of records.

Firstly, it may be observed that the use of groups with three records with no control of individual record mismatch with respect to the target spectral accelerations (mG3) tends to considerably overestimate the global response demands, with a deviation in terms of mean values from the aG7I results that can reach more than two times. Likewise, the level of variability in the response is extremely high, with CoV values of around 0.6 to 0.4. These limitations seem to be slightly overcome by introducing additional selection criteria based on the control of individual record mismatch relative to target spectrum (mG3I), although a deviation in terms of mean values of 50% from the aG7I results is still observed in these cases. As already concluded by Bommer and Acevedo (2004), the use of three to six records should be carried out with caution or even abandoned. However, these conclusions do not fully apply to the NZS 1170.5:2004 scaling method. With the exception of the results obtained for the GB and SB1 buildings at the NC limit state, it is observed

that the mG3I results were quite similar to the aG7I ones, both in terms of mean and CoV values, being the latter generally around 0.1. The selection and scaling procedure proposed by the New Zealand standard appears therefore to be an interesting approach to quantify global deformation demands with a lower number of records and thus with a lower computational effort. On the other hand, and as expected, the increase on the number of records considered in each set (aG7) significantly reduced the mean estimates and the variability of the response, although leading to some unstable results, particularly at the SD limit state of buildings GB and SB1 when using the ASCE41-13 procedure (Figure 3.2). The high CoV values observed in building GB at the SD and DL limit states were mainly due to the influence of a single outlier set of records that resulted in significantly higher levels of structural demands comparing to the other sets. Yet again, the adoption of alternative criteria to control the individual record mismatch relative to target spectrum (aG7I) improved the stability of the mean estimates of global demands, eliminating the existence of outliers and reducing its CoV to values of the order of 0.1. It is thus expected that a positive correlation exists between the record-to-record variability of the set and the variability of the structural demands. At last, and as already evidenced by Oyarzo-Vera and Chouw (2012) for simple single-degree-of-freedom systems, the ASCE scaling method generally appears as the most conservative one, while the New Zealand procedure results in a lower standard deviation of the response. It may be recognized that a narrower band of global drift ratio demands around the mean would be obtained if a higher number of group sets was adopted (Ang and Tang, 2007).

With respect to the local deformation demands, Figure 3.3 depicts the mean demand-to-capacity ratios (*DCRs*), i.e. ratio between the rotation demands obtained from the analysis and the rotation capacities defined by EC8-3 (CEN, 2005) assuming a KL3 knowledge level, and their respective CoV, obtained for buildings GB and the EC8 method. The full compilation of results may be found in Araújo et al. (2013). It is worth noting that in the adopted nomenclature of the structural members, letter *V* refers to beams, *C* to columns and *n* to their left and right nodes. The beam number increases from the top to the first floor. With regard to the columns, due to space limitations the results are presented only for the base of the first storey columns. Similar conclusions to those presented above for global deformation demands may be obtained for the local demands, being once again notorious the conservative nature of the mG3 and mG3I record selection strategies. However, it is observed that the level of variability of the local deformation demands increased significantly comparing to the global response results, to values that go

up to more than 1.0. This increase seems to be mostly associated with the effect of higher modes, which tend to become more relevant at the top floor beams, and in the direction along which the structural mechanism was formed. The fact that the formation of plastic hinges does not necessarily occur at both ends of a given beam, due to gravity load effects, implies that when the structural mechanism is developed, say in the positive direction, the plasticity will mostly concentrate at the right nodes of the beams; conversely, if the structural mechanism is developed in the opposite direction, the plasticity will tend to concentrate at the left nodes of the beams. Nevertheless, it may be seen that the use of groups with higher number of records and with the control of the individual record mismatch with respect to the code spectrum (aG7I) results in acceptable dispersion levels of local demands, which are around 0.25. These observations confirm the importance of considering the additional criterion based on the imposition of individual record mismatch limits of ±50% relative to the target spectrum. As previously discussed, the dispersion levels may be also reduced by adopting a larger number of records in the analysis, although this option will introduce additional computational effort that may not be feasible in current engineering practice.

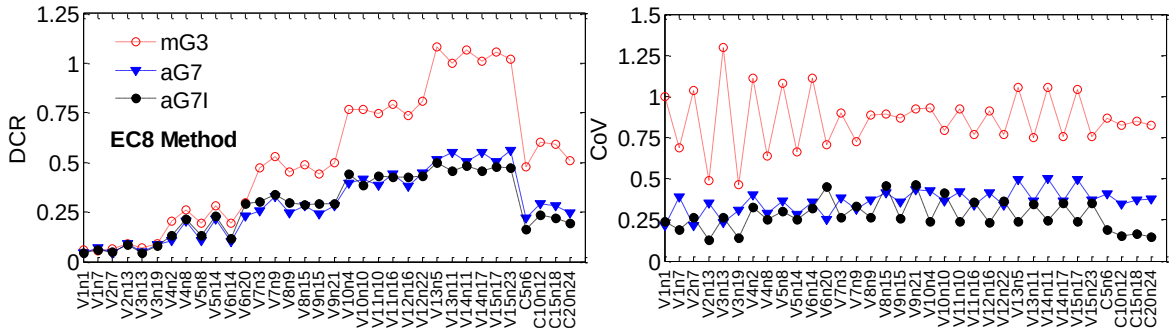

Figure 3.3 – Mean *DCR* and CoV values at the NC limit state of building GB using the 15 sets of records.

Notwithstanding the previous conclusions, Figure 3.4 depicts the percentage of groups of records that result on the exceedance of the DL, SD and NC limit states for building GB, thus allowing for a better understanding of the impact of each code-based record selection method on the demand-based assessment of structures. Ideally, the demand-based assessment process should be capable of providing a unique safety answer, independently of the group of records selected. However, the variability in the mean local deformation demands, which can reach CoV values of 0.5 even when groups of seven records are adopted (Figure 3.4), may significantly affect the demand-based safety verifications and lead to undesirable cases where groups of records selected according to similar criteria provide different safety answers. Such cases may be observed in Figure 4

for building GB, particularly when the maximum response of three records is considered, and eliminated either by increasing the number of records or by including the additional control of the spectral mismatch. Moreover, whereas the ASCE41-13 selection method seems to lead to less consistent demand-based assessments at the NC limit state using the G7I groups of records, the EC8-1 and NZS 1170.5:2004 procedures generally lead to similar results.

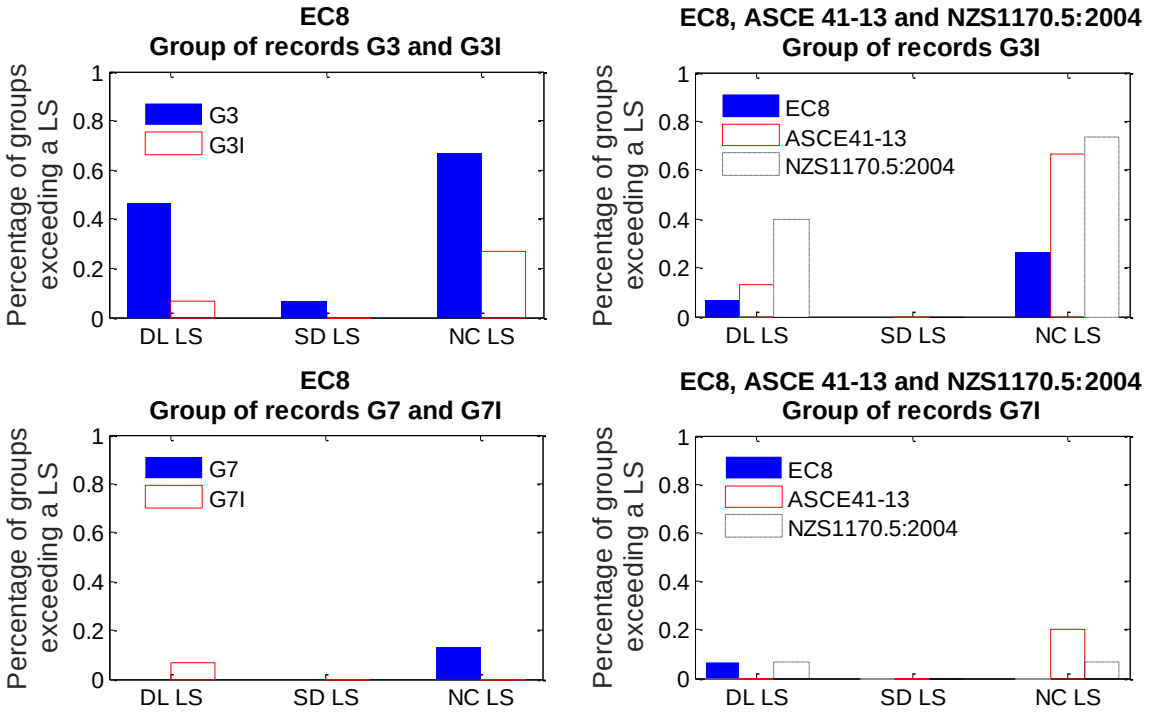

Figure 3.4 – Percentage of groups that exceeded the DL, SD and NC Limit States for building GB and considering the various groups of records.

As far as the safety assessment of the set of analysed buildings is concerned, and assuming the EC8-3 compliance criteria, it was seen that for the EC8-1 G7I group, building GB never exceeds the NC and SD LSs and only in 7% of the cases (1 in 15 sets) the DL LS is attained. In turn, the percentage of groups exceeding the NC LS was seen to increase to 13%, 27% and 67% when groups G7, G3I and G3 were considered, respectively. With the exception of building SB3, which does not exceed any damage state, similar results were observed for the remaining buildings. These findings seem to indicate that more consistent demand-based assessment results are obtained when groups of 7 records with control of spectral mismatch are adopted. Finally, rolling out from the outset the results obtained from groups G3 and G3I, which are seen to be too conservative, one may conclude that all buildings verify safety. Recall that a building is implicitly considered to be unsafe if at least one member fails its safety verifications. Although definitive conclusions can only be extracted based on detailed seismic risk analysis, these results

point out to the conservativeness of designing new buildings to EC8-1 with the control of *P*-Δ effects so that $0.1 < \theta \leq 0.2$ and $\theta < 0.1$ and the less stringent compliance criteria defined by EC8-3. The adoption of such designing criteria appear to have an important economic impact on the final cost of the structure. Comparing the steel weight of buildings SB1, SB2 and SB3 to building GB, an increase of 9%, 32% and 78% is observed, which may be said to be approximately proportional to the increase in the cost of the structures. Similar conclusion have already been drawn by Peres (2010), although further research on the impact of procedures that account for *P*-Δ effects on the seismic design of new steel structures is still needed.

3.6 Insights on the influence of code-based record selection methods on demand-based assessments of buildings

It has been shown that the accuracy of the structural demand estimates is of crucial importance in ensuring reliable application of demand-based safety assessment procedures. Several possible sources of bias in the estimation of structural demands have already been identified in previous works (Bradley, 2013; Cantagallo et a., 2014), such as the scaling of ground motion records, the pairs of *M*-*R* considered in the record selection or even the record-to-record variability within a given group, although no consensus has yet been achieved on how these parameters may actually influence the estimation of both local and global deformation demands. These various issues will be discussed in the next sections of the chapter with the aim of clarifying some open questions. Conclusions will be extracted based on the results obtained for each building under analysis.

3.6.1 Is the maximum response obtained from three response history analysis a conservative estimate of the "true" mean seismic response?

The question of what would be the likelihood that the maximum of three seismic response analysis is smaller than the "true" mean seismic response, already placed by Bradley (2011), is rather pertinent, in the sense that existing code-based record selection methods may be proposing the use of a conservative approach that is in fact associated with an undesirable probability of providing seismic demands lower than the "true" mean ones. This probability of obtaining non-conservative estimates of seismic demands using the maximum of the three responses should be quantified for every record selection

method, with the aim of assessing if the adoption of such approach is truly adequate from a code perspective and if its adequacy depends on the type of record selection method.

Following a similar procedure to that used by Bradley (2011), both local and global deformation demands obtained using groups G3 and G3I were divided by the "true" mean response, which was considered in this study to be defined, for each selection method, by the sample mean of the vector of G7I mean responses, defining a ratio R_i. The discrete cumulative probability of R_i was then computed and the probability of $R_i < 1.0$ quantified. Figure 3.5 shows the R_i values obtained considering all buildings and code-based selection methods.

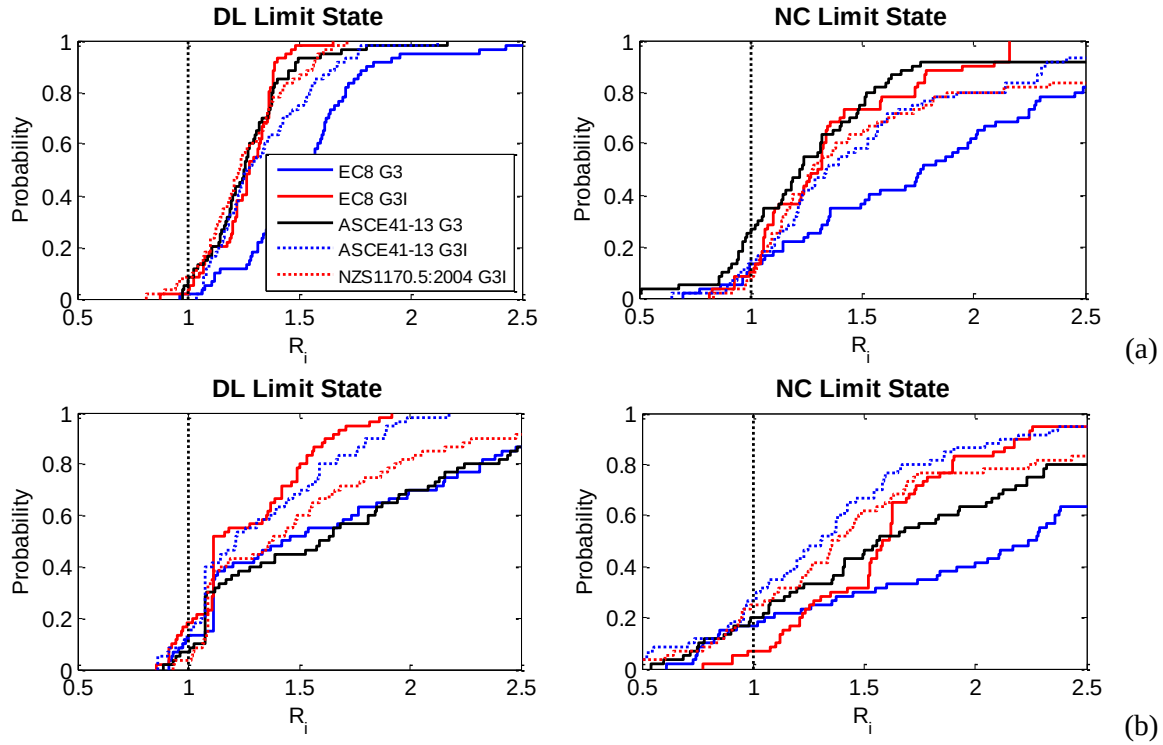

Figure 3.5 – Probability of the maximum of the three seismic responses being smaller than the "true" mean: (a) global deformation demands; (b) and local deformation demands.

The probability of the maximum of the three seismic responses being smaller than the "true" mean varies with the limit state and demand parameter under consideration. As it may be seen from Figure 3.5, at the DL limit state and when considering global deformation demands, the approach of taking the maximum of three responses is associated with systematically low probabilities of $R_i < 1.0$, which are below 10% and are independent of the record selection method adopted. Still, although the adequacy of such approach is ensured regardless the record selection method adopted, it may be seen by analysing the cumulative distribution of R_i that the inclusion of the additional control of spectral mismatch allows reducing the degree of conservativeness in the response estimates

to more acceptable levels (e.g., the mean R_i values reduce from 1.5 to around 1.25 in the EC8 method). These conclusions could have been previously anticipated from the inspection of Figure 1. At the NC limit state, whereas the EC8 method does not verify a probability of $R_i < 1.0$ greater than 20%, which may be considered acceptable from a code perspective, a higher probability of around 30% is observed using the ASCE41-13 and NZS 1170.5:2004 methods. However, the EC8 method systematically leads to higher mean R_i values, which resulted in rather conservative demand-based safety assessments (Figure 3.4). Moreover, although the inclusion of the additional control of spectral mismatch was seen to significantly reduce the mean R_i values, it did not influence the probability of $R_i < 1.0$.

3.6.2 Do the various code-based record selection methods lead to biased (statistically different) estimates of the global response of the buildings?

In order to answer this question, the ANOVA statistical technique (Moore et al., 2009) was employed. The purpose of ANOVA is to test the null hypothesis that all sample means are equal. A *p*-value under this null hypothesis lower than a certain significance level, say 5%, will suggest its rejection, meaning that at least one sample mean is significantly different than the other sample means. After rejecting the ANOVA null hypothesis, a multiple-comparisons procedure may be applied to identify which pairs of means differ from each other (Moore et al., 2009). Figure 3.6 depicts the multiple comparisons results obtained for buildings GB and SB3 at the SD and NC limit states. Not only it may be observed that the null hypothesis is rejected in all cases (*p*-value < 5%), but also that the differences in the sample means depend on the limit state and the building under consideration. Still, it can be concluded that the global deformation demands obtained using EC8 and NZS 1170.5:2004 always appear as statistically equal and hence, the methods proposed in both documents may be considered to lead to unbiased estimates of the global responses. In turn, ASCE41-13 generally leads to more conservative and statistically different estimates of global demands, particularly when compared to the EC8 results. It is interesting to note that although the variance in the global deformation demands obtained using ASCE41-13 has been reduced by introducing the additional control of the mismatch (G7I) at the individual record level (Figure 3.2), it also lead to biased response estimates with respect to the values obtained using EC8 G7I (Figure 3.6 (b)). These results could have been previously anticipated since ASCE41-13 proposes a

scaling method that is typically more conservative than the EC8 one, which would lead to potential bias in the response estimates as a result of a biased ensemble of ground motions. A discussion on the bias-variance trade-offs may be found in Bradley (2013).

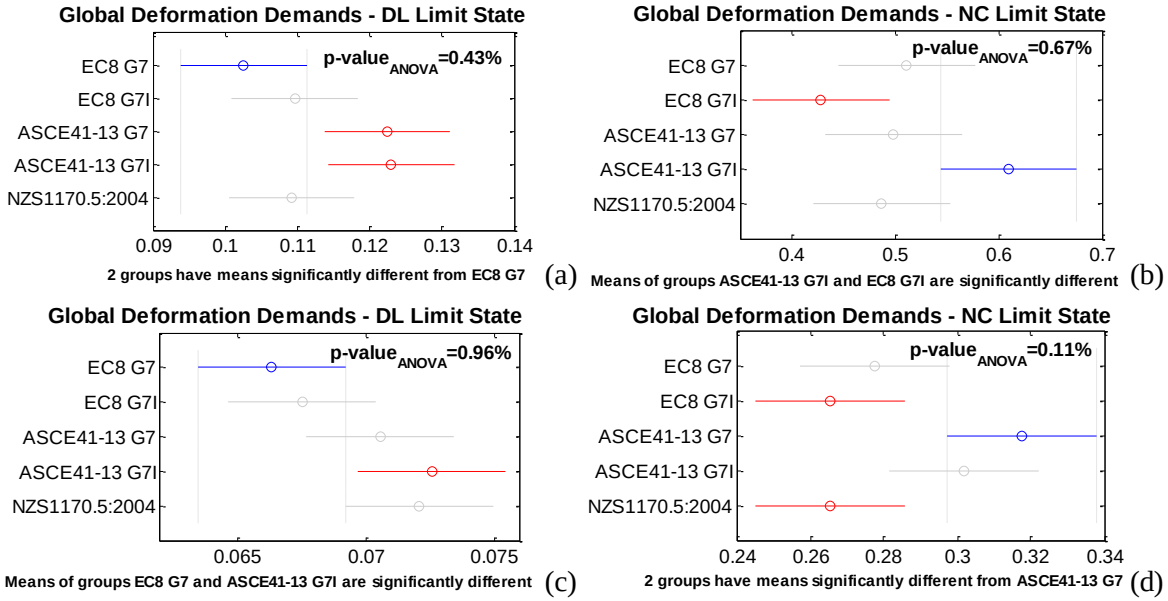

Figure 3.6 – Multiple comparisons of results obtained for building GB at the (a) DL and (b) NC LS and for building SB3 equally at the (c) DL and (d) NC LS.

3.6.3 Number of records required for a reliable estimate of seismic demands

The minimum number of records (i.e. seven records) proposed in design codes for estimating the mean seismic demand is based upon the guidance of the 1994 Uniform Building Code (UBC, 1994). As noted by Kircher (2005), this number was defined according to what the code drafting committee considered as a reasonable number of analysis to be conducted within an office environment and not on a scientific basis. Most of the previous studies that sought to address this issue simply focused on assessing the impact of the number of ground motion records on the estimation of stable global deformation demands, by considering a simplified single-degree-of-freedom system (Reyes and Kalkan, 2012), and inter-storey drift demands (Hancock et al., 2008). Although the inter-storey drift is a relevant response parameter that provides an overall picture of the distribution of local deformation demands within the structure, it does not reflect that the formation of plastic hinges at the member ends may be asymmetric due to the effect of gravity loads. This effect may introduce high variability in the estimation of curvature demands (Castro et al., 2008) which indicates the need of using a larger number of ground motion records.

To evaluate the influence of the number of records in the estimation of stable global (global drift ratios) and local (local rotation *DCRs*) deformation demands, the relative error between the demands obtained for an increasing number of records and the "true" mean seismic demand was quantified for each code-based record selection method. Moreover, in order to eliminate the influence of single sets of ground motions records, bootstrap simulation (Moore et al., 2009) was conducted. The mean demand was computed for each one of the generated 500 bootstrap samples and the 95% confidence interval of the relative error was then determined. The increase in the number of records was carried out by successively adding sets of 7 records equally scaled, so that its global mean also verifies the scaling conditions. Figure 3.7 presents the results obtained for building GB at the DL and NC limit states.

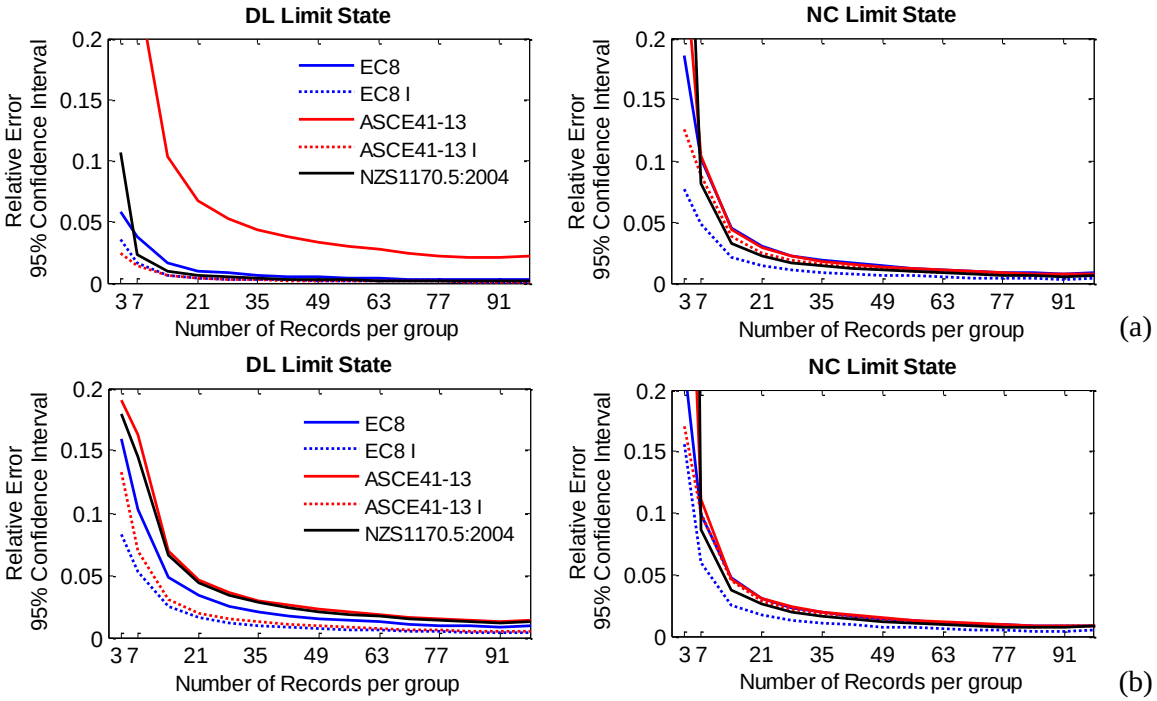

Figure 3.7 – Influence of the number of records in the estimation of stable seismic demands for building GB: (a) global deformation demands and (b) local deformation demands.

From the inspection of the figure, three conclusions can be readily drawn: (i) the number of ground motion records required to achieve more stable seismic demands increases from the DL to the NC limit states and if local deformation demands are being considered; (ii) the use of seven records per group seems to ensure relative errors lower than 10% if the control of the spectral mismatch is considered in the selection process. These relative errors significantly reduce to around, and less than, 5% in the case of building SB3 using both the EC8 and the ASCE41-13 methods with control of spectral mismatch and the NZS 1170.5:2004 method; (iii) a larger number of records, i.e. about 14

records, should be adopted to ensure systematic levels of error around, or lower than, 5%, particularly if no control of spectral mismatch is adopted. Moreover, special attention should be paid to the presence of offset records in the selected group, which may lead to outlier mean responses, as observed at the DL limit state for the ASCE41-13 group type (Figure 3.2). A group with more than 20 records would be necessary to eliminate the effect of outliers and provide relative errors around 5% in the response estimates.

3.6.4 Dependence of the structural response estimates on the record-to-record variability of the ground motion sets

It has been shown throughout this work that the accuracy of the structural demand estimates significantly increases with the consideration of the control of the mismatch of the spectral accelerations of each individual record with respect to the target spectrum. This observation suggests that the mean structural demand estimates are somehow dependent on the record-to-record variability of the corresponding group of records. To test this dependence, a linear regression analysis will be employed, so that $\ln EDP = \beta_o + \beta x$, where EDP is the engineering demand parameter under evaluation and x the parameter that measures the record-to-record variability of the set. The probability, given by a p-value, of the slope of the linear trend, β, being at least as large as that observed, given that its underlying true value is zero, will be also computed (Thothong and Luco, 2007). A p-value lower than a certain significance level (e.g. 5%) indicates that it is very unlikely that the true value of β is zero, i.e. that the record-to-record variability has a statistically significant effect in the structural response estimates. Figure 3.8 depicts the influence of the record-to-record variability of the ASCE41-13 group of records, defined in terms of the coefficient of variation of the spectral accelerations of the records, $\mathrm{CoV}_{Sa(T1)}$, at the fundamental period of vibration, T_1, on the global drift ratios (GDR) of building GB. It may be observed (Figure 3.8 (a)) that, based on the finite number of observations, the slope between ln GDR and $\mathrm{CoV}_{Sa(T1)}$ obtained for the ASCE41-13 group of records with no control of the spectral mismatch (G7 group type) is statistically significant (p-value < 5%) at both DL and SD limit states. Whilst, at the NC limit state and when the control of the spectral mismatch is adopted, the correlation between the global deformation demands of building GB and the record-to-record variability of the set becomes statistically insignificant. On the one hand, it may be concluded that the consideration of the additional criterion based on the control of the spectral mismatch at the individual record level seems to significantly improve the sufficiency of the selection process with respect to the record-

to-record variability of the set (Figure 3.8 (B)). In fact, these results were consistent for all buildings and for both EC8 and NZS 1170.5:2004 selection and scaling methods. However, it was interesting to note that, besides the control of the spectral mismatch has been ensured in the record selection to ASCE41-13, a statistically significant correlation between the global responses of buildings SB2 and SB3 and $CoV_{Sa(T1)}$ may still be found. These results may be again due to the previously referred bias-variance trade-off associated to the use of the more conservative ASCE41-13 scaling method.

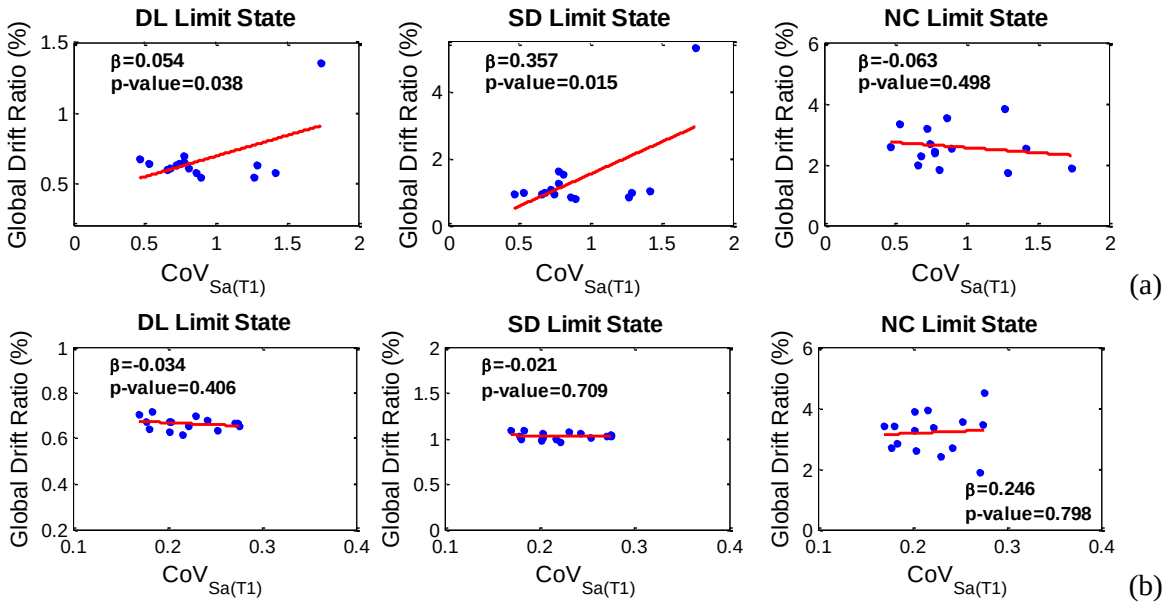

Figure 3.8 – Influence of the record-to-record variability ($CoV_{Sa(T1)}$) on the global drift ratio (GDR) estimates of building GB obtained for the ASCE41-13 G7 group of records: (a) dependence of GDR obtained without the control of the spectral mismatch on $CoV_{Sa(T1)}$; (b) and, dependence of GDR obtained with the control of the spectral mismatch on $CoV_{Sa(T1)}$.

On the other hand, the statistically insignificant correlation between GDR and $CoV_{Sa(T1)}$ at the NC limit state is possibly due to the lengthening of the fundamental period of vibration of the structure as it moves into its non-linear range of behaviour (Vamvatsikos and Cornell, 2005). Considering the EC8 G7 results, which were seen to give more representative values, a perfect correlation (i.e. coefficients of correlation ρ greater than 0.9) between the GDR variability obtained for a certain group of records, CoV_{GDR}, and the $CoV_{Sa(T1)}$ of that same group was observed at both DL and SD limit states, while at the NC limit state a negligible correlation was found (i.e. ρ lower than 0.1). This issue is, as a matter of fact, of critical importance when studying the appropriate range of periods within each code-based record selection and scaling criteria shall be verified, defined as $[0.2T_1; 2.0T_1]$, $[0.2T_1; 1.5T_1]$ and $[0.4T_1; 1.3T_1]$ in the European, the US and the New Zealand documents, respectively. Whereas the lower bound of the range of periods is just dependent on the period of vibration of the higher modes with more influence in the

response of the buildings, its upper bound should be defined so that it will not be exceeded by the elongation period. Beyer and Bommer (2007) have proposed a period range of [T_m; $\sqrt{\mu_\Delta}\,T_1$] for matching the record with the target spectrum, where T_m is the period of the highest mode which contributes significantly to the elastic response of the structure and μ_Δ is the displacement ductility of the structure. Therefore, aiming to provide an idea of the lengthening of the fundamental period of the buildings under analysis, a search across the $CoV_{Sa(Ti)}$ at all periods, T_i, was conducted to determine the one that exhibits the highest correlation with the variability of the response, CoV_{GDR}. Figure 3.9 presents the results obtained assuming, once again, the EC8 G7 results. It can be thus seen that a large correlation between CoV_{GDR} and $CoV_{Sa(Ti)}$ (i.e. ρ greater than 0.6) develops at the NC limit state at around $2.2T_1$, $1.8T_1$, $1.6T_1$ and $1.2T_1$ for buildings GB, SB1, SB2 and SB3, respectively. These results appear to be in agreement with the upper bound limit proposed by Beyer and Bommer (2007). For instance, by considering the mean GDR, of 2.7%, of building GB at the NC limit state for the EC8 G7 group of records and by taking from the capacity curve of the structure the value of the global drift at yield, approximately equal to 0.5%, a global drift ductility of the structural system, μ_Δ, of 5.4 is obtained, leading to an upper limit of the period range of interest of $2.3T_1$. As a result, despite Katsanos et al. (2012) have shown that the upper limit of $1.5T_1$ seems to be adequate to new buildings designed for low or moderate levels of ductility, in cases, such as of building GB, where the nonlinear capacity of the structure is almost fully exploited, this limit does not seem to hold true.

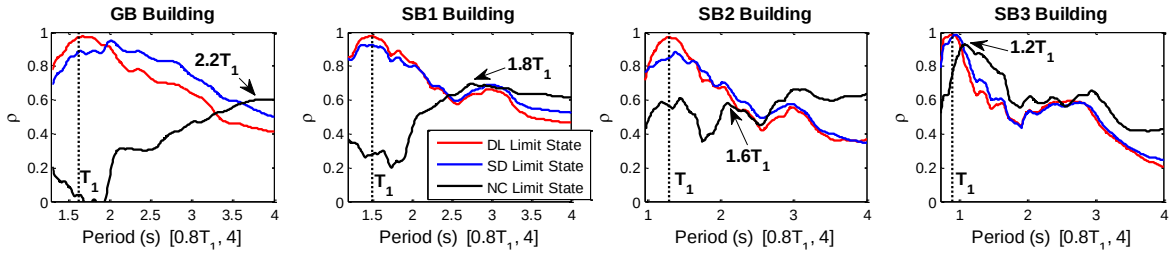

Figure 3.9 – Correlation between CoV_{GDR} and $CoV_{Sa(Ti)}$ along the period range of [$0.8T_1$, 4s].

With regard to the dependence of the local deformation demands (*DCR*) on $CoV_{Sa(T1)}$, no statistical significance has been observed, except for the specific case of building GB at the DL limit state and using the ASCE41-13 group of records (*p*-value=0.02). These results are consistent with those obtained when evaluating the correlation between the variability in the local deformation demands at the critical member of each building, CoV_{DCR}, and the global deformation demands variability, CoV_{GDR}. Practically no correlation between

CoV_{DCR} and CoV_{GDR} is observed at the DL and SD limit states for all buildings ($\rho \approx 0.2$), which will be mostly due to the higher mode effects. However, as the plastic incursions develop within the structure, and the participation of the first mode of vibration in the response increases, the correlation between the dispersions of both global and local deformation demands also increase to values of ρ of 0.5, 0.52, 0.58 and 0.83 at the NC limit state of buildings GB, SB1, SB2 and SB3, respectively. These results equally confirm that buildings with a greater lateral stiffness and strength that tend to develop more stable failure mechanisms exhibit, as it would be expected, a significantly higher correlation between CoV_{DCR} and CoV_{GDR} for increasing nonlinear behaviour incursions.

3.6.5 Dependence of the structural response estimates on the adopted scale factors

The dependence of the structural response estimates on linearly scaled ground motion records is now evaluated by means of linear regression analysis. However, before discussing the results obtained, a prior remark should be made on the scale factors adopted. Firstly, the scaling of the ground motion records to the SD LS target spectrum was conducted according to EC8 and ASCE41-13, with and without the control of the mismatch, by monitoring the maximum scale factors so as not to exceed a limit value of 2.0, thus leading to maximum scale factors at the NC limit state of 6.0. Additionally, in the case of the NZS 1170.5:2004 group of records, the scale factors adopted were defined by the product k_1k_2, where a maximum value of about 8.0 was obtained. Therefore, the inclusion of both constraints in the control of the maximum admissible scale factors will not allow further conclusions on the influence of high scale factors (e.g. greater than 10) on the response estimates. As presented in Figure 3.10 (a), which refers to building SB2 and the NZS 1170.5:2004 G7 group of records, the high *p*-values (i.e. >5%) indicate no statistical evidence of dependence of the global deformation demands on the mean scale factor of the corresponding group of records. This statistical independence was observed for all case study buildings and groups of records with no control of spectral mismatch. Nonetheless, it was interesting to observe that, when the control of the mismatch at the individual record level is included in the selection process, the logarithm of GDR and the mean scale factor become statistically significant for buildings SB2 and SB3 using the ASCE41-13 scaling method and, exceptionally, in building SB2 for the EC8 method. These results are even more consistent when local deformation demands are considered, which were seen to be statistically dependent on the mean scale factor in all buildings

using the ASCE41-13 scaling method with the control of the mismatch. Hence, it can be concluded that the consideration of the control of the mismatch at the record level may introduce bias in both local and global deformation demand estimates when using the ASCE scaling method. Similarly to what was observed by Cantagallo et al. (2014), the influence of the mean scale factors on the variability of both local and global structural demands, estimated with analysis conducted with code-based scaled records, seems to be characterized by a coefficient of correlation of about 0.4 to 0.5 (Figure 3.10 (B)).

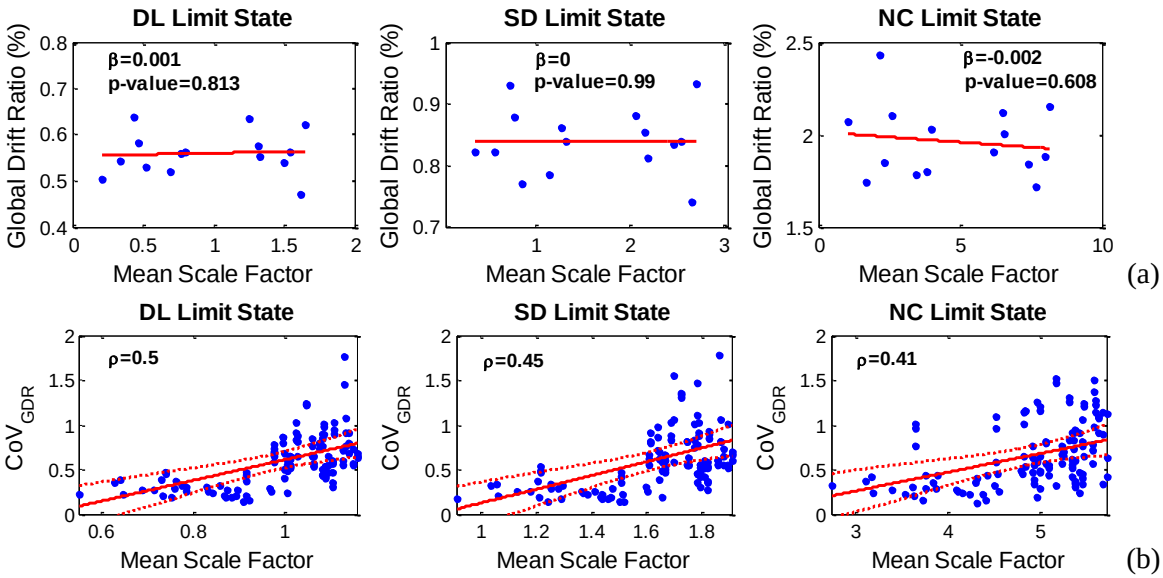

Figure 3.10 – (a) Influence of the mean scale factor of the NZS 1170.5:2004 G7 group of records on the global drift ratio (GDR) estimates of building SB2. (b) Correlation between the mean scale factor and CoV_{GDR} assuming all buildings and selection methods.

3.6.6 Dependence of the structural response estimates on the *M*-*R* pairs

The influence of the *M*-*R* pairs on the structural demand estimates is now carried out by employing a multiple linear regression analysis, so that ln EDP = $\beta_o + \beta_1 M + \beta_2 R$, where *M* and *R* refer to magnitude and distance, respectively. Two distinct analyses have been performed: (i) one focused on assessing the dependence of each individual global deformation demand on the *M*-*R* pair of the corresponding record; (ii) and a second one which intended to evaluate the dependence of the mean global drift ratio of the group of records on the respective group mean *M*-*R* pairs. Table 3.2 presents the *p*-values obtained from both analyses. Concerning the first analysis, the *p*-values computed with respect to the individual GDR indicate a strong statistical dependence on the *M*-*R* pairs, slightly reduced when the control of the spectral mismatch is adopted. On the other hand, regarding the second analysis, Table 3.2 allows concluding that the mean GDR of each group of records without control of spectral mismatch has low correlation with the mean *M*-*R* pairs.

Still, the inclusion of the additional control of spectral mismatch was seen to slightly increase the dependence of the mean GDR on the mean *M-R* pairs, which is statistically significant (*p*-value<0.05) for the SD LS of building GB and for the DL LS of building SB1, however remaining statistically insignificant for all the other cases. Recall that a prior selection of the records has been conducted on the basis of the seismological characteristics of the events that define the Portuguese type 1 and Zone 3 seismic action, which is characterized by magnitudes and epicentral distances higher than 5.5 and 20km, respectively. Therefore, these results are not conclusive on the influence of considering records randomly selected from an *M-R* bin, but still demonstrate that no bias seems to be introduced in the global response estimates when a pre-selection of the records is conducted considering the expected seismological characteristics of the seismic hazard scenario associated with the site location of the structure under analysis. These conclusions were also observed for the local deformation demand estimates. Finally, the influence of the mean *M-R* pairs on the variability of the global response demands, CoV_{GDR}, was seen to be characterized by a reduced coefficient of correlation of about 0.2 to 0.3.

Table 3.2 – *p*-values from linear regression on the *M-R* pairs.

		Dependence of individual GDR on the M-R pairs		Dependence of the group GDR on the group mean M-R pairs	
Building	Limit State	EC8 (G7)	EC8 (G7I)	EC8 (G7)	EC8 (G7I)
GB	DL	**0.00**	0.36	0.83	0.06
	SD	**0.00**	0.24	0.95	**0.01**
	NC	**0.00**	**0.00**	0.64	0.56
SB1	DL	**0.00**	0.29	0.79	0.40
	SD	**0.00**	0.09	0.63	0.38
	NC	**0.00**	0.30	0.94	0.40
SB2	DL	**0.00**	**0.02**	0.63	**0.02**
	SD	**0.00**	0.07	0.36	0.09
	NC	**0.00**	**0.01**	0.60	0.34
SB3	DL	**0.00**	**0.00**	0.46	0.93
	SD	**0.00**	**0.00**	0.69	0.63
	NC	**0.00**	**0.04**	0.79	0.22
Median		**0.00**	0.06	0.67	0.36

3.7 Probabilistic quantification of the design seismic demands

Most of the criteria found on codes dedicated to demand-based assessment of buildings, such as EC8-3, are based on the prediction of mean design seismic demands, which have been demonstrated to exhibit a degree of uncertainty that depends on the

group-to-group variability of selected ground motion records. Moreover, it has been shown in this chapter that the error associated with the estimates of the mean structural demand is deeply correlated with the record-to-record variability of the group of records selected. This error can be reduced by adopting a higher number of records or by imposing an additional selection criterion based on the control of the mismatch of each individual spectrum relative to the target spectrum. Notwithstanding the adoption of these additional measures, the design seismic demand estimates may still be associated with an unknown likelihood of being below the "true" mean value and, as shown in Figure 3.4, lead to undesirable cases where groups of records selected according to similar criteria provide different demand-based assessment answers. Therefore, bearing the above considerations in mind, Bradley (2011) has proposed a probability-based approach for the determination of the design seismic demands, X_d, so that:

$$X_d = \overline{X} \cdot R_{X,0.84} \tag{3.2}$$

where $\overline{X}$ is the sample mean of the seismic responses and $R_{X,0.84}$ is an amplification factor intended to add conservatism to the sample mean that is a function of the number of ground motion records considered, N_{gm}, and the uncertainty in the seismic responses, S_{lnX}, given by:

$$R_{X,0.84} = \exp\left[\frac{S_{\ln X}}{\sqrt{N_{gm}}} \cdot \left(\frac{N_{gm}}{20}\right)^{1/10}\right] \tag{3.3}$$

This procedure uses the 84th percentile of the distribution of the sample mean to obtain the deterministic design seismic demands, not only because it is commonly adopted in related topics such as seismic hazard analysis, but also due to the fact that it will give a constant and known 16% probability of the design seismic demands to be lower than the "true" mean seismic demand, which is considered to be a reasonable value (Bradley, 2011).

In order to demonstrate the applicability of such procedure to the present case study and to enforce its implementation in future generations of design and assessment codes, the 84th percentile of the discrete distribution of the sample mean, $\overline{X}_{0.84}$, is computed for each group of records and divided by the "true" mean response of that same group, μ_X, i.e. $R_{X,0.84} = \overline{X}_{0.84} / \mu_X$. Figure 3.11 and Figure 3.12 display the results of $R_{X,0.84}$ for both global and local deformation demands obtained from the seismic responses of the set of analysed buildings and from the application of the parametric approximation proposed by Bradley (2011). It may be thus observed from Figure 3.11 that, with respect to the quantification of the global deformation demands, the methodology proposed by Bradley (2011) provides

quite good results in comparison to those obtained from the actual seismic responses. In fact, even when considering a group of three records, with or without the consideration of the control of the spectral mismatch, the parametric approximation still gives consistent results.

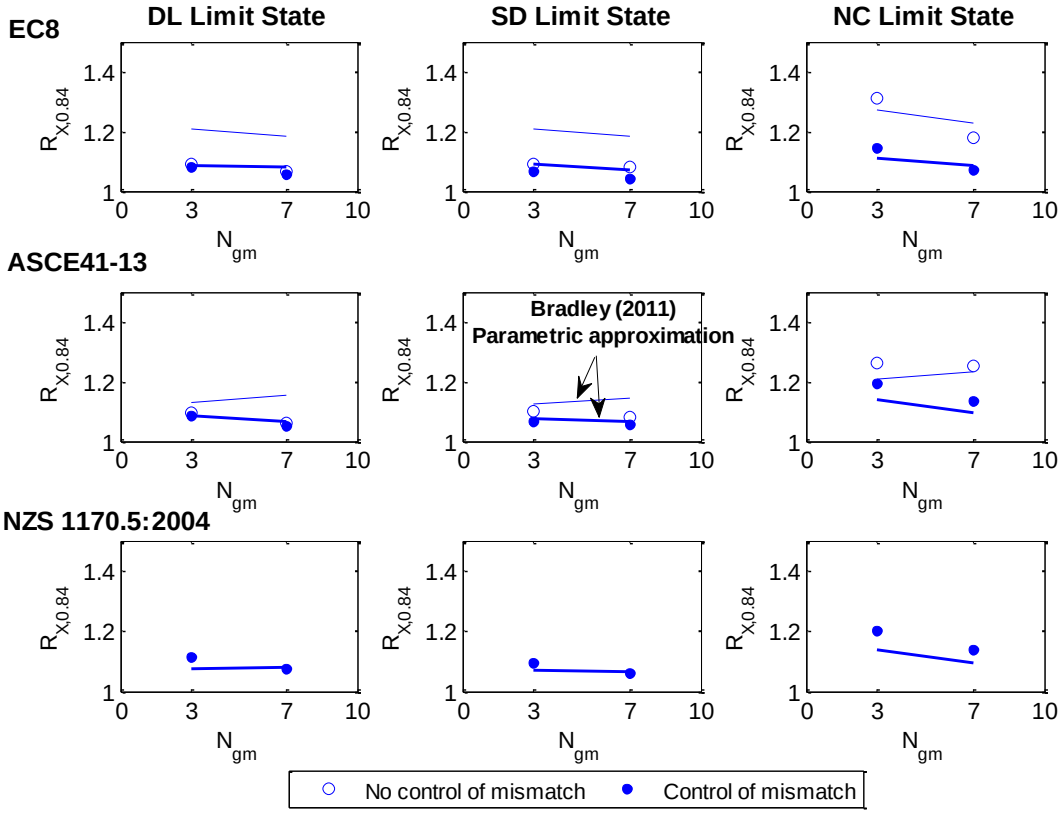

Figure 3.11 – Applicability of the probability-based approach proposed by Bradley (2011) in the estimation of the mean global deformation demands.

Likewise, regarding the determination of the local deformation demands, it may be observed from Figure 3.12 that the parametric approximation accurately captures the $R_{X,0.84}$ values obtained from the seismic responses using groups of seven records, with and without the control of the spectral mismatch. Since the lognormal standard deviation of the seismic responses, S_{lnX}, varies from group to group, the quantification of $R_{X,0.84}$ using the simplified approach was conducted considering the mean S_{lnX} of the 15 groups of records and its minimum and maximum values. Moreover, it was found that only for building GB at the DL and SD limit states, the application of the simplified approach resulted in values lower than those obtained from the seismic responses. Still, these differences are not representative and it may be concluded that the probability-based approach proposed by Bradley (2011) not only provides good estimates of $R_{X,0.84}$, but also, and most importantly, its use allows estimating mean design seismic demands, with constant and known

probability of being below the "true" mean demands, regardless the number of records or the variability of the group of records selected, which are particularly relevant to eliminate those undesirable cases where groups of records selected according to similar criteria provide different demand-based assessment answers.

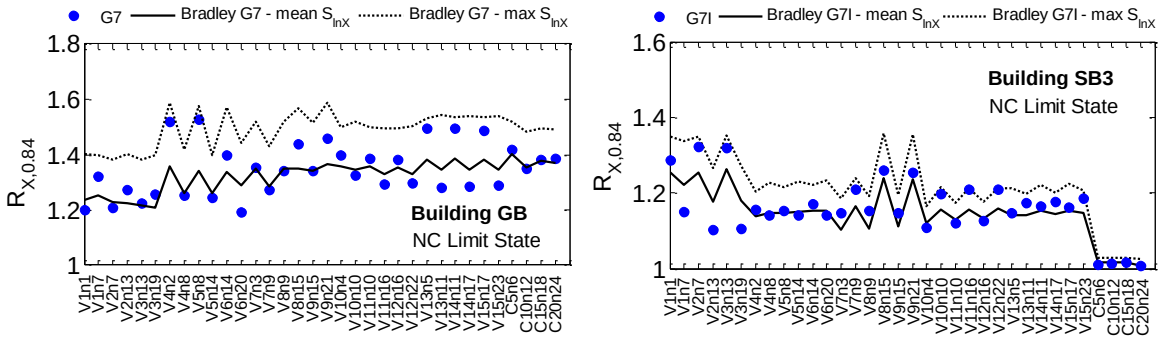

Figure 3.12 – Applicability of the probability-based approach proposed by Bradley (2011) in the estimation of the mean local deformation demands.

3.8 Conclusions

In this chapter a comparison between the methods available in the European, American and New Zealand provisions for selecting and scaling real ground motion records was presented in the context of the demand-based assessment of buildings. The accuracy, efficiency and consistency of the methods was evaluated and the influence of the number of ground motion records, scale factors and pairs of *M*-*R* on the seismic demand estimates was examined. A study on the suitability of a probability-based approach proposed by Bradley (2011) for determining the mean design seismic demands was also conducted. By employing this study to a set of four steel buildings with increasing lateral stiffness and strength, the following conclusions were drawn:

- Current codes for demand-based assessment of buildings rely on the estimation of mean seismic demands for conducting safety verifications. However, it has been shown throughout this work that the estimation of robust mean seismic demands is somehow uncertain and depends on the ground motion selection and scaling methods adopted. While the ASCE41-13 method was seen to lead to more conservative estimates of the mean seismic demands, the Eurocode 8 and NZS 1170.5:2004 methods generally conducted to similar results;
- The estimation of the mean seismic demands using both European and American methods was found to depend on the record-to-record variability of the group of ground motions selected. It has been demonstrated, though, that an improvement in the estimation is achieved if an additional criterion based on the control of the

mismatch between the spectra of the individual records in relation to the target spectrum is considered in the selection process. Such criterion clearly provided better control of the record-to-record variability of the group. Moreover, all record selection methods were seen to be sufficient with respect to the mean *M*-*R* pairs of the group of ground motions and scaling robust, namely the NZS 1170.5:2004 which is the most comprehensive method. However, these findings do not hold true for the ASCE41-13 method, which was seen to introduce potential bias in the mean seismic response estimates as the variance of the group of records was reduced, both by imposing the additional control of the mismatch or by increasing the number of records, thus leading to a classical bias-variance trade-off situation.

- The use of a minimum of seven records, as proposed by codes for determining mean seismic demands, was shown to be adequate if the additional control of the spectral mismatch was adopted; otherwise, it has been demonstrated that the minimum number of records that should be adopted is dependent on the seismic demands to be estimated, i.e. global or local deformation demands, and on the limit state under analysis.
- Finally, the probability-based approach proposed by Bradley (2011) was demonstrated to lead to accurate estimates of the 84^{th} percentile of the distribution of the sample mean when compared to the estimates obtained from the nonlinear dynamic analyses carried out on the set of buildings considered in this work. Its application and future implementation in design and/or assessment codes will clearly provide an important breakthrough in terms of the estimation of robust mean design seismic demands and consistent demand-based assessment answers, regardless of the number of records considered and/or if a more detailed selection of ground motions has been adopted

3.9 Acknowledgments

This work was performed within the framework of the research project ‘Development and calibration of seismic safety assessment methodologies for existing buildings according to the Eurocode 8 – Part 3’ founded by Foundation of Science and Technology (FCT) of Portugal. The authors would also like to thank Dr Brendon Bradley

and one anonymous reviewer for their thorough and constructive comments, which have undoubtedly helped to significantly improve the quality of the work.

3.10 References

Ang A, Tang W (2007) Probability concepts in engineering: Emphasis on applications in civil & environmental engineering, John Wiley & Sons, Inc., New York.

Araújo M, Macedo L, Castro JM, Delgado R (2013) Influence of code-based record selection methods on the seismic assessment of existing steel buildings, Proceedings of the 4th Thematic Conference on Computational Methods in Structural Dynamics and Earthquake Engineering, Kos Island, Greece.

ASCE (2010) Minimum design loads for buildings and other structures (ASCE/SEI 7-10), American Society of Civil Engineers, Reston, Virginia, USA.

ASCE (2014) Seismic evaluation and retrofit of existing buildings (ASCE/SEI 41-13), American Society of Civil Engineers, Reston, Virginia, USA.

Baker JW (2011) Conditional Mean Spectrum: Tool for ground motion selection, Journal of Structural Engineering, 137, 322-311.

Baker JW, Cornell C (2006) Spectral Shape, epsilon and record selection, Earthquake Engineering and Structural Dynamics, 35, 1077-1095.

Beyer K, Bommer J (2007) Selection and scaling of real accelerograms for bi-directional loadings: a review of current practice and code provisions, Journal of Earthquake Engineering, 11, 13-45.

Bommer J, Acevedo A (2004) The use of real earthquake accelerograms as input to dynamic analysis, Journal of Earthquake Engineering, 8, 43-91.

Bradley B (2011) Design seismic demands from seismic response analyses: A probability-based approach, Earthquake Spectra, 27, 213-224.

Bradley B (2013) A critical examination of seismic response uncertainty analysis in earthquake engineering, Earthquake Engineering and Structural Dynamics, 42, 1717-1729.

Bradley B, Dhakal R, MacRae G, Cubrinovski M (2010) Prediction of spatially distributed seismic demands in specific structures: Ground motion and structural response, Earthquake Engineering and Structural Dynamics, 39, 591-613.

Bradley BA (2012) The seismic demand hazard and importance of the conditioning intensity measure, Earthquake Engineering and Structural Dynamics, 41, 1417-1437.

Cantagallo C, Camata G, Spacone E (2013) Seismic demand sensitivity of reinforced concrete structures to ground motion selection and modification methods, Earthquake Spectra, in-press.

Castro JM, Dávila-Arbona FJ, Elghazouli AY (2008) Seismic design approaches for panel zones in steel moment frames, Journal of Earthquake Engineering, 12, 34-51.

CEN (2004) ENV 1998-1 Eurocode 8: Design of structures for earthquake resistance - Part 1: eneral rules, seismic actions and rules for buildings, European Committee for Standardization, Brussels, Belgium.

CEN (2005) ENV 1993-1 Eurocode 3: Design of steel structures - Part 1-1: General rules and rules for buildings, European Commitee for Standardization, Brussels, Belgium.

CEN (2005) ENV 1998-3 Eurocode 8: Design of structures for earthquake resistance - Part 3: Assessment and retrofitting of buildings, European Committee for Standardization, Brussels, Belgium.

CEN (2010) NP ENV 1998-1 Portuguese National Annex to Eurocode 8: Design of structures for earthquake resistance - Part 1: General rules, seismic actions and rules for buildings, Instituto Português da Qualidade, Lisboa Portugal.

Cimellaro GP, Reinhorn AM, D´Ambrisi A, De Stefano M (2011) Fragility analysis and seismic record selection, Journal of Structural Engineering, 137, 379-390.

Grant D, Diaferia R (2013) Assessing adequacy of spectrum-matched ground motions for response history analysis, Earthquake Engineering and Structural Dynamics, 42, 1265-1280.

Hancock J, Bommer J, Stafford P (2008) Numbers of scaled and matched accelerograms required for inelastic dynamic analyses, Earthquake Engineering and Structural Dynamics, 37, 1585-1607.

Haselton C, Whittaker A, Hortacsu A, Baker J, Bray J, Grant D (2012) Selecting and scaling earthquake ground motions for performing response-history analyses, Proceedings of the 15th World Conference on Earthquake Engineering, Lisbon, Portugal.

Haung Y, Whittaker A, Luco N, Hamburger R (2011) Scaling earthquake ground motions for performance-based assessment of buildings, Journal of Structural Engineering, 137, 311-321.

Iervolino I, Cornell A (2005) Record selection for nonlinear seismic analysis of structures, Earthquake Spectra, 21, 685-713.

Iervolino I, Maddaloni G, Cosenza E (2008) Eurocode 8 compliant real record sets for seismic analysis of structures, Journal of Earthquake Engineering, 12, 54-90.

Iervolino I, Manfredi G (2008) A Review of ground motion record selection strategies for dynamic structural analysis, Modern Testing Techniques for Structural Systems, 131-163. Springer Vienna.

Kappos AJ, Kyriakakis P (2000) A re-evaluation of scaling techniques for natural records, Soil Dynamics and Earthquake Engineering, 20, 111-123.

Katsanos E, Sextos A, Elnashai A. (2012) Period elongation of nonlinear systems modeled with degrading hysteretic rules, Proceedings of the 15th Word Conference on Earthquake Engineering, Lisbon, Portugal.

Katsanos EI, Sextos AG, Manolis GD (2010) Selection of earthquake ground motion records: a state-of-the-art review from a structural engineering perspective, Soil Dynamics and Earthquake Engineering, 30, 157-169.

Kircher C (2005) Current code and standard requirements for the selection and scaling of ground motion time histories and background on their development, Proceedings of the 2005 COSMOS Technical Session – Recommendations for the Selection and Scaling of Ground Motion Time Histories for Building Code Applications, California.

Krawinkler H, Median R, Alvi B (2003) Seismic drift and ductility demands and their dependence on ground motions, Engineering Structures, 25, 637-653.

Lucco N, Bazzurro P (2007) Does amplitude scaling of ground motion records result in biased nonlinear drift responses? Earthquake Engineering and Structural Dynamics, 35, 1813-1835.

Macedo L, Araújo M, Castro JM (2013) Assessment and calibration of the harmony search algorithm for earthquake record selection, Proceedings of the Vienna Congress on Recent Advances in Earthquake Engineering and Structural Dynamics, Vienna, Austria.

Moore D, McCabe G, Craig B (2009) Introduction to the practice of statistics, Sixth Edition. W. H. Freeman and Company, New York.

NEHRP (2011) Selecting and scaling earthquake ground motions for performing response-history analyses, NIST GCR 11-917-15 report, NEHRP Consultants Joint Venture.

NZS (2004) NZS 1170.5:2004 Structural design actions. Part 5: Earthquake actions – New Zealand, New Zealand Standard, Wellington, New Zealand.

Oyarzo-Vera C, Chouw N (2012) Comparisons of record scaling methods proposed by standards currently applied in different countries, Proceedings of the 15th World Conference on Earthquake Engineering, Lisbon, Portugal.

Özer B, Akkar S (2012) A procedure on ground motion selection and scaling for nonlinear response of simple structural systems, Earthquake Engineering and Structural Dynamics, 41, 1693-1707.

PEER (2011) OpenSees: Open system for earthquake engineering simulation, Pacific Earthquake Engineering Research Center, Universtiy of California, Berkeley, CA.

Peres R (2010) Comparison of European and American approaches for consideration of P-Δ effects in seismic design, MS.c. Dissertation, Istituto di Studi Superiori di Pavia, Pavia, Italy.

Reyes J, Kalkan E (2012) How many records should be used in an ASCE/SEI-7 ground motion scaling procedure? Earthquake Spectra, 28, 1223-1242.

Sextos A, Katsanos G, Manolis G (2011) EC8-based earthquake record selection procedure evaluation: validation study based on observed damage of an irregular R/C building, Soil Dynamics and Earthquake Engineering, 31, 583-597.

Shome N, Cornell CA, Bazzurro P, Carballo J (1998) Earthquakes, records and nonlinear responses, Earthquake Spectra, 14, 469-500.

Thothong P, Luco N (2007) Probabilistic demand analysis using advanced ground motion intensity measures, Earthquake Engineering and Structural Dynamics, 36, 1837-1860.

UBC (1994) Uniform building code 1994, International Conference of Building Officials, Washington.

Vamvatsikos D, Cornell CA (2005) Developing efficient scalar and vector intensity measures for IDA capacity estimation by incorporating elastic spectral shape information, Earthquake Engineering and Structural Dynamics, 34, 1573-1600.

Watson-Lamprey J, Abrahamson N (2006) Selection of ground motion time series and limits on scaling, Soil Dynamics and Earthquake Engineering, 26, 477-482.

Chapter 4

How reliable are linear analysis procedures for the seismic assessment of existing steel buildings to EC8-3?

Araújo M, Castro JM (2016) On the quantification of local deformation demands and adequacy of linear analysis procedures for the seismic assessment of existing steel buildings to EC8-3. Bulletin of Earthquake Engineering, 14 (6):1613–1642.

4.1 Summary

The application of performance-based design and assessment procedures requires an accurate estimation of local component deformation demands. In the case of steel moment-resisting frames, these are usually defined in terms of plastic rotations. A rigorous estimation of this response parameter is not straightforward, requiring not only the adoption of complex nonlinear structural models, but also of time-consuming numerical integration calculations. Moreover, the majority of existing codes and guidelines do not provide any guidance in terms of how these response parameters should be estimated. Part 3 of Eurocode 8 (EC8-3) requires the quantification of plastic rotations even when linear methods of analysis are used. Therefore, the aim of this work is not only to evaluate different methods of quantifying local component demands, but also to answer the question of how reliable are the estimates obtained using the EC8-3 linear analysis procedures in comparison to more accurate nonlinear methods of analysis, particularly when the linear analysis applicability criteria proposed by EC8-3 is verified.

4.2 Introduction

The implementation of performance-based design concepts and assessment procedures in seismic codes imposes the need for an accurate estimation of local component demands. In the case of framed structures, local component demands are

commonly expressed in terms of plastic rotations of steel members and chord rotations of RC members (CEN, 2005; ASCE, 2014). A rigorous estimation of these parameters is not straightforward, requiring not only the adoption of complex nonlinear structural models, but also of time-consuming numerical integration calculations. Moreover, the majority of existing guidelines and codes do not provide any guidance in terms of how these response parameters should be estimated. This situation arises, as discussed in Chapter 2, when applying the linear analysis procedures prescribed in Part 3 of Eurocode 8 (EC8-3) (CEN, 2005) to existing steel buildings. Despite the well-known limitation of this type of analysis in providing reliable predictions of inelastic response parameters, the safety checks prescribed in the European code are based on the control of plastic member rotations. As a result, during the assessment process, the analyst will be confronted with a rather ambiguous scenario: how can one perform the safety verifications if plastic rotations cannot be directly obtained from linear elastic methods of analysis?

A number of studies addressing the issue of the accuracy of linear elastic analysis in predicting the nonlinear response of buildings have been recently conducted (Kosmopoulos and Fardis, 2007; Browing et al., 2008; Günay and Sucuoglu, 2009, 2010; Romão et al., 2010a) On the basis of the results of over a thousand non-linear dynamic analyses, Panagiotakos and Fardis (1999) developed rules for the estimation of mean and upper-characteristic peak inelastic member chord rotations from linear analysis. These rules mainly involve the use of conversion factors on elastic chord rotations derived from response spectrum analysis or linear static analysis with inverted triangular equivalent lateral forces, which are for the mean value of about 1.0, while those for the upper-characteristic values are on average of about 1.5 over the height of the building. As referred by the authors, this proposal is essentially a generalization of the well-known equal-displacement rule of SDOF systems and its accuracy is justified with the fact that the fundamental period of the cracked elastic structures considered is beyond the corner period of the ground motion. However, the previous results were only derived from plan-wise regular and symmetric RC buildings and its range of applicability is therefore limited. As a result, Kosmopoulos and Fardis (2007) extended the previous work to asymmetric multi-storey RC buildings, having again concluded that elastic modal response spectrum analysis gives, on average, unbiased and fairly accurate estimates of member inelastic chord rotations. These conclusions were drawn from cases violating the linear analysis applicability criteria proposed by both EC8-3 and ASCE41-13 (ASCE, 2014), thus suggesting that there is room for re-examination and possible relaxation of the criteria, as

already discussed in previous works (Pinto and Franchin, 2008; Romão et al., 2010a). Additionally, Günay and Sucuoglu (2009, 2010) proposed an improved linear elastic analysis procedure based on reducing the stiffness of structural members that are expected to respond in the inelastic range in a single global iteration step, wherein inelastic chord rotations are determined on the basis of the equal displacement rule. The results obtained by the authors revealed that linear analysis can be effectively used with such a simple modification to predict the nonlinear seismic performance of structures, being at least as accurate as the prediction provided by nonlinear static procedures.

Local deformation demands can be alternatively measured in terms of story drifts (Gupta and Krawinkler, 2000). In this case, the safety of the structure is assessed by comparing those values with limit values specified in guidelines and codes for various performance levels (Bertero and Bertero, 2002; Gioncu and Mazzolani, 2002; Grecea et al., 2004). In a study carried out on a set of RC buildings, Browning et al. (2008) observed that, on average, the magnitude of the maximum story drift ratio calculated using nonlinear analysis is 1.5 times larger than that estimated using linear response spectrum analysis, with a coefficient of variation of approximately 0.39. The location of the maximum drift ratio was also seen to vary significantly when using nonlinear and linear analysis. Several works proposing approximate methods to estimate maximum lateral deformation demands may be found in the literature (Miranda and Reyes, 2002; Akkar and Miranda, 2005; Ruiz-García and Miranda, 2006; Whittaker and Huang, 2007).

Although there is a broad agreement that nonlinear procedures are a better tool to assess existing structures, linear elastic methods are, and will continue to be, used due to their relative simplicity and acquaintance of most design practitioners, as it was shown in a survey conducted by Paret et al. (2011). As pointed out by Toranzo-Dianderas (2009), further studies on linear analysis and proposals of new and more reliable procedures are still required. Therefore, and noting that the majority of studies already conducted mainly focused on RC buildings, the aim of this work is to answer the question of how reliable are the linear elastic procedures proposed by EC8-3 for the seismic safety assessment of existing steel buildings. Additionally, and since EC8-3 stipulates that the safety checks should be always performed in terms of plastic rotations, the following two questions will be discussed: (i) Is there any local deformation demand parameter compatible with the member plastic rotation demands that can be quantified from linear analysis? (ii) Do linear analysis procedures provide accurate estimates of plastic rotations, particularly when the linear analysis applicability criteria proposed by EC8-3 is verified?

4.3 Methods of quantifying local deformation demands

From a normative point of view, the assessment of existing buildings should be carried out by verifying the safety of each individual member of the structure. Most codes implicitly consider that if any primary member does not verify safety, then the building fails its assessment. According to EC8-3, for steel buildings these individual safety checks should be conducted in terms of plastic rotations. To understand the process associated with the quantification of this demand parameter, one can interpret a given member of a structural system as an isolated member responding under equivalent boundary conditions. A common cantilever beam example is usually assumed, although some approaches have been proposed, for comparison purposes, with experimentally tested elements (Gioncu and Petcu, 1997; Gioncu, 2000). Figure 4.1 represents a decomposition example of a simple structural system into a set of cantilever beams.

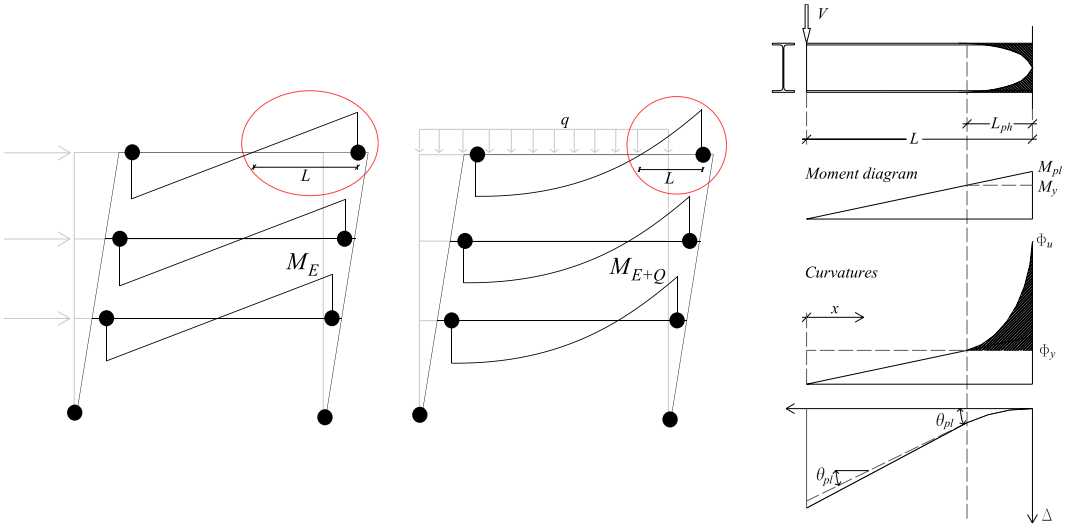

Figure 4.1 – Decomposition of a structure into a set of cantilever beams and the definition of plastic rotation (after Bruneau et al., 1998).

As demands locally increase in such cantilever members, cross-sectional plastification begins to take place at all sections of the element where the yield moment, M_y, is exceeded. Plasticity spreads from the flanges into the web, and eventually a fully plastified cross-section is formed with a plastic moment M_{pl}. The accurate evaluation of the member plastic rotation, θ_{pl}, can be defined as follows (Bruneau et al., 1998; Priestley et al., 2007):

$$\theta_{pl} = \int_{L-L_{ph}}^{L} \phi_{pl}(x)dx \tag{4.1}$$

where ϕ_{pl} (x) represents the plastic curvatures, which verify the condition ϕ (x) > ϕ_y, developed over L_{ph}, L is the length of the equivalent cantilever beam, defined as the distance from the member end to the point of contra-flexure and ϕ_y is the cross-sectional yield curvature defined as M_y/EI. Total rotation demands are then obtained by summing up the elastic component of the rotation, θ_{el}, to θ_{pl}, such that:

$$\theta_t = \theta_{pl} + \int_0^{L-L_{ph}} \phi(x)dx + \int_{L-L_{ph}}^{L} \phi_y dx \tag{4.2}$$

Alternatively, the member local deformation demands can be quantified in terms of chord rotations, which are defined as the angles between the chord connecting the end sections of the member to the contra-flexure point and the tangent to the member axis at the end section (Figure 4.2). This is the approach suggested by EC8-3 to assess RC members (Mpampatsikos et al., 2008; Romão et al., 2010b):

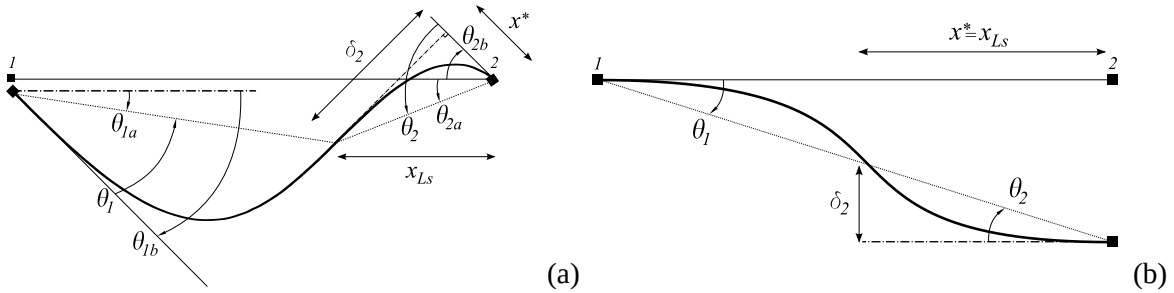

Figure 4.2 – Definition of chord rotation: (a) beam and (b) column.

The chord rotations, θ_1 and θ_2, of the two end of the structural member can be analytically obtained by means of the *Exact Integral Method* (*EIM*), as follows:

$$\theta_1 = \int_{x_{Ls}}^{L} \phi(x) \left(\frac{x_{Ls} - x}{L - x_{Ls}} \right) dx \tag{4.3}$$

$$\theta_2 = \int_{0}^{x_{Ls}} \phi(x) \left(\frac{x_{Ls} - x}{x_{Ls}} \right) dx \tag{4.4}$$

where x_{Ls} is the abscissa of the point of contra-flexure and L is the member length. However, the alternative *Exact Geometrical Method* (*EGM*) is commonly adopted due to easiness of application. In this case, chord rotations are defined in a geometrical way. It can be seen from Figure 4.2 that $tan(\theta_2) = \delta_2 / x^*$, which, under the hypothesis that θ_2 is small, leads to $x^* \approx x_{Ls}$ and $tan(\theta_2) \approx \theta_2$. As a result, θ_2 can be simplified as follows:

$$\theta_2 = \delta_2 / x_{Ls} \tag{4.5}$$

Since the calculation of δ_2 may not be straightforward, θ_2 is defined by:

$$\theta_2 = \theta_{2a} - \theta_{2b} \tag{4.6}$$

where θ_{2a} represents the contribution to the rotation due to the transversal deflection at x_{Ls} with respect to the initial member configuration and θ_{2b} corresponds to the nodal rotation, considering clockwise rotations as positive. Equally, θ_1 may be defined as:

$$\theta_1 = \theta_{1a} - \theta_{1b} \tag{4.7}$$

having θ_{1a} and θ_{1b} the same meaning of θ_{2a} and θ_{2b}, respectively. It has been found (Romão et al., 2010b) that in cases of frame elements under large deformation demands, θ_{1a} is approximately equal to θ_{2a}. Thus, in these situations an *Approximate Geometrical Method* (*AGM-DR*) that considers the member drift and nodal rotations for both beams and columns can be used to compute the chord rotation without having to evaluate x_{Ls}, by setting:

$$\theta_{1a} = \theta_{2a} = d_y / L \tag{4.8}$$

where d_y represents the relative transverse displacements of sections 1 and 2, neglecting the contribution of the axial deformation of the member. Assuming these approximations, θ_1 and θ_2 can be quantified without further difficulties from equations (4.6) and (4.7). More detailed information on the quantification of the chord rotation demands can be found elsewhere (Romão et al., 2010b).

4.4 Application of the various methods of quantifying local deformation demands

4.4.1 Case study description

The study presented herein was conducted considering the four 5-storey MRF steel buildings presented in Chapter 2. The analyses were carried out using the open-source software OpenSees (PEER, 2011). Two sets of structural models were developed in line with the type of analysis performed, linear and nonlinear. Again, it should be referred that, for the development of the numerical models for linear analysis, instead of the exact manufactured cross-section properties, approximate properties were adopted by neglecting the representation of the root radius between the flange and the web of the cross-sections. The aim was to provide a perfect fit between the results obtained from both linear and nonlinear analysis. Regarding the models used for nonlinear analysis, force-based beam-column elements were firstly adopted considering 10 Gauss-Lobatto integration points along its length. Also, a cross-section discretization solution by fibres was considered and

a bilinear elasto-plastic material model with 0.5% hardening was adopted for structural steel. However, this type of distributed plasticity numerical model is known to have several limitations (Calabrese et al., 2010; Macedo et al., 2015), namely the inability of representing both the local and torsional instability phenomena of steel members (D'Aniello et al., 2012). The quantification of plastic rotations based on curvature integration may lead to an unrealistic representation of the actual member response and also to significantly overestimate its capacity. As shown by Macedo et al. (2015), although distributed plasticity models provide, as expected, equal or more approximate results to those obtained using concentrated plasticity models that account for deterioration at slight and moderate damage state levels, respectively, they may lead to differences in the probability of exceedance of the collapse damage state greater than 90%. Therefore, a second set of structural models defined using the Ibarra et al. (2005) strength and stiffness hysteretic deterioration model and the parameters calibrated from Lignos and Krawinkler (2011) was considered. The effect of the panel zones was neglected in this study and the gravity loads were assumed as point loads applied at the mid-span of the beams and at each alignment of columns, representing the vertical loads transmitted from secondary frames. A modal analysis was firstly carried out for each frame in order to identify the dynamic characteristics of the buildings and fundamental periods of vibration of 1.63s, 1.50s, 1.20s and 0.90s were obtained for buildings GB, SB1, SB2 and SB3, respectively.

The main goal of the following example of application is not only to evaluate the effectiveness of each previously exposed method for quantifying the member deformation demands, but also to address the issue of how to estimate plastic rotations in the context of linear elastic analysis. It has been discussed in Chapter 2 that, while ASCE41-13 provides acceptance criteria for linear procedures defined on the basis of component strength demand-to-capacity ratios (*DCR*), so that a certain primary ductile member is safe if it verifies the inequality condition $mk \geq DCR$, where m expresses the expected ductility capacity of the member associated with given performance level and k is the knowledge factor, EC8-3 stipulates that safety checks should be performed in terms of deformations by ensuring $\theta_C / CF \geq \theta_D$, where θ_C refers to the member plastic rotation capacity, θ_D to the member plastic rotation demand and CF is the confidence factor. Accordingly, EC8-3 seems to lack on conceptual consistency, as it requires the analyst to derive plastic rotations from linear analysis. Thus, the key question on how to compute deformation demands from linear analysis that can be directly compared with the plastic rotation limits prescribed in EC8-3 has already been be placed. The most suitable answer was found to be

the determination of chord rotations, quantified on the basis of the *EGM* and *AGM-DR* methods described before. While the application of the *AGM-DR* is simple, based on the manipulation of nodal displacements and rotations, the *EGM* requires the calculation of the deflection at x_{Ls} to obtain θ_{1a} and θ_{2a}. This can be carried out by dividing each member into two cantilever beams with different lengths equal to L - x_{Ls} and x_{Ls} with reference to nodes 1 and 2, respectively (Figure 4.2). Each cantilever beam is then treated individually and the deflection (δ) at its free node calculated using the elastic integration method. In the present case study, since gravity loads were defined as point loads applied at the beam mid-span, resulting therefore in bending moment diagrams with linear variation, the deflection can be calculated from node 2 as:

$$\delta = \delta_2 + \theta_{2b} x_{Ls} - V\, x_{Ls}^{\,3} \big/ 3EI \tag{4.9}$$

where δ_2 is the vertical displacement of node 2 and V is the shear developed in the member, equal to M_2 / x_{Ls}, being M_2 the bending moment at node 2.

In order to evaluate the effectiveness of each method of quantifying the local deformation demands, pushover analyses were performed on both linear and nonlinear structural models. The aim was to exclude the dispersion in the deformation demand estimates associated with the type of analysis considered. A fixed load pattern, proportional to the mass and height of each storey, was defined and the results were computed for various levels of global drift ratios (i.e. top displacement divided by building height). The following aspects were considered in the discussion of results: (i) evaluation of the accuracy of the simplified *AGM-DR* method using nonlinear analysis (*AGM-DR*$_{NL}$) comparing to the reference *EIM* method in terms of the quantification of chord rotation demands when nonlinear material behaviour is considered (*EIM*$_{NL}$); (ii) assessment of the ability of linear analysis to provide reasonable estimates of chord rotation by means of the *EGM* and the *AGM-DR* methods (*EGM*$_L$ and *AGM-DR*$_L$); and, finally, (iii) a feasibility evaluation of the use of chord rotations as an alternative to plastic rotations, with and without considering strength degradation of the member.

4.4.2 Application to the set of steel buildings under analysis

Before discussing the previously highlighted aspects, a remark on the influence of gravity loads on the distribution of plasticity and quantification of deformation demands in beams should be made. A simplified expression to determine the rotation of the plastic hinge region, defined as $\theta_p = \delta / 0.5L$, where δ is the beam deflection at mid-span and L the

beam span, is commonly found in current seismic codes and guidelines (CEN, 2004; ASCE, 2014). This expression assumes that plasticity is symmetrically distributed along the beam length or, in other words, that equal plastic rotation demands develop at both ends of a beam. It is well known that, in most cases, this assumption is not valid (Castro et al., 2008), particularly when the level of gravity moments represents an important fraction of the beam flexural strength. In fact, it may be seen from Figure 4.3 (a) that when gravity loads are not considered in the analysis, the chord rotation demands are, as expected, equal at both beam ends (i.e. positive chord rotation values refer to the left node of the member, designated as node 1, and the negative values to its right node, designated as node 2).

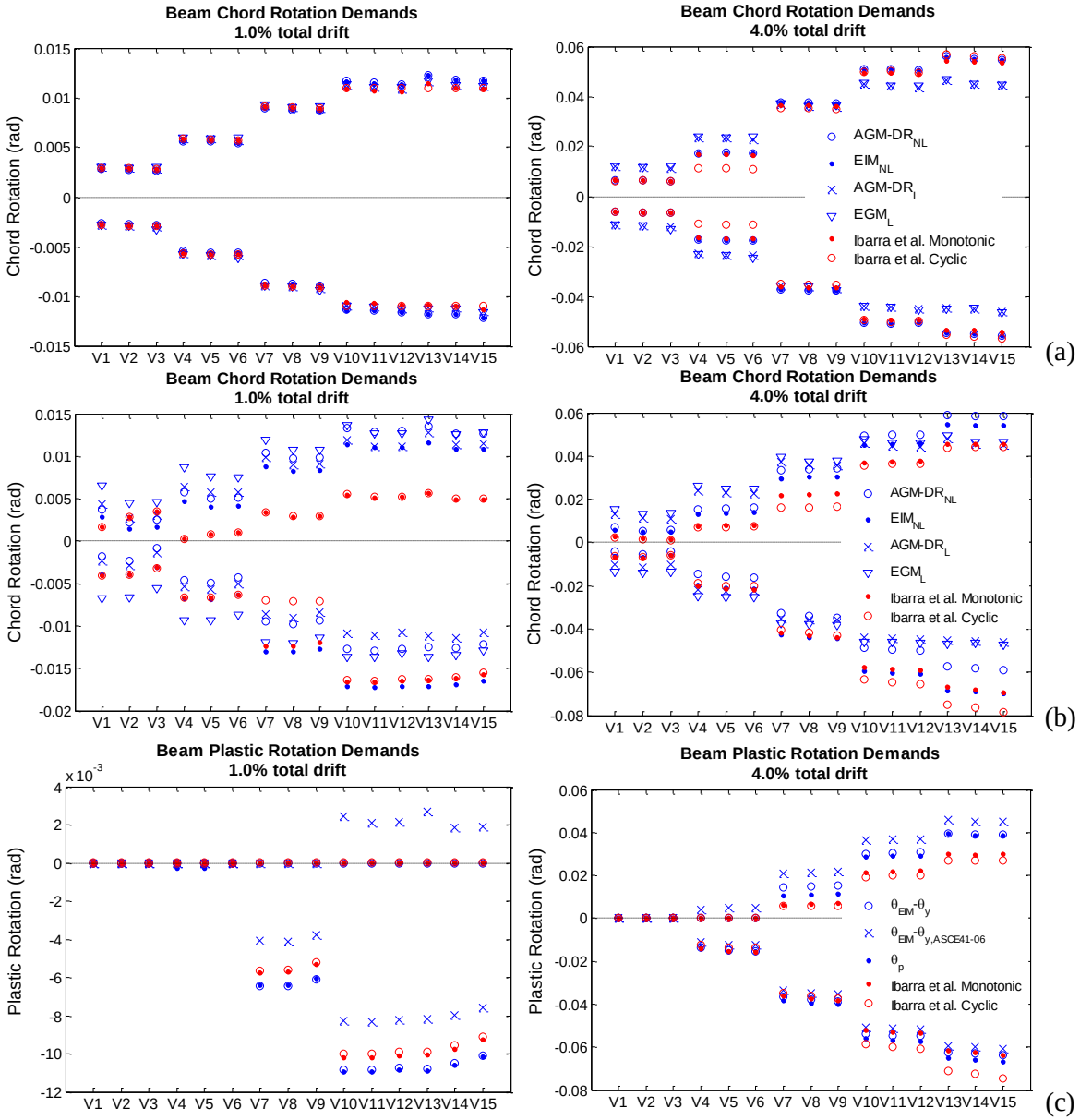

Figure 4.3 – Beam deformation demands for building GB: (a) chord rotations without gravity loads; (b) chord rotations with gravity loads; (c) and plastic rotation.

However, when comparing to the case in which gravity loads are considered (Figure 4.3 (b)), not only the maximum chord rotation values at node 2 of the critical beam (V15) decreases about 30% and 20% for total drift values of 1.0% and 4.0%, respectively, but also the symmetry in the distribution of the plasticity along the beam length is lost, which tends to concentrate at the right node (under positive moment) of these members. Thus, the use of the simplified expression proposed in most guidelines and codes for quantifying plastic rotations may underestimate the deformation demands in beams where gravity loads assume an important role. Although local deformation demands are often estimated from inter-story drifts (Gupta and Krawinkler, 2000), the latter cannot equally account for the unsymmetrical distribution of rotation demands between both nodes of the beams. Figure 4.4 depicts the inter-storey drift ratio distribution along the height of building GB for global drift values of 1%, 2.5% and 4%, wherein it may be observed that no significant variation in the inter-storey drift values is observed with (NLA_G) and without (NLA_{NG}) the inclusion of gravity loads in the nonlinear analysis. This may be explained by the fact that inter-storey drifts reflect the mean distribution of local deformation demands along both nodes of every floor beams. As an example, if one considers the inter-storey drift values at the first storey of building GB for a global drift of 4.0%, values of 0.056 and 0.058 may be observed with and without the consideration of the influence of gravity loads, respectively. These values are indeed consistent with those obtained by taking the average rotation values at both nodes of the first floor beams, which are approximately (0.055+0.056)/2=0.056rad and (0.054+0.069)/2=0.06rad, with and without gravity loads, respectively.

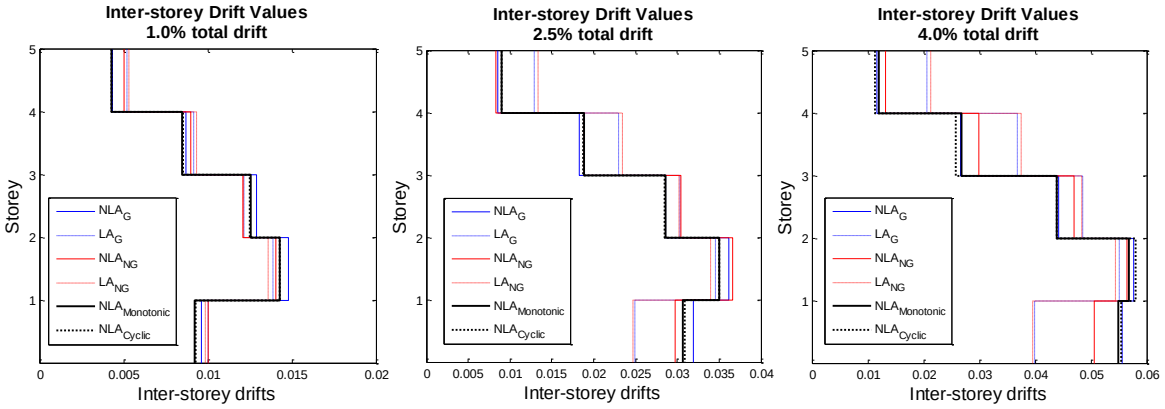

Figure 4.4 – Inter-storey drift ratio distribution along the height of building GB.

It should be noted that as the lateral stiffness and strength of the building increase (from buildings GB to SB3), an increasingly uniform distribution of plasticity along the height of the structure is observed. This behaviour reflects the development of a plastic

mechanism largely composed by beam hinging, which results in a more symmetrical distribution of rotational demands between both beam ends. Bojórquez et al. (2011) found similar results when assessing a set of buildings seismically designed according to the Mexico City Building Code, although referring that this equal distribution of rotation demands over the beams located at a particular story was due to the presence of rigid diaphragms.

With respect to the comparison of the various methods of quantifying the local deformation demands, it is observed from Figure 4.3 (b) that the approximate $AGM\text{-}DR_{NL}$ method using nonlinear analysis seems to underestimate the chord rotation demands in the most critical beams (V13, V14 and V15) in comparison to the EIM_{NL} method, particularly at the right node (node 2) of the beams. In fact, the $AGM\text{-}DR_{NL}$ method provides, as expected, values similar to those of the inter-storey drifts at the storey of these beams and does not have the ability to capture the unsymmetrical distribution of deformation demands between both nodes of the beams due to the effect of gravity loads. When the gravity loads are neglected, a perfect match is observed between both methods (Figure 4.3 (a)). In contrast, the $AGM\text{-}DR_{L}$ and the EGM_{L} methods yielded similar results when using linear analysis, although underestimating the demands at the lower stories of building GB in comparison to EIM_{NL}. These results are in agreement with the distribution of inter-storey drift ratios depicted in Figure 4.4. Similar findings were observed at the base of the first storey columns (P5, P10, P15 and P20), where linear analysis increasingly underestimated the chord rotation demands as the lateral deformation of the structure increased (Figure 4.5 (a)).

In order to evaluate the impact of the strength deterioration of steel members on the quantification of local deformation demands, the chord rotation demands are equally compared in Figure 4.3 with those obtained using the Ibarra et al. (2005) model. To include the influence of the cyclic deterioration of steel members, the parameters of the Ibarra et al. (2005) model were defined not only based on the monotonic behaviour of the members, using the Lignos and Krawinkler (2011) prediction equations, but also based on their cyclic envelopes, which were derived by conducting a prior pseudo-static nonlinear analysis of each single member using the SAC loading protocol (Krawinkler et al., 2000). More information on this procedure may be found in the work of Macedo et al. (2015). Moreover, it is demonstrated in Chapter 6 that the SAC loading protocol, which is representative of far-fault earthquakes, seems to lead to more conservative results in comparison with those obtained from the application of a set of real ground motion

records, whereas the monotonic response seems to match the responses obtained using loading protocols representative of near-fault earthquakes. Therefore, based on the above, it is expected that the modelling of the Ibarra et al. (2005) deterioration model, assuming both monotonic and cyclic responses, would lead to upper and lower bounds in the deviations of the deformation demand estimates, respectively, due to the deterioration of the members under real earthquake conditions. Hence, it can be observed from Figure 4.3 (b) that no substantial degradation of the GB building beams occurs for a global drift ratio of 4% when the deterioration model is defined assuming its monotonic response, and that a slight 12% increase in the rotation estimates of the most demanded beams (V13, V14 and V15) is obtained when assuming the cyclic envelope.

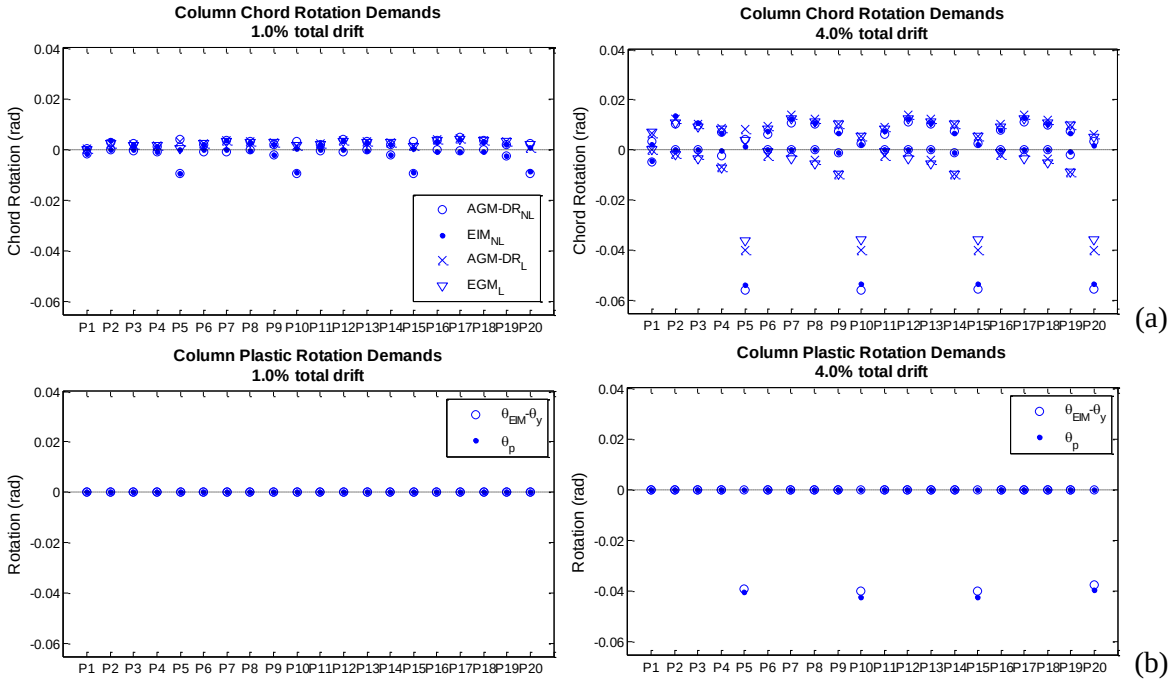

Figure 4.5 – Column deformation demands for building GB: (a) chord rotations; (b) and plastic rotations.

As far as the use of chord rotations as an alternative to plastic rotations is concerned, Figure 4.3 (c) and Figure 4.5 (b) demonstrate that it generally performs well in the prediction of plastic rotation demands, albeit some differences were observed at the left node (node 1) of the beams, which progressively reduced as the global drift increased. The elastic component of chord rotations was deducted to its total value so as to reproduce the plastic component of chord rotations to be compared with the plastic rotations. For comparison purposes, two approaches were adopted in the definition of the chord rotations at yielding: (i) the ASCE41-13- simplified approach, according to which the yielding chord rotation is defined for beams as:

$$\theta_y = M_{pl} L / 6EI \tag{4.10}$$

and for columns by,

$$\theta_y = M_{pl} L / 6EI \ \left(1 - N_{Ed} / N_{pl}\right) \tag{4.11}$$

where N_{ED} is the axial force installed in the element and N_{pl} is the expected axial capacity of the element; (ii) and the accurate approach, which consists in determining the actual value of the chord rotation at yielding at every step of the analysis. Since the ASCE41-13 simplified approach assumes that the member will develop a symmetric bending moment diagram, it does not include additional deflection due to shear deformation or second order effects, as already pointed out by Newell (2008), and thus may lead to non-conservative estimates of plastic rotations. Finally, from the linear analysis applicability point of view, consistent estimates of deformation demands using linear elastic analysis were seen to be only obtained for building SB3, despite the fact that EC8-3 and ASCE41-13 allow its application to all buildings for both the Significant Damage (SD) and Damage Limitation (DL) limit states and EC8-3 enables its use to buildings SB1 and SB2 at the Near Collapse (NC) limit state (Chapter 2). A further study is presented below with the objective of providing an insight into the evolution of the errors associated with the use of linear analysis and the accuracy of the various methods of quantifying local deformation demands for increasing levels of global drift ratios.

4.5 Prediction of the error associated with the use of linear analysis

The errors associated with the use of linear analysis in the quantification of local deformation demands will be determined both locally, at the critical element or storey that governs the safety of each building, and globally, considering the influence of all elements. Hence, the local error will be simply defined as the ratio between the reference quantity, Q_R, and the quantity under evaluation, Q_f, say our estimate, so that:

$$\Delta = Q_R / Q_f \tag{4.12}$$

and globally by adopting the Root Mean Square Error (*RMSE*) so as to aggregate the magnitudes of all local errors in the prediction:

$$RMSE = \sqrt{\frac{1}{n}\sum_{i=1}^{n}\left(Q_f / Q_R - 1\right)^2} \tag{4.13}$$

where n is the number of the element sections considered or the number of stories. The quantities Q_f and Q_R refer to different engineering demand parameters, as presented in the following subsections.

4.5.1 Errors in inter-storey drift predictions using linear analysis

The magnitude of the error in the estimation of inter-storey drifts when using linear analysis in comparison to reference nonlinear analysis is depicted in Figure 4.6. It can be seen that nonlinear analysis tends to concentrate plasticity at the first storey of each building and thus leads to higher inter-storey drift values at these levels in comparison to linear analysis. In turn, linear analysis tends to concentrate the demands at the top stories due to its inability to simulate internal force redistribution within the building as the lateral load increases. Thus, Figure 4.6 (a) shows how much linear analysis locally underestimates inter-storey drift demands at the first story in comparison to linear analysis. Two scenarios were considered: a case without gravity loads (*NG*) and another case with gravity loads (*G*). As expected, it is observed that both the error and the influence of gravity loads tend to be significantly reduced as the lateral stiffness increases from building GB to SB3.

Figure 4.6 (b) shows the *RMSE* calculated over all n stories of each building. Since the global error is expected to depend on the lateral distribution of forces initially imposed to the structure, three different lateral load patterns were considered: (i) a first one, designated as FP1, which is defined according to Annex B of EC8-3, so that:

$$F_i = \frac{m_i h_i^k}{\sum_1^n m_i h_i^k} V_b \tag{4.14}$$

where m_i are the storey masses, h_i are the heights of the masses m_i above the level of application of the seismic action (foundation or top of a rigid basement), k is an exponent that is function of the period of vibration of the structure, T, being 2.0 for $T \geq 2.5$ sec and 1.0 for $T \leq 2.5$ sec, while for values of T within this interval a linear interpolation shall be used, and V_b is the total base shear; (ii) a second one linearly proportional to the storey masses and heights, termed FP2; (iii) and a third one that is constant along the height of the buildings, designated by FP3. As one would might expect, the FP3 load pattern resulted in a higher overall error in comparison to the FP2 and FP1 load patterns, although the differences in the error estimates are not totally significant and tend to get very close as the total drift values increase.

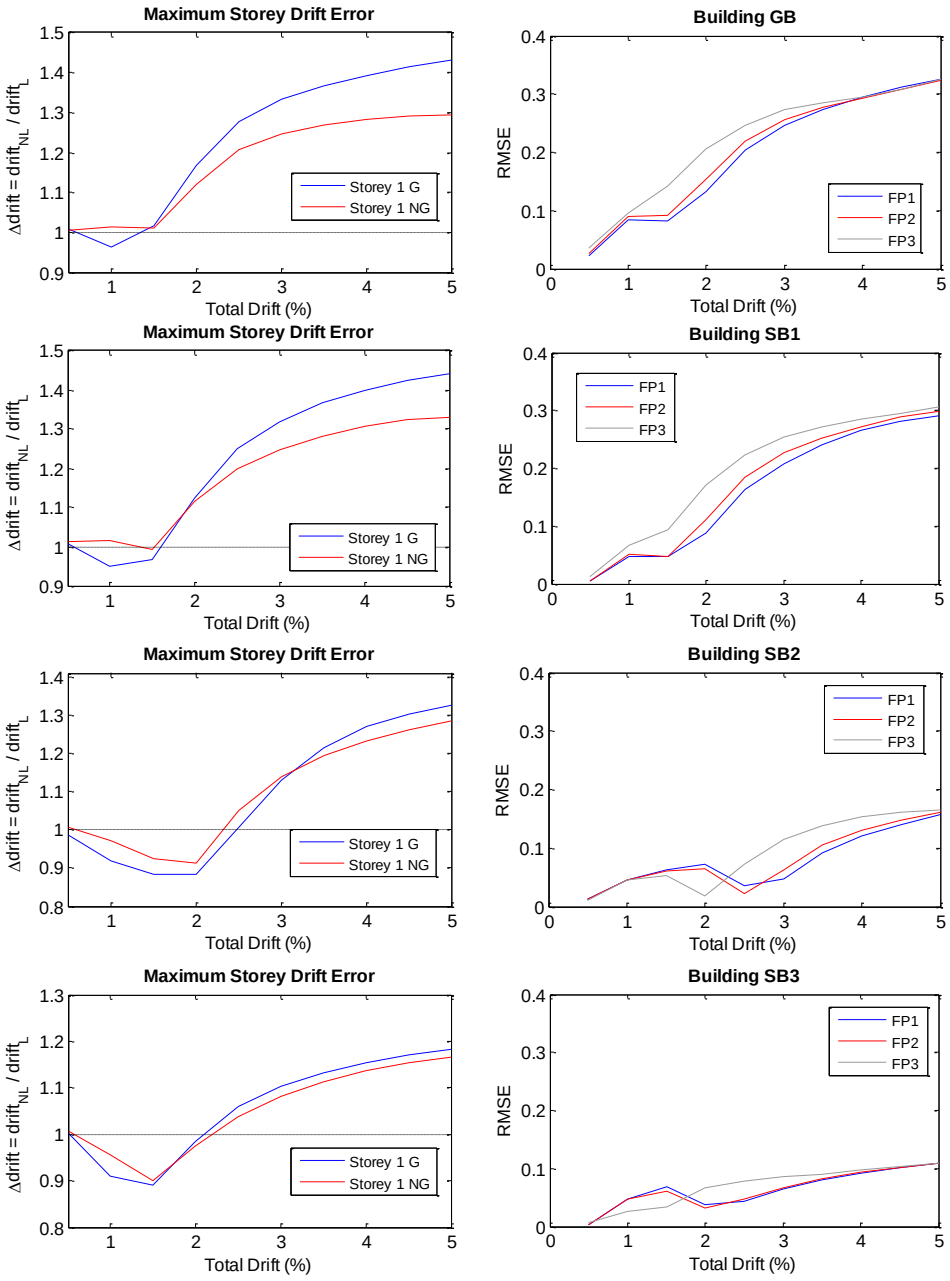

Figure 4.6 – Local and global linear vs nonlinear drift errors for buildings GB to SB3 (upper-to-lower figures) and increasing levels of total drifts: (a) ratio between nonlinear and linear inter-storey drifts at the first storey of each building; (b) and *RMSE* of the inter-storey drifts for load patterns FP1, FP2 and FP3.

Moreover, as shown in Chapter 2, total drift values of 0.7%, 1.12% and 3.31% correspond to the DL, SD and NC limit states of building GB when subjected to a Type 1 and Zone 3 seismic action (Lisbon) defined in the Portuguese National Annex of EC8 and considering the structure located in a soil type B. Thus, no major differences are observed in the inter-storey drift estimates, both in local and global terms, at the DL and SD limit states, being the latter limit state associated to an error of less than 10%. However, in the NC limit state, the local first storey error increased up to 40% and 20%, with and without

the influence of gravity loads, respectively, although the global error may be seen to be of about 25%. Similar conclusions may be drawn for building SB1, while in the case of buildings SB2 and SB3 the maximum local and global errors observed were of about 10%, indicating that linear analysis seems to perform well in these circumstances.

4.5.2 Errors in chord rotation predictions using linear analysis

With the use of chord rotations as an alternative to plastic rotations already validated, the level of error incurred when adopting linear analysis to estimate this deformation parameter is now assessed. Figure 4.7 depicts the comparison of the results obtained from the EGM_L method using linear analysis and the EIM_{NL} method using nonlinear analysis. It may be readily concluded that, generally speaking, linear analysis does not provide accurate estimates of local chord rotation demands, with levels of inaccuracy that can reach more than 50% for both beams and columns. This observation is verified even for buildings SB1 and SB2, which have been seismically designed. Furthermore, and in line with the findings previously extracted from Figure 4.3, the highest chord rotation prediction errors are found at the right and most demanded node of the beams and also when the shear deformation imposed by gravity loads play a critical role in the total deformation of these members. This is not the case of building SB3, for which almost similar prediction errors were obtained with and without considering the influence of gravity loads. Additionally, with respect to the chord rotation prediction errors at the base of the first storey columns, wherein plasticity is expected to be developed (Figure 4.5), it may be noted that similar results were obtained comparing to those of the inter-storey drifts at the first storey of the analysed buildings. In fact, it may be seen that although for total drift values in the range of 0.5% to about 2.0% the local inter-storey drift prediction errors seem to be systematically lower than the local chord rotation ones, for higher values of total drift ratios the local inter-storey drift prediction errors tend to match or even slightly exceed them. As a result, the linear analysis procedures proposed by EC8-3 to verify the seismic safety of existing steel buildings seem to potentially lead to erroneous deformation demand estimates, particularly as the global drift ratios increase. Still, these results need to be confronted with those obtained by applying linear and nonlinear methods of analysis to the analysed buildings, so as to understand how reliable this prediction error estimates actually are.

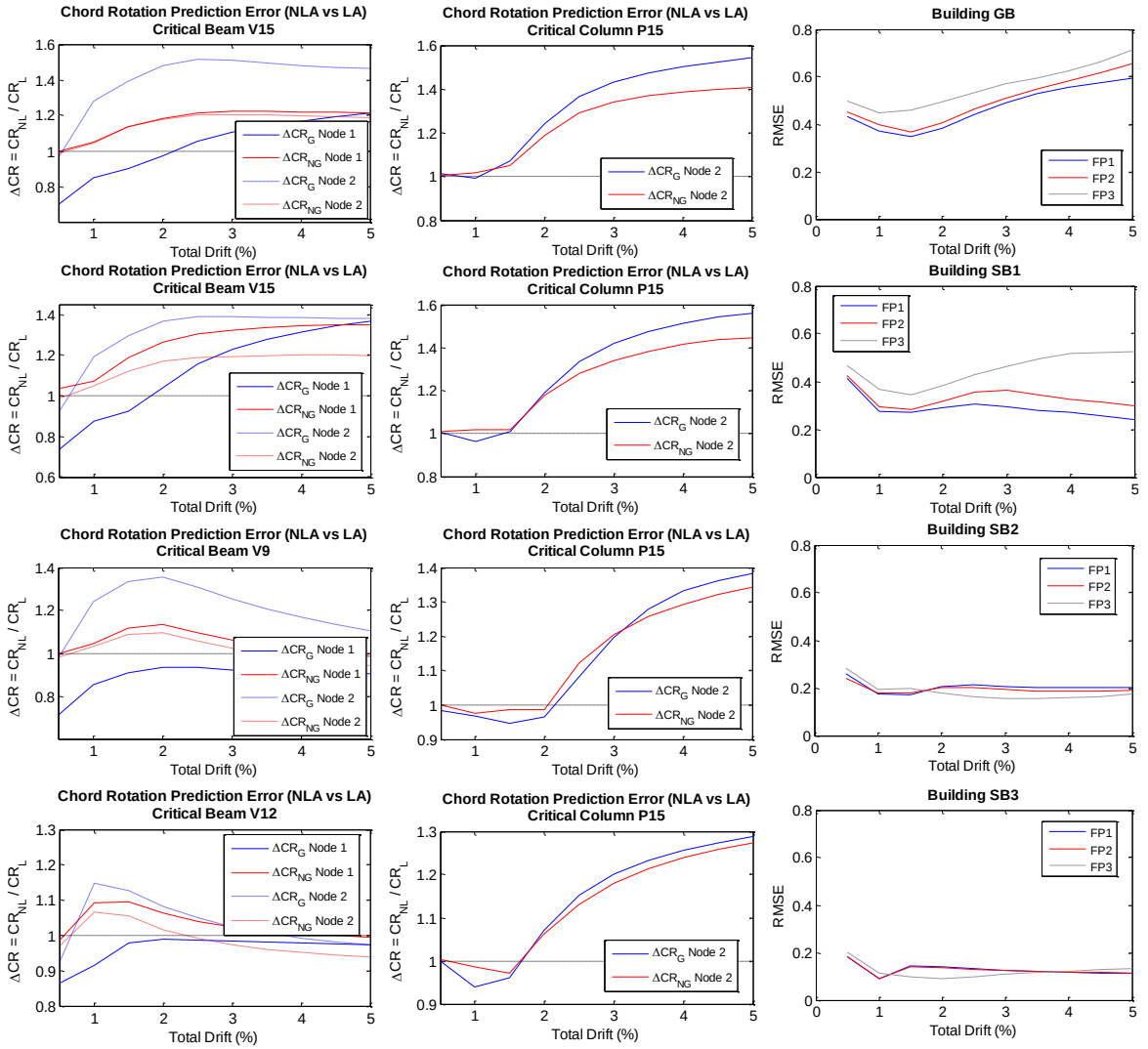

(a) (b) (c)

Figure 4.7 – Local and global nonlinear chord rotation *vs* linear chord rotation errors for buildings GB to SB3 (upper-to-lower figures) and increasing levels of total drifts: (a) error in the critical beam deformation demand estimates; (b) error in the critical column deformation demand estimates; (c) and *RMSE* for the beam deformation demand estimates and load patterns FP1, FP2 and FP3.

4.5.3 Errors in chord rotation predictions by applying linear and nonlinear methods of analysis

EC8-3 prescribes various methods of analysis for the seismic safety assessment of existing buildings, which can range from simpler force-based elastic methods, as the well-known lateral force method (LF) or the modal response spectrum method (MRSA), to more complex nonlinear methods, as the pushover or the time-history methods of analysis. By allowing the analyst to select a method of analysis from a wide range of alternatives, the Eurocode intends to provide more freedom to the analyst and encourage engineering judgment. Additionally, EC8-3 allows for the use of the *q*-factor approach, with a default

value of the behaviour factor, *q*, equal to 2.0 for steel structures. This value can be increased by about one-third when checking for the NC limit state or to higher values if analytically justified. However, the EC8-3 itself refers to this type of approach as generally not suitable to check the NC limit state and, with such small values of *q*, is in most cases, if not in all, expected to be too conservative.

A comparative analysis will be now carried out taking into account the main analysis procedures proposed by EC8-3, the results of which are presented in Figure 4.8 in terms of both local and global prediction errors. The pushover analyses (PA) were conducted using the EC8 N2 method considering a lateral force pattern proportional to the 1st mode shape ($PA_{1st}N2$) and a constant lateral force pattern along the height ($PA_{const}N2$), whereas the nonlinear time-history analysis (THA) has been performed considering 15 sets of seven ground motion records scaled to match the EC8 elastic spectrum defined, again, for a Portuguese type 1 and Zone 3 seismic action (Lisbon) located in a soil type B (Chapter 3). An additional criterion was included in the selection of each individual record, which consisted of imposing mismatch limits relative to the target spectrum of ±50%, being the respective group of ground motion records designated as G7I. This additional measure has been demonstrated in Chapter 3 to significantly reduce the variability in the structural response estimates. The analyses were performed for the DL, SD and NC limit states preconized by EC8-3.

It may be firstly observed from Figure 4.8 that the errors in the order of 50% previously found at the critical beams of buildings GB and SB1 (Figure 4.7 (a)), which were obtained by setting identical global drift ratios in both linear and nonlinear models, decreased to about 40% and 30%, respectively, when applying static linear and nonlinear methods of analysis, defined by the ratios between $LF/PA_{1st}N2$ and $LF/PA_{const}N2$. These observations could be explained by the fact that, for the buildings analysed in this study, the LF method itself lead to global drift ratios greater than those obtained from $PA_{1st}N2$ and $PA_{const}N2$ at the various limit states (Chapter 2). Nevertheless, the prediction errors at the NC limit state are still considerable, i.e. greater than 25% for most of the critical beams of buildings GB, SB1 and SB2. In turn, when comparing the MRSA results with those obtained from THA the following conclusions may be drawn: (i) if no additional control of the spectral mismatch is included in the selection of the set of ground motions (group G7), the greater variability in the chord rotation estimates may lead to prediction errors higher than those previously obtained for buildings GB and SB1, both locally at the most critical beam and globally as represented by the *RMSE* parameter.

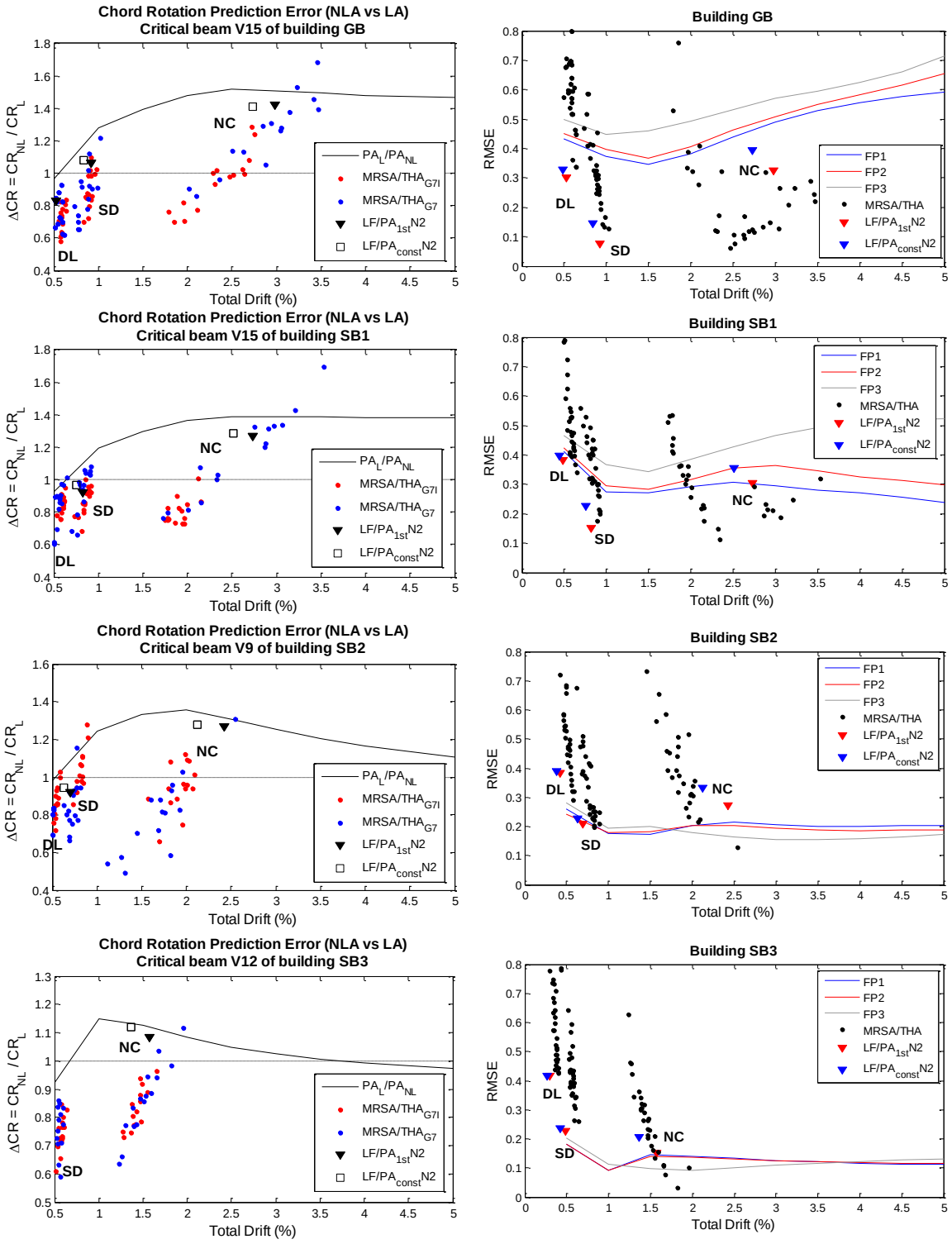

Figure 4.8 – Local and global prediction errors in the chord rotation estimates considering linear and nonlinear methods of analysis obtained for all the analysed buildings.

On the other hand, the linear MRSA generally leads to more conservative chord rotation estimates comparing to THA in buildings SB2 and SB3; (ii) if the additional control of the spectral mismatch is included in the selection of the set of ground motions (group G7I), the chord rotation prediction errors are considerably reduced, being the

underestimation of local deformation demands using linear analysis not greater than 20% for the most critical beam in all buildings; (iii) finally, the higher *RMSE* values may be explained by the influence of higher modes and by the fact that, as already mentioned, MRSA generally leads to higher estimates of global response in comparison with THA. Therefore, from the obtained results one may conclude that linear elastic analysis may provide unreliable estimates of chord rotation in buildings with the characteristics similar to those of buildings SB1 and GB, leading to levels of inaccuracy of the order of 30 to 40%. Moreover, although significant levels of prediction errors were observed for building SB2 using static methods of analysis, these were reduced due to the more conservative character of MRSA comparing to THA. Nonetheless, according to EC8-3, linear analysis procedures may be applied only if a set of applicability criteria is verified. Thus, the effectiveness of the local deformation demand prediction errors in the seismic safety assessment process has to be assessed by confronting these prediction errors with the applicability of linear analysis.

4.6 Linear analysis applicability criteria

4.6.1 Evaluation of the EC8-3 linear analysis applicability criteria

Part 3 of Eurocode 8 states that the applicability of linear analysis should be restricted to structures that comply with specific criteria related with the distribution of inelastic demands within the structure. In other words, EC8-3 allows the use of linear analysis for the estimation of local deformation demands in existing buildings if the ratio between the maximum and minimum demand-to-capacity ratios (*DCR*), defined in terms of bending moments in moment-resisting frames, over all primary elements, does not exceed a certain value ranging from 2 to 3. Only elements with *DCR* values higher than 1.0, say elements expected to respond inelastically, should be considered. Additionally, EC8-3 prescribes that, around beam-column joints, the *DCR* ratios only need to be evaluated at the sections where plastic hinges are expected to form on the basis of the comparison of the sum of the beam flexural capacities to that of columns. Since all buildings of the present case study verify the EC8-1 (CEN, 2004) weak-beam / strong-column condition at every joint, with the exception of top floor joints, only the *DCRs* of beams and of first storey columns (at the base cross-section) need to be considered. It should be referred that, conceptually, on the basis of the equal-displacement rule, the *DCR* ratios are expected to be about equal to the demand chord rotation ductility ratios.

Once again, pushover analyses were carried out for the various analysed buildings, simply assuming the linear elastic behaviour of the structures, with the goal of understanding the range of applicability of linear procedures with increasing levels of global drift ratios. Figure 4.9 depicts the obtained results assuming that linear analysis are not applicable if the ratio between the maximum and minimum *DCRs* is greater than 3. Two main observations promptly stand out from Figure 4.9. Firstly, a good perspective of the distribution of inelastic demands over the height of the building is obtained when evaluating the applicability criteria. In other words, the ladder shape of the applicability evaluation trend not only reflects the uniform concentration of the plasticity along the various floors of the building, but also the asymmetric formation of plastic hinges between the right and left nodes of the beams. As an example, the gap observed in the applicability evaluation trend of building GB between the total drift values of 4.5% and 5% is due to the onset formation of plastic hinges in the left node of the top floor beams, which led to a minimum *DCR* value of approximately 1.0. In the case of building SB3, the uniform distribution of plasticity along its height led to an applicability evaluation trend with only one constant plateau below the threshold of 1.0, thus allowing the applicability of linear analysis for total drift values up to 5%.

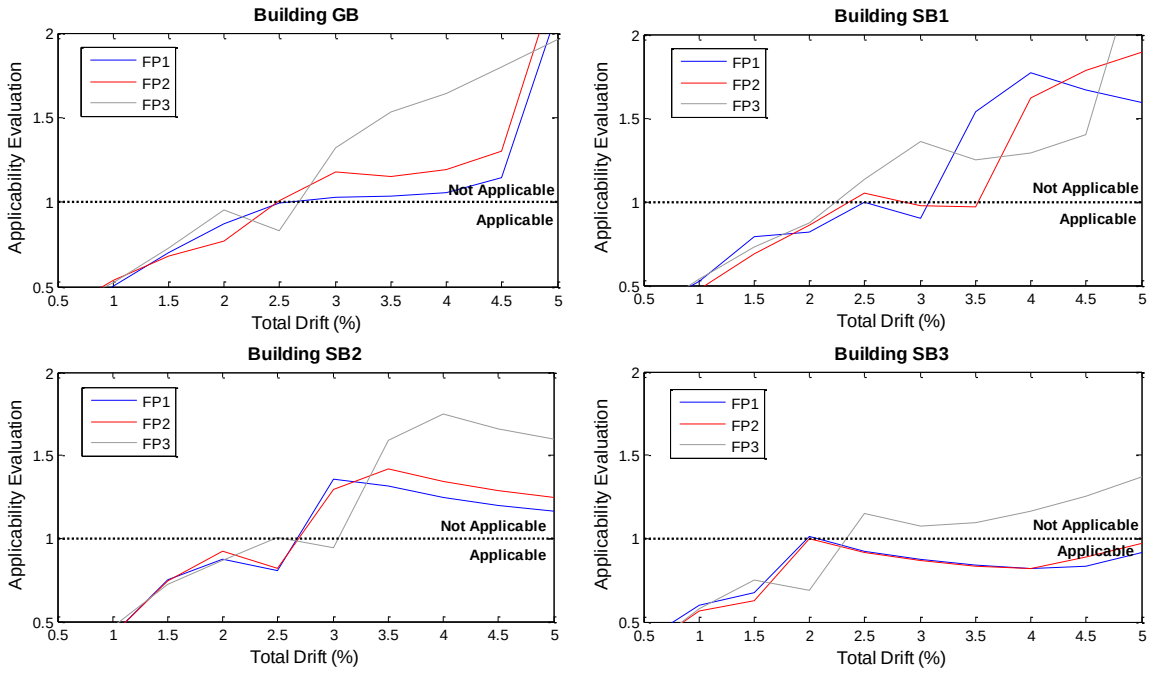

Figure 4.9 – Influence of the various force patterns in the applicability of linear analysis according to EC8-3.

Secondly, the EC8-3 applicability criterion appears to lead to somehow incoherent results. Not only it may be seen that the range of applicability of building SB1 is larger

than building SB2, despite its higher lateral stiffness and strength, but also in some particular cases linear analysis cannot be used at a certain total drift value, although being applicable at higher values of global drift, as it is the case of building SB1 for the FP2 lateral force pattern and a total drift value of 2.5%. Moreover, it can be seen that the EC8-3 criterion is considerably affected by the distribution of inertial forces along the height of the building, having the constant force pattern (FP3) resulted in more conservative results. These results appear to be in line with those presented in Chapter 2, wherein it has been demonstrated that although linear analysis could be used to assess the seismic safety of building SB1 at the NC limit state using the simplified LF method, the MRSA method failed its applicability verifications. It is expected that, due to the influence of higher modes, the MRSA method would lead to a distribution of forces along the height of the building closer to lateral force pattern FP3.

Furthermore, so as to understand the actual impact of the verification of the linear analysis applicability criteria in the accuracy of the chord rotation estimates, Figure 4.10 depicts the local chord rotation prediction error as a function of the different EC8-3 linear analysis applicability criteria, which are based on different DCR_{max}/DCR_{min} ratios. The ΔCR_G node 1 curves exhibited in Figure 4.7 (a) for each building are again represented in Figure 4.10 (a) at their respective fundamental periods of vibration, while the prediction errors displayed for the remaining periods of vibration have been interpolated so as to give an idea of possible evolution of the error with the increase in the lateral stiffness and strength of the building. Figure 4.10 (b) to (d) provide a picture of the evolution of the chord rotation prediction errors with the period of vibration of the buildings and the global drift ratios only in the cases where linear analyses are applicable in accordance to EC8-3 (Figure 4.9) (i.e. the blank region represents the cases where the linear analysis is not applicable). This way, one may actually assess the error associated with the use of linear analysis according to EC8-3. As mentioned above, EC8-3 allows the use of linear analysis if the ratio between the maximum and minimum *DCRs* does not exceed a certain value ranging from 2 to 3, being recommended a value of 2.5. Each one of these limit values has been assessed, being concluded that just when assuming an applicability limit value of 2.0, the local chord rotation prediction errors are within reasonable values. Still, the consideration of the 2.0 applicability limit value seems to be quite conservative in the case of buildings with higher lateral stiffness and strength, as it merely allows the use of linear analyses in building SB3 for global drift ratios below 2% (Figure 4.10 (d)), although this building exhibits an error lower than 15% regardless the level of deformation demand

observed (Figure 4.10 (a)). Also, the 2.0 limit would allow the use of linear analysis in building GB at global drift ratios that are associated with chord rotation prediction errors in the order of 30%. On the other hand, when the 2.5 and 3.0 applicability limit values were adopted, not only chord rotation prediction errors of about 40% were found in building GB, but also the previously referred incoherent results related to the inability of using linear analysis at a certain total drift value and the possibility of using them at higher total drift values are again observed (Figure 4.10 (b) and (c)). In Chapter 2 it was shown that the simplified linear LF method of analysis could be adopted at the NC limit state for both SB1 and SB2 buildings, which corresponds to global drift ratios of 3.12% and 2.30%, respectively. These values are in agreement with those presented in Figure 4.10 and demonstrate that the use of the EC8-3 linear analysis procedures may result in underestimates of local deformation demands of about 40%.

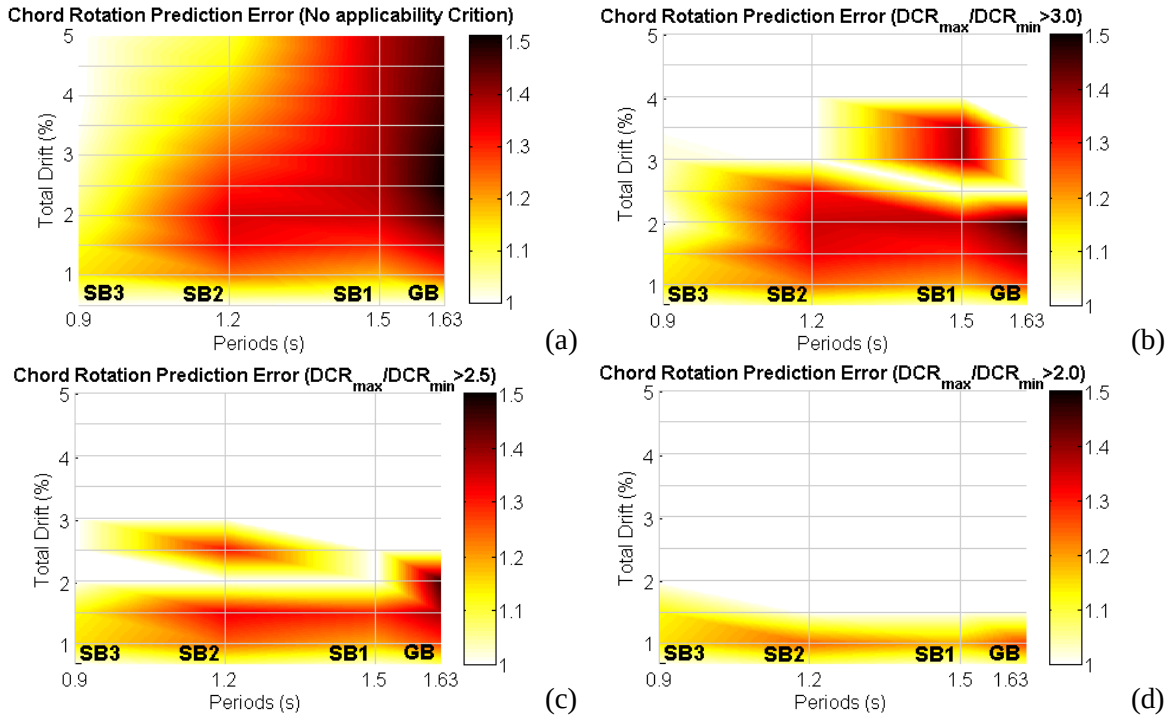

Figure 4.10 – Local chord rotation prediction errors as a function of different linear analysis applicability criteria: (a) no criteria; (b) DCR_{max}/DCR_{min} > 3.0; (c) DCR_{max}/DCR_{min} > 2.5; (d) and DCR_{max}/DCR_{min} > 2.0. The blank region represents the cases where linear analysis is not applicable.

4.6.2 Proposal of alternative criteria for evaluating the applicability of linear analysis procedures

While the ASCE41-13 linear analysis applicability criteria was shown in Chapter 2 to be too restrictive, EC8-3 allows the use of linear procedures in situations where significant local response deviations are expected relative to the ones obtained using

nonlinear analysis. Moreover, the EC8-3 applicability criteria was shown to be very dependent on the lateral load pattern adopted. Based on these observations, alternative linear analysis applicability criteria were sought and a proposal of a methodology defined by the verification of two criteria is herein discussed.

The first criterion aims at evaluating the regularity in the distribution of the plastic behaviour within the structure through the comparison of the maximum expected level of demand within a storey *i*, $mDCR_i$, with the maximum level of demand within storeys *i-1* and *i+1* that are immediately adjacent. The components of a storey *i* are herein characterized by the beam elements located at that floor. The main advantages of this criterion in comparison to the one proposed by EC8-3 are: (i) the disregarding of the minimum *DCR* value, which does not really reflects the level of demands in a storey, especially in cases where the effect of gravity loads is relevant, and may lead to somehow incoherent situations as previously observed for buildings SB1 and SB2; (ii) and the ability to provide a preliminary idea of the zones of the structure where higher concentrations of plasticity are expected to occur. Figure 4.11 (a) displays the results obtained for buildings GB and SB3. According to the distribution of inter-storey drifts over the height shown in Figure 4.4, one can conclude that the higher $mDCR_i/mDCR_{i\pm1}$ ratios are observed between storeys 4 and 3. Conversely, as the $mDCR_i/mDCR_{i\pm1}$ ratios tend to unity, it is found that the distribution of plasticity along the various levels of the structure will tend to become more uniform. The influence of the lateral force patterns FP1, FP2 and FP3 was equally evaluated, being observed that these will have a significant impact in the proposed criterion, namely in the most demanded storeys. In fact, setting building SB3 as benchmark due to its admissible levels of error, both locally and globally, excluding the $mDCR_i/mDCR_{i\pm1}$ ratio calculated between storeys 5 and 4 and considering the influence of the various lateral force patterns, the following applicability condition is proposed:

$$\frac{mDCR_i}{mDCR_{i\pm1}} \leq 1.30 \tag{4.15}$$

In other words, linear elastic methods of analysis may be applied if the ratio between the maximum *DCRs* of two adjacent storeys does not exceed more than 30%.

On the other hand, the second criterion aims at evaluating how asymmetric is the distribution of plasticity within a floor *i*. It was shown that symmetric distributions of demands between the two nodes of a member existing in a floor, which are typically due to the reduced influence of gravity loads and the higher lateral stiffness and strength of the building, produce better estimates of local deformation demands when comparing to

nonlinear analysis results. Hence, this second criterion consists of calculating the ratio between the maximum expected *DCR* within a floor *i*, $mDCR_i$, and the mean *DCR* at that same floor, $\overline{DCR_i}$. Only *DCRs* greater than 1.0 should be considered. Figure 4.11 (a) demonstrates that as the lateral stiffness and strength of the buildings increases, the ratio $mDCR_i/\overline{DCR_i}$ reduces. Also, its maximum value tends to be verified for every floor practically at the same global drift ratio, implying that a more uniform distribution of plasticity along the height would occur. Once again, setting building SB3 as benchmark and excluding the results obtained at the 5th floor, the following applicability condition is proposed:

$$\frac{mDCR_i}{\overline{DCR_i}} \leq 1.25 \tag{4.16}$$

In addition to the verification of the proposed applicability conditions, the EC8-1 (CEN 2004) weak-beam / strong-column condition at every joint should be checked. Otherwise, linear analysis is expected to fail in predicting the development of a possible soft-storey mechanism.

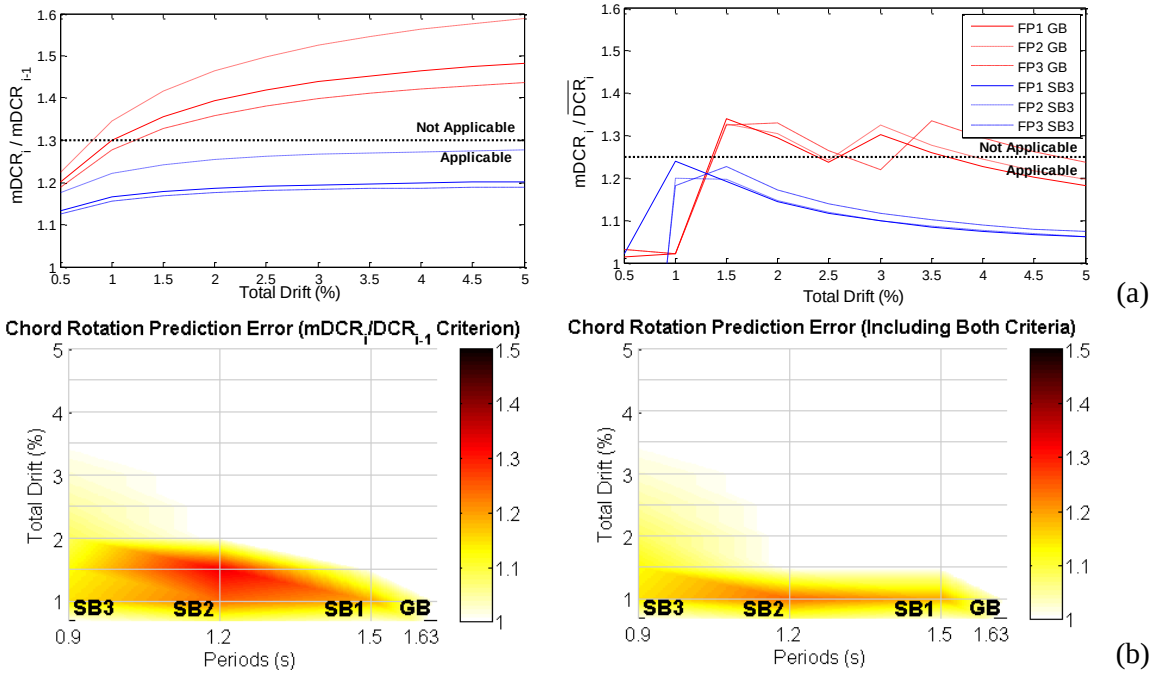

Figure 4.11 – (a) Applicability of linear analysis according to both conditions of the proposed methodology, (b) and corresponding local chord rotation prediction errors. The blank region represents the cases where linear analysis is not applicable.

Figure 4.11 (b) shows the evolution of the chord rotation prediction errors with the period of vibration of the buildings and the global drift ratios when the proposed applicability criteria are applied. It may be concluded that the use of the proposed criteria

is not only associated with a lower and more admissible level of error in the chord rotation estimates (below 20%), but also it is less stringent when compared to EC8-3, particularly in the case of robust buildings with higher lateral stiffness and strength (building SB3), which are expected to develop more stable collapse mechanisms. Despite the conclusions presented herein, further studies on the evaluation of these applicability criteria should be carried out, especially in the case of structures with different geometry, level of irregularity and hysteretic dissipation characteristics.

4.7 Conclusions

The quantification of reliable local deformation demands plays a crucial role in the seismic safety assessment process of a building. Various methods of quantifying these type of demands have already been discussed and evaluated by Romão et al. (2010b), although merely focusing on RC buildings and nonlinear analysis procedures. According to EC8-3, local deformation demands are defined in terms of plastic rotations, regardless of the type of analysis procedures adopted, thus confronting the analyst with a rather ambiguous scenario: how can one perform the safety verifications when using linear analysis if plastic rotations cannot be obtained from this type of analysis? The present work aimed to address this issue and presented chord rotations as a rational alternative to plastic rotations. It has been shown that chord rotations agree almost perfectly with plastic rotations, providing errors lower than 10% in the most demanded regions of the structural members.

However, generally speaking, linear analysis was seen to lead to rather unreliable chord rotation estimates comparing to those of nonlinear analysis, particularly in buildings with lower lateral stiffness and strength, leading to levels of inaccuracy of up to 40%. Even when the linear analysis applicability criteria proposed by the EC8-3 was verified, such high level of error was observed. As a result, an alternative methodology for assessing the applicability of linear analysis was proposed. This methodology not only accounts for the regularity in the distribution of plasticity over the height of the building, but also takes into consideration the asymmetric distribution of plasticity within the beams of a floor. A maximum error in the chord rotation estimates of about 20% was observed when using the proposed methodology. Still, it may be noted that the linear analysis applicability criteria is not expected to be satisfied by many existing steel buildings and thus the analysts will be unavoidably driven to carry out nonlinear analysis, despite not being, in most cases, acquainted with this type of analysis procedures.

Finally, a remark should be made regarding the common practice of evaluating local deformation demands simply in terms of inter-storey drifts. Although providing a fair picture of the level of inelastic demand within a storey, this approach is unable to capture the asymmetric concentration of plastic demands between the beam member ends due to the effect of gravity loads. Since code-based safety verifications shall be conducted individually at each member, this limitation may have a significant impact in the safety assessment of existing buildings.

4.8 Acknowledgments

This work was performed within the framework of the research project 'Development and calibration of seismic safety assessment methodologies for existing buildings according to the Eurocode 8 – Part 3' founded by Foundation of Science and Technology (FCT) of Portugal.

4.9 References

Akkar S, Miranda E (2005) Statistical evaluation of approximate methods for estimating maximum deformation demands on existing structures, Journal of Structural Engineering, 131, 160-172.

ASCE (2014) Seismic evaluation and retrofit of existing buildings (ASCE/SEI 41-13), American Society of Civil Engineers.

Bertero RD, Bertero VV (2002) Performance-based seismic engineering: the need for a reliable conceptual comprehensive approach, Earthquake Engineering and Structural Dynamics, 31, 627–652.

Bojórquez E, Terán-Gilmore A, Ruiz S, Reyes-Salazar A (2011) Evaluation of structural reliability of steel frames: Interstory drift versus plastic hysteretic energy, Earthquake Spectra, 27, 661-682.

Browning J, Warden B, Matamoros A, Lepage A (2008) Global and local seismic drift estimates for RC frames, Engineering Structures, 30, 1262–1271.

Bruneau M, Uang CM, Whittaker A (1998) Ductile design of steel structures, McGraw-Hill.

Calabrese A, Almeida JP, Pinho R (2010) Numerical issues in distributed inelasticity modeling of RC frame elements for seismic analysis, Journal of Earthquake Engineering, 14, 38-68.

Castro JM, Dávila-Arbona F, Elghazouli A (2008) Seismic design approaches for panel zones is steel moment frames, Journal of Earthquake Engineering, 12, 34-51.

CEN (2004) ENV 1998-1 Eurocode 8: Design of structures for earthquake resistance - Part 1: General rules, seismic actions and rules for buildings, European Committee for Standardization.

CEN (2005) ENV 1998-3 Eurocode 8: Design of structures for earthquake resistance - Part 3: Assessment and retrofitting of buildings, European Committee for Standardization.

D'Aniello M, Landolfo R, Piluso V, Rizzano G (2012) Ultimate behavior of steel beams under non-uniform bending. Journal of Constructional Steel Research, 78, 144-158.

Gioncu V (2000) Framed structures. Ductility and seismic response. General Report, Journal of Constructional Steel Research, 55, 125–154.

Gioncu V, Mazzolani F (2002) Ductility of seismic resistant steel structures, Spon Press, Taylor & Francis Group.

Gioncu V, Petcu D (1997) Available rotation capacity of wide-flange beams and beam-columns, Journal of Constructional Steel Research, 43, 219–244.

Grecea D, Dinu F, Dubina D (2004) Performance criteria for MR steel frames in seismic zones, Journal of Constructional Steel Research, 60, 739–749.

Günay MS, Sucuoglu H (2010) An improvement to linear-elastic procedures for seismic performance assessment, Earthquake Engineering and Structural Dynamics, 39, 907-931.

Günay MS, Sucuoglu, H (2009) Predicting the seismic response of capacity-designed structures by equivalent linearization, Journal of Earthquake Engineering, 13, 623-649.

Gupta A, Krawinkler H (2000) Behaviour of ductile SMRFs at various seismic hazard levels, Journal of Structural Engineering, 126, 98-107.

Ibarra LF, Medina RA, Krawinkler H (2005) Hysteretic models that incorporate strength and stiffness deterioration, Earthquake Engineering and Structural Dynamics, 35, 1489-1511.

Kosmopoulos A, Fardis M (2007) Estimation of inelastic seismic deformations in asymmetric multi-storey RC buildings, Earthquake Engineering and Structural Dynamics, 36, 1209–1234.

Krawinkler H, Gupta A, Medina R, Luco N (2000) Development of loading histories for testing of steel beam-to-column assemblies, Report prepared for the SAC Steel Project founded by the Federal Emergency Management Agency, Stanford University.

Lignos DG, Krawinkler H (2011) Deterioration modelling of steel components in support of collapse prediction of steel moment frames under earthquake loading, Journal of Structural Engineering, 137, 1291-1302.

Macedo L, Araújo M, Castro JM (2015) Comparison of modelling strategies for steel structures under cyclic loads, Proceedings of the 8th International Conference of Behaviour of Steel Structures in Seismic Areas.

Miranda E, Reyes CJ (2002) Approximate lateral drift demands in multi-storey buildings with nonuniform stiffness, Journal of Structural Engineering, 128, 840-849.

Mpampatsikos V, Nascimbene R, Petrini L (2008) A critical review of the R.C. frame existing building assessment procedure according to Eurocode 8 and Italian Seismic Code. Journal of Earthquake Engineering, 12, 52-82.

Newell JD (2008) Cyclic behaviour and design of steel columns subjected to large drift, Ph.D. Dissertation, University of California.

Panagiotakos T, Fardis M (1999) Estimation of inelastic deformation demands in multi-storey RC frame buildings, Earthquake Engineering and Structural Dynamics, 28, 501-528.

Paret TF, Searer GR, Freeman SA (2011) ASCE 31 and 41: Apocalypse Now. Structures Congress 2011.

PEER (2011) OpenSees: Open system for earthquake engineering simulation, Pacific Earthquake Engineering Research Center, Universtiy of California.

Pinto PE, Franchin P (2008) Assessing existing buildings with Eurocode 8 Part 3: a discussion with some proposals, Background documents for the "Eurocodes: Background and applications" workshop.

Priestley MJN, Calvi CM, Kowalsky MJ (2007) Displacement-Based Seismic Design of Structures, IUSS Press, Pavia, Italy.

Romão X, Delgado R, Costa A (2010b) Practical aspects of demand and capacity evaluation of RC members in the context of EC8-3, Earthquake Engineering and Structural Dynamics, 39, 473–499.

Romão X, Delgado R, Guedes J, Costa A (2010a) A comparative application of different EC8-3 procedures for the seismic safety assessment of existing structures, Bulletin of Earthquake Engineering, 8, 91–118.

Ruiz-García J, Miranda E (2006) Inelastic displacement ratios for evaluation of structures built on soft soil sites, Earthquake Engineering and Structural Dynamics, 35, 679–694.

Toranzo-Dianderas L (2009) Evaluation of the ASCE 41 linear elastic procedure for seismic retrofit of existing structures: Pros and cons of the method, Proceedings of the 2009 ATC & SEI Conference on Improving the Seismic Performance of Existing Buildings and Other Structures.

Whittaker S, Huang Y (2007) Simplified response analysis procedures, Background document of FEMA P-58/BD-3.7.4, Federal Emergency Management Agency

Chapter 5

Simplified procedure for the estimation of local inelastic deformation demands

Araújo M, Castro JM (2017) Simplified procedure for the estimation of local inelastic deformation demands for seismic performance assessment of buildings. Earthquake Engineering and Structural Dynamics, 46(3):491-514.

5.1 Summary

The implementation of performance-based design and assessment procedures in seismic codes leads to the need for an accurate estimation of local component demands. According to part 3 of Eurocode 8 (EC8-3) safety verifications should be always conducted in terms of plastic rotations even when linear-elastic methods of analysis are used. A simplified procedure that allows for the estimation of beam inelastic deformation demands using linear-elastic methods of analysis in an expeditious and conservative way is presented herein. A number of moment-resisting steel frames designed according to different criteria and exhibiting different column-to-beam moment ratios were analysed and used for the derivation of the proposed procedure. A comparative study between alternative methods of quantifying inelastic deformation demands using linear analysis is additionally carried out.

5.2 Introduction

Linear-elastic methods of analysis assume critical relevance in the context of the seismic safety assessment and rehabilitation of existing structures. Despite the broad agreement that nonlinear-based procedures are a better tool to assess existing buildings, linear-elastic procedures are, and will continue to be, used due to its relative simplicity and acquaintance to structural engineers (Paret et al., 2011). The survey presented in Chapters

1 and 2 among Portuguese practitioners revealed that a significant number of engineers (42%) is still not familiar with nonlinear procedures and only 20% of those who are have already applied this type of analysis in practice. Current guidelines and codes that specifically provide guidance for the seismic safety assessment and rehabilitation of existing buildings, such as the part 3 of Eurocode 8 (EC8-3) (CEN, 2005) or the American ASCE41-13 (ASCE, 2014), allow the use of both static and dynamic linear methods of analysis if a set of applicability criteria is previously verified. In a comprehensive study on the accuracy of linear analysis in predicting the nonlinear response of existing steel buildings, Chapters 2 and 4 have shown that the EC8-3 linear procedures systematically provide unreliable local deformation demands, with inaccuracy levels that can reach up to 40% even when the linear analysis applicability criteria is ensured. Similarly, Kunnath et al. (2004) demonstrated that linear procedures, as recommended in the American standard, do not consistently yield accurate inter-storey drift estimates and concluded that additional research is still needed to improve and enhance current code provisions before they can be used in routine practice.

The estimation of the maximum nonlinear deformation demands of existing buildings using linear analysis may be performed based on two distinct conceptual approaches, in line to what are the basis of various nonlinear static procedures (Akkar and Miranda, 2005; Lin and Miranda, 2009): the modification factor approach and the equivalent linearization approach. In the former approach, modification factors are applied to static linear analysis lateral force patterns so as to convert the linear system deformation demands into nonlinear demands. This is the approach followed by EC8-3, according to which the lateral force pattern applied to the structure under analysis should be corrected by a factor that depends on the type and period of vibration of that same structure. A factor of 1.0 should be adopted for low and medium frequency structures, recognizing the well-known equal displacement rule (Ruiz-Gárcia and Miranda, 2003), while a factor of 0.85 is proposed for high frequency structures, which are known to exhibit inelastic displacement demands that are significantly higher than their elastic counterparts (Kumar et al., 2011). Equally, ASCE 41-13 adopts specific modification factors that are function of the period of structure and the strength ratio R. On the other hand, in the second approach, a linear system with equivalent damping and stiffness is used to represent the ultimate response of a nonlinear system. Based on this, Günay and Sucuglou (2009; 2010) recently proposed an improved linear elastic procedure that consists on reducing the stiffness of structural members that are expected to respond in the inelastic range in a single global iteration step.

Likewise, Browing et al. (2008) developed a simple relationship that allows for the estimation of nonlinear maximum roof displacements using an effective period factor and elastic response spectrum with an equivalent damping. This procedure has been recently improved by Yaghmaei-Sabegh et al. (2014) to account for the influence of both far- and near-field ground motions and to provide estimates of the maximum inter-storey drift of nonlinear responding RC frames. Additional works on the proposal of approximate methods to estimate the maximum inter-storey drift demands may be found in the literature (Miranda and Reyes, 2002; Akkar and Miranda, 2005; Whittaker and Huang, 2007: Elghazouli et al., 2014).

The relevance of assessing the use of linear analysis to estimate reliable inelastic response parameters, particularly at a member level, increases to the extent that EC8-3 prescribes that, regardless the use of linear-elastic methods of analysis, the safety verifications should be always conducted in terms of plastic member rotations, rather than forces as it is proposed, for instance, by ASCE 41-13 and by part 1 of Eurocode 8 (EC8-1) (CEN, 2004) for the design of new buildings. Consequently, since plastic rotations cannot be obtained from linear-elastic analysis, a question on how the safety verifications should be performed in these cases may be naturally raised. It was found in Chapter 4 that the most suitable answer would be the use of chord rotations as an alternative to plastic rotations, quantified based on the geometry of the deformed shape of the member. Nevertheless, it was also found, as already referred, that linear procedures systematically lead to unreliable chord rotation estimates even when the linear analysis applicability criteria is verified.

The objective of this work is hence to propose a simplified procedure that allows for the estimation of local inelastic chord rotation demands using linear-elastic methods of analysis in an expeditious and conservative sort of way. The proposed procedure relies on empirical evidence that the ratio between nonlinear and linear chord rotations at beams increases almost proportionally to the ratio between the corresponding linear and nonlinear shear-spans. However, the applicability of the proposed procedure is conditioned to cases wherein column-sway mechanisms are not expected to be developed. A number of moment-resisting steel frames design according to different criteria and exhibiting different column-to-beam moment ratios were analysed so as to broaden the validity of the proposed procedure. Moreover, a comparative study was additionally carried out considering the equivalent linearization procedure developed by Günay and Sucuglou (2009; 2010) and the simplified procedure preconized by FEMA P58-1 (Whittaker and Huang, 2007; FEMA,

2012) with the aim of identifying possible advantages and limitations associated with the procedure proposed in this work.

5.3 Moment-resisting steel frame buildings considered in the present case study

5.3.1 Design details of frames

This study was conducted considering ten 5-storey MRSF buildings with regular configuration in plan and elevation similarly to those analysed in Chapter 2. Each building was designed according to different criteria. The first building, again denoted as GB, was simply designed to resist gravity loads, whilst the remaining nine buildings were seismically designed to EC8-1 (CEN, 2004). A medium ductility class (DCM) with a behaviour factor q of 4.0 was assumed, as well as different limits for the inter-storey drift sensitivity coefficient θ. Different column-to-beam moment ratios (*CBMR*) were considered. The design seismic action was set for Zone 3 of the Portuguese territory (Lisbon) and for a soil type B, defined by a soil factor S of 1.29 in accordance to the Portuguese National Annex of Eurocode 8. A grade S275 was assumed for the structural steel. The structural characteristics of the analysed buildings are summarized in Table 5.1.

Table 5.1 – Characteristics of the buildings analysed.

Storey	External Columns	External Columns	Beams	θ	*CBMR*			
Building GB (T_1 = 1.63s)								
5	HE240B	HE280B	IPE300	0.12	1.68	1.22	1.22	1.68
4	HE240B	HE280B	IPE300	0.23	3.35	2.44	2.44	3.35
3	HE240B	HE280B	IPE300	0.36	3.34	2.36	2.36	3.34
2	HE260B	HE300B	IPE300	0.45	3.62	2.46	2.46	3.62
1	HE260B	HE300B	IPE300	0.37	3.82	2.56	2.56	3.82
Building SB1 (T_1 = 1.50s)								
5	HE280B	HE280B	IPE300	0.12	2.44	1.22	1.22	2.44
4	HE280B	HE280B	IPE300	0.21	4.88	2.44	2.44	4.88
3	HE280B	HE280B	IPE300	0.29	4.88	2.36	2.36	4.88
2	HE300B	HE300B	IPE330	0.33	4.21	1.93	1.93	4.21
1	HE300B	HE300B	IPE330	0.28	4.51	2.01	2.01	4.51
Building SB2 (T_1 = 1.20s)								
5	HE300B	HE300B	IPE300	0.10	2.97	1.49	1.49	2.97
4	HE300B	HE300B	IPE300	0.16	5.95	2.97	2.97	5.95
3	HE400B	HE400B	IPE300	0.19	8.12	4.06	4.06	8.12
2	HE400B	HE400B	IPE330	0.20	8.04	3.96	3.96	8.04
1	HE450B	HE450B	IPE330	0.12	8.97	4.31	4.31	8.97

Building SB3 (T_1 = 0.90s)								
5	HE500B	HE500B	IPE300	0.06	7.66	3.83	3.83	7.66
4	HE500B	HE500B	IPE400	0.07	7.37	3.68	3.68	7.37
3	HE500B	HE500B	IPE400	0.09	7.37	3.68	3.68	7.37
2	HE500B	HE500B	IPE450	0.10	5.66	2.83	2.83	5.66
1	HE500B	HE500B	IPE450	0.08	5.66	2.80	2.80	5.66
Building SB4 (T_1 = 1.43s)								
5	HE200B	HE220B	IPE270	0.13	1.33	0.85	0.85	1.33
4	HE200B	HE220B	IPE300	0.24	2.04	1.28	1.28	2.04
3	HE220B	HE260B	IPE300	0.22	2.29	1.54	1.54	2.29
2	HE220B	HE260B	IPE450	0.21	0.91	0.65	0.65	0.91
1	HE220B	HE280B	IPE450	0.27	0.84	0.66	0.66	0.84
Building SB5 (T_1 = 1.47s)								
5	HE200B	HE220B	IPE270	0.15	1.33	0.85	0.85	1.33
4	HE200B	HE220B	IPE300	0.28	2.04	1.28	1.28	2.04
3	HE240B	HE260B	IPE300	0.27	2.68	1.54	1.54	2.68
2	HE240B	HE260B	IPE400	0.27	1.55	0.85	0.85	1.55
1	HE240B	HE280B	IPE400	0.30	1.45	0.87	0.87	1.45
Building SB6 (T_1 = 1.49s)								
5	HE220B	HE260B	IPE300	0.12	1.32	1.02	1.02	1.32
4	HE220B	HE260B	IPE300	0.23	2.63	2.03	2.03	2.63
3	HE220B	HE260B	IPE300	0.30	2.59	1.93	1.93	2.59
2	HE260B	HE280B	IPE360	0.30	1.99	1.22	1.22	1.99
1	HE260B	HE280B	IPE360	0.31	2.34	1.24	1.24	2.34
Building SB7 (T_1 = 1.45s)								
5	HE220B	HE260B	IPE300	0.12	1.32	1.02	1.02	1.32
4	HE220B	HE260B	IPE300	0.23	2.63	2.03	2.03	2.63
3	HE220B	HE260B	IPE300	0.30	2.59	1.93	1.93	2.59
2	HE260B	HE280B	IPE360	0.27	1.98	1.22	1.22	1.98
1	HE260B	HE280B	IPE400	0.28	1.82	0.96	0.96	1.82
Building SB8 (T_1 = 1.41s)								
5	HE220B	HE260B	IPE300	0.12	1.32	1.02	1.02	1.32
4	HE220B	HE260B	IPE300	0.23	2.63	2.03	2.03	2.63
3	HE220B	HE260B	IPE300	0.29	2.59	1.93	1.93	2.59
2	HE260B	HE300B	IPE360	0.26	1.98	1.39	1.39	1.98
1	HE260B	HE300B	IPE400	0.25	1.82	1.23	1.23	1.82
Building SB9 (T_1 = 1.46s)								
5	HE220B	HE260B	IPE300	0.12	1.3	1.0	1.0	1.3
4	HE220B	HE260B	IPE300	0.23	2.6	2.0	2.0	2.6
3	HE220B	HE260B	IPE300	0.30	2.6	1.9	1.9	2.6
2	HE260B	HE300B	IPE360	0.29	2.0	1.4	1.4	2.0
1	HE260B	HE300B	IPE360	0.28	2.3	1.6	1.6	2.3

The analyses were carried out using the open source software OpenSees (PEER, 2011) and two sets of structural models were developed in line with the type of analysis performed, linear and nonlinear, as discussed in Chapter 2. Although force-based beam-column elements were adopted, which do not account for strength and stiffness degradation of the members, it has been demonstrated in Chapter 4 that such elements provide reasonable results within the scope of this work.

5.3.2 Expected nonlinear behaviour of the buildings and accuracy of linear analysis

In modern design codes, the loss of available ductility of buildings due to development of undesirable collapse mechanisms is taken into account through design criteria that aim at controlling the strength hierarchy of the system, which should avoid column side-sway (soft-storey) mechanisms and ensure stable beam side-sway mechanisms (Mazzolani and Piluso, 1996; Priestley et al., 2007). The evaluation of weather a beam-sway or a column-sway inelastic mechanism is to be expected may be obtained by calculating the strength-based sway potential index S_i relating to the relative strength of beams and columns at the centroids of all j beam-to-column joints at a given floor level i of the frame (Bal et al., 2010), so that:

$$S_{ij} = \frac{\sum\left(M_{bl} + M_{br}\right)}{\sum\left(M_{ca} + M_{cb}\right)} \tag{5.1}$$

where M_{bl} and M_{br} are the beam expected flexural strengths at the left and the right of the joint, respectively, extrapolated to the joint centroid, and M_{ca} and M_{cb} are the expected column flexural strengths above and below the joint, also extrapolated to the joint centroid. The minimum value of column moment capacities within the range of column axial forces produced by the seismic design situation should be used (CEN, 2004). A remark should be made on the approach followed by EC8-3 to quantify the moment capacity of steel columns, which assumes a linear interaction between bending moment and axial force that is known to be oftentimes conservative (Trahair et la., 2008). Alternatively, the EC3 approach (Trahair et la., 2008) or the ASCE41-13 simplified approximation may be adopted. To calculate the moments at the centre of the joint, a component due to shear has to be taken into account (FEMA, 2005), though EC8-1 states that the loss in accuracy is miner if this shear allowance is neglected. Hence, if S_i is lower than 0.85, then a column-sway mechanism is unlikely to form; otherwise, if S_i is greater than 1.0 it is probable that a column-sway mechanism will develop (Priestley et al., 2007). EC8-3, in turn, preconizes that the column-sway mechanism is avoided if 1 / S_{ij}, designated as column-to-beam moment ratio (*CBMR*), is greater than 1.30. Different sway potential index approaches may be found in literature (Bal et al., 2010; Welch et al., 2014), having been demonstrated by Bal et al. (2010) that stiffness-based sway indices appear to be a useful and optimum solution to displacement-based assessments of existing buildings. Also, Gupta and Krawinkler (2000) concluded that the strong-column concept implemented in present

design guidelines and codes does not actually prevent the development of plastic hinges at columns. The *CBMR* values at every joint of the analysed buildings are summarized in Table 5.1 and since EC8-1 preconizes that the verification of the weak-beam / strong-column condition may be waived at the top level of multi-storey buildings, just buildings SB4 to SB8 are expected to develop soft-storey failure mechanisms.

Linear-elastic methods of analysis feature an inherent incapacity to capture the changes in the distribution of deformation demands over the height of the building as the level of seismic action increases, which is known to be strongly dependent on the structural and ground-motion characteristics (Gupta and Krawinkler, 2000; Elghazouli et al., 2014). In order to provide an overall picture of the expected nonlinear behaviour of the various MRSF buildings under analysis and the trustworthiness of the EC8-3 linear analysis in estimating inelastic local deformation demands, pushover analyses were conducted on both linear and nonlinear structural models for every building. A fixed load pattern defined as proportional to the mass and height of each storey was adopted and the structural responses (i.e. inter-storey drifts, chord rotations and plastic rotations) were computed for various increasing levels of total drift ratio (top displacement divided by building height). Information on the various methods of quantifying both plastic and chord rotations may be found in Chapter 4. Figure 5.1 depicts the results obtained and the following conclusions were drawn:

- Although buildings GB, SB1 and SB9 verify *CBMRs* greater than 1.30, the formation of plastic hinges at columns, excluding the bottom nodes of first storey columns, was not avoided (Figure 5.1 (a)). Nonetheless, the onset of hinging only occurred for levels of total drift greater than 2.5%, perhaps indicating that *P*-Δ effects could be leading to a reduction in the flexural moment developed at columns and to the violation of the weak-beam / strong-column capacity design criterion. A closer inspection on this will be provided later. All buildings non-conforming with the *CBMR* > 1.30 condition were seen to potentially develop soft-story failure mechanisms (Table 5.1 (b)).
- The observation of the evolution of the maximum plastic rotations developed at the critical beam of every building (Figure 5.1 (c) and (d)) provided clear insight on the distribution and lumping of plasticity within both beam-sway and column-sway mechanisms. The EC8-3 plastic rotation capacity limits were further confronted with the obtained plastic rotation demands so as to allow for a better understanding of the level of safety associated with each building. It was

found that the beams controlling the maximum plastic rotation demands changed as the total drift increased in buildings developing beam-sway mechanisms, namely in building SB9. These changes may be noted in slight deviations in the beam plastic rotations evolution trends and are a result of a variation in the distribution of deformation demands over the height of the structure, most likely due to the reduction in the stiffness of the storeys where hinging at columns occurred.

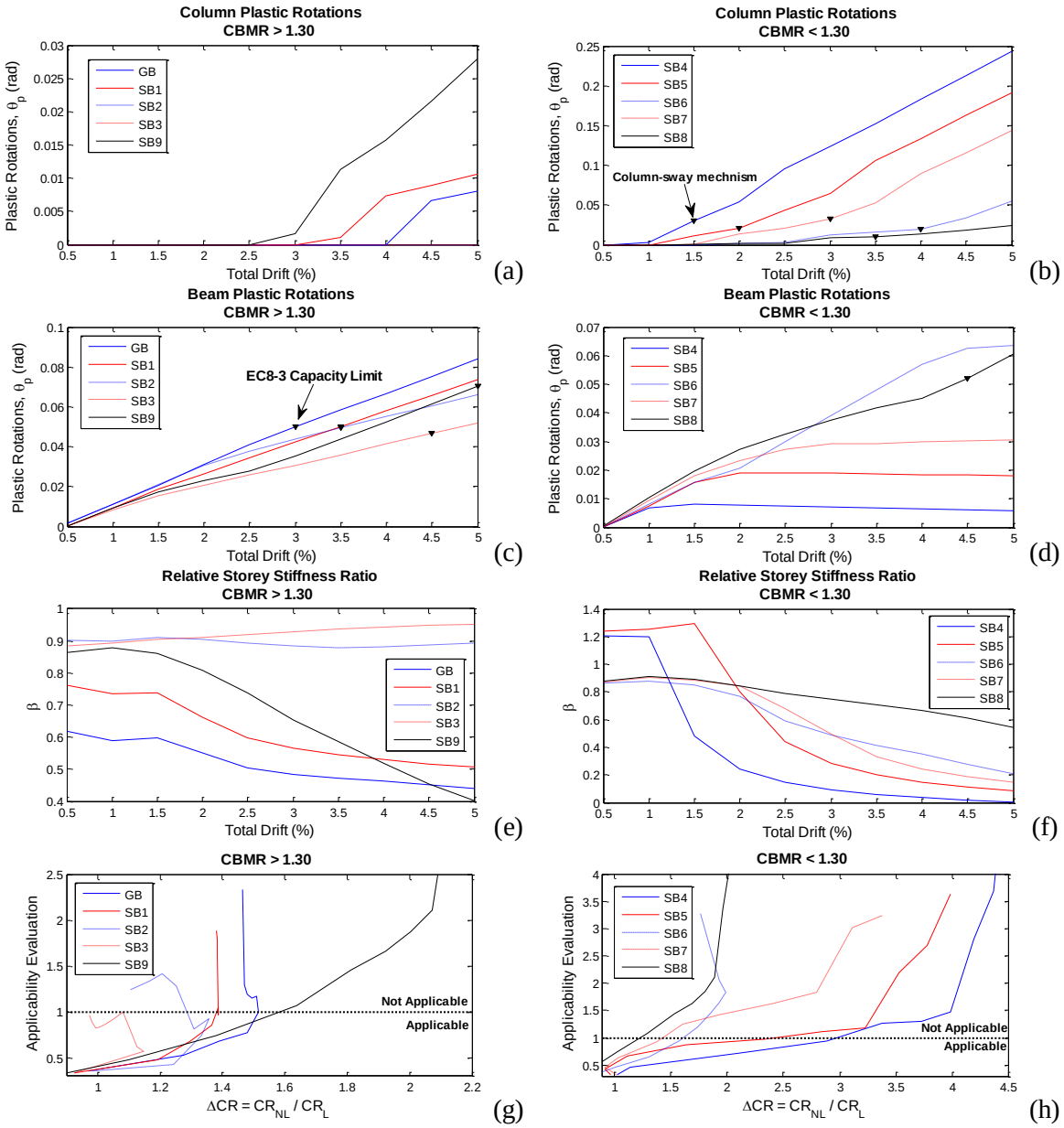

Figure 5.1 – Expected nonlinear behaviour of the buildings and accuracy of linear analysis: (a) and (b) plastic rotations at columns, excluding the bottom nodes of first storey columns; (c) and (d) plastic rotations at the critical beams; (e) and (f) evolution of the relative storey stiffness ratio β; and, (g) and (h) comparison between the applicability of linear analysis with the expected error in the nonlinear chord rotation estimates obtained from linear analysis.

In order to evaluate this demand distribution, the relative storey drift ratio β proposed by Kumar et al. (2013) was calculated, which is defined as the ratio between the maximum storey drift for the upper and lower halves of the frame. Figure 5.1 (e) and (f) display the results obtained for the two groups of buildings with *CBMRs* greater and lower than 1.30, respectively. It was observed that only buildings with a higher lateral stiffness and strength (buildings SB2 and SB3), associated to *CBMRs* greater than 2.80, do not experience significant demand distribution over its height, exhibiting β values that remain practically constant as the total drift increases. In turn, buildings GB and SB1 ($1.90 < CBMRs < 2.80$) and buildings SB6, SB8 and SB9 ($1.20 < CBMRs < 2.0$) present a reduction of about 70%, 30% and 50% in β, respectively. Finally, buildings developing early column-sway mechanisms are characterized by an abrupt reduction in β when the soft-storey is formed, as it would be expected, reaching practically 100% in buildings SB4. Still, it is noteworthy that β remains somehow constant until the mechanism is formed.

- The relevance of studying β increases as it may be seen as a measure for evaluating the suitability of linear analysis. Indeed, EC8-3 preconizes that linear analysis should be only applied if the ratio between the maximum and minimum demand-to-capacity ratios (*DCR*), defined in terms of bending moments in moment frames, over all primary elements, does not exceed a certain value ranging from 2 to 3. The assumption underlying this method is that linear analysis are considered to provide acceptably accurate estimates of inelastic displacements if the structure moves into inelastic range with an almost uniform distribution of demands (Chapters 2 and 4). The verification of this applicability criterion was confronted with the accuracy of linear analysis to estimate local inelastic deformation demands, defined as the ratio between the nonlinear and the linear chord rotations, ΔCR, at the most critical member (Chapter 4) (Figure 5.1 (g) and (h)). It may be seen that only building SB3 verifies both applicability criterion and levels of error below 20% for the whole range of total drift ratios considered. Contrarily, although buildings featuring *CBMRs* greater than about 2.0, particularly buildings GB and SB1, verified the applicability criterion for total drift ratios up to 2.5%, errors around 40 to 50% were observed. The feasibility of the applicability procedure should be even more tightly questioned when applied to buildings with characteristics identical to buildings

SB4 to SB9. In these cases, the error in the chord rotation estimates was seen to progressively increase with the global drift ratio, with linear analysis leading to chord rotation errors that reached 3 times the values of the nonlinear chord rotations. Note that the β values of buildings SB4 to SB8 vary little from 1.0 in the elastic range (total drift ratio of 0.5%), which defines a perfectly uniform distribution of demands. This may explain why the linear analysis applicability criterion was verified in all cases until a total drift ratio of 2% was reached and its inability to capture a potential formation of a soft-storey mechanism

The findings discussed above clearly draw attention for a need to revise the current EC8-linear analysis applicability criterion. However, the adoption of more stringent applicability criteria, as proposed in Chapter 4, may be too restrictive and consequently nonlinear analysis would have to be employed in the vast majority of cases. The lack of acquaintance of practitioners to the use of nonlinear analysis emphasizes the urge for the introduction of alternative and simplified analysis procedures in current guidelines and codes, as followed by the NZSEE (2006) and the JBDPA (1996) guidelines with the introduction of alternative procedures that aim at assessing the safety of existing buildings based on their probable global collapse mechanisms.

5.4 Methods of quantifying inelastic deformation demands using linear-elastic analysis

5.4.1 Equivalent linearization procedure proposed by Günay and Sucuoglu (2009; 2010)

A simple equivalent linearization procedure was initially developed by Günay and Sucuoglu (2009) for the inelastic seismic response prediction of capacity-design structures, being afterwards extended to existing structures (2010). This procedure basically consists on updating, in a single global iteration step, the stiffness of structural members that exceed their flexural capacities in an initial linear-elastic analysis. The methodology may be thus summarized in five steps (Günay and Sucuoglu, 2009; 2010): (i) firstly a linear elastic analysis is conducted on the initial structural system so as to determine the bending moments at the member ends and the modal spectral displacements; (ii) the bending moment capacities of beams and columns in both bending directions are further determined and the *CBMR* at all joints of the structure quantified to identify the potentially yielding member-ends. Column-ends are considered to potentially yield when $CBMR < 1.20$, while

beam-ends are probably yielding if *CBMR* > 0.80. Otherwise, all member-ends are potentially yielding; (iii) the distribution of yielding along the structure is estimated through the calculation of *DCRs*, so that if *DCR* >1.0 the member-end yields, otherwise the member-end behaves elastically; (iv) the update of the structure is then conducted by reducing the stiffness of yielded members so that $I' = I / R_M$, being I' the secant moment of inertia of the member, I the initial moment of inertia of the member and R_M the reduction factor (Table 5.2); (v) finally, a response spectral analysis is performed on the reduced system. An eigenvalue analysis should be firstly conducted to determine the new dynamic properties of the structure and the modal forces recalculated. These should be than combined using a standard combination technique (*SRSS* or *CQC*). This method was presented to be at least as accurate as standard nonlinear static procedures and as an effective method of predicting the nonlinear seismic performance of structures (Günay and Sucuoglu, 2010).

Table 5.2 – Stiffness reduction factors corresponding to different yielding situations (Günay and Sucuoglu, 2009; 2010).

Structural member	Reduction factor (RM)
All members with both ends not yielding	$R_M = 1{,}0$
Columns and beams with just one end yielding	$R_M = \dfrac{\sum M_E}{M_{rc,i} + \alpha M_{rc,j}} \quad \alpha = \begin{cases} CBMR & if\ CBMR < 1 \\ 1/CBMR & if\ CBMR > 1 \end{cases}$
Columns and beams with both ends yielding	$R_M = \dfrac{\sum M_E}{M_{rc,i} + M_{rc,j}}$

5.4.2 The FEMA P-58-1 simplified linear-elastic analysis procedure (Whittaker and Huang, 2007; FEMA, 2012)

Recently, FEMA (2012) published a new document that specifically addresses the seismic performance assessment of buildings on the basis of an extensive probabilistic framework that provides information in terms of potential casualties, repair and replacement costs, repair time and unsafe placarding resulting from earthquake damage. It thus takes a step forward in current performance-based design methodologies, providing information that is more meaningful and useful in the decision-making process comparing to standard discrete performance levels that are commonly adopted by codes. The document also proposes a simplified linear analysis procedure that is basically an extension of the ASCE 41-13 linear analysis. In other words, it consists on a first computation of the

floor displacements and story drift ratios, Δ_i, using the ASCE 41-13 lateral force method and then on the correction of those story drift ratios to account for the inelastic behaviour and the higher mode effects. The estimates of median story drift ratios, Δ_i^*, at each level i, are given by $\Delta_i^* = H_{\Delta i}(S, T_1, h_i, H)\,\Delta_i$, where $H_{\Delta i}(S, T_1, h_i, H)$ is the drift correction factor, defined as

$$ln(H_{\Delta i}) = a_0 + a_1 T_1 + a_2 S + a_3 \frac{h_{i+1}}{H} + a_4 \left(\frac{h_{i+1}}{H}\right)^2 + a_5 \left(\frac{h_{i+1}}{H}\right)^3 \quad (5.2)$$

where T_1 is the fundamental period of the structure, S is the strength ratio and h_i and H are the story and total heights of the structure, respectively. Values of $a_0 = 0.75$, $a_1 = -0.044$, $a_2 = -0.010$, $a_3 = -2.58$, $a_4 = 2.30$, $a_5 = 0$ are proposed for moment frame structures with 2 to 9 stories. This correction factor was defined on the basis of regression analysis of results of simplified and nonlinear analyses across a wide range of seismic intensities. Bilinear models were used for the nonlinear dynamic analysis and the degradation of strength and stiffness and second-order effects were neglected. Its applicability is thus limited to cases where the story drift ratios do not exceed 4 times the corresponding yield drift ratio and are below 4%. Correction factors for floor accelerations and velocities were also proposed in the same document, which is of open access. Another interesting feature of this procedure regards the definition of levels of dispersion associated with the response estimates, which aim to capture the uncertainty in the ground motion intensity, record-to-record variability and modelling. These will have a key role when conducting seismic loss estimations.

5.4.3 Simplified procedure for quantifying inelastic chord rotations using linear-elastic analysis

5.4.3.1 Proposal

A simplified procedure that enables the quantification of inelastic chord rotation demands at beams from linear-elastic analysis is presented herein. Despite it has been shown that buildings GB to SB3 exhibit a reduction in β values lower than 30%, which is expected to lead to a slight variation in the distribution of demands over the height of the building, the error in the chord rotation estimates using linear analysis reached more than 40%. Nevertheless, in Chapter 5 it was demonstrated that when gravity loads are excluded from the analysis, this level of error reduces to an admissible value of about 20%, particularly in the case of building GB. Thus, in order to identify the sources of deviation in these chord rotation estimates of beam elements using both linear (L) and nonlinear (NL)

analysis, Figure 5.2 displays the bending moments, chord rotations and curvature demands at member V15 of buildings GB and SB3 for a total drift ratio of 4%. A distinction was made between the results with (*G*+*E*) and without (*E*) considering the influence of gravity loads.

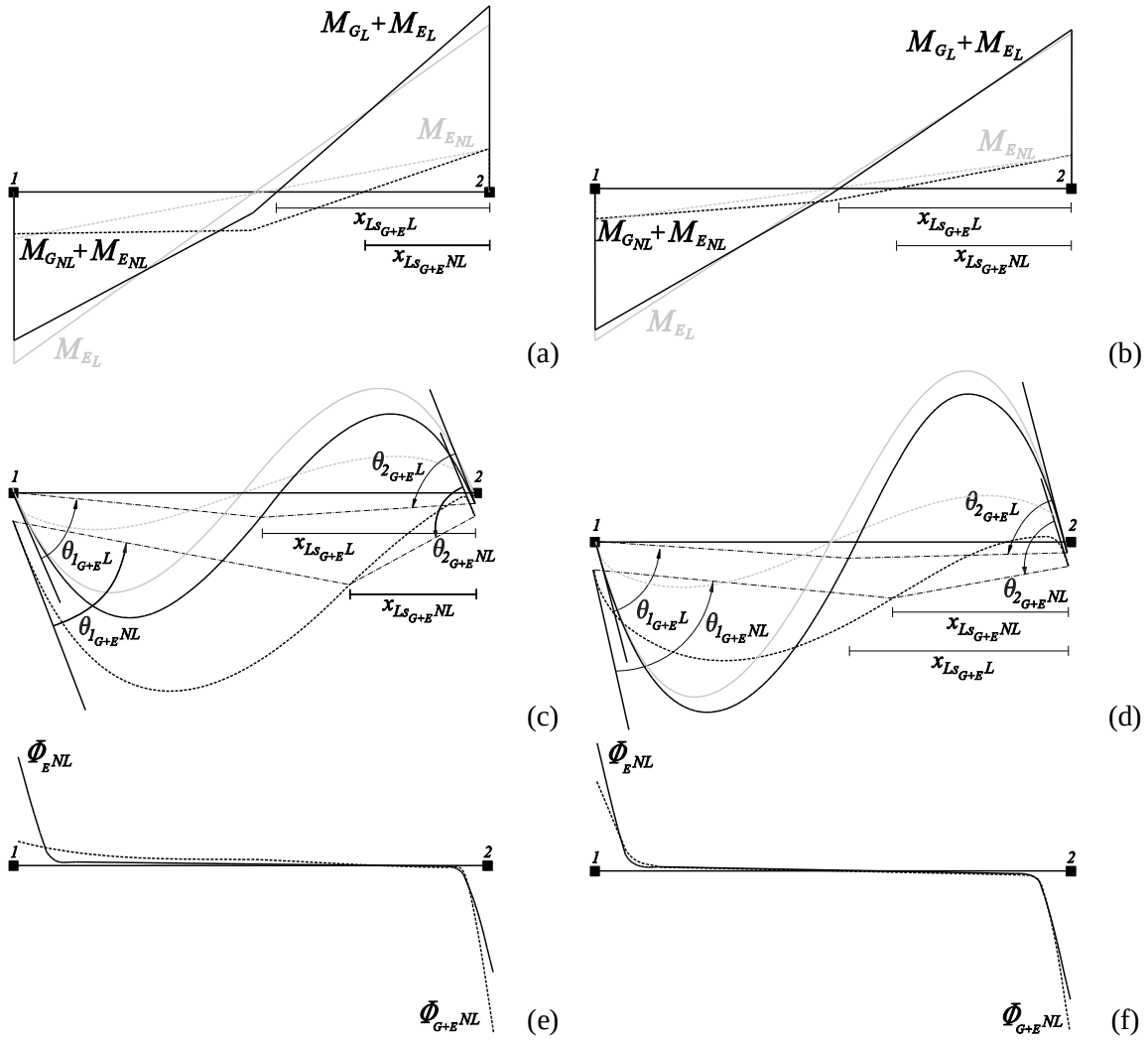

Figure 5.2 – Bending moments, chord rotations and curvature demands at member V15 of building GB ((a), (c) and (e)) and building SB3 ((b), (d) and (f)), with and without considering the effect of gravity loads, for both linear and nonlinear models and a 4% total drift ratio.

It may be first observed from Figure 5.2Table 5.2 that when the effect of gravity loads is neglected, or reduced (building SB3), the distribution of demands and plasticity along the two member ends of the beam is symmetric, as well as the shear span lengths x_{Ls} defined with reference to both member ends. The shear span length is known to play a key role in the chord rotation definition (Chapter 4). As a result, the equal linear and nonlinear shear span values found when no gravity loads are considered ($x_{Ls} = L/2$, being L the length of the beam) may explain the admissible level of chord rotation prediction errors obtained. The error of 20% observed in building GB without gravity loads, which decreased to

approximately 10% in building SB1 (Chapter 4), can be thus simply attributed to the intrinsic limitation of linear analysis to conveniently capture the nonlinear inter-storey drifts. On the other hand, when gravity loads are taken into account, the deviations in the chord rotation estimates significantly change with the level of nonlinear incursions and the lateral stiffness and strength of the building. In the elastic range both linear and nonlinear analysis led to similar response results and equal shear span values. However, as the total drift ratio increased, linear analysis failed to capture the distribution of demands and plasticity between both nodes of the member, resulting in rather different shear span values, particularly in building GB (Figure 5.2 (c)). In fact, linear analysis was seen to generally lead to higher chord rotation estimates at node 1 of beams and lower values at node 2 in comparison to nonlinear analysis. Finally, for higher levels of total drift ratio, the influence of gravity loads was seen to progressively decrease and the distribution of plasticity along the beam length became more and more symmetric, being this phenomenon more evident in the case of building SB3 (Figure 5.2 (d) and (f)). Consequently, the shear span length tended to approach the half of the length of the member and better chord rotation estimates using linear analysis were obtained.

Summing up the above findings, it seems evident that when the linear shear span lengths of beams approach the nonlinear ones, i.e. similar equivalent cantilever elements are defined, reasonable estimates of chord rotations are obtained. It may be noteworthy referring that the deviations in the chord rotation estimates of columns were seen to be practically dependent on the ability of linear analysis to correctly predict the inter-storey drifts at the various levels of total drift ratio. Hence, recognizing the impact of the shear span length in the quantification of beam chord rotation demands, the evolution of this parameter for increasing levels of total drift ratio and the correlation between the shear span predictions and the chord rotation estimates obtained using linear analysis were examined.

Figure 5.3 (a) depicts the evolution of x_{Ls}, defined with respect to node 2 of the critical beams (V15, V15, V9 and V12) of buildings GB, SB1, SB2 and SB3, respectively, for both linear and nonlinear analysis. These buildings were chosen due to their reduced variation in β values. Again, when gravity loads are neglected, a value of x_{Ls} of 50% of the total length of the member is found in all cases. Otherwise, a very distinct evolution of x_{Ls} may be seen for both linear and nonlinear analysis. While in the former case the x_{Ls} progressively increases to about 45% to 50% of the total length of the member, in the latter case x_{Ls} firstly reduces until both ends of the member yield, to about 25% to 35%, and from

that point on it remains practically constant, as expected since the member has practically attained its full flexural capacity.

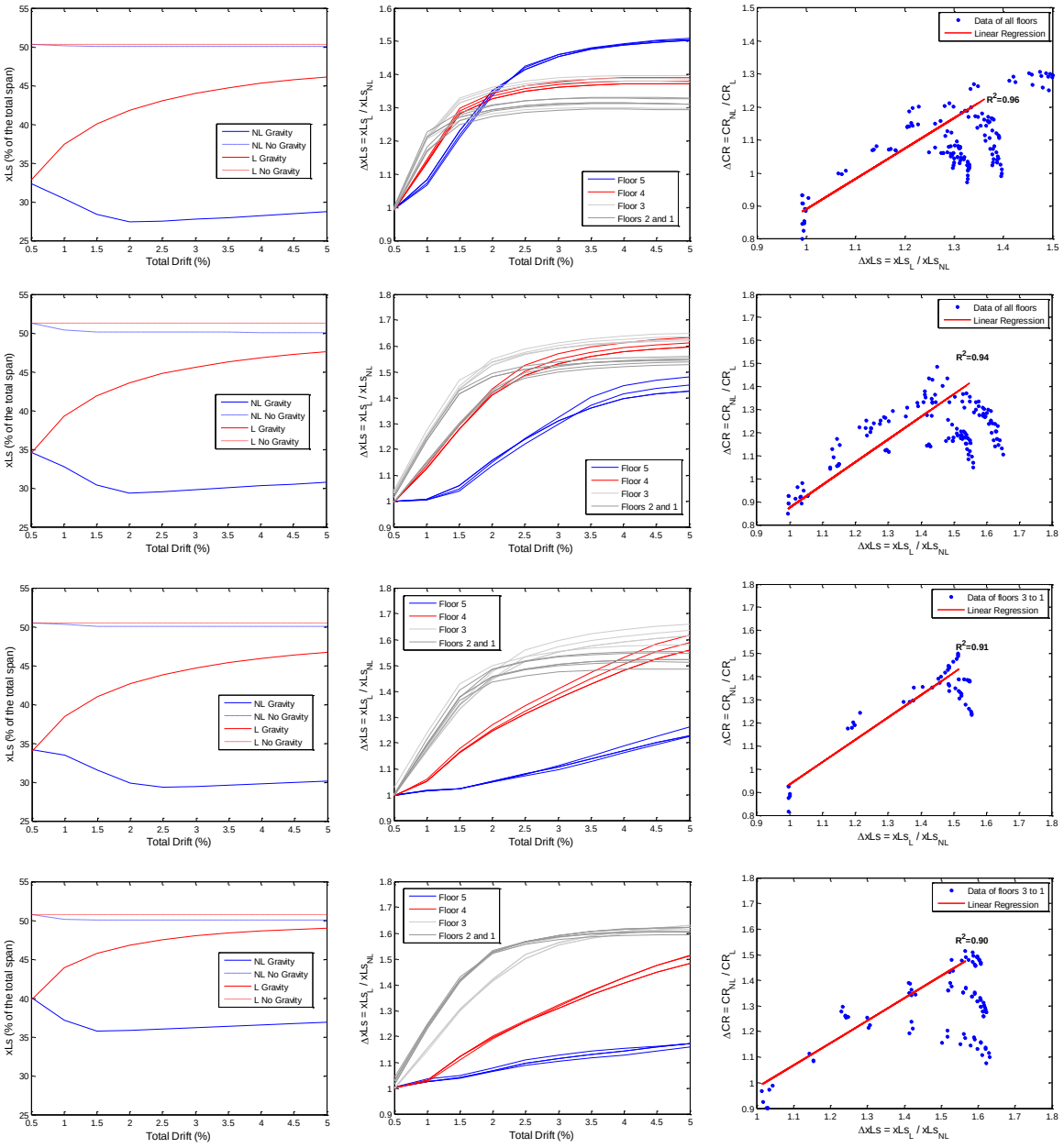

(a) (b) (c)

Figure 5.3 – Influence of the shear span length in the chord rotation estimates for buildings GB to SB3 (upper-to-lower figures): (a) evolution of the shear span length with the global drift ratios; (b) comparison between the linear and nonlinear shear span lengths; (c) correlation between shear span predictions and the chord rotation estimates using linear analysis.

Moreover, as the stiffness and strength of the member increases, and hence the influence of gravity loads becomes less relevant, the minimum value of x_{Ls} attained also increases (building SB3), which consequently reduces the deviations between the linear and nonlinear estimates of x_{Ls}, designated by Δx_{Ls}. It may be also noted that since stiffer and stronger buildings uniformly distribute deformation demands over its height, a similar

evolution of Δx_{Ls} was observed within the various floor levels (Figure 5.3 (b)). Figure 5.3 (c) displays the correlation between the shear span predictions, Δx_{Ls}, and the nonlinear and linear chord rotation deviations, ΔCR. Two trends of correlation may be distinguished: (i) a linear one, characterized by coefficients of determination R^2 equal or greater than 0.9, indicating that the chord rotation deviations linearly increase with Δx_{Ls} until the maximum value of ΔCR is reached; (ii) and a second one, which is notoriously nonlinear and results from a decrease in ΔCR, more evident in the less demanded members, for small variations of Δx_{Ls}, which are due to the attainment of the full flexural capacity of the member. It should be remarked that, in the case of buildings GB and SB1, only the results obtained at the beams of floors 1 to 3 were considered, since at the remaining ones the ΔCR values were lower than 1.0. Nonetheless, as one is simply interested in the positive increase of ΔCR, only the linear trend of the correlation needs to be considered. Hence, the simplified procedure proposed in this study basically consists on defining the nonlinear chord rotation of a certain beam member end in terms of a corrected equivalent linear chord rotation $\theta_{L,corr}$, so that:

$$\theta_{L,corr} = \theta_L \frac{xLs_L}{xLs_{NL}} \tag{5.3}$$

where θ_L is the linear chord rotation at the beam member end under consideration, defined for instance through the Exact Geometrical Method (*EGM*) or the Approximate Geometrical Method (*AGM*) as described in Chapter 4, and $x_{Ls\ L}$ and $x_{Ls\ NL}$ are the linear and nonlinear shear span lengths defined with reference to that same member end. Since it has been shown that linear analysis already led to conservative estimates of chord rotations at node 1 of the beams, with $x_{Ls\ L}$ values lower then $x_{Ls\ NL}$, (Figure 5.2 (c) and (d)) it was decided to apply equation (3) just to node 2 of the beams. A brief parallelism with the case of two elastic cantilever beams with different lengths but similar cross-section and material properties may be also made. By subjecting those cantilevers to similar maximum flexural moments, the ratio between their elastic chord rotations will be equal to the ratio between their lengths.

The results obtained from the application of the proposed procedure to predict the nonlinear chord rotations at all critical nodes of beams of buildings GB to SB3 for increasing total drift ratios from 0.5% to 5% are presented in Figure 5.4. The linear chord rotations θ_L obtained using the *EGM* are equally presented. The proposed procedure may be thus seen to perform quite well, allowing for the estimation of nonlinear chord rotations

using linear-elastic analysis at least in a slightly conservative way in the most demanded members. In the case of the top floor members of buildings GB and SB1, wherein values of ΔCR lower than 1.0 were obtained due to the incapacity of linear analysis to accurately predict nonlinear inter-storey drifts, the procedure was found to be even more conservative. Yet, these values will not have a great impact in the global response of the structure and consequently on safety checks.

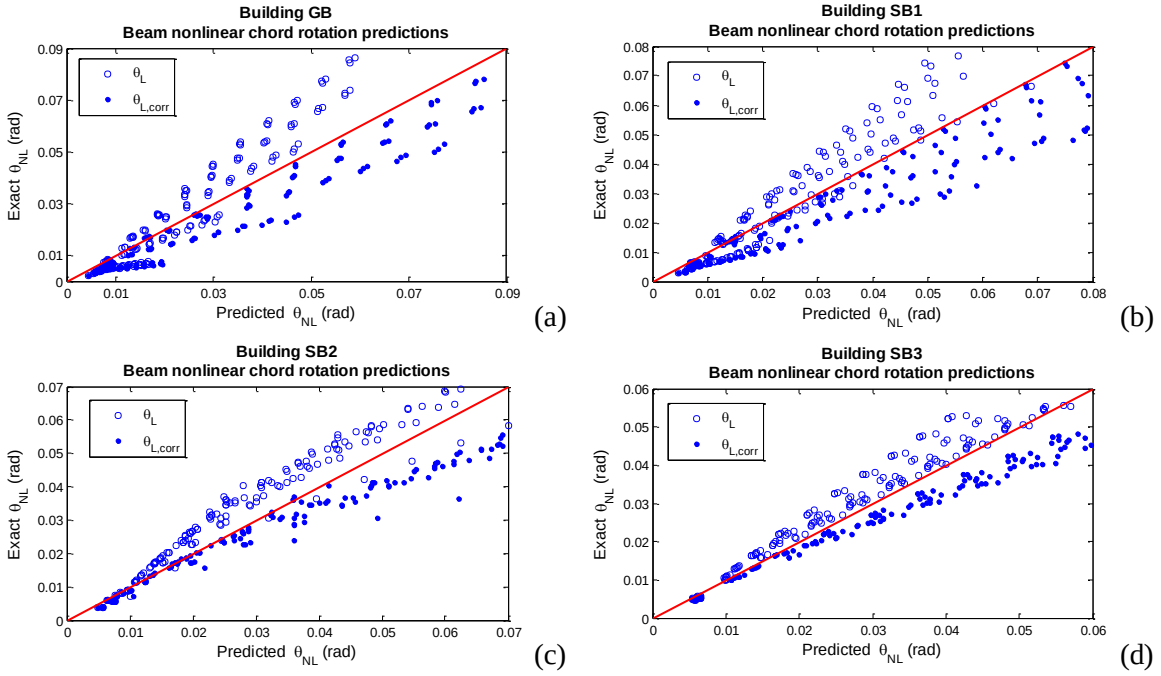

Figure 5.4 – Application of the proposed methodology for predicting nonlinear chord rotations at beams: (a) building GB; (b) building SB1; (c) building SB2; (d) and building SB3.

Notwithstanding the attractiveness of this approach as a simplified and expeditious assessment tool, an important drawback may be naturally noted, which is associated with the definition of $x_{Ls\ NL}$ without having to adopt nonlinear analysis. The solution to this limitation involves the calculation of an approximate $x_{Ls\ NL}$ value, defined on the basis of the capacity design principles. For instance, if one considers a simplified fixed-end beam with a point gravity load P applied at its mid-span, as it is the case of the buildings under analysis in this study, the value of x_{Ls} at the onset of yielding in the right node of the member, $x_{Ls\ Y,}$ can be easily obtained as represented in Figure 5.5 (a). Likewise, neglecting the effect of over-strength and assuming that both member ends have reached their full flexural capacities, the minimum value of $x_{Ls\ NL}$ (Figure 5.3 (a)) may be approximately determined as represented in Figure 5.5 (b). Thus, $x_{Ls\,NL}$ can be defined as follows:

$$xLs_{NL} = \frac{M_p\ L}{2\left(M_p + M_G\right)} \tag{5.4}$$

where M_p refers in the case of steel members to the plastic flexural capacity, M_G to the gravity bending moment at the mid-span of the member and L to the length of the member. Naturally, as this expression is only valid for a single loading situation, it should be extended and validated for other loading scenarios. More generic expressions may be found in the works of Gioncu and Petcu (1997) and Priestley et al. (2007). Table 5.3 presents the estimates of the minimum value of $x_{Ls\ NL}$ using equation (5.4). It may be observed that this expression provides fairly reasonable results, within an error of 10%, which tend to approximate the exact nonlinear analysis results as the lateral stiffness and strength of the structure increases. Still, although equation (5.4) always provides a minimum $x_{Ls\ NL}$ estimate comparing to the exact nonlinear one, thus ensuring a conservative estimate of nonlinear chord rotations from equation (5.3), a better estimate of $x_{Ls\ NL}$ may be obtained by including the over-strength effects, so that $\gamma_{ov}M_p$, being γ_{ov} equal to 1.25 as proposed by EC8-1.

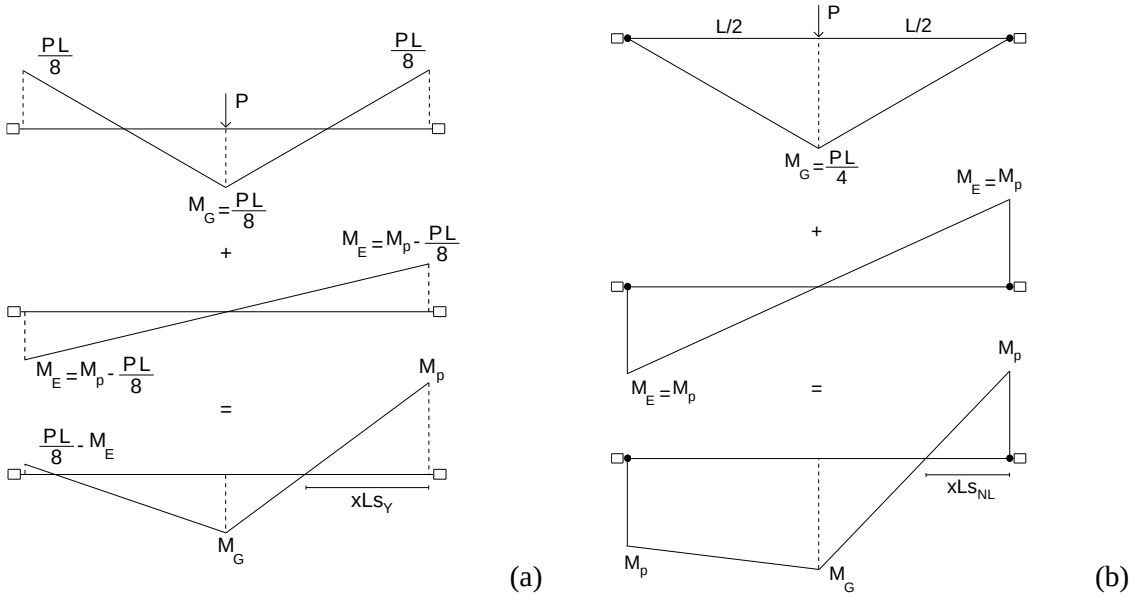

Figure 5.5 – Computation of the x_{Ls} value: (a) at the begging of yielding in node 2 of the member, $x_{Ls\ Y}$; (b) at the yielding of both member ends, $x_{Ls\ NL}$.

Table 5.3 – Minimum nonlinear shear span estimates with respect to node 2 of beams V15 of buildings GB to SB3.

Parameter		GB		SB1		SB2		SB3	
		Proposed	Observed	Proposed	Observed	Proposed	Observed	Proposed	Observed
xLs_{NL}	without γ_{ov}	1.48m	1.64m	1.61m	1.76m	1.61m	1.76m	2.11m	2.15m
	with γ_{ov}	1.64m		1.77m		1.77m		2.29m	
xLs_Y		1.93m	1.94m	2.05m	2.07m	2.05m	2.04m	2.38m	2.38m

Another interesting feature of equation (5.4), as a mean of predicting $x_{Ls\ Y}$, is related with the definition of the EC8-3 plastic rotation capacity limits at the end of steel members.

EC8-3 defines the plastic rotation capacity limits of compact steel elements at the limit states of damage limitation, significant damage and near collapse as $1.0\theta_y$, $6.0\theta_y$ and $8.0\theta_y$, respectively, being θ_y the value of the chord rotation at yielding. ASCE41-13 preconizes a simplified equation to quantify θ_y, which assumes that the member will develop symmetric double-bending, so that $\theta_y = M_p\ L\ /\ 6EI$. This approach does not include additional deflection due to shear deformation, as exhibited in Figure 5.2 and already pointed out by Newell (2008), and may thus lead to non-conservative estimates of plastic rotations (Chapters 2 and 4). Hence, alternatively, θ_y can be defined as an equivalent cantilever beam with length equal to $x_{Ls\ Y}$, or even more conservatively equal $x_{Ls\ NL}$, recognizing that the shear span length varies for increasing nonlinear incursions. The chord rotation at yielding may be thus defined as $\theta_y = M_p\, x_{Ls\ Y} / 3EI$.

However, despite the inclusion of the above improvement, the proposed procedure still has a slight handicap associated with the quantification of linear chord rotation demands, θ_L, which is not intuitive in many situations, nor straightforward. In order to overcome this difficulty, an alternative way of defining θ_L will be proposed in the following. Assuming, once again, an equivalent cantilever beam now with length equal to $x_{Ls\ L}$, the linear chord rotation at the end node of a certain beam element could be given by $\theta_L = M_{E+G\ L}\, x_{Ls\ L} / 3EI$, being $M_{E+G\ L}$ the bending moment at the end node under consideration obtained from linear analysis for the seismic combination of loads (Figure 5.2 (a) and (b)). Recalling that $M_{E+G\ \ L}$ may be defined from the demand-to-capacity ratio, so that $M_{E+G\ \ L} = M_p\ DCR$, the following expression to determine the equivalent linear chord rotation, $\theta_{L,eq}$, is proposed:

$$\theta_{L,eq} = \frac{M_p\, xLs_L}{3EI}\, DCR \tag{5.5}$$

The accuracy of adopting this approximate expression is depicted in Figure 7 for all members of buildings GB to SB3 and various total drift ratios, from 0.5% to 5%. The linear chord rotation predictions are compared with those computed either from the *EGM* and the *AGM*. It may be thus concluded that the proposed approximate expression derives quite accurate estimates of linear chord rotations. Finally, by applying the correction ratio of equation (5.3) to equation (5.6), the following expression for quantifying nonlinear chord rotation demands using linear analysis is obtained:

$$\theta_{L,eq,corr} = \frac{M_p}{3EI}\, DCR\, \frac{xLs_L^{\ 2}}{xLs_{NL}} \tag{5.6}$$

where $x_{Ls\,NL}$ may be defined from equation (5.4). The procedure proposed in this work may be thus seen as a rational, user-friendly and reliable tool that allows structural engineers for the estimation of approximate inelastic chord rotation demands from linear-elastic analysis at least on the safety side. If more precise predictions of inelastic chord rotations, particularly at columns, are intended, more robust nonlinear methods of analysis should be alternatively adopted. Recall that equation (5.6) was simply derived for cases where no significant changes in the distribution of demands over the height of the building are expected to occur.

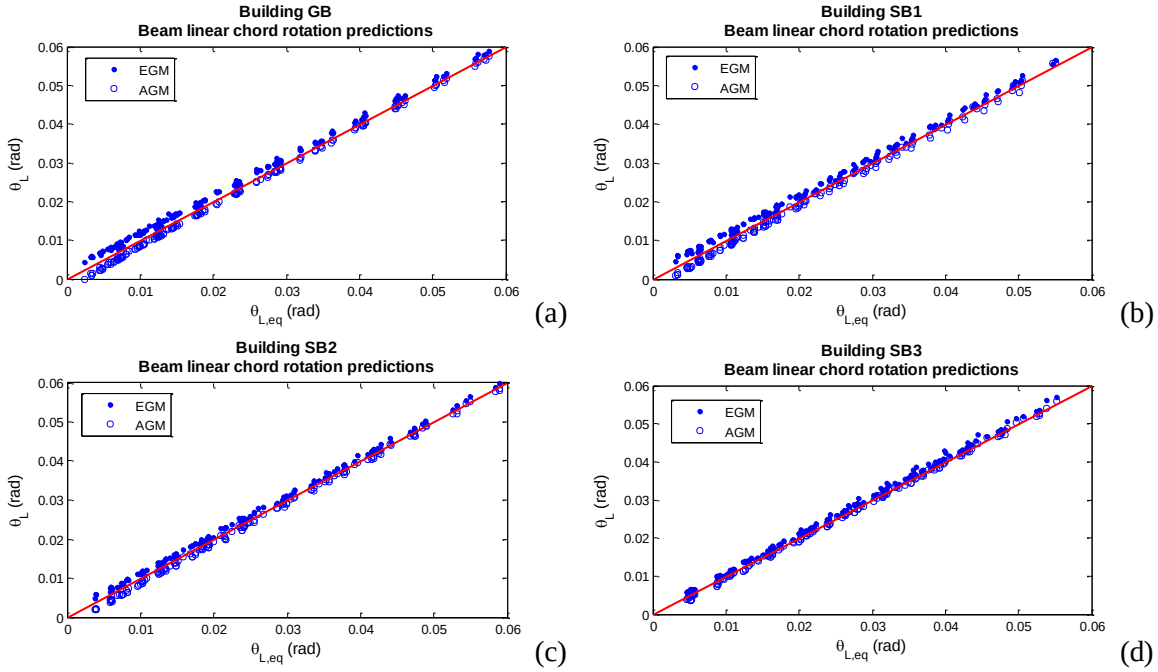

Figure 5.6 – Comparison of $\theta_{L,eq}$ with the exact linear chord rotation demands obtained for all beams of: (a) building GB; (b) building SB1; (c) building SB2; (d) and building SB3.

Albeit buildings SB6 to SB9 feature a reduction in β values greater than 40%, reaching 80% in buildings SB6 and SB7 with the development of a soft-storey mechanism, constant β values were found until a total drift ratio of about 2% was attained (Figure 5.1). As a matter of fact, the significant reduction in β values was seen to be triggered by the onset of plastic incursions at the top node of the first storey columns and both nodes of the second to fifth storey columns. Therefore, the applicability of equation (5.6) is expected to hold true until a significant reduction in the β values is observed, which is related with the onset of plastic hinging at columns. It is considered herein that more robust nonlinear methods of analysis should be adopted when hinging at columns occurs, which should incorporate stiffness and strength degradation (Lignos and Krawinkler, 2011) and axial load effects, as they have been seen to play a critical role in the response of steel columns (Elkady and Lignos, 2014a; 2013; Chapter 6).

5.4.3.2 Range of applicability

An early work carried out by Popov et al. (1975) revealed that the cyclic behaviour of steel columns is a function of the applied axial load and magnitude of inter-storey drifts. The normalized axial load v limit of 0.3 adopted by most codes is historically tied to this series of tests (Bruneau et al., 1998). Later, Roeder et al. (1993) and Schneider et al. (1993) shown that weak-column/strong-beam frames seem to initiate rapid strength and stiffness deterioration when the columns are subjected to normalized axial loads equal to about 0.25 and that P-Δ effects do not appear to be critical for displacement levels of less than 5% storey drift. Medina and Krawinkler (2005) also observed that regular frames exhibit potential for column plastic hinging even for *CBMRs* greater than 3.0 and concluded that more stringent strong-column/weak-beam criteria appear to be called for. Median *CBMRs* of about 2.0 would be required during design to ensure a behaviour factor q of around 4.0. Equally, it was shown that actual column flexural demands can be much larger than anticipated in design since column moment diagrams can deviate significantly during inelastic response from the double-curvature shape assumed in elastic analysis. More recently, Elkady and Lignos (2014b) concluded that MRSFs designed with *CBMRs* greater than 1.5 or 2.0 achieve a uniform and acceptable probability of collapse over 50 years and recommended that further analytical studies on the identification of the optimum *CBMR*s to be used in the seismic design of steel moment frames should be carried out. In order to propose a criterion for the identification of the onset of plastic hinging at columns some of these aspects will be examined.

Figure 5.7 (a) depicts a comparison between the design *CBMRs* (Table 5.1) and the inter-storey drifts (*ISD*) at the onset of plastic hinging at the top and bottom nodes of the columns of the corresponding column-to-beam joint for every analysed building. These results were also compared with the error in the nonlinear chord rotation estimates, defined as the ratio between the exact (θ_{NL}) and predicted ($\theta_{L,eq,corr}$) nonlinear chord rotations at the critical beam of each joint. It may be observed that joints featuring *CBMRs* greater than 2.80 do not develop plastic hinges at columns, whereas joints with *CBMRs* greater than 1.0 seem to initiate plastic hinging at columns when an *ISD* ratio of about 2.0% is reached. Moreover, all joints with *CBMRs* lower than 1.50, with the exception of building SB9, developed plastic hinges at columns for *ISD* ratios lower or equal to 3%. A relationship between the design *CBMR* and the *ISD* at the onset of plastic hinging at columns was found to exist. Moreover, it was be concluded that, at the onset of plastic hinging at columns, the proposed simplified procedure generally leads to conservative estimates of

beam nonlinear chord rotations when θ_{NL} / $\theta_{L,eq,corr}$ < 1.0 and to acceptable levels of error, below 20%, at the most demanded beams when θ_{NL} / $\theta_{L,eq,corr}$ > 1.0. Based on these observations, a regression model was fitted to data so as to provide an expression that establishes the range of applicability (i.e. buildings where plastic hinging at columns has not occurred or is initiating) of the proposed procedure in terms of a limit *ISD*, ISD_{limit}, obtained from linear analysis that is function of the design *CBMR* (Figure 5.7 (b)). Hence, if the minimum ISD_{limit} of a storey, obtained for every column-to-beam joint, is exceeded by the *ISD* of that same storey obtained from a linear-elastic analysis, then the proposed simplified procedure fails its applicability.

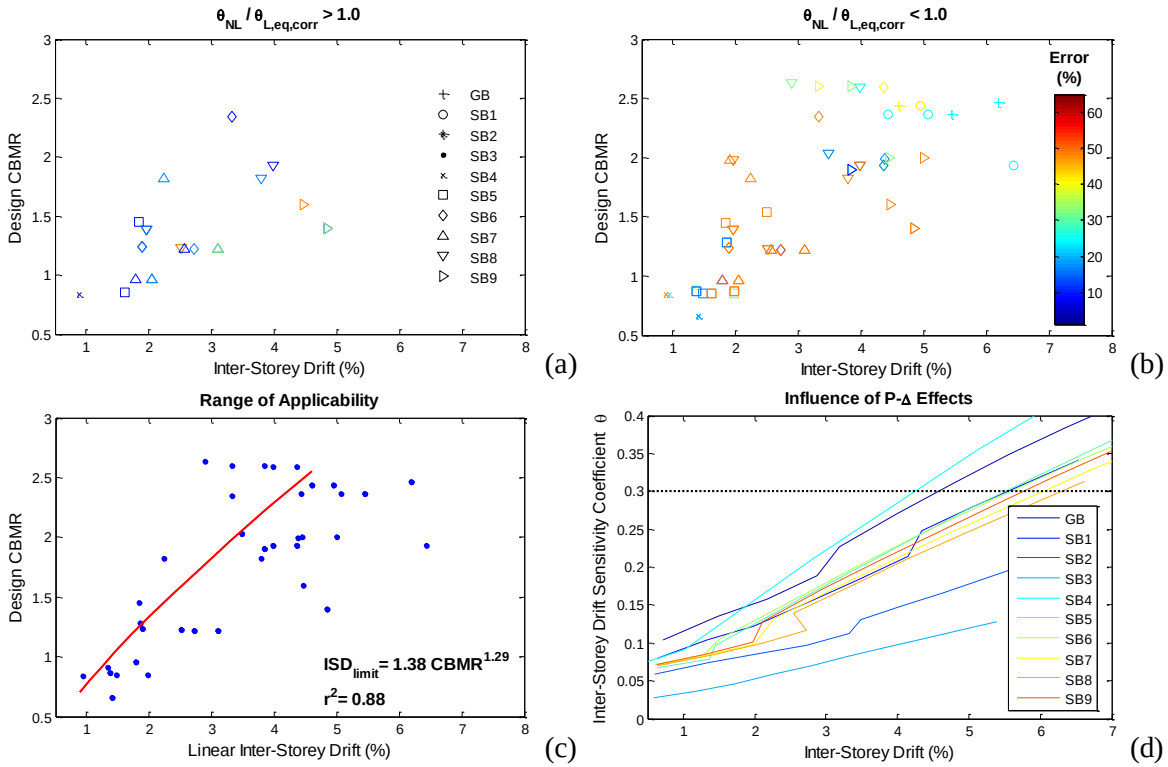

Figure 5.7 – Range of applicability of the proposed procedure: (a) confrontation of the design *CBMR* with the *ISD* at the onset of plastic hinging at the joint columns and comparison with the accuracy of the proposed procedure in estimating the nonlinear chord rotations at the beams of the corresponding joint; (b) fitting of the regression model to data; (c) and evaluation of the influence of *P*-Δ effects in the structural response of each building.

The influence of *P*-Δ effects in the structural response of the buildings was equally evaluated by assessing the inter-storey drift sensitivity coefficient θ, already presented in Table 5.1 for the seismic design of every building. Figure 5.7 (c) displays the evolution of θ for increasing levels of *ISD*, being observed that not only the influence of *P*-Δ effects significantly reduces with the lateral stiffness and strength of the building, as it would be previously expected, but also that θ always exhibits values below 0.3 for the *ISDs* at the onset of plastic hinging at columns. Thus, the proposed applicability criterion seems to

equally ensure acceptable levels of *P*-Δ effects. It may be referred that the maximum normalized axial load *v* at columns was found to be practically constant at every building and of about 0.2.

A proof of concept of the proposed procedure is presented in Figure 5.8 by laterally pushing buildings GB and SB6 to global drift ratios (*GDR*) of 2.0% and 4.0%. Building GB is associated to a governing ISD_{limit} of 4.4% at the 2nd storey, which is exceeded for a *GDR* of approximately 3.0%. As a result, the proposed procedure is applicable until a *GDR* of 3.0% is reached. However, although building GB fails to verify the proposed procedure applicability criterion for a *GDR* of 4.0%, it still provides satisfactory, although rather conservative, nonlinear chord rotation estimates, contrarily to conventional linear-elastic analysis (Figure 5.8 (a)). For a *GDR* of 2.0%, the proposed procedure was seen to perform quite accurately. On the other hand, Building SB6 is associated to a governing ISD_{limit} of 1.8%, equally at the 2nd storey, that is exceeded for *GDRs* greater than 2.0%. In accordance to this range of applicability, it may be observed from Figure 5.8 (b) that the proposed simplified procedure provides good estimates of nonlinear chord rotations for *GDRs* lower than 2.0% and fails to capture the variation in the distribution of deformation demands over the height of the building, from the 3rd to the 1st storey, for greater values of *GDR*. Recall that building SB6 is expected to develop a soft-storey mechanism at a *GDR* of about 4% (Figure 5.1).

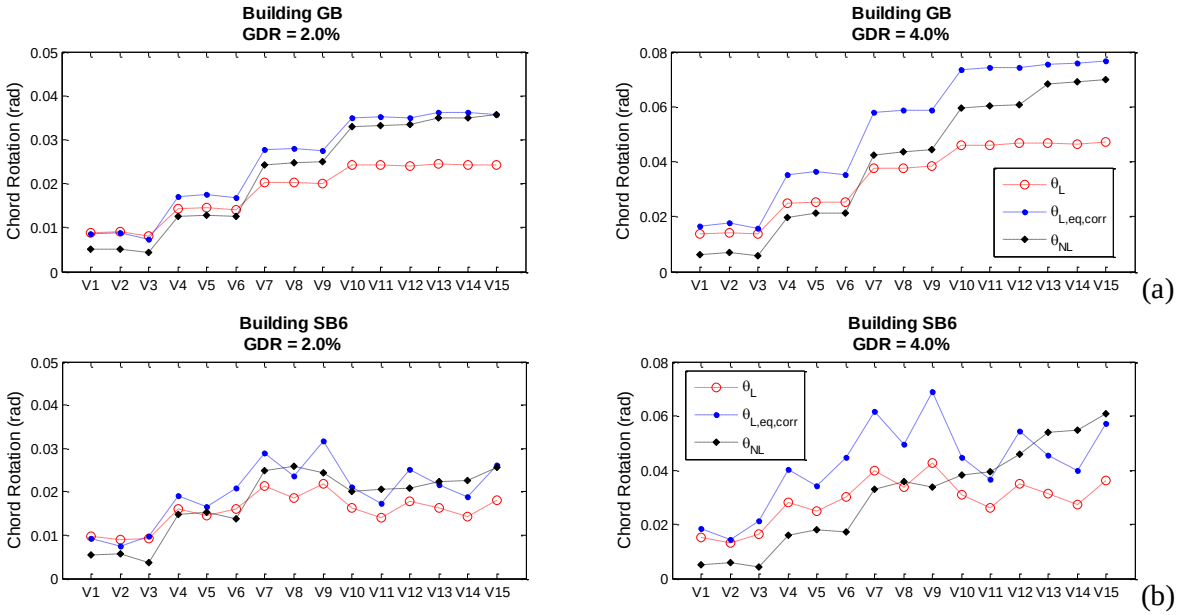

Figure 5.8 – Example of application of the proposed procedure to (a) building GB and (b) building SB6 for different values of global drift ratio, *GDR*.

5.5 Comparative study and evaluation of the proposed procedure

In this section, the different methods of quantifying inelastic chord rotation demands using linear-elastic analysis procedures are evaluated and compared with the results obtained from nonlinear methods of analysis. Linear-elastic static and dynamic analyses were conducted using the EC8-3 lateral force method (LF) and the modal response spectrum method (MRSA), respectively, while nonlinear static and dynamic analyses were conducted using the EC8 N2 method and time-history analysis (THA), respectively. In the latter case, 15 sets of seven ground motion records scaled to match the EC8 elastic spectrum defined, again, for a Portuguese type 1 and Zone 3 seismic action (Lisbon), located in a soil type B, were adopted. An additional criterion was included in the selection of each individual record by imposing mismatch limits relative to the target spectrum of ±50%. This additional measure has been demonstrated in Chapter 3 to significantly reduce the variability in the structural response estimates. The analyses were performed for the Damage Limitation, Significant Damage and Near Collapse limit states, as defined by EC8-3 for return period values T_r of 225, 475 and 2475 years, which correspond to PGA values of 0.091g, 0.15g and 0.451g, respectively.

Figure 5.9 depicts the comparison between the various methods of quantifying chord rotations at the Near Collapse limit state of buildings GB, SB2 and SB3, which were seen to verify the proposed procedure applicability criterion defined by ISD_{limit}. Similar conclusions to those obtained for these buildings were observed in building SB1. Firstly, it may be concluded that the proposed procedure ($\theta_{L,eq,corr}$) always provides satisfactory and conservative results when compared to nonlinear analysis (θ_{NL}), contrarily to conventional linear analysis (θ_L), which, as previously stated, systematically underestimates nonlinear chord rotations. Note that the θ_{NL} values obtained from dynamic THA are defined as the mean of the chord rotation values of the 15 sets of ground motion records and that the shaded area reflects the associated variability. Moreover, the significant overestimates of chord rotations observed in the static analysis results when using the Günay and Sucuoglu (2009; 2019) approach ($\theta_{L,Gunay}$) at buildings SB2 and SB3 and the proposed procedure at building SB2 are due to the correction factor λ of the EC8 LF method, which should be equal to 1.0 for structures with a fundamental period of vibration T_1 greater than 1.20s, and 0.85 otherwise. In fact, the increase in T_1 of building SB3 due to the reduction of stiffness of the members proposed by Günay and Sucuoglu (2009; 2019), changed λ from 0.85 to

1.0 and consequently lead to higher structural response demands. In Chapter 2 and 4 it has been already demonstrated that both linear static and dynamic methods of analysis generally lead to higher global drift demands when comparing to nonlinear methods of analysis. Better estimates could be eventually obtained by using an elastic response spectrum with an equivalent damping as proposed by Yaghmaei-Sabegh et al. (2014). Finally, the FEMA P-58-1 procedure ($\theta_{L,FEMAP58}$) was seen to fail to provide good chord rotation estimates.

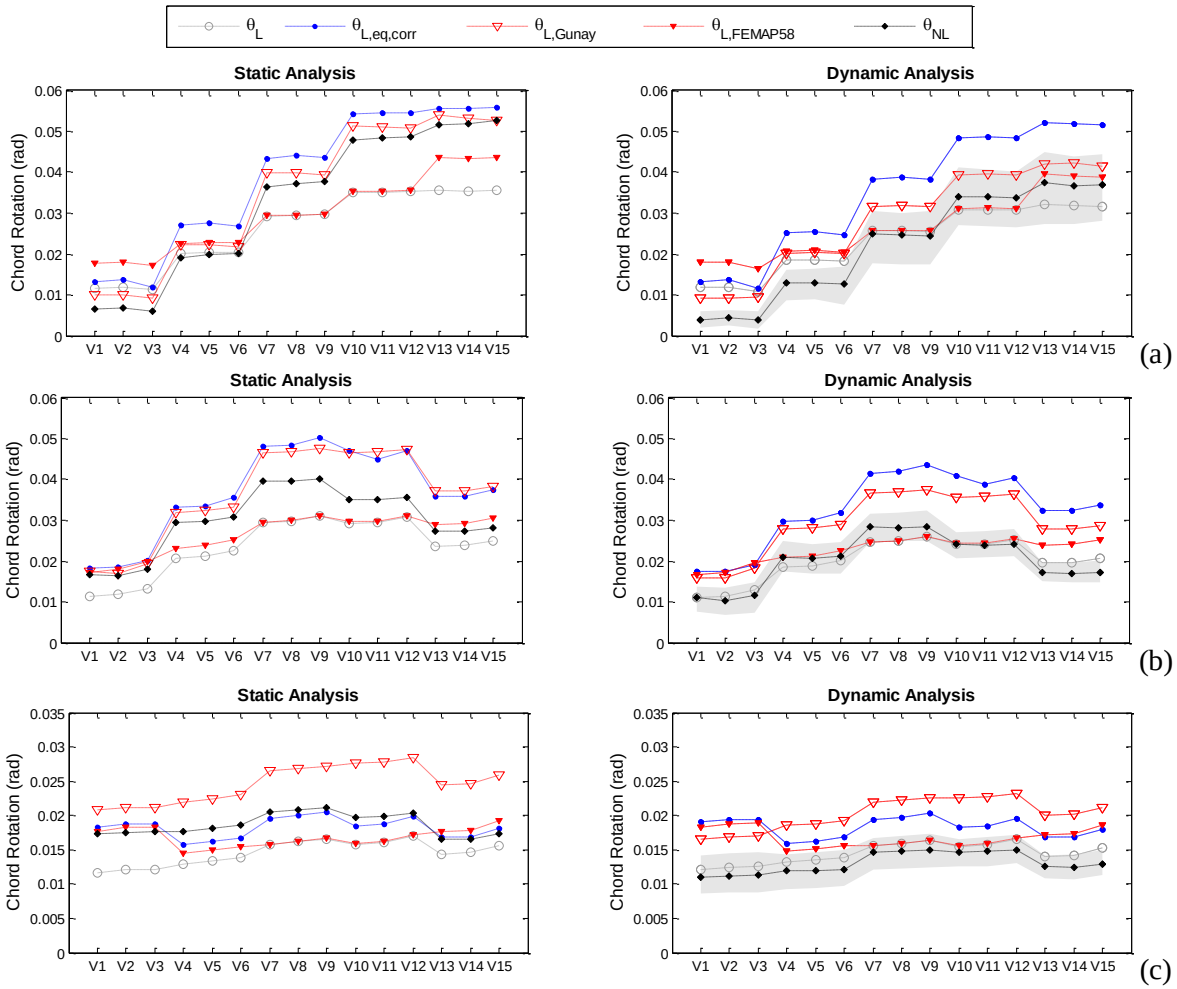

Figure 5.9 – Comparison between the different methods of quantifying chord rotations at the Near Collapse limit state of: (a) building GB; (b) building SB2; (c) and building SB3.

The comparison between the various methods of quantifying chord rotations at the Near Collapse limit state of buildings SB6, SB7 and SB9, which do not verify the proposed procedure applicability criterion, is displayed in Figure 5.10. Indeed, the proposed procedure was unable to capture the variation in the distribution of deformation demands over the height of the buildings. *GDRs* around 2.6% were obtained for each one of these buildings at the Near Collapse limit state using pushover analysis, being expected that buildings SB6 and SB7 would exhibit a significant concentration of plastic deformation

demands at the 1st storey columns and could be about to develop a soft-storey mechanism (Figure 5.1).

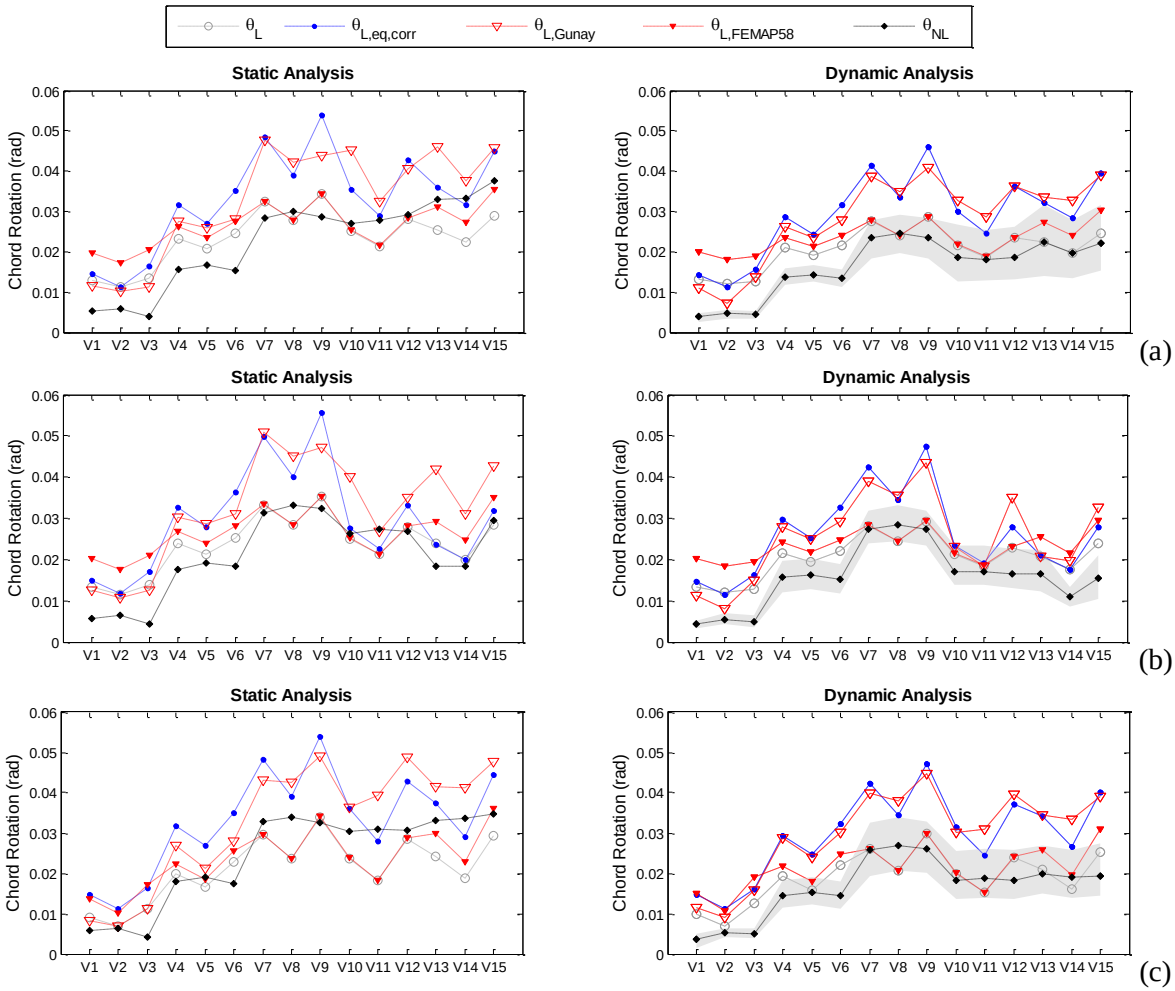

Figure 5.10 – Comparison between the different methods of quantifying chord rotations at the Near Collapse limit state of: (a) building SB6; (b) building SB7; (c) and building SB9.

Alternatively, although the Günay and Sucuoglu (2009; 2010) procedure provides chord rotation demands at beams similar to those obtained using the procedure proposed herein, it has as an advantage the ability to estimate the nonlinear chord rotations at columns through their stiffness updating, thus being equally applicable in the case of buildings exhibiting significant variations in the distribution of deformation demands, such as buildings SB6, SB7 and SB9. Figure 5.11 demonstrates the accuracy of the Günay and Sucuoglu (2009; 2010) procedure in predicting nonlinear chord rotations at the base of the 1st storey columns of buildings SB6 and SB7, which developed soft-storey mechanisms at 2 records and 1 record of the 15 sets of ground motions adopted, respectively. A soft-storey mechanism was considered to be develop not only when plastic hinges were developed at both top and bottom nodes of all columns of a certain storey, but also when the maximum deformation demands were concentrated at that storey columns and not at

beams. Similar findings were observed for buildings SB4 and SB5. Günay and Sucuoglu (2010) had already demonstrated the ability of the method to capture the development of eventual soft-storeys. On the contrary, linear analysis was seen to provide acceptable chord rotation θ_L estimates, which also refer to those of the proposed procedure, at the base of columns P5, P10, P15 and P20 of buildings SB8 and SB9. Recall that the proposed procedure simply corrects beam chord rotations and assumes that column chord rotations may be directly obtained from linear-elastic analysis. Hence, the applicability criterion defined by ISD_{limit} may be equally seen to be slightly conservative in the case of buildings SB8 and SB9. This conservative character may be explained by the fact that the onset of plastic hinging at columns may not necessarily imply significant variations in the distribution of demands along the height of the buildings. In turn, the Günay and Sucuoglu (2009; 2010) procedure overestimated column chord rotation demands at buildings SB8 and SB9 (Figure 5.11).

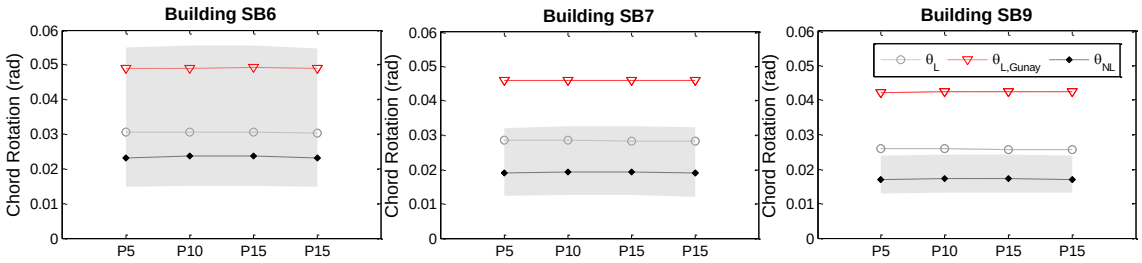

Figure 5.11 – Chord rotations at the base of the 1st storey columns of buildings SB6, SB7 and SB9 obtained from dynamic analysis.

To assess the performance of the applicability criterion defined by ISD_{limit}, Figure 5.12 presents the comparison between the β values computed for each one of the sets of ground motion records at the various limit states of buildings SB6, SB7 and SB9 and the ratio between the nonlinear *ISDs* obtained from THA and the proposed ISD_{limit}. The variation in the distribution of demands over the height of the building, represented by a significant variation in β, may be thus seen to be conveniently captured by ISD_{limit}, particularly at buildings SB6 and SB7, which are more susceptible to the development of soft-storey mechanisms. To conclude, Figure 5.13 depicts a comparison between the various methods of quantifying chord rotations at the Significant Damage limit state of buildings SB2 and SB7, being shown that the proposed procedure, which is now applicable to building SB7, still provides slightly conservative, though fairly reasonable, chord rotation estimates comparing to those obtained from nonlinear analysis. The Günay and Sucuoglu (2009; 2010) procedure, in turn, tends to approach the 'exact' nonlinear chord rotation values, which are defined as the mean of the chord rotations obtained for each set

of ground motion records. Still, whilst the Günay and Sucuoglu (2009; 2010) procedure is based on an iterative step analysis that requires substantial work in updating the reduced stiffness of the members, the procedure proposed herein allows for a prompt estimation of nonlinear chord rotations in a single step.

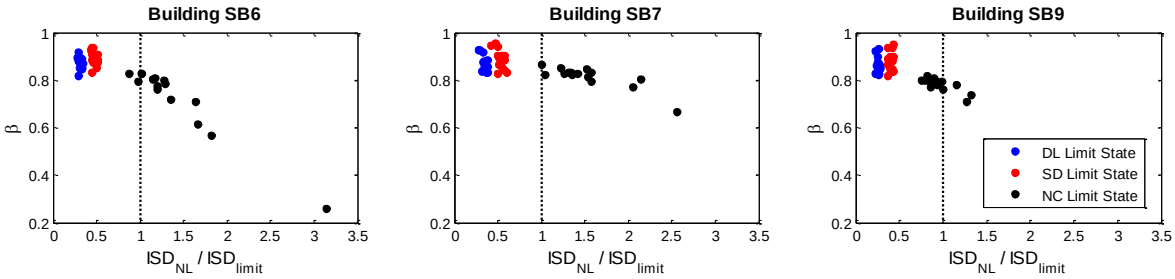

Figure 5.12 – Comparison between the β values computed for every set of ground motion records at the various limit states of buildings SB6, SB7 and SB9 and the ratio between nonlinear *ISD* and ISD_{limit}.

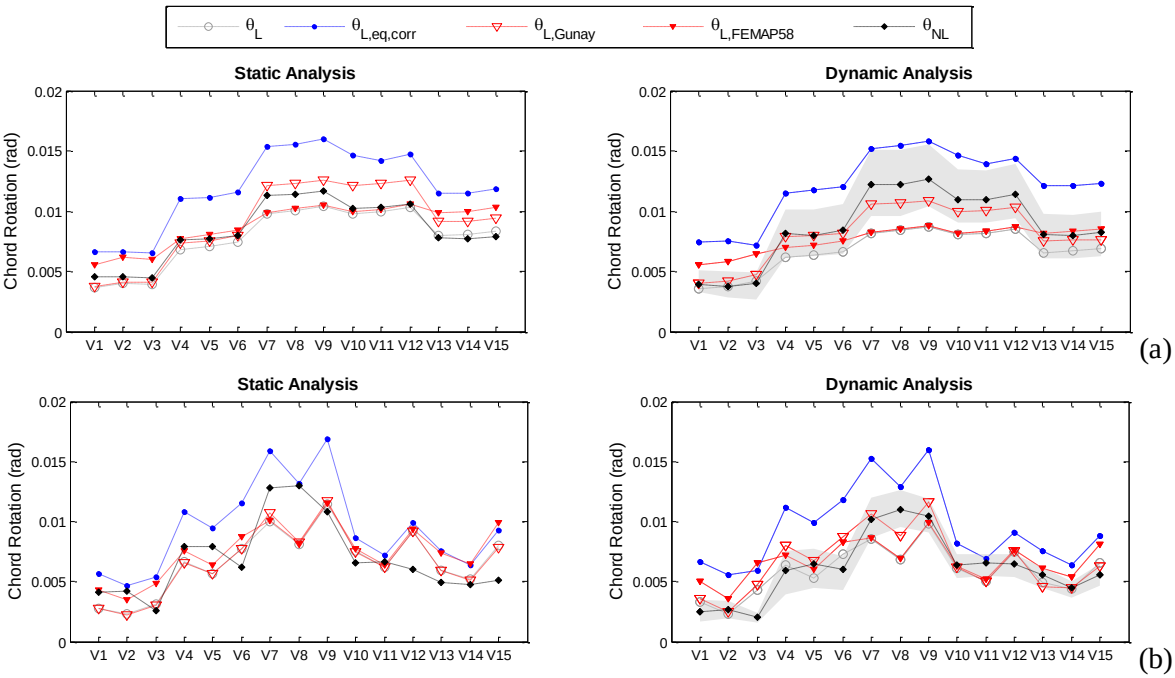

Figure 5.13 – Comparison between the different methods of quantifying chord rotations at the Significant Damage limit state of: (a) building SB2; (b) and building SB7.

5.6 Conclusions

In this chapter, a simplified procedure that allows for the estimation of beam inelastic chord rotations using linear-elastic methods of analysis in an expeditious and conservative way is presented. A number of moment-resisting steel frames designed according to different criteria and exhibiting different column-to-beam moment ratios (*CDMR*) were analysed and served as the basis for the derivation of the procedure proposed herein. This procedure relies on empirical evidence that the ratio between nonlinear and linear chord

rotations at beams increases almost proportionally to the ratio between the corresponding linear and nonlinear shear-spans. An expression for determining the nonlinear shear-spans was derived for the case studies under analysis based on the capacity-design principles, while an approximate method for estimating linear chord rotations was used by considering an equivalent linear-elastic cantilever beam. Moreover, the proposed procedure was derived for buildings that are expected to develop stable beam-sway mechanisms and are not expected to exhibit significant variations in the distribution of deformations demands over their height. An applicability criterion was thus defined aiming to extend the use of this simplified procedure to a broader number of cases. It was demonstrated that the proposed procedure consistently leads to good and conservative estimates of nonlinear chord rotations. This conservative character was seen to increase as the seismic action increases. Nevertheless, further studies on the evaluation of the proposed procedure and calibration of the applicability criterion should be carried out, particularly in the case of irregular structures.

A comparative study was additionally conducted considering the equivalent linearization procedure developed by Günay and Sucuglou (2009) and the simplified procedure preconized by FEMA P58-1. Although the Günay and Sucuglou (2009; 2010) procedure was seen to provide quite good estimates of nonlinear chord rotation demands, even for buildings exhibiting an important variation of deformation demands over their heights, it required a substantial amount of work in updating the reduced stiffness of all members of the structure. On the other hand, the FEMA P-58-1 procedure failed to provide reasonable estimates of inelastic chord rotations.

5.7 Acknowledgments

This work was performed within the framework of the research project ‘Development and calibration of seismic safety assessment methodologies for existing buildings according to the Eurocode 8 – Part 3’ founded by Foundation of Science and Technology (FCT) of Portugal.

5.8 References

Akkar S, Miranda E (2005) Statistical evaluation of approximate methods for estimating maximum deformation demands on existing structures, Journal of Structural Engineering, 131, 160-172.

ASCE (2014) Seismic evaluation and retrofit of existing buildings (ASCE/SEI 41-13), American Society of Civil Engineers.

Bal IE, Crowley H, Pinho R (2010) Displacement-based earthquake loss assessment: method development and application to Turkish building stock, IUSS Press, Pavia, Italy.

Browning J, Warden B, Matamoros A, Lepage A (2008) Global and local seismic drift estimates for RC frames, Engineering Structures, 30, 1262–1271.

Bruneau M, Uang CM, Whittaker A (1998) Ductile design of steel structures, McGraw-Hill, New York.

Castro JM, Dávila-Arbona FJ, Elghazoulli AY (2008) Seismic design approaches for panel zones in steel moment frames. Journal of Earthquake Engineering; 12, 34-51.

CEN (2004) ENV 1998-1 Eurocode 8: Design of structures for earthquake resistance - Part 1: general rules, seismic actions and rules for buildings, European Committee for Standardization, Brussels, Belgium.

CEN (2005) ENV 1998-3 Eurocode 8: Design of structures for earthquake resistance - Part 3: Assessment and retrofitting of buildings, European Committee for Standardization, Brussels, Belgium.

Elghazouli AY, Kumar M, Stafford PJ (2014) Prediction and optimisation of seismic drift demands incorporating ground motion frequency content, Bulletin of Earthquake Engineering, 12, 255-276.

Elkady A, Lignos DG (2014a) Analytical investigation of the cyclic behavior and plastic hinge formation in deep wide-flange steel beam-columns, Bulletin of Earthquake Engineering, 13, 1097-1118.

Elkady A, Lignos GD (2014b) Modeling of the composite action in fully restrained beam-to-column connections: implications in the seismic design and collapse capacity of steel special moment frames, Earthquake Engineering and Structural Dynamics, in press.

Elkady A, Lignos DG (2013) Collapse assessment of steel moment resisting frames with deep members, Proceedings of the Vienna Congress on Recent Advances in Earthquake Engineering and Structural Dynamics, Vienna.

FEMA (2005) FEMA 350 Recommended seismic design criteria for new steel moment-frame buildings, Document developed by the SAC Joint Venture for the Federal Emergency Management Agency, Washington, D.C., USA.

FEMA (2012) FEMA P-58-1 Seismic performance assessment of buildings. Volume 1 – Methodology, Federal Emergency Management Agency, Washington, D.C., U.S.A.

Gioncu V, Petcu D (1997) Available rotation capacity of wide-flange beams and beam-columns, Journal of Constructional Steel Research, 43, 219–244.

Günay MS, Sucuoglu H (2010) An improvement to linear-elastic procedures for seismic performance assessment, Earthquake Engineering and Structural Dynamics, 39, 907–931.

Günay MS, Sucuoglu, H (2009) Predicting the seismic response of capacity-designed structures by equivalent linearization, Journal of Earthquake Engineering, 13, 623-649.

Gupta A, Krawinkler H (2000) Behavior of ductile SMRFs at various seismic hazard levels, Journal of Structural Engineering, 126, 98-107.

JBDPA (1996) Recommendations for seismic diagnosis and upgrading of existing steel buildings, Japan Building Disaster Prevention Association, Tokyo, Japan (in Japanese).

Kumar M, Castro JM, Stafford PJ, Elghazouli AY (2011) Influence of the mean period of ground motion on the inelastic dynamic response of single and multi degree of freedom systems, Earthquake Engineering and Structural Dynamics, 40, 237-256.

Kumar M, Stafford PJ, Elgazouli AY (2013) Influence of ground motion characteristics on drift demands in steel moment frames designed to Eurocode 8, Engineering Structures, 52, 502-517.

Kunnath SK, Nghiem Q, El-Tawil S (2004) Modeling and response prediction in performance-based seismic evaluation: case studies of instrumented steel moment-steel buildings, Earthquake Spectra, 20, 883-915.

Lin YY, Miranda E (2009) Evaluation of equivalent linear methods for estimating target displacements of existing structures, Engineering structures, 31, 3080-3089.

Lignos DG, Krawinkler H (2011) Deterioration modelling of steel components in support of collapse prediction of steel moment frames under earthquake loading, Journal of Structural Engineering, 137, 1291-1302.

Mazzolani FM, Piluso V (1996) Theory and design of seismic resistant steel frames, E & FN Spon, London, UK.

Medina RA, Krawinkler H (2005) Strength demand issues relevant for the seismic design of moment-resisting frames, Earthquake Spectra, 21, 415-439.

Miranda E, Reyes CJ (2002) Approximate lateral drift demands in multi-storey buildings with nonuniform stiffness, Journal of Structural Engineering, 128, 840-849.

Newell JD (2008) Cyclic behaviour and design of steel columns subjected to large drift, PhD Dissertation, University of California, San Diego, CA.

NZSEE (2006) Assessment and improvement of the structural performance of buildings in earthquake. Recommendation of a NZSEE study group on earthquake risk buildings, New Zealand Society for Earthquake Engineering, New Zealand.

Paret TF, Searer GR (2011) Freeman SA (2011) “ASCE 31 and 41: Apocalypse Now.”, Structures Congress, Las Vegas, Nevada.

PEER (2011) OpenSees: Open system for earthquake engineering simulation, Pacific Earthquake Engineering Research Center, Universtiy of California, Berkeley, CA.

Popov EP, Bertero VV, Chandramouli S (1975) Hysteretic behaviour of steel columns, Earthquake Engineering Research Center Report UCB/EERC-75-11, University of California, Berkley, USA.

Priestley MJN, Calvi CM, Kowalsky MJ (2007) Displacement-Based Seismic Design of Structures, IUSS Press, Pavia, Italy.

Roeder CW, Schneider SP, Carpenter JE (1993) Seismic behavior of moment-resisting steel frames: analytical study, Journal of Structural Engineering, 119, 1866-1884.

Ruiz-Gárcia J, Miranda E (2003) Inelastic displacement ratios for evaluation of existing structures, Earthquake Engineering and Structural Dynamics, 32, 1237-1258.

Schneider SP, Roeder CW, Carpenter JE (1993) Seismic behavior of moment-resisting steel frames: experimental study, Journal of Structural Engineering, 119, 1885-1902.

Trahair NS, Bradford MA, Nethercot DA, Gradner L (2008) The behavior and design of steel structures to EC3. Fourth edition, Taylor & Francis, New York, USA.

Welch DP, Sullivan TJ, Calvi GM (2014) Developing direct displacement-based procedures for simplified loss assessment in performance-based earthquake engineering, Journal of Earthquake Engineering, 18, 290-322.

Whittaker S, Huang Y (2007) Simplified response analysis procedures, Background document of FEMA P-58/BD-3.7.4, Federal Emergency Management Agency, Washington, D.C.

Yaghmaei-Sabegh S, Neekmanesh S, Lumantarna E (2014) Nonlinear response estimates of RC frames using linear analysis of SDOF systems. Earthquake Engineering and Structural Dynamic, 43, 769-790.

Chapter 6

On the estimation of the deformation capacity of European steel members. How adequate are the EC8-3 deformation limits?

Araújo M, Macedo L, Castro JM (2017) Evaluation of the rotation capacity limits of steel members defined in EC8-3. Journal of Constructional Steel Research 135:11–29.

6.1 Summary

One issue of major importance on the application of seismic assessment guidelines is that of the deformation capacity limits prescribed for the various limit states. In the case of existing steel structures, Part 3 of Eurocode 8 (EC8-3) defines the limits in terms of plastic rotations, which are only valid for normalized axial load levels lower than 0.3 and cross-section classes of type 1 and 2. These limits resemble the ones defined in ASCE41-13, suggesting a direct reproduction from the latter document despite their derivation on the basis of typical American profiles. Hence, this Chapter aims at evaluating the deformation capacity of European steel members and answers the question of how adequate are the EC8-3 limits. Based on detailed FE models, the influence of member imperfections, axial load and real ground motion records is assessed. Fracture is taken into account and general expressions for predicting the rotation capacity of a wide number of European cross-section profiles are proposed.

6.2 Introduction

Under earthquake loading conditions, excessive levels of deformation in one or several members of a structural system triggers local strength and stiffness deterioration and consequently produces loss of structural integrity, which may be characterized by significant damage or even collapse of the building. Reliable collapse or damage-state

assessments of existing buildings are greatly dependent on the accuracy of the analytical models adopted and their ability to capture the expected level of degradation within a member. The deformation capacity of steel elements and its impact in the collapse prediction of existing buildings are key issues when conducting performance-based analysis and have been the focus of very recent research studies (Krawinkler and Zareian, 2007; Zareian et al., 2010; Lignos et al., 2011; 2013; Dimakopoulou, 2013).

Furthermore, the deformation capacity limits of structural members equally play an unequivocal role in the seismic safety assessment process, namely during the safety verifications stage (Chapter 2). In this context, a relevant aspect regarding the application of the part 3 of Eurocode 8 (EC8-3) (CEN, 2005a) should be highlighted. Not only, the deformation capacity limits proposed by EC8-3 for steel members are only valid for cases of normalized axial load lower than 0.3, but also these limits are simply defined for cross-section classes of type 1 and 2, as defined in the part 1 of Eurocode 3 (EC3) (CEN, 2005b), without any distinction being made between beam or column elements. As a matter of fact, the resemblance between the values proposed by EC8-3 and the American standard ASCE 41-13 (ASCE, 2014) suggests a direct reproduction of the capacity limits defined by the latter standard for beams and columns with a normalized axial load, ν, equal to 0.2, which were derived for typical American cross-section sizes. As a result, further revision of the capacity limits proposed by EC8-3 is required and must be placed as a first priority.

Recently, a joint experimental campaign involving the Universities of Naples and Salerno has promoted a series of scientific works (Brescia, 2009; Tortorelli et al., 2011; D'Aniello et al., 2012; Corte et al., 2013) that focused on the issue of the quantification of the deformation capacity and over-strength of European steel members. This experimental program not only made possible the access to a set of experimental results of great interest for the scientific community, but also has strengthened the idea that the quantification of the deformation capacity of steel members simply based on its monotonic behaviour leads to rather conservative results when comparing to its cyclic behaviour, with ratios in the order of 2 to 3.5 times. Nevertheless, the results provided by this experimental program are limited, particularly regarding the currently used I or H cross-section profiles, whereby the fulfilment of extensive systematization studies on the deformation capacity of steel elements that include a wide number of European metallic profiles are presently required.

Alternative approaches for the quantification of the deformation capacity of steel members have been proposed by Kazantzi et al. (2008) and Lignos and Krawinkler (2011), which are based on univariate and multivariate regression analysis performed on the basis

of experimental results available in the literature, respectively. In both cases, the compilation of results was conducted in a virtually undifferentiated fashion, with respect to the type of experimental setup adopted and structural element tested, thus leading to levels of uncertainty considerably high. According to FEMA 461 (FEMA, 2007; Bradley, 2010), the following sources of epistemic uncertainty shall be accounted for in the definition of the fragility functions of structural members: (i) testing of a component isolated from its real in-situ conditions; (ii) incorrect simulation of boundary conditions; (iii) extrapolation to in-situ conditions not fully simulated in laboratory; (iv) variability in the configuration of the member; (v) uncertainty in the definition of the various damage states and the input load at which they initiate; (vi) and, finally, the variability associated to the material properties, level of imperfections, fabrication and construction methods and details. Likewise, the PEER/ATC-72-1 (ATC, 2010) draws attention to the influence of the slab effect and the axial restraint in the quantification of the deformation capacity of steel members and to the fact that, unfortunately, the majority of currently available experimental test data come from tests that do not include these type of effects. At the present, the American National Earthquake Hazards Reduction Program has initiated a research project addressing the study of the seismic behaviour and design of deep, slender wide flange structural steel beam-column (NEHRP, 2011), being expected further breakthroughs in this field of knowledge.

The present work aims hence at the evaluation of the plastic rotation capacity limits currently proposed by EC8-3 on the basis of detailed FE analyses of steel elements under combined uniaxial bending and axial compression. Special attention is given to the modelling of the member imperfections, being the numerical models validated by comparison with experimental test data (D'Aniello et al., 2012). The main demand parameters are quantified for both monotonic and cyclic loading protocols, as well as for a set of real ground motion records. These values are compared with the estimates obtained using expressions available in the literature. A parametric study is also performed in order to examine the influence of the geometrical imperfections and the level of axial load in the deformation capacity of this type of elements. A wide number of section sizes and values of plate slenderness typical of steel sections common in European practice are evaluated and a multivariate regression analysis is then conducted so as to provide empirical equations for quantifying the deformation capacity of steel members in a sufficiently accurate and expeditious way. Finally, since the ultimate strength and ductility of steel members may be often controlled by ductile fracture, ultra-low cycle fatigue (ULCF),

which occurs at very small number of cycles (<100 cycles) (Pereira et al., 2014), is additionally investigated.

6.3 Experimental data and comparison with existing prediction models

The experimental data adopted in this work was provided by D'Aniello et al. (2012) and respects to the bending capacity of three steel beam-columns with cross-sections HEB 240, HEA 160 and IPE 300. It readily stands out from the observation of Figure 6.1 that all specimens exhibit lower rotation capacities under cyclic loading conditions, when comparing to those obtained from monotonic loading. This decrease is in the order of 1.7 to 2.5 times and is larger in more compact cross-sections, namely in the member with cross-section HEB 240. The latter was also seen to dissipate a higher amount of energy as the number of cycles grew. Moreover, as pointed out in previous studies (Torabiam and Schafer, 2014; Shokouhian and Shi, 2014), the height of the web plastic mechanism was found to increase for increasing flange widths, which is associated with a reduction in the rotation capacity of the member. Each specimen experienced a coupled in-plane and out-of-plane instability mechanism despite the presence of torsional restraints at both ends (D'Aniello et al., 2012). These results are in line with the observations provided by Gioncu and Anastasiadis (2014), according to which out-of-plane buckling is associated with a local sectional deformation, rather than the global member deformation as lateral/torsional buckling, thus leading to a rapid strength and ductility degradation. The failure mode of all specimens was also characterized by the development of cracks at the flange (Brescia, 2009). Furthermore, regarding the flexural over-strength of steel members, it was found that the H and I profiles tend to exhibit values under cyclic loading conditions somehow similar to those observed under the monotonic loading (Güneyisi et al., 2013).

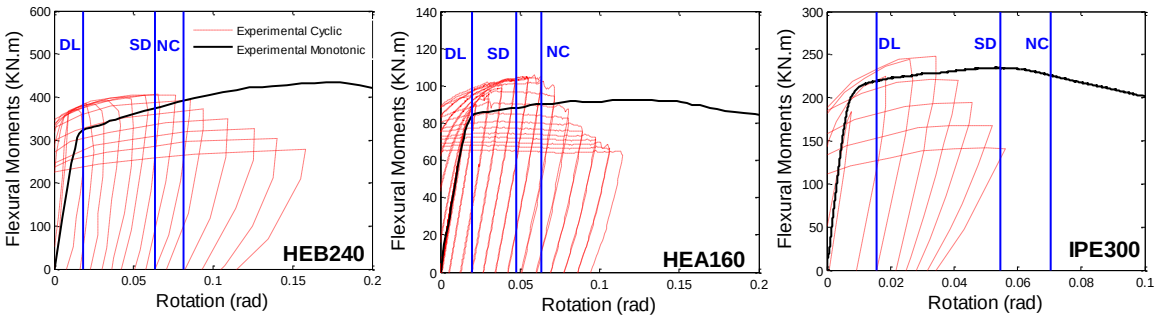

Figure 6.1 – Comparison of the experimental results obtained from D'Aniello et al. (2012) and the EC8-3 deformation capacity limits.

EC8-3 establishes that a certain structure achieves appropriate levels of protection if a number of limit states (LSs) is satisfied, which are defined as: Near Collapse (NC), Significant Damage (SD) and Damage Limitation (DL). According to this code, beams should develop their full plastic moments without local buckling at the SD limit state, while no axial and flexural yielding or buckling should occur in columns. In turn, at the NC limit state limited local buckling may occur in beams, although no reference is made for columns. Additionally, Mergos and Beyer (2014) refer that the EC8-3 deformation capacities at the NC limit state are related to a 20% drop in the member's peak strength obtained by imposing a loading protocol that should represent a seismic hazard level with 2% of probability of exceedance in 50 years. The deformation capacity at the SD limit state may be then determined as a 75% fraction of the NC deformation capacity. The plastic rotation capacity limits proposed by EC8-3 are defined for the DL, SD and NC limit states by $1\theta_y$, $6\theta_y$, and $8\theta_y$, for a cross-section of class 1 and by $0.25\theta_y$, $2\theta_y$, and $3\theta_y$, for a cross-section of class 2, respectively, being θ_y the chord rotation at yield which is given for a cantilever beam-column element by $\theta_y \approx M_p\ L\ /\ 3EI$. Figure 6.1 depicts the comparison between the limits proposed by EC8-3 and the experimental results. Note that the HEA 160 profile features a flange slenderness ratio greater than the EC3 limit set for plastic cross-sections of class 1. Hence, it may be found that although the EC8-3 limits appear to conveniently fit the HEA 160 and HEB 240 cyclic results, they fail to match those from the IPE 300 profile, being closer to its monotonic experimental results.

These results seem to suggest that the rotation capacity limits proposed by EC8-3 for deep members need to be revised. Similar findings have been recently drawn by Elkady and Lignos (2013; 2014). Although Newell and Uang (2008) have shown that stocky sections are able to sustain drifts of 7-9% radians prior to a 10% reduction in the maximum flexural capacity when subjected to a normalized axial load ranging from 0.35 to 0.75, Elkady and Lignos (2013; 2014) demonstrated that steel components with local slenderness ratios close to the seismic compactness requirements and subjected to a constant normalized axial load of 0.5 tend to lose their flexural capacity before reaching drifts in the order of 3% radians. Moreover, the PEER/ATC-72-1 (ATC, 2010) guidelines refer that despite the ASCE 41-13 deformation limits already account for cyclic deterioration, smaller rotation values at the onset of local buckling appear to be found from real experimental data.

Several prediction models for estimating the deformation capacity of steel members have already been proposed by many authors (Sawyer, 1961; Lay and Galambos, 1967;

Southward, 1969; Susuki and Ono, 1977; Kato and Akiyama, 1981; Kemp and Deller, 1991; Spangemacher and Sedlacek, 1992; Daali and Korol, 1994; Daali, 1995; Mazzolani and Piluso, 1996; Mitani et al., 1997; White and Barth, 1998; Kemp, 2003; Kemp, 2003). However, these are based on rather distinct modelling approaches, varying from: (i) analytical models; (ii) empirical cyclic models; (iii) empirical monotonic models; (iv) and FEM models. Figure 6.2 displays the rotation capacity of steel members at the onset of local buckling obtained from different existing prediction models for the HEB 240 specimen tested by D'Aniello et al. (2012). The root mean square error (RMSE) was calculated relative to the experimental result, providing an idea of the level of epistemic uncertainty (Bradley, 2010) associated with the use of the various prediction models. The high level of error, in the order of 50%, acknowledges the need for a cautious selection of the prediction model that most conveniently represents the real in-situ conditions of the member under evaluation, which will naturally have an important impact in providing reliable collapse or damage-state assessments.

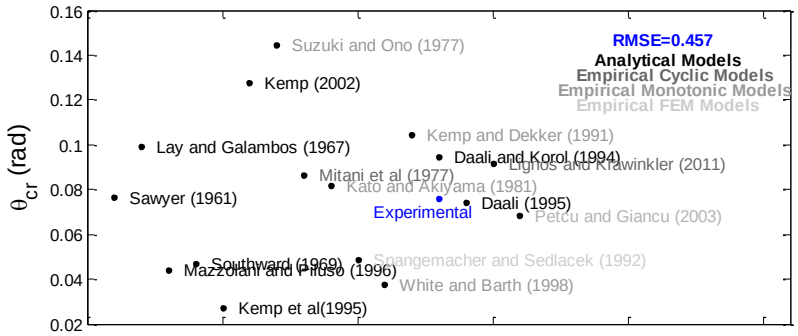

Figure 6.2 – Estimation of the rotation capacity of the HEB 240 column at the onset of local buckling.

6.4 Numerical assessment of the deformation capacity of steel members

6.4.1 Calibration of the numerical models

In order to conduct the present study, a Finite Element (FE) model capable of simulating the monotonic and cyclic response of steel members was firstly developed and calibrated on the basis of the results of the specimens tested by D'Aniello et al. (2012). For such, the ANSYS (2009) structural analysis software package was adopted. The modelled cantilever member has a length of 1.885m and aims to reproduce the behaviour of beam-columns in actual frames subjected to seismic action. The hot rolled HEB 240, HEA 160 and IPE 300 cross-sections previously referred were considered. Thin-walled

elements of type SHELL181 were used with 5 points of Gauss along its thickness. A mesh size of 0.02 x 0.02 m was adopted at the first third of the length of the member so as to conveniently capture the local buckling phenomenon, being doubled at the remaining two-thirds with the aim of providing higher computational efficiency. A mesh sensitivity study was conducted to support the proposed meshing solution. Furthermore, two distinct material models were assumed to reproduce the cyclic and the monotonic behaviour of the members. The monotonic behaviour was modelled by using a multilinear kinematic material model with hardening, designated in ANSYS by KINH. In this case, the engineering stress-strains obtained experimentally (D'Aniello et al., 2012) were converted into true stress-strains (Arasaratnam et al., 2011) and introduced directly in the FE model. Particular attention was paid to the inclusion of local geometrical imperfections in the model, which was found to be of critical importance in numerically capturing the exact experimental response. In the present study three types of local geometrical imperfections were defined taking into account the geometrical tolerances specified for fabrication according to EN 10034 (CEN, 1993) (Figure 6.3). While Model 1 seeks to simulate a scenario where just the top flange of the member is imperfect, being this imperfection defined by the first local buckling mode, both Models 2 and 3 were obtained from a combination of the first local buckling mode with a symmetric and negative symmetric first local buckling mode, respectively. The goal was to simulate two alternative scenarios of symmetrical local geometrical imperfections along the longitudinal axis of the member, equally represented in Figure 6.4.

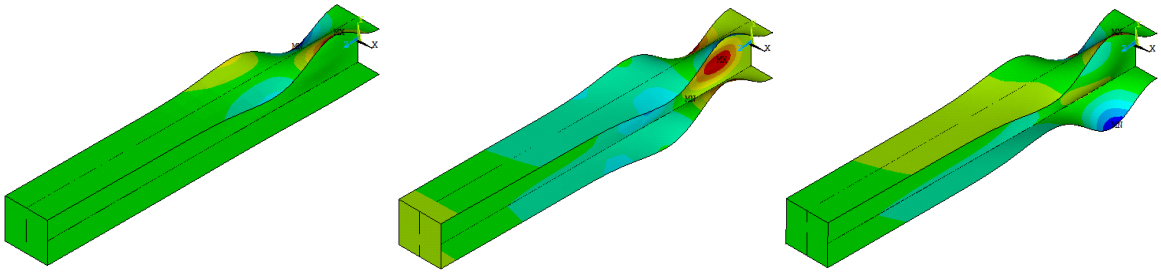

Figure 6.3 – Definition of local geometrical imperfections in Models 1 to 3 (*left-to-right* figures) for the HEB 240 member.

To reproduce the conditions of the experimental tests, the monotonic loading was imposed laterally at the top of the member through in-plan displacements (δ_y), while its out-plan displacements (δ_x) were restrained to avoid the occurrence of flexural-torsional instabilities (D'Aniello et al., 2012). Fully fixed boundary conditions were applied at the base of the member. Figure 6.4 depicts the monotonic response of the HEB 240 member in

both positive (PA^+) and negative (PA^-) y-axis directions. The nomenclature adopted in the identification of the local geometrical imperfections, *k+k'*, is in agreement with the one established by EN 10034 (CEN, 1993). The imposed local geometrical imperfections were scaled until a reasonable match between the numerical and the experimental results was obtained. Once again, it may be seen from Figure 6.4 that the non-inclusion of local geometrical imperfections in the model, case *k+k'=0*, delays the onset of the local buckling observed experimentally. The Model 2, on the other hand, was found to better capture the experimental monotonic response of the member in both loading directions, being adopted in the following studies.

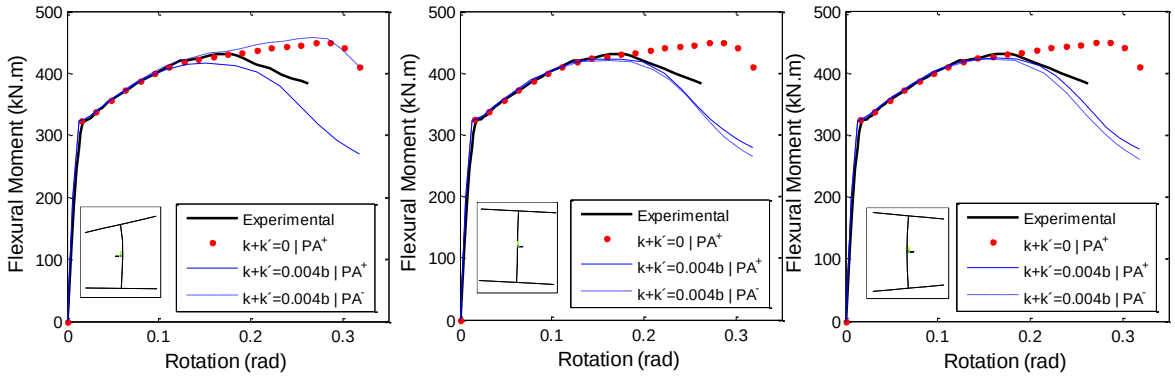

Figure 6.4 – Monotonic response of the HEB 240 member assuming different local geometrical imperfection of Models 1 to 3 (*left-to-right* figures).

Figure 6.5 displays the ability of the FE model to capture local instabilities adequately, in particular the coupled in-plane and out-of-plane instability mechanism observed more clearly in the IPE 300 member despite the presence of torsional restraints at both ends (Figure 6.5 b).

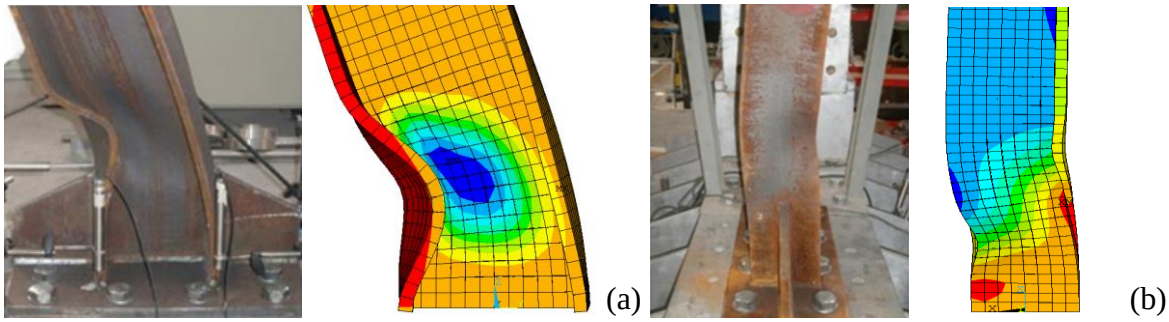

Figure 6.5 – Comparison between the numerical and the experimental deformation mode patterns: (a) monotonic instability mechanism of the HEB 240 member; (b) cyclic coupled in-plan and out-of-plan instability mechanism of the IPE 300 member.

The cyclic behaviour was simulated by adopting the nonlinear kinematic material model with hardening, designated in ANSYS by CHABOCHE, combined with a nonlinear isotropic hardening model, designated by NLISO. The isotropic component defines the

change of the size of the yield surface σ^o as a function of equivalent plastic strain ε^p, being given by:

$$\sigma^o = \sigma|_0 + Q_\infty \left(1 - e^{-b_{iso}\varepsilon^p}\right) \tag{6.1}$$

where $\sigma|_o$ is the yield stress at zero equivalent plastic strain (i.e. the yield stress f_y), Q_∞ is the maximum change in the size of the yield surface and b_{iso} is the rate at which the size of the yield surface changes as plastic strain increases (Lemaitre and Chaboche, 1990; Chaboche, 2008; Nip et al., 2010). For its turn, the kinematic component of the model establishes the change of backstress α, which is related to the translation of the yield surface, so that:

$$\alpha = \frac{C_{kin}}{\gamma}\left(1 - e^{-\gamma\varepsilon^p}\right) + \alpha_1 e^{-\gamma\varepsilon^p} \tag{6.2}$$

being C_{kin} and γ constants calibrated by test data from stabilised cycle (Lemaitre and Chaboche, 1990). The ratio C_{kin}/γ represents the maximum change in backstress and γ determines the rate at which the backstress varies as the plastic strain increases. Experimental cyclic stress-strain curves can be found in literature (Kaufmann et al., 2001; Nip et al., 2010). Nip et al. (2010) calibrated the parameters of the nonlinear combined isotropic/kinematic hardening model based on hot-rolled steel coupons of grade S355 and shown that there is high variability associated to each individual parameter. In this work, both C_{kin} and γ constants were calibrated so as to provide a good agreement between the numerical and experimental cyclic responses of the members tested by D'Aniello et al. (2012). Values of C_{kin} and γ of 7000 MPa and 50, 17000 MPa and 150 and 10000 MPa and 170 were obtained for the HEB 240, HEA 160 and IPE 300 members, respectively. The parameters Q_∞ and b_{iso} can be equally acquired from constant amplitude cycle tests and values of 150 MPa and 2 (Elkady and Lignos, 2014) were considered, respectively. Furthermore, the AISC (2005) loading protocol, herein designated by SAC loading protocol in accordance with the name of the project that lead to its development (Elkady and Lignos, 2014), was employed in line with the experimental tests.

Figure 6.6 depicts the numerical predictions of the monotonic and cyclic behaviour for the three beam-column members under analysis. In general, it may be observed that all FE models conveniently capture the onset of local buckling, i.e. the point from which the deterioration of the member initiates, and the actual strength deterioration when the negative tangent stiffness is attained. The experimental cyclic envelopes, or skeleton curves, were also accurately predicted by the models. Although the Bauschinger

component of the hysteretic behaviour and the unloading stiffness deterioration (Jiao et al., 2011) were not completely reproduced in the HEB 240 member, resulting in slightly fatter hysteretic loops and higher energy dissipation levels, the prediction of the strength deterioration of the member with the number and amplitude of cycles was not affected. In the case of the IPE 300 member, the numerical model was equally able to accurately capture the unloading stiffness deterioration initiated by the out-of-plane local buckling exhibited in Figure 5b. To conclude, one may refer that all numerical models lead to fairly suitable and reliable member responses.

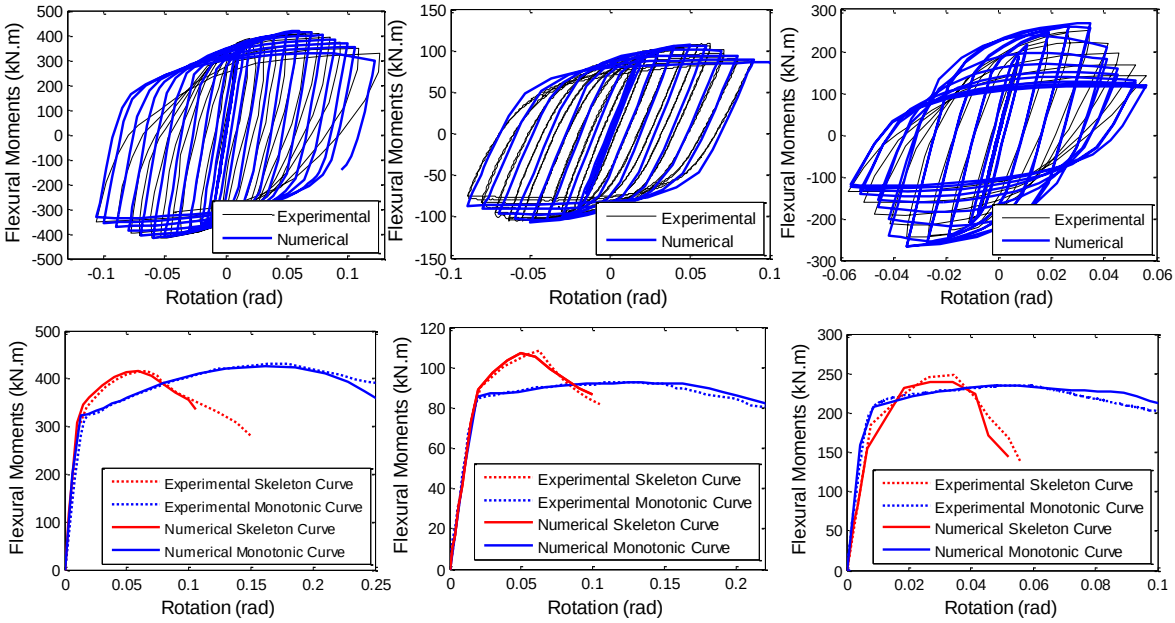

Figure 6.6 – Prediction of the monotonic and cyclic behaviour of the HEB 240, HEA 160 and IPE 300 (*left-to-right* figures) members.

6.4.2 Damage and ultra-low cycle fatigue predictions

Fracture is often a controlling mode of failure in steel structures, generally initiating in a ductile mode and transitioning into a brittle mode during crack growth (Kuwamura, 1997; Kanvinde and Deierlein, 2006). Under earthquake loading conditions, however, fracture typically propagates rapidly after initiation. Thus, in these cases, crack initiation may be considered as a reasonable limit state to evaluate structural performance (Kanvinde and Deierlein, 2007). Earthquake-induced crack initiation occurs after a few cycles (<100 cycles) of large plastic strain amplitude in the so-called ultra-low cycle fatigue (ULCF) regime. A number of methods for predicting such phenomenon may be found in the literature (Pereira et al., 2014) and grouped into strain-based fatigue-life prediction models (Coffin, 1971; Ge and Kang, 2012; Zhou et al., 2014) or micro-mechanics based fracture models (Kanvinde and Deierlein, 2006; 2007).

Strain-based models rely on the classical Coffin-Mason rule (Coffin, 1971), which assumes that the fatigue life (number of cycles to failure) and the plastic strain range follow a linear relationship in the logarithmic space. Several methods for estimating the Coffin-Manson's relationship parameters have been proposed in the past (Meggiolaro and Castro, 2004), still, owing to the lack of experimental data for different strain ranges and structural steel types, the more generic Mason's universal slope equation was adopted in the present work due to its recognized conservative character (Howdyshell et al., 1991; Meggiolaro and Castro, 2004), being given by:

$$\Delta\varepsilon = 3.5\frac{\sigma_u}{E}N_f^{-0.12} + \varepsilon_f^{0.6}N_f^{-0.6} \tag{6.3}$$

where N_f is the number of cycles to failure at a strain range level $\Delta\varepsilon$, σ_u is the ultimate strength and ε_f is the true strain at fracture, which is around 20% for the present case study members (Brescia, 2009). To account for variable-amplitude loading cases, a cumulative damage rule, such as the Palmgren-Miner rule (Miner, 1945), is required, so that:

$$D = \sum_{i=1}^{n}\frac{n_i}{N_{f_i}} \tag{6.4}$$

where N_{fi} is the number of cycles to failure at a strain level $\Delta\varepsilon_i$, and n_i are the number of cycles for which that particular strain level is applied. Fatigue occurs when the damage index, D, reaches unity. As pointed out by Nip et al. (2010), various factors should be taken into account when extracting strains from the numerical models, such as the measure and the location of strains and the through-thickness effects. In the present work, average strains over the buckled region were used to predict damage and calculate fatigue, as they are known to be less sensitive to mesh size (Nip et al., 2010). Furthermore, previous authors (Xia et al., 1996; Gong and Norton, 1999; Castiglioni, 2005) have shown that plastic deformations accumulated in the buckled region causes ratcheting strain (cyclic creep strain), which leads to additional damage and results in shorter fatigue lives. To account for this issue, the approach proposed by Gong and Norton (1999) to include the effects of mean strain in fatigue life predictions was adopted.

On the other hand, micro-mechanics based models, such as the cyclic void growth model (CVGM) proposed by Kanvinde and Deierlein (2007) for cyclic loading conditions, aim to represent the mechanisms (void growth and coalescence) that govern the physical process of ULCF. According to the CVGM, crack initiation is expected to occur once the cyclic void growth index, $\mathrm{VGI}_{\mathrm{cyclic}}$, exceeds its critical value, $\mathrm{VGI}_{\mathrm{cyclic}}^{\mathrm{critical}}$. The void growth and

shrinkage during cyclic loading is captured by subdividing the cycles into tensile and compressive based on the sign of triaxiality, T (i.e. the ratio between the hydrostatic pressure and von Mises equivalent stress), being expressed by:

$$\mathrm{VGI}_{\mathrm{cyclic}} = \sum_{T>0} \int_{\bar{\varepsilon}_1^p}^{\bar{\varepsilon}_2^p} \exp\left(|1.5T|\right) d\bar{\varepsilon}_p - \sum_{T<0} \int_{\bar{\varepsilon}_1^p}^{\bar{\varepsilon}_2^p} \exp\left(|1.5T|\right) d\bar{\varepsilon}_p \tag{6.5}$$

where $d\bar{\varepsilon}_p$ is the incremental equivalent plastic strain. The critical cyclic void growth index is defined by an exponential decay function of the critical void growth index obtained under monotonic loading, $\mathrm{VGI}_{\mathrm{monotonic}}^{\mathrm{critical}}$, which is treated as a material property that is invariant to stress and strain sates (Kanvinde and Deierlein, 2007), so that:

$$\mathrm{VGI}_{\mathrm{cyclic}}^{\mathrm{critical}} = \mathrm{VGI}_{\mathrm{monotonic}}^{\mathrm{critical}} \exp\left(-\lambda \bar{\varepsilon}_p^{accumulated}\right) \tag{6.6}$$

where $\bar{\varepsilon}_p^{accumulated}$ is the equivalent plastic strain that has accumulated up to the beginning of each tensile excursion of loading and λ is a material-dependent damage-ability coefficient.

Nevertheless, both models possess some known inconsistencies. Whilst the Coffin-Manson law tends to overestimate the cyclic life under ULCF conditions (Anastasiadis et al., 2015), the CVGM uses a regression-based approach wherein a damage law is fitted to observations of failure and does not consider the implications of non-failure cycles (Myers et al., 2014). Figure 6.7 (a) exhibits a comparative application of both ULCF models to the IPE 300 member. Three distinct loading protocols were adopted (SAC, SACNF and reduced SACNF), which will be discussed later on in this work. Note that the reduced SACNF protocol consists on an amplification of the initial steps of the SACNF protocol so as to represent a more evident pulse-like response of the member, commonly observed when the member is subjected to real ground motions records. A closer inspection on this will be equally provided later. Values of $\mathrm{VGI}_{\mathrm{monotonic}}^{\mathrm{critical}}$ and λ of 2.8 and 0.38 were adopted, respectively, based on the steel materials investigated by Kanvinde and Deierlein (2007). It was observed that the strain-based model underestimates crack initiation at every loading condition when compared to the CVGM, being this underestimation more evident as the response of the member approximates its monotonic behaviour. Still, with the exception of the reduced SACNF protocol, wherein the CVGM did not predict crack initiation, both models provided estimates of the initiation of the crack at the same loading cycle, thus leading to equal rotation capacities of the member before fracture. A similar comparative study was conducted on the HEB 240 member, being again observed quite identical estimates of crack initiation, which not only occurred at the same cycle, but also at the

same loading/unloading branch of the hysteretic response. In this case, the CVGM slightly underestimated crack initiation using the SACNF protocol. The influence of each loading protocol on the evolution of the cyclic void growth demand and capacity indices of the IPE 300 member is represented in Figure 6.7 (b).

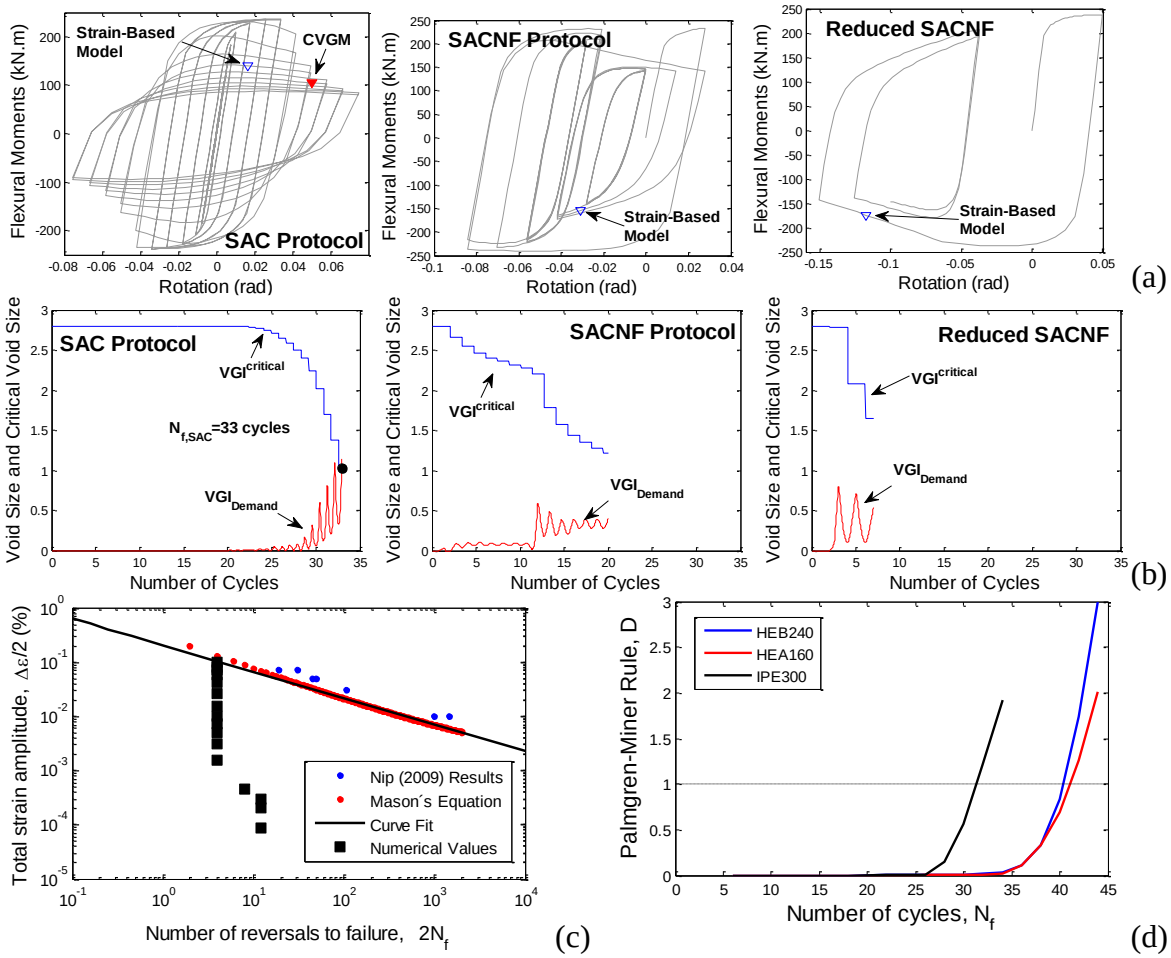

Figure 6.7 – ULCF crack initiation predictions: (a) comparative application of the strain-based model and the CVGM to the IPE 300 member; (b) influence of loading protocols on the evolution of the cyclic void growth demand and capacity indices; (c) comparison between the Mason's universal slop equation and numerical results obtained for the HEB 240 member; (d) and evolution of the damage index *D* with the number of cycles.

Based on this preliminary comparative study, the strain-based model was chosen to be mostly adopted throughout this work due to its easiness of application. Figure 6.7 (c) displays the comparison between the amplitudes of the total strains obtained numerically for the number of cycles of the SAC loading protocol imposed to the HEB 240 member and the amplitudes of the total strains obtained from equation (6.3). In accordance to Brescia et al. (2009) and D'Aniello et al. (2012), which reported the occurrence of cracks at the flanges under tension already buckled in compression of all specimens, fatigue failure occurred in all members. Figure 6.7 (d) depicts the evolution of damage, given by

D, for increasing cycles of the SAC loading protocol, being observed that the HEB 240 and HEA 160 members reach fatigue failure after 40 and 41 cycles, which correspond to values of rotation at fracture, θ_f, of 0.092 and 0.095 radians, respectively, while the IPE 300 member was seen to fracture after 31 cycles, corresponding to a θ_f of 0.050 radians. Interestingly, these values seem to be in agreement with the estimates of θ_f of 0.101 radians, 0.107 radians and 0.051 radians obtained for the HEB 240, HEA 160 and IPE 300 members, respectively, using the simplified approach proposed by Gioncu et al. (2014). Moreover, one may note that the rotation at fracture was found to be around 1.40 times the rotation at the onset of the strength deterioration in all members.

The propagation of damage was additionally evaluated by monitoring the amplitude of the buckling wave at both flanges, ΔU_f, and web, ΔU_w, of the member, as represented in Figure 6.8 (a). Its evolution with the rotation of the members is displayed in Figure 6.8 (b). Maximum values of ΔU_f of 80.7 mm, 57.7 mm and 65.8 mm and of ΔU_w of 21.1 mm, 30.5 mm and 42 mm were observed for the HEB 240, HEA 160 and IPE 300 members, respectively, which seem to be in line with those presented by Stojadinovic (2003).

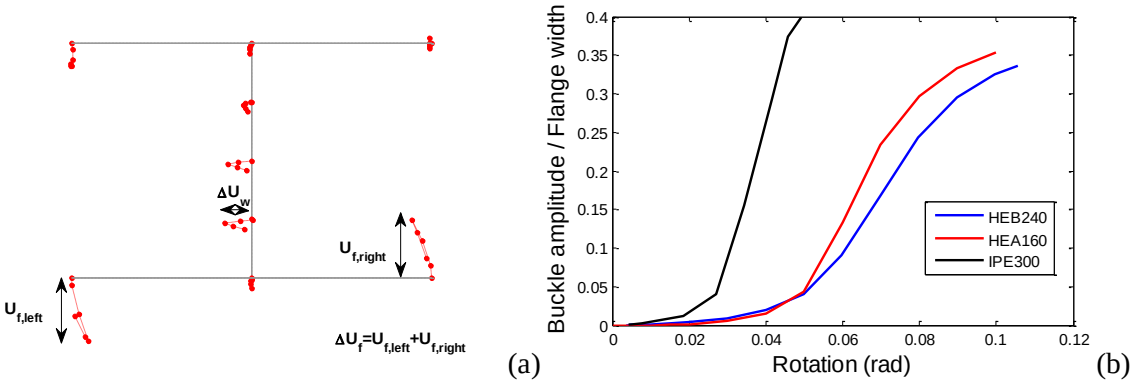

Figure 6.8 – Representation of the amplitude of the buckling wave at both flanges and web (a) and evolution of the flange buckle amplitude with the rotation of the members (b).

6.4.3 Parametric study

A parametric study was conducted with the objective of identifying potential sources of variability in the deformation capacity of steel members. The influence of the local and global geometrical imperfections, the axial load and the type of loading in the behaviour of the HEB 240, HEA 160 and IPE 300 members was evaluated. Three types of global geometrical imperfections of *L/300*, *L/666* and *L/1000*, where *L* is the length of the member, were assumed, as well as of local geometrical imperfections, so that *k+k'=0*, *k+k'=0.01 b* and *k+k'=0.06 b*, being *b* the base of the cross-section (CEN, 1993). Five

levels of normalized axial load, from ν=0 to ν=0.4, and a group of distinct loading protocols and real ground motion records were adopted.

6.4.3.1 Monotonic behaviour

Figure 6.9 presents the results of the parametric study relative to the monotonic response of all members. The results are depicted assuming two distinct scenarios: (i) a first scenario that aims to assess the maximum bending moment developed in beam-column elements without accounting for the influence of *P*-Δ effects, being the bending moment simply given by the base shear, *V*, multiplied by the height of the member, *L* (Figure 6.9 (a)); (ii) and a second scenario that seeks to evaluate the influence of the axial load in the capacity of steel members. In this case, the flexural capacity was calculated by adding the flexural component due to *P*-Δ effects, which is given by the product of the axial load, *N*, with the lateral displacement of the member top end, δ (Figure 6.9 (b)). It may be thus observed from Figure 6.9 (a) that an increase in the axial load from ν=0 to ν=0.4 produces an important reduction, of about 38%, 29% and 18%, in the maximum bending moment developed in the IPE 300, HEB 240 and HEA 160 members, respectively. In fact, for ν=0.4, the HEA 160 member was merely capable of developing a maximum bending moment about equal to its flexural yielding moment. This issue has particular importance when designing or assessing moment resisting steel frames based on capacity-design principles, i.e. when ensuring the weak-beam / strong-column condition. Whereas beams (ν=0) are expected to experience a significant increase in their flexural capacity due to over-strength effects, columns will be greatly affected by the level of axial load applied. Furthermore, it may be equally observed from Figure 6.9 (b) that the deformation capacity of steel members, defined by the chord rotation at the onset of strength deterioration, experiences an important decrease, in the order of 60%, 51% and 55% in the HEB 240, HEA 160 and IPE 300 members, respectively, with the increase of the axial load from ν=0 to ν=0.4. This axial load increase also hastens strain hardening. In other words, higher levels of compressive axial load produce higher cross-sectional strain levels, which consequently anticipate local buckling and over-strength effects. An important deterioration mechanism due to column axial shortening will be equally associated with higher compressive axial loads, as discussed by Elkady and Lignos (2013; 2014). The HEA 160 member, which cross-section features a flange slenderness ratio c/t = 8.88 greater than both class 1 and 2 limits proposed by EC3 (CEN, 2005b) of 9ε and 10ε, was found to be more sensitive, as expected, to the influence of the axial load. Still, although

the HEB 240 cross-section may be classified as class 1, with a flange slenderness ratio equal to 7.05, both HEA 160 and HEB 240 members exhibit similar rotation capacity values. This fact could be associated with the similar web slenderness ratios exhibited by both HEA 160 and HEB 240 cross-sections. In turn, the higher web slenderness ratio featured by the IPE 300 profile may explain its lower rotation capacity.

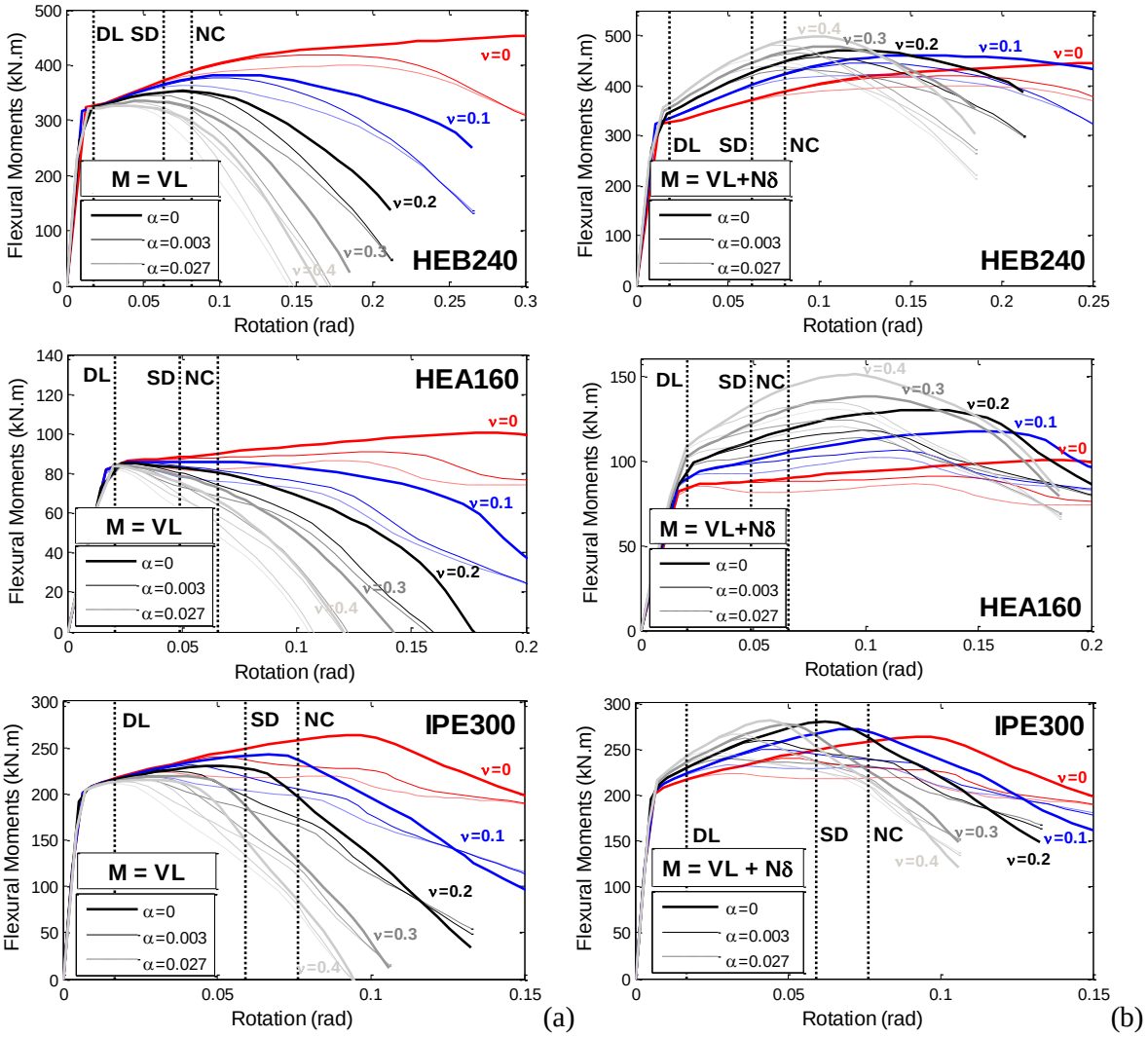

Figure 6.9 – Parametric study on the monotonic behaviour of the members: (a) maximum bending moment developed in the members without accounting for *P*-Δ effects; (b) cross-sectional capacity of the members.

The influence of global geometrical imperfections in the deformation capacity of all members was found to be practically insignificant. Contrarily, local geometrical imperfections, which are herein presented in terms of the scaling factor, α, applied to the buckling mode to provide the intended level of imperfection, led to a significant loss of deformation capacity that reached more than 60% when no axial load was applied. Note that the imperfection tolerance established in the manufactures table is defined by $k+k' \leq 0.02\ b$ (CEN, 1993) and so the higher imperfection level considered (α = 0.027) intends to

assess the impact of a highly amplified local geometrical imperfection that is not expected to occur. As the level of axial load increased, the influence of local imperfections was seen to progressively decrease to about 30%.

6.4.3.2 Loading protocols

According to FEMA 461 (FEMA, 2007) and as already evidenced by previous works (Conseza et al., 1995; Krawinkler, 1999; 2009; Chen et al., 2013), the type of loading protocol has an important impact on the deformation capacity estimates of steel members. A number of different loading protocols was assumed in the present work, whose general description may be found in the Krawinkler (2009), Jiao et al., (2011) and Chen et al. (2013). Additionally, the recently proposed loading protocols for European regions of low to moderate seismicity (Mergos and Beyer, 2014), herein designated as M&B, were considered, admitting a Fat-Takeda hysteresis law and a fundamental period of vibration equal or greater than 0.5s. The results obtained are displayed in Figure 6.10 (a), being interesting to observe that, apart from the SAC Near Fault (SACNF) loading protocol, which intends to reproduce the effect of a near-fault earthquake, the protocols preconized by most guidelines and codes led to practically identical rotation capacity estimates. Still, the SAC loading protocol was seen to be slightly conservative. On the other hand, the results obtained by adopting the M&B loading protocols suggest that the M&B P1 protocol, which was defined for the median response of low to moderate seismicity earthquakes, tend to better fit the results obtained from the SAC Near Fault loading protocol; whereas the M&B P4 protocol, which was defined for the 84th percentile of the response of high seismicity earthquakes, agreed better with the results obtained by most guideline and code protocols.

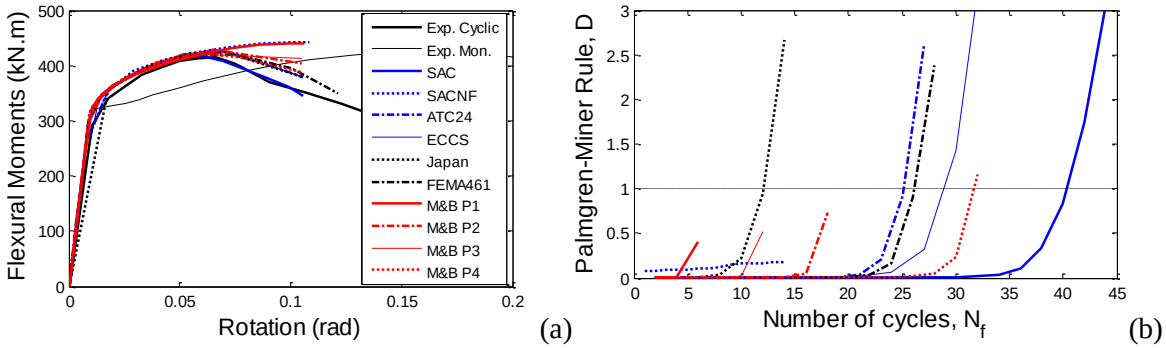

Figure 6.10 – Influence of loading protocols the response of the HEB 240 member: (a) comparison of the skeleton curves obtained for each loading protocol; (b) and evolution of the damage index *D*.

Gioncu et al. (2014) distinguish two member collapse criteria as a function of the type of loading: (i) a first one based on the maximum fracture strain, being governed by the corresponding fracture rotation (near-fault earthquakes); (ii) and a second one based on low-cycle fatigue, being governed by cumulative plastic rotation (far-field earthquakes). Table 6.1 summarizes the influence of loading protocols on the propagation of damage over the HEB 240 member. Accordingly, it may be seen that whilst loading protocols representative of far-field earthquakes produce higher levels of cumulative damage (Figure 10b) and earlier rotation values at fracture (Table 6.1), the applied loading protocols representative of near-fault earthquakes have not exploited the full strain capacity of the member, and thus no fracture occurred.

Table 6.1 – Characteristics of the buildings analysed.

Damage parameter	Loading Protocol									
	SAC	SACNF	ATC24	ECCS	Japan	FEMA461	M&B P1	M&B P2	M&B P3	M&B P4
ΔU_f (mm)	80.7	24.6	75.3	75.2	75.3	81.1	47.8	62.2	54.4	70.9
θ_f (rad)	0.092	-	0.107	0.099	0.107	0.102	-	-	-	0.101

6.4.3.3 Time-history analysis using sets of ground motion records

The use of loading protocols as a mean of deriving and assessing the deformation capacity of structural components disables the ability to account for the variability introduced by the specific characteristics of ground motions, such us the number of cycles, the duration or the frequency content. Moreover, as noted by Mergos and Beyer (2014), most protocols have been developed for regions of high seismicity, which may underestimate the actual deformation capacities of structural components located in regions of low to moderate seismicity. Time-history analysis was thus conducted to further evaluate the 'real' deformation capacity of steel members. A set of 21 real ground motion records scaled to match the EC8 elastic spectrum defined for a Portuguese type 1 (far-field) and Zone 3 seismic action (Lisbon) located in a soil type B was adopted. An additional criterion was included in the selection of each individual record by imposing mismatch limits relative to the target spectrum, which have been demonstrated in Chapter 3 to significantly reduce the variability in the structural response estimates. The records were firstly selected and scaled to match the SD limit state, defined by a *PGA* of 0.15g, being afterwards linearly scaled to 5 different *PGA* levels (0.091g, 0.225g, 0.30g, 0.375g and

0.451g). Note that the *PGA* values of 0.091g and 0.451g refer to the DL and the NC limit states, respectively.

To characterize the members' deformation capacity, two rotation values were computed: (i) the rotation, $\theta_{max,}$ at the maximum developed flexural strength, M_{max}, which aims to identify the onset of local buckling and member deterioration. In cases where the definition of θ_{max} is not straightforward, the θ_{max} rotation was considered to be attained when a 5% ratio between the buckle amplitude and the flange width (Figure 6.8 (b)) was verified; (ii) and the rotation, $\theta_{80\%,}$ corresponding to a 20% reduction in M_{max}. If the 20% reduction in M_{max} is not achieved, the maximum rotation value is considered, θ_{deg}. Alternative approaches may be found in literature to quantify the maximum deformation capacity of steel members (D'Aniello et al., 2012; Elkady and Lignos, 2014), although the criterion herein adopted, which is based on a 20% drop in the member's peak strength (Mergos and Beyer, 2014), seems to be in agreement with the limited local buckling requirement preconized by EC8-3 for the NC limit state. As depicted in Figure 6.8 (b), a curvature of the buckled flange of around 0.3 is expected to be obtained at $\theta_{80\%}$.

Figure 6.11 (a) displays the hysteretic responses of the HEB 240 member for a single ground motion record scaled to match two elastic spectra with *PGA* levels of 0.375g and 0.451g. The computation of both θ_{max} and $\theta_{80\% \text{ or } deg}$ is equally represented, being verified that for a target *PGA* level of 0.375g ($S_{a,\,Target}(T_1)$ = 0.73g) the 20% drop in M_{max} has not yet been attained and that the θ_{max} value remained practically unchanged despite the increasing plastic incursions and ratcheting observed at the higher target *PGA* level of 0.451g ($S_{a,\,Target}(T_1)$ = 0.87g). In fact, it was found that the mean θ_{max} rotation capacity of the member does not vary much with the increase in the target seismic intensity (Figure 6.11 (b)), herein defined in terms of the target ductility modification factor R_μ (ASCE, 2014), and its variability, characterized by a coefficient of variation (CoV) around 26%, may be almost entirely explained by the record-to-record variability ($CoV_{S_a(T_1)}$), which at $S_a(1.5\,T_1)$, where 1.5 T_1 aims to account for the period elongation of the member (Chapter 3), is about 27%. Pearson's coefficients of correlation ρ of 76%, 80% and 53% were observed between θ_{max} and the $S_a(1.5\,T_1)$ of each individual record for target R_μ levels of 8.2, 10.2 and 12.3, respectively, suggesting that although the mean θ_{max} values remained practically constant, the θ_{max} rotation capacity increases for increasing levels of seismic intensity, nearing evermore the monotonic θ_{max} rotation capacity (Figure 6.6). Comparing the mean θ_{max} predictions with those obtained from the application of the various loading protocols, it may be seen that the SAC loading protocol leads to rather conservative

capacity estimates, as already expected due to its higher number of incremental displacements and cycles, whereas the M&B P2 loading protocol yields results closer to time-history analysis, with a θ_{max} value around 0.08 radians. Similarly, the SAC loading protocol was seen to derive conservative $\theta_{80\%}$ capacity estimates (Figure 6.11 (c)), as well as lower predictions of the over-strength factor s when comparing to those obtained for higher R_μ levels (Figure 6.11 (d)).

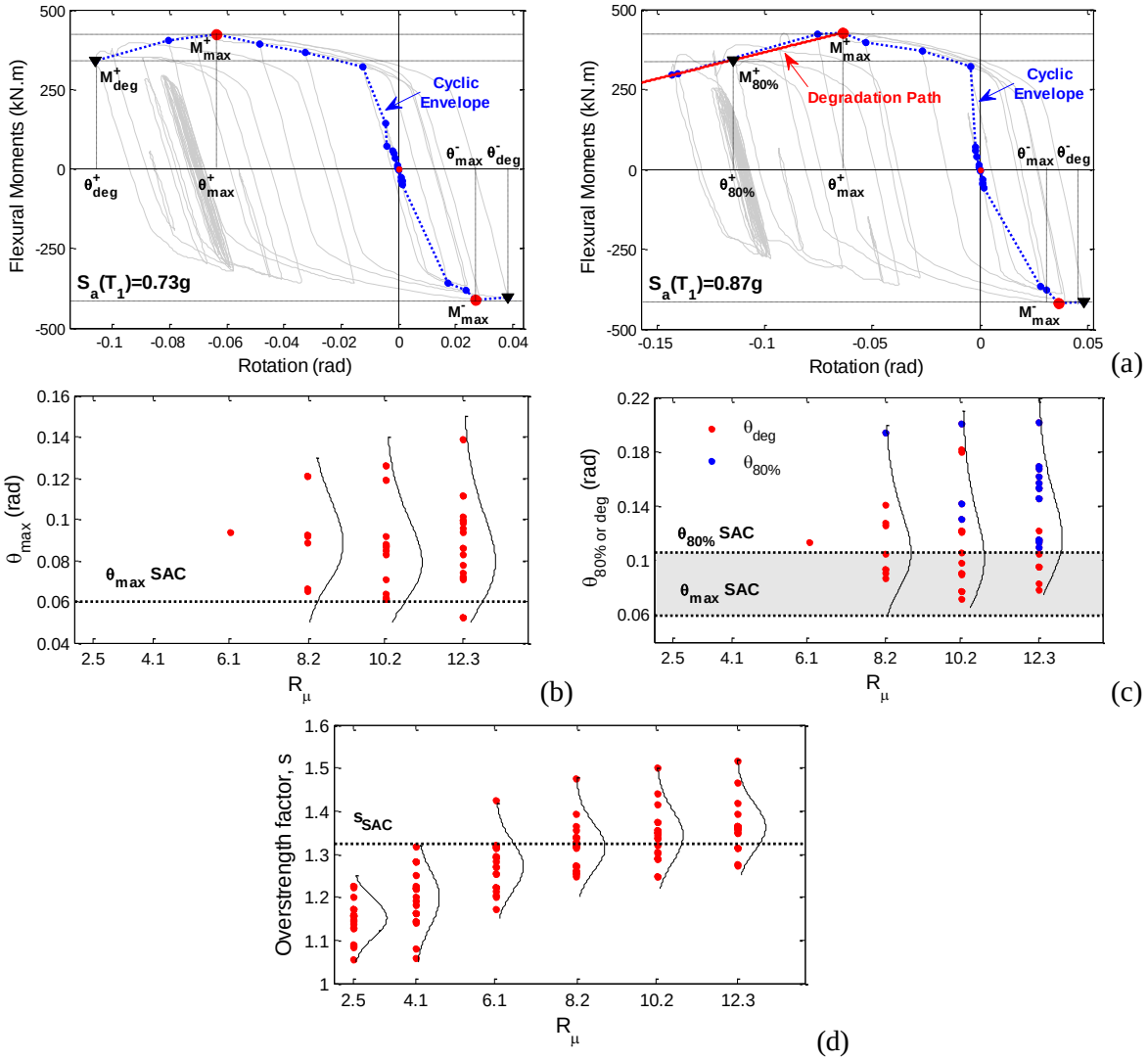

Figure 6.11 – Response of the HEB 240 member to real ground motion records: (a) hysteretic responses for a single record scaled to match two spectra with increasing *PGA* levels (0.30g and 0.375g); (b) evolution of θ_{max} with R_μ; (c) evolution of $\theta_{80\%\ or\ deg}$ with R_μ; (d) and evolution of overstrength factor s with R_μ.

The propagation of damage for increasing levels of R_μ is displayed in Figure 6.12. A mean curvature of the buckled flange (ratio between ΔU_f and b_f) of 0.21 (CoV = 33%) was obtained at the NC limit state (Figure 6.12 (a)), which varies almost 40% from the curvature estimated using the SAC protocol and is around 2 times the one estimated from the SACNF protocol (Table 6.1). In order to determine the number of strain cycles and

quantify the fatigue life of the member using a strain-based approach, the Rainflow counting method was adopted (Kondo, 2003). Figure 6.12 (b) presents the evolution of the damage index D of the HEB 240 member with R_μ, being observed that most code-based protocols, which were derived for high seismicity near-fault earthquakes, seem to underestimate crack initiation of steel members. In fact, the protocol proposed by Mergos and Beyer (2014) for low to moderate seismicity regions, particularly the one based on the 84th percentile (M&B P2), was found to provide better deformation capacity and damage propagation estimates. Regarding the possibility of occurring fatigue fracture, a mean damage index D of 0.31, which is significantly below the unit fracture limit, was obtained from time-history analysis at the NC limit state. The higher D values observed for R_μ levels of 8.2, 10.2 and 12.3 were attained for a single ground motion record that imposed a pulse-like excitation in the member (Earthquake 3 of Figure 6.14 (a)). In other words, a first high amplitude cycle, similar to the one produced by the SACNF protocol, was initially developed, causing significant ratcheting strain and being followed by a series of cycles of variable and lower amplitude wherein the effect of mean strain played an important role in the fatigue life predictions.

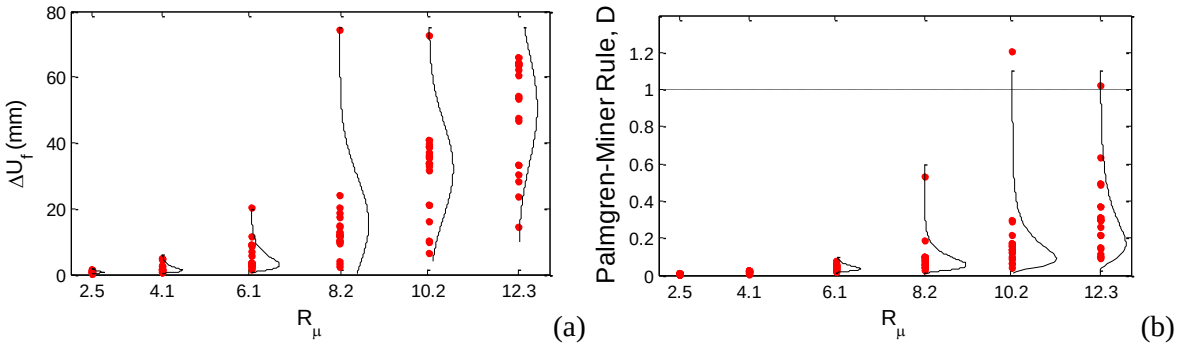

Figure 6.12 – Influence of loading protocols the response of the HEB 240 member: (a) comparison of the skeleton curves obtained for each loading protocol; (b) and evolution of the damage index D.

A practically linear relationship between the rotation demand θ of the HEB 240 member and the respective levels of damage, $ln\ \Delta U_f$ and $ln\ D$, was equally verified, being characterized by coefficients of correlation ρ of 86% and 91%, respectively. Based on this, a simple linear regression analysis was conducted (Figure 6.13) so that the mean predicted rotation demand could be related with the respective level of damage and given by $\theta = \beta_1\ ln\ X + \beta_o$, where X is the damage parameter under consideration. Values of the slope of the linear trend, β_1, of about 0.02 and 0.03 were found for parameters ΔU_f and D, respectively, while β_o can be defined by the maximum deformation capacity of the member obtained from a monotonic analysis, which is about 0.18 radians. Similar findings were drawn for

the IPE 300 member and β_1 values of about 0.01 were obtained for both damage parameters. The proposal of prediction equations that correlate the member's deformation with the respective level of damage is of great interest when preforming seismic loss assessments of structures, still its derivation from time-history analysis and robust FE models requires a high computational onus, hampering its generalization to a wide range of cross-section profiles.

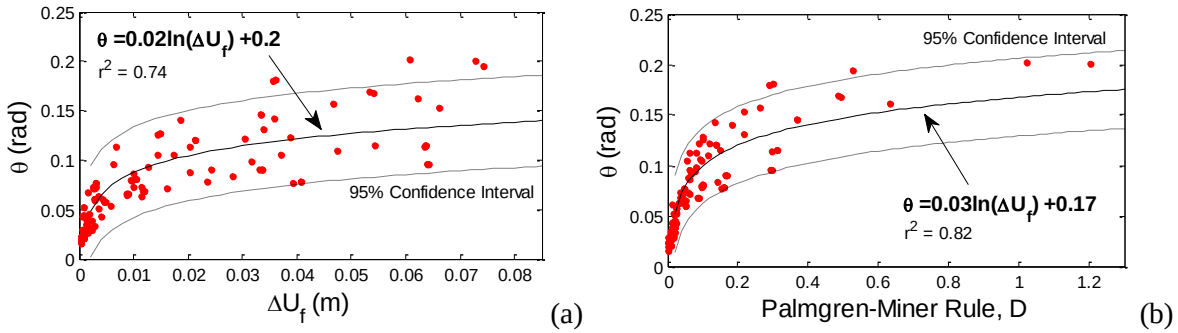

Figure 6.13 – Correlation between the deformation capacity of the HEB 240 member and the developed level of damage: (a) flange buckle amplitude; (b) and damage index *D*.

It has been demonstrated that the deformation capacity of steel members is greatly dependent on the characteristics of ground motions. Indeed, Gioncu et al. (2014) have already pointed out that the available ductility of steel members should be firstly evaluated under monotonic loads and corrected by a factor that accounts for the specific features of the earthquake type. Moreover, Elkady and Lignos (2014) have shown that the ASCE 41-13 rotation capacity limits, which are identical to those preconized by EC8-3, more a less agree with the capacity estimates obtained from FE analysis of a set of wide-flange sections using the SAC loading protocol. This protocol was equally found to underestimate the deformation capacity of steel members. Bearing these initial premises in mind, a correction factor capable of converting the rotation capacities predicted by applying the SAC loading protocol to account for the actual dynamic response of the member was sought.

The cumulative dissipated energy appears to be an interesting parameter to define such correction factor. Whilst the SAC loading protocol imposes a symmetrical and incremental increase in deformation demands, leading to a continuous growth in the total dissipated energy and anticipating the onset of strength degradation, real ground motion records cause ratcheting and asymmetric responses characterized by lower levels of total dissipated energy and higher capacity values. Figure 6.14 (a) illustrates the dependency between the cumulative dissipated energy and the deformation capacity of the HEB 240

member. It may be observed that as the μ_t parameter increases, which represents a sort of dissipated energy ductility factor obtained by bi-linearizing the cumulative dissipated energy curve, the deformation capacity $\theta_{80\%}$ of the member equally increases. A linear correlation between the $\theta_{80\%}$ computed for the NC limit state (i.e. for the R_μ level at which the 80% reduction in M_{max} occurred in practically all responses) and $ln\ \mu_t$ was found, being defined by a high coefficient of correlation ρ of 81%. A similar coefficient of correlation was observed for the IPE 300 member.

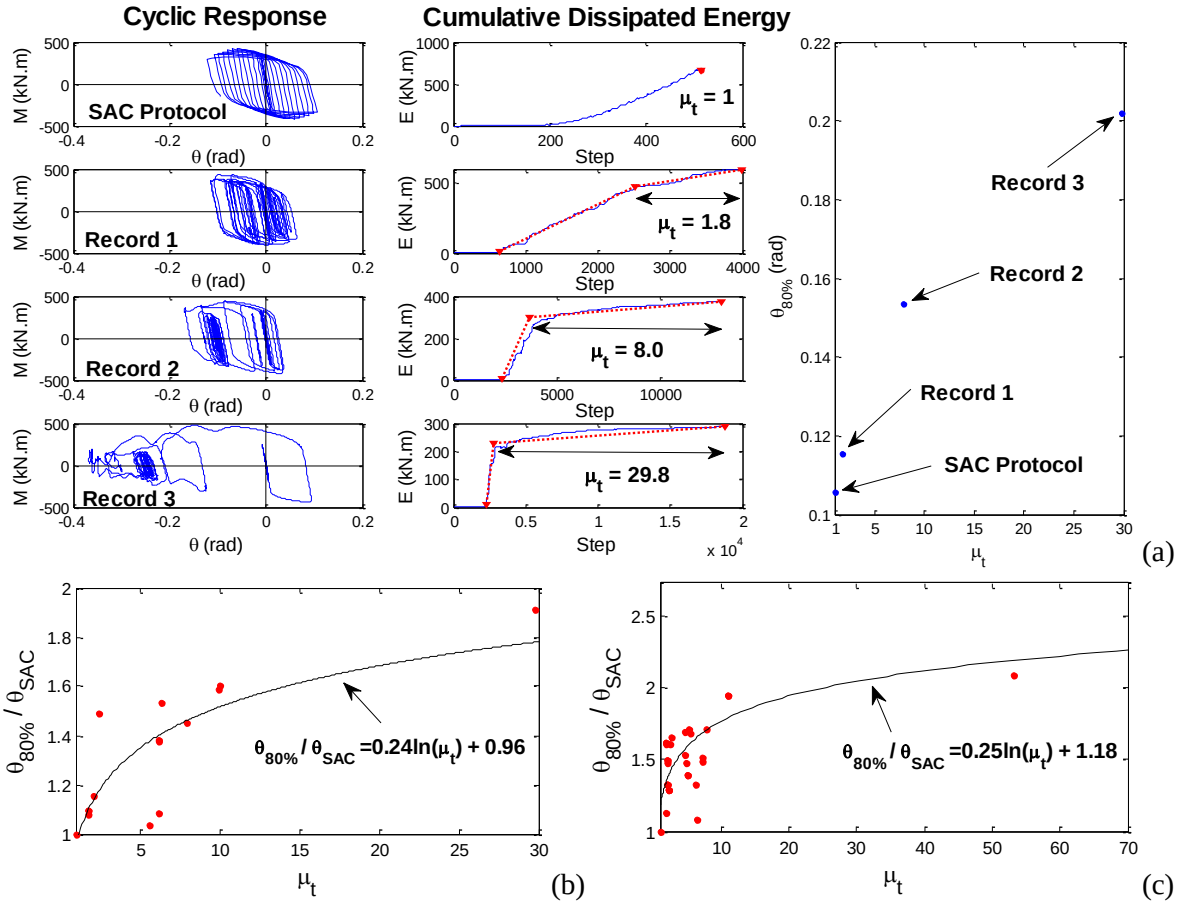

Figure 6.14 – (a) Schematic representation of the influence of the cumulative dissipated energy in the deformation capacity of steel members and linear regression analysis for both (b) HEB 240 and (c) IPE 300 members.

Hence, once again, a simple linear regression analysis was conducted between the $\theta_{80\%}$ values normalized with respect to the deformation capacity of the member at a 20% reduction in M_{max} obtained using the SAC loading protocol, θ_{SAC}, and $ln\ \mu_t$ for both HEA 240 and IPE 300 members (Figure 6.14 (b) and (c)). Values of the linear trend slope β_1 of 0.24 and 0.25 were estimated, respectively, as well as values of β_o around the unit, as expected since for a unit μ_t the $\theta_{80\%}$ value equals θ_{SAC}. The use of such correction factors may have particular interest in reducing the degree of conservatism associated to the

seismic safety verifications of steel members preformed on the basis of rotation capacity limits defined by θ_{SAC}. Still an extension of such linear relationships to a wider range of cross-section profiles is deemed necessary.

6.4.3.4 Cyclic behaviour

The influence of the axial load and geometrical imperfections in the cyclic response of steel members assuming the SAC loading protocol is now discussed. Figure 6.15 presents the response of the HEB 240 member for two distinct axial load levels (ν=0 and ν=0.4) and local imperfection levels (α=0 and α =0.003). Global imperfections were found to have a practically negligible impact in the response of the members, while local imperfections increased the member's potential of degradation, anticipating the onset of local buckling and reducing the value of θ_{max} by around 1/3 for both axial load levels. The unloading stiffness deterioration was equally affect by local imperfections.

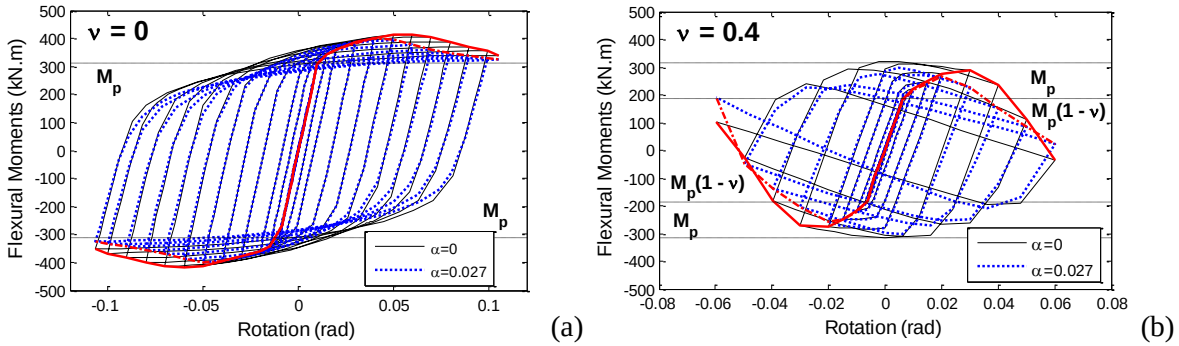

Figure 6.15 – Cyclic response of the HEB240 member assuming different axial load levels: (a) ν = 0; (b) and ν = 0.4.

Likewise, the axial load appeared as a critical parameter in the determination of the deformation capacity of steel components, in such a way that not only it produced a 50% to 75% reduction in θ_{max} from ν = 0 to ν = 0.4 (recall the 60% reduction in the monotonic case), but also it precluded the member to develop its full plastic moment M_p due to P-Δ effects (Figure 6.15 (b)). This drop in the plastic moment may be captured by assuming the well-known simple linear interaction equation, so that M_p (1-ν). A similar reduction in the yielding moment was observed in the monotonic response of the member, although being somehow unnoticed due to the fast strain hardening effect. By including P-Δ effects, the hysteretic loops rotate counter-clockwise, evidencing that at a cross-sectional level the full plastic moment M_p is still reached. Figure 6.16 presents the results of the parametric study relative to the cyclic response of all members. The results are again depicted in terms of the maximum developed bending moment without including P-Δ effects (Figure 6.16 (a)) and the members' cross-section flexural capacity (Figure 6.16 (b)).

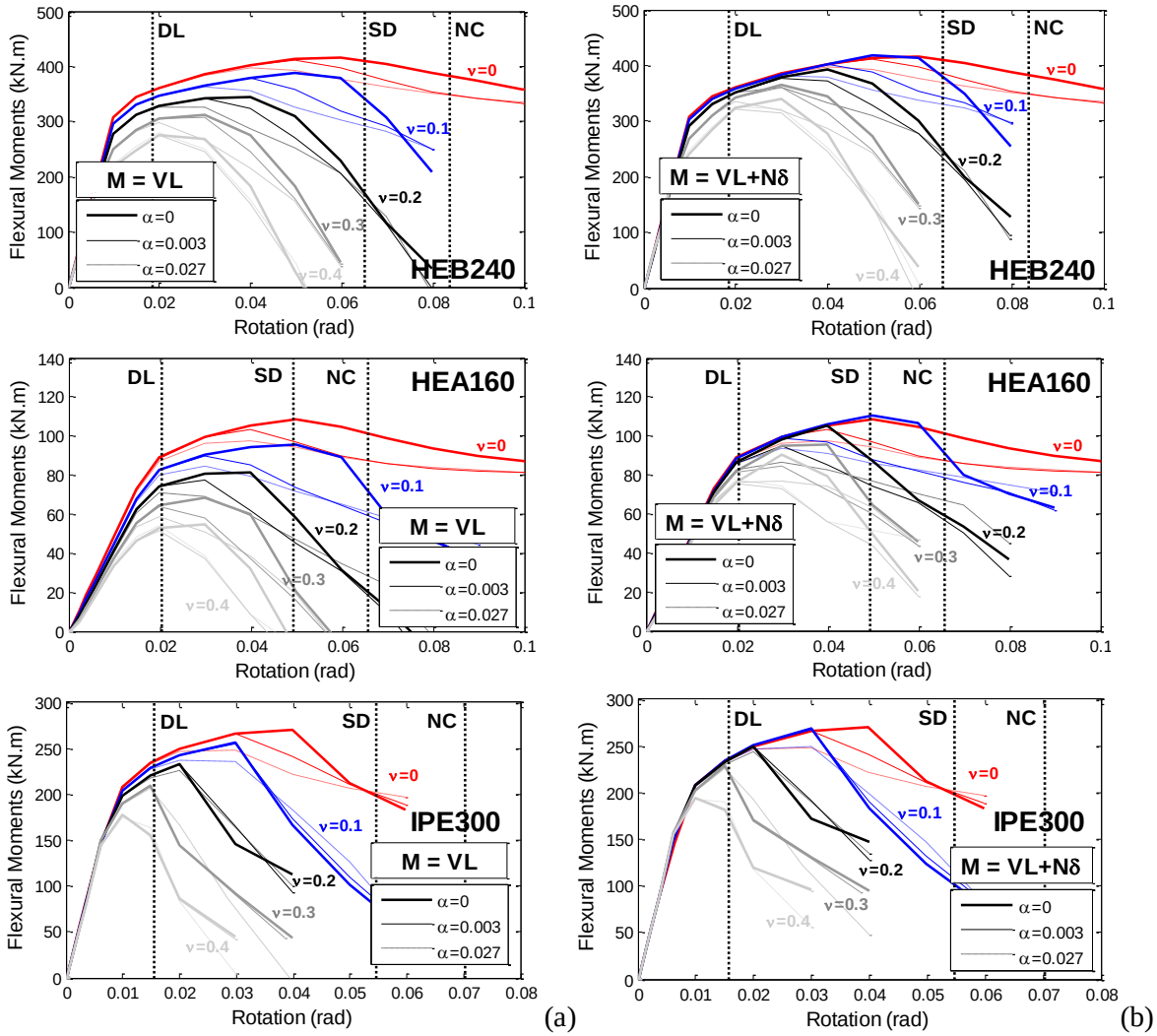

Figure 6.16 – Parametric study on the cyclic behaviour of the members: (a) maximum bending moment developed in the members without accounting for *P*-Δ effects; (b) cross-sectional capacity of the members.

In comparison with the responses obtained from the monotonic loading cases, the increase in the axial load (ν = 0 to ν = 0.4) was found to produce a similar reduction in M_{max} of 37% and 31% in the IPE 300 and HEB 240 members (EC3 class 1 cross-sections), respectively, whereas a higher reduction in M_{max} of 45% was observed in the HEA 160 member (EC3 class 3 cross-section). Moreover, the impact of the axial load in the cyclic rotation capacity of the HEB 240 and HEA 160 members was found to decrease about 20% relative to their monotonic counterpart, yet it increased 27% in the IPE 300 member. Nevertheless, a higher ratio between the monotonic and cyclic θ_{max} values was observed for increasing levels of axial load, which rose from 1.7 to 3 times in the IPE 300 member and from 2.5 times to 4 times in the HEB 240 and HEA 160 members. Castiglioni (2005) has evidenced that local buckling can be regarded as a notch effect, as it induces local stress concentrations in the buckled area and cracks in the base material at plastic hinge

locations. Concurrently, the axial load is known to amplify such stress concentrations and worsen local buckling phenomena. Table 6.2 presents the influence of the axial load in the rotation at fracture θ_f of all members. A reduction in the fatigue life of the members about equal to that observed in the rotation at the onset of local buckling was found as the axial load increased from $v = 0$ to $v = 0.4$.

Table 6.2 – Influence of the axial load in the fatigue life θ_f (rad) of the analysed members.

Member	Normalized Axial Load				
	ν = 0	ν = 0.1	ν = 0.2	ν = 0.3	ν = 0.4
HEB 240	0.092	0.072	0.052	0.042	0.039
HEA 160	0.095	0.088	0.069	0.059	0.049
IPE 300	0.050	0.022	0.013	0.012	0.009

The amplification of the buckled region imposed by higher axial load levels is represented in Figure 6.17. When no local geometrical imperfection is considered, the increase in the axial load was seen to lead to an elephant's foot-like buckling mode and to a significant concentration of plastic strains at the edge of flanges and web-to-flange corners. In this case, crack initiation is expected to occur at 1/16 of the total height of the member.

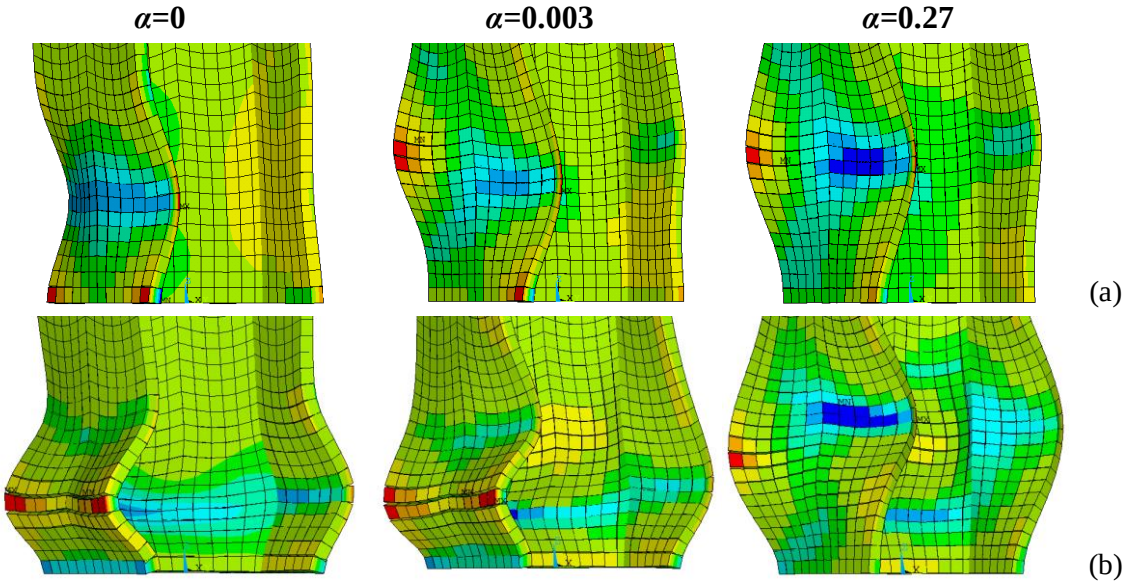

Figure 6.17 – Local buckling mechanisms developed in the HEB 240 member considering different local geometrical imperfection levels (α=0, α=0.003 and α=0.27) and two distinct axial load levels: (a) v=0; (b) and v=0.4.

The inclusion of a local geometrical imperfection within the fabrication tolerance limit (α = 0.003) significantly affected the local buckling wave when no axial load was introduced, concentrating plastic strains at 1/8 of the total height of the member. The

increase in the axial load again aggravated local buckling, although the initially imposed local geometrical imperfection was found to have a positive effect in reducing the concentration of plastic strains, as it leads to a buckling mode opposite to the one developed by the axial load, increasing the fatigue life by about 20%. The positive effect of local geometrical imperfections is even more evident when the amplified imperfection (α = 0.027) is considered, which completely changed the local buckling mechanism at the higher axial load level.

6.4.3.5 Comparison with the limits proposed by EC8-3 and ASCE 41-13

The numerical estimates of the member's deformation capacity obtained for increasing levels of axial load and assuming a local geometrical imperfection within the manufactures tolerance limit (α = 0.003) were compared with the limits proposed by EC8-3 and ASCE41-13. The aim was to provide a first answer to the question initially placed on how adequate are the deformation limits proposed by EC8-3. As previously referred, EC8-3 preconizes that beams should develop their full plastic moments without local buckling at the SD limit state and limited local buckling may occur in beams at the NC limit state; therefore the θ_{max} and $\theta_{80\%}$ rotation capacity values were considered to define each limit state, respectively. Also, information is missing in EC8-3 regarding the admissible levels of damage to be developed in columns, particularly at the NC limit state, and the no axial and flexural yielding level of damage proposed for the SD limit state seems to be quite conservative and neglects, for instance, the end node of 1st storey columns of structures developing potential beam-sway mechanisms. Hence, identical levels of damage are herein set for both beam and column members. Moreover, EC8-3 proposes deformation capacity limits that are independent on the level of axial load and are valid for values of v not greater than 0.3. These limits are in fact equal to those proposed by ASCE41-13 for v levels below 0.2. Still, according to the American standard, if the axial load level is within $0.2 < v < 0.5$, the plastic rotation capacity limits shall be defined by $8(1 - 5/3v)\ \theta_y$ and $11(1 - 5/3v)\ \theta_y$ for the SD and NC limit states, respectively, of stocky cross-sections (EC3 class 1) and by $0.5\ \theta_y$ and $0.8\ \theta_y$ for other cross-sections. Figure 6.18 presents the comparison between the numerical estimates and both codes capacity limits. Not only one may conclude that EC8-3 provides overestimated capacity limits for members with EC3 class 1 cross-sections (HEB 240 and IPE 300), being this overestimation more significant in the case of deep cross-sections (IPE 300), at the SD limit state and for higher axial load levels, but also the limits proposed for cross-sections of higher EC3 classes (HEA 160) seem to be

generally in good agreement with numerical results at the NC limit state. Additionally, the alternative values proposed by ASCE41-13 to account for the influence of the axial load were found to better adjust to numerical results, although remaining rather conservative in the member with a deeper cross-section profile.

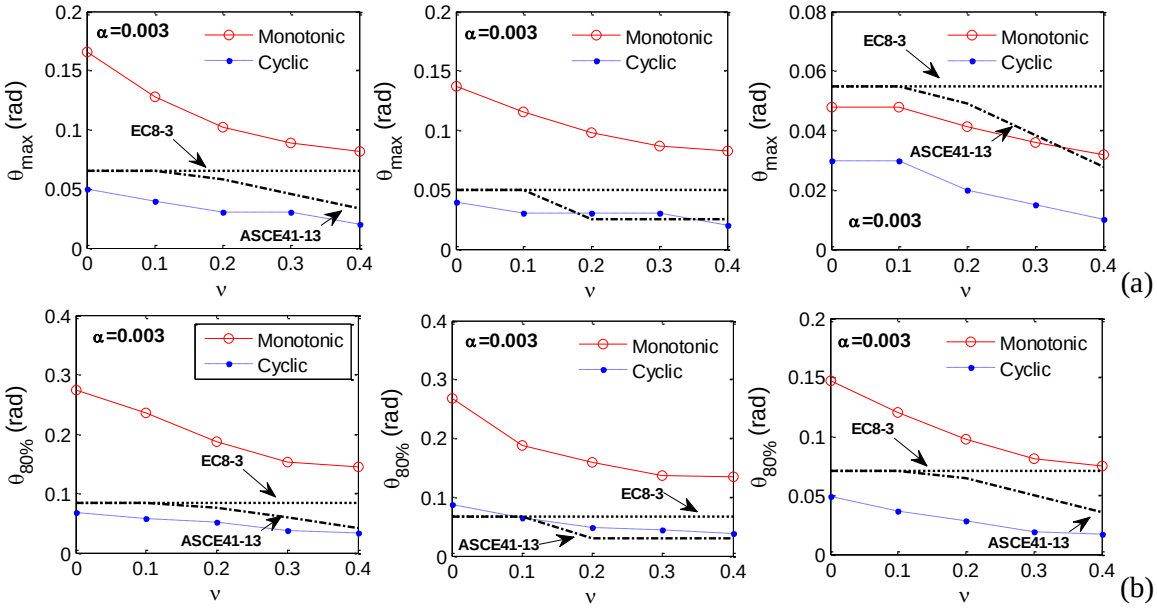

Figure 6.18 – Comparison between the numerical rotation capacity estimates and the limits proposed by EC8-3 and ASCE 41-13 for (a) the SD limit state and (b) the NC limit state of members HEB240, HEA160 and IPE300 (*left-to-right* figures).

6.5 Expressions for predicting the rotation capacity of laterally restrained steel members

6.5.1 Behaviour of steel members with different European cross-section profiles

Extensive studies on the evaluation of the deformation capacity of steel members subjected to combined axial load and inelastic deformations with a wide range of European section sizes are practically inexistent. Hence, with the aim of contributing to the current database of available results and extending the assessment study on the accuracy of the deformation capacity limits proposed by EC8-3, a set of steel beam-column members with typical IPE (80* to 600), HEA, HEB and HEM (100 to 1000) cross-section profiles was evaluated. Cantilever members with variable length were modelled so as to avoid the occurrence of inelastic buckling when the influence of the axial load is taken into account. A power law was fitted to the stress-strain experimental results provided for every member tested by D'Aniello et al. (2012), which served as the basis for the multilinear kinematic material model with hardening used in the monotonic analyses. Likewise, mean C_i = 11333

N/mm2 and $\gamma_{i,mean}$ = 123 values of those obtained from the initial calibration of the HEB240, IPE300 and HEA160 members were adopted in the nonlinear kinematic material model with hardening. To assess the adequacy of the EC8-3 capacity limits to steel beam-column members with a wide-range of European cross-section profiles, the numerical estimates of θ_{max} and $\theta_{80\%}$ for axial load levels of ν = 0 and ν = 0.4 are plotted in Figure 6.19 and Figure 6.20, respectively, versus the web slenderness ratio λ_w of the sections. The main observations are summarized as follows:

- For stocky wide-flange cross-sections (HEA, HEB and HEM profiles), the EC8-3 limits appear to be in reasonable agreement with the numerical capacity estimates obtained for ν = 0, particularly of $\theta_{80\%}$. Nevertheless, some discrepancies may be observed in the estimation of θ_{max} for HEA and HEB profiles with web slenderness ratios lower than about 25, where EC8-3 provides rotation capacity estimates up to 2 times the numerical ones, and in the estimation of θ_{max} and $\theta_{80\%}$ for HEM profiles with web slenderness ratios greater than around 18, where, in turn, EC8-3 significantly underestimates their deformation capacity. Note that the break in EC8-3 limits curve of the HEB profiles refers to cross-sections with flange slenderness ratios of class 2. Furthermore, it was found that as the web slenderness ratio of stocky sections increases, θ_{max} tends to a minimum value of 0.03 radians and $\theta_{80\%}$ to about 0.05 radians. On the contrary, EC8-3 systematically provides non-conservative estimates of the deformation capacity for deep wide-flange cross-sections (IPE profiles).
- In agreement with the previous findings of Newell and Uang (2008), the deformation capacity of heavy and wide-flange column sections, particularly the HEM profiles, was found to be practically unaffected by the increase in the axial load. The effect of the stocky web may explain the delay on the onset of flange local buckling and may be contributing to the higher deformation capacities (Newell and Uang, 2008). Still, as pointed out by Elkady and Lignos (2014), the occurrence of local buckling in deep wide-flange profiles is hastened by higher levels of axial load, reducing the member's deformation capacity. Accordingly, IPE and slender web HEA and HEB profiles were seen to undergo a significant reduction in their rotation capacity, which may further aggravate the inadequacy of the EC8-3 limits and thus lead to rather unsafe scenarios during the seismic safety assessment process of existing steel buildings.

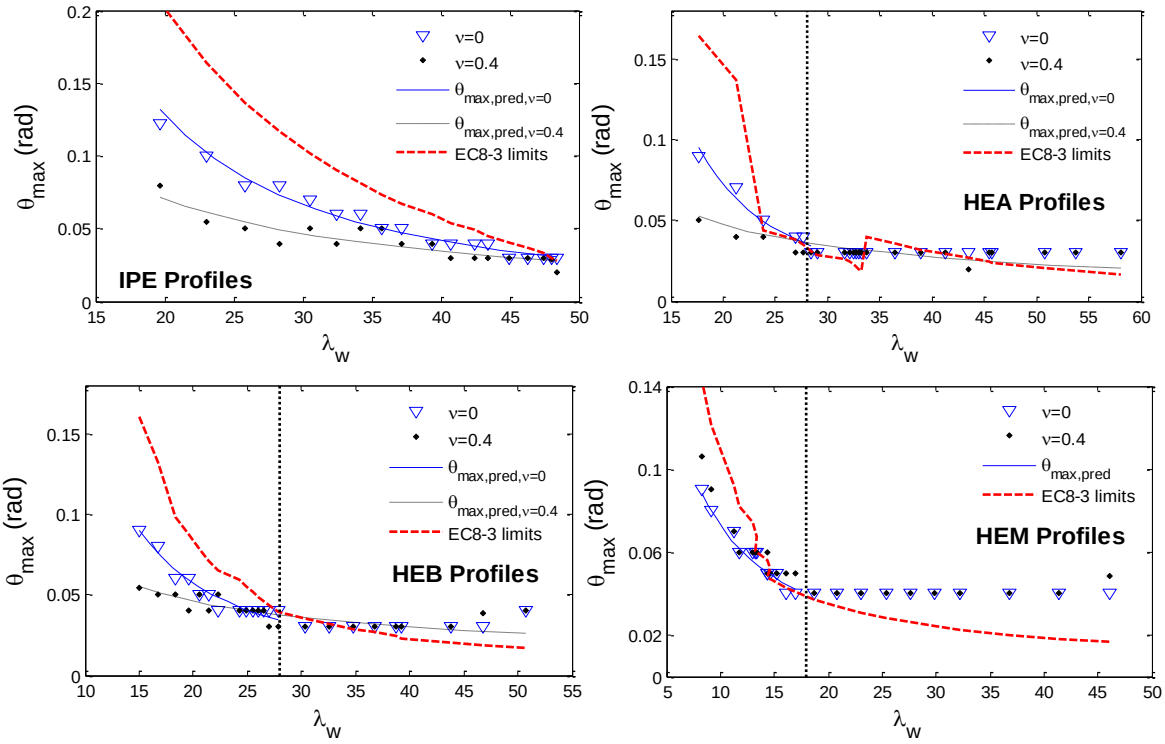

Figure 6.19 – Comparison between the numerical θ_{max} estimates and the EC8-3 SD limit state capacity limits for wide-range of European cross-section profiles.

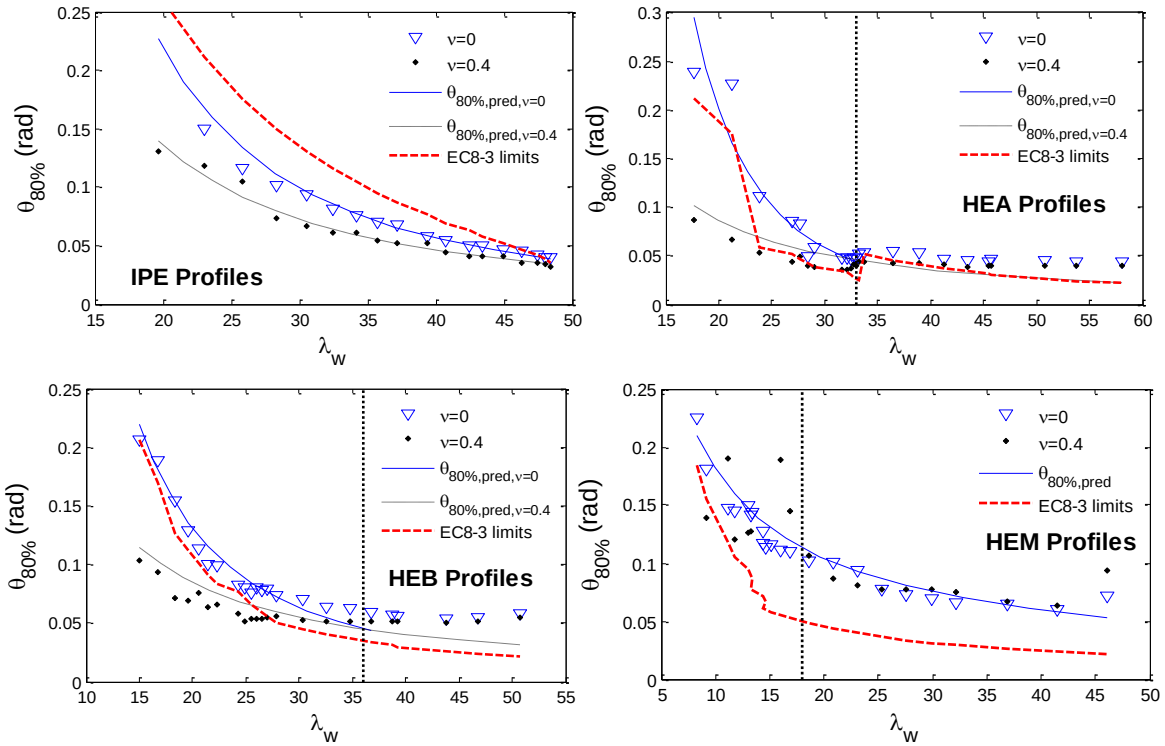

Figure 6.20 – Comparison between the numerical $\theta_{80\%}$ estimates and the EC8-3 NC limit state capacity limits for wide-range of European cross-section profiles.

Anastasiadis et al. (2015) have already highlighted two opposite effects associated with the increase in the rotation capacity of steel members: (i) a first natural positive effect

that respects to the improvement of the building's structural performance; (ii) and second negative effect that is related to the fact that no filter will exist against large strain rates, thus increasing the potential of brittle cracking. In other words, steel members with thick and larger cross-sections may fracture in a brittle manner preceding the occurrence of buckling instability phenomena (Kuwamura, 1997). Hence, aiming to account for the occurrence of brittle fracture before the onset of local buckling or the attainment of $\theta_{80\%}$, which, as previously referred, controls the collapse of steel members, the fatigue life of the set of cross-section profiles was evaluated. Figure 6.21 shows the comparison between the fatigue life predictions and the θ_{max} and $\theta_{80\%}$ rotation capacity estimates. Brittle fracture prior to the onset of local buckling was found to potentially occur in the case of more compact deep wide-flange sections (i.e. with λ_w values lower that around 28). Interestingly, the CVGM equally predicted the possibility of occurring brittle fracture in HEB and HEM profiles with high λ_w ratios, which initiated at constant rotation values of about 0.018 radians. For the remaining cross-section profiles, fracture occurred around or before reaching $\theta_{80\%}$, thus allowing to conclude that θ_f seems to be a more rational parameter to characterize the deformation capacity of steel members at the NC limit state.

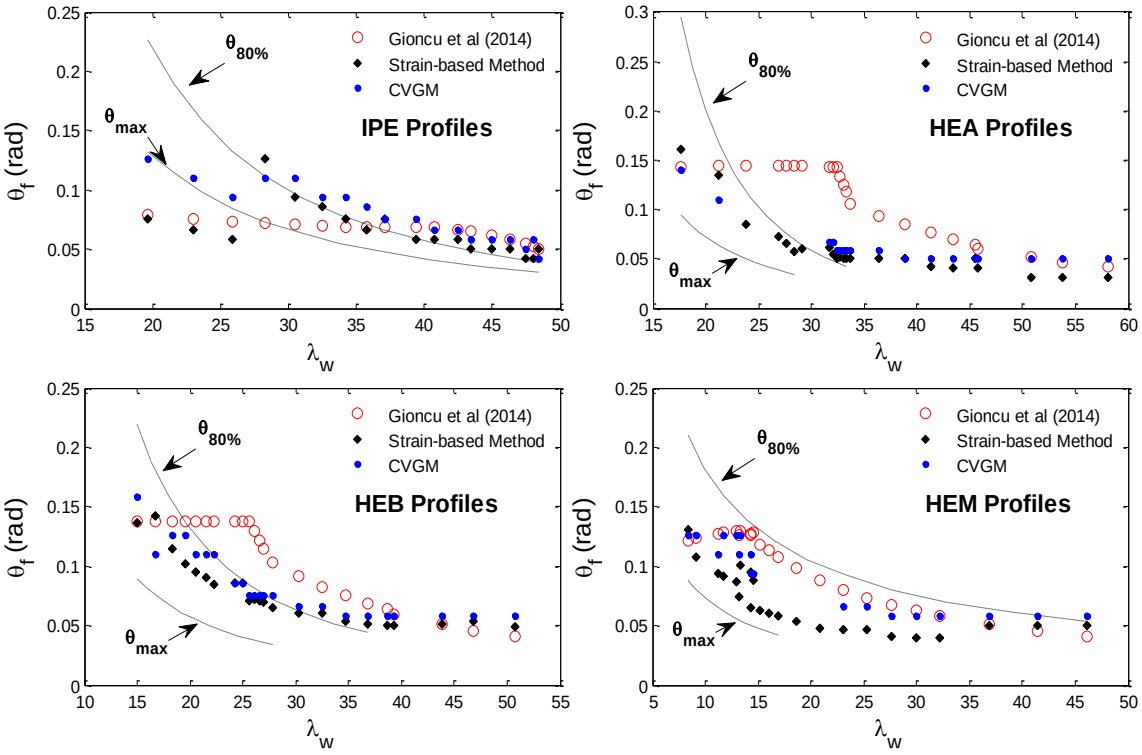

Figure 6.21 – Confrontation of crack initiation with the numerical estimates of θ_{max} and $\theta_{80\%}$ and comparison between different methods of quantifying θ_f.

Regarding the comparison between the various methods of quantifying θ_f, both strain-based and cyclic void growth models were found to generally lead to similar results,

with the exception to the referred predictions of θ_f in the case of HEB and HEM profiles with high λ_w ratios. Additionally, the estimates of θ_f were compared with those obtained from the simplified approach proposed by Gioncu et al. (2014). This approach is based on the estimation of fracture at flanges under a monotonic loading characteristic of a near-fault earthquake with high pulse-velocity, which induces high strain-rate levels. A quite good agreement between the predictions obtained from the simplified approach and the strain-based and CVG models was observed for the IPE profiles, while for stocky sections the simplified approach generally overestimated θ_f.

Finally, Anastasiadis et al. (2012) stated that a lowering in the deformation capacity of steel members could be observed as the member span increases and the steel quality becomes higher. Although the influence of the member span has not been taken into account, the effect of the steel quality was assessed by re-evaluating the cyclic response of the set of cross-section profiles assuming a S355 steel grade with the nonlinear kinematic material model parameters proposed by Nip et al. (2010), i.e. $\sigma|_o$ = 465 MPa, C = 23554 MPa and γ = 139. It was observed that the deformation capacity of the members did not vary much with the increase in the steel grade, being verified deviations in θ_{max} not greater than 25%. Still, it is worth noting that the backstress parameters adopted in this case are different from those previously adopted. Hence, further probabilistic and sensitivity analysis on the impact of the adopted modelling parameters in the final response estimates of the member seems to be deemed necessary.

6.5.2 Fitting of nonlinear regression models

It has been demonstrated by others (D'Aniello et al., 2012; Lignos and Krawinkler, 2011) and throughout this work, that the rotation capacity of steel members is highly dependent on the characteristic of the member, namely the depth of the cross-section, the span-to-depth ratio and both web and flange slenderness. On the basis of the numerical data herein presented, empirical equations for predicting the capacity of laterally restrained steel members have been derived by means of nonlinear regression analyses (Lignos and Krawinkler, 2011) and assuming the flange and web slenderness as predictor variables. The nonlinear model used to predict the capacity of the members, R_C, is given by:

$$R_c = a_1 \left(\frac{b_f}{2t_f} \right)^{a_2} \left(\frac{h}{t_w} \right)^{a_3} \tag{6.7}$$

where a_1, a_2 and a_3 are the regression coefficients, b_f and t_f are the flange width and thickness and h and t_w are the web depth and thickness. Figure 6.22 shows a fitting example of the nonlinear regression model to the numerical cyclic responses of the IPE profiles. It was found that an almost perfect match ($R^2 \approx 1.0$) between the prediction equations and the numerical results is obtained when the model is fitted separately for each group of cross-section profiles. Table 6.3 summarizes the values of a_1, a_2 and a_3, as well as the goodness-of-fit coefficient R^2 and the residuals standard deviation σ_{ln}, estimated for each capacity parameter with $v = 0$, namely both cyclic and monotonic capacities at the onset of local buckling, θ_{max}^{cyclic} and $\theta_{max}^{monotonic}$, the cyclic capacity at 80% of M_{max}, $\theta_{80\%}^{cyclic}$, the cyclic rotation at fracture, θ_f, and both cyclic and monotonic over-strength factors, s^{cyclic} and $s^{monotonic}$. Figure 6.19 and Figure 6.20 display the applicability of the θ_{max}^{cyclic} and $\theta_{80\%}^{cyclic}$ prediction models for each group of cross-section profiles.

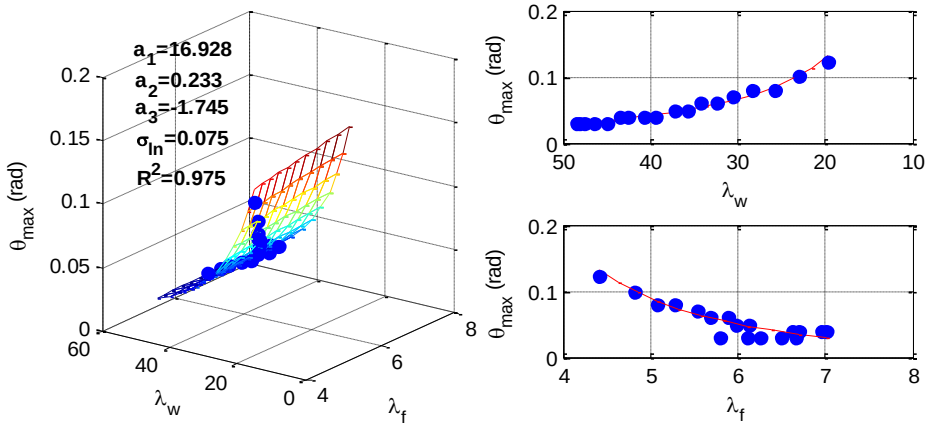

Figure 6.22 – Fitting example of the nonlinear regression model to the numerical cyclic responses of the IPE profiles obtained using the SAC loading protocol.

It should be referred that no fitting was conducted to the monotonic rotation capacities at $0.8M_{max}$ since this rotation level was not attained at every member and lead to poor goodness-of-fit levels. Nevertheless, a general abrupt loss of strength was observed after the initiation of local buckling. This delay in the onset of local buckling may equally explain the higher monotonic over-strength factors observed in compact cross-sections when compared to cyclic ones. The nonlinear regression models presented for $\theta_{max}^{monotonic}$ and $s^{monotonic}$ have particular interest in defining the monotonic backbone curve of lumped plasticity models that incorporate strength and stiffness deterioration, such as the one proposed by Ibarra et al. (2005). This model accounts for cyclic deterioration by defining a cumulative plastic rotation parameter Λ, which may be calibrated having θ_{max}^{cyclic} and $\theta_{80\%}^{cyclic}$ as reference member responses. The calibration of Λ is currently under way by the group at

University of Porto based on the application of robust Harmony Search optimization algorithms (Araújo et al., 2015).

Table 6.3 – Prediction equations for quantifying the capacity of laterally restrained steel members with $\nu = 0$.

Profile		Onset of local buckling		Capacity at 80%M_{max}	Fracture	Over-strength factor	
		$\theta_{max}^{monotonic}$	$\theta_{max}^{cyclic\,1}$	$\theta_{80\%}^{cyclic\,2}$	θ_f	$s^{monotonic}$	s^{cyclic}
IPE	a_1	17.978	16.928	33.838	2.669	9.273	1.547
	a_2	1.008	0.233	0.105	0.957	-0.12	-0.053
	a_3	-1.798	-1.745	-1.785	-1.469	-0.447	-0.010
	R^2	0.833	0.98	0.996	0.883	0.911	0.796
	σ_{ln}	0.180	0.075	0.028	0.113	0.044	0.005
HEA	a_1	223.135	94.739	1165.677	3.244	8.474	1.899
	a_2	-1.252	0.807	-0.680	-0.308	-0.493	-0.096
	a_3	-1.384	-2.924	-2.453	-0.943	-0.255	-0.050
	R^2	0.857	0.954	0.933	0.817	0.794	0.787
	σ_{ln}	0.142	0.113	0.168	0.089	0.056	0.011
HEB	a_1	5.606	4.565	32.353	3.099	10.608	1.641
	a_2	-0.067	-0.764	-0.600	-0.066	-0.634	-0.047
	a_3	-0.981	-0.997	-1.487	-1.078	-0.231	-0.036
	R^2	0.956	0.958	0.989	0.905	0.898	0.728
	σ_{ln}	0.071	0.062	0.042	0.087	0.060	0.007
HEM	a_1	0.747	1.024	1.295	0.326	1.891	1.547
	a_2	0.553	0.425	-0.342	0.370	-0.034	-0.041
	a_3	-0.710	-1.349	-0.702	-0.624	-0.061	-0.023
	R^2	0.956	0.957	0.948	0.914	0.856	0.907
	σ_{ln}	0.074	0.055	0.085	0.106	0.027	0.004

[1] Constant values of θ_{max}^{cyclic} of 0.03 and 0.04 radians should be adopted for HEA and HEB profiles with $\lambda_w \geq 28$ and HEM profiles with $\lambda_w \geq 16$, respectively.

[2] Constant values of $\theta_{80\%}^{cyclic}$ of 0.045 and 0.055 radians should be adopted for HEA profiles with $\lambda_w \geq 28$ and HEB profiles with $\lambda_w \geq 37$, respectively.

Moreover, the values of $s^{monotonic}$ and s^{cyclic} equally play an important role in the verification of the strong-column / weak-beam capacity design principal, according to which the sum of the flexural capacities of the joint columns should be equal or greater

than the sum of the flexural capacities of the joint beams multiplied by the over-strength factor *s* and a partial safety factor γ_{ov} that takes into account the material variability (D'Aniello et al., 2012). Recall that significant variability around the quantification of *s* may be found as a function of the input seismic intensity (Figure 6.11 (d)). Finally, the θ_{max}^{cyclic} and θ_f rotation capacities could be adopted to define the EC8-3 limits. Whereas the SD limit state rotation capacity may be defined by $min\ \{\theta_f\ ;\ \theta_{max}^{cyclic}\}$ so as to avoid the occurrence of local buckling and brittle fracture, the NC limit state rotation capacity may be simply given by θ_f. In comparison to the limits proposed by EC8-3, the present values have the additional advantage of being independent on the yield rotation θ_y, which is expected to significantly change during the inelastic response of the member (Chapters 4 and 5). Still, the rotation capacity limits should be reduced in the presence of the axial load as discussed below.

6.5.3 Inclusion of axial load effects

The influence of the axial load in the deformation capacity of steel members has been thoroughly assessed throughout the previously conducted parametric study, wherein a reduction of about 60% was evidenced in agreement with the findings of Elkady and Lignos (2013; 2014). Figure 6.23 (a) depicts the ratio between the rotation capacity of the HEB 240, HEA 160 and IPE 300 members already analysed for different axial load levels and their respective rotation capacity without the inclusion of axial load, defining a sort of axial load reduction factor η_v. Both monotonic and cyclic rotation capacities at θ_{max} and $\theta_{80\%}$ are represented, as well as the cases with varying local geometrical imperfections. It may be observed that, contrarily to the axial load reduction factor proposed by ASCE41-13, which is linearly proportional to 1-5/3*v*, the influence of the axial load seems to approximately follow a parabolic trend, tending to a constant value as *v* increases. Based on this evidence, a power law and a polynomial function were fitted to the axial load reduction factors η_v presented in Figure 6.23 (a) by giving more weight to the cyclic responses of the members. A more generic relationship was sought, which additionally includes the influence of local geometrical imperfections. These relationships may be afterwards multiplied by the rotation capacity prediction models (Table 6.3) to account for axial load effects. However, as demonstrated in Figure 6.19 and Figure 6.20, whilst web slender and deep cross-section profiles were seen to be more affected by axial load effects, the rotation capacity of heavy and stocky web cross-sections remained practically

unchanged as the axial load increased from zero to ν =0.4. In order to include the influence of the geometrical features of different cross-section profiles in the fitted power law function of η_ν, chosen due to its simplicity, a nonlinear regression model was derived based on the η_ν reduction factors obtained for the set of cross-section sizes, so that:

$$\eta_\nu = 1 - \left(2.2 - k_1 \lambda_f^{\,k_2} \lambda_w^{\,k_3}\right) \nu^{0.53} \tag{6.8}$$

where k_1, k_2 and k_3 are the regression coefficients presented in Table 6.4 for each group of cross-section profiles. The suitability of equation (6.8) is depicted in Figure 6.23 (b) to (d), wherein it may be also observed that the disregard of the characteristics of cross-sections, namely the flange and web slenderness, could lead to substantial conservative rotation capacity estimates. Note that constant values of $\theta_{max}^{monotonic}$ and $\theta_{80\%}^{cyclic}$ should be adopted in the case of HEA and HEB profiles in accordance to Table 6.3 and regardless the axial load level, while no reduction is needed in the case of HEM profiles.

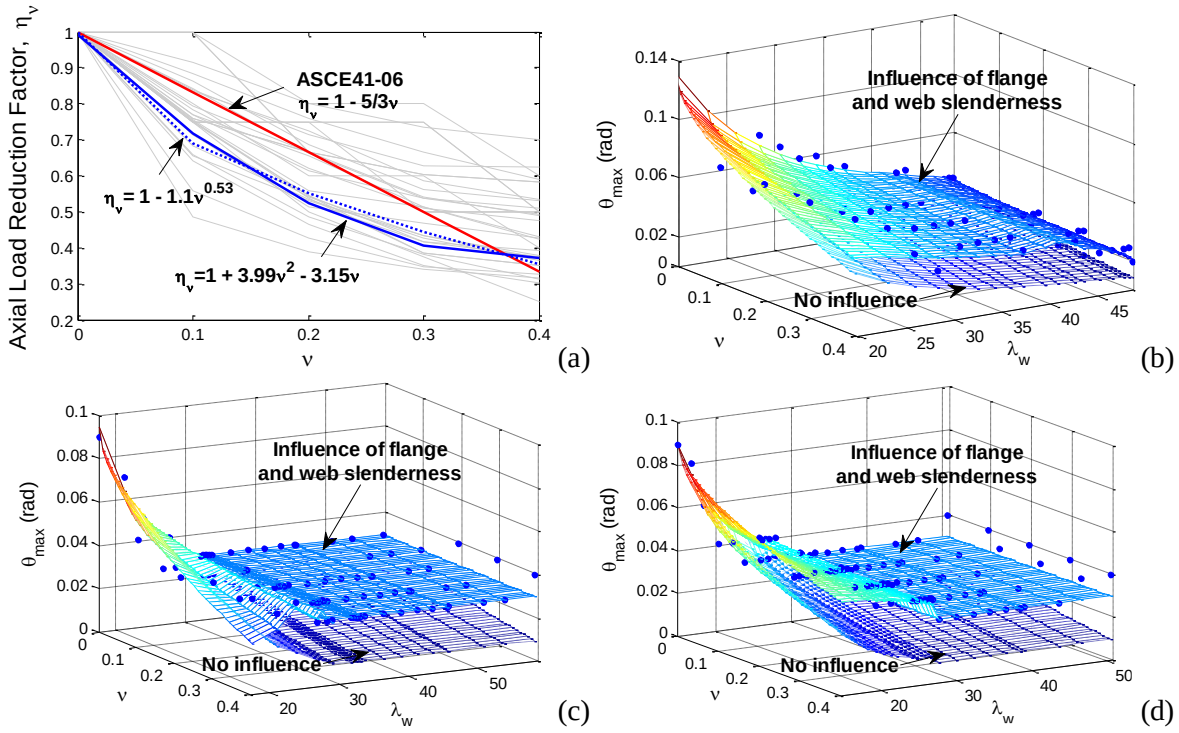

Figure 6.23 – Definition of the axial load reduction factor η_ν: (a) derivation based on the results of the HEB 240, HEA 160 and IPE 300 members; and extension to the (b) IPE profiles, (c) HEA profiles and (d) HEB profiles.

Table 6.4 – Parameters of the axial load reduction factor prediction equations.

Profile	Parameters				
	k_1	k_2	k_3	R^2	σ_{ln}
IPE	0.183	1.211	0.038	0.51	0.17
HEA	0.079	2.039	-0.424	0.13	0.89
HEB	0.164	0.634	0.406	0.12	0.64

6.6 Conclusions

This work focuses on the estimation of the deformation capacity of laterally restrained European beam-column elements and investigates the suitability of the deformation capacity limits preconized in the Part 3 of Eurocode 8 (EC8-3). Numerical FE models capable of simulating the experimental monotonic and cyclic responses obtained by D'Aniello et al. (2012) were developed and served as the basis for a comprehensive parametric study that aimed at assessing the influence of global and local geometrical imperfections, the axial load level and real ground motion records on the deformation capacity of steel members. Fracture was taken into account by adopting strain-based and cyclic void growth models. The FE model was finally extended to a set of cross-section profiles with the purpose of providing more general conclusions and expressions for predicting the rotation capacity of steel members.

In summary, the EC8-3 limits were seen to systematically overestimate the deformation capacity of deep and slender web cross-section profiles, being further aggravated by the increase in the axial load. Additionally, these limits do not avoid the occurrence of fracture, which, in turn, is the expected governing failure mode of stocky wide-flange cross-section profiles. Therefore, answering the question initially placed, the EC8-3 deformation limits were found to be in general inadequate and its revision should be placed as a first priority.

6.7 Acknowledgments

This work was performed within the framework of the research project 'Development and calibration of seismic safety assessment methodologies for existing buildings according to the Eurocode 8 – Part 3' founded by Foundation of Science and Technology (FCT) of Portugal.

6.8 References

AISC (2005) Seismic provisions for structural steel buildings, American Institute of Steel Construction, Chicago, Illinois.

Anastasiadis A, Mosoarca M, Gioncu V (2012) Prediction of available rotation capacity and ductility of wide-flange beams, Part 2, Application, Journal of Constructional Steel Research, 68, 176-191.

Anastasiadis A, Mosoarca M, Gioncu V (2015) Investigation of the cyclic inelastic capacity of steel beams through the use of plastic collapse mechanism, Bulletin of Earthquake Engineering, 13, 1377-1403.

ANSYS (2009) ANSYS Structural Analysis Guide, ANSYS, Inc., Canonsburg.

Arasaratnam P, Sivakumaran KS, Tait MJ (2011) True stress-true strain models for structural steel elements, International Scholarly Research Network.

Araújo M, Macedo, L, Castro JM (2015) Calibration of strength and stiffness deterioration hysteretic models using optimization algorithms, Proceedings of the 8th International Conference on Behaviour of Steel Structures in Seismic Areas, Shangai, China.

ASCE (2014) Seismic evaluation and retrofit of existing buildings (ASCE/SEI 41-13), American Society of Civil Engineers, Reston, Virginia, USA.

ATC (2010) ATC-72-1 Modeling and acceptance criteria for seismic design and analysis of tall buildings, Prepared for Pacific Earthquake Engineering Research Center by Applied Technology Council, Redwood City, CA.

Bradley B (2010) Epistemic uncertainties in component fragility function, Earthquake Spectra, 26, 41-62.

Brescia M, Landolfo R, Mammana O, Iannone F, Piluso V, Rizzano G (2009) Preliminary results of an experimental program on the cyclic response and rotation capacity of steel members, Proceedings of the STESSA09 conference on the Behavior of Steel Structures in Seismic Areas, Philadelphia.

Castiglioni CA (2005) Effects of the loading history on the local buckling behavior and failure mode of welded beam-to-column joints in moment-resisting steel frames, Journal of Engineering Mechanics, 131, 568-585.

CEN (1993) EN 10034 Structural steel I and H sections – Tolerances on shape and dimensions, European Committee for Standardization, Brussels, Belgium.

CEN (2005a) ENV 1998-3 Eurocode 8, Design of structures for earthquake resistance - Part 3, Assessment and retrofitting of buildings, European Committee for Standardization, Brussels, Belgium.

CEN (2005b) ENV 1993-1 Eurocode 3, Design of steel structures - Part 1-1, General rules and rules for buildings, European Committee for Standardization, Brussels, Belgium.

Chaboche JL (2008) A review of some plasticity and viscoelastic constitutive theories, International Journal of Plasticity, 24, 1642-1693.

Chen Y, Sun W, Chan TM (2013) Effect of loading protocols on the hysteric behavior of hot-rolled structural steel with yield strength up to 420 MPa, Advances in Structural Engineering, 16, 707-719.

Coffin LF (1971) A note on low cycle fatigue laws, Journal of Materials, 6, 338-402.

Conseza E, Manfredi G, Martin AD (1995) Experimental testing for the analysis of the cyclic behavior of steel elements, an overview of the existing procedures, In Mazzolani M and Gioncu V (eds), Behaviour of Steel Structures in Seismic Areas, E & FN Spon, London.

Corte GD, D'Aniello M, Landolfo R (2013) Analytical and numerical study of plastic over-strength of shear links, Journal of Constructional Steel Research, 82, 19-32.

D'Aniello M, Landolfo R, Piluso V, Rizzano G (2012) Ultimate behaviour of steel beams under non-uniform bending, Journal of Constructional Steel Research, 78, 144-158.

Daali ML (1995) Damage assessment in steel structures, Proceedings of the 7th Canadian Conference on Earthquake Engineering, Montreal, Canada.

Daali ML, Korol R (1994) Local buckling rules for rotation capacity, Engineering Journal, Second Quarter, 41-47.

Dimakopoulou V, Fragiadakis M, Spyrakos C (2013) Influence of modelling parameters on the response of degrading systems to near-field ground motions, Engineering Structures, 53, 10-24.

Elkady A, Lignos DG (2013) Collapse assessment of steel moment resisting frames with deep members, Proceedings of the Vienna Congress on Recent Advances in Earthquake Engineering and Structural Dynamics, Vienna.

Elkady A, Lignos DG (2014) Analytical investigation of the cyclic behavior and plastic hinge formation in deep wide-flange steel beam-columns, Bulletin of Earthquake Engineering, 13, 1097-1118.

FEMA (2007) FEMA 461 Interim testing protocols for determining the seismic performance characteristics of structural and non-structural components, Federal Emergency Management Agency, Washington DC, Maryland.

Ge H, Kang L (2012) A damage index-based evaluation method for predicting the ductile crack initiation in steel structures, Journal of Earthquake Engineering, 16, 623-643.

Gioncu V, Anastasiadis A (2014) Plastic coupled instabilities of I-shapes steel beams, Thin-Walled Structures, 81, 67-77.

Gioncu V, Mosoarca M, Anastasiadis A (2014) Local ductility of steel elements under near-field earthquake loading. Journal of Constructional Steel Research, 101, 33-52.

Gong Y, Norton M (1999) Cyclic response and fatigue of steels subjected to strain control with non-zero means. Journal of Testing and Evaluation 1999, 27, 15-30.

Güneyisi EM, D'Aniello M, Landolfo R, Mermerdas K (2013) A novel formulation of the flexural overstregth factor for steel beams, Journal of Constructional Steel Research, 90, 60-71.

Howdyshell P, Trovillion JC, Wetterich JL (1991) Low-cycle fatigue of structural materials, Proceedings of the 5th ASCE Materials Engineering Congress, Reston.

Ibarra LF, Medina RA, Krawinkler H (2005) Hysteretic models that incorporate strength and stiffness deterioration, Earthquake Engineering and Structural Dynamics, 34, 1489-1511.

Jiao Y, Yamada S, Kishiki S, Shimada Y (2011) Evaluation of plastic energy dissipation capacity of steel beams suffering ductile fracture under various loading histories, Earthquake Engineering and Structural Dynamics, 40, 1553-1570.

Kanvinde AM, Deierlein GG (2006) Void growth model and stress modified critical strain model to predict ductile fracture in structural steels, Journal of Structural Engineering, 132, 1907-1918.

Kanvinde AM, Deierlein GG (2007) Cyclic void growth model to assess ductile fracture initiation in structural steels due to ultra low cycle fatigue, Journal of Engineering Mechanics, 133, 701-712.

Kato B, Akiyama H (1981) Ductility of members and frames subjected to buckling, ASCE Convention, New York.

Kaufmann EJ, Metrovich BR, Pense AW (2001) Characterization if cyclic inelastic strain behavior on properties of A572 Gr.50 and A913 Gr.50 rolled sections, National Center for Engineering Research on Advanced Technology of Large Structural Systems, Lehigh University, Bethlehem.

Kazantzi A, Righiniotis TD, Chryssanthopoulos MK (2008) The effect of joint ductility on the seismic fragility of a regular moment resisting steel frame designed to EC8 provisions, Journal of Constructional Steel Research, 64, 987-996.

Kemp A (2003) Designing for ductility, The Structural Engineer, 81, 13-14.

Kemp A, Dekker N (1991) Available rotation capacity in steel and composite beams, The Structural Engineer, 69, 88-97.

Kemp A, Dekker N, Trinchero P (1995) Differences in inelastic properties of steel and composite beams, Journal of Constructional Steel Research, 34, 187-206.

Kondo Y (2003) Fatigue under variable amplitude loading, Comprehensive Structural Integrity, Cyclic loading and fatigue, Milne I, Ritchie RO, Karihaloo BL, eds., Elsevier.

Krawinkler H (1999) Cyclic loading histories for seismic experimental on structural components, Earthquake Spectra, 12, 1-12.

Krawinkler H (2009) Loading histories for cyclic tests in support of performance assessment of structural components, Proceeding of the 3rd International Conference on Advances in Experimental Structural Engineering, San Francisco.

Krawinkler H, Zareian F (2007) Prediction of collapse - How realistic and practical is it and what can we learn from it? The Structural Design of Tall and Special Buildings, 16, 633-653.

Kuwamura H (1997) Transition between fatigue and ductile fracture in steel, Journal of Structural Engineering, 123, 864-870.

Lay M, Galambos T (1967) Inelastic beams under monotonic gradient, Journal of Structural Division, 93, 381-399.

Lemaitre J, Chaboche JL (1990) Mechanics of solid materials, Cambridge University Press, English ed, UK.

Lignos DG, Hikino T, Matsuoka Y, Nakashima M (2013) Collapse assessment of steel moment frames based on E-defense full-scale shake table collapse tests, Journal of Structural Engineering, 139, 120-132.

Lignos DG, Krawinkler H (2011) Deterioration modeling of steel components in support of collapse prediction of steel moment frames under earthquake loading, Journal of Structural Engineering, 137, 1291-1302.

Lignos DG, Krawinkler H, Wittaker AS (2011) Prediction and validation of sidesway collapse of two scale models of a 4-storey steel moment frame, Earthquake Engineering and Structural Dynamics, 40,807-825.

Mazzolani F, Piluso V (1996) Theory and design of seismic resistant steel frames, E&EF Spon, London, UK.

Meggiolaro MA, Castro JTP (2004) Statistical evaluation of strain-life fatigue crack initiation predictions, International Journal of Fatigue, 26, 463-476.

Mergos PE, Beyer K (2014) Loading protocols for European regions of low to moderate seismicity, Bulletin of Earthquake Engineering, 12, 2507-2530.

Miner MA (1945) Cumulative damage in fatigue, Journal of Applied Mechanics, 12, A159-A164.

Mitani I, Makino M, Matsui C (1997) Influence of local buckling on cyclic behavior of steel beam-column, Proceedings of the 6th World Conference on Earthquake Engineering, New Delhi, India.

Myers AT, Kanvinde AM, Deierlein GG, Baker JW (2014) Probabilistic formulation of the cyclic void growth model to predict ultralow cycles fatigue in structural steel, Journal of Engineering Mechanics, 140.

NEHRP (2011) Research plan for the study of seismic behavior and design of deep, slender wide flange structural steel beam-column members, NIST GCR 11-917-13 report, NEHRP Consultants Joint Venture, Reston, Virginia.

Newell JD, Uang CM (2008) Cyclic behavior of steel wide-flange columns subjected to large drift, Journal of Structural Engineering, 134, 1334-1342.

Nip KH, Gardner L, Elghazouli AY (2010) Cyclic testing and numerical modelling of carbon steel and stainless steel tubular bracing members, Engineering Structures, 32, 424-441.

Nip KH, Gradner L, Davies CM, Elghazouli (2010) Extremely low cycle fatigue tests on structural carbon steel and stainless steel, Journal of Constructional Steel Research, 66, 96-110.

Pereira JCR, de Jesus AMP, Xavier J, Fernandes AA (2014) Ultra low-cycle fatigue behaviour of a structural steel, Engineering Structures, 60, 214-222.

Petcu D, Gioncu V (2003) Computer program for available ductility analysis of steel structures, Computers and structures, 81, 2149-2164.

Sawyer A (1961) Post-elastic behavior of wide-flange steel beams, Journal of Structural Division, 87,134-141.

Shokouhian M, Shi Y (2014) Classification of I-section flexural members based on member ductility, Journal of Constructional Steel Research, 95, 198-210.

Southward R (1969) Local buckling in universal sections, Engineering Department of the University of Cambridge, Cambridge, UK.

Spangemacher R, Sedlacek G (1992) On the development of a computer simulation for tests of steel structures, Proceedings of the Constructional Steel Design World Developments, Acapulco, Mexico.

Stojadinovic B (2003) Stability and low-cycle fatigue limits of moment connection rotation capacity, Engineering Structures, 25, 691-700.

Susuki T, Ono T (1977) An experimental study on inelastic behavior of steel members subjected to repeated loading, Proceedings of the 6th World Conference on Earthquake Engineering, New Delhi, India.

Torabiam S, Schafer WB (2014) Role of local slenderness in the rotation capacity of structural members, Journal of Constructional Steel Research, 95, 32-43.

Tortorelli S, D'Aniello M, Landolfo R (2011) Prediction of the flexural capacity of steel beams, Proceedings of the 6th European Conference on Steel and Composite Structures, Budapest, Hungary.

White D, Barth K (1998) Strength and ductility of compact flange I-girders in negative bending, Journal of Constructional Steel Research, 45, 241-280.

Xia Z, Kujawski D, Ellyin F (1996) Effect of mean stress and ratcheting strain on fatigue life of steel. International Journal of Fatigue, 18, 335-341.

Zarein F, Krawinkler H, Ibarra L, Lignos D (2010) Basic concepts and performance measures in prediction of collapse of buildings under earthquake ground motions, The Structural Design of Tall and Special Buildings, 19,167-181.

Zhou H, Wang Y, Yang L, Shi Y (2014) Seismic low-cycle fatigue evaluation of welded beam-to-column connections in steel moment frames through global-local analysis, International Journal of Fatigue, 64, 97-113.

Chapter 7

Seismic losses to property and business activity of industrial buildings - Modelling assumptions and property losses

Araújo M, Castro JM, Marques M (2019) Seismic losses to property and business activity of industrial buildings. Part 1: modelling assumptions and property losses, *Earthquake Spectra* (submission).

7.1 Summary

The industrial building stock of countries located in seismic prone regions may be exposed to suffer extensive property damage and losses, which may result in even higher losses to production or business closure. Still, very few works focusing on the estimation of property losses and on the proposal of fragility and vulnerability functions for industrial steel buildings, which represent a substantial slice of the industrial building stock of many countries, have been conducted up to date. Hence, this work aims to contribute to such research needs through the proposal of vulnerability functions for typical industrial steel buildings that account for damage to structural and non-structural components and contents specific of different industrial activities. Property losses within a 95% confidence interval to industrial buildings located in mainland Portugal were estimated and seen to reach up to 12.30% of the building replacement cost in 50 years.

7.2 Introduction

Recent seismic events that occurred in highly industrialized regions, e.g. the 1999 Kocaeli, the 2011 Tohoku or the 2012 Emilia earthquakes, revealed an unexpected high vulnerability of the industrial building stock to earthquakes (Durukal and Erdik, 2008; Krusmann et al., 2010; Nakashima et al., 2014; Grimaz, 2014). The significant industrial

physical losses, around 49% of the average total losses in the Izmir region after the 1999 Kocaeli earthquake (Kurita et al., 2004; Durukal and Erdik, 2008), somehow counteracted the general assumption that industrial buildings are expected to withstand strong earthquakes due to its lightweight and design governed by wind loads. The inexistence of proper seismic design regulations and insufficient joint capacities were some of the main reasons for a number of RC precast industrial building collapses observed after the Kocaeli and Adana-Ceyhan earthquakes (Rahnama and Morrow, 2000), and very recently after the 2012 Emilia earthquake (Casotto et al., 2015). The latter has, in fact, triggered a series of works focused on the assessment of the seismic performance of precast RC buildings and on the proposal of strengthening techniques (Bournas et al., 2014; Magliulo et al., 2014). Similarly, industrial steel buildings were seen to be relatively vulnerable to earthquakes, suffering a number of partial collapses during the 1989 Loma Prieta earthquake (Phipps et al., 1992) and substantial damage during the last 2011 Christchurch and 2011 Tohoku earthquakes (Clifton et al., 2011; Nakashima et al., 2014). However, very few studies focused on the seismic performance assessment and development of physical fragility functions for industrial steel buildings have been conducted up to date (Ozakgul et al., 2011; Petruzzelli et al., 2012a; 2012b). Such specific studies are in fact of particular relevance to allow for a more rigorous assessment of the risk to which the existing industrial building stock of a number of countries, such as Portugal, Spain or Greece, is exposed to. According to the Precasteel Project (RFCS, 2013), the industrial building stock of the referred countries is mostly composed by steel buildings, which range from 60% to 80% of the total industrial building stock. In Italy, on the other hand, practically 70% of the total industrial building stock is made of concrete. This level of exposure is coherent with the high physical losses observed in precast RC buildings after the 2012 Emilia earthquake.

The partial collapse of industrial buildings, e.g. failure of roof girders, and the significant damage to non-structural components, e.g. fell down of cladding panels (Magliulo et al., 2015), oftentimes result in the destruction of the machinery and equipment bellow, terminating production (Krusmann et al., 2010). The losses to non-structural components, contents (i.e. furnishings and equipment) and business inventories may, in fact, significantly overcome structural losses (Dowrick and Rhoades, 1993; 1995; Durukal et al., 2008). After the 1994 Northridge earthquake, almost 70% of the businesses with damage reported that the damage was non-structural, 56% reported damage to furnishings and practically 50% reported damage to equipment and stock or inventory (Tierney, 1997).

Significant damage to non-building structures, e.g. pressurized tanks, vessels, power generators, storage areas, chimneys or cranes, was equally observed in past events (Durukal et al., 2008; Salzano et al., 2009). Direct losses to production and indirect losses due to business interruption, or downtime, which are function of the businesses dependency on input factors, infrastructures and supply chain, may contribute to an important portion of the total industrial losses. A more thorough discussion on this may be found in Chapter 9.

Hence, this work aims at the estimation of property losses associated to a typical industrial steel building located in Portugal Mainland. The geometrical characteristics of the building are defined based on data made available by the Precasteel Project (RFCS, 2013) and on mean geometrical properties obtained from a survey conducted by the authors among more than 200 industrial building design projects and a number of site-visits to national firms (Chapter 9). A comprehensive 3-dimensional model is developed to accurately capture the main failure modes of steel buildings observed in previous post-earthquake reconnaissance campaigns and every particular modelling aspect is discussed. Novel physical fragility and vulnerability functions for typical industrial steel buildings are proposed, accounting not only for structural components, but also for non-structural components and contents. Finally, in order to provide a wider picture of the expected property losses, the later are estimated assuming the case study industrial steel building to be located in any region of Portugal Mainland, defined at the county level.

7.3 Review of previous post-event damage to industrial property

The seismic performance of industrial steel buildings is governed by a number of particular aspects that have been the focus of very little research in the past, particularly in comparison to other types of structures. With the aim of identifying and characterizing the main failure mechanisms developed in industrial buildings, a compilation of the damage to property typically observed in previous post-earthquake reconnaissance campaigns is presented in Table 7.1. In brief, the main structural failure modes observed in industrial steel buildings consist on several brace buckling and net-section fracture, distortion and fracture of the gusset plates and pull-out of column base plates due to fracture of anchor bolts. Damage to non-structural components was typically observed in partitions, ceiling tiles, sprinklers and piping systems, whether equipment and machinery was not only

indirectly damaged by the falling of structural and non-structural members, but also directly damaged by the ground motion. Moreover, the performance of industrial facilities was seen to vary substantially depending on the age and type of structures at the plant. Heavy industrial facilities, typically older, larger and taller, were found to perform poorly when compared to light industrial facilities (EPRI, 1991; Rahnama and Morrow, 2000; Durukal and Erdik, 2008), generally newer and seismically designed. In the latter case, building damage turned out to be primary reason for most direct and indirect losses observed after the 1999 Kocaeli earthquake (Durukal and Erdik, 2008).

Table 7.1 – Property damage observed in previous post-earthquake reconnaissance campaigns.

Earthquakes	Observed Damage	References
1989 Loma Prieta, 1994 Northridge and 2001 Nisqually earthquakes	• Bucking of the bracing system, cracking of floors and window walls and damage to non-structural components (e.g. sprinklers and piping) were the most common types of damage observed in steel facilities. After the 1994 Northridge earthquake almost 70% of the facilities damaged simply indicated damage to non-structural components, such as furnishings, equipment and stock or inventory. The most common non-structural component failures observed following the Nisqually earthquake were related to suspended ceiling systems, cracking of interior partition walls and shattering of glass windows.	Phipps et al. (1992); Tierney (1997); FEMA (2014); Filiatrault and Sullivan (2014).
1992 Erzincan, 1996 Adana-Ceyhan, 1999 Kocaeli and 1999 Düzce earthquakes	• Fell down of precast girders due to insufficient seat lengths, inadequate joint capacities and/or lack of horizontal bracing in the roof plane. Although no damage was observed in facilities with steel joist roof girders after the 1992 Erzincan earthquake, damage was reported to steel frame structures in the 1999 Kocaeli earthquake due to inadequate lateral load resistance. Failure of the roof truss to column connections and column anchor bolts, fracture of brace connections, buckling of braces and structural instability were observed. The partial collapse of buildings (e.g. girders and concrete panels) destroyed the machinery and equipment bellow, terminating production. Equipment was equally directly damaged by the ground motion. Disarraying and toppling of machinery was observed. • Excessive disproportionate in-plane displacements due to column slenderness resulted in permanent offsets. Out-of-plane deformations limited by the masonry infills forming the side walls of the factory resulted in differential movements between the mid-span columns and those at the sides. Shell buckling at the base of tanks resulted in oil leakage and fire that spread to other structures (e.g. a cooling tower was completely destroyed).	Wenk et al. (1998); Rahnama and Morrow (2000); Adalier and Aydingun (2001); Arslan et al. (2006); Durukal and Erdik (2008)
The 2010 and 2011 Christchurch series of earthquakes	• Pre-tensioned brace bars were found to be sagging by much as 200mm, both in the vertical and roof diaphragm braced bays. Fracture of the connections near their pin end also occurred. In a few cases, the gusset plates to which the braces were connected suffered bearing failures. Non-structural damage in these structures was substantially more significant. • Tensile failure of a row of bolts in a base-plate connection in a portal frame building. Local fractures between the beam flange and column flange also occurred. In pavilions, the anchorage of tilt-up walls to steel structures failed, leading to the buckling in compression of roof beams and roofing collapse.	Burneau et al. (2010); Clifton et al. (2011);
2004 Mid Niigata and 2011 Tohoku earthquakes	• Buckling and net-section fracture of brace members and joints, buckling of diagonal members of latticed column, damage of connection between RC columns and steel roof frames, deflection, buckling and fracture of roof horizontal braces and cracking of column base concrete were observed, mostly in steel structures (e.g. gymnasiums) designed under the previous code and that have not suffered retrofitting measures. Some gusset plates fractured as a result of a large number of repeated bending. The damage to exposed base plates points out that, unless the anchor bolts fractured, residual storey drift and structural damage to the building was minimal. Otherwise, severe residual storey	Nakashima et al. (2014); Nishiyama et al. (2012); Midorikawa et al. (2012); Koyama et al. (2012a, 2012b)

	drift was observed. Again, the most common non-structural type of damage was related to dropping of ceilings and exterior walls and breakage of windows.	
2010 Chilean earthquake	• Fracture of bracing members, either at the gusset plate or at the intersection between braces and crushing of the concrete pedestal in the base of columns, probably due to low quality of grouting and poor rebar detailing. Permanent drifts occurred as a result of the buckling of the single diagonal member in a braced frames (lack of redundancy). A large number of anchor bolts yielded and fractured in base plate connections.	RMS (2011); Herrera et al. (2012); Tremblay et al. (2013)
2009 L'Aquila and 2012 Emilia earthquakes	• Damage to non-structural components (e.g. partitions and ceiling tiles) and contents (e.g. industrial equipment) due to lack of anchorage between the elements and the structure. A silo collided with the adjacent precast warehouse, crushing the concrete wall. A number of roofs and cladding panels of precast buildings collapsed causing deaths and destroying the equipment below.	Liberatore et al. (2013); Magliulo et al. (2014); Bournas et al. (2014); Grimaz (2014);

7.4 Damage states for industrial steel buildings

The compilation of most common types of property damage observed in previous post-earthquake reconnaissance campaigns given in Table 7.1 provides valuable information to support and more clearly identify damage levels for industrial steel buildings, which are key in deriving consistent physical fragility curves. Few studies have been conducted in the past focused on the definition of damage states (or limit states) to industrial facilities. Based on data collected after the 1999 Kocaeli earthquake, Durukal and Mustafa (2008) proposed a set of four structural and non-structural damage state levels qualitatively described, which are similar to those defined by the Hazus – MH MR5 framework (FEMA, 2010), although the later also provides quantitative values defined in terms of inter-storey drifts. However, such limits have been defined just for a single direction of analysis, which seems to be associated with the moment resisting frame of the building, and regardless, for instance, the base plate connection adopted. In fact, stiffer portal frames with rigid base plate connections are expected to attain lower drifts and to develop more damage at moment frame members, in comparison to more flexible portal frames with, for instance, nominally pinned base plate connections. Hence, to account for the specificities of a certain industrial steel building, the damage states were defined considering the damage to every individual structural component and bearing in mind the information provided in Table 7.1 and by previous works.

7.4.1 Structural damage states

Structural damage to industrial steel buildings was seen to be mostly circumscribed to moment resisting frame (MRF) members (i.e. girders and columns), to roof and lateral bracing systems and to base plate connections. Current practices in Portugal typically

consist on adopting bolted column-to-girder connections with haunches (with a length that varies from 10% to 20% of the portal frame span), top apex connections and stiffened panel zones that are expected to perform well under earthquake conditions. Thus, damage to such elements will not be considered. To facilitate the definition of criteria for every component damage state, the damage limitation (DL), significant damage (SD) and near collapse (NC) limit states established by part 3 of Eurocode 8 (EC8-3) (CEN, 2005a) were adopted. Table 7.2 describes the structural damage states for every component and their respective assessment criteria.

Table 7.2 – Structural damage states.

Component	Damage Limitation (DL)	Significant Damage (SD)	Near Collapse (NC)
Base plate connections	• Development of type 1 (plate failure), type 2 (contemporary bolt and plate failure) or type 3 (bolt failure) mechanisms or concrete crushing (Aviram et al., 2008; Latour and Rizzano, 2013; Latour et al., 2014). • Type 1, 2 or 3 mechanism or concrete crushing defined according to EC3 component method (Latour et al., 2014).	• Onset of strength deterioration, e.g. due to grout spalling, and initiation of ductile fracture at the fusion line between the column flange and the baseplate weld (Deierlen and Victorsson, 2008). • Onset of strength deterioration occurs at 2/3 of the ultimate rotational capacity of steel base joints, Φcd (Takamatsu and Tamai, 2005). • Initiation of ductile fracture expected to occur at a median drift of around 0.042 radians (Myers et al., 2009).	• Failure due to type 1, 2 or 3 mechanism and complete fracture of the column weld and dislocation of column relative to the base plate (Latour and Rizzano, 2013; Latour et al., 2014). • Ultimate rotational capacity of steel base joints, Φcd, defined according to Latour and Rizzano (2013). • Complete fracture of the column weld expected to occur at a median drift of around 0.07 radians (Myers et al., 2009)
MRF members	• Yielding of moment resisting frame (MRF) members, i.e. columns or girders (Chapter 6).	• Onset of strength deterioration triggered by local instability phenomena. Capacity defined according to expressions proposed in Chapter 6 for European steel profiles.	• Member failure due to an excessive drop in the member's peak strength or fracture. Capacity defined according to expressions in Chapter 6 for European steel profiles.
Bracing system	• Yielding or global bucking of braces. Limits defined by Lignos and Karamanci (2013) or EC8-3 (CEN, 2005a). • Local yield or buckling of gusset plates defined according to Hsiao et al. (2012).	• Local buckling of braces. Limits defined by Lignos and Karamanci (2013) or EC8-3 (CEN, 2005a). • Initial tearing of the gusset plate to column or beam weld. Experimental drift values provided by Lehman et al. (2008).	• Brace fracture. Limits defined by Lignos and Karamanci (2013) or EC8-3 (CEN, 2005a). • Complete fracture of the gusset plate to column or beam weld (Lehman et al., 2008).
Permanent drifts	• Loss of functionality due to excessive permanent drifts and necessity of demolishing the structure (Bojórquez and Ruiz-García, 2013). Probability of having to demolish the structure defined as proposed by Ramirez and Miranda (2012), using a median 1.0% residual drift ratio and a dispersion of 0.3.		

It may be referred, with regard to the lognormal probability of having to demolish the structure conditioned on the peak residual inter-storey drift (Ramirez and Miranda, 2012),

that a median 1.0% residual drift ratio was considered according to Iwata et al., (2006). Such residual drift ratio is expected to cause human discomfort (e.g. dizziness, headaches, and nausea), loss of functionality and loss of reparability, i.e. direct repair cost greater than the direct replacement cost.

7.4.2 Non-structural and contents damage states

Damage to non-structural components and contents is an issue of major concern to both scientific community and stakeholders, as it has been found to significantly contribute to direct losses produced in past earthquake events. Numerous works focused on the definition of fragility functions for every single non-structural component and content that comprises a building structure, e.g. mechanical, electrical and plumbing equipment, furnishings, etc., have already been carried out (Hutchinson and Chaudhuri, 2006; Porter et al., 2010; FEMA, 2012; Filiatrault and Sullivan, 2014). However, because there are often so many individual items of non-structural components, machinery and equipment, particularly in the case of industrial buildings with different activities, it would be impractical to define such fragility functions (Dowrick and Rhoades, 1993; 1995). Therefore, more general fragility functions obtained based on the non-structural damage states defined within the Hazus – MH MR5 framework (FEMA, 2010) were adopted. According to Hazus – MH MR5, non-structural damage is considered to be independent of the building taxonomy and is divided into damage to drift-sensitive (e.g. partitions, wall panels, veneer and finishes) and acceleration-sensitive (e.g. general mechanical, storage tanks, trussed towers, piping and HVAC systems) non-structural components. Hence, whilst the DL, SD and NC limit states of drift-sensitive non-structural components were defined by storey drifts of 0.8%, 2.5% and 5.0%, respectively, the DL, SD and NC limit states of acceleration-sensitive non-structural components were defined by floor accelerations of 0.6g, 1.2g and 2.4g, respectively. Moreover, Hazus – MH MR5 considers that damage to contents (e.g. overturning of cabinets and equipment or equipment sliding of tables and counters) is a function of building accelerations, and thus acceleration sensitive non-structural damage is assumed as a good indicator of contents damage.

7.5 Description of the case study

Light industry and warehousing facilities usually represent a high percentage of a country's industrial building stock, which is naturally associated with its industrial capacity and clustering, e.g. light industry facilities and warehousing represent 90% and 70% of the

total Portuguese and German industrial building stock, respectively (RFCS, 2013). The study presented herein thus aims at representing a typical one storey, single bay, light industry or warehousing facility located in Portugal Mainland. A moment-resisting portal frame system and a bracing system constitute the in-plane and out-of-plane structural systems of the building, respectively, in accordance with the most common practices in Portugal (RFCS, 2013). Figure 7.1 (a) schematically represents the case study industrial steel building. The geometric characteristics were defined based on mean values collected from a survey conducted by the authors among more than 200 industrial building design projects and a number of site-visits to national firms (Chapter 9). An in-plan span length, $2L$, of 20m, a girder slope, θ_{rafter}, of 6.73º, a number, nPF, and spacing, sPF, of portal frames of 8 and 6m, respectively, a purlins spacing, $s_{purlins,}$ of 1.62m, a column height, H, of 6.2m, and, finally, a haunch length, L_{haunch}, of $0.3L$ were adopted. Additional geometrical and detailing information, particularly with regard to the exposed base plate (Figure 7.1 (c) and (d)) and gusset plate connections (Figure 7.1 (e) and (f)), is provided thorough the chapter.

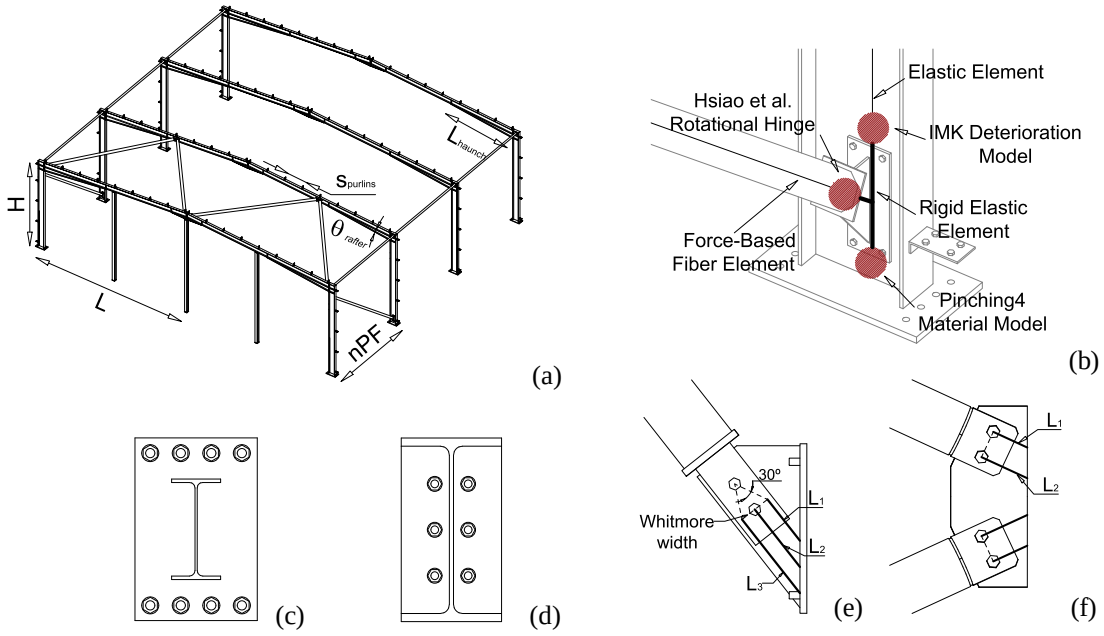

Figure 7.1 – Symmetric representation of the case study industrial steel building (a), modelling assumptions (b), semi-rigid (c) and pinned (d) base plate connections and gusset plate connections of the lateral (e) and roof (f) braces.

Over the years, most Portuguese practitioners have been simply designing industrial buildings to laterally withstand wind loads. To account for this issue, the present case study building was simply designed to gravity, snow and wind loads in accordance to the Portuguese design actions and loads code (RSA, 1983) and Eurocode 3 (EC3) (CEN, 2005b), which is conceptually identical to the former Portuguese steel building design code

(REAE, 1986). A grade S275 was assumed for structural steel and IPE360 and IPE400 cross-section profiles were adopted at girders and columns, respectively, CHS 108x6 cross-section profiles were adopted at both roof and lateral braces, CHS 76.1x6.3 profiles were adopted at the beams of the out-of-plane frames and Z140-1.5 profiles were adopted at purlins. Moreover, based on information collected in the conducted survey (Chapter 9) and on the feedback of Portuguese practitioners, the type of building support usually adopted (i.e. pinned or rigid) was seen to vary substantially. Some practitioners even adopt both rigid and pinned supports during the design of the same portal frame to facilitate safety verifications at both serviceability and ultimate limit states. However, it is expected that the adoption of different base column supports significantly affect the seismic response of industrial buildings, particularly of non-structural components sensitive to drifts and accelerations. Therefore, three different column base support conditions were considered in the present case study: (i) a totally fixed condition, designated as FBPC; (ii) a semi-rigid condition, designated as SBPC; (iii) and a nominally pinned condition, designated as PBPC. A discussion on the modelling assumptions of each condition is provided later.

Property losses were estimated considering an interval of time of 50 years, an admissible lifetime span for this type of structures. Mean and 5% - 95% quantile hazard maps were obtained for that same interval of time on the basis of a probabilistic seismic hazard analysis carried out using the OpenQuake-engine (Pagani et al., 2014) and by adopting the ground-shaking and rupture characteristics previously defined by Silva et al. (2015). A rock soil type was adopted for simplicity and a county-level resolution was considered (i.e. Portugal Mainland has 278 counties), consistent with the NUTS IV European local administrative territorial unit. Information on the Portuguese industrial activity is also provided by the Portuguese National Institute of Statistics (INE) for that same territorial unit. Moreover, to derive the building fragility curves, suits of 20 records were selected and scaled using the Generalized Conditional Intensity Measure approach proposed by Bradley (2010) and considering the hazard curve obtained for Lisbon as target-spectrum. The used number of records has been demonstrated by Marques et al. (2014) to be sufficient and to provide accurate loss estimates when robust ground motion selection and modification methods are adopted. Also, different suits of records should have been selected for each individual county, so as to obtain fragility functions that more accurately account for the record-to-record variability introduced by the specific nature of each county hazard curve. Nevertheless, since the building is expected to respond mostly

in the transverse and longitudinal fundamental modes of vibration, it was found reasonable to simply derive fragility functions using suits of records selected on the basis of the hazard curve obtained for Lisbon (Figure 7.2).

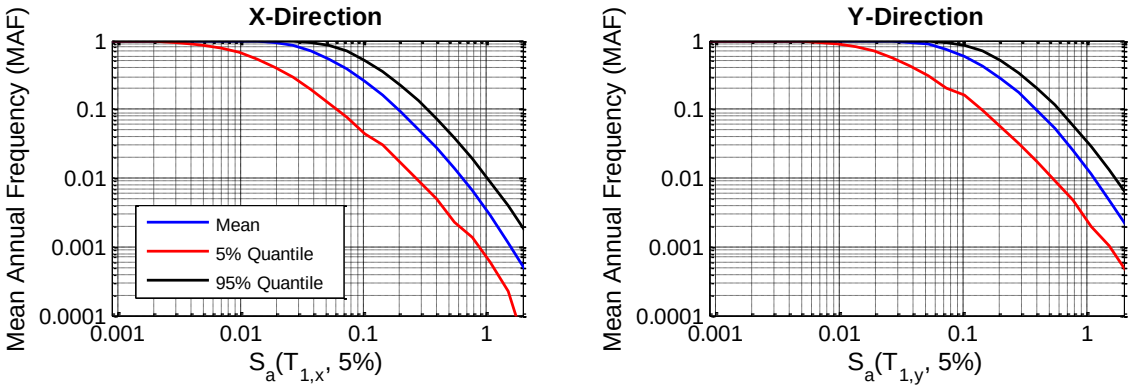

Figure 7.2 – Mean and 5% - 95% hazard curves for Lisbon defined with respect to the 5% damping spectral accelerations at the fundamental periods of vibration of the buildings in both *x*- and *y*-directions.

A modal analysis was firstly carried out using the open-source software OpenSees (PEER, 2011) to identify the dynamic characteristics of the buildings. Periods of vibration respective to the five initial transverse *x*-direction modes, T_1,x, of around 0.56s were obtained, whose mode shapes were seen to be practically governed by single portal frames. In the longitudinal *y*-direction, a fundamental mode of vibration, T_1,y, of 0.3s was found. The influence of overhead traveling cranes, which may significantly affect the dynamic response of industrial buildings, as well as the influence of cladding panels and roof decks (Shrestha et al., 2009; Magliulo et al., 2015) was not considered for simplicity, being assumed that the roof bracing system and purlins conveniently transfer horizontal loads to the vertical braces. Similar fundamental periods of vibration were obtained for all FBPC, SBPC and PBPC buildings, thus allowing the use of the same suits of records in the derivation of each building fragility curves.

Finally, to account for the ground motion directivity and to assess its impact on the derivation of fragility curves, four groups of records were selected: (i) a *x*-direction group of records that consists on single horizontal component records selected and scaled by setting the 5% damping spectral acceleration at T_1,x, S_a (T_1,x, 5%), as the main intensity measure. The single component records were applied along the *x*-direction of the buildings; (ii) a *xy*-direction group of records composed by two horizontal component records selected and scaled using the geometric mean of the 5% damping spectral accelerations of the two horizontal *x* and *y* components at T_1,x, $S_{a,x}$ (T_1,x, 5%) and $S_{a,y}$ (T_1,x, 5%), respectively, as the main intensity measure. A discussion on the selection and scaling

of real records for bi-directional analysis may be found in the work of Beyer and Bommer (2007). The *x* and *y* horizontal components were applied, respectively, along the *x*- and *y*-directions of the buildings. (iii) a *yx*-direction group of records, selected similarly to the later, although considering as the main intensity measure the geometric mean of the 5% damping spectral accelerations of the two *x* and *y* horizontal components at T_1,*y*, $S_{a,x}$ (T_1,*y*, 5%) and $S_{a,y}$ (T_1,*y*, 5%), respectively. The two horizontal components were again applied in simultaneously along the *x*- and *y*-directions of the buildings; (iv) and finally a *y*-direction group of records that consists on single horizontal components selected and scaled by setting the 5% damping spectral acceleration at T_1,*y*, S_a (T_1,*y*, 5%), as the main intensity measure. The records were applied along the *y*-direction of the buildings.

7.6 Modelling assumptions and structural responses

A comprehensive 3-dimensional model has been developed using the open-source software OpenSees (PEER, 2011) to accurately capture the main failure modes observed in previous post-earthquake reconnaissance campaigns and that characterize each structural damage state (Table 7.1 and Table 7.2). Every modelling assumption adopted is discussed next.

7.6.1 Base plate connections

In Europe, the monotonic behaviour of base plate connections is typically defined in accordance with the Eurocode 3 (CEN, 2005c) component method (Latour et al., 2014). This method will be adopted herein, considering the extensions proposed by Latour et al. (2014) to determine the rotational stiffness and the approach proposed by Latour and Rizzano (2013) to define the ultimate rotational capacity, Φ_{cd}. Modelling approaches to characterize the cyclic behaviour of base plate connections have been equally developed, such as the mechanical model proposed very recently by Latour and Rizzano (2015), which relies on previous studies concerning the cyclic behaviour of bolted T-stubs. However, since none of the models have yet been implemented in OpenSees, the Pinching4 material model available in OpenSees was adopted and its parameters were calibrated based on experimental results provided by Gomez (2010). Figure 7.3 presents a comparison between the monotonic and cyclic curves defined analytically based on the EC3 component method and the conducted calibration, respectively, and the experimental results obtained by Gomez (2010). Two experimental tests were selected: (i) a first monotonic and cyclic test (#1 and #2) that was found to sustain significant plate and grout damage and to develop a

pinching response at zero moment due to the interaction of the anchor rods with the base plate; (ii) and a cyclic test (#4) characterized by a more pronounced flag-type pinching effect due to opening and closing of a gap between the base plate and grout or the anchor rod nut and the base plate, which was imposed by the axial load and reflects a cyclic behaviour mostly governed by the anchor bolts. Hence, whereas the #1 and #2 tests would be more representative of EC3 type 1 and 2 mechanisms, the #4 test would represent an EC3 type 3 mechanism. As it may be observed in Figure 7.3 , an over-strength factor of 1.4 was adopted to simulate tests #1 and #2, the peak strength was assumed to be attained at 2/3 Φ_{cd}, as proposed by Takamatsu and Tamai (2005), and a ratio of strength developed upon unloading from negative load to the minimum strength developed under monotonic loading, which sets M_{unl}, equal to zero was defined. Conversely, in test #4, an over-strength factor of 1.1 was adopted, mainly to assure convergence stability, and M_{unl} was defined assuming a ratio of strength of -0.4.

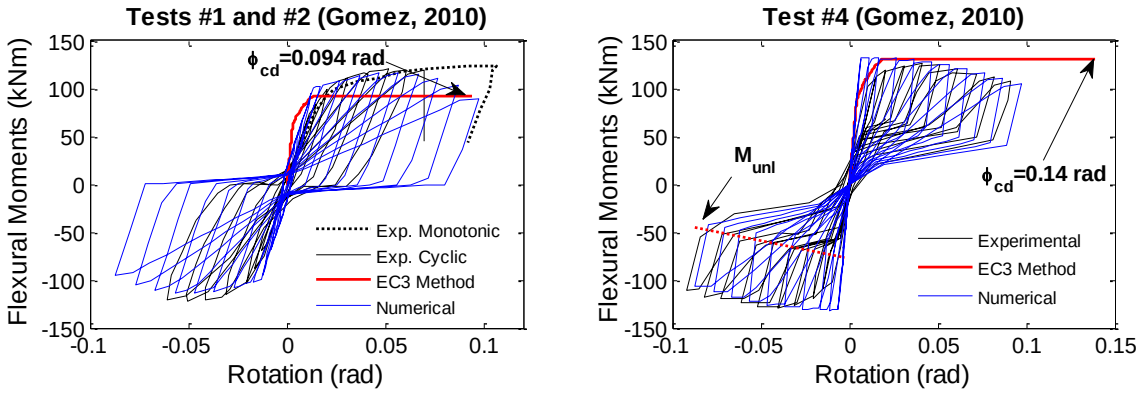

Figure 7.3 – Calibration of the Pinching4 material model based on experimental data provided by Gomez (2010).

Figure 7.1 (c) shows the semi-rigid base plate connection adopted in the SBPC building. On the basis of the information collected from the conducted survey on the most common industrial steel building design practices in Portugal (Chapter 9), a base plate with 25mm thickness and a high 1.7 times greater than height of the column cross-section was adopted. M22 anchor bolts of 8.8 class with a length of 500mm, concrete footing of C20/25 class, 60MPa grouting with 35mm thickness, a S275 steel grade and welds with 8mm were considered. The base plate connection was designed according to part 8 of Eurocode 3 (CEN, 2005c), being characterized by a type 1 mechanism and classified as semi-rigid. A flexural resistance of 226kNm, a rotational stiffness of 125940kNm and an ultimate rotation capacity of 0.22rad were obtained. With regard to the nominally pinned base plate connection adopted in the PBPC building (Figure 7.1 (d)), similar geometrical and material properties were considered, although in this case a base plate with height

equal to that of the column cross-section and M20 anchor bolts were used. This connection was also characterized by a type 1 mechanism. A flexural resistance of 171kNm, a rotational stiffness of 57083kNm and an ultimate rotation capacity of 0.18rad were obtained. Finally, a fixed support was adopted in the FBPC building.

7.6.2 Moment-resisting frame members

Column and girder members were modelled using the Ibarra et al. (2005) IMK model (Figure 7.1 (b)), so as to accurately capture strength and stiffness deterioration triggered by local instability phenomena (Macedo et al., 2015). The Ibarra et al. (2005) model parameters were derived for each specific European cross-section profile following the procedure proposed by Araújo et al. (2015), which consists on calibrating those parameters through the application of Harmony Search optimization algorithms to member responses previously obtained from advanced Finite Element analysis. The application of the procedure proposed by Araújo et al. (2015) requires the members to be conveniently laterally restrained. Although such restrained conditions are imposed by codes, it was found from the inspection of a number of industrial building design projects that those code requirements are sometimes neglected. Nevertheless, the present case study building was designed and assessed assuming the members to be fully laterally restrained. Additionally, the region of the girder with the haunch (Figure 7.1 (a)) was modelled to behave elastically with a corrected moment of inertial that simulates the variable height of the haunch, assumed to be cut from a profile with the same size of the girder. The restrained conditions imposed in the top of the column by the height of the haunch were modelled using a rigid elastic element.

7.6.3 Bracing system

Braces exhibit a complex behavior under earthquake loading conditions, being characterized by buckling in compression, yielding in tension, fracture and significant pinching when the deformation reverses (D'Aniello et al., 2013). To simulate such behavioral aspects, the brace component model was adopted following the recommendations provided by Karamanci and Lignos (2014). This steel brace model consists of two force-based fiber elements (Figure 7.1 (b)) that are offset with an initial camber of $L_s/700$ (Wijesundara et al., 2014), where L_s is the length of the brace, in the mid-length to trigger global buckling. Fracture resulting from low cycle fatigue is simulated using the fatigue material model available in OpenSees. The influence of the gusset plate

connection was equally accounted for by adopting the model proposed by Hsiao et al. (2012). This model consists of a zero-length rotational spring, simulates the out-of-plane rotational behaviour of the gusset plate connections and provides more accurate boundary conditions to braces. Different models were adopted in the lateral and roof brace gusset plate connections, as shown in Figure 7.1 (e) and (f), respectively. In order to determine the rotational stiffness and flexural strength of the zero-length nonlinear spring, the Whitmore width has to be defined assuming a 30º projection angle, as well as the L_{ave} length, which is the average of lengths L_1, L_2 and L_3 represented in Figure 7.1 (e) and (f). A 20mm plate thickness was considered. As expected due to the reduced Whitmore widths and plate thicknesses, low rotational stiffness values were obtained, equal to 60kNm and 84kNm in the lateral and roof brace connections, respectively. Rigid elements were used for the remainder of the gusset plate connection as shown in Figure 7.1 (b).

7.6.4 Structural responses

Before deriving the case study physical fragility and vulnerability functions, a prior pushover analysis was conducted with the aim of validating the structural models and providing a picture of the expected collapse mechanisms. Figure 7.4 presents the transverse collapse mechanisms of buildings FBPC and PBPC, being observed, as expected, that the stiffer building with rigid base plate connections attained a lower storey drift ratio (SDR) at collapse, around 4.1%, when compared to the more flexible building with nominally pinned base plate connections, which reached collapse at a SDR of around 6.3%. Also, whereas damage to the FBPC building was found to be mostly concentrated at the end of columns (i.e. loss of capacity of columns would trigger partial collapse of the building), damage to the PBPC building was concentrated at the top of columns and at the right node of the girder, next to the haunch (i.e. failure of girder would trigger collapse of the building roof). These collapse mechanisms were seen to be developed in the adjacent portal frames immediately after. In turn, in the longitudinal direction, the collapse mechanisms of the three buildings were governed by lateral braces. Similarly, based on the nonlinear time-history analysis conducted using the groups of records presented above, which have been selected and scaled for nine intensity measure levels (S_a (T_1, 5%) equal to 0.1g, 0.4g, 0.7g, 1.0g, 1.4g, 1.8g, 2.2g, 2.6g and 3.0g), mean and 5% - 95% confidence intervals of SDR values were obtained for each one of the DL, SD and NC limit sates. The limit states were assumed to be attained when 20% of the elements that govern the response of the building

in a certain direction of analysis were at that same limit state, in accordance with the criteria defined in Table 7.2. The EC8-3 limits were used in braces.

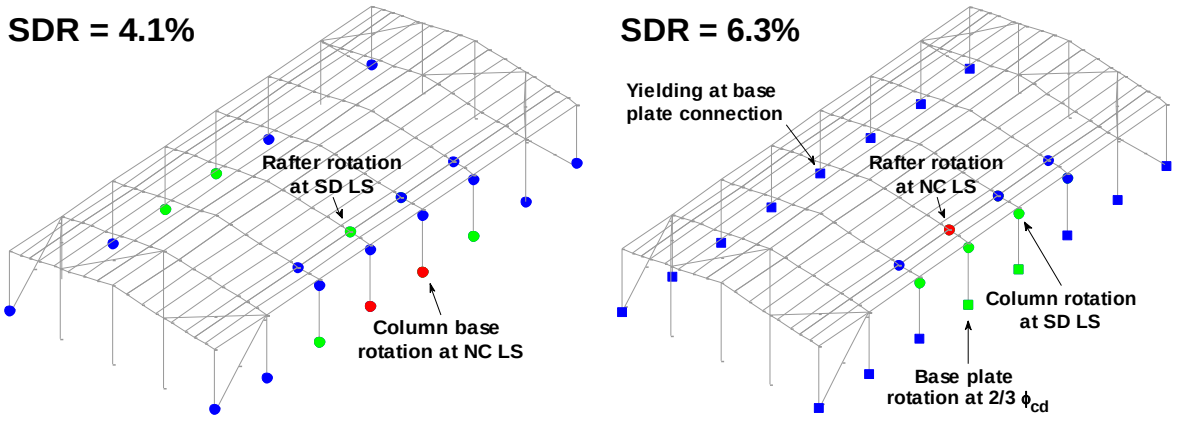

Figure 7.4 – Transverse collapse mechanisms of the building with fixed base plate connections, FBPC, (*right*) and the building with nominally pinned base plate connections, PBPC (*left*).

Figure 7.5 shows the correlation between SDR and the percentage of elements exceeding each limit state, being interesting to observe that despite the high intensity measure levels only one ground motion produced a member collapse and the building was found to be mostly responding in the DL limit state. These results are coherent with the general assumption that steel portal frames perform well under earthquake loading conditions.

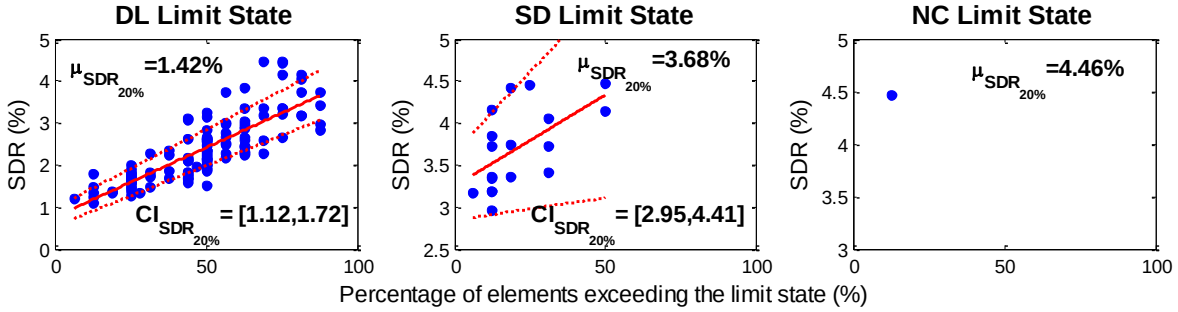

Figure 7.5 – Correlation between the storey drift ratio (SDR) and the percentage of members exceeding a certain limit state for building FBPC assessed in the *x*-direction.

Table 7.3 compiles the SDR values obtained for each building and the two main directions of analysis. Comparing the *x*-direction SDR values with the limits proposed by Hazus – MH MR5, it was seen that the latter provides more conservative drift limits at the DL and SD limit states, which vary from 0.51% to 0.8% and 1.28% to 2.40%, respectively, depending on the design code level, and similar drifts at the NC limit state, which vary from 3.50% to 7.00%. In the *y*-direction, the SDR values were found to be, somehow, in agreement with those proposed by Lignos and Karamanci (2013), particularly at the DL and SD limit states.

Table 7.3 – Mean and 5% - 95% confidence interval storey drift ratios (SDR) when 20% of elements exceed a certain limit state.

Model	GM direction	Damage Limitation (DL)		Significant Damage (SD)		Near Collapse (NC)	
		μ_{SDR} (%)	CI_{SDR} (%)	μ_{SDR} (%)	CI_{SDR} (%)	μ_{SDR} (%)	CI_{SDR} (%)
FBPC	*x*-dir.	1.42	[1.12; 1.72]	3.68	[2.95; 4.41]	4.46	-
	y-dir.	0.11	[0.05; 0.17]	0.75	[0.49; 1.01]	1.15	[0.74; 1.55]
SBPC	*x*-dir.	0.96	[0.69; 1.22]	5.28	[3.74; 6.82]	7.20	-
	y-dir.	0.17	[0.05; 0.39]	0.70	[0.46; 0.93]	1.01	[0.73; 1.29]
PBPC	*x*-dir.	1.14	[0.63; 1.66]	5.07	[4.03; 6.11]	7.31	-
	y-dir.	0.08	[0.07; 0.09]	1.14	[0.34; 0.95]	1.23	[0.76; 1.71]

7.7 Physical vulnerability functions

Physical vulnerability functions are defined by converting fragility functions (i.e. probability of exceeding a number of limit states for a set of intensity measure levels) through the employment of a consequence model (i.e. ratio between the repair and replacement costs for each damage state), thereby providing loss ratios for increasing intensity measure levels (Silva et al., 2015a; 2015b). Structural and nonstructural component fragility functions were derived herein by adopting a multiple stripes analysis following the recommendations provided by Baker (2015) and assuming, as previously referred, nine intensity measure levels. The obtained fragility and vulnerability (including contents) functions are presented below.

7.7.1 Structural components fragility functions

Figure 7.6 depicts the structural fragility functions obtained for the three buildings and ground motion directivities. In the transverse *x*-direction, the fragility of the buildings was seen to be simply governed by the moment resisting frame elements and by the permanent drifts criterion. The probabilities of failure were found to increase with the flexibility of the base plate connections. Whereas in the FBPC building low and practically none probabilities of failure were observed within the S_a (T_1,*x*) interval of 0 to 3g (e.g. median S_a (T_1,*x*) values of 0.7g and 2.8g were obtained at the DL and SD limit states, respectively), higher probabilities of failure were observed in the SBPC (Figure 7.6) and PBPC buildings (e.g. median S_a (T_1,*x*) values of 0.25g and 1.5g were obtained at the DL and SD limit states, respectively, of building PBPC), which were governed by damage to base plate connections and permanent drifts. In the skewed *xy*- and *yx*-directions and longitudinal *y*-direction, the fragility of all buildings was seen to be governed by damage to lateral braces, being the influence of permanent drifts more representative in the PBPC

building and the damage to moment resisting frame elements reduced from the *xy*-direction to practically none in the *y*-direction. In general, the *xy*-direction provided the most demanding responses and conservative fragility curves (e.g. median $S_a(T_{1,x})$ values of 0.2g and 0.8g were obtained at the DL and SD limit states, respectively, of building PBPC), so that one may conclude that it defines the most critical direction of analysis of this type of structures. Although few roof braces were seen to buckle and some damage to girders and columns occurred, the fragility of the buildings was basically controlled by lateral braces, permanent drifts and base plate connections. The latter equally played a key role in the dynamic responses of the buildings.

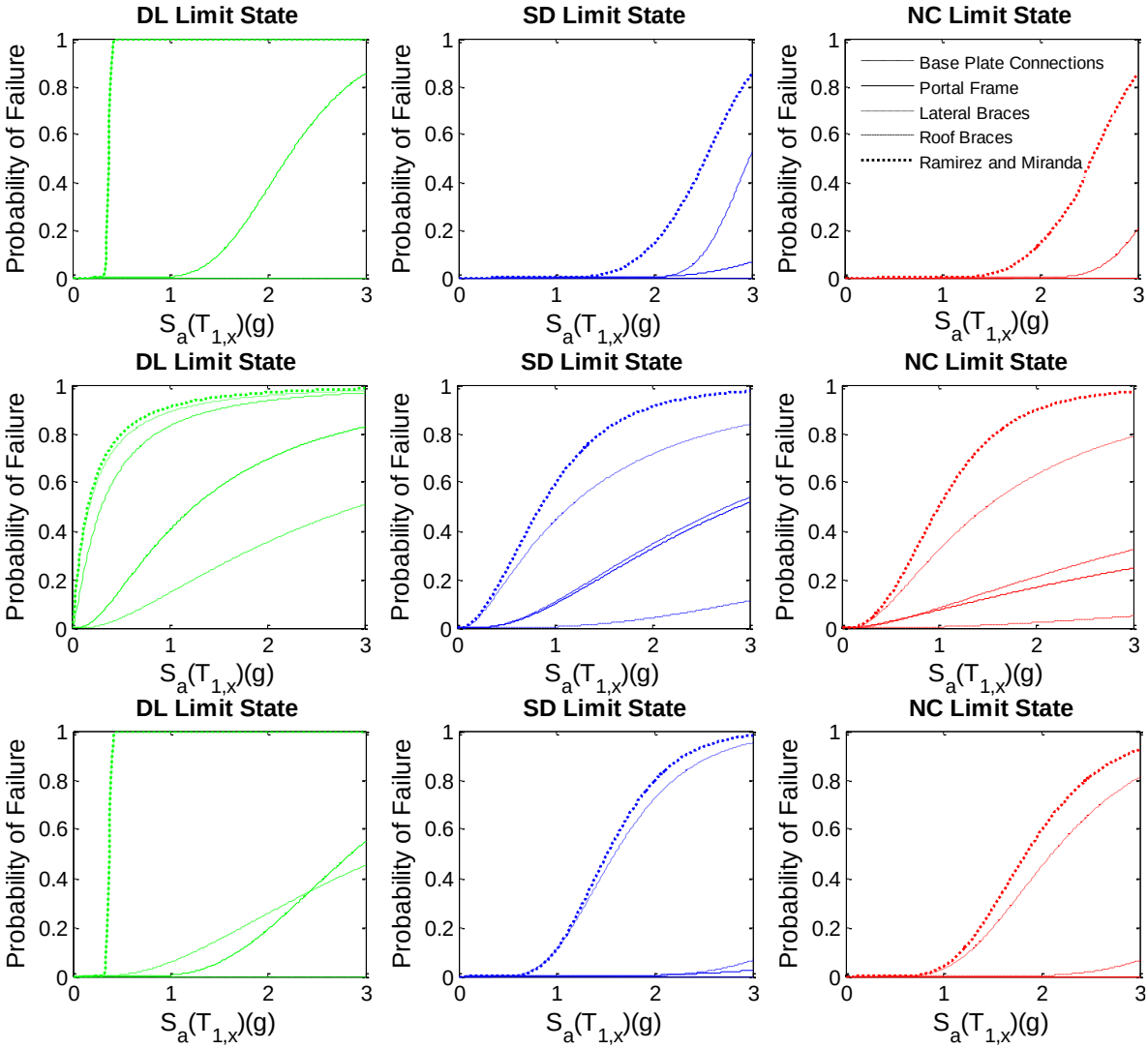

Figure 7.6 – Structural fragility functions for building SBPC in the *x*-direction of analysis (*top*), building PBPC in the *xy*-direction of analysis (*middle*), and building FBPC in the *y*-direction of analysis (*bottom*).

7.7.2 Non-structural components and contents fragility functions

Figure 7.7 shows the non-structural drift-sensitive and acceleration-sensitive/contents fragility functions. As it would be expected, it was observed that drift-sensitive non-structural components are more susceptible to damage in more flexible buildings (i.e. PBPC building) and ground motions striking in the *x*-direction (i.e. no damage to drift-sensitive non-structural components was observed at both SD and NC limit states in the *y*-direction). On the other hand, the acceleration-sensitive fragility functions were seen not to vary much with the support boundary conditions, in accordance with the buildings' dynamic characteristics, and to decrease, though slightly, from the *x*- to the *y*-directions of analysis, as expected since the buildings' periods of vibration are middling in the plateau region of the elastic spectrum.

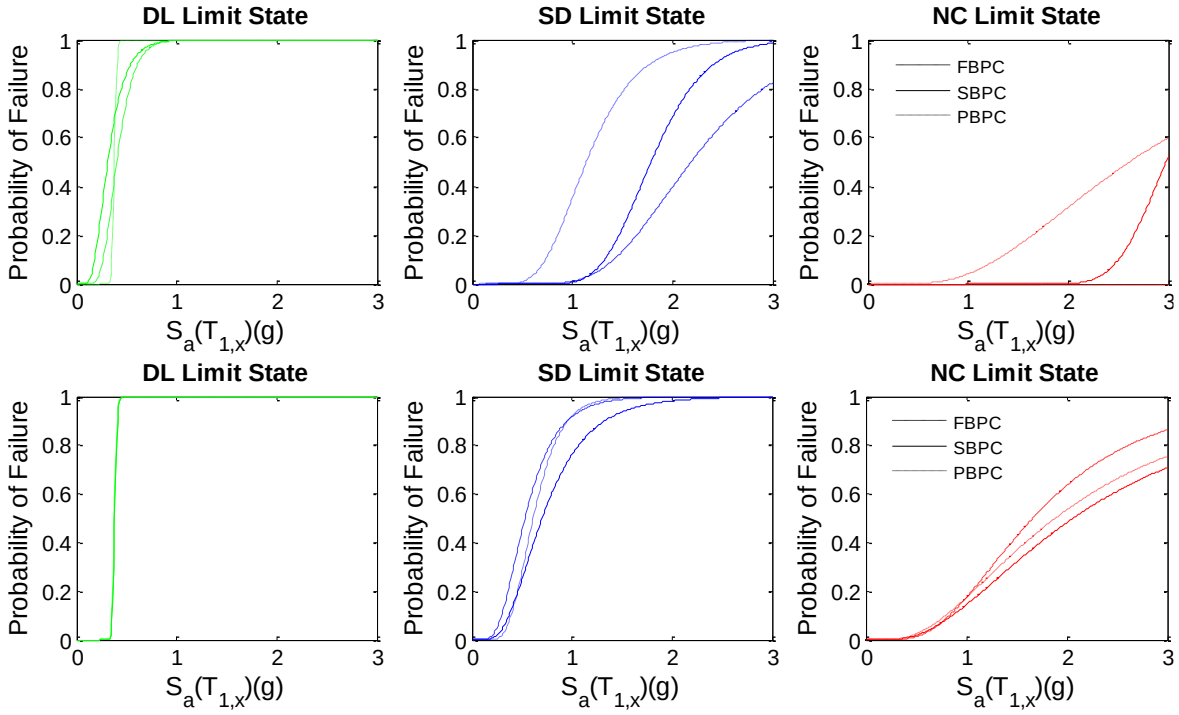

Figure 7.7 – Non-structural drift-sensitive (*top*) and acceleration-sensitive/contents (*bottom*) fragility functions for the transverse *x*-direction of analysis.

7.7.3 Structural and non-structural components and contents damage-to-loss consequence models

Consequence models defining the distribution of cost ratios for a set of damage states have already been proposed for RC industrial buildings for earthquake insurance pricing in Turkey (Eren and Luş, 2015). However, to the author's knowledge, specific consequence models for industrial steel buildings, that also distinguish damage to structural and non-

structural components and contents, have just been proposed within the Hazus – MH MR5 framework. Hence, this model will be adopted herein. Nevertheless, as discussed by Silva et al. (2015), the cost ratios for a given damage state may vary greatly. This uncertainty should be propagated to vulnerability models, as it may significantly affect loss estimates. In order to do so, a multivariate random generation of cost ratios was conducted using Copulas (Figure 7.8), by assuming that each damage state cost ratio follow a beta distribution (Silva et al., 2015) and that the ratios of each damage state are linearly correlated with a correlation coefficient of 0.8. The mean of the beta distributions was defined by the cost ratios proposed within the Hazus – MH MR5 framework and by coefficients of variation of 0.3, 0.2 and 0 for the DL, SD and NC limit sates, respectively, based on the work of Silva et al. (2015). Figure 7.8 depicts the cost ratios adopted for structural and non-structural components, which are defined in terms of the building replacement cost.

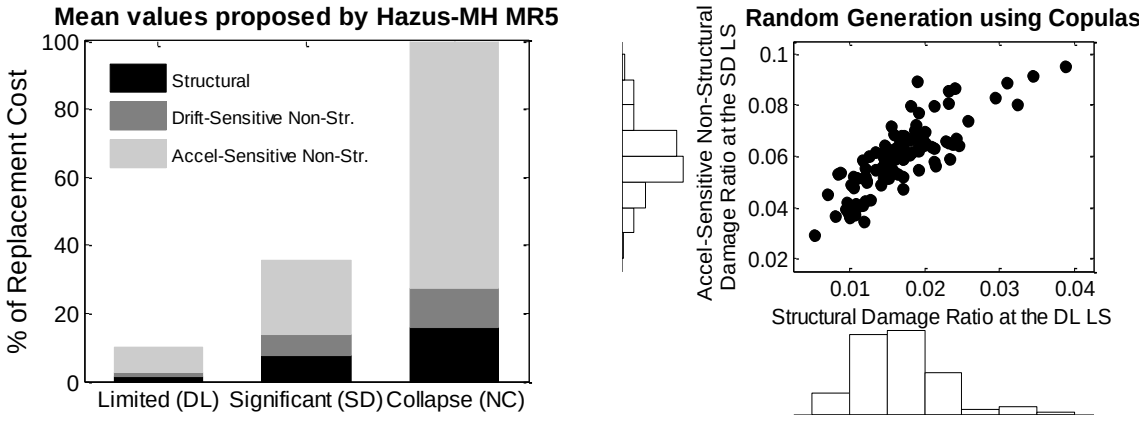

Figure 7.8 – Consequence model for structural and non-structural components.

In the case of contents, mean cost ratios of 5%, 25% and 50% were defined with respect to contents replacement cost for the DL, SD and NC limit states, respectively, according to Hazus – MH MR5 and assuming that significant salvage of contents will take place even at collapse. A multivariate random generation was equally carried out using Copulas, considering beta distributions with identical coefficients of variation for each damage state. Moreover, to facilitate the quantification of losses, the contents cost ratios were homogenized and converted into cost ratios defined in terms of the building replacement cost. This conversion is performed by Hazus – MH MR5 assuming the value of contents as 1.5 times the structure value. According to the same document, the structure cost represents 15.7% of the total building replacement cost. Still, this unique content-to-structure value ratio (*CSVR*) does not reflect the variability in the value of contents associated with different industrial activity types. Hence, the *CSVR* values collected by the

U.S. Army Corps of Engineers (USACE, 2006) for flood damage reduction studies on non-residential buildings with different industrial activities, defined in terms of the U.S. 3-digit Standard Industrial Codes (SIC), were adopted. These *CSVR* values (excluding business inventory) were converted to the 2-digit industrial activity classification of the Portuguese Standard Industrial Classification System (CAE). In industrial activities with no direct correspondence of *CSVRs*, values from similar CAE activities were adopted. Moreover, the USACE (2006) report not only defines *CSVRs* based on mean values, but also provides corresponding standard deviation values. According to this report, the *CSVRs* should follow a normal distribution. Table 7.4 presents the *CSVRs* mean and standard deviation values for each industrial activity of the 2-digit Portuguese CAE.

Table 7.4 – Normal probability distribution parameters for content-to-structure value ratios (*CSVRs*) defined based on the Portuguese 2-digit industrial activity classification (CAE).

Industrial Activity	Mean Value	Standard Deviation
Extractive Industries	7.2	1.0
Food Industry	0.4	0.4
Beverages Industry	0.4	0.4
Tabaco Industry	4.7	0.4
Textiles Manufacturing	4.7	0.4
Clothing Industry	4.7	0.3
Leather Industry	4.7	0.3
Wood and Cork Products	0.6	0.1
Pulp, Paper and Paper Products	2.1	1.1
Publishing, Printing and Reproduction of Recorded Media	2.1	0.5
Coke and Refined Petroleum Products	7.2	1.0
Chemical Products and Fibres	7.2	1.0
Pharmaceutical Products	7.2	1.0
Rubber and Plastic Products	1.4	0.3
Non-Metallic Mineral Products	1.6	0.2
Base Metallurgical Industry	2.3	0.3
Metal Products (Except Machinery and Equipment)	7.2	0.5
Communication, Electronic and Optical Equipment	5.1	0.2
Electric Equipment	0.9	0.3
Machinery and Equipment Manufacturing	0.9	0.3
Motor Vehicles Manufacturing	0.9	0.3
Other Transportation Equipment Manufacturing	0.9	0.3
Furniture and Mattresses Products	0.6	0.1
Other Manufacturing Industries	0.9	0.3
Repair, Maintenance and Installation of Machinery and Equipment	0.9	0.3
Retail	0.6	0.2
Transportation and Warehousing	0.6	0.2

7.7.4 Physical vulnerability functions

Figure 7.9 exhibits the structural and non-structural components vulnerability functions obtained for the main transverse and longitudinal *x*- and *y*-directions of analysis. Not only it may be observed that the acceleration-sensitive non-structural components represent the most significant part of total losses, but also that the losses to drift-sensitive non-structural components reduce from values similar to the structural components in the *x*-direction to practically zero in the *y*-direction.

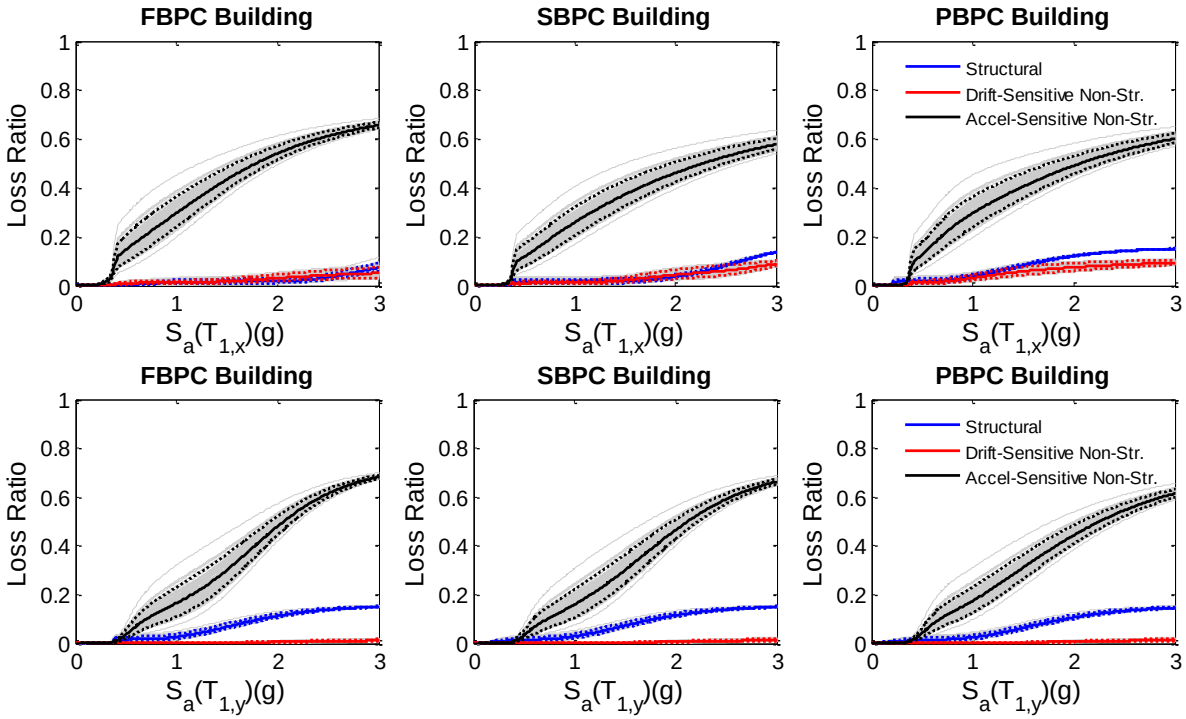

Figure 7.9 – Mean and 5%-95% confidence interval structural and non-structural components vulnerability functions for the two main transverse and longitudinal *x*- (*upper*) and *y*- (*lower*) directions of analysis.

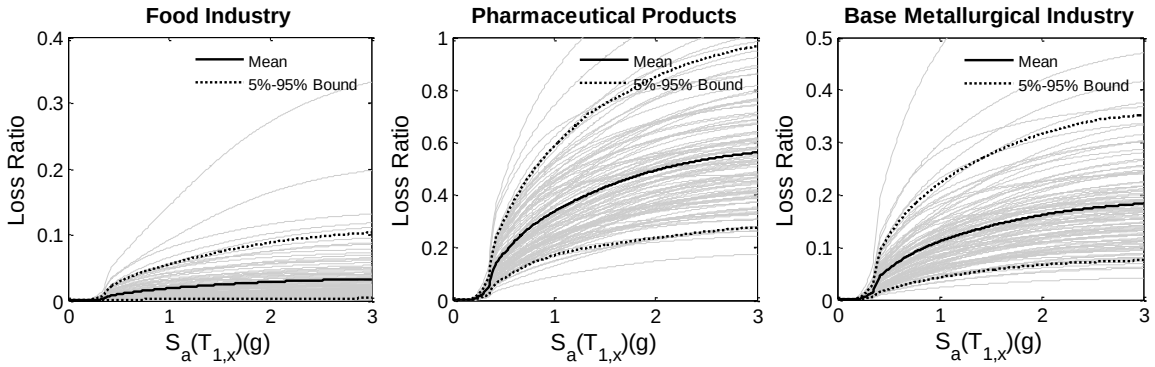

Figure 7.10 – Mean and 5%-95% confidence interval contents vulnerability functions for the FBPC building in the skewed *xy*-direction of analysis with different industrial CAE activities.

On the other hand, Figure 7.10 presents the contents vulnerability functions obtained for building FBPC, in the *xy*-direction, with different industrial CAE activities, i.e. food

industry, base metallurgical industry and pharmaceutical products manufacturing. As intended, these functions recognize that industrial sectors with a high capital demand (i.e. machinery and equipment and value of production equipment) might be hit harder by earthquakes than others.

7.8 Losses to property of typical industrial steel buildings located in Mainland Portugal

Losses to property are obtained by convoluting the vulnerability functions with the earthquake hazard, defined in this case study for an interval of time of 50 years, and by multiplying the result of that convolution with the respective building replacement cost (Silva et al., 2015b), in accordance with the consequence model (i.e. cost ratios) previously defined. Hence, replacement cost values for typical industrial steel buildings located in Mainland Portugal, as well as property losses in 50 years, are provided in the following.

7.8.1 Replacement cost values for Mainland Portugal

In order to propose building replacement costs for industrial steel buildings with transverse portal frames, the CYPE (2008) prices generator software module for Portugal was adopted. This module provides structural replacement costs, defined in €/m^2, for standard industrial steel buildings with different span lengths and spacing between portal frames, located in various regions of Portugal Mainland. The total building replacement costs were then determined assuming, as defined by Hazus-MH MR5, that the structural costs represent 15.7% of the total building cost. Figure 7.11 presents replacement cost maps obtained for two span length and portal frame spacing conditions.

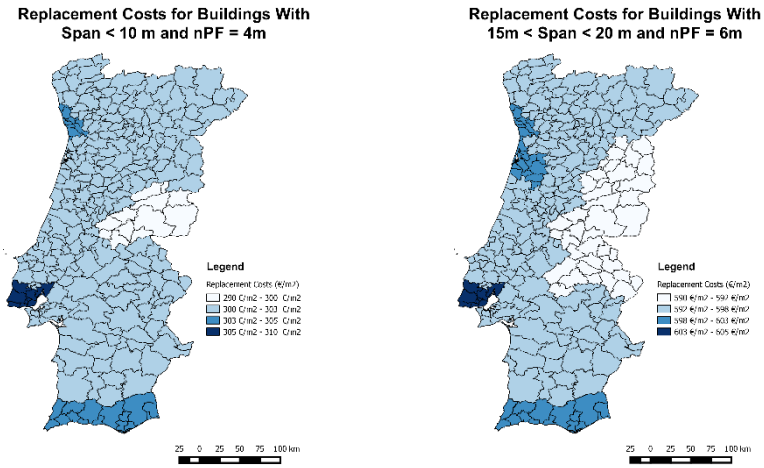

Figure 7.11 – Replacement costs for industrial steel buildings with different span lengths and portal frames spacing located in Portugal Mainland.

To assess the validity of the replacement cost maps derived (Figure 7.11), market values for the main cities of Lisbon and Oporto were taken from the Guide to Property Investment in Portugal (AICEP, 2014) and compared to those obtained. According to that market guide, industrial building construction costs may vary from 300€/m^2 to 450€/m^2 in warehouses and from 350€/m^2 to 600€/m^2 in factories. It may be thus concluded that the replacement costs derived (Figure 7.11) are in agreement with those provided by the real estate sector. Moreover, as noted in IGCN (2012), when national cost reference values are adopted to estimate building construction costs, the impact of economies of scale should be taken into account. The fundamental reason to include such effects is related to the fact that all construction processes involve fixed costs that are spread over the larger number of units as the construction volume increases. The use of specialized equipment and the learning curve effect may also contribute to such effect. Hence, the impact of economies of scale was equally accounted for in this study by assuming an exponential relationship, with an exponent of 0.9, between a size factor (i.e. ratio between the building size and a reference building size) and a cost multiplier that accounts for that effect (IGCN, 2012). A reference building size of 784.4 m^2 was defined based on the mean size (i.e. implementation area) of the buildings collected from the survey conducted by the authors (Chapter 9). Finally, a lognormal distribution was used to simulate the uncertainty in the replacement costs, adopting coefficients of variation of 0.28, 0.25 and 0.23 for the DL, SD and NC limit states, respectively, similar to those proposed by the FEMA P-58-1 framework (FEMA, 2012) for structural steel members.

7.8.2 Losses to property of typical industrial steel buildings

Loss estimations to property of industrial steel buildings provide useful metrics to support building owners and stakeholders in risk management decision-making (e.g. business relocation due to highly exposed assets, implementation of retrofitting measures or life-cycle costs analysis). Whereas insurance companies usually require the estimation of probable maximum losses (PML) to quantify insurance rates (Eren and Luş, 2015), other measures, such as the annual expected loss (AEL), the expected loss within a certain interval of time (e.g. lifetime of the building), the value at risk (VAR) or the tail value at risk (TVAR) (Yoshikawa and Goda, 2014), may be of interest to stakeholders and decision-makers. The average losses to property within the expected lifetime of the industrial steel building (50 years) were considered in this work. Figure 7.12 and Figure 7.13 depicts the mean and 5%-95% confidence interval structural and non-structural

components and contents losses obtained considering the industrial building to be located in the city of Lisbon.

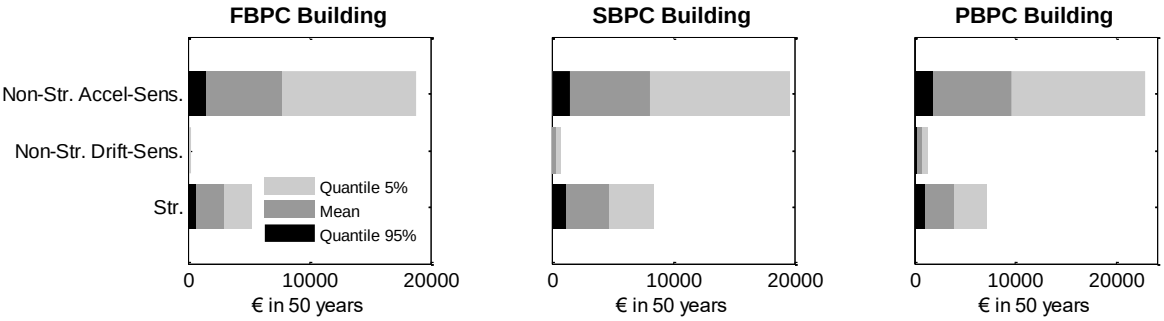

Figure 7.12 – Mean and 5%-95% confidence interval property losses in 50 years for buildings located in the city of Lisbon and considering the *xy*-direction of analysis.

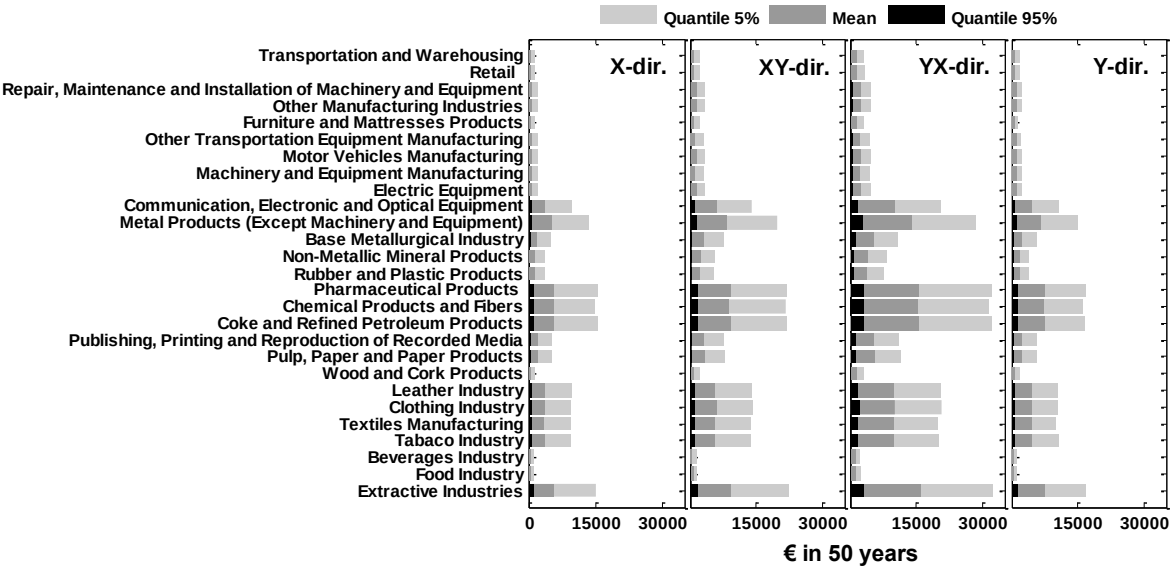

Figure 7.13 – Mean and 5%-95% confidence interval content losses in 50 years for the various ground motion directions of analysis and building FBPC located in the city of Lisbon.

Losses to structural and non-structural components, with a 95% probability of not being exceeded, in the order of 5.96% of the building replacement cost (i.e. the building mean replacement cost is 503900€) were obtained for the interval of time of 50 years, where 68% of the losses correspond to acceleration-sensitive non-structural components, 29% to structural components and only 3% to drift-sensitive non-structural components (Figure 7.12). These losses may increase to 12.30%, 10.0%, 8.10% or 6.90% of the building replacement cost when the losses to contents of chemical industries (e.g. chemical and pharmaceutical products manufacturing), communication and optical equipment manufacturing industries, textile and leather industries or beverages and food industries, respectively, are included. Hence, it may be concluded that, overall, the estimated property losses for a lifetime period of 50 years seem to be within acceptable limits and such level

of risk may be easily transferred by the building owner to private institutions, such as insurance companies. However, a remark should be made to the fact that direct and indirect losses to business production and inventories were not accounted for in this study. Moreover, although the losses to property were not seen to vary much with the column base support conditions in the *x*-, *xy*- and *y*-directions of analysis, differences of 50% were observed between buildings FBPC and PBCP in the *yx*-direction of analysis. The stiffer FBPC building was seen to exhibit higher acceleration-sensitive non-structural components and contents losses, as it may be observed from the inspection of Figure 7.13. Likewise, variations of 60% and 35% in property losses were observed for the *x*- and *y*-directions of analysis, respectively, with respect to those obtained in the *xy*-direction of analysis considering the SBPC building. It may be thus concluded that both the industrial building support conditions and the ground motion directivity play a critical role in loss estimates, in such a way that their disregard may significantly underestimate property losses.

With respect to the estimation of the average losses to property of a building located in any region of mainland Portugal, it may be observed from Figure 7.14 that the higher mean property losses in 50 years are expected to occur in the region of Lisbon and the Tagus Valley, which vary from 3.5% to 4% of the building replacement cost.

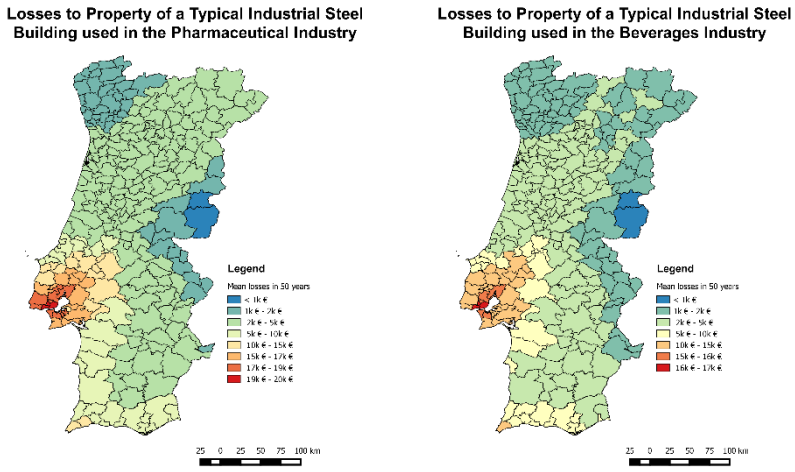

Figure 7.14 – Maps of mean losses to property in 50 years of FBPC buildings used in different industrial activities (pharmaceutical and beverages) assessed in the *xy*-direction of analysis.

This distribution of potential losses to the industrial building stock should be of great concern due to the fact that the region of Lisbon and the Tagus Valley represents a rather dynamic industrial hub in Europe and is one of the most important in Portugal, hosting essential metallurgic, machinery, chemical, electronics, food and beverages, automobile assembly, wood pulp and cork industries. This region, together with the Porto-Aveiro-Braga industrial region in the northwest of mainland Portugal, account for approximately

three-fourths of the counties' net industrial output. Lower mean property losses in 50 years, varying from 0.4% to 1% of the building replacement cost, were obtained at the latter region. Finally, a reference should be made to the coastal Sines industrial hub, located about 140 kilometers south of Lisbon, which comprises a major deep-water port and a heavy industrial complex (oil refinery and petrochemical industry), where mean property losses in 50 years of 2% of the building replacement cost were obtained.

7.9 Conclusions

This work has examined the losses to property of an industrial steel building with typical dimensions and geometrical characteristics of a building located in Portugal. Novel physical fragility and vulnerability functions were proposed, accounting not only for structural components, but also for non-structural components and contents. A comprehensive 3-dimensional structural model was developed to accurately capture the main failure modes identified in a brief review of the most common types of damage observed in past post-earthquake reconnaissance campaigns and to allow monitoring pre-established structural damage states criteria. The influence of different column base plate connections and the ground motion directivity was equally considered, which were found to play a critical role in loss estimates, in such a way that their disregard may underestimate property losses up to 60%. Contents vulnerability functions specific of the industrial activity of a certain industrial building were proposed, recognizing that industrial sectors with a high capital demand might be hit harder by earthquakes than others, as well as industrial steel building replacement cost maps for mainland Portugal that are coherent with values provided by the real estate market.

The results obtained herein suggest that industrial steel buildings located near the Portuguese capital, in Lisbon and Tagus Valley region, which is the economic heart of Portugal, are expected to suffer structural and non-structural losses in 50 years of 5.96% of the building replacement cost with a 95% probability of not being exceeded. These losses may increase up to 12.30% of the building replacement cost when losses to contents are included. Despite the fact that such level of losses to individual industrial buildings seem to be within acceptable and transferable limits, the highly exposed industrial assets, particularly those located in the Lisbon and Tagus Valley region, point out for the need of further studies focused on the estimation of industrial losses at a national scale for Portugal.

7.10 Acknowledgments

This work has been performed within the framework of the research project PTDC/ECM-EST/3062/2012 'Earthquake loss of the Portuguese building stock' founded by the Foundation of Science and Technology (FCT) of Portugal. The Authors are also grateful for all support provided by Dr. Luís Sousa from the University of Porto.

7.11 References

Adalier K, Aydingun, O (2001) Structural engineering aspects of the June 27, 1998 Adana-Ceyhan (Turkey) earthquake, Engineering Structures, 23, 343-355.

AICEP (2014) Guide to property investment in Portugal, Report prepared for the Portuguese Agency for Investment and External Commerce (AICEP) by Curshman & Wakefield and Uría Menendez – Proença de Carvalho, Lisbon, Portugal.

Araújo M, Macedo L, Castro JM (2015) Calibration of strength and stiffness deterioration hysteretic models using optimization algorithms, In Proceedings, 8th International Conference on Behaviour of Steel Structures in Seismic Areas STESSA, Shanghai, China.

Arslan MH, Korkmaz HH, Gulay FG (2006) Damage and failure pattern of prefabricated structures after major earthquakes in Turkey and shortfalls of the Turkish Earthquake code, Engineering Failure Analysis, 13, 537–557.

Aviram A, Stojadinovic B, Der Kiureghian A (2008) Reliability of exposed column-base plate connection in special moment-resisting frames, In Proceedings, 14th World Conference on Earthquake Engineering, Beijing, China.

Baker JW (2015) Efficient analytical fragility function fitting using dynamic structural analysis, Earthquake Spectra, 31, 570-599.

Beyer K, Bommer JJ (2007) Selection and scaling of real accelerograms for bi-directional loading: a review of current practice and code provisions, Journal of Earthquake Engineering, 11, 13-45.

Bojórquez E, Ruiz-García J (2013) Residual drift demands in moment-resisting steel frames subjected to narrow-band earthquake ground motions, Earthquake Engineering and Structural Dynamics, 42, 1583-1598.

Bournas DA, Negro P, Taucer FF (2014) Performance of industrial buildings during the Emilia earthquake in Northern Italy and recommendations for their strengthening, Bulletin of Earthquake Engineering, 12, 2383-2404.

Bradley BA (2010) A generalized conditional intensity measure approach and holistic ground motion selection, Earthquake Engineering and Structural Dynamics, 39, 1321-1342.

Burneau M, Anagnostopoulou M, MacRae G, Clifton C, Fussell A (2010). Preliminary report on steel building damage from the Darfield earthquake of September 4, 2010, Bulletin of the New Zealand Society for Earthquake Engineering, 43, 351-369.

Casotto C, Silva V, Crowley H, Nascimbene R, Pinho R (2015). Seismic fragility of Italian RC precast industrial structures, Engineering Structures, 94, 122-136.

CEN (2005a) ENV 1998-3 Eurocode 8: design of structures for earthquake resistance – Part 3: assessment and retrofitting of buildings, European Committee for Standardization, Brussels, Belgium.

CEN (2005b) NP ENV 1993-1-1 Eurocode 3: design of steel structures – Part 1-1: general rules and rules for buildings, European Committee for Standardization, Brussels, Belgium.

CEN (2005c) NP ENV 1993-1-8 Eurocode 3: design of steel structures – Part 1-8: design of joints, European Committee for Standardization, Brussels, Belgium.

Clifton C, Bruneau M, MacRae G (2011) Steel structures damage from the Christchurch earthquake series of 2010 and 2011, Bulletin of the New Zealand Society for Earthquake Engineering, 44, 297-318.

CYPE (2008) Prices generator software for Portugal, CYPE Ingenieros, S.A., Alicante, Spain.

D'Aniello M, La Manna Ambrosino G, Portioli F, Landolfo R (2013) Modelling aspects of the seismic response of steel concentric braced frames, Steel and Composite Structures, 15, 539-566.

Dierlein G, Victorsson V (2008) Fragility curves for components of steel SMF systems, Background document for FEMA P-58/DB-3.8.3, Federal Emergency Management Agency, Washington, D.C.

Dowrick DJ, Rhoades DA (1993) Damage costs for commercial and industrial property as a function of intensity in the 1987 Edgecumbe Earthquake, Earthquake Engineering and Structural Dynamics, 22, 869-884.

Dowrick DJ, Rhoades DA (1995) Damage ratios for plant, equipment and stock in the 1987 Edgecumbe, New Zealand Earthquake, Bulletin of the New Zealand National Society for Earthquake Engineering, 28, 65-278.

Durukal E, Erdik M (2008) Physical and economic losses sustained by the industry in the 1999 Kocaeli, Turkey earthquake, Natural Hazards, 46, 153-178.

Durukal E, Erdik M, Uçkan E (2008) Earthquake risk to industry in Istanbul and its management, Natural Hazards, 44, 199-212.

EPRI (1991) The October 17, 1989, Loma Prieta earthquake: Effects on selected power and industrial facilities, Report prepared by EQE Engineering, Inc. for the Electric Power Research Institute, California.

Eren C, Luş H (2015) A risk based PML estimation method for single-storey reinforced concrete industrial building and its impact on earthquake insurance rates, Bulletin of Earthquake Engineering, 13, 2169-2195.

FEMA (2010) Multi-hazard loss estimation methodology. Earthquake Model. HAZUS – MH MR5 Technical Manual, Federal Emergency Management Agency, Mitigation Division, Washington, D. C.

FEMA (2012) FEMA P-58-1 Seismic performance assessment of buildings. Volume 1 – Methodology, Federal Emergency Management Agency, Mitigation Division, Washington, D. C.

Filiatrault A, Sullivan T (2014) Performance-based seismic design of non-structural building components: The next frontier of earthquake engineering, Earthquake Engineering and Engineering Vibration, 13, 17-46.

Gomez IR (2010) Behavior and design of column base connections, PhD thesis, University of California, Davis, CA.

Grimaz S (2014) Can earthquakes trigger serious industrial accidents in Italy? Some considerations following the experiences of 2009 L'Aquila (Italy) and 2012 Emilia (Italy) earthquakes, Bullettino di Geofisica Teorica ed Applicata. 55, 227-237.

Herrera RA, Beltran JF, Aguirre C, Verdugo A (2012) Seismic performance of steel structures during the 2010 Maule earthquake, In Proceedings, 7th International Conference on Behavior of Steel Structures in Seismic Areas STESSA, Santiago, Chile.

Hsiao PC, Lehman DE, Roeder CW (2012) Improved analytical model for special concentrically braced frames, Journal of Constructional Steel Research, 73, 80-94.

Hutchinson TC, Chaudhuri SR (2006) Simplified expression for seismic fragility estimation of sliding-dominated equipment and contents, Earthquake Spectra, 22, 709-732.

Ibarra LF, Medina RA, Krawinkler H (2005) Hysteretic models that incorporate strength and stiffness deterioration, Earthquake Engineering and Structural Dynamics, 35, 1489-1511.

IGCN (2012) 2012 Residential and commercial cost tables: overview of methodology, Indiana Government Center North, Department of Local Government Finance of the State of Indiana, Indianapolis, Indiana.

Iwata Y, Sugimoto H, Kuguamura H (2006) Reparability limit of steel structural buildings based on the actual data of the Hyogoken-Nanbu earthquake, In Proceedings, 38th Joint Panel Meeting, Wind and Seismic effects, NIST Special Publication, Washington, D.C.

Karamanci E, Lignos DG (2014) Computational approach for collapse assessment of concentrically braced frames in seismic regions, Journal of Structural Engineering, 140, in press.

Koyama T, Iyama J, Yamada S, Matsumoto Y, Kishiki S, Shimada Y, Asada H, Ikenaga M (2012) Damage to steel educational facilities in the 2011 East Japan earthquake: Part 2 Damage to minor structural components and damage due to the tsunami, In Proceedings, 15th World Conference on Earthquake Engineering, Lisbon, Portugal.

Koyama T, Iyama J, Yamada S, Matsumoto Y, Kishiki S, Shimada Y, Asada H, Ikenaga M (2012) Damage to steel educational facilities in the 2011 East Japan earthquake: Part 1 Outline of the reconnaissance and damage to major structural components, In Proceedings, 15th World Conference on Earthquake Engineering, Lisbon, Portugal.

Krausmann E, Cruz AM, Affeltranger B (2010) The impact of the 12 May 2008 Wenchuan earthquake on industrial facilities, Journal of Loss Prevention in the Process Industries, 23, 242-248.

Kurita T, Annaka T, Fukushima S (2004) Seismic risk estimation for principal cities in Turkey, In Proceedings, 13th World Conference on Earthquake Engineering, Vancouver, Canada.

Latour M, Piluso V, Rizzano G (2014) Rotational behavior of column base plate connections: experimental analysis and modelling, Engineering Structures, 68, 14-23.

Latour M, Rizzano G (2013) A theoretical model for predicting the rotational capacity of steel base joints, Journal of Constructional Steel Research, 91, 89-99.

Latour M, Rizzano G (2015) Cyclic behaviour of exposed column base joints: experimental analysis and mechanical modelling, In Proceedings, 8th International Conference on Behaviour of Steel Structures in Seismic Areas STESSA, Shanghai, China.

Lehman DE, Roeder CW, Herman D, Johnson S, Kotulka B (2008) Improved seismic performance of gusset plate connections, Journal of Structural Engineering, 134, 890-901.

Liberatore I, Sorrentino L, Liberatore D, Decaini LD (2013) Failure of industrial structures induced by the Emilia (Italy) 2012 earthquakes, Engineering Failure Analysis, 35, 629-647.

Lignos DG, Karamanci E (2013) Drift-based and dual-parameter fragility curves for concentrically braced frames in seismic regions, Journal of Constructional Steel Research, 90, 209-220.

Macedo L, Araújo M, Castro JM (2015) Comparison of modelling strategies for steel structures under cyclic loads, In Proceedings, 8th International Conference on Behaviour of Steel Structures in Seismic Areas STESSA, Shanghai, China.

Magliulo G, Ecolino M, Petrone C, Coppola C, Manfredi G (2014) Emilia earthquake: the seismic performance of precast RC buildings, Earthquake Spectra, 30, 891-912.

Magliulo G, Ercolino M, Manfredi G (2015) Influence of cladding panels on the first period of one-story precast buildings, Bulletin of Earthquake Engineering, 13, 1531-1555.

Marques M, Macedo L, Araújo M, Martins L, Castro JM, Sousa L, Silva V, Delgado R (2014) Influence of record selection procedures on seismic loss estimates, In Proceedings, Vulnerability, Uncertainty and Risk. doi: 10.1061/9780784413609.176.

Midorikawa M, Nishiyama I, Tada M, Terada T (2012) Earthquake and tsunami damage on steel buildings caused by the 2011 Tohoku Japan earthquake, In Proceedings, International Symposium on Engineering Lessons Learned from the 2011 Great East Japan Earthquake, Tokyo, Japan.

Myers AT, Kanvinde AM, Deielein, GG, Fell BV (2009) Effect of weld details on the ductility of steel column baseplate connections, Journal of Constructional Steel Research, 65, 1366-1373.

Nakashima M, Lavan O, Kurata M, Luo Y (2014) Earthquakes engineering research needs in light of lessons learned from the 2011 Tohoku earthquake, Earthquake Engineering and Engineering Vibration, 13, 141-149.

Nishiyama I, Okawa I, Fukuyama H, Okuda Y (2012) Building damage by the 2011 off the Pacific coast of Tohoku earthquake and coping activities by NILIM and BRI collaborated with the administration, In Proceedings, International Symposium on Engineering Lessons Learned from the 2011 Great East Japan Earthquake, Tokyo, Japan.

Ozakgul K, Caglayan O, Tezer O (2011) Investigation of buckled brace system of an existing industrial building, Engineering Failure Analysis, 18, 455-463.

Pagani M, Monelli D, Weatherill G, Danciu L, Crowley H, Silva V, Henshaw P, Butler L, Nastasi M, Panzeri L, Simionato M, Vigano D (2014) OpenQuake-engine: an open hazard (and risk) software for the global earthquake mode, Seismological Research Letters, 85, 692-702.

PEER (2011) OpenSees: open system for earthquake engineering simulation, Pacific Earthquake Engineering Research Center, University of California, Berkeley, CA.

Petruzelli F, Della Corte G, Ievolino I (2012a) Seismic risk assessment of an industrial steel building. Part 1: Modelling and analysis, In Proceedings, 15th World Conference on Earthquake Engineering, Lisbon, Portugal.

Petruzelli F, Della Corte G, Ievolino I (2012b) Seismic risk assessment of an industrial steel building. Part 2: Fragility and failure probabilities, In Proceedings, 15th World Conference on Earthquake Engineering, Lisbon, Portugal.

Phipps MT, Jirsa JO, Picado M, Karp R (1992) Performance of high technology industries in the Loma Prieta earthquake, In Proceedings, 10th World Conference on Earthquake Engineering, Balkema, Rotterdam.

Porter K, Johnson G, Sheppard R, Bachman R (2010) Fragility of mechanical, electrical and plumbing equipment, Earthquake Spectra, 26, 451-472.

Rahnama M, Morrow G (2000) Performance of industrial facilities in the August 17, 199 Izmit Earthquake, In Proceedings, 12th World Conference on Earthquake Engineering, Auckland, New Zealand.

Ramirez, MC, Miranda E (2012) Significance of residual drifts in building earthquake loss estimation, Earthquake Engineering and Structural Dynamics, 41, 1477-1493.

REAE (1986) Regulamento de estruturas de aço para edifícios, Decreto-Lei nº 211/86, Lisbon, Portugal.

RFCS (2013) Prefabricated steel structures for low-rise buildings in seismic areas, Research Found for Coal and Steel, European Commission, Brussels, Belgium.

RMS (2011) The 2010 Maule, Chile earthquake, Lessons and future challenges. Risk Management Solutions, Inc.

RSA (1983) Regulamento de segurança e acções para estruturas de edifícios e pontes, Decreto-Lei nº 235/83, Lisbon, Portugal.

Salzano E, Agreda AG, Di Carluccio A, Fabbrocino G (2009) Risk assessment and early warning systems for industrial facilities in seismic zones, Reliability Engineering and System Safety, 94, 1577–1584.

Shrestha K, Franquet J, Rogers CA, Tremblay R (2009) OpenSees modeling of the inelastic seismic response of steel roof diaphragms, Proceedings, 6th International Conference on Behavior of Steel Structures in Seismic Areas STESSA, Philadelphia, Pennsylvania.

Silva V, Crowley H, Varum H, Pinho R (2015b) Seismic risk assessment for mainland Portugal, Bulletin of Earthquake Engineering, 13, 429-457.

Silva V, Crowley H, Varum H, Pinho R, Sousa L (2015ª) Investigation of the characteristics of Portuguese regular moment-frame RC buildings and development of a vulnerability model, Bulletin of Earthquake Engineering, 13, 1455-1490.

Silva V, Marques M, Castro JM, Varum H (2015) Development and application of a real-time loss estimation framework for Portugal, Bulletin of Earthquake Engineering, 13, 2493-2516.

Takamatsu T, Tamai H (2005) Non-slip-type restoring force characteristics of an exposed-type column base, Journal of Constructional Steel Research, 61, 942-961.

Tierney KJ (1997) Business impacts of the Northridge Earthquake, Journal of Contingencies and Crisis Management, 5, 87-97.

Tremblay R, Mitchell D, Tinawi R (2013) Damage to industrial structures due to the 27 February 2010 Chile earthquake, Canadian Journal of Civil Engineering, 40, 735-749.

USACE (2006) Depth-damage relationships for structures, contents and vehicles and content-to-structure value ratios (CSVR) in support of the Donaldsonville to the Gulf, Louisiana, feasibility study, Report prepared for the U.S. Army Corps of Engineers, New Orleans, Louisiana.

Wenk T, Lacave C, Peter K (1998) The Adana-Ceyhan Earthquake of June 27, 1998, Report on the Reconnaissance Mission from July 6-12, 1998, Swiss Society of Earthquake Engineering and Structural Dynamics.

Wijesundara KK, Nascimbene R, Rassati GA (2014) Modeling of different bracing configurations in multi-storey concentrically braced frames using a fiber-beam based approach, Journal of Constructional Steel Research, 101, 426-436.

Yoshikawa H, Goda K (2014) Financial seismic risk analysis of building portfolios, Natural Hazards Review, 15, 112-120.

Chapter 8

Seismic losses to property and business activity of industrial buildings – Business activity losses

Araújo M, Castro JM, Marques M (2019) Seismic losses to property and business activity of industrial buildings. Part 2: business activity losses, *Earthquake Spectra* (submission).

8.1 Summary

Earthquakes may imply substantial losses to capital, production or revenues of firms located in seismic-prone regions, or even to those located in unaffected regions due to ripple effects. Despite the evident socio-economic relevance of this issue, works focusing on the microeconomic behaviour of firms to natural disaster are lacking on the literature. Hence, this Chapter aims at the estimation of stock, relocation and production losses due to business interruption, including indirect effects resultant from input factor, infrastructures and supply chain disruptions, to industrial buildings located in seismic prone regions. Losses to industrial buildings located in mainland Portugal were seen to reach, with 95% confidence, 41.7% of the building replacement cost in 50 years in the most vulnerable industrial sectors, warning for the potential risks to which some industrial activities located the region of Lisbon and Tagus Valley may be exposed to.

8.2 Introduction

Natural disasters (e.g. earthquakes, floods, hurricanes) may have severe economic impacts on industrial facilities. Such impacts vary with the type of natural hazard and industrial activity and are commonly distinguished between direct and indirect impacts to property and production (Rose, 2009; Merz et al., 2013; Khazai et al., 2013). Whereas impacts to property mostly comprise damage to structural and non-structural components

and contents (Chapter 7), production impacts are mainly caused by the length of production downtime, i.e. business interruption, which result from direct property damage and indirect supply chain disruptions and outages in critical infrastructures (FEMA, 1991; Rose and Lim, 2002; Li et al., 2013). Business interruptions may even propagate, in a cascade sort of way, to firms that have not been directly affected by the natural disaster due to the complex integration of businesses within globally interlaced supply networks (Merz et al., 2007). Concomitantly, cascading effects can affect property, e.g. ancillary fires or hazardous material releases, and result in highly devastating, though rare, technological accidents triggered by natural disasters, the so-called Natechs (Cruz and Steinberg, 2005; Cruz and Okada, 2008). Other indirect impacts can result from reduced investments or subsequent charging on costs of remediation measures and negative market effects, e.g. general rise of material prices, competitive disadvantages over non-affected competitors and overall damage to the company's reputation (Merz et al., 2007; Hiete and Merz, 2009). In some industrial sectors, indirect impacts can overcome direct impacts several-fold, in the order of 3 to 10 times (Kleindorfer and Saad, 2005).

Disaster impacts to production, i.e. business interruption, may, in contrast, be positively reduced by the ability of businesses to recover from the natural event, i.e. economic resilience, namely the ability to conserve or substitute away from inputs in short supply, technological change, business relocation or production recapturing (Rose, 2007; Rose, 2009; Park et al., 2011). Promoting a preparedness culture in firms is key to foster economic resilience (UNDP, 2013; Xiao and Peacock, 2014), as well as the access to (re)insurance payments (Swiss Re, 2004; De Mel et al., 2011; GRF, 2014).

In Chapter 7 it was demonstrated that direct seismic losses to property of a typical industrial building located in mainland Portugal may reach, with 95% confidence, up to 12.30% of the building replacement cost in 50 years. Although such property losses are within acceptable and transferable limits, they can expand to unbearable values if production losses are equally accounted for. Studies focused on the microeconomic-individual behaviour of industrial businesses (Rose, 2009) to earthquakes seem to be lacking on the literature, despite is recognized importance and high vulnerability observed in previous events, as in the 1994 Northridge or the 1999 Kocaeli earthquakes (Rose et al.. 1997; Dahlhamer and Tierney, 1998; Durukal et al., 2008). Therefore, this Chapter aims at the estimation of seismic business losses, i.e. direct and indirect business losses, associated to an industrial steel building located in mainland Portugal, as well as at the derivation of industrial business vulnerability, or loss, functions. The industrial steel building developed

in Chapter 7 is employed herein and every industrial activity of the 2-digit Portuguese Standard Industrial Classification System (CAE) considered. Moreover, the Hazus – MH MR5 framework (FEMA, 2010) is followed and specific amendments accounting for the Portuguese industrial context, particularly regarding the definition of the industrial assets at risk, is conducted.

8.3 Business activity loss modelling and case study

Losses to business activity caused by earthquakes are quite complex to model and are affected by a number of variables that are oftentimes difficult to measure and to account for. Whilst direct business losses are relatively simpler to model, as they are function of the physical damage to the built environment, indirect business losses are more complicated to evaluate, and are mainly caused by business interruptions resultant from the disruption of input factors, lifelines and supply chains (Dorra et al., 2013; Merz et al., 2013). Hence, due to the complexity on modelling business activity losses to earthquakes, the study presented herein relies on the more general framework proposed by Hazus – MH MR5 (FEMA, 2010), which is extended to the Portuguese industrial context. Nevertheless, before giving an overview on the Hazus – MH MR5 framework, a brief review of previous post-event losses to business activity is conduct with the aim of clarifying the various sources of loss at stake.

8.3.1 Brief review of post-event losses to business activity

Table 8.1 compiles the review of business activity losses and factors influencing business interruption observed in past earthquake events. In general, the speed of reopening was seen to be key in business recovery, which mostly depended on repair and clean up works, access to capital, i.e. negotiation with loaners or insurance companies, and preparedness measures (Chang and Falit-Baiamonte, 2002). The cordoning of the Christchurch's Central Business District was a good example of the latter, which forced businesses to relocated, even those that remained undamaged, and caused more losses in businesses that were least prepared (Chang et al., 2014). The speed of reopening also varied with the business characteristics, e.g. size, age, financial condition or number of employees (Tierney, 1997; Rose et al., 1997), particularly accessing capital, and the construction capacity of the region, e.g. the engagement of most construction workers at the Ceyhan Industrial Park was most likely the reason why no reconstruction works were elapsing at the residential district (Wenk et al., 1998). Business relocation was carried out

by a number of business to allow resuming production (Sapountzaki, 2005; Chang et al., 2014). Nevertheless, despite the speed of reopening, a number of businesses was still not able to resume production due to disruptions in electricity and water services, transportation infrastructures and supply chains, e.g. the Renesas Electronics Corporation's Naka plant failure, which held 40% of the world's share of microcontrollers used for automobiles, had an significant economic impact on the worldwide automobile production (Carvalho et al., 2014).

Table 8.1 – Business activity losses and factors influencing business interruption observed in previous earthquake events.

Earthquakes	Business Losses and Factors Influencing Business Interruption	References
1989 Loma Prieta, 1994 Northridge and 2001 Nisqually earthquakes	• Largest losses were reported after the Northridge earthquake by manufacturing and construction firms. Property losses were confined to building contents, inventory and leasehold improvements, as 75% of the business spaces were loaned, rather than owned. Even businesses that remained property undamaged were forced to close due to failure of critical facilities. Over 60% of businesses lost electricity (restored in 24 hours) and 20% lost water and natural gas service (restored in 2 days). Failure of transportation services caused 39% of business losses in 43% of firms, affecting costumer and employee access to business location, shipping delays, utility cut-offs and repair/clean up. On average, Northridge businesses were closed for 2 days. The speed of reopening was found to be one of the most important determinants in business recovery. Businesses with smaller size, poor financial condition and facing discretionary demand (i.e. locally oriented and undiversified businesses in highly competitive and unstable markets face the risk that their customers may easily switch to competition and may have been as well impacted by the disaster) had a particularly difficult recovery. While, in general, small businesses had to apply for government or commercial loans, as a result of few capital reserves, large business had rapid access to capital (e.g. higher business reserves or insurance payments).	Kroll et al. (1990); Tierney (1997); Rose et al. (1997); Boarnet (1998); Dahlhamer and Tierney (1998); Rose and Lim (2002); Chang and Falit-Baiamonte (2002); Rose and Liao (2005)
1996 Adana-Ceyhan and 1999 Kocaeli earthquakes	• In many cases, the loss of production costed much more than the repair of the building. After the 1999 Kocaeli earthquake, around 1500 small enterprises (5-10 people) were severely damaged and insurance coverage for small and micro enterprises was very limited (53%). About 20 000 small businesses terminated their operation leaving behind about 140 000 jobless people. Average business interruption of 35 days, with 44% of production capacity restored after 1 month and 77% after six months. In the most heavily damaged regions (IX MMI), business interruption losses were about 5% to 10% of the annual turnover in most industrial sectors. In the chemical, textile and automotive sectors the losses reached 50%, 30% and 20%, respectively. In VIII MMI regions the losses varied between 2 and 3%.	Wenk et al. (1998); Moat et al. (2000); Kurita et al. (2004); Durukal and Erdik (2008); Durukal et al. (2008)
1999 Athens earthquake	• Only 15% of 'yellow' and 'red' tagged firms were eager to relocate from their pre-disaster location. Beverage and food businesses were more susceptible to machinery damage. Various illegal practices, such as the use of heavy machinery in unprepared buildings and the placement of staff in inadequate manufacturing areas increased the exposure to damage.	Moat et al. (2000); Sapountzaki (2005)
The 2010 and 2011 Christchurch series of earthquakes	• A cordon placed around the Christchurch's Central Business District (CBD) forced 64% and 11% of the Canterbury firms to temporarily and permanently close, respectively. The median duration of closure was 16 days. The estimated cost to restore damage to commercial property in Canterbury was 4 billion New Zealand Dollars. The damage and disruption caused many businesses to relocate to other areas (i.e. 50 000 CBD jobs at 6000 businesses were displaced by the cordon). The most disruptive factor to businesses was seen to be related with the decrease in costumer's number, spending and demand of different services.	Potter et al. (2015)

1995 Kobe and 2011 Tohoku earthquakes	• Non-structural damage and loss of electricity caused major disruption to businesses and breakage of supply chains. After the 1995 Kobe earthquake, the economy recovery was characterized by a three to four year temporary boost in reconstruction activities. Still, this recovery varied considerably between economic sectors, with services gaining, but manufacturing, construction (in the long run), and wholesale and retail trade experiencing 20% to 35% losses in output compared with pre-disaster levels. After the 2011 Tohoku earthquake, despite the small share of economic activities in the area, many firms from outside were surprised by the ripple effects that the production halt caused through their supply chain. The earthquake, excluding the tsunami, caused a 34% loss of production capacity in the region.	Chang (2010); Krausmann and Cruz (2013); Nakashima et al. (2014); Carvalho et al. (2014)
2010 Chilean earthquake	• All commercial activity was suspended in the affected area for a few days and some major industries (e.g. pulp paper production, wine making and oil refining) had no, or significantly reduced, commercial activity for months. Business interruption losses were in the list of top losses, summing up to 1150 million dollars. A 5% decline in national economic activity was assessed by the Bank of Chile and 50% to 60% of losses were covered by insurance.	Muir-Wood (2011)

8.3.2 The Hazus-MH MR5 framework for direct and indirect economic loss assessment

The Hazus – MH MR5 framework (FEMA, 2010) provides a loss assessment methodology defined in strict economic terms, so that buildings and inventories represent capital investments that produce income and the value of the building and inventory will be the capitalized value of the income produced by the investment created. Hence, and based on Rose (2009), property damage will represent a decline in stock (i.e. quantity at a single point in time) value and usually leads to a decrease in service flows (i.e. outputs of stocks over time). Business interruption losses are a measure of this reduction in the flow of goods and services and must consider the time dimension of losses. Figure 8.1 provides an overview of the Hazus – MH MR5 framework for direct and indirect economic loss assessment.

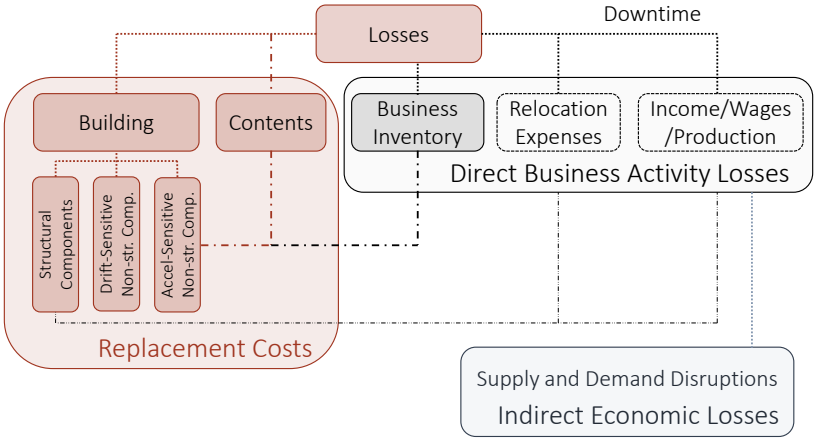

Figure 8.1 – Overview of the Hazus – MH MR5 framework for direct and indirect economic loss assessment

Direct losses are divided in losses to stocks, i.e. property and inventory, and losses to service flows, i.e. relocation expenses and proprietor's income or production, that depend on the business interruption or downtime. Downtime, or building's loss of function time, is considered to be controlled by damage to structural components, while damage to inventory is a function of building accelerations, similarly to acceleration-sensitive non-structural components and contents. Losses to inventory have been herein separated from losses to building and contents, as the latter have already been quantified in Chapter 7. Indirect losses, on the other hand, reflect the effects of supply and demand disruptions and are modelled in the Hazus – MH MR5 framework based on input-output (IO) methodologies. Such macro-economic modelling approaches have already been implemented in a number of previous works, including traditional IO analysis (Rose et al., 1997; Dorra et al., 2013; Shi et al., 2014) or Computable General Equilibrium (CGE) analysis (Rose and Liao, 2005; Wu et al., 2012), however, they offer little insight into disaster impacts at the firm level (Rose, 1997) and would require an exhaustive work to account for every disruption effect, i.e. electricity and water services, transportation infrastructures and supply chains, in the businesses' interruption time. Alternatively, a number of modelling approaches may be found in the literature (Ouyang, 2014), such as the composite indicator model developed very recently to assess the vulnerability of industrial sectors to indirect disaster losses (Hiete and Merz, 2009; Khazai et al., 2013; Merz et al., 2013). This composite indicator model will be employed herein and will be presented in more detailed later.

8.3.3 Description of the case study

The present case study gives continuity to the study initiated in Chapter 7, which focuses on the estimation of direct seismic losses to property of an industrial steel building most representative of the as-built Portuguese industrial building stock (Chapter 9). The derivation of physical fragility functions was carried out based on nonlinear time-history analyses preformed on a comprehensive 3-dimentional structural model that accounts for every single failure mode observed in previous post-event reconnaissance campaigns (Chapter 7). Three distinct industrial building structural models were additionally considered to reflect the influence of different types of column base plate connection, namely of fixed base plate connections (FBPC), semi-rigid base plate connections (SBPC) and nominally pinned base plate connections (PBPC). Moreover, the effects of ground motion directivity were equally included by conducting nonlinear time-history analyses

along the *x*-, *xy*-, *yx*- and *y*-direction axes of the buildings. Physical fragility and vulnerability functions that comprise damage to structural and non-structural components and contents, as well the hazard definition, may be found in Chapter 7, which will be key in interpreting some of the findings and conclusion withdrawn throughout this work. Moreover, in order to provide a wider picture of the expected losses, the industrial building is considered to be located in any region of mainland Portugal, assuming a county-level resolution (Portugal Mainland has 278 counties) consistent with the NUTS IV European local administrative territorial unit. In accordance, the variation in space of the industrial asset values at risk (Merz et al., 2007; Seifer et al., 2010) was defined considering Portuguese regional specifications and data collected from the Portuguese National Institute of Statistics (INE) and from the OECD statistics database for that same territorial unit and 2-digit CAE industrial activities.

8.4 Business inventory vulnerability functions

Business inventory, i.e. stocks of products that are available to sell, constitute a major source of losses, particularly in the case of businesses devoted to the production of final and durable goods (more difficult to replenish), hi-tech businesses (typically associated with higher inventory ratios) or businesses in retail and transportation and warehousing. As an example, textile and leather manufacturing and chemical and petroleum products industries exhibited higher stock losses after the 1999 Kocaeli earthquake in the most affected regions (Durukal and Erdik, 2008). Still, these losses are representative of the exposed industrial assets of the Kocaeli region and may not reflect other regional economies featuring, for instance, different economic sectors or sectors with a tendency to form industrial clusters. Hazus – MH MR5 recognizes this dependency and provides some guidance on how to derive such regional-specific business inventories for the US. In brief, business inventories are defined by multiplying industry-specific inventory ratios (defined as a percentage of annual production outputs or sales) with the respective industrial activity annual production outputs or sales per unit of building size (e.g. implementation area in m^2) and the size of the building under analysis (e.g. in m^2). Business inventory values for mainland Portugal were thus determined for every county and 2-digit industrial CAE activities, as presented next.

8.4.1 Industrial activity production values per m^2

Industrial activity annual production or sales values per m^2 should be quantified ensuring that, if loss assessments at a regional or national scale are conducted, the product between this quantity, the average size of industry-specific buildings and the number of firms of that industry within the region is equal to the regional overall annual production or sales values of the sector. To do so, the annual production of every 2-digit industrial CAE activities was firstly divided by the number of firms of each sector and for every county, thus providing a measure of mean annual production per firm (or establishment, as the number of firms and establishments was found to be roughly equal based on the data collected from INE) and by activity. Average building size values per industry-specific firms were then obtained by multiplying sectorial firm-employment ratios (i.e. number of firms divided by employment) with employment density ratios (i.e. number of full time employees, FTE, per gross internal area of building, m^2). Typically, employment density ratios of 80, 58.4 and 37.1 m^2 per FTE are observed in warehousing and distribution, light industry and other industrial facilities in the UK, respectively (HCA, 2010). For the US, values of 54.8, 50.2, 67.8, 27.9, 83.6 and 76.6 m^2 per FTE were provided by Hazus – MH MR5 for heavy, light, food-drugs-chemicals, metals-mineral processing and high technology industrial facilities and wholesale trade and retail facilities, respectively. The latter reflects more clearly the influence of the industrial activity on the employment density ratios, i.e. businesses that produce perishable goods are expected have higher employment densities, and of the technological environment, i.e. the technological development tend to increase the floor-space per head (HCA, 2010).

Table 8.2 presents the industrial asset values at risk collected and quantified just for mainland Portugal, though values for every county were equally determined. The employment density ratios were defined based on HCA (2010) and Hazus – MH MR5, assuming similar values for identical 2-digit CAE activities. Furthermore, the average building size values presented in Table 8.2 were confronted with building sizes, i.e. implementation areas, collected from a survey of more than 200 design projects (Chapter 9) and from the AICEP Global Find platform. The values derived based on the country's economic statistical information were found to be statistically consistent, i.e. Kolmogorov-Smirnov goodness-of-fit test satisfied at a significance level of 5%, with those obtained from as-built industrial steel buildings located in Portugal (Figure 8.2), thus ensuring

coherence between the industrial assets defined and the physical fragility functions derived from the model developed in Chapter 7.

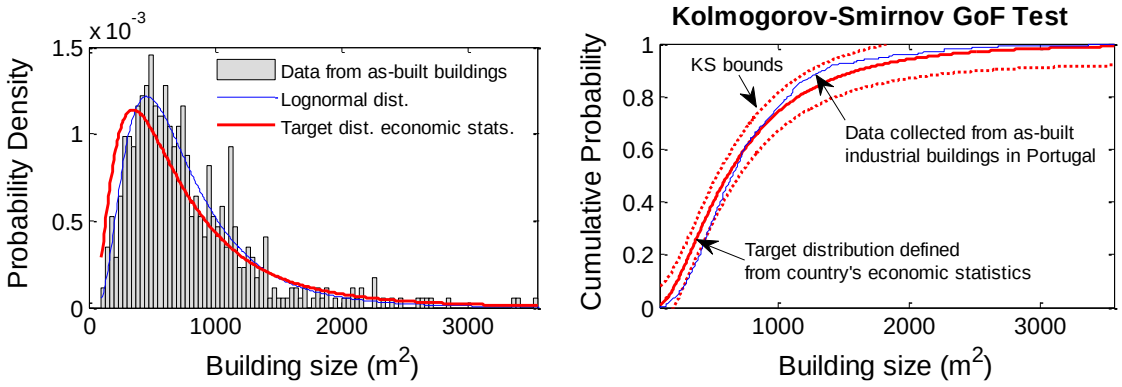

Figure 8.2 – Assessment of statistical consistency between building sizes derived from economic statistics of mainland Portugal and building sizes collected from a survey on the characteristics of the Portuguese as-built industrial building stock (Chapter 9).

8.4.2 Industrial activity inventory ratios

The inventory value at a certain period of time (e.g. days or months) is estimated by multiplying the average time to sell the inventory (i.e. the average duration of stocks) with the cost of goods sold converted to that same period of time (Weygandt et al., 2013). It is affected by the regional economic and technological environment, e.g. market saturation, change in customer preferences, technologies or pricing, as well as by firm characteristics, e.g. activity, dimension, type of products sold or efficiency. INE provides regional statistical information on the value of the merchandise in stock sold per industrial activity and average duration of stocks of raw materials and merchandise depending on the firm's size, small (less than 20 employees) or big (more than 20 employees). The Portuguese economy is basically composed by small firms, which represent more than 95% of the overall business structure. Big firms, in turn, are associated to heavy industry, pharmaceutical (26% of sector firms) and tobacco (75% of sector firms) activities. Once again, one may recall the consistency in using the structural model developed in Chapter 7 to represent the Portuguese industrial context. Table 8.2 presents mean values for stock durations (in months) and inventory ratios (i.e. inventory value divided by the respective sector production output) per industrial sector, which were defined by preforming a weighted mean considering the percentage of small and big firms within the region. It may be observed that the obtained inventory ratios are in agreement and in the order of those provided by Hazus – MH MR5, and reflect expected economic trends. Sectors that produce perishable goods display lower duration of stocks and inventory ratios (e.g. food industry),

while hi-tech industries (e.g. communication, electronic and optical equipment) and businesses in retail exhibit higher inventory ratios.

8.4.3 Business inventory consequence model and vulnerability functions

Vulnerability functions represent the evolution of losses, or more commonly loss ratios, for increasing ground motion intensity levels (Silva et al., 2015). When analytical models are used, these functions are typically obtained by converting fragility functions on the basis of damage-to-loss consequence models. Damage to inventories usually results from stacks of inventory falling over or objects falling off shelves (FEMA, 2010), and, according to Hazus – MH MR5, may be predicted by acceleration sensitive non-structural damage. As a result, the acceleration sensitive non-structural components fragility functions derived in Chapter 7 will be employed herein to represent inventory damage. These functions were derived by setting the 5% damping spectral acceleration at the *x*- and *y*-direction transverse and longitudinal fundamental periods of vibration of the buildings, S_a (T_1,*x*, 5%) and S_a (T_1,*y*, 5%), as the main intensity measure. Three damage states, i.e. damage limitation (DL), significant damage (SD) and near collapse (NC), were defined in accordance with damage observed from previous post-event reconnaissance campaigns. Existing damage-to-loss consequence models typically refer to structural damage (Eren and Luş, 2015). Specific models for business inventories are lacking in the literature and may be simply found, to the author's knowledge, within the Hazus – MH MR5 framework. The latter considers that average losses of 5%, 25% and 50% of the total exposed business inventory would occur at the DL, SD and NC damage sates, respectively, assuming that some salvage of inventory would take place even if collapse of non-structural components occurs. Nevertheless, as pointed out by Silva et al. (2015), loss ratios for a given damage state vary greatly and their uncertainty should be propagated into vulnerability functions. This uncertainty propagation was done by employing the technique adopted in Chapter 7, which consists on a multivariate random generation of loss ratios using Copulas, assuming that each damage state loss ratio follows a beta distribution and that the ratios of each damage state are linearly correlated with a correlation coefficient of 0.8. Coefficients of variation of 0.3, 0.2 and 0 were adopted for the DL, SD and NC limit sates, respectively.

Figure 8.3 depicts the mean and 5%-95% bound inventory vulnerability functions obtained for mainland Portugal and different 2-digit industrial CAE activities. To highlight the influence of column base plate connections and ground motion directivity, vulnerability functions derived from different structural models and directions of analysis are presented.

Losses to inventory per unit of building size (€/m^2) were adopted so as to give a more general perspective. In brief, it may be observed that the derived vulnerability functions reflect the intended sectorial economic behaviour. For instance, sectors that produce perishable goods (e.g. food industry) have lower vulnerability to inventory losses in comparison to hi-tech industries (e.g. communication, electronic and optical equipment). Mean losses to food industry inventories of around 3700€ and 8000€ (approximately 16% and 35% of total inventory) would be expected for S_a (T_1,x) levels equal to 0.5g and 1.5g, which are associated to mean annual frequencies (MAF) of occurrence in 50 years of 0.014 and 0.0012, respectively, at the city of Lisbon (Chapter 7). Such losses would increase in communication, electronic and optical equipment industry inventories to values of around 10500€ and 63000€ (approximately 4% and 26% of the total inventory) for S_a (T_1,y) levels equal to 0.5g and 1.5g, which, in turn, correspond to MAF values in 50 years of 0.052 and 0.0049, respectively, for the same city. Regarding the influence of the support conditions and ground motion directivity, although their impact on acceleration-sensitive fragility functions was found not to be very pronounced (Chapter 7), they significantly affected the uncertainty propagation to the inventory vulnerability functions. For example, the abrupt increase in the food industry inventory losses shown in Figure 8.3 for lower S_a (T_1,x) levels resulted from a DL limit state fragility function with vertical shape and practically null uncertainty. Comparing the obtained inventory vulnerability functions with the mean empirical stock loss ratio (including all industrial sectors) observed after the 1999 Kocaeli earthquake at IX MMI regions (estimated PGA of 0.3g), which is around 23% (Durukal and Erdik, 2008; Durukal et al., 2008), it was observed that the obtained vulnerability functions provide somehow similar values, which range from 11% to 25% considering a S_a (T_1,x) of 0.75g (roughly corresponds to a PGA of 0.3g) and all CAE activities

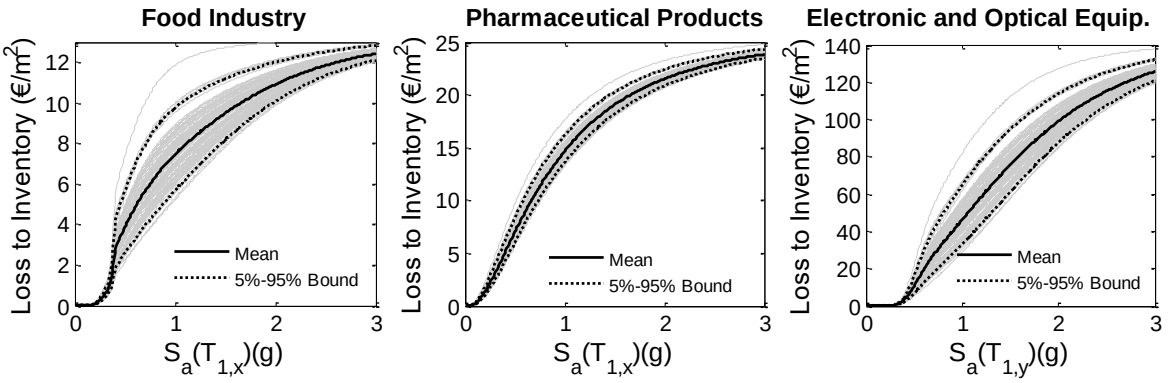

Figure 8.3 – Mean and 5%-95% confidence interval inventory vulnerability functions for mainland Portugal and different industrial CAE activities obtained based on fragility functions derived from the FBPC building analysed in the *x*-direction (*left*), the SBPC building analysed in the *xy*-direction (*middle*) and the PBPC building analysed in the *y*-direction (*right*).

Table 8.2 – Industrial assets at risk for mainland Portugal.

Industrial Activity (2-digit Portuguese CAE)	Number of establishments	Number of employees	Employee per m²	Building area (m²)	Production per area (€/m²)	Duration of stocks (months)	Inventory ratios	DL LS recovery time (days)	SD LS recovery time (days)	NC LS recovery time (days)	Income per area per day (€/m²/day)	Wage per area per day (€/m²/day)
Extractive Industries	1411	10254	0.0196	371.3	2081	1.95	0.57%	53.0	289.5	442.5	0.17	1.1
Food Industry	10973	88782	0.0199	405.9	2430	1.44	1.10%	46.0	273.5	427.5	0.10	0.8
Beverages Industry	1354	13821	0.0199	512.1	3997	1.44	0.75%	46.0	273.5	427.5	-0.12	1.3
Tobacco Industry	6	174	0.0199	1454.9	13253	1.37	4.03%	46.0	273.5	427.5	3.31	10.4
Textiles Manufacturing	3361	39935	0.0182	651.3	1255	3.10	1.01%	53.0	289.5	442.5	-0.08	0.7
Clothing Industry	9384	83876	0.0182	489.9	615	3.10	1.37%	53.0	289.5	442.5	-0.03	0.5
Leather Industry	3077	43366	0.0182	772.5	967	2.55	0.58%	53.0	289.5	442.5	0.01	0.6
Wood and Cork Products	5945	30223	0.0196	259.8	1651	2.98	2.68%	53.0	289.5	442.5	0.00	0.7
Pulp, Paper and Paper Products	484	10657	0.0182	1206.9	6267	1.97	0.17%	53.0	289.5	442.5	1.26	1.2
Publishing, Printing and Reproduction of Recorded Media	3009	16179	0.0182	294.7	1103	1.90	0.47%	53.0	289.5	442.5	0.00	0.8
Coke and Refined Petroleum Products	17	1733	0.0196	5208.9	116117	1.89	0.00%	53.0	289.5	442.5	2.85	4.2
Chemical Products and Fibres	971	12117	0.0199	626.0	7261	1.89	0.90%	46.0	273.5	427.5	0.48	1.7
Pharmaceutical Products	141	6449	0.0199	2294.5	3415	1.69	1.51%	46.0	273.5	427.5	0.55	1.6
Rubber and Plastic Products	1177	23696	0.0199	1010.0	2875	1.40	0.54%	46.0	273.5	427.5	0.27	1.1
Non-Metallic Mineral Products	4711	40937	0.0147	589.3	1253	2.09	1.66%	52.0	293.5	446.5	0.17	0.7
Base Metallurgical Industry	394	8200	0.0147	1411.5	4788	2.34	0.38%	52.0	293.5	446.5	0.09	0.9
Metal Products (Except Machinery and Equipment)	12631	79354	0.0147	426.1	942	2.36	1.01%	52.0	293.5	446.5	0.08	0.7
Communication, Electronic and Optical Equipment	334	8809	0.0359	735.1	5684	2.15	4.98%	61.0	365.0	523.5	-0.45	2.3
Electric Equipment	740	17312	0.0359	652.0	5467	2.16	1.70%	61.0	365.0	523.5	0.84	2.2
Machinery and Equipment Manufacturing	1667	20610	0.0359	344.6	3905	2.59	0.92%	61.0	365.0	523.5	0.42	1.9
Motor Vehicles Manufacturing	534	30187	0.0359	1575.5	7651	1.88	0.22%	61.0	365.0	523.5	0.08	2.1
Other Transportation Equipment Manufacturing	211	4027	0.0359	531.9	2413	1.98	1.19%	61.0	365.0	523.5	-0.40	1.8
Furniture and Mattresses Products	5327	30847	0.0182	317.4	728	2.98	1.19%	53.0	289.5	442.5	-0.01	0.5
Other Manufacturing Industries	3347	13216	0.0196	201.8	1352	2.34	4.30%	53.0	289.5	442.5	0.09	0.7
Repair, Maintenance and Installation of Machinery	3468	17405	0.0182	275.1	1279	2.61	2.01%	53.0	289.5	442.5	0.19	1.1
Retail	262238	754745	0.0101	284.2	395	1.84	48.10%	52.5	316.5	454.5	0.04	0.4
Transportation and Warehousing	25217	153068	0.0125	485.6	1450	1.26	0.19%	52.5	316.5	454.5	-0.04	0.8

8.5 Downtime due to building loss of function

Downtime, or recovery time, so-called in resilience studies, refers to the period necessary to restore the functionality of a facility or business to closer, identical or even better levels of operation (Cimellaro et al., 2010). It consists on a highly uncertain random variable, resultant from the lack of detailed data and dependence on numerous factors outside of the control of engineers, contractors and building owners (Comerio, 2006). In general, downtime estimation approaches can be divided into: (i) general approaches that provide crude values representative of large portfolios of buildings, such as Hazus – MH MR5; (ii) and building-specific approaches (Porter et al., 2001; Porter and Ramer, 2012). Whereas the former give more generic values based on expert opinion and empirical post-event information, the latter requires the knowledge of every single subsystem repair time and the modelling of their linkages using scheduling techniques (i.e. Gant chart) or logic-trees. Since it would be unpractical to obtain such singular information for every industrial activity subsystem, the more generic Hazus – MH MR5 approach will be adopted herein. As discussed by Jain and Guin (2009), downtime to supply chain independent businesses is equal to the sum of pre-repair times (i.e. finance, design and permits) and repair times, relocation times or continued business interruption times (Hsu et al., 2013), conditioned to restoration times of access to property and utilities. The time to businesses regain their previous pre-event market share can be equally included to account for market share losses. In the case of supply chain dependent businesses, the downtime can be aggravated by supply chain disruptions, i.e. supply shortages or demand reductions. Hazus – MH MR5 defines downtime as the sum of pre-repair time and clean-up and repair times, assuming that supply chain business interruption losses will be accounted for from indirect economic analysis and that realistic building and service downtimes will be reproduced by a set of proposed multipliers.

Table 8.2 depicts the median building recovery times (in days) defined per structural damage state and 2-digit industrial CAE activity. To better simulate the dependency of recovery times on the industrial sector, i.e. large businesses perform business-impact analysis and have continuity plans that accelerate restoration times or contents in hi-tech manufacturing facilities are more difficult to replace than the typical contents (Jain and Guin, 2009), and to account for the uncertainty on recovery times, the ATC-13 lower and upper bound repair times provided by Hazus – MH MR5 in Appendix 15A were adopted.

Such lower and upper bounds were set as the 5% and 95% quantiles of a lognormal distribution (adopted by Porter et al. (2001) to represent repair times), allowing to estimate the respective median and standard deviation values. Coefficients of variation of 0.1, 0.43 to 0.54 and 0.24 to 0.27 (the lower and higher values refer to light and hi-tech industries) were obtained for the DL, SD and NC damage states, respectively. The median repair times were then summed up to median pre-repair times and the random generation of restoration times was carried out assuming that every damage state restoration times are fully correlated. Furthermore, the Hazus – MH MR5 time multipliers were, thereafter, applied to the recovery times. Time multipliers of 0.5 and 1.0 were defined at the DL and SD-NC limit states, respectively, for heavy industry activities, whereas times multipliers of 0.1 to 0.2, 0.3 and 0.4 were defined at the DL, SD and NC limit states, respectively, for other industries. These multipliers reflect, for instance, the fact that at slight damage states the repair times are shorter and clean-up by staff may occur simultaneously, in some activities the repair time is almost irrelevant since firms can rent alternative spaces and resume production, or at moderate damage, some businesses may close, while others may promptly open after some days of clean-up (FEMA, 2010).

Figure 8.4 presents the mean and 5%-95% bound downtime functions for mainland Portugal and different CAE activities obtained by convoluting the structural fragility functions derived in Chapter 7 with the restoration times randomly generated. It may be observed, as intended, that light industries (e.g. food industry) exhibit lower restoration times, but also that the ground motion directivity and the support boundary conditions, which were seen to significantly influence the structural fragility of industrial steel buildings, greatly affect downtime and its evolution with the ground motion intensity levels.

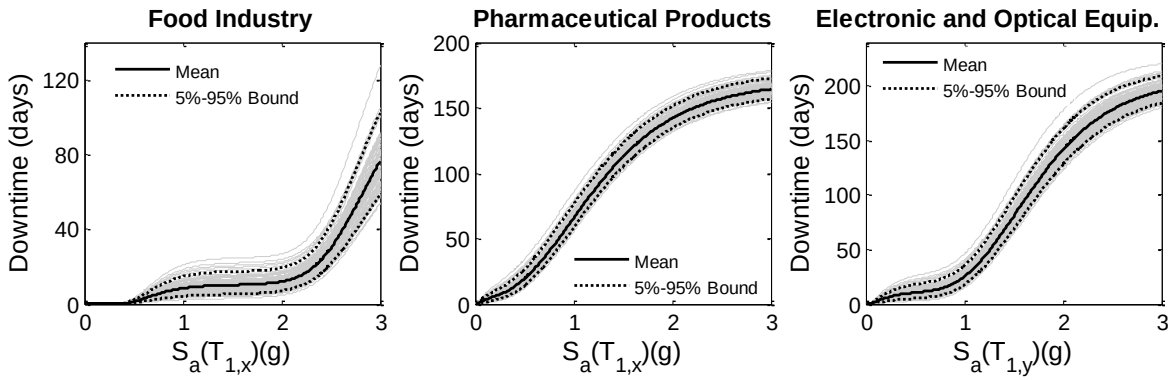

Figure 8.4 – Mean and 5%-95% confidence interval downtime functions for mainland Portugal and different industrial CAE activities obtained based on structural fragility functions derived from the FBPC building analysed in the *x*- (*left*) and *xy*-directions (*middle*) and the PBPC building analysed in the *y*-direction (*right*).

Moreover, comparing the functions derived with the mean downtime (including all industrial activities) of 80 days observed after the 1999 Kocaeli earthquake at IX MMI regions, it was observed that the obtained downtime functions provide similar values for the *xy*-direction of analysis and buildings SBPC and PBPC, equal to 83 days and 88 days considering all industrial activities, respectively. However, a significantly smaller value of 7 days was obtained for building FBPC in the *x*-direction of analysis.

8.6 Relocation expenses vulnerability functions

As above-mentioned, the property loss of function or other uncontrolled causes that may limit its access, e.g. the cordoning of the CBD of Christchurch (Chang et al., 2014), most likely make businesses relocate. If the building is not owner occupied though, the burden of relocation is not expected to be borne by the renter (i.e. the tenant would cease paying the rent and would only pay to the new landlord), but instead by the building owner (FEMA, 2010). These was actually the case of 75% of the businesses analysed by Tierney (1997) after the 1994 Northridge earthquake. Nevertheless, according to Hazus – MH MR5, 55% of hi-tech and 75% of the remaining businesses are owner occupied, respectively. Specific ownership rates for Portugal are difficult to ascertain, being only available values respective to households ownership rates, which are around 74% according to the Eurostat. The case study building was considered to be owner occupied. Moreover, relocation expenses not only include rental costs, but also disruption costs associated to shifting and transferring, which are quite difficult to estimate and are around 0.79% to 1.53% of the total building replacement cost within the Hazus – MH MR5 framework. The rental costs, on the other hand, are regional-specific and economy dependent. Real estate market values for Portugal indicate that current industrial building rental costs vary between 2.75 €/m^2/month and 6.50 €/m^2/month in the city of Lisbon and are around 3.50 €/m^2/month in city of Oporto (AICEP, 2014). Since rental cost values for every county of mainland Portugal are not readily available, it was considered reasonable to geographically distribute these costs based on the building replacement cost maps developed in Chapter 7, provided that similar real estate market values would be obtained at Lisbon and Oporto. Figure 8.5 depicts the rental cost maps derived for mainland Portugal and different building configurations. The relocation expenses vulnerability functions may be afterwards easily obtained by multiplying the downtime functions, which already account for the fact that firms can rent alternative spaces in order to resume

production, with the county-specific relocation cost. For example, considering the downtime functions obtained for the pharmaceutical industry FBPC building struck in the *xy*-direction (Figure 8.4), mean recovery times of around 20 days and 112 days would be expected for S_a (T_1,*x*) levels equal to 0.5g and 1.5g, respectively, which would correspond to rental losses, assuming a maximum rental cost of 6.5€/m^2/month, equal to 3360€ and 18816€ (approximately 0.7% and 3.7% of the building replacement cost), respectively. These would increase to 2.2% and 5.2% of the building replacement cost if the disruption costs were included.

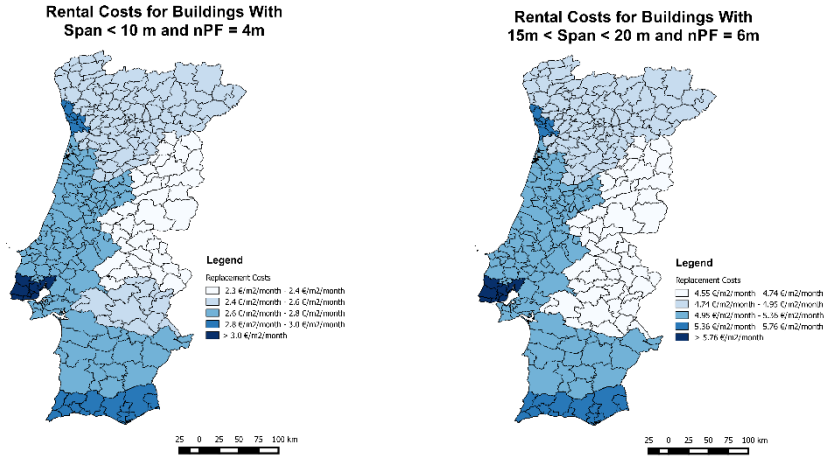

Figure 8.5 – Replacement costs for industrial steel buildings with different span lengths and portal frames spacing located in Portugal Mainland.

8.7 Income or production vulnerability functions

The vulnerability of a firm to natural disasters depends on the size of its investment and revenue exposures combined with the disruptions to the firm's production, logistics, manpower, clientele and supply chain (Olson and Wu, 2010). In other words, losses to firm's revenue, or income, occur due to downtime disruption of economic activity (FEMA, 2010), and are greater the higher the income assets exposed to risk are. Notwithstanding the latter, firm's tend to display some resilience after the disaster (Rose and Lim, 2002), either by relocating or rescheduling production, i.e. by making up, or recapturing, lost production at a later date by overtime work or working extra shifts, since demand tends to persist even if the supply is disrupted (Park et al., 2010).

8.7.1 Recapturing of lost production

Very recently, Park et al. (2010) proposed an approach for modeling the recapture of lost production. The model depends on the characteristics of the sector and time, i.e. firms heavily dependent on time would more difficulty recoup losses, and relies on the

assumption that the path of recapturing the lost production follows a normal cumulative distribution function and that the initial recapture factor vary with an exponential decay function (General Recapture Factor Model). If the downtime period is less than 3 months, the initial recapture factor starts from 0.99 and has the Hazus – MH MR5 (or those observed by Rose and Lim, 2002) recapture factor at the period of 3 months; in turn, if the downtime period is over 3 months, the initial recapture factor starts from the Hazus – MH MR5 recapture factor and attains 0.01 after 12-month. This model is, in fact, an extension of the recapture factors proposed by Hazus – MH MR5, who recognizes that the proposed factors are deemed appropriate for business disruptions lasting up to three months, but that, for more advanced studies, users may choose to adjust recapture factors downward for longer disruptions (FEMA, 2010). Figure 8.6 depicts the recapture factor function derived from the General Recapture Factor Model for every industrial sector in accordance with Hazus – MH MR5, which proposes an identical recapture factor of 0.98 regardless the industrial activity. This value is consistent with that of Rose and Lim (2002), which found output reductions after the 1994 Northridge earthquake of 0.95 at food and nondurable manufacturing industries and 0.99 at durable manufacturing and petroleum refining industries. An example of application to a food industry FBPC building with the ground motion striking in the *xy*-direction is also presented in Figure 8.6, being expected direct production reductions of 0.02% and 0.43% at S_a (T_1,*x*) levels equal to 0.5g and 1.5g, respectively.

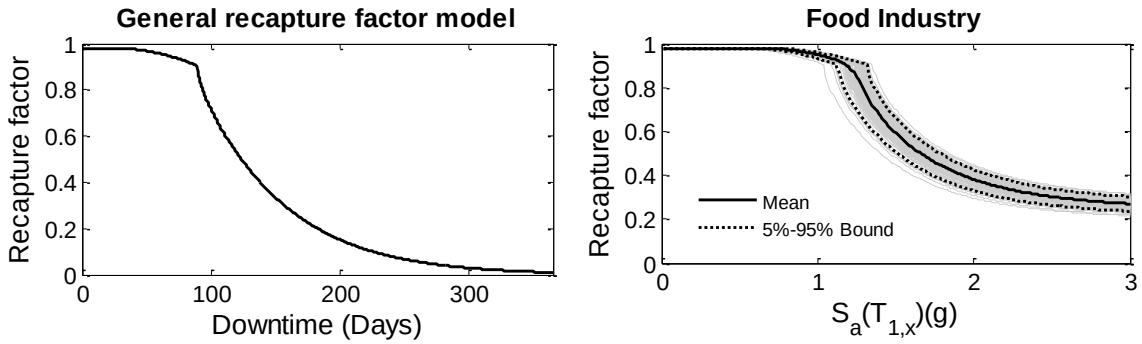

Figure 8.6 – Initial recapture factor function defined from the General Recapture Factor Model (*left*) and application to a food industry FBPC building with the ground motion striking in the *xy*-direction (*right*).

8.7.2 Income or production exposed assets at risk and vulnerability functions by sector

Income (and wage) values per m^2 were derived (Table 8.2) similarly to the annual production values per m^2 presented above. Every measure was divided per unit of time (in

days) so as to allow providing estimates of the respective losses when business interruption (downtime) is considered. Moreover, since the income varies with time as consequence of economic trends (Seifer et al., 2010), a three year average was considered in accordance to Hazus – MH MR5. Figure 8.7 provides a picture of some direct business activity vulnerability functions resultant from the convolution of the asset at risk and the recapture function.

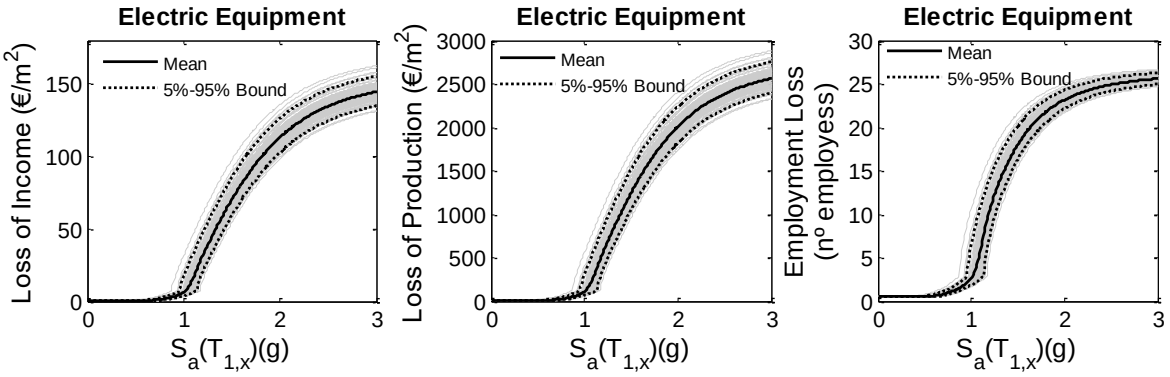

Figure 8.7 – Mean and 5%-95% confidence interval income, production and employment vulnerability functions for mainland Portugal and different industrial CAE activities obtained based on structural fragility functions derived from the FBPC building analysed in the *xy*-direction.

8.8 Indirect industrial activity vulnerability

Modelling indirect business losses is a difficult task, mostly because of the complexity of the interdependencies between all variables at stake. A rational way of dealing with this issue is by adopting conceptual indicator frameworks, such as the framework developed by Hiete and Merz (2009), and recently implemented by Merz et al. (2013) and Khazai et al. (2013), to assess the vulnerability of industrial sectors to indirect disaster losses. This framework relies on production theory (i.e. production loss might occur when production factors are not available as required and when critical infrastructures or material and information flows within supply chains are disturbed) and defines three sub-indicators groups: (i) input factor (equipment and labor) dependency; (ii) infrastructure dependency; (iii) and supply chain dependency. The framework will be adopted herein. A detailed description of the variables that explain each sub-indicator may be found in Merz et al. (2013). Since data describing supply chain dependencies (i.e. backward and forward multipliers based on the Leontief and Gosh Inverses) are just available at a national scale from the Input-Output OECD database, the vulnerability indices derived will be more representative of average national indirect losses. Information on the importance factor of power and water services by industrial activity was collected from FEMA (1991). Figure 8.8 presents the obtained indirect Industrial Vulnerability

Indices (IVIs) per 2-digit CAE activities and sub-indicator group. Overall, it may be seen that supply chain disruptions contribute the most to indirect losses and that hi-tech and heavy activities exhibit higher levels of indirect vulnerability.

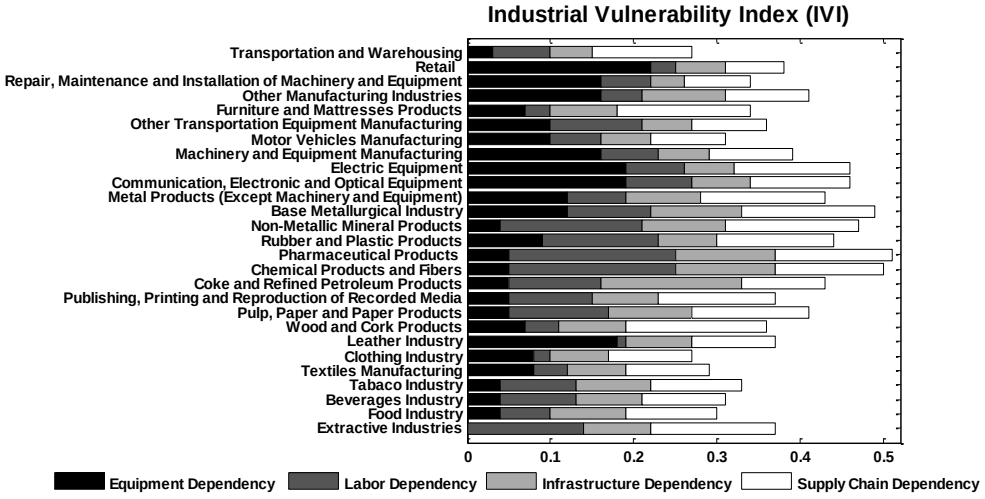

Figure 8.8 – Sector-specific indirect Industrial Vulnerability Index (IVI) for mainland Portugal.

The IVI composite indicator can be afterwards integrated with direct losses using Moncho's equation (Burton et al., 2014; EMI, 2015) in order to obtain total loss estimates. For instance, the direct production capacity losses of 0.02% and 0.43% at S_a (T_1,x) levels equal to 0.5g and 1.5g, respectively, observed in Figure 8.6 for food industry would increase to 0.26% and 0.56%, respectively, if indirect vulnerability is taken into account. Once again, comparing the developed model with the mean overall business interruption losses at IX MMI regions observed for every sector after the 1999 Kocaeli earthquake (Durukal and Erdik, 2008), of around 9.8%, similar mean losses of 11% (including all sectors) were obtained for a S_a (T_1,x) level of 0.75g considering the ground motion striking in the *xy*-direction. Though, these mean business interruption losses may reduce to around 2.8% if the *x*-direction of analysis is considered.

8.9 Losses to business of a typical industrial steel building located in Portugal Mainland

Earthquakes may potentially imply substantial losses (e.g. capital, production or revenues) to firms located in seismic-prone regions or even to those that, hopping to enhance their market value, scout for opportunities in such regions. Risk management and loss quantification are essential to support firms on developing strategies and measures for the reduction of natural disaster losses, e.g. mitigation of investments, financial protection or use of risk transfer mechanisms, such as cat-bonds or insurance (Olson and Wu, 2010).

Therefore, with the aim of providing a contribute to such needs, the potential average losses to different sectorial industrial businesses were quantified for a time span of 50 years, following the work conducted in Chapter 7.

Figure 8.9 depicts the direct business losses in 50 years obtained for a FBPC building located in the city of Lisbon and assessed in the *xy*-direction of analysis. This figure provides valuable information, not only, in terms of the expected losses per unit size of the building, but also in terms of their inter-sectorial variations. It may be firstly observed that sectors associated to non-durable goods and high stock turnover ratios are expected to exhibit quite low inventory losses in 50 years, around 1€/m^2 assuming a 95% confidence bound, whereas hi-tech industries (e.g. communication, electronic and optical equipment), retail and the tobacco industry would exhibit inventory losses of 7.4€/m^2, 5.3€/m^2 and 14€/m^2, respectively. Secondly, with regard to direct business interruption, higher downtimes would be expected in heavy industrial activities (e.g. coke and petroleum refining, base metallurgical industry, machinery, equipment and vehicles manufacturing) as a result of the higher recovery time multipliers (lower resilience to cope with damage), reaching 20 days with a 95% confidence level. Downtime values varying from 5 to 10 days would be expected for other industries. Proportional relocation losses up to 4.1€/m^2 with a 95% confidence would be also observed. Moreover, such expected downtime values would be potentially overcome by production rescheduling (i.e. recapture factor of 0.98), allowing to mitigate production output or income losses. In accordance with the assets at risk of Table 8.2, higher production losses would be expected in hi-tech (e.g. electronic equipment), heavy (particularly automobile manufacturing) and tobacco (cluster in the region of Lisbon) industries. Hi-tech industrial production losses would reach 40€/m^2 within the 95% bound. In the case of textile related industries, on the other hand, such losses would not exceed 2€/m^2. A remark should be additionally made on coke and refined petroleum products and motor vehicles manufacturing industries, which exhibit particularly high production assets at risk. These heavy industrial activities are typically associated to large industrial complexes, whose structural fragility could be misrepresented by the case study building (geared towards light industrial facilities and warehousing). Furthermore, it may be observed that motor vehicle and other transportation equipment manufacturing, base metallurgical and beverages industries seem to be more vulnerable to natural disasters and could even worsen their later bad years (negative income) in the case of a seismic event.

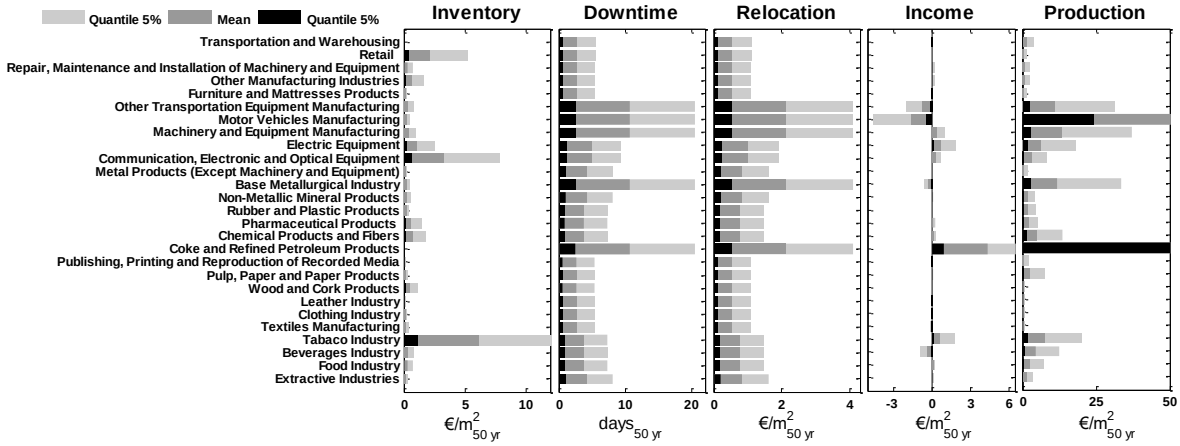

Figure 8.9 – Mean and 5%-95% confidence interval direct business losses in 50 years for a FBPC building assessed in the *xy*-direction of analysis located in the city of Lisbon.

Indirect business interruptions, due to input factor, infrastructure and supply chain disruptions, would increase, with 95% confidence, relocation expenses up to 6.1€/m^2 (respective to base metallurgical industry) and production losses up to 58.4 €/m^2 (respective to hi-tech industry and excluding coke and petroleum products and motor vehicle manufacturing industries) in 50 years.

As far as the geographical distribution of losses along mainland Portugal is concerned, Figure 8.10 shows that higher mean business losses, in 50 years, are expected to occur in the region of Lisbon and Tagus Valley, which is associated to an expected mean business interruption time of around 5 days. As stated in Chapter 7, this region represents one of the most important industrial hubs in Portugal, and together with the Porto-Aveiro-Braga industrial region in the northwest of mainland Portugal, account for approximately three-fourths of the counties' net industrial output. Still, significantly lower mean downtimes in 50 years, of around 1 day, were obtained at the latter region. These results call attention for the potentially high risk to which firms located in the region of Lisbon and Tagus Valley may be exposed to. In fact, considering both the property losses derived in Chapter 7 and the direct and indirect business losses quantified herein, mean total losses in 50 years up to 2.9% of the building replacement cost (6.6% within the 95% bound) were obtained for warehousing, 4.1% (10.2% within the 95% bound) for food and light industrial activities, 6.23% (15.3% within the 95% bound) for chemicals and hi-tech industries, 7.3% (18% within the 95% bound) for the tobacco industry and 15.3% (41.7% within the 95% bound) for heavy industries. In the case of the coke and refined petroleum products, the mean losses would surpass almost 2 times (5.5 times within the 95% bound) the building replacement cost. Nevertheless, these losses refer to the most critical direction of analysis of the case study building, and, if in turn, the *x*-direction of analysis was

considered, a substantial reduction on the mean total losses would be observed, to values around 4% of the building replacement cost in the coke and refined petroleum products sector and varying from 0.9% to 2% for the remaining sectors.

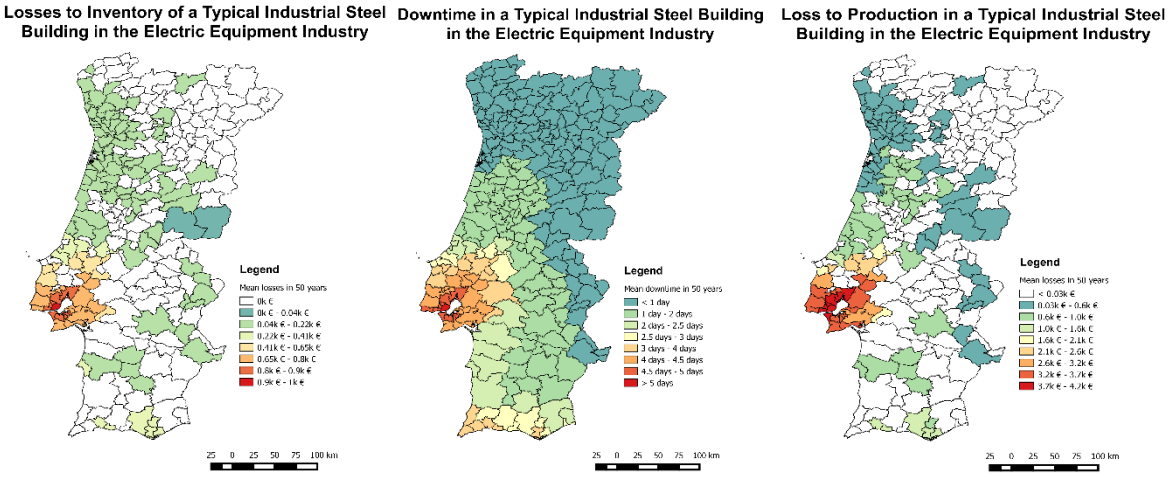

Figure 8.10 – Maps of mean direct business losses and downtime in 50 years of FBPC buildings used in the electric equipment industry assessed in the *xy*-direction of analysis.

To sum up the above findings, Table 8.3 presents, for more general groups of industrial sectors, the contribution of business losses (including inventory, relocation expenses and production) to total losses observed in a FBPC building struck in both *x*- and *xy*-directions, providing, in this way, an overview of the vulnerability of each sectorial group to business losses, as well as its dependency on ground motion directivity. It has been shown in Chapter 7 that, whilst acceleration-sensitive fragility functions (i.e. govern damage to property) vary slightly with the ground motion directivity, structural fragility functions (i.e. predict business interruption) are greatly dependent on the earthquake direction, which may introduce variations up to 60% in the property loss estimates. These observations support the present findings, explaining why the contribution of business losses to the total losses decreases so markedly in the *x*-direction of analysis (Table 8.3).

Table 8.3 – Contribution of business (direct and indirect) losses to total losses by sectorial group.

Direction of Analysis	Transportation and Warehousing	Food and Light Industries	Chemicals and Hi-Tech Industries	Tobacco Industry	Heavy Industries	Coke and Refined Petroleum Products
x-dir.	1.3%	6.5%	20%	32%	21%	58%
xy-dir.	23%	36%	53%	56%	85%	98%

8.10 Conclusions

Natural disaster, e.g. earthquakes, may imply substantial losses to firms and significantly affect the economy of a region, or even of unaffected regions due to ripple effects. This Chapter has examined such businesses losses to firms, through the consideration of an industrial steel building with typical dimensions and geometrical characteristics of as-built buildings located in mainland Portugal. Every industrial activity of the 2-digit Portuguese Standard Industrial Classification System (CAE) was equally considered. Novel sectorial business vulnerability, or loss, functions accounting to inventory (or stocks), relocation expenses and production output (or income, sales, etc.) losses were proposed on the basis of the Hazus – MH MR5 conceptual framework. Extensions to the framework were also implemented, particularly the modelling of the damage-to-loss ratios uncertainty propagation, the inclusion of recapture factor functions and the integration of a sub-indicator framework to quantify indirect losses. Exposure models for every economic asset at risk were also developed for mainland Portugal considering a county-level resolution. The corresponding losses were, at last, quantified.

The results obtained herein suggest that industrial sectors with higher capital demand, extensive material requirements and higher degree of specialization of the production equipment and labor (e.g. chemicals, hi-tech or heavy activity industries) would be hit harder by disasters. In these sectors, business losses are expected to contribute up to 85% to total losses in 50 years. Still, this contribution would reduce significantly to around 36% in food and light activity industries and 23% in transportation and warehousing, as anticipated by their high activity dependency on property. Concomitantly, whilst the total losses in 50 years to light and hi-tech industries were seen to be within acceptable and affordable limits, reaching, with 95% confidence, 15.3% of the building replacement cost, in the case of heavy industrial activities the losses may reach values around 41.7% of the building replacement cost. These findings aware for the potential risks of heavy industrial activities in mainland Portugal, particularly those located in the region of Lisbon and Tagus Valley, and provide crucial information for future implementation of loss reduction strategies. Still, it was equally found that the ground motion directivity plays a critical role in the total loss estimates, leading to variations greater than 80%. Moreover, a remark should be made on the high mean losses in 50 years observed to the coke and refined petroleum products industry, which were found to surpass almost 2 times the building replacement cost. Still, these are simply indicative results, since the actual fragility of large

industrial facilities characteristic of this sector may be misrepresented by the case study building. Studies focusing on the assessment of the risk to large industrial complexes that equally account for the dependencies within the complex have already been initiated in the context of the REAKT project (Lopes et al., 2012; Oliveira et al., 2014), although further research is still needed. Likewise, the losses observed along the south-western coastal region of mainland Portugal, particularly in the highly industrialized Lisbon and Tagus Valley region, point out for the need of further studies focusing on the estimation of industrial losses at a national scale for Portugal.

8.11 Acknowledgments

This work has been performed within the framework of the research project PTDC/ECM-EST/3062/2012 'Earthquake loss of the Portuguese building stock' founded by the Foundation of Science and Technology (FCT) of Portugal. The authors would like to express their gratitude to Dr. Joana Neto, Marketing Director of AICEP Global Parques, for providing access to the AICEP Global Find platform database.

8.12 References

AICEP (2014) Guide to property investment in Portugal, Report prepared for the Portuguese Agency for Investment and External Commerce (AICEP) by Curshman & Wakefield and Uría Menendez – Proença de Carvalho, Lisbon, Portugal.

Boarnet MG (1998) Business losses, transportation damage and the Northridge Earthquake, Journal of Transportation and Statistics, 1, 50-63.

Burton CG, Khazai B, Silva V (2014) Social vulnerability and integrated risk assessment within the Global Earthquake Model, In Proceedings, 10th National Conference in Earthquake Engineering, Earthquake Engineering Research Institute, Anchorage, AK.

Carvalho VM, Nieri M, Saito YU (2014) Supply chain disruptions: evidence from the Great East Japan earthquake, The Research Institute of Economy Trade and Industry.

Chang SE (2010) Urban disaster recovery: a measurement framework and its application to the 1995 Kobe earthquake, Disasters, 34, 303−327.

Chang SE, Falit-Baiamonte A (2002) Disaster vulnerability of business in the 2001 Nisqually earthquake, Environmental Hazards, 4, 59-71.

Chang SE, Taylor EJ, Elwood JK, Seville E, Brunsdon D, Gartner M (2014) Urban disaster recovery in Christchurch: The central business cordon and other critical decisions, Earthquake Spectra, 30, 513-532.

Cimellaro, G.P., Reinhorn, A.M., and Bruneau, M., 2010. Framework for analytical quantification of disaster resilience. Engineering Structures, 32, 3639-3649.

Comerio M (2006) Estimating downtime in loss modelling, Earthquake Spectra, 22, 349-365.

Cruz AM, Steinberg LJ (2005) Industry preparedness for earthquakes and earthquake-triggered hazmat accidents in the 1999 Kocaeli earthquake, Earthquake Spectra, 21, 285-303.

Cruz AM, Okada N (2008) Consideration of natural hazards in the design and risk management of industrial facilities, Natural Hazards, 44, 213-227.

Dahlhamer JM, Tierney KJ (1998) Rebounding from disruptive events: business recovery following the Northridge earthquake, Social Spectrum: Mid-South Sociological Association, 18, 121-141.

De Mel S, McKenzie D, Woodruff C (2011) Enterprise recovery following natural disasters, The Economic Journal, 122, 64-91.

Dorra EM, Stafford PJ, Elghazouli AY (2013) Earthquake loss estimation for Greater Cairo and the national economic implications, Bulletin of Earthquake Engineering, 11, 1217-1257.

Durukal E, Erdik M (2008) Physical and economic losses sustained by the industry in the 1999 Kocaeli, Turkey earthquake, Natural Hazards, 46, 153-178.

Durukal E, Erdik M, Uçkan E (2008) Earthquake risk to industry in Istanbul and its management, Natural Hazards, 44, 199-212.

EMI (2015) A guide to measuring urban risk resilience. Principles, tools and practice of urban indicators, Pre-release draft. Earthquake and Megacities Initiative, Quezon City, Philippines.

Eren C, Luş H (2015) A risk based PML estimation method for single-storey reinforced concrete industrial building and its impact on earthquake insurance rates, Bulletin of Earthquake Engineering, 13, 2169-2195.

FEMA (1991) FEMA 224 - Seismic vulnerability and impact of disruption of lifelines in the conterminous United States, Federal Emergency Management Agency, Washington, D.C.

FEMA (2010) Multi-hazard loss estimation methodology. Earthquake Model. HAZUS – MH MR5 Technical Manual, Federal Emergency Management Agency, Mitigation Division, Washington, D. C.

GRF (2014) Global reinsurance: strengthening disaster risk resilience, The Global Reinsurance Forum, Basel, Switzerland.

HCA (2010) Employment densities guide. 2nd Edition, Document prepared for Homes & Communities Agency by Drivers Jonas Deloitte.

Hiete M, Merz M (2009) An indicator framework to assess the vulnerability of industrial sectors against indirect disaster losses, In Proceedings, 6th Conference on Information Systems for Crisis Management, Gothenburg, Sweden.

Hsu WK, Chiang WL, Chen CW (2013) Earthquake risk assessment and optimal risk management strategies for Hi-Tech Fabs in Taiwan, Natural Hazards, 65, 2063-2076.

Jain VK, Guin J (2009) Modeling business interruption losses for insurance portfolios, In Proceedings, 11th America Conference on Wind Engineering, San Juan, Puerto Rico.

Khazai B, Merz M, Schulz C, Borst D (2013) An integrated indicator framework for spatial assessment of industrial and social vulnerability to indirect disaster losses, Natural Hazards, 67, 145-167.

Kleindorfer PR, Saad HG (2005) Managing disruption risks in supply chains, Production and Operations Management, 14, 53-68.

Krausmann E, Cruz AM (2013) Impact of the 11 March 2011, Great East Japan earthquake and tsunami on the chemical industry, Natural Hazards, 67, 811-828.

Kroll C, Landis J, Shen Q, Stryker S (1990) The economic impacts of the Loma Prieta Earthquake: a focus on small business, Berkeley Planning Journal, 5, 39-58.

Kurita T, Annaka T, Fukushima S (2004) Seismic risk estimation for principal cities in Turkey, In Proceedings, 13th World Conference on Earthquake Engineering, Vancouver, Canada.

Li J, Crawford-Brown D, Syddall M, Guan D (2013) Modelling imbalanced economic recovery following a natural disaster using input-output analysis, Risk Analysis, 33, 1908-1923.

Lopes M, Pais I, Oliveira CS, Mota de Sá F (2012) Methodologies for the analysis of the seismic vulnerability of an industrial complex, In Proceedings, 15th World Conference on Earthquake Engineering, Lisbon, Portugal.

Merz M, Bertsch V, Rentz O, Gerdermann J (2007) Assessment of industrial asset values at risk, In Proceedings, 4th Conference on Information Systems for Crisis Management, Delft, the Netherlands.

Merz M, Hiete M, Comes T, Schultmann F (2013) A composite indicator model to assess natural disaster risks in industry on a spatial level, Journal of Risk Research, 16, 1077-1099.

Moat AM, Morrison AJT, Wond S (2000) Performance of industrial facilities during 1999 earthquakes: implications for risk managers, In Proceedings, Euro Conference on Global Change and Catastrophe Risk Management, Earthquake Risks in Europe, Laxenburg, Austria

Muir-Wood R (2011) Designing Optimal Risk Mitigation and Risk Transfer Mechanisms to Improve the Management of Earthquake Risk in Chile, OECD Working Papers on Finance, Insurance and Private Pensions, OECD Publishing.

Nakashima M, Lavan O, Kurata M, Luo Y (2014) Earthquakes engineering research needs in light of lessons learned from the 2011 Tohoku earthquake, Earthquake Engineering and Engineering Vibration, 13, 141-149.

Oliveira CS, Lopes M, Pais I, Ferreira MA, Mota de Sá F (2014) Reduction of seismic impacts at an industrial complex, In Proceedings, 2nd European Conference on Earthquake Engineering and Seismology, Istanbul, Turkey.

Olson DL, Wu D (2010) Enterprise risk management models, Springer - Verlag Berlin Heidelberg, Berlin, Germany.

Ouyang M (2014) Review on modeling and simulation of interdependent critical infrastructure systems, Reliability Engineering and System Safety, 121, 43-60.

Park JY, Cho J, Rose A (2011) Modeling a major source of economic resilience to disasters: recapturing lost production, Natural Hazards, 58, 163-182.

Porter K, Ramer K (2012) Estimating earthquake-induced failure probability and downtime of critical facilities, Journal of Business Continuity & Emergency Planning, 5, 352-364.

Porter KA, Kiremidjian AK, LeGrue JS (2001) Assembly-based vulnerability of buildings and its use in performance evaluation, Earthquake Spectra, 17, 291-312.

Potter SH, Becker JS, Johnston DM, Rossiter KP (2015) An overview of the impacts of the 2010-2011 Canterbury earthquakes, International Journal of Disaster Risk Reduction, in press.

Rose A, Lim D (2002) Business interruption losses from natural hazards: conceptual and methodological issues in the case of the Northridge earthquake, Environmental Hazards, 4, 1-14.

Rose A (2007) Economic resilience to natural and man-made disasters: multidisciplinary origins and contextual dimensions, Environmental Hazards, 7, 383-398.

Rose A (2009) A Framework for analyzing the total economic impacts of terrorist attacks and natural disasters, Journal of Homeland Security and Emergency Management, 6.

Rose A, Liao S (2005) Modeling regional economic resilience to disasters: a computable general equilibrium analysis of water service disruptions, Journal of Regional Science, 45, 75-112.

Rose A, Benavides J, Chang SE, Szczesniak P, Lim D (1997) The regional economic impact of an earthquake: direct and indirect effects of electricity lifeline disruption, Journal of Regional Science, 37, 437-458.

Sapountzaki K (2005) Coping with seismic vulnerability: small manufacturing firms in western Athens, Disasters, 29, 195-212.

Seifert I, Thieken AH, Merz M, Borst D, Werner U (2010) Estimation of industrial and commercial asset values for hazard risk assessment, Natural Hazards, 52, 453-479.

Shi Y, Jin S, Seeland K (2015) Modelling business interruption impacts due to disrupt highway network of Shifang by the Wenchuan earthquake, Natural Hazards, 75, 1731–1745.

Silva V, Crowley H, Varum H, Pinho R (2015) Seismic risk assessment for mainland Portugal, Bulletin of Earthquake Engineering, 13, 429-457.

Swiss Re (2004) Business Interruption Insurance, Swiss Reinsurance Company, Zurich, Switzerland.

Tierney KJ (1997) Business impacts of the Northridge Earthquake, Journal of Contingencies and Crisis Management, 5, 87-97.

UNDP (2013) Small businesses: impact of disasters and building resilience, Global assessment report on Disaster Risk Reduction prepared by United Nations Development Programme, Geneve, Switzerland.

Wenk T, Lacave C, Peter K (1998) The Adana-Ceyhan Earthquake of June 27, 1998, Report on the Reconnaissance Mission from July 6-12, 1998, Swiss Society of Earthquake Engineering and Structural Dynamics.

Weygandt JJ, Kimmel PD, Kieso DE (2013) Accounting Principles, 11th Edition. John Wiley & Sons, Incorporated.

Wu J, Li N, Hallegatte S, Shi P, Hu A, Liu X (2012) Regional indirect economic impact evaluation of the 2008 Wenchuan Earthquake, Environment Earth Science, 65, 161-172.

Xiao Y, Peacock WG (2014) Do hazard mitigation and preparedness reduce physical damage to business in disaster? Critical role of business disaster planning, Natural Hazards Review, 15.

Chapter 9

Industrial seismic risk assessment for Mainland Portugal

Araújo M, Castro JM, Marques M (2019) Industrial seismic risk assessment for Mainland Portugal, *Natural Hazards* (submission).

9.1 Summary

Industry plays a key role in the economy of a country, people welfare and socio-economic resilience to natural disasters. However, notwithstanding the negative impacts that earthquakes may cause to industrial property and activity, oftentimes resulting in businesses closure, production and job losses or damage to industrial buildings, the industrial building stock has been continuously excluded from seismic risk models developed for Portugal, as it is normally assumed that industrial buildings are expected to withstand strong earthquakes due to their lightweight and design governed by wind loads. The aim of this Chapter is thus to give a first contribution to the industrial seismic risk assessment at a national scale for mainland Portugal and to provide loss estimates to industrial property and production of most valuable importance to future emergency planning and seismic vulnerability reduction programs. Hazard and industry-specific exposure and vulnerability models, which set the basis of any risk assessment study, were developed, thoroughly evaluated and afterwards implemented in a web-based platform for seismic loss estimation recently developed at the University of Porto under the nationally founded PRISE project that provides user-friendly and interactive cloud-based computing and data visualization. The expected direct and indirect industrial losses to property, production and employment for a probability of exceedance of 10 % in 50 years were quantified.

9.2 Introduction

Portugal is the westernmost country of Europe and is supported by a high-income service-oriented economy, in which industrial activities contribute to around 21% of the national GDP and to around 24% of the country's employment (AICEP, 2015). Over the past few years, Portugal has been under external economic and financial assistance as a result of the European debt crisis that initiated in the year of 2009 and struck quite hardly the Portuguese economy, reducing the country's industrial production capacity to almost 70% (Bank of Portugal, 2015). Presently, in line with the current economic growth, the country's industrial capacity has been recovering and reaching pre-crisis levels, although, it still remains grounded on rather vulnerable microenterprises that fulfil 95% of the country's overall business structure and are heavily dependent on the domestic banking sector (European Commission, 2015). The lack of capital reserves and difficulties in securing loans were barriers found by many struggling microenterprises in previous earthquake events (Chang and Falit-Baiamont, 2002; Sapountazki, 2005). The Portuguese industrial structure is also characterized by highly localized clusters, mostly along the costal Porto-Lisbon corridor (Guimarães et al., 2004; 2007), associated to a large number of traditional sectors (e.g., tannery, jewellery, textiles, and footwear industries) and technologically advanced industries (e.g., tobacco, fabrication of pharmaceutical products, artificial and synthetic fibres, automobiles, and measuring and controlling devices). On the other hand, Portugal is located in a seismic-prone region exposed to offshore inter-plate seismic events of large to very large magnitude, e.g., the 1755 Lisbon earthquake, and to onshore intra-plate earthquakes with moderate to large magnitude, e.g., the 1909 Benavente (40 km away from Lisbon) earthquake (Silva et al., 2015a). As a result, the agglomeration of such an important share of the Portuguese industrial capacity around the Lisbon and Tagus Valley region, which together with the Porto-Aveiro-Braga industrial hub accounts for almost three-fourths of the countries' net industrial output, may be associated to potentially high industrial seismic losses, especially in the current economic panorama of greater vulnerability and recovery. Nevertheless, and notwithstanding the expected alarming scenarios for Portugal (Silva et al., 2015a; Oliveira, 2013; Sousa and Costa, 2015), e.g., Silva et al. (2015a) estimate that a future seismic event with a return period of 475 years will produce mean economic losses to the current residential building stock of around 30% of the Portuguese national GDP, and the increasing public awareness recently strengthened by a Parliament Resolution on seismic risk reduction and new

legislation on Critical Infrastructure Protection (Lopes et al., 2012), no risk studies have yet been conducted for Portugal incorporating an economic model that accounts for industrial losses.

Previous events have shown the devastating impacts that earthquakes may cause to fairly industrialized regions. In the aftermath of the 1999 Kocaeli earthquake, losses to industrial facilities and small businesses of around 2 and 1 billion dollars, respectively, were observed (Erdik, 2000; Durukal and Erdik, 2008; Durukal et al., 2008) and reached up to 7% of the Turkish national GDP when indirect socio-economic losses were included (Erdik, 2000). These economic losses were reported to represent almost 60% of the total industrial stock within that region (Cruz and Steinberg, 2005; Senel and Kayhan, 2010). The World Bank (1999) estimated that around 20000 small businesses terminated their operations leaving behind almost 140000 jobless people. More recently, the 2012 Emilia earthquake produced damage to 500 factories and disrupted other 3000. At least 15000 workers were laid off or lost their jobs. The importance of Emilia-Romagna region in the Italian national GDP (1%), which is considered crucial to the national economic recovery from the prevailing recession, may have severer mid- and long-term economic impacts (EPICentre, 2012). Unprecedented business interruption losses of 6.5 billion dollars and a staggering 100 billion dollars were also observed after the 1994 Northridge and 1995 Kobe earthquakes, respectively (National Academy of Sciences, 1999; Toyoda, 2008). The disruption of factories, utilities and ports within the Kobe region for almost a year generated direct and indirect losses in the economy of 5 to 10 times the structural losses (Cochrane, 1996). In 1999, the worst blackout ever in northern Taiwan caused by the Chi-Chi earthquake lead to indirect business interruption losses of around 2.2 billion dollars, mostly associated to semiconductor manufacturing and silicon processing firms, whose two week disruption generated a worldwide shortage of computer chips (Shaw, 2000). The share prices of Dell Computer went down 7% in a single day (Papadakis, 2000; Hsu et al, 2013). Likewise, the failure of a microcontrollers for automobiles producer plant located in the Tohoku region implied a generalized drop in the world's automobile production after the great 2011 earthquake and tsunami (Carvalho et al, 2014; Sampognaro and Sicsic, 2012). To sum up, the lessons learned from past events should aware and alert Portuguese companies, investors and public authorities to the potentially high industrial and economic seismic losses that the country may be exposed to.

This work hence aims to provide a first projection of the seismic losses to industrial property and economic activity at a national scale for mainland Portugal. The expected

economic stimulus due to rebuilding and construction (Cochrane, 1996) will not be taken into account, as the intention is to simply provide an estimate of the potential industrial capacity reduction and how it may cripple the national economy and hinder the resumption of normal activity. For such, comprehensive industrial exposure and vulnerability models were developed for mainland Portugal based on economic statistical information collected from the Portuguese National Institute of Statistics (INE), considering every industrial activity from the 2-digit Portuguese Standard Industrial Classification (CAE) system, and based on an extensive survey of more than 200 industrial building design projects and site-visits to national firms. The industrial property (i.e., structural and non-structural components and contents) and direct and indirect activity (i.e., stocks, relocation expenses and production losses) vulnerability functions proposed in Chapters 7 and 8 were herein extended to account for the uncertainty introduced by the variability in the characteristics of the existing industrial building stock. The hazard model, in turn, was constructed based on the ground-shaking used by Silva et al. (2015b) and rupture characteristics defined within the European SHARE project (Stuchi et al. 2013). The developed hazard, exposure, vulnerability models, which set the basis of any risk assessment study, were afterwards implemented in a web-based seismic loss estimation platform created at the University of Porto under the nationally founded PRISE project, which relies on the open-source OpenQuake engine developed within the Gobal Earthquake Model initiative (Silva et al., 2014) and provides user-friendly and interactive cloud-based computing and data visualization.

9.3 Industrial seismic risk model for Mainland Portugal

Seismic risk assessments typically involve the convolution of three distinct components, namely: (i) the seismic hazard, i.e. the probability of a seismic event striking a certain geographical area within a certain time-span; (ii) the physical and/or socio-economic vulnerability, i.e. the percentage of losses, commonly defined by the ratio between the repair cost and replacement cost of the building property or by business interruption related loss ratios, for increasing levels of seismic intensity; (iii) and, finally, the exposure model, i.e. the number and type of physical and financial assets at risk (Chapters 7 and 8). In the particular case of the quantification of the industrial seismic risk at national scales, holistic seismic risk models should be developed bearing in mind the need to account for: (i) industrial property losses, including structural and non-structural

components and contents (e.g. industry-specific machinery, equipment and furniture); (ii) industry-specific inventory (or stock) losses; (iii) business relocation expenses, i.e. the cost of renting additional spaces due to loss of function of the building to allow resuming production; (iv) and, industry-specific production losses, i.e. the loss of production due to business interruption; and by incorporating composite indicators of indirect industrial vulnerability that simulate the impact of input factor, infrastructures and supply chain disruptions. A deeper discussion on these various aspects and types of losses may be found in Chapter 8. Lastly, to better clarify every modelling assumption taken in the development of the present industrial seismic risk model for mainland Portugal, each component of the model, i.e. the hazard, the exposure and the vulnerability, will be presented and discussed below.

9.3.1 Hazard model

As noted by Oliveria (2008), great advances have been made in recent years to understand the tectonic setting in the vicinity of the boundary between the Eurasian and African plates where Portugal is located. However, since strong-motion data are still missing for major earthquakes, most hazard studies conducted up to date for Portugal simply rely on macro-seismic information (Vilanova and Fonseca, 2007). This lack of data that supports a unique comprehensive model for inter- and intra-plate regions, has resulted in the proposal of a number of seismic source models for Portugal, and corresponding recurrence rates (Sousa and Oliveira, 1997; Vilanova and Fonseca, 2007; Montilla and Casado, 2002). Moreover, the current database of instrumentally recorded seismic activity does not allow for the deduction of ground motion attenuation models compatible with the maximum magnitude values expected for those seismic sources (Rodrigues et al., 2014), being thus necessary to rely on studies developed for regions with similar crustal characteristics (Vilanova and Fonseca, 2007). The identification of reliable equations for the prediction of ground-motion parameters of interest, together with measures of uncertainty, which are the factor that probably influences most the seismic hazard (Crowley et al., 2005), have been the focus of most discussion in previous works (Villanova and Fonseca, 2007; Delavaud et al., 2012; Silva et al., 2015a), mainly with respect to the construction of logic trees capable of describing epistemic uncertainties that are to be considered in a seismic hazard analysis (Silva et al., 2014). In the present case study, it was considered reasonable to adopt the seismic source model recently developed for Europe and made available within the SHARE project (Stuchi et al. 2013) and the logic

tree proposed by Silva et al. (2015a) to account for ground motion epistemic uncertainties, which consists in the Atkinson and Boore (2006) and Akkar and Bommer (2010) ground motion prediction equations (GMPEs) applied to the whole region with weights of 0.70 and 0.30, respectively. The influence of site effects was accounted for similarly to the work of Silva et al. (2015a). At last, it may be also referred that a novel seismic hazard model for Portugal is currently being developed within the PRISE project that incorporates the ground motion attenuation relationships proposed by Rodrigues et al. (2014) and Carvalho (2007) for mainland Portugal based on the stochastic modelling of the seismic action and accounting for different soil types.

9.3.2 Exposure model

Quantitative risk assessments require the knowledge of the spatial distribution of physical and financial assets at risk on a disaggregated scale at an explicit raster level so as to be intersected with the hazard and the vulnerability of each individual asset at that same scale (Merz et al., 2007; Seifert et al., 2010). In other words, if industrial property risk maps are intended to be obtained, for every single industrial activity, with a county-level resolution, then the spatial distribution of the number of industrial buildings for each industrial activity, the replacement cost of the buildings (i.e. commonly defined in €/m^2) and the size of the buildings (i.e. in m^2) have to be provided for that same county-level resolution (Chapter 8). Moreover, industrial buildings with different structural typologies (e.g. precast RC buildings, lattice steel buildings or steel portal frame buildings) are expected to exhibit different levels of seismic vulnerability, and eventually different replacement costs and sizes. The modelling of the spatial distribution of the industrial building stock exposed to risk thus has to be also conducted distinguishing every single structural topology. Hence, ultimately, the exposure model should not only comprise the representation of the spatial distribution of industrial assets (e.g. production or inventory per m^2 and industrial activity; average building sizes, in m^2, per industrial activity; replacement or rental costs per m^2 ; number of industrial building or number of employees per industrial activity) at a national scale for mainland Portugal, but also the identification of categories of buildings, typically referred to as building taxonomies (Silva et al., 2015c; Bal et al., 2008b), associated to similar financial and physical levels of seismic vulnerability.

However, when data regarding post-earthquake damage levels are not available and no information exists with respect to the expected seismic vulnerability of different

building categories, analytical methodologies have to be employed both to predict the vulnerability of the existing building stock and to group it into different taxonomies (Silva et al., 2015c). These analytical methodologies involve the generation of a sufficient number of synthetic buildings representative of the existing building stock that should be afterwards seismically assessed to increasing levels of ground motion intensities so as to derive their corresponding fragility and vulnerability functions. The probabilistic modelling of such a wide range of synthetic buildings is made by assuming that the variation in the material properties and geometrical characteristics within a building category can be represented as a random variability, although, as noted by Crowley et al. (2005), this variation is an epistemic uncertainty since its exact distribution could be determine by detailed inspection of all buildings. Therefore, similarly to the work of Silva et al. (2015c), Crowley et al. (2004) and Bal et al. (2008a), probabilistic distributions were fitted to data of a set of geometric parameters of industrial buildings, with years of construction ranging from 1995 to 2014, obtained from the inspection of more than 200 blueprint drawings from design offices and steelworks companies. These distributions were posteriorly employed in the random generation of samples of buildings using simulation techniques, e.g. Monte Carlo Sampling Method or Latin Hypercube Sampling Method (Moore et al, 2009). The statistical parameters of the probabilistic distributions were derived using the maximum likelihood approach and the good-of-fit of each distribution was evaluated using the Chi-square test for significance levels of 1%, 5% and 10%. If any distribution satisfied the latter condition, the Kolmogorov-Smirnov test was alternatively applied for the same significance levels and the probability plots were visually inspected, being the best-fit assessed on the basis of a parametric bootstrap simulation on the correlation coefficient using 1000 samples.

After the random generation of each industrial building, the cross-section sizes of all structural members were designed in accordance with the Portuguese regulations that were in force over the past 50 years, so as to generate synthetic buildings that more accurately represent the lateral stiffness and strength of the existing Portuguese industrial building stock. Since most Portuguese practitioners have been simply designing industrial buildings to laterally withstand wind loads, particular attention was paid to past regulation that specifically addresses this issue. The wide range of random generated synthetic industrial buildings was, at last, statistically analysed based on their structural and dynamic characteristics in order to support the proposal of novel taxonomies for industrial buildings.

9.3.2.1 Spatial distribution of industrial assets at risk

The information on the existing Portuguese industrial assets at risk was taken from the Portuguese National Institute of Statistics (INE), which provides economic statistical data with a maximum resolution at the county level (Portugal Mainland has 278 counties). Every industrial activity of the 2-digit Portuguese Standard Industrial Classification (CAE) system was considered (28 industrial activities). This aggregation of assets at the county-level may be, however, rather inaccurate for a more detailed appraisal of the industrial loss potential, as the ground motion at the area centroid might be significantly different from that at the actual location of the assets (Silva et al., 2015a). To overcome this limitation, the assets were distributed by an evenly spaced grid with a 30 arc sec resolution based on additional information on the geographical distribution of industrial assets collected from the OpenStreet Maps, the European Environment Agency CORINE Land Cover inventory and from the AICEP Global Find platform. The distribution of the assets within the county was carried out considering the inverse distance weighting criterion, depicted in Figure 9.1 for the total number of industrial firms, which, as already pointed out in Chapter 8, was found to be identical to the number of industrial buildings. Another difficulty encountered in the definition of the assets was related with the fact that some information (e.g. annual production, annual cost of goods sold, etc.) was found to be occasionally missing in the INE database for specific counties and industrial activities. In order to cope with this difficulty, the missing data was replaced by assets predicted on the basis of a weighted percentage of the number of firms and employees of a certain industrial activity within a county. Such an assumption relies on the underlying rationale that regions with higher number of firms and employees are associated to a higher value of assets (Merz et al., 2007; Seifert et al., 2010). Finally, the procedure previously adopted in Chapter 8 to define the spatial distribution of daily industrial activity production values per m^2 and the expected industrial activity inventory ratios was equally followed herein, allowing to further estimate the industrial production and inventory (or stocks) losses. The former is defined with respect to downtime, which is commonly set in days. The replacement cost maps derived in Chapter 7 and the rental costs maps derived in Chapter 8, both for mainland Portugal, were herein refined to a 30 arc sec resolution and used to quantify the potential industrial property and business relocation losses.

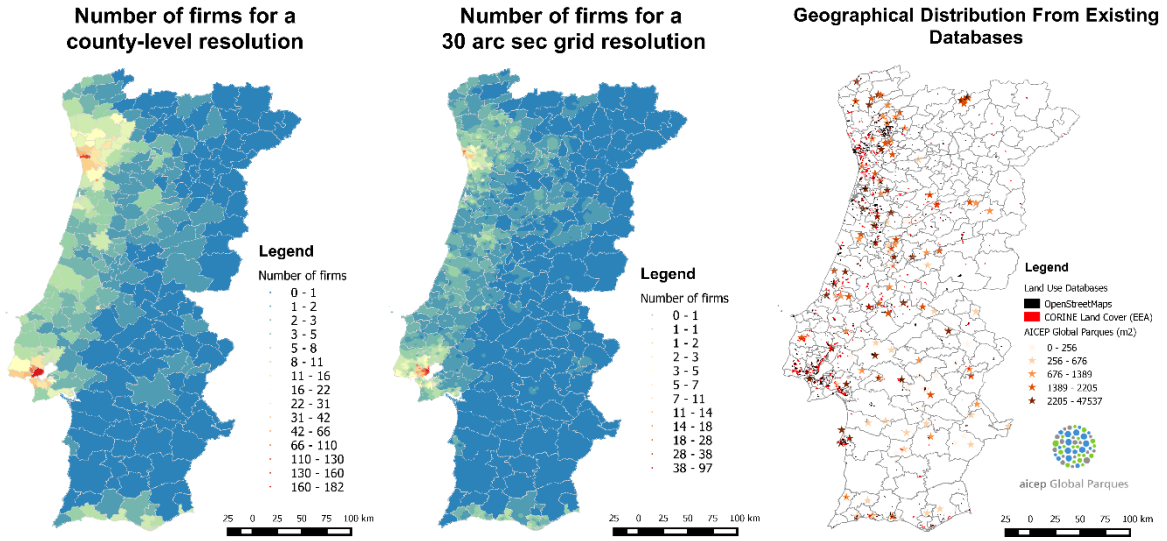

Figure 9.1 – Exposure models for mainland Portugal with a county-level resolution and a 30 arc sec grid resolution defined based on the geographical distribution of the industrial stock collected from existing databases.

9.3.2.2 Geometric characteristics of the as-built industrial building stock

A report recently elaborated within a European founded research project, the Precasteel project (RFCS, 2013), indicates that practically 60% of the Portuguese existing industrial building stock is made of steel, 30% refers to reinforced concrete structures and 10% uses other structural solutions. Despite the high vulnerability exhibited by the Italian pre-fabricated RC industrial building stock during the 2012 Emilia-Romagna earthquake, which resulted in substantial building collapses, mostly due to the brittle failure of the pre-fabricated RC girders and columns joints (Casotto et al., 2015), this type of building typology was not examined herein for simplicity as a result of its lower level of exposure in comparison to the industrial steel building stock. Regarding the latter, it was observed from the conducted survey that 30% of the as-built Portuguese steel buildings stock adopts lattice structures and that 70% was built with portal frame structures. This distribution of building typologies is in complete agreement with that indicated by the Precasteel project (RFCS, 2013), therefore validating the information collected in the conducted survey and following statistical analyses. In order to streamline the presentation and interpretation of the collected data, namely the fitting of the probability distribution functions to the buildings' geometrical parameters that will support the random generation of a wide range of synthetic industrial steel buildings, a brief discussion on the main features of the as-built Portuguese industrial building stock is presented below.

- *Dependence on the type of industrial activity*: No statistical evidence was found that supports the dependency of the structural typology (e.g., portal frame or

lattice structures) on the industrial activity, as it could be previously anticipated since lattice buildings typically have greater dimensions, when comparing to portal frame buildings, and could tend to be associated to industrial activities, rather than warehousing. By disaggregating the collected information, such a dependency was not found to exist, as 57% of lattice buildings and 45% of portal frame buildings were seen to be associated to light industry, respectively, while the remaining 43% and 55% were seen to be associated to warehousing. These percentages are, in fact, in accordance with the Precasteel project (RFCS, 2013), which refers that 45% of the Portuguese as-built industrial building stock is associated to light industry, 45% to warehousing and only 10% to heavy industry.

- *Structural Steel Class*: Most buildings inspected (93%) were built with a structural steel of class S275 and a small minority (7%) was built with a structural steel of class S235.
- *Number and distance between consecutive frames*: On the basis of logistic regression analysis (Moore et al., 2009), statistical dependency was found to exist between the number (p-value = 0.01) and distance of frames (p-value = 0.07) and the building typology. Whereas lattice structural solutions are mainly adopted in longer buildings, i.e. with more than 15 frames and a spacing between them that can reach 18m, portal frame solutions are usually used in shorter buildings, with 3 to 15 frames and a spacing between them lesser than 8m. With respect to the fitting of the probability distribution functions, it was found that the number and distance between consecutive frames of lattice buildings follow a lognormal distribution, with mean and coefficient of variation shown in Figure 9.2, satisfying the Chi-square and Kolmogorov-Smirnov goodness-of-fit tests for a significance level of 1%. In turn, regarding the portal frame buildings, the number of frames was found to follow a normal distribution and the distance between consecutive frames follow a lognormal distributions, Figure 9.3, passing the Kolmogorov-Smirnov test with a significance level of 1%. According to discrete information provided by the Precasteel project (RFCS, 2013), 65% of the Portuguese industrial buildings have up to 11 frames and 90% have a spacing between 5m to 7m. Confronting these values with those obtained from the fitted probability distribution functions, i.e. 78% of the

buildings have up to 11 frames and 84% have a spacing between 5m to 7m, one may conclude that they are in somehow good agreement.

- *Number and length of spans:* The Portuguese as-built industrial steel building stock typically displays a single span (65%), a small percentage displays two (17%) or three (11%) spans and a minority displays more than four spans (7%). It should be noted, however, that although industrial steel buildings with multiple spans refer to a small share of the existing industrial building stock, this building typology can be more susceptible to seismic actions as a result of the common removal of internal columns for space optimization and accommodation of the production layout. Similarly to previous geometric parameters, it was found that the length of spans follows a lognormal distribution, satisfying the Chi-square test for a significance level of 1%, as depicted in Figure 9.2 and Figure 9.3. On average, the span length was seen to be around 23m in the case of lattice structures and around 20m in the case of portal frame structures. According to the Precasteel project (RFCS, 2013), 15% of Portuguese buildings have spans with less than 20m, 50% have spans between 20m to 25m, 25% have spans between 25m and 30m and 10% have spans with more than 30m. Confronting this percentages with those obtained using the probability distribution functions fitted for lattice structures, values of 16%, 56%, 24% and 4%, were obtained, respectively, thus strongly supporting the collected data. Still, these values were seen to diverge from those obtained for portal frame structures, which are around 48%, 46%, 5.8% and 0.2%, respectively, and reflect the lower span lengths exhibited by this building typology. Furthermore, by conducting correlation analyses between the span length and the remaining geometric parameters, a moderate and positive correlation, i.e. coefficient of correlation ρ of 0.41, between the span length and the number of frames was found to exist, which could be previously anticipated due to space implications and needs. At last, it should be referred that IPE cross-section profiles were seen to be typically adopted in portal frame structures (90%) and that, on average, the portal frame girders exhibit a 7º slope that follows a lognormal distribution with the parameters presented in Figure 9.3. Current practices in Portugal consist on adopting hunched bolted column-to-girder connections with haunch lengths that vary from 10% to 20% of the span length.

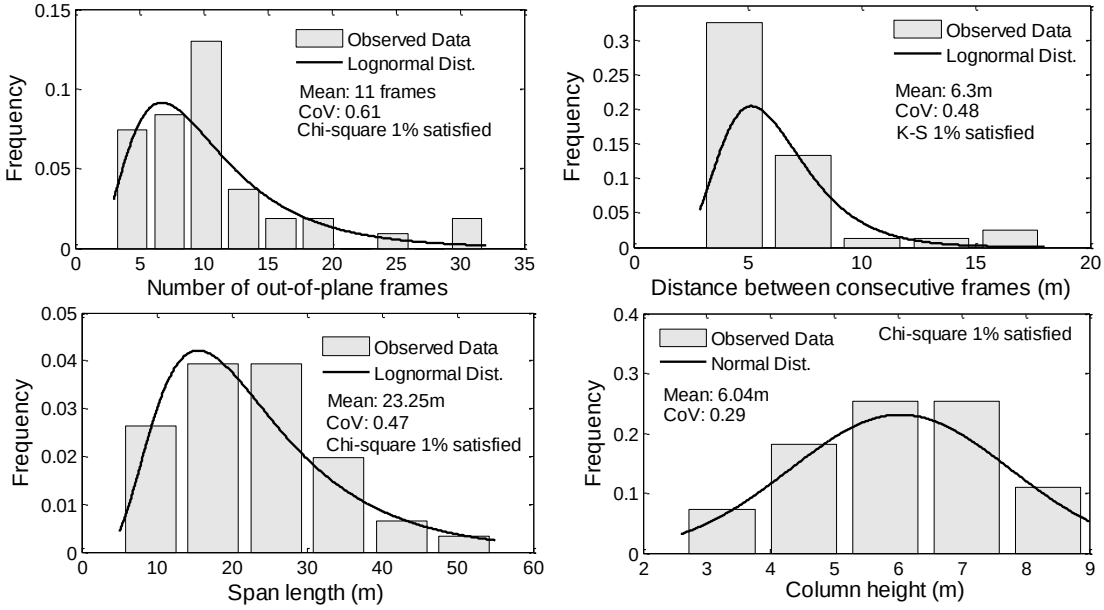

Figure 9.2 – Fitting of probability distributions to the geometrical characteristics of industrial lattice buildings.

- *Type and height of columns:* Generally speaking, it was seen that RC columns are usually adopted in lattice buildings (75% of cases) and that steel columns are characteristic of portal frame buildings (95% of cases), being used with more frequency, in the latter case, IPE cross-section profiles (75%). Once again, on the basis of regressions logistic analysis, a statistical dependence between the height of columns and the number of floors was found to exist (p-value = 0.02), as previously expected. Nevertheless, since only 6% of the collected buildings has more than one floor, it was assumed that this building typology is not representative of the existing building stock. Furthermore, it was observed that the height of columns, for both lattice and portal frame structures, follow a lognormal distribution with parameters presented in Figure 9.2 and Figure 9.3, satisfying the Chi-square test for a significance level of 1%.
- *Structural systems in the transverse and longitudinal directions:* The collected information indicates that the Portuguese industrial steel building stock is typically characterized by unbraced moment-resisting frame systems in the in-plane transverse direction. This information is in agreement with that of the Precasteel project (RFCS, 2013), which refers that in-plan moment-resisting frames represent 90% of the Portuguese building stock and that only 10% is characterized by systems with concentric or eccentric braces. In turn, in the

longitudinal out-of-plane direction, it was observed that 70% of portal frame buildings are braced, mostly with diagonal concentric braces, and that 74% of lattice buildings adopt common moment-resisting frame solutions. Again, on the basis of logistic regression analysis, statistical dependencies between the use of bracing system and the year of construction (p-value = 0.03) and between the use of bracing system and the height of columns (p-value = 0.02) were found to exist. These dependencies may be explained, on the one hand, by the fact that lattice structures have been more commonly adopted in the past, which, as already referred, are typically characterized by in-plane moment-resisting frames, and, on the other hand, by the fact that higher columns tend to be associated to unbearable flexural demand levels in the direction of the weak axes, thus requiring the use of bracing systems.

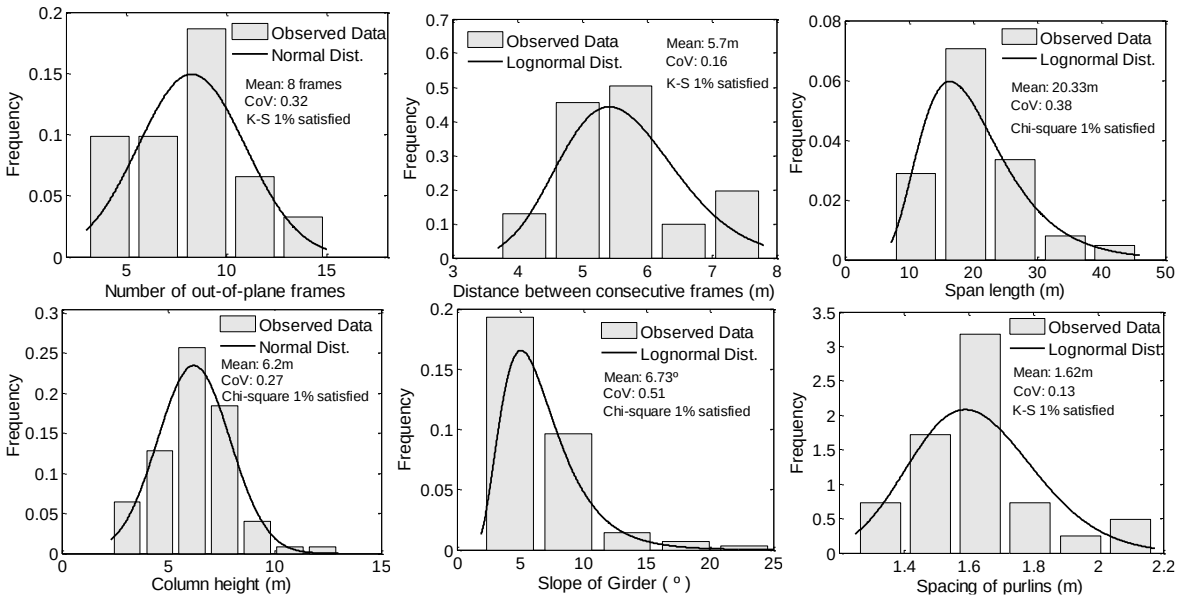

Figure 9.3 – Fitting of probability distributions to the geometrical characteristics of industrial portal frame buildings.

- *Type of column base plate connections:* Although it was not possibly to identify any tendency on the most common type of base plate connections adopted in Portugal, two major groups were defined: (i) exposed base plate connections with single rows of four bolts outside both flanges of the column cross-section, herein designated as SBPC connections. These connections typically have plates with 25mm thickness and a high 1.7 times greater than the height of the column cross-section. M22 anchor bolts of 8.8 class with a length of 500mm, concrete footing of C20/25 class, 60MPa grouting with 35mm thickness, S275 steel grades and welds with 8mm are usually adopted; (ii) and, exposed base plate

connections with single rows of two or three bolts at both sides of the web and inside the flanges of the column cross-section, designated as PBPC connections. In this case the base plate typically has a height equal to that of the column cross-section and M20 anchor bolts are adopted.

- *Non-structural components:* The disaggregation of the collected information allowed observing that 90% of the inspected buildings adopt sandwich panels on the roof and that the remaining 10% have roofs made of fibrocement. In turn, with regard to side claddings, whilst 7% of the inspected buildings have masonry walls, the reaming buildings use corrugated metal sheets (52%) and sandwich panels (41%). Moreover, it was additionally observed that the existing industrial building stock typically adopts cold-formed steel purlins (78%), usually with Z cross-section profiles (54%) and U or L cross-section profiles (24%), having an average spacing between them of 1.62m. The latter was found to follow a lognormal distribution as depicted in Figure 9.3.

Since the use of overhead travelling cranes is mostly related to heavier industrial activities (RFCS, 2013), their influence will be neglected herein, although being recognized the importance of such components on the dynamic response of industrial buildings and the potential losses that their failure and falling down may cause in the contents below, as observed in previous earthquake events (Moat et al., 2000).

9.3.2.3 Portuguese codes for design of industrial steel buildings

Due to the prevalence of industrial steel buildings in the Portuguese industrial building stock, which are typically characterized by portal frame solutions, the revision of past Portuguese regulations that provide guidance to the design of industrial buildings will be oriented towards the specific case of industrial portal frame steel buildings. This type of structural solution was implemented in Portugal around 30 years ago.

The first design code specifically dedicated to the design of steel buildings in Portugal, hitherto based on other European regulations and specifications preconized within the design code for steel bridges (RPM, 1929), was introduced in the mid-60s (REAE, 1965). This code was mainly based on the allowable tension method and incorporated local instability phenomena by importing specific design criteria form the Belgium code in force at that time. A single commercial mild steel type with a characteristic yield strength of 210 MPa was available. The introduction of REAE was triggered by the publication of RSEP (1961), which was the first code to provide

provisions regarding the definition of design actions and loads for buildings and bridges. Later, in 1983, RSEP was replaced by a new and more demanding design code, the RSA (1983), which is still the most commonly used nowadays (Chapter 1 and 2). Again, the introduction of this new code motivated the revision of REAE, and a final version was published in 1986 reflecting the European normalization efforts promoted by the European Convention for Steel Construction and the CEB European International Concrete Committee. These efforts resulted, in the early 90's, in the introduction of Eurocodes in Portugal, in particular of Eurocodes 1 and 3, and their constant subsequent revised versions.

With respect to the seismic design of industrial steel buildings, it is typically assumed by Portuguese practitioners that this type of structures is expected to withstand strong earthquakes due to its lightweight and design governed by wind loads, thus neglecting seismic design. As a result, the evolution of the wind load prescriptions for Portugal over the past 50 years is key to understand the actual seismic vulnerability of the existing Portuguese industrial steel building stock. In brief, the first prescriptions for wind design were introduced by RSEP (1961) and two wind zonations were defined: (i) areas very exposed to wind loads located in altitudes greater than 600m or at a 5km coastal strip; (ii) and areas with normal exposure referring to the remaining territory. These areas are associated to reference wind velocities of 38m/s and 35m/s, respectively, and no reference is made to the terrain aerodynamic roughness, so that the evolution of the wind velocity with the height of the building is simply provided by a single abacus defined regardless the surrounding terrain characteristics. RSA (1983) adopted the same wind zonations and introduced two terrain roughness types: (i) a type I roughness that refers to urban areas characterized by mid- and high-rise buildings; (ii) and a type II roughness that refers to the remaining locations, being thus representative of industrial areas. Wind velocities of 42.9m/s and 39m/s, which correspond to mean wind velocities of 27.5m/s and 25m/s, were defined for terrains with type II roughness in very exposed and normally exposed areas, respectively. For terrains with type I roughness the values previously proposed by RESEP were adopted. At last, the recent Portuguese National Annex of part 4 of Eurocode 1 (CEN, 2010) adopted the same wind zonations, although a set of new terrain roughness categories has been additionally introduced. Terrains of types II and III are those that better associate to industrial areas and have mean wind velocities of 30m/s and 23m/s for very exposed areas and mean wind velocities of 27m/s and 20m/s for normally exposed areas, respectively. These values are somewhat similar to those provided by RSA. Therefore,

summing up the above review on the evolution of the Portuguese wind design provisions, it may be overall concluded that the Portuguese wind design criteria have not suffered significant changes over the last 50 years and thus, since the REAE design prescriptions are in general identical to that of Eurocode 3, no significant variations in the seismic vulnerability of the existing industrial steel building stock have been introduced.

Hence, the wide range of random generated synthetic industrial steel buildings was herein designed according to RSA, as it is still typically adopted by Portuguese practitioners nowadays (Chapter 2 and 3), and to Eurocode 3 (CEN, 2005), with the confidence that they will conveniently represent the actual lateral stiffness and strength of the existing industrial steel building stock. Furthermore, it should be referred that wind effects are expected to be more relevant in buildings with height-to-span ratios greater than 0.5 or located in regions of high dynamic pressure, e.g., at higher altitudes, (SCI, 2004). Snow loads will equally play a key role in the design of portal frame structures, particularly for industrial buildings located at higher altitudes. RSA defines more demanding snow design criteria when compared to Eurocode 1 (Simões et al., 2007), and to some extent to RSEP, excepting for altitudes lower than 200m where RSA and RSEP preconize that no snow design is needed. Although the use of RSA will most probably result in structures located at higher altitudes with higher lateral stiffness and strength, thus structurally less vulnerable to seismic losses, it will be used herein, once again, since it has been widely adopted in the past by Portuguese practitioners.

9.3.2.4 Taxonomies for industrial steel buildings

The proposal of novel taxonomies for industrial buildings will be herein carried out based on the statistical analysis of the dynamic and structural responses of the wide range of random generated synthetic buildings. For the sake of simplicity, and bearing in mind the information collected in the survey, the sampling of synthetic buildings representative of the Portuguese industrial building stock was performed assuming the as-built portfolio to be simply characterized by industrial portal frame steel buildings. The geometric probabilistic distributions presented above, as well as information collected from literature on the probabilistic characterization of the material properties of structural steel and the capacity of steel members, were applied to randomly generate the wide range of synthetic buildings using a multivariate Latin Hypercube method for spurious correlation reduction in the generated sample (Owen, 1994; Olsson et al., 2003; Marques, 2011). The uncertainty in the behaviour of beam-column elements was modelled based on the recent work of

Kazanti et al. (2014). This work provides a probabilistic characterization of the behaviour of steel components that relies on the numerical model adopted in Chapter 7 to simulate the response of steel elements, which is also adopted herein. It was assumed that the construction of the steel members followed regular (i.e., average) construction practices. Furthermore, the uncertainty in the material properties of structural steel, namely the yield and the ultimate tensile strengths and strains of structural steel S275, was defined based on the information provided by Melcher et al. (2004), Kala et al. (2009) and Simões da Silva et al. (2009). These random variables were the input for the brace component model used herein to simulate the response of both lateral and roof bracing systems, which is defined by two force-based fiber elements and two gusset plate rotational springs at each end that aim at capturing global buckling phenomena (Chapter 7). Geometrical imperfections in the thickness of the CHS cross-section of braces were equally accounted for assuming an identical level of uncertainty to that of regular I profiles (Melcher et al., 2004; Kala et al., 2009). Due to the reduced Whitmore widths and plate thicknesses of the gusset plates, which are associated to low rotational stiffness values, and consequently, to a pinned behaviour (Chapter 7), no variability was included in these elements. At last, the variability in the response of base plate connections was modelled based on the study recently carried out by Latour and Rizzano (2013). Since this work simply provides an idea of the uncertainty associated to the maximum strength of base plate connections, and no information may be found on the literature regarding the uncertainty associated to their stiffness and deformation capacity, similar levels of variability were assumed for the strength, stiffness and deformation capacity of base plate connections. The random generated synthetic buildings consist of complex 3-dimentional numerical models constructed using OpenSees (PEER, 2011) with a moment-resisting portal frame in the transverse *x*-direction and a braced system with diagonal braces in the longitudinal *y*-direction, in accordance with the most common Portuguese practices. The numerical models have been developed with the aim of capturing all main failure mechanisms observed in industrial steel buildings in previous post-earthquake reconnaissance campaigns. A thorough discussion on the various modelling assumptions adopted may be found in Chapter 7, whose numerical model sets the basis of the present work.

To simulate the impact of the geographical location of the buildings in the seismic vulnerability of the portfolio, and by acknowledging, as previously referred, the importance of the altitude in wind and snow designs, six groups of fifty industrial buildings were generated and designed to gravity, wind and snow loads considering values of

altitude of 100m, 250m, 400m, 600m, 800m and 1000m, respectively. Moreover, since any tendency was identified in the survey regarding the most common type of column base plate connections, the six groups of fifty buildings were designed, firstly, assuming fixed connections at the base of columns and, afterwards, assuming pinned connections at the base of columns. The objective was to create groups of buildings that reflect the uncertainty in the seismic vulnerability of the industrial building stock introduced by the influence of different support conditions. Hence, three distinct support conditions were assumed in the present case study: (i) a totally fixed condition, designated as FBPC; (ii) a semi-rigid condition that considers the SBPC connections identified in the survey; (iii) and a nominally pinned condition that considers the PBPC connections identified in the survey.

A modal analysis was firstly carried out to assess the dynamic characteristics of the synthetic buildings and their fundamental periods of vibration. When analytical methodologies are employed to derive vulnerability and exposure models, it is important to verify whether the structures that are being generated are reasonable and in agreement with the real characteristics of the building stock (Silva et al., 2015c). Information on the real dynamic properties of industrial steel buildings is scarce, particularly for Portugal. One of the very few works conducted up to date was carried out by Lamarche et al. (2009). In this work, the results of an ambient vibration testing campaign on single storey steel frame buildings, both under service and construction conditions, located in Canada is presented. However, practically all tested buildings have bracing systems in both longitudinal and transverse directions, thus displaying fundamental periods of vibration more representative and similar to the average *y*-direction longitudinal period of vibration of 0.3s of the portfolio of generated assets. In order to assess the *x*-direction longitudinal period of vibration, some values made available by Lamarche et al. (2009) had to be filtered. The comparison between the *x*-direction period of vibration of the synthetic collection of assets with different support conditions and the real measured data is presented in Figure 9.4. Although it may be readily concluded that the measured periods of vibration seem to be in agreement with those obtained herein, the real periods of vibration are still somehow lower than the ones analytically obtained. This may be due to the fact that, again, the real data respect to single-storey braced steel frame buildings, but also, and most importantly, due to the influence of non-structural (e.g. cladding) components. By measuring the fundamental periods of vibration of steel buildings under the construction phase (i.e. without non-structural components) and at service (i.e. with non-structural components), Lamarche et al. (2009) observed that the introduction of non-structural components may reduce the

fundamental period of vibration of single storey industrial buildings up to 34%. Nevertheless, it was considered that the developed numerical models provide fairly reasonable results, although further studies may be additionally conducted in the future to assess the influence of flexible diaphragms (Shrestha, et al. 2009) in the seismic vulnerability of industrial steel buildings.

Secondly, multivariate regression analysis and ANOVA analysis (Moore et al., 2009) were employed, on the one hand, to evaluate if any strong statistical dependency exists between the fundamental period of vibration and any geometrical parameter of the buildings, which would allow the proposal of novel prediction equations for industrial porta frame steel buildings, and, on the other hand, to understand whether or not the buildings can be grouped into different taxonomies according to the statistics of the periods of vibration. It was found that the geometric parameters with greater inference on the fundamental period of vibration in the *x*-direction vary with the type of support condition. In the FBPC case, the ratio between the height of the building, H, and the height of the column cross-section, h_c, was found to have greater explanatory power with respect to period of vibration (p-value = 0; r^2 = 0.79). In turn, in the SBPC and PBPC cases, the height of the building (p-value = 0; r^2 = 0.75) and the column base plate connection stiffness ratio (p-value = 0; r^2 = 0.79), which is given by $S_{j,ini}H$ / (EI_c), where $S_{j,ini}$ is the initial stiffness of the base plate connection, I_c is the inertia of the column cross-section and E is the elastic modulus of steel, where found to have greater statistical inference on the periods of vibration of the SBPC and PBPC buildings. Based on this findings, the following prediction equations for the quantification of the fundamental period of vibration in the transverse direction of industrial portal frame steel buildings with fixed, T_{FBPC}, semi-rigid, T_{SBPC}, and nominally pined base plate, T_{PBPC}, are proposed, being associated to goodness-of-fit coefficients of determination, r^2, equal to 0.63, 0.65 and 0.73, respectively.

$$T_{FBPC} = 28.19\frac{\mathrm{H}}{\mathrm{h_c}} + 0.61$$

$$T_{SBPC} = 0.022\mathrm{H} + 0.014\frac{\mathrm{S_{j,ini}}H}{\mathrm{EI_c}} + 0.136 \tag{9.1}$$

$$T_{PBPC} = 0.046\mathrm{H} + 0.029\frac{\mathrm{S_{j,ini}}H}{\mathrm{EI_c}} + 0.067$$

It should be referred that these expressions may be of great interest, not only, to promptly estimate the dynamic characteristics of the Portuguese industrial steel building stock, but

also in studies focused on the seismic risk assessment and prioritization of industrial portfolios (Petruzzelli, 2013). With respect to the ANOVA analysis, the aim of this statistical technique is to test the null hypothesis that all sample means (e.g., the mean period of vibration of different groups of buildings) are equal. A *p*-value under this null hypothesis lower than a certain significance level, say 5%, will suggest its rejection, meaning that at least one sample mean is significantly different than the other sample means (Moore et al., 2009). This rejection would imply, in this particular case, that at least one group of buildings would have mean dynamic properties, and eventually mean seismic responses, significantly different from other groups. Grouping the collection of assets according to the height of the building and the altitude was found to reject such null hypothesis (*p*-value < 0.05). Furthermore, multiple comparisons, i.e. analysis of variances from one group to the others, where conducted to understand how the buildings should be grouped. Hence, as depicted in Figure 9.4, it was found that buildings with heights lower than 5.5m have dynamic properties (i.e. period of vibration) statistically different (*p*-value < 0.05) from buildings with heights between 5.5m and 6.7m and buildings with heights greater than 6.7m. In turn, buildings located at altitudes lower than 100m and higher than 1000m have periods of vibration significantly different from buildings at other altitudes.

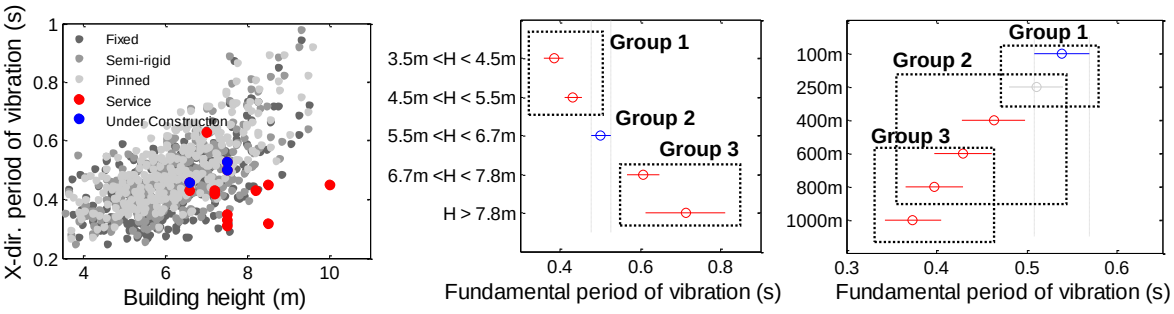

Figure 9.4 – Comparison between the period of vibration of the collection of assets with real data obtained by Lamarche et al. (2009) based on ambient vibration testing (*left*) and multi comparisons ANOVA analysis with respect the height of the building (*middle*) and altitude (*right*).

Based on the foregoing, six taxonomies for industrial portal frame steel buildings were considered regarding the level of design to wind actions, namely: (i) low wind design (LWD), i.e. altitudes lower that 100m; (ii) average wind design (MWD), i.e. altitudes between 100m and 800m; (iii) and high wind design (HWD), i.e. altitudes higher than 800m; and regarding the building height, namely: (i) low height buildings (LH), i.e. height lower than 5.5m; (ii) and high height buildings (HH), i.e. height greater than 5.5m. It was considered reasonable, and for simplicity, to group the buildings with heights between 5.5m and 6.7m with the buildings with heights greater than 6.7m. The proposed

taxonomies were validated by inspecting the overall stiffness and strength of the buildings of each taxonomy based on their mean capacity curves (Figure 9.5). The total base shear of the buildings was divided by their length to allow for the comparison between them. It may be additionally observed from the inspection of Figure 9.5, as expected, that the type of base plate connection will also constitute a different taxonomy. Buildings with SBPC connections, which are oftentimes adopted by Portuguese practitioners as fixed supports, exhibit a markedly lower lateral stiffness and strength when compared to buildings with FBPC connections.

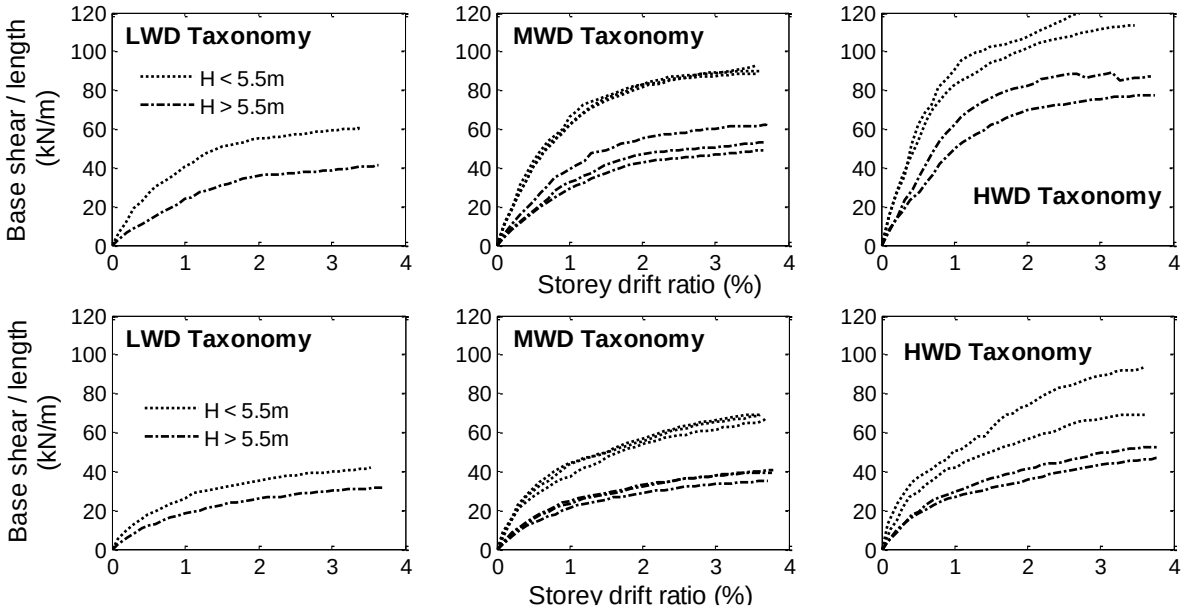

Figure 9.5 – Capacity curves obtained for each taxonomy assuming fixed FBPC connections (*upper*) and semi-rigid SBPC connections (*lower*).

Finally, the assets were geographically distributed according to their taxonomy, namely to the altitude at which they are located and their height. Based on the normal distribution fitted to the height of industrial portal frame steel buildings (Figure 9.3), it may be readily estimated that LH buildings (i.e. height lower than 5.5m) correspond to 33.7% of the industrial building stock, whereas HH buildings (i.e. height higher than 5.5m) correspond to the remaining 66.3%. The assets were geographically distributed for the whole country according to this percentages. With respect to the altitude, an altimetry map for mainland Portugal was defined with a 30 arc sec resolution based on information provided by the DIVA-GIS Database. The assets were thus accordingly geographically distributed, as depicted in Figure 9.6.

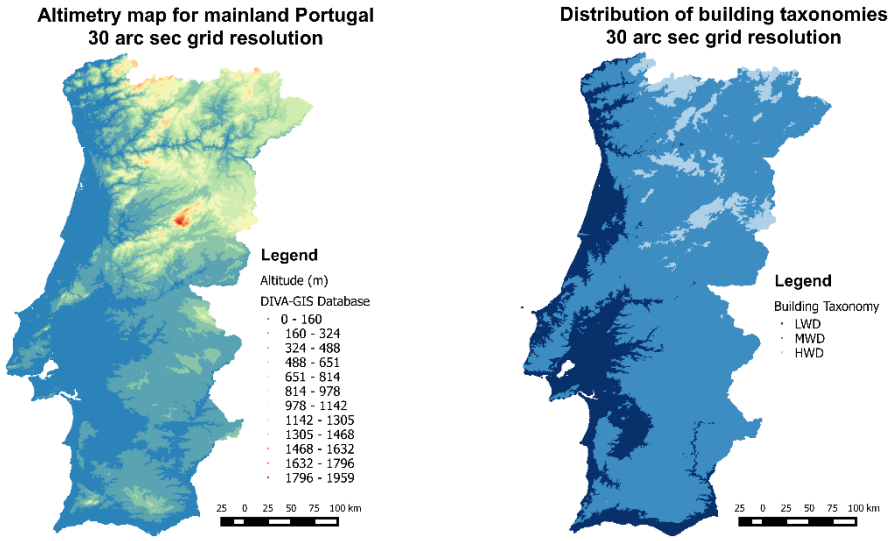

Figure 9.6 – Altimetry map for mainland Portugal (*left*) and geographical distribution of assets by taxonomy (*right*).

9.3.3 Vulnerability model

To analytically derive the present vulnerability model, the collection of synthetic assets generated was subjected to a suit of twenty ground motion records selected and scaled using the Generalized Conditional Intensity Measure approach proposed by Bradley (2010). The geometric mean of the 5% damping spectral accelerations of the two horizontal *x* and *y* components at the transverse fundamental period of vibration T_x, $S_{a,x}$ (T_x, 5%) and $S_{a,y}$ (T_x, 5%), respectively, was set as main intensity measure for record selection and scaling. To keep the computational effort at a reasonable level, the ground motions were cut off based on their significant duration, which is defined by the length of time over which the Cumulative Arias Intensity is between 5% and 95%. Thousands of bi-direction nonlinear dynamic analysis were conducted using OpenSees with the aim of assessing the response of the building portfolio in the most critical *xy*-direction of analysis identified in Chapter 7. Although it has been shown in Chapter 7 that the ground motion directivity may introduce differences in the loss estimates that may reach 60%, thus the consideration of the most critical direction of analysis will most probably lead to conservative estimates of losses, it was still considered reasonable due to the impracticability of conducting various multi-directional analyses. Structural, non-structural drit- and acceleration-sensitive and contents fragility functions (i.e. probability of exceeding a number of limit states for a set of intensity measure levels) were afterwards derived. The structural damage states proposed in Chapter 7 and non-structural and contents damage states defined within the Hazus – MH MR5 framework (FEMA, 2010)

were adopted. The fragility functions were convoluted with the consequence model (i.e., loss ratios) defined in Chapter 7, which relies on the mean loss ratios proposed within the Hazus – MH MR5 framework and models uncertainty through a multi-variate random generation of loss ratios using Copulas, to finally derive the vulnerability functions for each building taxonomy. Moreover, due to the fact that the property losses, which include losses to structural and non-structural components and contents, may vary according to the type of industrial activity, i.e. industrial sectors with a higher capital demand (e.g., machinery and equipment and value of production equipment) might be hit harder by earthquakes, as well as business losses (i.e. losses to inventory or stocks or losses to production), the building taxonomies previously defined were extended to include the 27 industrial activities of the 2-digit Portuguese CAE classification system. Overall, 486 vulnerability functions were derived for every combination of building taxonomies, including the type of column base plate connection, and industrial activities.

The industrial economic impacts of earthquakes may be distinguished between direct and indirect impacts to property and production (Rose, 2004; Merz et al., 2013; Khazai et al., 2013). Whilst direct impacts to property comprise losses to structural, non-structural components and contents, direct impacts to production mainly result from the length of production downtime, i.e. business interruption, which may be caused by the loss of function of the building as a result of the former direct losses to property (i.e., loss of use of collapsed buildings, broken equipment and disarrayed production lines or loss of access to buildings red or blue tagged in emergency responses in the aftermath of an earthquake event). Moreover, the disruption of forward and backward linkages of supply chains and outages in critical infrastructures (e.g., electricity and water services, transportation networks, ports, etc.) may have significant indirect impacts to production, which, as observed in the practically one year disruption of utilities and ports within the Kobe region (Cochrane, 1996), may imply significant ripple effects into the economy. Indirect impacts to property may equally occur a result of hazard material releases or ancillary fires, which may trigger highly devastating, though rare, cascading effects and technological accidents (Cruz and Okada, 2008). Although acknowledging the extreme relevance of this indirect impacts to property, they will not be included herein. Indeed, further studies should be conducted aiming to assess the risk of occurrence of such technological accidents in Portugal and to support emergency and contingency planning. Businesses have also demonstrated in previous earthquake events to have high capacity of recovery, i.e. economic resilience, through renting of alternative spaces to resume production or by

recapturing lost production, i.e. rescheduling of lost production at a later date by overtime work or working extra shifts (Rose, 2007; Park et al, 2010). Based on the foregoing, vulnerability functions, i.e. percentage or measure of losses for increasing levels of seismic intensity, were derived accounting for direct losses to property and inventories, relocation expenses due to renting of alternative spaces to resume production and production losses due to business interruption. The industrial indirect vulnerability will be modelled similarly to the work conducted in Chapter 7.

9.3.3.1 Property and inventory vulnerability model

Figure 9.7 presents mean and 5%-95% quantile property vulnerability functions derived based on the methodology proposed in Chapter 7 for different building taxonomies and two, i.e. food and pharmaceutical, industrial activities. Three main observations may be readily drawn from the inspection of Figure 9.7, namely: (i) HWD-LH taxonomy buildings with FBPC connections, i.e. located at altitudes greater than 800m and with height lower than 5.5m, exhibit higher loss potential comparing to other taxonomies. This is due to the fact that this category of buildings is associated to an overall higher lateral stiffness (Figure 9.4), thus potentially reaching higher levels of acceleration demands, which, as shown in Chapter 7, contribute the most to total property losses (i.e. non-structural acceleration-sensitive components and contents). A remark should be made on the deviations between the vulnerability functions at lower S_a (T_x) levels, which are associated to higher probabilities of occurrence, and thus have greater impact on loss quantifications; (ii) similarly to the latter, buildings with more flexible column base plate connections (e.g. PBPC connections), which tend to develop higher drift demands in non-structural drift-sensitive components, although with lesser importance in total property loss quantifications, are generally associated to lower seismic vulnerability levels. In the considered *xy*-direction of analysis, structural damage was found to be mostly governed by lateral braces, permanent drifts and base plate connections, similarly to what was observed in Chapter 7, however, like non-structural drift-sensitive cost ratios, structural repair cost ratios are expected to have lower impact in total building replacement costs when compared to non-structural acceleration-sensitive components and contents; (iii) industrial activities with higher input dependency, i.e. higher equipment and labour intensity and degree of labour specialization (Merz et al., 2013), such as the pharmaceutical industry, are more vulnerable to earthquakes. The vulnerability of these industrial activities is also associated to higher levels of uncertainty, mostly because of the high variability in the

value of the fixed assets (e.g. machinery and equipment). Moreover, to highlight the impact of the various building taxonomies on the property loss quantifications, Figure 9.8 depicts the 95% quantile of the average loss ratios in 50 years (i.e. ratio between the repair and the replacement costs of the building) obtained for each one of the six building taxonomies with respect to altitude and height, considering a FBPC support condition and the building to be located in the Lisbon. The seismic hazard was defined on the basis of a probabilistic seismic hazard analysis, carried out using the OpenQuake-engine (Vitor et al., 2014), equally for a time-span of 50 years. Hence, it may be again seen that stiffer buildings are associated to higher property losses, which may reach 16% of the building replacement cost in hi-tech and heavy industries, and variations up to 50% may be found between the property losses of taxonomies HWD-LH and LWD-HH.

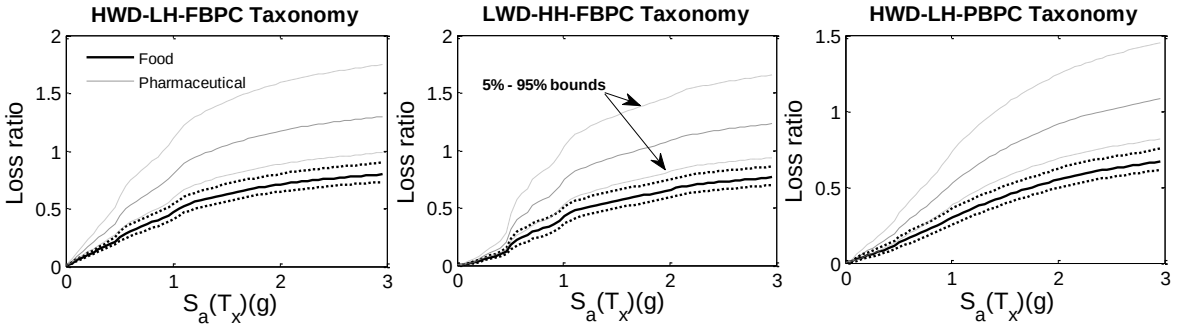

Figure 9.7 – Industrial property vulnerability functions for different building taxonomies and food and pharmaceutical industries: HWD-LH taxonomy with FBPC connection (*left*), LWD-HH taxonomy with FBPC connection (*middle*) and HWD-LH taxonomy with PBPC connection (*right*).

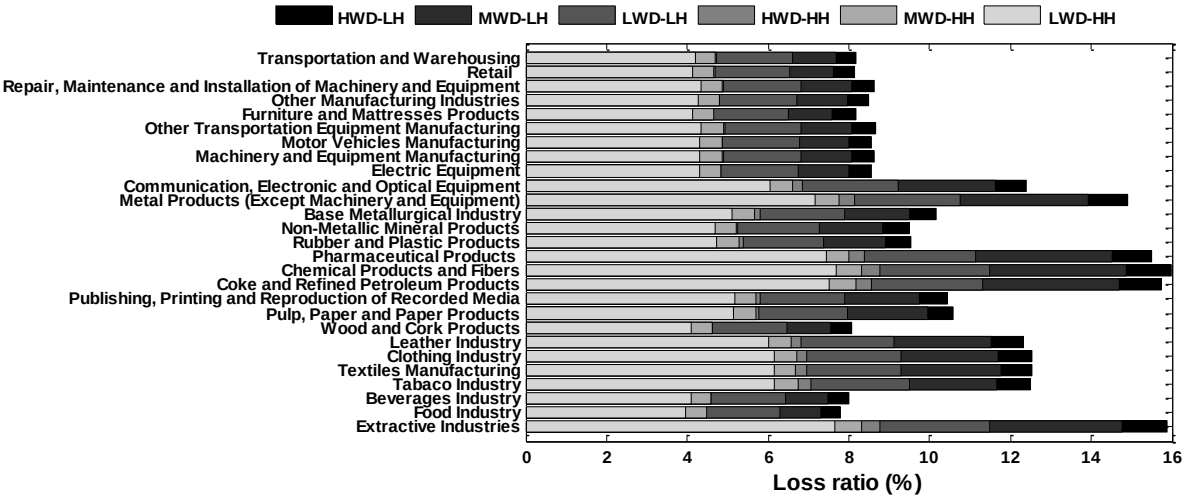

Figure 9.8 – Influence of building taxonomy vulnerabilities with FBPC connections in the 95% quantile of average property losses in 50 years for the city of Lisbon.

Damage to inventory, or stocks, usually result from stacks of inventory falling over or objects falling off from shelves, thus being predicted similarly to acceleration-sensitive non-structural damage (Chapter 8). The inventory losses are estimated by convoluting such

acceleration-sensitive vulnerability functions with industry-specific inventory asset values, usually defined as a percentage of the annual production output of a specific industrial activity. Therefore, the inventory vulnerability functions were derived independently of the industrial activity, just as a function of the building taxonomy. Figure 9.9 depicts the inventory vulnerability functions (i.e. ratio of losses to inventory) derived for different building taxonomies. Similarly to the above mentioned, laterally stiffer building taxonomies, such as the HWD-LH-FBPC taxonomy, are expected to develop greater acceleration demands and to exhibit a higher inventory vulnerability to earthquakes, when comparing to more flexible building taxonomies, such as the HWD-LH-PBPC.

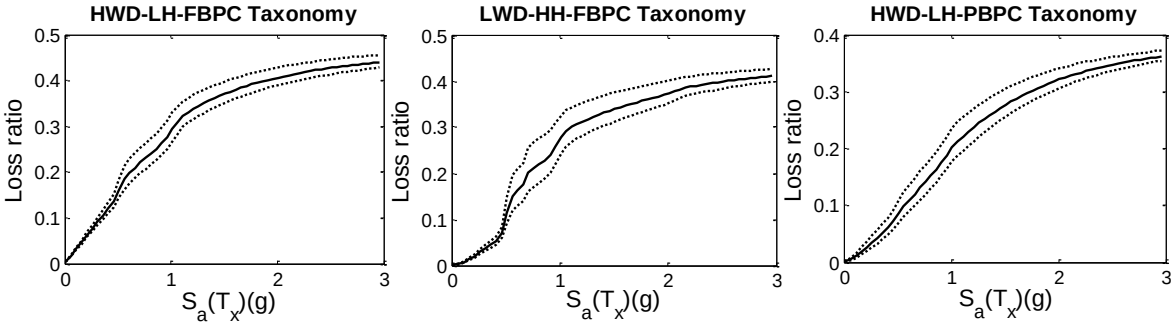

Figure 9.9 – Acceleration-sensitive inventory vulnerability functions for different building taxonomies.

9.3.3.2 Downtime and production vulnerability model

A key aspect in loss estimation is related with the fact that losses to goods and service flows should be measured in terms of the value of resources used or destroyed at prices that represent their efficient allocation, and not necessarily market prices, so as to avoid double-counting and to cover all resources, including non-market ones (Rose, 2004; 2009). Business interruption losses due to production downtime are generally a good proxy for such loss valuations, not only to reduce valuation problems, but also because businesses, insurers, and governments typically make decisions on the basis of such metric, such as gross lost sales (i.e. production) or net profits (i.e. income). A thorough discussion on the economics of the impacts of natural hazards may be found in Rose (2004; 2009). Hence, the economic direct impacts to industrial production will be herein defined in terms of production downtime, both to estimate the relocation expenses associated with the need of renting alternative spaces to resume production and to estimate production losses due to business interruption, accounting for the positive resilient effect of recapturing lost production by rescheduling at a later date overtime work or extra shifts. In brief, downtime refers to the period necessary to restore the functionality of a facility or a business to closer, identical or even better levels of operation (Cimellaro et al., 2010), and typically

includes pre-repair times (i.e. time to get financial support, design and permits), repair times (i.e. construction and reconstruction works), relocation times and times conditioned to the restauration of access to property and utilities (Chapter 8). Downtime, or time of loss of function of the building, is essentially a result of structural damage (Phipps et al., 1992). The methodology followed in Chapter 8 to estimate industry-specific downtimes will be adopted herein and extended to the proposed building taxonomies.

Figure 9.10 shows the downtime functions derived for increasing ground motion intensity levels, different building taxonomies and for textiles manufacturing and machinery and equipment manufacturing industries. These functions reflect the expected overall structural damage developed in each building taxonomy under earthquake loading conditions, which, as above mentioned, is mostly governed by lateral braces, permanent drifts and base plate connections. For what concerns the building categories with flexible column base plate connections (e.g. PBPC connection), the downtimes at lower S_a (T_x) levels were seen to be mostly governed by the initiation of structural damage at the transverse moment-resisting frames, namely at development of base plate connection failure mechanisms (i.e. plate yielding, contemporary anchor bolt and plate yielding or anchor bolt yielding). However, since these failure mechanisms exhibit high ductility and deformation capacities, it was observed that, for greater S_a (T_x) levels, the structural damage was essentially controlled by damage to lateral braces and, most importantly, by permanent drifts, i.e. excessive permanent drifts may imply loss of functionality of the building and the need to demolish the structure (Chapter 7). These findings are in agreement with the observations of Midorikawa et al. (2012), who, based on the inspection of the structural damage to steel structures after the 2011 Tohoku earthquake, observed that if anchor bolt failure mechanisms were developed, substantial column dislocations and severe residual story drifts occurred, otherwise minor residual story drifts were found.

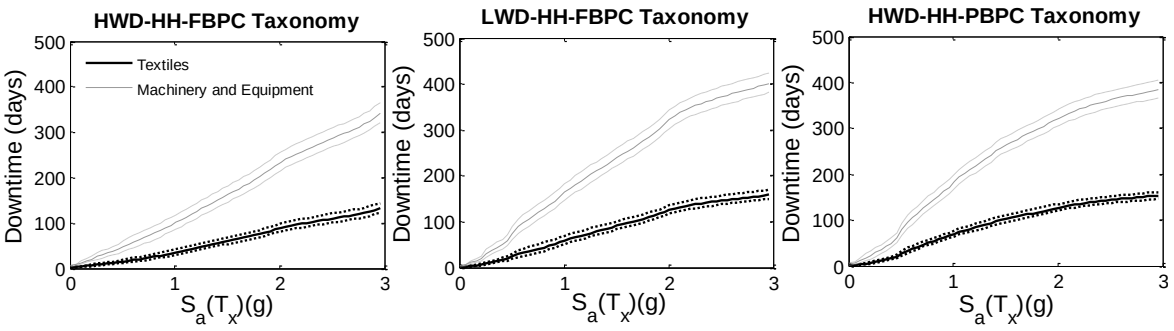

Figure 9.10 – Downtime functions for different building taxonomies and textiles manufacturing and Machinery and Equipment manufacturing industries.

The lower downtimes associated to buildings with fixed base plate connects (FBPC) may be thus explained by the lower residual drift demands. On the other hand, as it would be expected, buildings located at higher altitudes and designed to sustain higher lateral wind loads (HWD buildings) exhibit lower structural vulnerability when compared to LWD buildings, hence being also associated to lower downtimes. The downtime functions derived herein per industrial activity and building taxonomy, which reflect the length of time of loss of use of the building, will be used to estimate the relocation expenses (i.e. rent and shifting costs) associated with the need of businesses to rent additional spaces to resume production. However, it is important to refer that the burden of relocation is only expect to be borne by companies that own the building. Otherwise companies would cease paying the rent and would only pay to the new landlord. Since industrial building ownership rates for Portugal are difficult to ascertain, and having as benchmark that household ownership rates are around 74% (Araújo et al., 2016b) and that owning the property may be a potentially good investment for companies, it was assumed herein, for simplicity, that all buildings are owner occupied.

With respect to production losses, the resilient capacity of businesses to recapture lost production by overtime work or working extra shifts, which is supported by the fact that demand tends to persist even if the supply is disrupted, was modelled according to Park et al. (2010), similarly to the work conducted in Chapter 8. The actual business interruption, or lost production, times for different building taxonomies and industrial activities are presented in Figure 9.11.

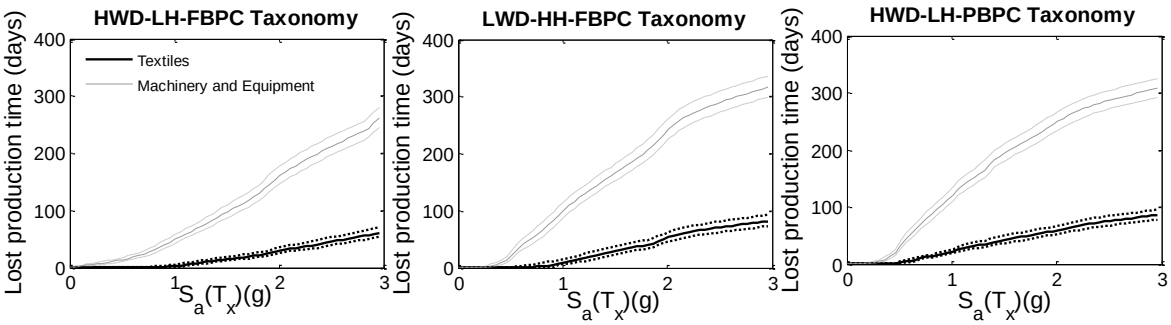

Figure 9.11 – Functions of lost production time, including production recapturing, for different building taxonomies and textiles manufacturing and Machinery and Equipment manufacturing industries.

9.3.3.3 Indirect industrial vulnerability model

The modelling of indirect economic impacts to industrial activity due to input factor (equipment and labour), infrastructure or supply chain disruptions is a rather intricate task because of the complexity of the interdependencies between all variables at stake.

Therefore, the conceptual indicator framework implemented by Merz et al. (2013) and Khazai et al. (2013), was adopted herein, which offers a good trade-off between accuracy and simplicity. This framework relies on production theory (i.e. production loss might occur when production factors are not available as required and when critical infrastructures or material and information flows within supply chains are disturbed) and defines three sub-indicators groups: (i) input factor (equipment and labour) dependency; (ii) infrastructure dependency; (iii) and supply chain dependency. Final composite Industrial Vulnerability Indices per industrial activity are computed, which could be afterwards integrated with direct losses using Moncho's equation (EMI, 2015). More information on the quantification of the Industrial Vulnerability Indices may be found in Chapter 8.

9.4 Implementation in a web-based platform for seismic loss estimation

Performing risk assessment studies at regional and national scales requires managing an enormous amount of data, in terms of assets information, vulnerability models for each single group of collected assets or seismic hazard information, e.g., source models. The treatment of such huge amount of information may be quite time-consuming, delicate, highly susceptible to error and stressful. To simply this process, every model constructed herein (hazard, exposure and vulnerability) was implemented in a web-based platform for seismic loss estimation recently developed at the University of Porto under the nationally founded PRISE project. This web-based platform relies on the open-source OpenQuake engine (Silva et al., 2014) and provides user-friendly and interactive cloud-based computing and data visualization. It also offers to users the possibility of implementing newly developed models or using previously uploaded ones. The output information is stored in a PostgreSQL relational database, allowing for an interactive post-processing of the results. This web-based platform not only aims at providing an easier way of dealing with risk assessment and management studies, while using the open-source OpenQuake engine, but also, and most importantly, aims at facilitating the dissemination of loss assessment results and supporting decision-making. Figure 9.12 depicts a screenshot of the web-based interface in the listing and selecting of the intended vulnerability model and in the displaying of loss estimates at different scales.

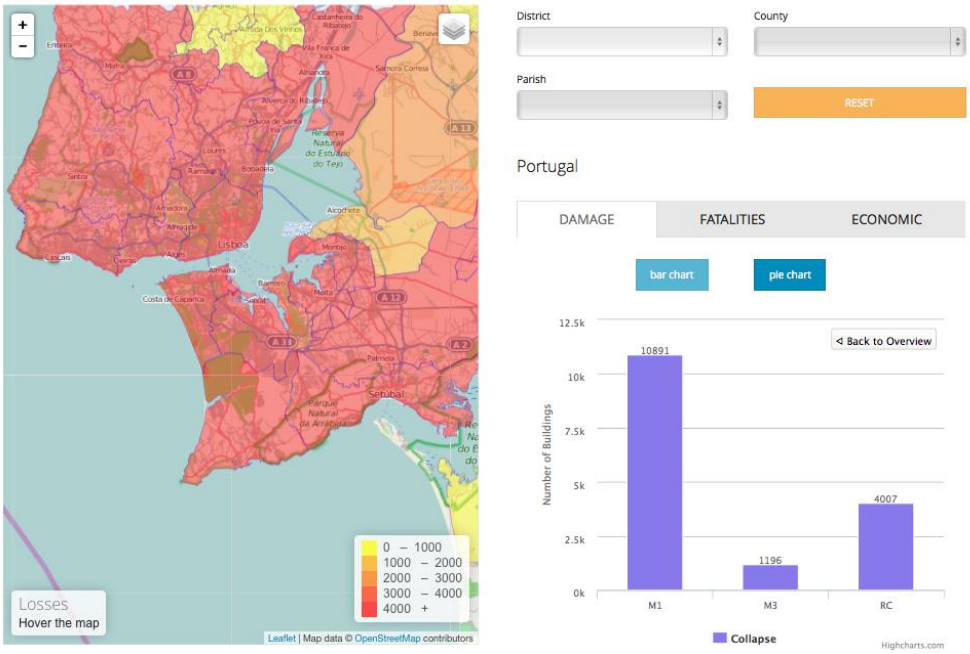

Figure 9.12 – Screenshot of the web-based interface showing the selection of the vulnerability model and presentation of loss results.

9.5 Industrial seismic risk assessment for Mainland Portugal

The industrial seismic risk assessment for Mainland Portugal was carried out using the web-based platform developed within the PRISE project. To compute specific property and industrial activity loss maps, the seismic hazard has to be previously computed and afterwards convoluted with the exposure and vulnerability models already developed. The PRISE project web-based platform, which relies on the OpenQuake Engine (Silva et al., 2014), allows carrying out different types of seismic hazard analysis, such as: (i) Classical Probabilistic Seismic Hazard Analysis (PSHA) following the integration procedure formulated by Field et al. (2003); (ii) Event-Based Probabilistic Seismic Hazard Analysis by calculating a set of ground-motion fields from generated stochastic event sets; (iii) or Scenario-Based Seismic Hazard Analysis by calculating ground motion fields for a single earthquake rupture scenario taking into account the ground-motion aleatory variability (Crowley et al., 2005). Whereas the probabilistic event-based approach allows to conveniently aggregate the losses throughout a certain region of interest by taking into consideration the spatial correlation of the intra-event residuals (Jayaram and Baker, 2009) and the correlation of loss ratios between buildings of the same vulnerability class, i.e., the losses are calculated event-by-event leading to an aggregated loss exceedance curve with higher probabilities of exceeding large losses (Silva et al., 2015a), the classical PSHA approach may underestimate the total aggregated loss value, particularly at high return

periods (Silva et al., 2015a). However, since the use of the probabilistic event-based approach at a national scale for Mainland Portugal would require a high computational onus and time and, as noted by Silva et al (2015a), a wide spectrum of uncertainties is still present in a study of this magnitude, it is herein considered that the aggregation of losses using the classical PSHA approach may still provide a reasonable estimate of the total industrial losses. Hence, the classical PSHA approach was adopted to compute the hazard curves at each site (i.e., a 30 arc sec resolution was considered in agreement with the exposure model previously developed) for a time span of 50 years. The mean was calculated from this set of hazard curves and the hazard map presented in Figure 9.13 for a probability of exceedance of 10% in 50 years (return period of 475 years) obtained. The spatial distribution and range of the peak ground accelerations obtained in this study seem to be in agreement with the hazard maps computed by Silva et al. (2015a) and Vilanova and Fonseca (2007), although a different seismic source model, as proposed within the SHARE project, has been adopted in the present study. It should be referred that Silva et al. (2015a) used the seismic source model of Vilanova and Fonseca (2007) and a different GMPE scheme. Overall, it may be observed from Figure 9.13 that a higher hazard is obtained in the Lisbon and Tagus Valley region and Algarve, similarly to what was found by Silva et al. (2015a) and Vilanova and Fonseca (2007), with peak ground acceleration (PGA) values ranging between 0.11g and 0.25g. This range of PGA values seems to be slightly lower than that obtained by Silva et al. (2015a) and Vilanova and Fonseca (2007), particularly at the Lisbon and Tagus Valley region, which is greater than 0.18g.

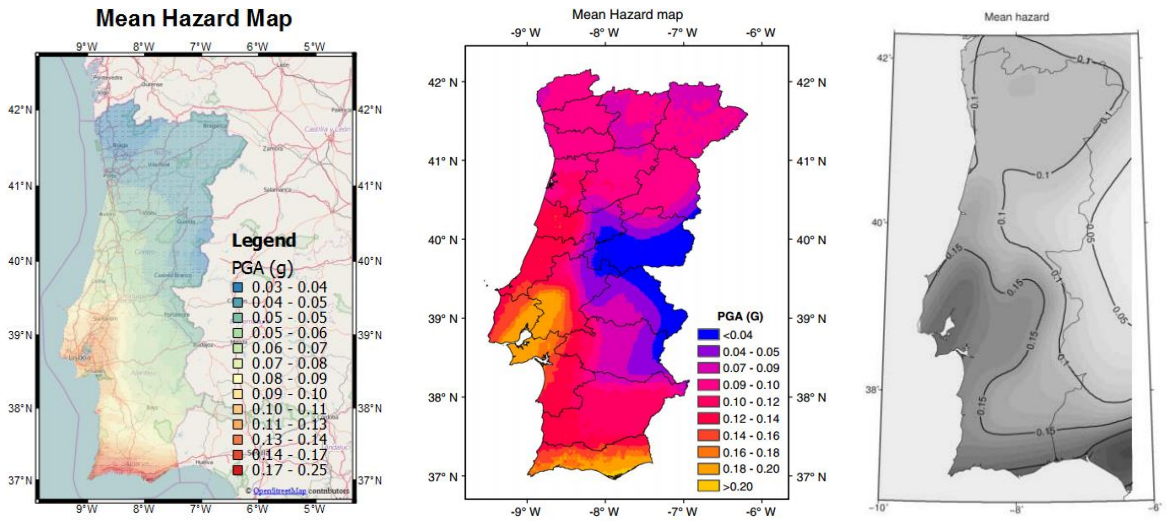

Figure 9.13 – Mean seismic hazard map in peak ground accelerations (PGA) for a probability of exceedance of 10% in 50 years obtained in this study (*left*), by Silva et al. (2015a) (*middle*) and Vilanova and Fonseca (2007) (*right*).

Despite the slight differences observed between the obtained mean hazard map and those obtained by Silva et al. (2015a) and the Vilanova and Fonseca (2007) in terms of the spatial distribution of the hazard around the northeast region of Mainland Portugal and the range of PGA values observed around the Lisbon and Tagus Valley region, it may be considered that the developed hazard model provides reasonable and expectable results, being thus conveniently validated.

Building on the OpenQuake Engine classical PSHA-based risk calculator (Silva et al., 2014), the PRISE project web-based platform convolutes the hazard, exposure and vulnerability models in order to calculate loss exceedance curves for each asset considering each possible path of the logic tree. Again, based on the set of loss exceedance curves obtained for each asset, the mean loss maps for a 10 % probability of exceedance in 50 years were computed and presented in Figure 9.14.

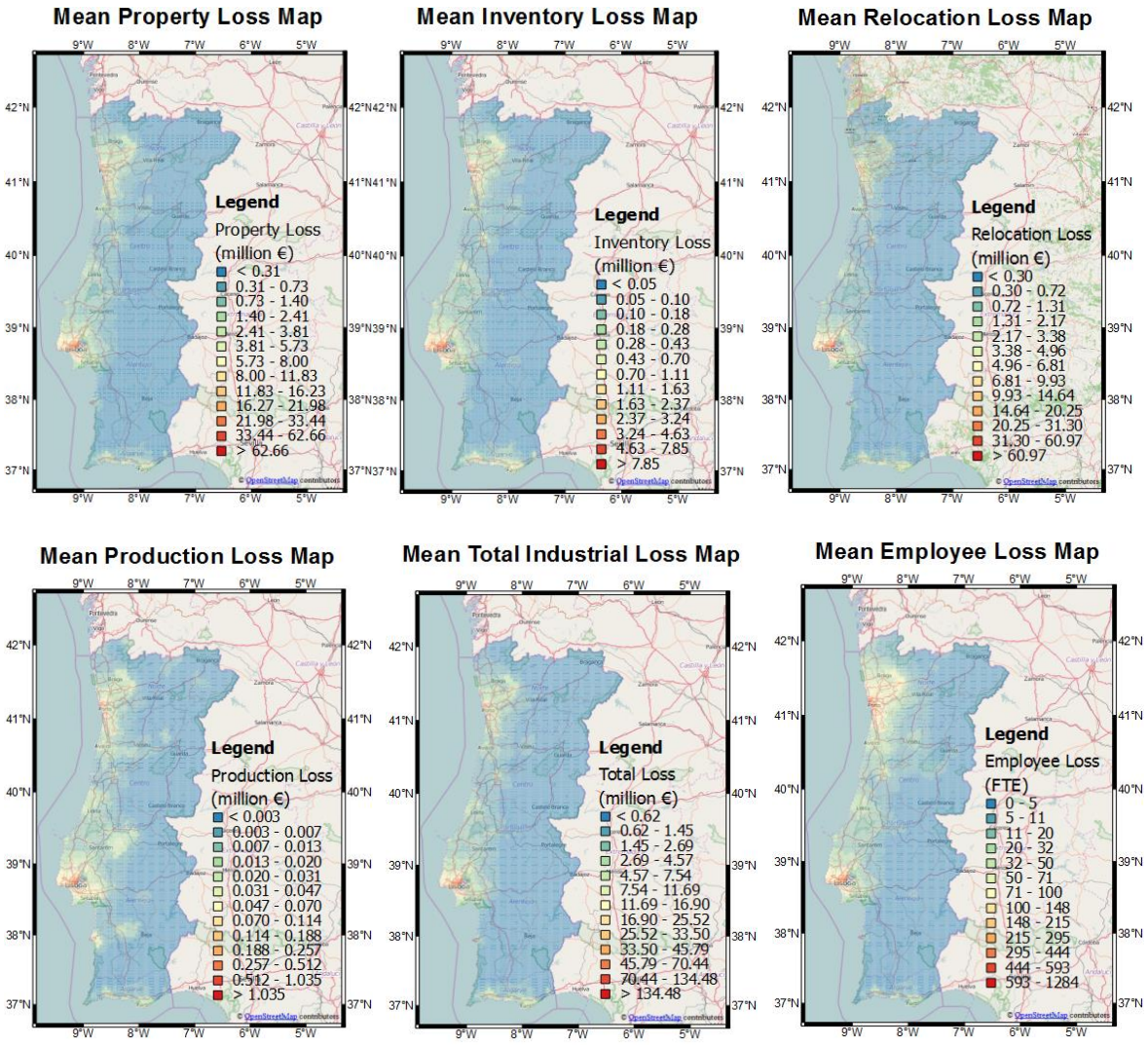

Figure 9.14 – Mean property, production and industrial activity, total (direct and indirect) and employment losses industrial loss for a probability of exceedance of 10% in 50 years.

The obtained spatial distribution of industrial property and activity losses in mainland Portugal is coherent with both the spatial distribution of the hazard observed in Figure 9.13 and the geographical distribution of the industrial assets (e.g., number of firms) presented in Figure 9.1. As already discussed in Chapters 7 and 8, the higher industrial losses are observed along the south-western coastal region of mainland Portugal, being the region of Lisbon and the Tagus Valley expected to be hit harder by an event with a 475 years return period, wherein the total direct and indirect losses to industrial property and activity may overcome 134 million € within a 30 arc sec grid spacing (approximately 1km). Figure 9.14 allows observing that the direct losses to industrial property, including not only structural and non-structural components, but also contents (such as production equipment, machinery, furniture, etc.) are expected to significantly contribute to the overall industrial losses. In turn, the losses to production may be seen to have a reduced expression in the overall industrial loss estimates due to the businesses' resilient capacity to recapture the lost production by renting alternative places, which losses are expressed in terms of relocation losses, and working extra hours. Moreover, it may be interesting to observe from Figure 9.14 that the spatial distribution of the mean industrial production losses slightly vary from that shown in the mean property and relocation loss maps. Whereas in the latter cases the spatial distribution is mostly a result of the geographical distribution of the industrial buildings (or firms) and employees (used to derived the unitary building area by industrial activity) throughout the mainland, in the case of the mean production loss maps some localized losses may be observed as a result of a reduced number of firms with high annual production outputs, as it is the case of the Sines industrial hub, which hosts important Coke and Refined Petroleum Products companies such as Galp and Repsol.

Nevertheless, this spatial distribution of industrial losses around the Lisbon and Tagus Valley region and Algarve varies between different industrial activities. By disaggregation the direct industrial property losses, Figure 9.15 presents the spatial distribution of the mean property losses obtained for the Textile Manufacturing, the Motor Vehicle Manufacturing and the Pharmaceutical Products industries. It may be observed that a significant distribution of losses to the Textile Manufacturing industry is obtained in the Northern region of mainland Portugal, particularly around the Ave Valley region, which is known to be the heart of the Portuguese textile and clothing industry, despite its lower seismic hazard level. Similarly, significant mean property losses to the Motor Vehicle Manufacturing industry were obtained in the Setúbal region (e.g., location of Volkswagen AutoEuropa), south of Porto (e.g., location of Salvador Caetano) and Viseu

(e.g., location of the PSA production plant), northeast of Santarém (e.g., location of Mitsubishi-FUSO) and around the Lisbon and Tagus Valley and Porto-Aveiro-Braga regions, wherein about 200 automotive supplier companies are located. In turn, most mean industrial property losses to the Pharmaceutical Products industry are concentrated within the Great Lisbon Metropolitan area.

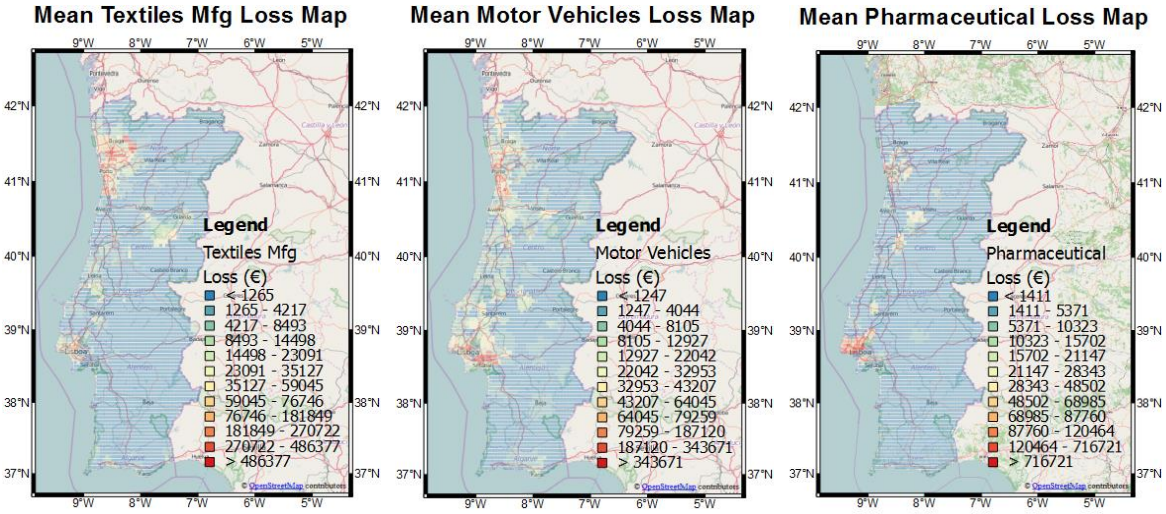

Figure 9.15 – Mean property losses for different industrial activities, i.e. Textiles Manufacturing (left), Motor Vehicles Manufacturing (*middle*) and Pharmaceutical Products (*right*), for a probability of exceedance of 10% in 50 years.

Table 9.1 lists the mean aggregated direct property losses, the mean aggregated direct and indirect industrial activity losses, the mean aggregated total direct and indirect industrial losses and the mean aggregated employment losses by industrial activity for a return period of 475 years. Higher mean aggregated total losses were observed in the food, clothing, metal and non-metallic mineral products industries, being greater or around 0.1 billion €, and in the retail and transportation and warehousing sectors, reaching up to 2.7 billion €. The overall mean aggregated industrial loss for mainland Portugal has been estimated to be around 3.8 billion €, which represents 2.2% of the Portuguese GDP in 2014. Since the Portuguese industrial sector roughly contributes to 21% of the national GDP (AICEP, 2015), it may be concluded that a potential 10% reduction in the country's industrial annual revenue could be expected for a return period of 475 years. Also, a mean aggregated loss of more than 15000 full time employment (FTE) jobs has been estimated. Nevertheless, despite the devastating consequences to the country's economy, people's welfare and potential job loss, the estimated overall industrial losses of 2.2% of the Portuguese GDP may be seen to just represent 7% of total losses estimated by Silva et al. (2015a) for the Portuguese residential building stock.

Table 9.1 – Mean industrial losses with 10% probability of exceedance in 50 years.

Industrial Activity (2-digit Portuguese CAE)	Direct Property Losses (million €)	Direct Industrial Activity Losses (million €)	Indirect Industrial Activity Losses (million €)	Total Losses (million €)	Mean Employment Losses (FTE)
Extractive Industries	11.48	5.38	1.99	18.85	104
Food Industry	66.10	48.60	14.59	129.29	664
Beverages Industry	10.04	7.35	2.35	19.75	115
Tobacco Industry	0.09	0.10	0.03	0.22	1
Textiles Manufacturing	31.59	11.07	3.33	45.99	330
Clothing Industry	69.88	24.19	6.28	100.36	611
Leather Industry	36.30	12.51	4.63	53.44	489
Wood and Cork Products	20.37	10.86	3.91	35.13	297
Pulp, Paper and Paper Products	9.52	4.69	1.97	16.18	125
Publishing, Printing and Reproduction of Recorded Media	17.02	8.57	3.09	28.68	160
Coke and Refined Petroleum Products	1.96	5.84	2.45	10.25	20
Chemical Products and Fibres	18.97	10.17	4.98	34.11	207
Pharmaceutical Products	10.77	5.98	3.00	19.75	110
Rubber and Plastic Products	18.52	11.57	5.09	35.19	315
Non-Metallic Mineral Products	46.39	31.96	14.70	93.05	562
Base Metallurgical Industry	9.91	16.49	7.92	34.32	135
Metal Products (Except Machinery and Equipment)	114.96	54.65	23.50	193.11	967
Communication, Electronic and Optical Equipment	5.10	4.39	2.03	11.52	126
Electric Equipment	8.55	8.39	3.86	20.80	267
Machinery and Equipment Manufacturing	8.31	15.37	5.99	29.67	234
Motor Vehicles Manufacturing	14.49	28.51	9.13	52.12	284
Other Transportation Equipment Manufacturing	1.81	3.35	1.23	6.40	44
Furniture and Mattresses Products	21.32	10.42	3.44	35.19	280
Other Manufacturing Industries	10.46	6.01	2.46	18.92	160
Repair, Maintenance and Installation of Machinery	18.35	10.62	3.51	32.48	156
Retail	1190.61	881.65	335.03	2407.29	7657
Transportation and Warehousing	195.44	113.26	28.32	337.02	875
Total	**1968.30 million €**	**1352.96 million €**	**498.81 million €**	**3819.07 million €**	**15297 FTE**

It should be noted that the present study does not account for the economic situation of each individual business or sector, nor for the influence of the businesses' dimension in securing loans and assuring sufficient capital reserves, which may have an important impact in vulnerability or resilient capacity of the industry to recover from a natural disaster (Chang and Falit-Baiamont, 2002). Furthermore, it has been herein considered for the sake of simplicity that the Portuguese industrial building stock is simply characterized by industrial steel buildings with transverse Portal Frames, which are not fully representative of reality as the Portuguese industrial building stock also comprehends pre-cast industrial RC buildings (30% of the industrial building stock) and industrial buildings with steel lattice roofs (18% of the industrial building stock). Further studies aiming at incorporating such building categories in the vulnerability model developed herein are hence needed.

9.6 Conclusions

This chapter has investigated the industrial seismic risk for mainland Portugal and has provided a first projection of the seismic losses to the region's industrial property and activity by using newly developed hazard, exposure and vulnerability models, state-of-the-art methods and up-to-date data. The models were implemented in a web-based platform for seismic loss estimation developed at the University of Porto under the nationally founded PRISE project, thus allowing for the computation of mean industrial loss maps and the overall aggregated losses for mainland Portugal.

Economic statistical information collected from the Portuguese National Institute of Statistics (INE) for every industrial activity of the 2-digit Portuguese Industrial Classification (CAE) System was employed to derive a novel and comprehensive industrial exposure model for mainland Portugal, which has been refined to a 30 arc sec resolution with the support of additional information on the spatial distribution of the region's industrial building stock collected from existing databases. Novel industrial steel building taxonomies defined based on the height of the building, wind design level and base plate connection have been included in the exposure model and derived considering the dynamic characteristics and expected seismic performances of a large amount of synthetic industrial buildings randomly generated using data collected from the inspection of more than 200 blueprint drawings from Portuguese design offices and steelwork companies. The developed exposure model revealed highly exposed industrial assets along the costal Porto-

Lisbon corridor, wherein industrial steel buildings designed to sustain low to moderate wind load levels are located. Moreover, a detailed vulnerability model was analytically developed from thousands of bi-directional time-history analysis conducted using the set of randomly generated synthetic industrial steel buildings so as to represent the evolution of losses ratios with the increase in the ground-motion intensity for each one of the proposed building taxonomies. Losses to industrial property accounting for structural and non-structural components and contents, as well as direct and indirect losses to industrial activity, i.e., inventory, relocation or production, were included in the vulnerability model following the frameworks presented in Chapter 7 and 8. It was herein concluded that whilst industrial steel buildings with higher lateral stiffness and strength are expected to be more seismically vulnerable, mostly because of the higher losses to acceleration sensitive non-structural components, industrial buildings with higher lateral flexibility, e.g., taller buildings designed to sustain lower wind loads, are expected to be less susceptible to seismic losses. Finally, an updated hazard model of that previously developed by Silva et al. (2015a) that employs the area and fault source model from the SHARE project was used in this study.

The inspection of the mean industrial loss maps computed using the PRISE project web-based platform revealed the Lisbon and Tagus Valley and Algarve regions as the most prone to industrial property and activity losses. Nevertheless, the spatial distribution of losses was found to vary from sector-to-sector. The food, clothing, metal and non-metallic mineral products industries, as well as the retail and transportation and warehousing sectors, were seen to be the most risk-prone activities, being associated to mean aggregated losses for a return period of 475 years greater than 0.1 billion € and 2.7 billion €, respectively. An overall mean aggregated industrial loss for mainland Portugal has been estimated to be around 3.8 billion €, representing 2.2% of the Portuguese GDP in 2014 and a 10% reduction in the country's industrial annual revenue. More than 15000 full time employment (FTE) jobs have been estimated to be lost.

Despite the novelty of the developed industrial seismic risk model and the pertinence of projected losses, further developments to the present model should be conducted in future studies, such as the inclusion of vulnerability models respective of pre-cast industrial RC buildings and industrial buildings with steel lattice roofs or the inclusion of socio-economic indicators capable of explaining the capacity of business to securing loans and assuring sufficient capital reserves, which may significantly increase the seismic vulnerability of businesses or increase their resilient capacity to cope with natural disasters.

9.7 Acknowledgments

This work has been performed within the framework of the research project PTDC/ECM-EST/3062/2012 'Earthquake loss of the Portuguese building stock' founded by the Foundation of Science and Technology (FCT) of Portugal. The authors would like to express their gratitude to Dr. Joana Neto, Marketing Director of AICEP Global Parques, for providing access to the AICEP Global Find platform database, and to Eng.ª Alexandra Feliz and Eng.º José Manuel Silva from the steelworks company "O Feliz" and to Eng.º Marco Beleza Vieira from the design office "Projegui" for their availability and support in the survey conducted on the geometrical characteristics of the industrial Portuguese building stock.

9.8 References

AICEP (2015) Portugal – Basic Data, Portuguese Agency for Investment and External Commerce (AICEP), Lisbon, Portugal.

Akkar S, Bommer JJ (2010) Empirical equations for the prediction of PGA, PGV and spectral accelerations in Europe, the Mediterranean region and the Middle East, Seismological Research Letters, 81, 195-206.

Atkinson G, Boore D (2006) Earthquake ground-motion prediction equations for eastern North America, Bulletin of the Seismological Society of America, 96, 2181-2205.

Bal EI, Crowley H, Pinho R (2008a) Displacement-based earthquake loss assessment for an earthquake scenario in Istanbul, Journal of Earthquake Engineering, 12,12-22.

Bal EI, Crowley H, Pinho R, Gülay FG (2008b) Detailed assessment of structural characteristics of Turkish RC building stock for loss assessment models, Soil Dynamics and Earthquake Engineering, 28, 914-932.

Bank of Portugal (2015) Projections for the Portuguese Economy: 2015-2017. Projection assumptions, Economic Bulletin, Bank of Portugal, Lisbon, Portugal.

Bradley BA (2010) A generalized conditional intensity measure approach and holistic ground motion selection, Earthquake Engineering and Structural Dynamics, 39, 1321-1342.

Carvalho A (2007) Stochastic modelling of the seismic action for Mainland Portugal. PhD dissertation thesis, Instituto Superior Técnico, Lisbon, Portugal.

Carvalho VM, Nieri M, Saito YU (2014) Supply chain disruptions: evidence from the great east Japan earthquake, The Research Institute of Economy Trade and Industry.

CEN (2005) NP ENV 1993-1-1 Eurocode 3: design of steel structures – Part 1-1: general rules and rules for buildings, European Commitee for Strandardization, Brussels, Belgium.

CEN (2010) NP ENV 1991-1-4 Eurocode 1: actions on structures – Part 1-4: general actions – wind actions, European Commitee for Strandardization, Brussels, Belgium.

Chang SE, Falit-Baiamont A (2002) Disaster vulnerability of business in the 2001 Nisqually earthquake, Environmental Hazards, 4, 59-71.

Cimellaro GP, Reinhorn AM, Bruneau M (2010) Framework for analytical quantification of disaster resilience, Enginering Structures, 32, 3639-3649.

Cochrane, H (1996) Catastrophic earthquakes and the prospect of indirect losses, Post-Earthquake Rehabilitation and Reconstruction, Cheng FY, Wang YY (eds.), Elsevier B.V., Oxford, U.K.

Crowley H, Bommer JJ, Pinho R, Bird J (2005) The impact of epistemic uncertainty on an earthquake loss model, Earthquake Engineering and Structural Dynamics, 34, 1653-1685.

Crowley H, Pinho R, Bommer JJ (2004) A probabilistic displacement-based vulnerability assessment procedure for earthquake loss estimation, Bulletin of Earthquake Engineering, 2, 173-219.

Cruz AM, Okada N (2008) Consideration of natural hazards in the design and risk management of industrial facilities, Natural Hazards, 44, 213-227.

Cruz, AM, Steinberg LJ (2005) Industry preparedness for earthquakes and earthquake-triggered hazmat accidents in the 1999 Kocaeli earthquake, Earthquake Spectra, 21, 285-304.

Delavaud E, Cotton F, Akkar S, Scherbaum F, Danciu L, Beauval C, Drouet S, Douglas J, Basili R, Sandikkaya MA, Segou M, Faccioli E, Theodoulidis N (2012) Toward a ground-motion logic tree for probabilistic seismic hazard assessment in Europe, Journal of Seismology, 16, 451-473.

Durukal E, Erdik M (2008) Physical and economic losses sustained by the industry in the 1999 Kocaeli, Turkey earthquake, Natural Hazards, 46, 153-178.

Durukal E, Erdik M, Uçkan E (2008) Earthquake risk to industry in Istanbul and its management, Natural Hazards, 44, 199-212.

EMI (2015) A guide to measuring urban risk resilience. Principles, tools and practice of urban indicators. Pre-release draft, Earthquake and Megacities Initiative, Quezon City, Philippines.

EPICentre (2012) The 29th May 2012 Emilia Romagna Earthquake, EPICentre Field Observation Report, University College London, London, United Kingdom.

Erdik, M (2000) Report on 1999 Kocaeli and Düzce (Turkey) earthquakes, Proceedings of the Euro Conference on Global Change and Catastrophe Risk Management, Earthquake Risks in Europe, Laxenburg, Austria.

European Commission (2015) Country Report Portugal 2015 including an in-depth review on the prevention and correction of macroeconomic imbalances, European Commission, Brussel, Belgium.

FEMA (2010) Multi-hazard loss estimation methodology. Earthquake Model, HAZUS – MH MR5 Technical Manual, Federal Emergency Management Agency, Mitigation Division, Washington, DC.

Field EH, Jordan TH, Cornell AC (2003) OpenSHA: A developing community-modelling environment for seismic hazard analysis, Seismological Research Letters, 74:406-419.

Guimarães P, Figueiredo O, Woodward F (2007) Location modelling and the localization of Portuguese manufacturing, Proceedings of the 44th European Congress of the European Regional Science Association, Porto, Portugal.

Guimarães P, Figueiredo O, Woodward F (2007) Measuring the localization of economic activity: a parametric approach, Journal of Regional Science, 47, 753-774.

Hsu WK, Chiang, WL, Chen CW (2013) Earthquake risk assessment and optimal risk management strategies for hi-tech fabs in Taiwan, Natural Hazards, 65, 2063-2076.

Jayaram N, Baker JW (2009) Correlation model for spatially distributed ground-motion intensities, Earthquake Engineering and Structural Dynamics, 38:1687-1708.

Kala Z, Melcher J, Puklick L (2009) Material and geometrical characteristics of structural steel based on statistical analysis of metallurgical products, Journal of Civil Engineering and Management, 15, 299-307.

Kazantzi AK, Vamvatsikos D, Lignos DG (2014) Seismic performance of a steel moment-resisting frame subject to strength and ductility uncertainty, Engineering Structures, 78, 69-77.

Khazai B, Merz M, Schulz C, Borst D (2013) An integrated indicator framework for spatial assessment of industrial and social vulnerability to indirect disaster losses, Natural Hazards, 67, 145-167.

Lamarche CP, Proulx J, Paultre P, Turek M, Ventura CE, Le TP, Lévesque C (2009) Toward a better understanding of the dynamic characteristics of single-storey braces steel frame buildings in Canada, Canadian Journal of Civil Engineering, 36, 969-979.

Latour M, Rizzano G (2013) Full strength design of column base connections accounting for random material variability, Engineering Structures, 48, 458-471.

Lopes M, Pais I, Oliveira S, Sá FM (2012) Methodologies for the analysis of the seismic vulnerability of an industrial complex, Proceedings of the 15th World Conference on Earthquake Engineering, Lisbon, Portugal.

Marques M (2011) Seismic safety probabilistic assessment of buildings. PhD dissertation thesis, Department of Civil Engineering, Faculty of Engineering of the University of Porto, Oporto, Portugal.

Melcher J, Kala Z, Holický M, Fajkus M, Rozlívka K (2004) Design characteristics of structural steels based on statistical analysis of metallurgical products, Journal of Constructional Steel Research, 60, 795-808.

Merz M, Bertsch V, Rentz O, Gerdermann J (2007) Assessment of industrial asset values at risk, Proceedings of the 4th Conference on Information Systems for Crisis Management, Delft, the Netherlands.

Merz M, Hiete M, Comes T, Schultmann F (2013) A composite indicator model to access natural disaster risks in industry on a spatial level, Journal of Risk Research, 16, 1077-1099.

Midorikawa M, Nishiyama I, Tada M, Terada T (2012) Earthquake and tsunami damage on steel buildings caused by the 2011 Tohoku Japan earthquake, Proceedings of the International Symposium on Engineering Lessons Learned from the 2011 Great East Japan Earthquake, Tokyo, Japan.

Moat AM, Morrison AJT, Wond S (2000) Performance of industrial facilities during 1999 earthquakes: implications for risk managers, Proceedings of the Euro Conference on Global Change and Catastrophe Risk Management, Earthquake Risks in Europe, Laxenburg, Austria.

Montilla JAP, Casado CL (2002) Seismic hazard estimate at the Iberian Peninsula, Pure and Applied Geophysics, 159, 2699-2713.

Moore DS, McGabe GP, Craig BA (2009) Introduction to the practice of statistics (6th eds.), WH Freeman and Company, New York, USA.

National Academy of Sciences (1999) The impacts of Natural Disasters. A framework for loss estimation, National Academy of Sciences, National Academy Press, Washington, D.C.

Oliveira CS (2008) Lisbon earthquake scenarios: a review on uncertainties, from earthquake source to vulnerability modelling, Soil Dynamics and Earthquake Engineering, 28, 890-913.

Oliveira CS (2013) Studies made since early nineteen ninety in Portugal reducing the seismic risk, Proceedings of the Vienna Congress on Recent Advances in Earthquake Engineering and Structural Dynamics, Vienna, Austria.

Olsson A, Sandberg G, Dahlblom O (2003) On Latin Hypercube sampling for structural reliability analysis. Structural safety, 25, 47-68.

Owen AB (1994) Controlling correlations in Latin Hypercube samples, Journal of America Statistical Association, 89.

Papadakis IS (2000) The disruption of global markets by earthquakes: risk analysis of PC supply chains, Proceedings of the Euro Conference on Global Change and Catastrophe Risk Management, Earthquake Risks in Europe, Laxenburg, Austria.

Park JY, Cho J, Rose A (2011) Modeling a major source of economic resilience to disasters: recapturing lost production, Natural Hazards, 58, 163-182.

PEER (2011) OpenSees: open system for earthquake engineering simulation. Pacific Engineering Research Center, University of California, Berkeley, CA.

Petruzzelli F (2013) Scale-dependent procedures for seismic risk assessment and management of industrial building portfolios, PhD dissertation thesis, Department of Structures for Engineering and Architecture, University of Naples Federico II, Napoles, Italy.

Phipps MT, Jirsa JO, Picado M, Karp R (1992) Performance of high technology industries in the Loma Prieta earthquake, Proceedings of the 10th World Conference on Earthquake Engineering, Balkema, Rotterdam.

REAE (1965) Regulamento de estruturas de aço para edifícios, Decreto-Lei nº 46160, Diário do Governo, Imprensa Nacional, Casa da Moeda, Lisbon, Portugal.

REAE (1986) Regulamento de estruturas de aço para edifícios, Decreto-Lei nº 211/86, Diário da República, Imprensa Nacional, Casa da Moeda, Lisbon, Portugal.

RFCS (2013) Prefabricated steel structures for low-rise buildings in seismic areas, Research Fund for Coal and Steel, European Commission, Brussels, Belgium.

Rodrigues J, Carvalho A, Delfim R, Gomes R (2014) Sesmic attenuation model for mainland Portugal considering the type of soil, Proceedings of the 5th Portuguese Conference on Structural Engineering, Lisbon, Portugal.

Rose A (2004) Economic principles, issues and research priorities in hazard loss estimation, Modelling Spatial and Economic Impacts of Disasters, Okuyama, Chang (eds.), Springer V.A., Berlin, Germany.

Rose A (2007) Economic resilience to natural and man-made disasters, Environmental Hazards, 7, 383-398.

Rose A (2009) A framework for analyzing the total economic impacts of terrorist attacks and natural disasters, Journal of Homeland Security and Emergency Management, 6.

RPM (1929) Regulamento de Pontes Metálicas, Decreto-Lei nº 16781, Diário do Governo, Imprensa Nacional, Casa da Moeda, Lisbon, Portugal

RSA (1983) Regulamento de segurança e acções para edifícios e pontes, Decreto-Lei nº 235/83, Diário da República, Imprensa Nacional, Casa da Moeda, Lisbon, Portugal.

RSEP (1961) Regulamento de solicitações em edifícios e pontes, Decreto-Lei nº 44041, Diário do Governo, Imprensa Nacional, Casa da Moeda, Lisbon, Porugal.

Sampognaro R, Sicsic M (2012) The impact of Japan's earthquake on the global economy, Trésor-Econonomics, Ministère de l'Économie des Finances et de l'Industrie, No. 100, p.8.

Sapountzaki K (2005) Coping with seismic vulnerability: small manufacturing firms in western Athens, Disasters, 29, 195-458.

SCI (2004) Design of single-span steel portal frames to BS 5950-1:2000, The Steel Construction Institute, Berkshire, UK.

Seifert I, Thieken AH, Merz M, Borst D, Werner U (2010) Estimation of industrial and commercial asset values for hazard risk assessment, Natural Hazards, 52, 453-479.

Senel, SM, Kayhan AH (2010) Fragility based damage assessment in existing precast industrial buildings: A case study for Turkey, Structural Engineering and Mechanics, 34, 39-60.

Shaw D (2000) Emergency relief measures and rehabilitation policies in the aftermath of the 921 Chi-Chi (Taiwan) earthquake, Proceedings of the Euro Conference on Global Change and Catastrophe Risk Management, Earthquake Risks in Europe, Laxenburg, Austria.

Shrestha K, Franquet J, Rogers CA, Tremblay R (2009) OpenSees modeling of the inelastic seismic response of steel roof diaphragms, Proceedings of the 6th International Conference of Behavior of Steel Structures in Seismic Areas, Philadelphia, Pennsylvania.

Silva V, Crowley H, Pagani M, Modelli D, Pinho R (2014) Development of the OpenQuake Engine, the Global Earthquake Model's open-source software for seismic risk assessment, Natural Hazards, 72, 1409-1427.

Silva V, Crowley H, Varum H, Pinho R (2015a). Seismic risk assessment for mainland Portugal. Bulletin of Earthquake Engineering, 13, 429-457.

Silva V, Crowley H, Varum H, Pinho R, Sousa L (2015c) Investigation of the characteristics of Portuguese regular moment-frame RC buildings and development of a vulnerability mode, Bulletin of Earthquake Engineering, 13, 1455-1490.

Silva V, Marques M, Castro JM, Varum H (2015b). Development and application of a real-time loss estimation framework for Portugal. Bulletin of Earthquake Engineering, 13, 2493-2516.

Simões da Silva L, Rebelo C, Nethercot D, Marques L, Simões R, Vila Real PMM (2009) Statistical evaluation of the lateral-torsional buckling resistance of steel I-beams. Part 2: Variability of steel properties, Journal of Constructional Steel Research, 65, 832-849.

Simões P, Fernandes C, Varum H (2007) Comparative analysis in the quantification of snow action in accordance to RSA, the Spanish standard NBE and EC1, Journal of Civil Engineering, Department of Civil Engineering, University of Minho, 29, 45-56.

Sousa ML, Costa AC (2015) Evolution of earthquake losses in Portuguese residential building stock, Bulletin of Earthquake Engineering (in press).

Sousa ML, Oliveira CS (1997) Hazard mapping based on macroseismic data considering the influence of geological conditions, Natural Hazards, 14, 207-225.

Stucchi M, Rovida A, Gomez Capera AA, Alexandre P, Camelbeeck T, Demircioglu MB, Gasperini P, Kouskouna V, Musson RMW, Radulian M, Sesetyan K, Vilanova S, Baumont D, Bungum H, Fäh D, Lenhardt W, Makropoulos K, Martinez Solares JM, Scotti O, Živčić M, Albini P, Batllo J, Papaioannou C, Tatevossian R, Locati M, Meletti C, Viganò D, Giardini D (2013). The SHARE European Earthquake Catalogue (SHEEC) 1000–1899, Journal of Seismology, 17, 523-544.

Toyoda T (2008) Economic impacts of Kobe earthquake: a quantitative evaluation after 13 years, Proceedings of the 5th International ISCRAM Conference, Washington DC, USA.

Vilanova S, Fonseca J (2007) Probabilistic seismic-hazard assessment for Portugal, Bulletin of the Seismological Society of America, 97, 1702-1717.

Whittaker S, Huang Y (2007) Simplified response analysis procedures. Background document of FEMA P-58/BD-3.7.4, Federal Emergency Management Agency.

World Bank (1999) Turkey, Marmara Earthquake Assessment, September 14, 1999, Turkey Country Office, The World Bank.

Chapter 10
Closure

10.1 Summary

In this thesis, the seismic safety and risk assessment of existing steel buildings was investigated. Current guidelines and codes for safety assessment were reviewed and their conceptual frameworks and procedures were assessed. Particular attention was given to the inconsistencies encountered in the use of Part 3 of Eurocode 8 (EC8-3) (CEN, 2005). A new simplified procedure for estimating local inelastic deformations demands using linear-elastic analysis as well as prediction equations for quantifying the deformation capacity of laterally restrained steel members with any European cross-section profile were proposed. The former procedure was validated against more accurate nonlinear dynamic analysis conducted using ground motion records selected and scaled in a sufficient, efficient and consistent manner, whereas the latter prediction equations were previously calibrated based on experimental results provided by D'Aniello et al. (2012). A novel industrial seismic loss model for Mainland Portugal was developed and the expected losses for a probability of exceedance of 10% in 50 years that the country might be exposed to were projected.

10.2 Conclusions and key contributions

Specific conclusions and contributions related to each topic addressed were given within the body of this thesis. Hereafter, the key contributions alongside with important conclusions are summarised.

10.2.1 Current inconsistencies and limitations of the EC8-3 procedures for seismic safety assessment of existing steel buildings

- EC8-3 preconizes more relaxed performance criteria, in comparison to Part 1 of Eurocode 8 (EC8-1) (CEN, 2004), that do not aim at upgrading existing buildings to comply with the design seismic level, but rather to ensure acceptable levels of damage or to prevent collapse. Still, it was not clear the probability of collapse that sets the baseline for such performance criteria. On the other hand, the EC8-1 performance requirements seem to be conservative, particularly when the linear analysis simplified approach that excludes the consideration of P-Δ effects is adopted in the seismic design.
- The restriction of EC8-3 to use linear methods of analysis when the level of knowledge of the structure is limited, as well as its confidence factor value of 1.35, need to be revised, as linear analysis itself was found to be associated to an error in local deformation demands that may reach 1.50, without accounting for material and geometrical uncertainties.
- The EC8-3 linear analysis applicability criterion seems to lead to rather ambiguous situations, due to its dependency on the lateral force patter applied, and to be associated with unacceptable levels of error, even for buildings with column-to-beam moment ratios (*CBMR*) greater than 2. Moreover, the EC8-3 applicability criterion seems to be incapable of capturing the formation of column-sway mechanisms. Local deformation demands at beams 3 times higher than those of nonlinear analysis were observed in buildings developing soft-storey mechanisms and verifying the applicability criterion. The EC8-3 linear analysis applicability criterion was found to urge for revision. This may consist on borrowing the more conservative applicability criteria from the America standard ASCE 41-13 (ASCE, 2014).
- Nonlinear static analysis was seen to provide, in line with the findings from previous works, conservative safety assessments results.
- The studies conducted in this thesis have shown that the record selection method preconized by Eurocode 8 is consistent, i.e. to provide unbiased mean global deformation demands, and scaling robust. Additionally, it was demonstrated that the Eurocode 8 method fails to be efficient, i.e. is associated to high dispersion in mean deformation demands, and sufficient with respect to the magnitude and

distance of the ground motions. It was concluded in this thesis that the efficiency and sufficiency of the Eurocode 8 record selection and scaling method may be assured by: (i) increasing the minimum number of ground motion records to 14; (ii) or imposing spectral mismatch limits relative to the target spectrum of ±50% for each individual record. The record selection and scaling should by conducted within the period range of interest proposed by Beyer and Bommer (2007). The approach of taking the maximum of three response history analysis preconized by Eurocode 8 was found to be associated to reasonable probabilities of failing, below 10%, although providing fairly conservative results.

- EC8-3 preconizes that safety verifications shall be always performed in terms of plastic rotation demands regardless the type of analysis employed. However, no particular guidance is provided by the European code in the case of linear-elastic methods of analysis. The EC8-3 acceptance criteria thus need to be revised by: (i) guiding practitioners on how to approximately estimate plastic rotations using linear analysis; (ii) or carrying out safety verifications in terms of forces similarly to the ASCE 41-13 *m*-factor approach. The later approach, which relies on the equal displacement rule, should be also validated.
- The resemblance between the deformation capacity limits preconized by EC8-3 and those defined in ASCE 41-13, suggest a direct reproduction of the EC8-3 limits from the latter document, despite the fact that American cross-section sizes are known to be significantly different from those adopted in Europe. Moreover, EC8-3 defines limits that are independent on the level of axial load and are only valid for values of normalized axial load, ν, not greater than 0.3. For stocky wide-range cross-section profiles (HEA, HEB and HEM), the EC8-3 limits were seen to be within reasonable values when the axial load is zero; however significant deviations may occur in cross-sections with web slenderness ratios greater than 18 and for higher levels of axial load. In the case of deep wide-flange IPE profiles, EC8-3 systematically provides non-conservative deformation capacity limits, which are aggravated with higher levels of axial load. The revision of the EC8-3 deformation capacity limits is deemed necessary, as it may be affecting the code performance requirements. The gravity building GB was seen to change its maximum mean local deformation demand-to-capacity ratio (*DCR*) to 0.89 (prior around 0.5) when the deformation capacity limits were updated and to be associated to a higher annual probability

of failure of 0.46×10^{-4} (β=3.91). The probability of collapse at the EC8-1 design seismic level PC|*gm* increased to 0.101 (prior around 1.01×10^{-3}) and to 0.801 (prior around 0.24) at EC8-3 near collapse limit state seismic level.

- It was demonstrated in this thesis that the current form of the EC8-3 deformation capacity limits, which depend on the chord rotation at yielding, θ_y, should be revised. The code does not provide any guidance on how to estimate θ_y, and does not recognize and call for attention for its high dependency on the shear-span length, x_{Ls}. Quantifying θ_y assuming an x_{Ls} equal to half of the length of the member, particularly at beams, was seen to significantly overestimate plastic rotation capacities in cases where gravity loads play an important role.

10.2.2 Quantification of local deformation demands

- The use of chord rotations as an alternative to plastic rotations was seen to perform, in general, fairly well, even in cases where gravity loads assume particular relevance. Conversely, despite the unequivocal value of inter-storey drifts in proving a measure of the overall damage within a storey, they failed to estimate local deformation demands when gravity loads were present and significant.
- It was observed that the Approximate Geometrical Method (*AGM-DR*) underestimates chord rotations in comparison to the more accurate Exact Integral Method (*EIM*), as it is more representative of inter-storey drifts. These results seem to contradict those of Romão et al. (2010) obtained for RC members, who recommend the use of *AGM-DR* in both columns and beams.
- Despite it has been demonstrated that, for the present case study buildings, the use of more realistic strength and stiffness deterioration models is associated to an acceptable increase in local deformation demands of 12% when compared to distributed plasticity models and for a global drift ratio up to 4%, it is important to emphasize that this observation was specific of the buildings under analysis and cannot be generalized to other cases, as discussed by Macedo et al. (2015).
- This thesis has thoroughly assessed the quantification of chord rotations using linear analysis as a mean of overcoming the limitation encountered in the EC8-3 acceptance criteria. The use of the Approximate Geometrical Method (*AGM-DR*) and the Exact Geometrical Method (*EGM*) to quantify linear chord rotations was herein investigated. It was found that both methods yield similar results,

which are in agreement with those of linear inter-storey drift ratios. However, and most importantly, linear chord rotation estimates were found to be associated to errors greater than 40% when compared to nonlinear chord rotations, and consequently to plastic rotations. These observations allowed concluding, as above mentioned, that the current EC8-3 linear analysis procedure is associated to unacceptable levels of error and should be revised.

- The Günay and Sucuoglu (2009; 2010) and the American FEMA P-58-1 (FEMA, 2012) procedures for quantifying inelastic local deformation demands using linear analysis were assessed in this dissertation. The former was found to provide acceptable, and generally slightly conservative, inelastic chord rotation demands, even in buildings with significant variations in the distribution of demands over their height. Nevertheless, the Günay and Sucuoglu (2009; 2010) procedure was seen to require a substantial amount of work in updating the reduced stiffness of all members and should be used with caution in buildings were hinging at columns is expected to occur, as the behaviour of steel columns was seen to be typically associated to significant stiffness and strength degradation due to axial load effects. The American procedure failed to provide reasonable estimates of inelastic chord rotations.

10.2.3 Deformation capacity of steel members with European profiles

- Several prediction models existing in the literature for estimating the deformation capacity of steel members were appraised in this thesis and compared to experimental results. An epistemic uncertainty associated with the use of various prediction models of around 46% was found, reflecting the different modelling approaches followed in their derivation. It has been acknowledge in this thesis the need for a cautious selection of the prediction model that most conveniently represents the real in-situ conditions of the member under evaluation.
- A detailed Finite Element (FE) model was developed and calibrated based on experimental data made available by D'Aniello et al. (2012). The FE model revealed being capable of conveniently capturing local in-plane and out-of-plane instability mechanisms observed in the experimental tests, as well as the onset of local buckling and post-buckling strength degradation. The calibration of the model was found to be highly sensitive to local geometrical imperfections,

particularly in the monotonic response, whereas global geometrical imperfections were seen not have particular influence.

- The parametric study conducted in this thesis revealed that the deformation and the over-strength capacities of steel beam-column members are highly dependent on local geometrical imperfections, axial loads and loading conditions. On the one hand, the over-strength capacity of steel members was seen to reduce up to 38% due to the effect of the axial load and to depend on the seismic intensity. Excessive levels of axial load were found to even preclude the member to develop its full plastic moment. This issue has particular importance when designing or assessing moment resisting steel frames based on capacity-design principles, as beams are expected to experience a significant increase in their flexural capacity due to over-strength effects, whereas columns will evidence a reduced maximum flexural capacity due to axial load effects. On the other hand, the deformation capacity of steel members was seen to drastically reduce up to 75% with the increase in the axial load to $v = 0.4$, to be highly dependent on the loading protocol adopted and on the characteristics of the ground motion.
- It has been demonstrated that the SAC loading protocol (Krawinkler, 2009) leads to conservative estimates of the deformation capacity of steel members. A relationship between the deformation capacity of the steel members and a so-called dissipated energy ductility factor, obtained by bi-linearizing the cumulative dissipated energy curve, was found to exist.
- This thesis corroborated the previous findings of Newell and Uang (2008), and demonstrated that the deformation capacity of heavy and wide-flange column sections, particularly of HEM profiles, is practically unaffected by the increase in the axial load. The effect of the stocky web may explain the delay on the onset of flange local buckling and may be contributing to the higher deformation capacities. This thesis further demonstrated that deep wide-flange IPE profiles and slender web HEA and HEB profiles undergo a significant reduction in their deformation capacities due to the hastening of local buckling by higher levels of axial load.
- The initiation of ductile facture due to ultra-low cycle fatigue was evaluated using strain-based and micro-mechanics approaches. Overall, both approaches were found to lead to similar results, particularly in the case of IPE and HEA

profiles, although, contrarily to the strain-based approach, the micro-mechanics approach predicted the possibility of occurring brittle fracture in HEB and HEM profiles with high λ_w ratios. Brittle fracture prior to the onset of local buckling was found to potentially occur in steel members with more compact deep wide-flange cross-sections. For the remaining cross-section profiles, fracture occurred around or before the 20% reduction in the maximum flexural capacity was reached. The axial load was seen to have a negative impact on the fatigue life of steel members similar to that observed at the onset of local buckling. Local imperfections should be treated with caution when controlling fracture initiation, as they may unrealistically change the buckle shape and affect the notch effect.

10.2.4 Contributions to EC8-3 seismic safety assessment procedures

- The Bradley (2010) procedure for probabilistic quantification of the design seismic demands was assessed. Its applicability and accuracy have been demonstrated. This thesis strongly enforced its implementation in future generations of design and assessment codes, as it clearly provides consistent mean design seismic demands with known 16% probability of being exceeded.
- More rational linear analysis applicability criteria have been proposed to account for the regularity in the distribution of plasticity over the height of the building and for the asymmetric distribution of plasticity within the beams of a floor. However, these applicability criteria are not expected to be verified by many existing buildings. Alternatively, a simplified procedure for the estimation of acceptable and conservative local inelastic deformation demands using linear-elastic analysis has been proposed. Its applicability is conditioned to buildings where hinging at columns has not or is about to initiate. Otherwise, nonlinear methods of analysis should be adopted, incorporating stiffness and strength degradation and axial load effects, as they were seen to play a critical role in the behaviour of steel columns.
- Prediction equations for the estimation of the deformation capacity of steel members with European cross-section profiles have been derived. These prediction equations account for fracture due to ultra-low cycle fatigue, as well as axial load effects. Since these prediction equations have been conservatively derived based on the SAC loading protocol, the deformation capacity may be

further relaxed on the basis of the cumulative dissipated energy, e.g., according to the dissipated energy ductility factor, as discussed in this thesis.

10.2.5 Seismic vulnerability of industrial steel buildings

- The seismic vulnerability of industrial steel buildings has been addressed in this thesis. Post-earthquake damage observed in previous reconnaissance campaigns was reviewed. More comprehensive structural damage states were defined to include all components expected to fail or suffer damage during an earthquake event. The damage states have been employed alongside with a 3-dimentional numerical model developed to allow monitoring the pre-established damage criteria. Structural fragility curves for industrial steel buildings accounting for the ground motion directivity and different column base plate connections were derived.
- It has been concluded in this thesis that column base plate connections and ground motion directivity play a critical role in loss estimates, in such a way that their disregard may considerably underestimate property losses up to 60%. Ground motions striking on the skewed *xy*-direction of analysis were found to lead to more demanding results, being the *x*-direction characterized by a moment-resisting portal frame and the *y*-direction by diagonal bracing systems. The fragility of industrial buildings with nominally pinned base plate connections was found to be mostly governed by damage to base plate connections and permanent drifts. In turn, the fragility of industrial buildings with rigid base plate connections was seen to be practically governed by damage to braces and permanent drifts.
- Vulnerability functions were derived based on the consequence models proposed within the HAZUS-MH MR5 framework (FEMA, 2010) by incorporating the uncertainty associated to the loss ratios using a multivariate random generation using Copulas. Industrial property vulnerability functions accounting for non-structural components and contents were further obtained by introducing the uncertainty in the value of contents according to different industrial activity types. Property related to manufacturing of chemical, pharmaceutical, metal and coke/refined products and to extractive industries were found to be more vulnerable to earthquakes. At least two facilities were seen to collapse after the

- In this thesis, industrial business activity vulnerability functions were built upon the HAZUS-MH MR5 framework and extended to the Portuguese industrial structure. The economic resilience to recapture the lost production, as well as to relocate so as to resume production were modelled considering current industry-specific production output values and rent prices representative of the real estate market. Indirect industrial vulnerability due to input factor, infrastructure and supply chain disruptions was equally accounted for. Industrial sectors with higher capital demand, extensive material requirements and higher degree of specialization of the production equipment and labour (e.g. chemicals, hi-tech or heavy activity industries) were seen to be expected to be hit harder by disasters.
- A thorough characterization of the Portuguese industrial steel building stock has been conducted in this thesis on the basis of a survey of more than 200 industrial building design projects and site-visits to national firms. The data collected set the background for the random generation of hundreds of synthetic industrial buildings. The influence of the geometrical characteristics and other parameters involved in the design on the fundamental period of vibration of industrial steel buildings was appraised. Taxonomies for industrial steel building were proposed.

10.2.6 Industrial seismic loss model for Mainland Portugal

- A comprehensive industrial seismic loss model for Mainland Portugal has been developed in this thesis. An exposure model incorporating economic statistical information respective to 28 industrial activities from the 2-digit Portuguese Standard Industrial Classification geographically distributed with high refinement based on the OpenStreet Maps, the CORINE Land Cover and the AICEP Global Find databases was proposed. The Porto-Lisbon costal corridor was found, as expected, to be significantly more exposed. The seismic vulnerability functions derived for typical industrial steel buildings were extended to the Portuguese building stock on the basis of the building taxonomies proposed, constituting the industrial vulnerability model developed.
- The overall mean aggregated industrial loss for mainland Portugal has been estimated to be around 2.2% of the Portuguese GDP and to represent a 10% reduction in the country's industrial annual revenue for a return period of 475 years. These losses should aware public authorities, business owners and

investors for the need of the implementation of future mitigation measures, such as the creation of specific capital reserves or an insurance pool.

10.3 Limitations and future works

The work presented in this thesis dealt with the seismic safety and risk assessment of existing steel buildings in detail, covering various conceptual, analytical and numerical aspects that, for the sake of practicability, required simplifications and assumptions. In the course of this research, several topics were also identified as requiring further examination. They are summarised in the following.

10.3.1 Codes and procedures for seismic safety assessment of existing steel buildings

- Further work focusing on the Eurocode 8 performance requirements of both parts 1 and 3 is required to understand their consistency, associated probabilities of failure and if there is room for future revision, eventually by introducing the concept of risk-target maps (Silva et al., 2015).
- The confidence factors proposed by EC8-3 should be revised for existing steel buildings similarly to what has already been conducted for RC (Franchin et al., 2012) and masonry (Cattari et al., 2015) buildings. The uncertainty that may arise from on-site inspection and testing and other procedures to check the actual condition of the structure should be equally accounted for (Romão et al., 2012). A review of existing steel property measurement techniques should be conducted and further recommendations should be implemented in the code (Castro and Araújo, 2013).
- Additional work seems to be required to support and improve the EC8-3 guidance on the retrofitting and strengthening measures, particularly those related to repair of damages members (Castro and Araújo, 2013).
- The simplified procedure for quantification of inelastic deformation demands using linear elastic analysis, as well as the linear analysis applicability criteria were proposed on the basis of a limited number of mid-rise buildings with elevation regularity. Further studies are deemed necessary to demonstrate the robustness of the proposed procedures and introduce additional amendments if needed. Analytical probabilistic frameworks consisting on the random

generation of hundreds of buildings within specific categories (e.g. mid- and high-rise buildings, irregular buildings, buildings with setbacks, 3-dimensional buildings) should be employed to support these works.

10.3.2 Behaviour and deformation capacity of steel elements

- The prediction equations proposed herein for the quantification of the deformation capacity of steel beam-column elements with European cross-sections sizes are exclusive of laterally restrained members. Further studies should be conducted to extend the prediction equations to other boundary conditions. A revision of the most common restraining solutions adopted in practice, which are oftentimes different from those preconized by codes, should be conducted (e.g. industrial steel building, residential buildings, non-building structures). The slab effect, which increases over-strength capacity in positive bending, and hastens the onset of local buckling in negative bending (Lee et al., 2016), should be investigated.
- The University of Porto group is currently conducting a probabilistic assessment of the deformation capacity of steel members with a wide range of European cross-section sizes. This work initiated within the scope of this thesis and is being carried out in close collaboration with Dr. Luís Macedo and with the supervision of Prof. José Miguel Castro. Sensitivity analysis on material and geometrical properties that are expected to mostly affect the deformation capacity of steel members are being conducted using robust statistical methodologies. Measures of uncertainty are expected to be obtained and will have particular interest in supporting the definition of the EC8-3 confidence factors, as well as to conduct future seismic risk assessments of steel buildings. Harmony search optimization algorithms are being employed to calibrate the parameters of strength and stiffness deterioration hysteretic models to be used in the modelling of a wide range of European cross-section sizes (Araújo et al., 2015; Macedo et al., 2015).
- Despite the unequivocal advantages of the Cyclic Void Growth Model (CVGM) proposed by Kanvinde and Deierlein (2007), the predictions of fracture initiation are seen to be highly dependent on the $VGI_{monotonic}^{critical}$ adopted, which is function of the λ parameter or the Charpy V-Notch impact test results (Silva, 2014).

However, values for such parameters are lacking on the literature for European structural steels. Further studies and experimental testes are required.

10.3.3 Industrial seismic risk model incorporating cascading effects for Mainland Portugal

- The industrial vulnerability functions derived in this thesis relied on the mean damage-to-loss consequence models proposed within the HAZUS-MH MR5 framework, which is simply based on expert opinion. Works focusing on the proposal of novel damage-to-loss models to industrial property and inventories are highly needed. Future surveying and data collection on the value of contents of industrial buildings and number of non-building structures (e.g. silos, tanks, towers, etc.) by industrial activity are desperately needed, particularly for Portugal, where no information exists. Logic-tree and system analysis using Bayesian networks (Porter et al., 2001; Porter and Ramer, 2012; Bensi et al., 2013) should be adopted to identify the most critical inter-linked production systems associated to various industrial activities, which would allow supporting the definition of damage-to-loss ratios (e.g. expected repair costs by damage state) and associated downtimes.
- The industrial seismic loss model for mainland Portugal should be further extended to incorporate indirect cascading effects and pre-cast RC industrial buildings. Additional work focused on the response of industrial buildings under fire triggered by earthquakes should be conducted. At least two industrial facilities collapsed after the 2012 Emilia-Romagna earthquake due to earthquake loading and following fire (EPICentre, 2012). Moreover, future attention should be devoted to the impacts of hazardous material releases triggered by earthquakes. According to Grimaz (2014), in Italy, the probability that an earthquake will trigger major dangerous substance releases from anchored and unanchored atmospheric steel tanks is higher than the probability that it will cause significant structural damage on old masonry buildings. Future studies should be dedicated to the assessment of the NatTech potential of the 127 industrial facilities located in Portugal Mainland covered by the Seveso II directive. Alarmingly, according to the Portuguese Environmental Agency (Palma, 2006), the higher number of facilities covered by the Seveso II directive are located in regions with higher industrial risk, such as Lisbon and Setúbal.

10.4 References

Araújo M, Macedo L, Castro JM (2015) Calibration of strength and stiffness deterioration hysteretic models using optimization algorithms, In Proceedings, 8th International Conference on Behaviour of Steel Structures in Seismic Areas STESSA, Shanghai, China.

ASCE (2014) Seismic evaluation and retrofit of existing buildings (ASCE/SEI 41-13), American Society of Civil Engineers.

Bensi M, Der Kiureghian A, Straub C (2013) Efficient Bayesian network modeling of systems, Reliability Engineering and System Safety, 112, 200-213.

Beyer K, Bommer J (2007) Selection and scaling of real accelerograms for bi-directional loadings: a review of current practice and code provisions, Journal of Earthquake Engineering, 11, 13-45.

Bradley B (2011) Design seismic demands from seismic response analyses: A probability-based approach, Earthquake Spectra, 27, 213-224.

Castro JM, Araújo M (2013) Assessment and rehabilitation of the seismic safety of existing buildings to part 3 of Eurocode 8: The case of steel, International Seminar on Strengthening and Rehabilitation – Materials and Technologies, Faculty of Engineering of the University of Porto and Hilti, Porto, Portugal.

Cattari S, Logomarsino S, Bosiljkov V, D'Ayala D (2015) Sensitivity analysis for setting up the investigation protocol and defining proper confidence factors for masonry buildings, Bulletin of Earthquake Engineering, 13, 129-151.

CEN (2004) ENV 1998-1 Eurocode 8: Design of structures for earthquake resistance - Part 1: General rules, seismic actions and rules for buildings, European Committee for Standardization, Brussels, Belgium.

CEN (2005) ENV 1998-3 Eurocode 8: Design of structures for earthquake resistance - Part 3: Assessment and retrofitting of buildings, European Committee for Standardization, Brussels, Belgium.

EPICentre (2012) The 29th May 2012 Emilia Romagna Earthquake, EPICentre Field Observation Report, University College London, London, United Kingdom.

FEMA (2010) Multi-hazard loss estimation methodology. Earthquake Model. HAZUS – MH MR5 Technical Manual, Federal Emergency Management Agency, Mitigation Division, Washington, D. C.

FEMA (2012) FEMA P-58-1 Seismic performance assessment of buildings. Volume 1 – Methodology, Federal Emergency Management Agency, Washington, D.C., U.S.A.

Franchin P, Pinto PE, Rajeev R (2012) Confidence factor? Journal of Earthquake Engineering, 14, 989-1007.

Grimaz S (2014) Can earthquakes trigger serious industrial accidents in Italy? Some consideration following the experiences of 2009 L'Aquila (Italy) and 2012 Emilia (Italy) earthquakes, Bullettino di Geofisica Teorica ed Applicata, 55, 227-237.

Günay MS, Sucuoglu H (2010) An improvement to linear-elastic procedures for seismic performance assessment, Earthquake Engineering and Structural Dynamics, 39, 907–931.

Günay MS, Sucuoglu, H (2009) Predicting the seismic response of capacity-designed structures by equivalent linearization, Journal of Earthquake Engineering, 13, 623-649.

Kanvinde AM, Deierlein GG (2007) Cyclic void growth model to assess ductile fracture initiation in structural steels due to ultra-low cycle fatigue, Journal of Engineering Mechanics, 133, 701-712.

Krawinkler H (2009) Loading histories for cyclic tests in support of performance assessment of structural components, Proceeding of the 3rd International Conference on Advances in Experimental Structural Engineering, San Francisco.

Lee CH, Jung JH, Kim SY, Kim JJ (2016) Review of composite slab effect on the seismic performance of welded steel moment connections, Journal of Constructional Steel Research, in press.

Macedo L, Araújo M, Castro JM (2015) Comparison of modelling strategies for steel structures under cyclic loads, Proceedings of the 8th International Conference of Behaviour of Steel Structures in Seismic Areas.

Newell JD, Uang CM (2008) Cyclic behavior of steel wide-flange columns subjected to large drift, Journal of Structural Engineering, 134, 1334-1342.

Palma MC (2006) Application of the Seveso II directive in Portugal, II Iberian Meeting on Industrial Safety and Fire Protection Engineering. New challenges for the XXI century, Porto, Portugal.

Porter K, Ramer K (2012) Estimating earthquake-induced failure probability and downtime of critical facilities, Journal of Business Continuity & Emergency Planning, 5, 352-364.

Porter KA, Kiremidjian AK, LeGrue JS (2001) Assembly-based vulnerability of buildings and its use in performance evaluation, Earthquake Spectra, 17, 291-312.

Romão X, Delgado R, Costa A (2010) Practical aspects of demand and capacity evaluation of RC members in the context of EC8-3, Earthquake Engineering and Structural Dynamics, 39, 473–499.

Romão X, Gonçalves R, Costa A, Delgado (2012) Evaluation of EC8-3 confidence factors for the characterization of concrete strength in existing structures, Material and Structures, 45, 1737-1758.

Silva T (2014) Influence of ultra-low cycle fatigue on the deformation capacity assessment of structural steel elements, MSc dissertation thesis, Faculty of Engineering of the University of Porto, Porto, Portugal.

Silva V, Crowley H, Bazzurro P (2015) Exploring risk-targeted hazard maps for Europe, Earthquake Spectra, in press.